

Version 1.0, May 25, 2019

Neutrino masses and mixings and...

Alessandro Strumia

Dipartimento di Fisica dell’Università di Pisa and INFN, Italia

Francesco Vissani

INFN, Laboratori Nazionali del Gran Sasso, Theory Group, I-67010 Assergi (AQ), Italy

Abstract

We review experimental and theoretical results related to neutrino physics with emphasis on neutrino masses and mixings, and outline possible lines of development.

We try to present the physics in a simple way, avoiding unnecessary verbosity, formalisms and details. Comments, criticisms, etc are welcome. We want to upgrade this ‘review’ or ‘book’ at the light of future developments: therefore for the moment we publish it only on

[arXiv.org/abs/hep-ph/0606054](https://arxiv.org/abs/hep-ph/0606054) and www.cern.ch/astrumia/review.html

in electronic form. Nowadays it has several advantages over printed form, but prevents an official refereeing process. We asked some experts to privately referee the parts less connected to our research activity. The review is organized as follows:

- Chapter 1: a brief overview.
- Chapters 2, 3, 4: the basic tools.
- Chapters 5, 6: the established discoveries (solar and atmospheric).
- Chapters 7, 8: future searches for neutrino oscillation and neutrino masses.
- Chapter 9: unconfirmed anomalies.
- Chapters 10, 11: neutrinos in cosmology and astronomy.
- Chapters 12, 13, 14: speculative lines of development.

Acronyms are listed in appendix A. Appendix B summarizes basic facts concerning statistics. The last pages contain the detailed index.

Chapter 1

Introduction

Neutrinos physics is interesting because neutrino experiments recently discovered something new, rather than giving only more precise measurements of SM parameters, or stronger bounds on unseen new physics. ‘Solar’ and ‘atmospheric’ data directly show that lepton flavour is not conserved.

The next step is identifying the new physics responsible of these anomalies. Theoretical simplicity suggests oscillations of massive neutrinos, which can fit data provided that mixing angles among the SM neutrinos are unexpectedly large. The observed flavour conversions could be produced by other mechanisms. Present data strongly disfavor alternative exotic possibilities, such as neutrino decay or oscillations into extra ‘sterile’ neutrinos ν_s (i.e. light fermions with no SM gauge interactions, as opposed to the three ‘active’ SM neutrinos) and show some hints for the characteristic features of oscillations.

Future experiments should confirm and complete this picture. Oscillations can be directly seen by precise reactor and long-baseline beam experiments, that are nowadays respectively testing the solar and atmospheric anomalies. Other so far unseen oscillation effects (‘atmospheric’ oscillations into ν_e , and CP-violation) could be discovered soon or never, depending how large they are. Future non-oscillation experiments should detect neutrino masses, and test if they violate lepton number. Realistically, these developments could be achieved in the next 10 or 20 years. Understanding neutrino propagation will allow to do astrophysics, cosmology, geology using neutrinos.

At this point we will still have to understand the origin of the neutrino mass scale, $m_\nu \sim (0.01 \div 0.05)$ eV. Presumably neutrino masses are of Majorana type and are the first manifestation of a new scale in nature, $\Lambda_L \sim v^2/m_\nu \sim 10^{14}$ GeV. This could be the mass of new particles, maybe 3 right-handed neutrinos with a 3×3 matrix of Yukawa couplings. Experiments drove the recent progress but cannot directly test such high energies. Leptogenesis, $\mu \rightarrow e\gamma$ and related processes could be other manifestations of the new physics behind neutrino masses.

Alternatively, experiments could discover something different, e.g. some new light particle, and require a significant change in the above picture. This would be the case if an anomaly, seen so far only by the LSND experiment, will be confirmed.

Before starting, we present a quick overview. We employ standard, usually self-explanatory notations, precisely defined in the next sections.

1.1 Past

After controversial results, in 1914 Chadwick established that the electrons emitted in radioactive β decays have a continuous spectrum, unlike what happens in α and γ decays. It took some time to ensure that, if the β decay process were ${}_Z^A X \rightarrow {}_{Z-1}^{A-1} X e$ with only two particles in the final state, energy conservation would unavoidably imply a monochromatic electron spectrum. (Today we also know that Lorentz invariance requires an even number of fermions in decays).

On 4 december 1930 Pauli proposed a ‘desperate way out’ to save energy conservation, postulating the existence a new neutral particle, named “neutron”, with mass ‘of the same order of magnitude as the electron mass’ and maybe ‘penetrating power equal or ten times bigger than a γ ray’ [1]. The estimate of the cross-section was suggested by the old idea that particles emitted in β decays were previously bound in the parent nucleus (as happens in α decays) — rather than created in the decay process. In a 1934 paper containing ‘speculations too remote from reality’ (and therefore rejected by the journal *Nature*) Fermi overcame this misconception and introduced a new energy scale (the ‘Fermi’ or ‘electroweak’ scale) in the context of a model able of predicting neutrino couplings in terms of β -decay lifetimes. Following a joke by Amaldi, the new particle was renamed neutrino¹ after that the true neutron had been identified by Chadwick. Neutrinos were finally directly observed by Cowan and Reines in 1956 in a nuclear reactor experiment and found to be left-handed in 1958.

In those years $K^0 \leftrightarrow \bar{K}^0$ effects were clarified, and this lead Pontecorvo to discuss $\nu \leftrightarrow \bar{\nu}$ oscillations with maximal mixing in a 1957 paper [2]. In 1962 $\nu_e \leftrightarrow \nu_\mu$ ‘virtual transmutations’ were mentioned by Maki, Nakagawa and Sakata in the context of a wrong model of leptons bound inside hadrons [3]. For these reasons some authors now name ‘MNS’ (or ‘MNSP’, or ‘PMNS’) the neutrino mixing matrix, although this seems as improper as naming ‘indians’ the native habitants of America. The work that lead to the first evidence for a neutrino anomaly was done by Bahcall et al. (that predicted the solar ν_e flux) and by Davis et al. (that, using a technique suggested by Pontecorvo [4], since 1968 measured a ν_e flux smaller than the predicted one) [4]. Despite significant efforts, up to few years ago, it was not clear if there was a solar neutrino problem or a neutrino solar problem. Phenomenologists pointed out a few clean signals possibly produced by oscillations, but could not tell which ones are large enough to be detected. Since doing experiments is the really hard job, only in 2002 two of these signals have been discovered. The SNO solar experiment found evidence for $\nu_{\mu,\tau}$ appearance and the KamLAND experiment confirmed the solar anomaly discovering disappearance of $\bar{\nu}_e$ from terrestrial (japanese) reactors.

In the meantime, analyzing the atmospheric neutrinos, originally regarded as background for proton decay searches, in 1998 the japanese (Super)Kamiokande experiment established a second neutrino anomaly, confirmed around 2004 by K2K, the first long base-line neutrino beam experiment.

1.2 Present

Table 1.1 summarizes the oscillation interpretation of the two established neutrino anomalies:

¹In italian the suffixes for small and large are -ino and -one. The root of neutrino is ‘ne uter’, ‘not either’ in latin. Presently adopted pronunciations differ from the latin-italian pronunciation. E.g. japanese experimentalists recently gave a main contribution to neutrino physics, but pronounce it as ニュートリノ (‘nyu to ri no’), doubly distorted due to limitations of hiragana (to) and english (nyu) phonetics.

Oscillation parameter	central value	99% CL range
solar mass splitting	$\Delta m_{12}^2 = (8.0 \pm 0.3) 10^{-5} \text{ eV}^2$	$(7.2 \div 8.9) 10^{-5} \text{ eV}^2$
atmospheric mass splitting	$ \Delta m_{23}^2 = (2.5 \pm 0.2) 10^{-3} \text{ eV}^2$	$(2.1 \div 3.1) 10^{-3} \text{ eV}^2$
solar mixing angle	$\tan^2 \theta_{12} = 0.45 \pm 0.05$	$30^\circ < \theta_{12} < 38^\circ$
atmospheric mixing angle	$\sin^2 2\theta_{23} = 1.02 \pm 0.04$	$36^\circ < \theta_{23} < 54^\circ$
‘CHOOZ’ mixing angle	$\sin^2 2\theta_{13} = 0 \pm 0.05$	$\theta_{13} < 10^\circ$

Table 1.1: *Summary of present information on neutrino masses and mixings from oscillation data.*

- The **atmospheric** evidence. SuperKamiokande [5] observes disappearance of ν_μ and $\bar{\nu}_\mu$ atmospheric neutrinos, with ‘infinite’ statistical significance ($\sim 17\sigma$). If interpreted as oscillations, one needs $\nu_\mu \rightarrow \nu_\tau$ with quasi-maximal mixing angle. The other possibilities, $\nu_\mu \rightarrow \nu_e$ and $\nu_\mu \rightarrow \nu_s$, cannot explain the anomaly and can only be present as small sub-dominant effects. The SK discovery is confirmed by ν_μ beam experiments: K2K [6] and NuMI [7]. Table 1.1 reports global fits for oscillation parameters.
- The **solar** evidence. Various experiments [4, 8, 9, 10] see a 8σ evidence for a $\sim 50\%$ deficit of solar ν_e . The SNO experiment sees a 5σ evidence for $\nu_e \rightarrow \nu_{\mu,\tau}$ appearance (solar neutrinos have energy much smaller than m_μ and m_τ , so that experiments cannot distinguish ν_μ from ν_τ). The KamLAND experiment [11] sees a 6σ evidence for disappearance of $\bar{\nu}_e$ produced by nuclear reactors. If interpreted as oscillations, one needs a large but not maximal mixing angle, see table 1.1. Other oscillation interpretations in terms of a small mixing angle enhanced by matter effects, or in terms of sterile neutrinos, are excluded.

There are few unconfirmed anomalies related to neutrino physics.

1. **LSND** [12] sees a $(3 \div 7)\sigma$ $\bar{\nu}_\mu \rightarrow \bar{\nu}_e$ anomaly (the statistical significance varies depending on how data are analyzed, so that it is presented as a 3σ anomaly), maybe due to oscillations with $\Delta m^2 \sim 1 \text{ eV}^2$ and small mixing. KARMEN [13] excludes part of the oscillation region suggested by LSND. A $\bar{\nu}_\mu \rightarrow \bar{\nu}_s \rightarrow \bar{\nu}_e$ interpretation is disfavored by other experiments.

The three possible oscillation effects (solar, atmospheric, LSND) require three different ranges of Δm^2 . Therefore with oscillations of three neutrinos it is possible to fit only two anomalies: usually one drops the LSND anomaly. In order to fit all anomalies, one can try to add one extra sterile neutrino. However this does not provide a satisfactory fit because none of the three anomalies is well fitted by sterile oscillations. If all experiments were confirmed, it is likely that some unexpected new physics is involved.

2. **NuTeV** [14] claims a 3σ anomaly in neutrino *couplings*: the measured ratio between the $\nu_\mu/\text{iron NC and CC}$ couplings is about 1% lower than some SM prediction. Specific QCD effects that cannot be computed in a reliable way could be the origin of the NuTeV anomaly.
3. A reanalysis [15] of the **Heidelberg-Moscow** data [16] claims a 4σ hint for violation of lepton number. The simplest interpretation would be in terms of Majorana neutrino masses, implying approximatively degenerate neutrinos with mass $m \sim 0.4 \text{ eV}$. In our opinion these data contain a $(2 \div 3)\sigma$ hint at most.

Furthermore, there are some important constraints

- LEP data tell that there are **only 3 neutrinos** lighter than $M_Z/2$. Extra light fermions with no gauge interactions might exist, and could play the rôle of ‘sterile neutrinos’.
- Together with atmospheric and K2K data the CHOOZ bound on the $\bar{\nu}_e$ survival probability restricts θ_{13} , the last unseen mixing angle that induces $\nu_e \leftrightarrow \nu_{\mu,\tau}$ **oscillations at the atmospheric frequency** Δm_{atm}^2 to be

$$\sin^2 2\theta_{13} = 0 \pm 0.05.$$

- Under plausible *assumptions*, cosmology implies that **neutrinos are lighter than about 0.2 eV**. Assuming that neutrinos have Majorana masses, bounds on $0\nu2\beta$ decay imply $m_\nu \lesssim 1 \text{ eV}$. Bounds on β decay imply $m_\nu \lesssim 2 \text{ eV}$. Astrophysics gives somewhat weaker bounds.

1.3 Future?

The recent discoveries have been achieved studying natural phenomena with neutrino detectors. Solar, atmospheric, supernova, terrestrial and reactor neutrinos are freely available, and are interesting not only for fundamental physics. Further progress is expected along these lines, but maybe no new discoveries. To discover new effects which might affect natural neutrinos in a minor way, it will be necessary to first produce the physical system to be later studied, as already customary in collider physics. Even if significant improvements seem possible, the necessity of building appropriate neutrino beams will make progress more expensive and slow, as illustrated in table 1.2. Fig. 1.1 shows the regions of the (L, E_ν) plane which have so far explored, with at least one neutrino flavour.

2006 On 17 June at the Neutrino 2006 conference, the **MiniBoone** collaboration will announce if the LSND anomaly is confirmed. **KamLAND** will try to establish the distortion in the $\bar{\nu}_e$ energy spectrum characteristic of oscillations. **Borexino** and maybe KamLAND begins to study the monochromatic ${}^7\text{Be}$ neutrinos.

2007 **long-baseline** experiments (the already running NuMI and the presumably later CNGS) will better measure the atmospheric parameters, testing oscillations and maybe discovering θ_{13} (i.e. $\nu_\mu \rightarrow \nu_e$ oscillations at the atmospheric frequency).

2008 **LHC** begins to explore physics at the TeV scale, maybe having some indirect relevant impact on neutrino physics.

IceCube, located at south pole, tries to start neutrino astronomy at energies larger than about a TeV. Other projects that use sea water instead of ice are being discussed (ANTARES, NEMO, NESTOR).

The **MEG** $\mu \rightarrow e\gamma$ experiment [17] might give the first results.

AUGER has collected enough cosmic rays up to 10^{20} eV , saying the final word about the GZK anomaly [18].

experiment	status	name	start	cost in M€
WC (3 kton)	terminated	Kamiokande	1983	5
WČ (50 kton)	running	SuperKamiokande	1996	100
WČ (1000 kton)	proposals	HyperK, UNO?	2015?	500?
Solar B	running	SNO	2001	100 + 500 (target)
Solar Be	construction	Borexino	2006?	25
Solar pp	running	Gallex \approx SAGE/2	1991	1 + 15 (target)
Solar pp	proposals	many or none	2010?	100??
Reactor	terminated	CHOOZ	1997	1.5
Reactor	running	KamLAND	2002	20
Reactor	proposal	Double-CHOOZ	2009	10
Long baseline	terminated	K2K	1999	(beam)
Long baseline	construction	CNGS	2006	50 (beam) + 80 (detectors)
Long baseline	construction	NuMI	2004	110 (beam) + 60 (detector)
Long baseline	proposal	Nova	2011	160
Long baseline	approved	T2K	2009	130
Long baseline	proposals	super-beam	2010?	500?
Long baseline	discussions	ν factory	2020?	2000?
CR observatory	construction	Auger	2005	50
ν telescope	approved	ANITA	2007	35
ν telescope	approved	IceCube	2010?	200
β decay at 0.2 eV	approved	Katrin	2008?	35
$0\nu 2\beta$ at 0.01 eV	proposals		2010?	100?
ν couplings	terminated	NuTeV	1996	
$e\bar{e}$ collider (103 GeV)	terminated	LEP	1989	1200
$e\bar{e}$ collider (1 TeV)	proposals	ILC	2020?	10000?
pp collider (7 TeV)	construction	LHC	2008	3000
pp collider (20 TeV)	not approved	SSC		10000?
Satellite	running	WMAP	2003	150
Satellite	construction	GLAST	2008	200
Gravit. wave detector	running	LIGO + VIRGO	2002	250 + 100
Super B factory	discussions	BarbaBelle?	2015?	600?
Space station	running	ISS	2006?	50000?

Table 1.2: *Main neutrino experiments. Costs are estimated approximating 億¥ \approx M\$ \approx M€, which is about the total life salary of a physicist. This allows to estimate that manpower costs (not included) are often comparable to the cost of the experiment. Some experiments obtained their target material as free rent, but bigger experiments will have to produce it. Among the many caveats, we emphasize that costs of future experiments are rarely underestimated.*

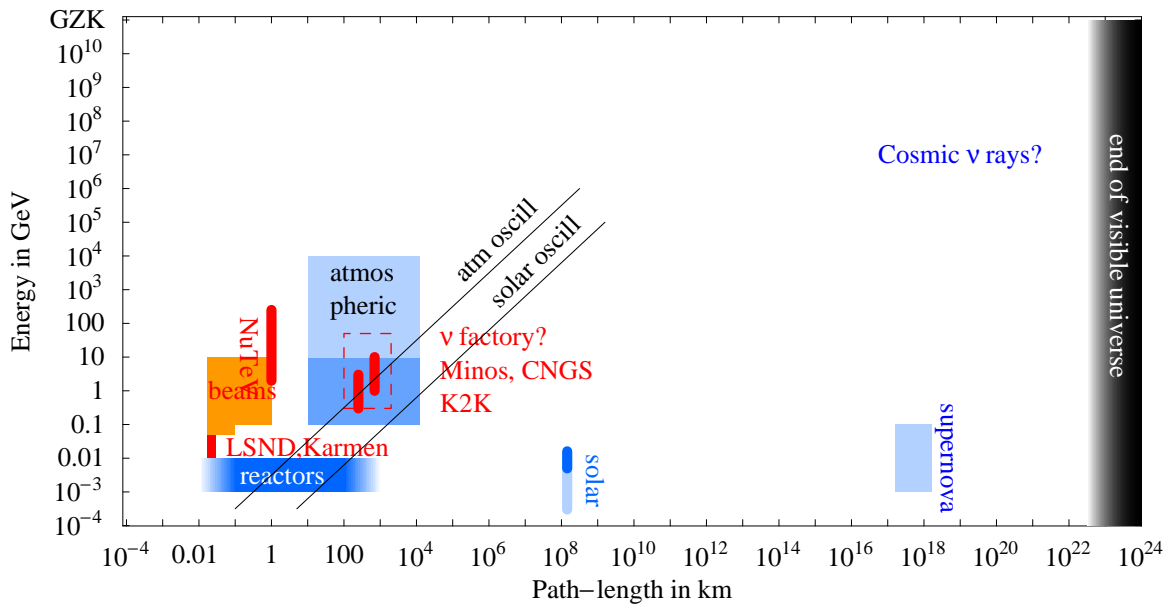


Figure 1.1: *Regions explored using natural (blue) or artificial (red) neutrino sources. Solar and atmospheric oscillations occur below the black lines.*

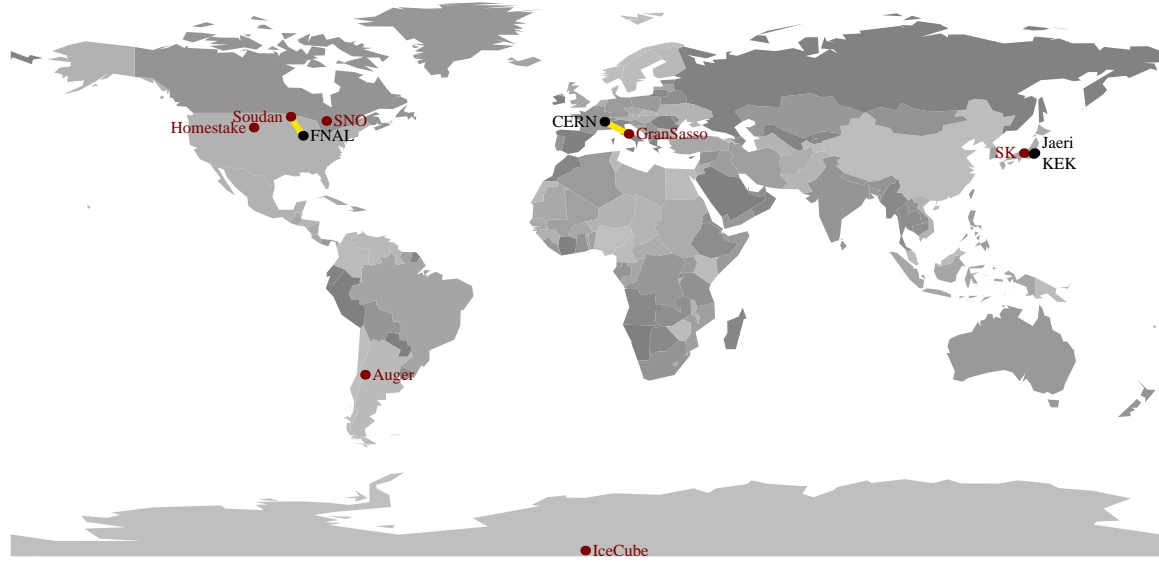


Figure 1.2: *Location of main neutrino-related observatories.*

Source	Mechanism	Flavour	Typical energy	Rate
Sun	nuclear fusion	ν_e	(0.1 \div 20) MeV	known
Atmosphere	π, μ decays	$(\bar{\nu})_{e,\mu}$	(0.1 \div 1000) GeV	known
Big-Bang	thermal	all	\sim meV	too small
Supernovæ	thermal	all	\lesssim 50 MeV	poorly known
Astrophysics	π, μ decays?	$(\bar{\nu})_{e,\mu}$?	?	?
Sun, Earth	DM annihilations	all	$< m_{\text{DM}}$?
Earth	nuclear decays	$\bar{\nu}_e$	\lesssim few MeV	poorly known
Fission reactors	nuclear fission	$\bar{\nu}_e$	\lesssim 10 MeV	known
Conventional beams	π or μ decay	$(\bar{\nu})_{e,\mu}$	tunable, \sim GeV	known
ν -factory	μ^- decay	$\nu_\mu, \bar{\nu}_e$	tunable, \sim 10 GeV	well known
ν -factory	μ^+ decay	$\bar{\nu}_\mu, \nu_e$	tunable, \sim 10 GeV	well known
β -beams	Nuclear decay	ν_e or $\bar{\nu} - e$	tunable, \sim GeV	well known

Table 1.3: *Possible neutrino sources.*

2009 **T2K** and **NO ν A**. Around 2009 two intense ν_μ beam experiments will start. Their main goal is completing the measurement of neutrino oscillation parameters: θ_{13}, \dots . The T2K experiment will use SK as detector, that could sooner or later be upgraded up to a ‘Hyper-Kamiokande’ Mton WČ, relevant also for proton decay and other searches.

The high-intensity beam also allows tests of neutrino couplings and searches for lepton-flavour violating μ decays.

200? Some big **neutrino-less double-beta decay** experiment will search for violation of lepton number (e.g. Majorana ν masses). Some experiment could precisely study **sub-MeV solar neutrinos**.

2010 A sensitivity to neutrino masses $m_\nu \gtrsim 0.1$ eV could be reached by the **Katrin** β -decay experiment.

2020 A **neutrino factory** or **beta-beam** could perform the ‘ultimate’ search for oscillation effects.

20?? Few thousands of neutrino events will be detected at the next core-collapse galactic **supernova** explosion allowing to study astrophysics and maybe neutrino oscillations.

2030 december 4: ν centennial. This is the only safe expectation.²

²Most of the expectations for the years 2002—2005 present in our first drafts have been realized.

Chapter 2

Neutrino masses

2.1 Massless neutrinos in the SM

In all observed processes baryon number B and lepton number L are conserved. Searches for proton decay and for neutrino-less double-beta decay (section 8.4) give the dominant constraints. The SM provides a nice interpretation of these results, missed by old pre-SM models where e, ν, p, n, π were considered as point-like fundamental particles. Yukawa introduced a $pn\pi^-$ coupling in order to account for nuclear forces. However, the analogous Yukawa-type coupling $p\nu\pi^-$, obtained by replacing n with ν , would give rise to unseen p decay. These models do not explain why the proton is stable, but explain why the electron is stable: electric charge is conserved and the electron is the lightest ‘charged’ particle. Therefore theorists introduced a new conserved charge, called baryon number B , under which the proton is the lightest charged particle. This makes the proton stable and forbids all other B -violating processes, like $pp \rightarrow \bar{e}\bar{e}$.

Conservation of lepton number was introduced for analogous reasons. In particular it forbids unseen L -violating neutrino mass terms without forbidding the neutron mass term. Exact conservation of B and L was widely considered on the same footing of conservation of electric charge.

The advent of gauge theories and of the SM changed the situation: today B and L automatically emerge as approximatively conserved charges.

The key difference between n and ν is that the neutron is a bound state of quarks. In the SM the Yukawa coupling $pn\pi^-$ arises from renormalizable strong interactions of quarks, while the $p\nu\pi^-$ coupling would correspond to a non renormalizable $qqq\nu$ interaction. In fact the most general $SU(3)_c \otimes SU(2)_L \otimes U(1)_Y$ gauge-invariant renormalizable Lagrangian that can be written with the SM fields (the Higgs doublet H and the observed fermions: the three lepton doublets $L = (\nu, \ell_L)$, the lepton singlets $E = \ell_R$, etc. See table 4.1 at page 45 for the full list.) beyond ‘minimal’ terms (kinetic and gauge interactions) can only contain the following Yukawa and Higgs-potential terms

$$\mathcal{L}_{\text{SM}} = \mathcal{L}_{\text{minimal}} + (\lambda_E^{ij} E^i L^j H^* + \lambda_D^{ij} D^i Q^j H^* + \lambda_U^{ij} U^i Q^j H + \text{h.c.}) + m^2 |H|^2 - \frac{\lambda}{4} |H|^4 \quad (2.1)$$

where $i, j = \{1, 2, 3\}$ are flavour indices. No term violates baryon number B and lepton flavour L_e, L_μ, L_τ (and in particular lepton number $L = L_e + L_\mu + L_\tau$), that therefore naturally emerge as *accidental* symmetries.¹ In the SM there is no need of imposing by hand a stable proton and

¹To be more precise, quantum anomalies modify the situation in a way which will be relevant only when

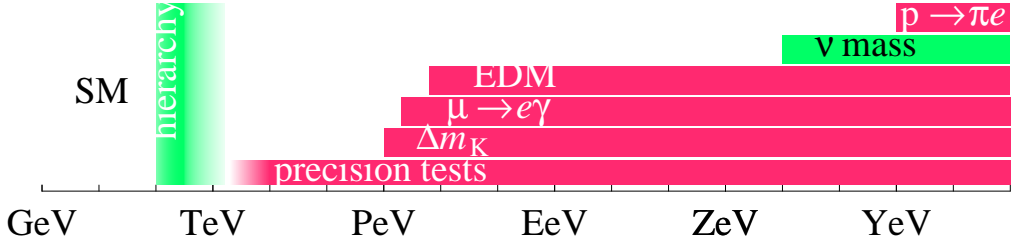


Figure 2.1: *Bounds on the scale Λ that suppresses non-renormalizable operators that violate B, L, CP, L_f, B_f and affect precision data. Maybe the ‘hierarchy problem’ suggests new-physics around few hundred GeV.*

massless neutrinos. This line of reasoning leads to more successful predictions: baryon flavour and CP are violated in a very specific way, described by the CKM matrix, giving rise (among other things) to characteristic rates of $K^0 \leftrightarrow \bar{K}^0$, $B^0 \leftrightarrow \bar{B}^0$ transitions. Since CKM CP violation is accompanied by flavour mixing, CP-violating effects which do not violate flavour, like electric dipoles, are strongly suppressed, in agreement with experimental data.²

The Higgs vev breaks $SU(2)_L \otimes U(1)_Y \rightarrow U(1)_{\text{em}}$

$$\langle H \rangle = (0, v) \quad \text{with} \quad v \approx 174 \text{ GeV}, \quad (2.2)$$

and gives Dirac masses to charged leptons and quarks³ mass terms $m_i = \lambda_i v$

$$m_E \ell_R \ell_L + m_D d_R d_L + m_U u_R u_L$$

but neutrinos remain massless. Within the SM, neutrinos are fully described by the Lagrangian term

$$\bar{L} i \not{D} L$$

i.e. a kinetic term plus gauge interactions with the massive vector bosons, $\bar{\nu} Z \nu$ and $\bar{\nu} W \ell_L$.

discussing baryogenesis in section [19]. To be less precise, massless neutrinos were already suggested, before the SM, by the $V - A$ structure of weak interactions.

²Most of these theoretical successes would be lost if extensions of the SM motivated by the hierarchy ‘problems’, such as the MSSM, will be confirmed by future data.

³Dirac and Majorana quadri-spinors are usually presented following the historical development and notation, but this is confusing. Quadri-spinors are representations of the Lorentz group and of parity, that was believed to be an exact symmetry. Since we now know that this is not the case, it is more convenient to use the basic fermion representations of the Lorentz group: the 2-dimensional Weyl spinors. The only Lorentz invariant mass term that can be written with a single Weyl fermion ψ is the Majorana term ψ^2 . This mass term breaks a $U(1)$ symmetry $\psi \rightarrow e^{iq\psi} \varphi \psi$ under which ψ might be charged (it could be electric charge, hypercharge, lepton number, ...). For example, a Majorana neutrino mass is possible if the electric charge of neutrinos is exactly zero. With two Weyl fermions ψ and ψ' one can write three mass terms: ψ^2 , ψ'^2 and $\psi\psi'$. In many interesting cases (all SM fermions, except maybe neutrinos) the Lagrangian has an unbroken $U(1)$ symmetry (electromagnetism, in the SM) under which ψ and ψ' have opposite charges, so that then $\psi\psi'$ is the only allowed mass term. It is named ‘Dirac mass term’, and one can group ψ and ψ' in one 4-component Dirac spinor $\Psi = (\psi, \bar{\psi}')$. The electron gets its mass from a Dirac term, that joins two different Weyl fermions that are therefore named e_L and e_R rather than ψ and ψ' . If one knows what is doing this is the simplest notation. Since e_L and e_R have opposite electric charges one usually prefers to use names like ‘ \bar{e}_R ’ or ‘ e_R^c ’ or ‘ e_L^c ’ in place of ‘ e_R ’. For a clean recent presentation of Weyl spinors see [20].

2.2 Massive neutrinos beyond the SM

Observations of neutrino masses call for an extension of the SM, and plausible extensions of the SM suggested neutrino masses.

The new physics can be either lighter or heavier than 100 GeV, the maximal energy that has been experimentally explored so far.

Since LEP excluded new particles coupled to the Z boson and lighter than $M_Z/2$, the first case can only be realized by adding light *right-handed neutrinos* ν_R . Unlike other right-handed leptons and quarks, ν_R are neutral under all SM gauge interactions: gauge invariance allows a Majorana mass term for right-handed neutrinos, $N\nu_R^2/2$, that breaks lepton number. Neutrinos can acquire Dirac masses like all other fermions if conservation of lepton number (that in the SM is automatic) is imposed by hand, such that $M = 0$. In such a case, the neutrino Yukawa coupling $\lambda_N \nu_R L H$ gives the Dirac neutrino mass $m_\nu = \lambda_N v \approx 0.1$ eV for $\lambda_N \sim 10^{-12}$.

Alternatively, generic new physics too heavy for being directly studied manifests at low energy as non renormalizable operators (NRO), suppressed by heavy scales Λ . NRO give small corrections, suppressed by powers of E/Λ , to physics at low energy $E \ll \Lambda$, that is therefore well described by a renormalizable theory. The SM is the low energy effective theory of something and we would like to know what this something is. Experimentally, this something can be searched in various ways: a) going to higher energies; b) searching for small effects in precision experiments at low energies; c) searching for small effects enhanced by a large coherence factor; d) studying rare processes; e) searching processes that cannot be generated by renormalizable operators.

This last possibility is how the Fermi scale made its first appearance. The 1896 discovery of radioactivity by Becquerel (β -rays were soon identified by Rutherford) lead Fermi to add to the QED Lagrangian non renormalizable $pne\nu$ operators suppressed by the electroweak scale.

History might repeat now. Adding NRO to the SM Lagrangian, L_e, L_μ, L_τ, B are no longer accidentally conserved:

$$\mathcal{L} = \mathcal{L}_{\text{SM}} + \frac{(LH)^2}{2\Lambda_L} + \frac{1}{\Lambda_B^2} \left[c_1(\bar{U}\bar{D})(QL) + c_2(QQ)(\bar{U}\bar{E}) + c_3(QQ)(QL) + \right. \quad (2.3)$$

$$\left. c_4(Q\tau^a Q)(Q\tau^a L) + c_5(\bar{D}\bar{U})(\bar{U}\bar{E}) + c_6(\bar{U}\bar{U})(\bar{D}\bar{E}) + \text{h.c.} \right] + \dots \quad (2.4)$$

With only one light higgs doublet there is only one kind of dimension-5 operator: $(LH)^2 = (\nu h^0 - e_L h^+)^2$. Inserting the Higgs vev v , this operator gives a Majorana neutrino mass term, $m_\nu \nu_L^2/2$, with $m_\nu = v^2/\Lambda_L \sim 0.1$ eV for $\Lambda_L \sim 10^{14 \div 15}$ GeV. Neutrino masses might be the first manifestation of a new length scale Λ_L in nature.

The six dimension-6 operators violate B and conserve $B - L$ giving rise to proton decay into anti-leptons: $p \rightarrow \bar{e}\pi^0, \bar{\nu}\pi^+, \dots$ with width $\tau_p^{-1} \sim m_p^5/\Lambda_B^4$. The first two B -violating operators can be mediated by tree-level exchange of heavy vector bosons, and are predicted by unification models. The strongest constraint on the proton life-time τ_p comes from the SK experiment, which monitored about 10^{10} moles of protons for a few years. Therefore the present bound is

$$\tau_p \gtrsim 10^{10} N_A \text{ yr} \approx 10^{34} \text{ yr} \quad \text{i.e.} \quad \Lambda_B \gtrsim 10^{15} \text{ GeV.} \quad (2.5)$$

Observing proton decay would open another window on physics at high energy scales.

Furthermore, other operators (not shown) give additional sources of CP and hadronic flavour violation, or affect precision LEP data. Fig. 2.1 summarizes present bounds. In conclusion, we

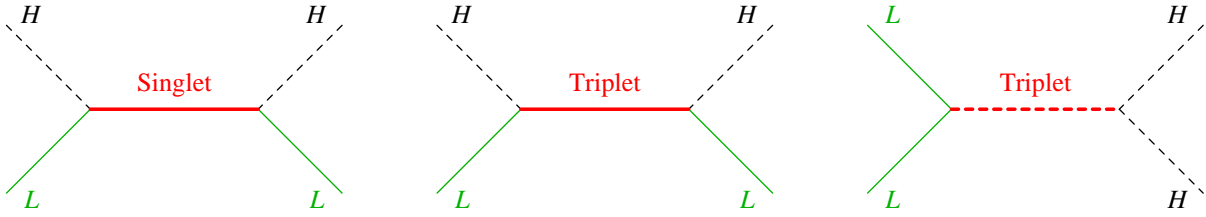


Figure 2.2: The neutrino Majorana mass operator $(LH)^2$ can be mediated by tree level exchange of: I) a fermion singlet ('see-saw'); II) a fermion triplet; III) a scalar triplet.

today have three evidences for non-renormalizable interactions. Two of them are the solar and neutrino anomalies. The third one corresponds to case c), and is gravity: the non renormalizable gravitational couplings, suppressed by E/M_{Pl} , sum coherently over many particles giving the well known Newton force.

2.3 See-saw

It is tempting to speculate about which renormalizable extensions of the SM can generate Majorana neutrino mass operator $(LH)^2$. However, the considerations in the previous section indicate that this might be untestable metaphysics: whatever is the source of the $(LH)^2$ operator, this operator is all what we can see at low energy; different sources cannot be discriminated.⁴

Tree level exchange of 3 different types of new particles can generate neutrino masses: right-handed neutrinos, and fermion or scalar $SU(2)_L$ triplets, as we now discuss. The first possibility is known as 'see-saw', although some authors apply the same name to all three possibilities.

2.3.1 Extra fermion singlets

The simplest possibility is adding new fermions with no gauge interactions, that play the rôle of 'right-handed neutrinos', $N = \nu_R$. As already anticipated they can have both a Yukawa interaction λ_N and a Majorana mass M_N :

$$\mathcal{L} = \mathcal{L}_{\text{SM}} + \bar{N}_i i \not{D} N_i + (\lambda_N^{ij} N^i L^j H + \frac{M_N^{ij}}{2} N_i N_j + \text{h.c.}) \quad (2.6)$$

such that neutrinos generically have a 6×6 Majorana/Dirac mass matrix

$$\begin{matrix} & \nu_L & \nu_R \\ \nu_L & \left(\begin{matrix} 0 & \boldsymbol{\lambda}_N^T v \\ \boldsymbol{\lambda}_N v & \boldsymbol{M}_N \end{matrix} \right) \end{matrix} \quad (2.7)$$

where bold-face reminds that $\boldsymbol{\lambda}_N$ and \boldsymbol{M}_N are 3×3 flavour matrices. The values of λ_N and M_N could be related to the unification scale, or to supersymmetry-breaking or to the size of extra

⁴We will present our best hopes of making progress on this issue: the matter/antimatter asymmetry (that however is only one number) in section 10.3 and weak-scale supersymmetry (that however has not yet been discovered) in section 13.5.

dimensions or to some other ‘fundamental’ physics, but in practice we do not know. We focus on two interesting extreme limits:

Pure Majorana neutrinos. If $M_N \gg \lambda_N v$ the full 6×6 mass matrix gives rise to 3 (almost) pure right-handed neutrinos with heavy Majorana masses \mathbf{M}_N , and to 3 (almost) pure left-handed neutrinos with light Majorana masses $\mathbf{m}_\nu = -(v\boldsymbol{\lambda}_N)^T \mathbf{M}_N^{-1} (v\boldsymbol{\lambda}_N)$.

We now rederive the same result proceeding in a different way. Integrating out the heavy neutrinos gives a non-renormalizable effective Lagrangian that only contains the observable low-energy fields. Fig. 2.2a shows that ν_R exchange generates the Majorana mass operator $(L_i H)(L_j H)/2$ with coefficient $-(\boldsymbol{\lambda}_N^T \mathbf{M}_N^{-1} \boldsymbol{\lambda}_N)_{ij}$. This ‘see-saw’ mechanism [21] works naturally and fits nicely in grand unified extension of the SM. It generates the 9 measurable neutrino mass parameters (see section 2) from $\boldsymbol{\lambda}_N$ and \mathbf{M}_N , that contain 18 unknown parameters. Still, it might be not impossible to test it experimentally (sections 10.3, 13.5).

Pure Dirac neutrinos. If $M_N \ll \lambda_N v$ the full 6×6 mass matrix gives 3 Dirac neutrinos $\Psi = (\nu_L, \bar{\nu}_R)$ with mass $m_\nu = \lambda_N v$. The vanishing of M_N can be justified if conservation of lepton number is *imposed* (rather than obtained, as in the SM). In order to get the observed neutrino masses one needs $\lambda_N \sim 10^{-12}$ — much smaller than all other SM Yukawa couplings. While Majorana masses arise ‘naturally’, one needs to ‘force’ the theory in order to get Dirac neutrinos. Due to these æstethical considerations, Majorana neutrinos are considered as more likely. If Dirac neutrinos will turn out to be the right possibility, after complementing the SM with a few more fermions one should understand why they are so surprisingly light.

In general, M_N can be anywhere: e.g. $M_N \sim v$ (again giving light Majorana neutrinos) or $M_N \sim \lambda_N v$ (giving 6 mixed neutrinos with comparable masses).

2.3.2 Extra fermion triplets

The extra fermion N added in the previous section could be a $SU(2)_L$ triplet, rather than a singlet. One has analogous $\boldsymbol{\lambda}_N$ and \mathbf{M}_N flavour matrices. As long as $M_N \gg v$ (triplets lighter than $M_Z/2$ have been excluded by LEP) everything works in the same way: triplet exchange generates the Majorana mass operator, $(LH)^2$. This mechanism is sometimes known as ‘type III see-saw’.

2.3.3 Extra scalar triplet

We have seen how neutrino masses can be obtained adding new *fermionic* (‘matter’) fields. Alternatively, one can add one *scalar* (‘Higgs’) triplet T^a ($a = \{1, 2, 3\}$) with hypercharge $Y_T = 1$, such that the most generic renormalizable Lagrangian is

$$\mathcal{L} = \mathcal{L}_{\text{SM}} + |D_\mu T|^2 - M_T^2 |T^a|^2 + \frac{1}{2} (\lambda_T^{ij} L^i \epsilon \tau^a L^j T^a + \lambda_H M_T H \epsilon \tau^a H T^{a*} + \text{h.c.}) \quad (2.8)$$

where λ_T is a symmetric flavour matrix, ϵ is the permutation matrix, and τ^a are the usual $SU(2)_L$ Pauli matrices. Integrating out the heavy triplet generates the Majorana neutrino masses operator $(LH)^2$ (see fig. 2.2b) inducing neutrino masses $m_\nu^{ij} = \lambda_T^{ij} \lambda_H v^2 / M_T^2$. This mechanism is sometimes known as ‘type II see-saw’. A smaller number of unknown flavour parameters are needed to describe one extra scalar triplet than the extra fermion scalars or triplets.



Figure 2.3: Possible neutrino spectra: (a) normal (b) inverted.

To conclude, we discuss how these possible sources of neutrino masses are consistent with plausible extensions of the SM: gauge unification, supersymmetry and thermal leptogenesis.

SU(5) and SO(10) gauge unification allow to understand the charges of the observed fermions and suggest a new ‘unification’ scale of about 10^{16} GeV, between Λ_L and the Planck scale. According to this theoretical framework the most attractive way of generating neutrino masses is adding one right-handed neutrino per family: it is predicted by SO(10), it does not affect running of gauge coupling constants and its decays can generate the observed baryon abundance (section 10.3). Certain unification models naturally accomodate scalar triplets, while fermion triplets seem more problematic from this point of view.

Furthermore, all three possibilities are compatible with supersymmetry. Singlet and triplet fermions can be straightforwardly promoted to superfields. As well known the SM scalar Higgs must be extended to two Higgs superfields H_d and H_u with opposite gauge charges. Likewise, the scalar triplet T must be extended to two triplet superfields T and \bar{T} with opposite gauge charges. In the relevant superpotential

$$\mathcal{W} = \mathcal{W}_{\text{MSSM}} + M_T T \bar{T} + \frac{1}{2} (\lambda_T^{ij} L^i L^j T + \lambda_{H_d} H_d H_d T + \lambda_{H_u} H_u H_u \bar{T})$$

\bar{T} does not couple to leptons and neutrino masses are obtained as $m_\nu^{ij} = \lambda_T^{ij} \lambda_{H_u} v_u^2 / M_T$.

Finally, all scenarios allow successful thermal leptogenesis (section 10.3).

2.3.4 Loop mediation of neutrino masses

Mediation by loop effects can be realized in many ways: adding extra particles A, B with couplings of the form LAB and HAB (we do not list all the possibilities), one loop exchange of A and B generates the $(LH)^2$ operator. For example, one can consider the standard see-saw scenario, and replace the Higgs doublet with another scalar doublet with vanishing vev, coupled to the standard Higgs doublet.

See [22] for alternative speculative possibilities.

We now study in detail the special cases of pure Majorana and Dirac neutrino masses. We describe how many and which parameters can be measured in the two cases by low energy experiments.

2.4 Pure Majorana neutrinos

We extend the SM by adding to its Lagrangian the non-renormalizable operator $(LH)^2$ and no new fields. Below the $SU(2)_L$ -breaking scale, $(LH)^2$ just gives rise to Majorana neutrino masses. In this situation, charged lepton masses are described as usual by a complex 3×3 matrix \mathbf{m}_E , and neutrino masses by a complex symmetric 3×3 matrix \mathbf{m}_ν :

$$-\mathcal{L}_{\text{mass}} = \ell_R^T \cdot \mathbf{m}_E \cdot \ell_L + \frac{1}{2} \nu_L^T \cdot \mathbf{m}_\nu \cdot \nu_L.$$

How many independent parameters do they contain? Performing the usual unitary flavour rotations of right-handed $E = \ell_R$ and left-handed $L = (\nu_L, \ell)$ leptons, that do not affect the rest of the Lagrangian,⁵ we reach the standard mass eigenstate basis of charged leptons, where $m_E = \text{diag}(m_e, m_\mu, m_\tau)$. It is still possible to redefine the phases of e_L and e_R such that m_e and m_ν^{ee} are real and positive; and similarly for μ and τ . Therefore charged lepton masses are specified by 9 real parameters and 3 complex phases: the 3 real parameters m_e , m_μ , m_τ ; the 3 real diagonal elements of m_ν ; the 3 complex off-diagonal elements of m_ν .

It is customary to write the mass matrices as

$$m_E = \text{diag}(m_e, m_\mu, m_\tau), \quad m_\nu = V^* \text{diag}(m_1 e^{-2i\beta}, m_2 e^{-2i\alpha}, m_3) V^\dagger \quad (2.9)$$

where $m_{e,\mu,\tau,1,2,3} \geq 0$. The neutrino mixing matrix V , that relates the neutrinos with given mass, ν_i , to those with given flavour,

$$\nu_\ell = V_{\ell i} \nu_i, \quad (2.10)$$

can be written as a sequence of Euler rotations

$$V = R_{23}(\theta_{23}) \cdot R_{13}(\theta_{13}) \cdot \text{diag}(1, e^{i\phi}, 1) \cdot R_{12}(\theta_{12}) \quad (2.11)$$

where $R_{ij}(\theta_{ij})$ represents a rotation by θ_{ij} in the ij plane and $i, j = \{1, 2, 3\}$. In components

$$\begin{pmatrix} V_{e1} & V_{e2} & V_{e3} \\ V_{\mu 1} & V_{\mu 2} & V_{\mu 3} \\ V_{\tau 1} & V_{\tau 2} & V_{\tau 3} \end{pmatrix} = \begin{pmatrix} c_{12}c_{13} & c_{13}s_{12} & s_{13} \\ -c_{23}s_{12}e^{i\phi} - c_{12}s_{13}s_{23} & c_{12}c_{23}e^{i\phi} - s_{12}s_{13}s_{23} & c_{13}s_{23} \\ s_{23}s_{12}e^{i\phi} - c_{12}c_{23}s_{13} & -c_{12}s_{23}e^{i\phi} - c_{23}s_{12}s_{13} & c_{13}c_{23} \end{pmatrix}. \quad (2.12)$$

Within this standard parameterization⁶, the 6+3 neutrino parameters are the 3 neutrino mass eigenvalues, m_1, m_2, m_3 , the 3 mixing angles θ_{ij} and the 3 CP-violating phases ϕ , α and β . ϕ is the analogous of the CKM phase, and affects the flavour content of the neutrino mass eigenstates. α and β are called ‘Majorana phases’ [23] and do not affect oscillations (see section 3).

We now justify this parameterization.

1. Two parameters, θ_{23} and θ_{13} , are necessary to describe the flavour of the most splitted neutrino mass eigenstate

$$|\nu_3\rangle = s_{13}|\nu_e\rangle + c_{13}s_{23}|\nu_\mu\rangle + c_{13}c_{23}|\nu_\tau\rangle.$$

Complex phases can be rotated away by redefining the phases of $L_{e,\mu,\tau}$ and $E_{e,\mu,\tau}$ leaving $m_{e,\mu,\tau}$ real and positive. Physically, this means that *two* mixing angles, θ_{23} and θ_{13} , give rise to CP-conserving oscillations at the larger frequency Δm_{23}^2 .

⁵Gauge interactions are the same in any flavour basis, because kinetic energy and gauge interaction originate from the same Lagrangian term, $\bar{L} \not{D} L$. This well known but non-trivial fact rests on solid experimental and theoretical grounds.

⁶Other commonly employed parameterizations have the complex phase in different positions (e.g. with complex V_{e3}) or different names for the mixing angles (e.g. $\theta_1, \theta_2, \theta_3$ or ψ, ϕ, ω in place of $\theta_{23}, \theta_{13}, \theta_{12}$).

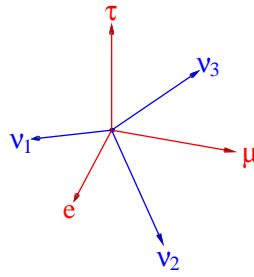


Figure 2.4: The neutrino mass eigenstates $\nu_{1,2,3}$ in 3-dimensional flavour-space. The neutrino mixing matrix suggested by present data is a rotation with angle $\approx 56^\circ$ along the axis that corresponds to the point of view used in this figure.

2. Since the flavours of $|\nu_2\rangle$ and $|\nu_3\rangle$ must be orthogonal, a single complex mixing angle (decomposed as one real mixing angle, θ_{12} , plus one relative phase, ϕ) are needed to describe the flavour of $|\nu_2\rangle = \sum_\ell V_{\ell 2}^* |\nu_\ell\rangle$. Since there is no longer any freedom to redefine the phases of $\nu_{e,\mu,\tau}$, the overall phase of $|\nu_2\rangle$, α , is physical.
3. Finally, no more parameters are needed to describe the flavour of ν_1 , that must be orthogonal to ν_2 and ν_3 . The overall phase of ν_1 , β , cannot be rotated away and is a physical parameter.

Finally, we specify the full allowed range of the parameters.

We order the neutrino masses m_i such that m_3 is the most splitted state and $m_2 > m_1$, and define $\Delta m_{ij}^2 = m_j^2 - m_i^2$. With this choice, Δm_{23}^2 and θ_{23} are the ‘atmospheric parameters’ and $\Delta m_{12}^2 > 0$ and θ_{12} are the ‘solar parameters’, whatever the spectrum of neutrinos (‘normal hierarchy’ so that $\Delta m_{23}^2 > 0$; or ‘inverted hierarchy’ so that $\Delta m_{23}^2 < 0$, see fig. 2.3). With this choice the physically inequivalent range of mixing angles is

$$0 \leq \theta_{12}, \theta_{23}, \theta_{13} \leq \pi/2, \quad 0 \leq \phi < 2\pi \quad 0 \leq \alpha, \beta \leq \pi.$$

The flavour composition of the neutrino mass eigenstates $\nu_{1,2,3}$ suggested by present data (table 1.1) is indicated in fig. 2.3 in a self-explanatory pictorial way. Fig. 2.4 illustrates again the neutrino mixing matrix in an alternative, non-standard, way: for present best-fit values the neutrino mixing matrix is a real rotation $V = R_n(\theta \approx 56^\circ)$ around the axis

$$\hat{n} = 0.78|\nu_e\rangle + 0.24|\nu_\mu\rangle + 0.58|\nu_\tau\rangle = 0.78|\nu_1\rangle + 0.24|\nu_3\rangle + 0.58|\nu_3\rangle. \quad (2.13)$$

2.5 Pure Dirac neutrinos

We extend the SM by adding three neutral singlets (one per family), named ‘right-handed neutrinos’, ν_R . We forbid ν_R^2 mass terms by imposing conservation of lepton number (or of its anomaly-free cousin $B - L$). The most generic renormalizable Lagrangian contains the additional term

$$\mathcal{L} = \mathcal{L}_{\text{SM}} + \bar{\nu}_R i\bar{\partial}\nu_R + \lambda_N \nu_R L H + \text{h.c.} \quad (2.14)$$

In this situation, charged lepton masses are described as usual by a complex 3×3 matrix \mathbf{m}_E , and neutrino masses by a complex 3×3 matrix $\mathbf{m}_\nu = \boldsymbol{\lambda}_N^T v$:

$$-\mathcal{L}_{\text{mass}} = \ell_R^T \cdot \mathbf{m}_E \cdot \ell_L + \nu_L^T \cdot \mathbf{m}_\nu \cdot \nu_R$$

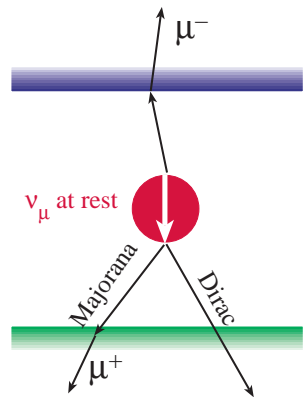
We have more matrix elements and more fields that can be rotated than in the pure Majorana case. One can repeat the steps 1, 2, 3 above, with the only modification that the ‘Majorana phases’ can now be rotated away (reabsorbed in the phases of the ν_R) leaving only the CKM phase.

In fact, the flavour structure (2 mass matrices for 3 kinds of fields) is identical to the well known structure present in quarks (2 mass matrices for the up and down-type quarks, contained in the 3 fields u_R , d_R and $Q = (u_L, d_L)$). However, a numerical difference makes the physics very different: neutrino masses are small. Up and down-type quarks and charged leptons are produced in ordinary processes as mass eigenstates, while neutrinos as flavour eigenstates. So far, we can produce a ν_μ , but we are not able of getting a ν_3 . For this reason, tools analogous to the ‘unitarity triangle’ (used to visualize CKM mixing among quarks, and useful because experiments can measure both its sides and its angles) have no practical use in lepton flavour.

Before concluding, let us discuss the physical difference between Majorana and Dirac neutrinos. In both cases $\nu_\ell = V_{\ell i} \nu_i$ implies $\bar{\nu}_\ell = V_{\ell i}^* \bar{\nu}_i$. While Dirac masses conserve lepton number, that distinguish leptons from anti-leptons, in the Majorana case there is no Lorentz-invariant distinction between a neutrino and an anti-neutrino. They are different polarizations of a unique particle that interacts mostly like a neutrino (an anti-neutrino) when its spin is almost anti-parallel (parallel) to its direction of motion. While ideally an anti-neutrino becomes a neutrino, if seen by an observer that moves faster than it, in practice these effects are suppressed by $(m_\nu/E_\nu)^2$. This factor is usually so small that only in appropriately subtle situations it might be possible to detect it.

A gedanken experiment allows to appreciate the physical difference between Majorana and Dirac neutrinos in a simple way. Suppose that it were practically possible to put at rest a massive ν_μ neutrino with spin-down in the middle of the room. If accelerated up to relativistic energies in the up direction, when it hits the roof can produce a μ^- trough a CC interaction. If accelerated up to relativistic energies in the down direction, when it hits the floor it can produce a μ^+ (if it is a Majorana particle) or have no interaction (if it is a Dirac particle).

Coming to realistic experiments, in the next section we show that oscillation experiments cannot discriminate Majorana from Dirac neutrinos. No signal induced by neutrino masses other than oscillations has so far been seen. It seems that the only realistic hope of experimentally discriminating Majorana from Dirac neutrino masses is based on the fact that Majorana masses violate lepton number, maybe giving a signal in future neutrino-less double β decay searches (section 8.4).



2.6 Formalism

One can define the usual neutrino field operators, neutrino creation and destruction operators, neutrino states, neutrino wave-functions, etc. At least in the relevant ultra-relativistic limit

(where ν and $\bar{\nu}$ are trivially distinguished), there should be no doubt of how to implement flavour mixing within the standard QFT formalism. See [20] for a clean presentation of Majorana and Dirac fermions in terms of Weyl spinors.

We could skip these details. However we follow the standard formalism and notation, and we must warn the reader that it contains one unfortunate choice that becomes relevant when computing the sign of CP-violating effects. The point is that (by convention) a field operator creates anti-particles while an anti-field operator creates particles. As a consequence one must be careful in distinguishing V from V^* . The correct relations between mass eigenstates and flavour eigenstates are:

$$\begin{aligned} \text{Field operators } \nu: \quad & \nu_\ell = V_{\ell i} \nu_i, & \bar{\nu}_\ell = V_{\ell i}^* \bar{\nu}_i \\ \text{One-particle states } |\nu\rangle: \quad & |\nu_\ell\rangle = V_{\ell i}^* |\nu_i\rangle & |\bar{\nu}_\ell\rangle = V_{\ell i} |\bar{\nu}_i\rangle \\ \text{Wave-functions } \nu(x) \equiv \langle x | \nu: \quad & \nu_\ell(x) = V_{\ell i}^* \nu_i(x), & \bar{\nu}_\ell(x) = V_{\ell i} \bar{\nu}_i(x) \end{aligned} \quad (2.15)$$

In common-practice all these quantities are often denoted as ν : to do things properly one should understand physics rather than relying on precise formalisms.

2.6.1 Inverting the see-saw

Assuming that three heavy right-handed neutrinos mediate Majorana neutrino masses according to the see-saw Lagrangian of eq. (2.6), the most generic high energy parameters that give rise to any desired neutrino masses m_{ν_i} and mixings V can be parameterized as [24]

$$M_N = \text{diag}(M_1, M_2, M_3), \quad \lambda_N = \frac{1}{v} M_N^{1/2} \cdot R \cdot \text{diag}(m_{\nu_1}, m_{\nu_2}, m_{\nu_3})^{1/2} \cdot V^\dagger. \quad (2.16)$$

One can always work in the mass eigenstate basis of right-handed neutrinos, where M_i is real and positive. R is an arbitrary complex orthogonal matrix (i.e. $R^T \cdot R = 1$), that can be written in terms of 3 complex mixing angles. In total the high-energy see-saw theory has 9 real unknown parameters.

Chapter 3

Oscillations

We start discussing oscillations in vacuum, without hiding subtle points and giving practical formulæ. Next, we discuss oscillations in matter, and describe how neutrinos oscillate in continuously varying density profiles (e.g. in the sun and in supernovæ).¹

3.1 Oscillations in vacuum

One-particle quantum mechanics is the appropriate language for describing neutrino oscillations. In all cases of practical interest neutrino fluxes are sufficiently weak that multi-particle Fermi-Dirac effects can be neglected. Concerning this aspect, a neutrino beam is simpler than an electro-magnetic field, that can be composed by inequivalent configurations of many photons. Therefore, one should

1. **Build a neutrino wave-packet** [27], taking into account the dynamics of the specific process that produces it. For example, atmospheric and beam neutrinos are mostly produced in π and μ decays. Solar ν_e are produced in collisions and decays of light nuclei inside the sun. Reactor $\bar{\nu}_e$ in decays of fragments of fissioned heavy radioactive nuclei. Supernova neutrinos are produced mostly thermally.
2. **Study its evolution.** Different mass eigenstates acquire different phases, giving rise to oscillations. The mass difference also generates other effects. The lighter mass eigenstate moves faster than the heavier one: at some point their wavepackets no longer overlap, destroying oscillations. While in neutrinos this effect is usually negligible, the mass differences between quarks are so large that there are no oscillations between quarks: e.g. the down-type quark q produced in decays of charmed hadrons, $c \rightarrow q\ell\bar{\nu}$, is $|q\rangle = \cos\theta_C|d\rangle + \sin\theta_C|s\rangle$, giving rise to a π with probability $\cos^2\theta_C$ and to K with probability $\sin^2\theta_C$ — not to $\pi \leftrightarrow K$

¹Solar and atmospheric anomalies have been discovered studying natural sources of neutrinos. To correctly interpret data one needs to understand how these systems work. The oscillation formalism was developed around 1980. The recent experimental progress stimulated new interest and all these issues have been critically reconsidered. This generated some healthy confusion, that should not give a wrong impression. All newly claimed effects turned out to be wrong or already known: old results have been confirmed [25]. Many papers discuss if the standard oscillation phase should be corrected with extra $\mathcal{O}(1)$ factors: to verify that this is not the case one can simply notice that the standard oscillation formula reduces to well known physics in two limiting regimes of small and large oscillation phase (respectively to first-order perturbation theory and to multiplication of probabilities, see page 23). These discussions correctly showed that the ‘standard derivation’ of the vacuum oscillation formula is over-simplified: following [26] we present a simple meaningful derivation.

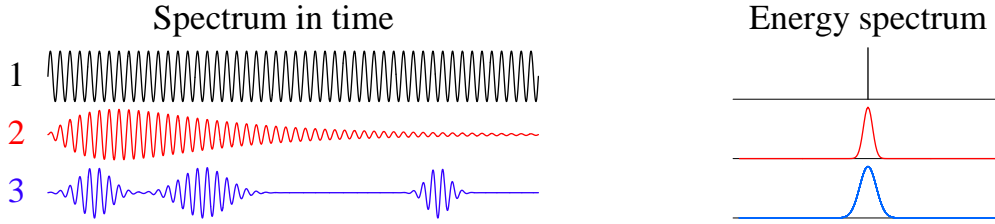


Figure 3.1: **1:** a monochromatic wave; its energy spectrum is a line. **2:** a pulse of ‘monochromatic’ neutrinos; its energy spectrum is almost a line. **3:** a few wave packets of ‘monochromatic’ neutrinos; their energy spectrum is roughly a line.

oscillations. (Furthermore the heavier quarks decay fast, while the heavier neutrinos seem to be almost stable).

3. **Compute the observable to be measured**, taking into account what the detector is really doing. Oscillations are a quantum interference effect. The necessary coherence is destroyed if the neutrino mass is measured (for example by measuring the neutrino energy and momentum) with enough precision to distinguish which one of the different neutrino mass eigenvalues has been detected.

We can derive a general and simple result, bypassing the cumbersome wave-packet analysis, if we restrict our attention to a *stationary* flux of neutrinos or to experiments that only look at *time-averaged* observables [26]. We now show that in these conditions a neutrino wave is *fully described by its energy spectrum* (and of course by its direction, flavour and possibly polarization). This means that a plane wave is the same thing as a mixture of short wavepackets, just as the same light can be obtained as a mixture of circular or linear polarizations.

The basic observation is so simple that it might be difficult to understand it. It is convenient to work in the basis of eigenstates of the Hamiltonian. The most generic *pure* state is a superposition of them. In stationary conditions all interferences between states with different energy average to zero, $\langle e^{i(E-E')t} \rangle = 0$, when computing any physical observable. Therefore the relative phases between neutrinos with different energies are not observable, and the conclusion follows. This is illustrated in fig. 3.1.

We need to generalize this proof to a neutrino flux described by a density matrix ρ . In fact, let us consider e.g. a neutrino produced in π decay, $\pi \rightarrow \nu_\mu \bar{\mu}$. A wave function describes the neutrino and the muon. As usual, when we want we restrict to a subset (the neutrino) of the full system (neutrino and muon), we are forced to introduce mixed states. Furthermore, the particle that produces the neutrino usually interacts in a non negligible way with the environment (e.g. a stopped π at FermiLab, or a ${}^7\text{Be}$ in the sun): using a density matrix for neutrinos is simpler than studying the wave function of FermiLab, or of the sun. Again, the result simply follows by the fact that the off-diagonal terms of ρ oscillate in time as $e^{i(E-E')t}$ and therefore average to zero. More formally, $i\dot{\rho} = [H, \rho] = 0$ in stationary conditions, so that the off-diagonal elements of ρ between states with different energy vanish. The diagonal elements of ρ tell the neutrino energy spectrum.

Our simplifying conditions are valid in all realistic experiments: an experiment that can measure the time of neutrino detection with $\Delta t \sim \text{ns}$ is not sensible to interference among

neutrinos with $E - E' \gg 1/\Delta t \sim 10^{-6}$ eV, which is much smaller than any realistic energy resolution. Deviations from the oscillation probabilities that we now derive are negligible even when considering a pulsed neutrino beam or a short supernova neutrino burst.

Neutrinos with different mass and the same energy oscillate, as we now describe. We start considering the simplest case, and we do not employ density matrices, which are the appropriate and convenient formalism for more complex computations.

3.1.1 Vacuum oscillations of two neutrinos

We consider two generation mixing, so that we just have one mixing angle, θ , and no CP violation. We assume that at the production region, $x \approx 0$, ν_e are produced with energy E . To study their propagation it is convenient to utilize the basis of neutrino mass eigenstates $\nu_{1,2}$, and write $|\nu(x=0)\rangle = |\nu_e\rangle = \cos\theta|\nu_1\rangle + \sin\theta|\nu_2\rangle$. Since ν_1 and ν_2 have different masses, the initial ν_e becomes some other mixture of ν_1 and ν_2 , or equivalently of ν_μ and ν_e . At a generic x

$$|\nu(x)\rangle = e^{ip_1 x} \cos\theta|\nu_1\rangle + e^{ip_2 x} \sin\theta|\nu_2\rangle.$$

The probability of ν_μ *appearance* at the detection region $x \approx L$ is

$$P(\nu_e \rightarrow \nu_\mu) = |\langle \nu_\mu | \nu(L) \rangle|^2 = \sin^2 2\theta \sin^2 \frac{(p_2 - p_1)L}{2} \simeq \sin^2 2\theta \sin^2 \frac{\Delta m_{12}^2 L}{4E}. \quad (3.1)$$

Since in all cases of experimental interest $E \gg m_i$, in the final passage we have used the ultra-relativistic approximation $p_i = E - m_i^2/2E$, valid at dominant order in the small neutrino masses and defined $\Delta m_{12}^2 \equiv m_2^2 - m_1^2$.²

By swapping the names of the two mass eigenstates, $\nu_1 \leftrightarrow \nu_2$, one realizes that the couples $(\theta, \Delta m_{12}^2)$ and $(\pi/2 - \theta, -\Delta m_{12}^2)$ describe the same physics. On the contrary $(\theta, \Delta m_{12}^2)$ and $(\pi/2 - \theta, \Delta m_{12}^2)$ are physically different. However, eq. (3.1) shows that *vacuum oscillations depend only on* $\sin^2 2\theta$ and do not discriminate these two cases. Oscillation effects are maximal at $\theta = \pi/4$.

The ν_e *disappearance* probability is

$$P(\nu_e \rightarrow \nu_e) = |\langle \nu_e | \nu(L) \rangle|^2 = 1 - P(\nu_e \rightarrow \nu_\mu).$$

A convenient numerical relation is found restoring \hbar and c factors:

$$S_{ij} \equiv \sin^2 \frac{c^3 \Delta m_{ij}^2 L}{\hbar 4E} = \sin^2 1.27 \frac{\Delta m_{ij}^2}{\text{eV}^2} \frac{L}{\text{Km}} \frac{\text{GeV}}{E}. \quad (3.2)$$

The oscillation wave-length is

$$\lambda = \frac{4\pi E}{\Delta m^2} = 2.48 \text{ km} \frac{E}{\text{GeV}} \frac{\text{eV}^2}{\Delta m_{ij}^2}. \quad (3.3)$$

²We sketch the standard over-simplified derivation. It proceeds writing the evolution in *time* as $|\nu(t)\rangle = e^{-iHt}|\nu(0)\rangle$. Assuming that neutrinos with different mass have equal momentum, the hamiltonian is $H \approx p + mm^\dagger/2p$. This gives the correct final formula, if one does not take into account that different neutrinos have different velocity. It is not clear which ‘time’ one should use (e.g. when neutrinos are produced by slow decays), as no real experiment measures it: experiments measure the *distance* from the production point.

Furthermore, in many realistic cases neutrinos actually oscillate in space but not in time, because their wave-packets have a much larger spread in momentum than in energy. This happens because the particle that decays into neutrinos often interacts with a *big* environment and therefore behaves like a ball that bounces in a box: it keeps the same energy but changes momentum.

All this discussion applies to oscillations, not only to neutrino oscillations.

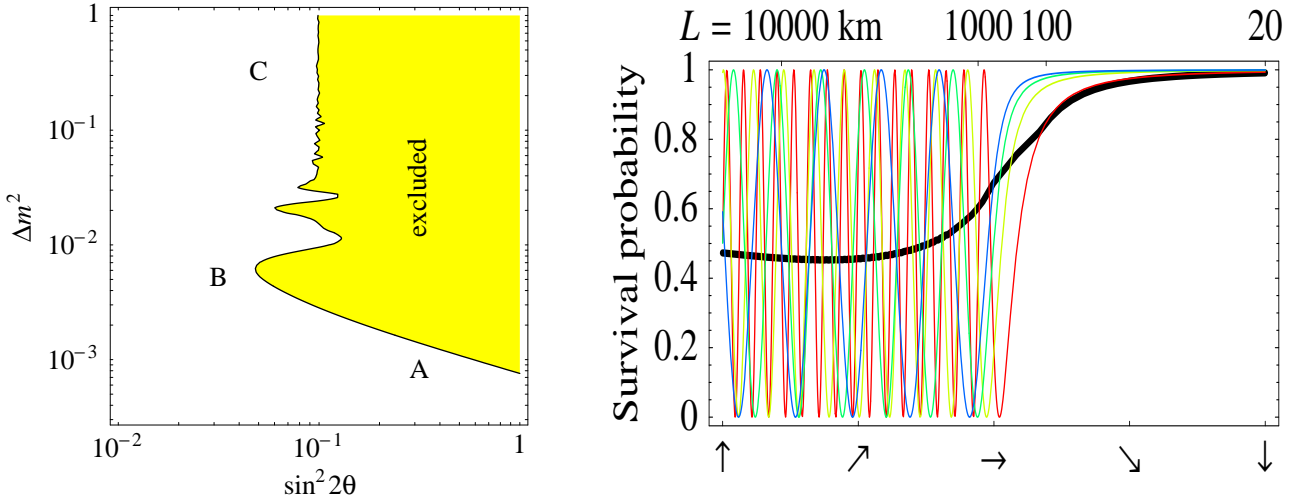


Figure 3.2: (a) Typical bound on oscillations. (b) Averaging oscillations over neutrinos with different energies (here represented with different colors) gives a smooth survival probability (thick curve). This plot holds for atmospheric neutrinos, where the path-length (upper axis) is measured from the direction of arrival (lower axis).

Like decays, oscillations are suppressed at large energy by the m/E ‘time-dilatation’ Lorentz factor, well known from relativity. In order to see oscillations one needs neutrinos of low enough energy, that have small detection cross sections (section 4). Furthermore some reactions are kinematically allowed only at high enough energies. For example, a ν_τ can be seen by detecting a scattered τ : using the $\nu_\tau e \rightarrow \nu_e \tau$ reaction one needs $E_{\nu_\tau} > m_\tau^2/2m_e \approx 3$ TeV, while using $\nu_\tau n \rightarrow \tau p$ one needs $E_{\nu_\tau} > m_\tau + m_\tau^2/2m_N \approx 3.5$ GeV.

3.1.2 Limiting regimes

In a realistic setup, the neutrino beam is not monochromatic, and the energy resolution of the detector is not perfect: one needs to average the oscillation probability around some energy range ΔE . Furthermore, the production and detection regions are not points: one needs to average around some path-length range ΔL . Including these effects, in fig. 3.2a we show a typical experimental bound on oscillations. We can distinguish three regions:

A Oscillations with short base-line, where $S_{ij} \ll 1$. In this limit oscillations reduce to first-order perturbations:³

$$P(\nu_e \rightarrow \nu_\mu) \simeq (H_{e\mu} L)^2 \quad \text{with} \quad H_{e\mu} \equiv \frac{(m_\nu m_\nu^\dagger)_{e\mu}}{2E_\nu} = \frac{\Delta m^2}{E_\nu} \sin 2\theta.$$

³Notice that the standard oscillation factor follows from first-order perturbation theory. In this simple limit, one could explicitly study how $e^{i(E-E')t}$ averages to zero, i.e. take into account the negligible phenomenon of oscillations among neutrinos with different energies E and E' .

This explains the slope of the exclusion region in part A of fig. 3.2a. Since $P(\nu_e \rightarrow \nu_\mu) \propto L^2$, and since going far from an approximatively point-like neutrino source the neutrino flux decreases as $1/L^2$, choosing the optimal location for the detector is usually not straightforward.

C Averaged oscillations, where $\langle S_{ij} \rangle = 1/2$ as illustrated in fig. 3.2b. In this limit one has

$$P(\nu_e \rightarrow \nu_\mu) = \frac{1}{2} \sin^2 2\theta, \quad P(\nu_e \rightarrow \nu_e) = 1 - \frac{1}{2} \sin^2 2\theta. \quad (3.4)$$

The information on the oscillation phase is lost due to the insufficient experimental resolution in E or L . Consequently, one can rederive the transition probabilities (3.4) by combining *probabilities* rather than *amplitudes*. Using the language of quantum mechanics, one refers sometimes to this case as the “classical limit”. The computation proceeds in full analogy to the our π/K example at page 20, as illustrated by the following figure:



At $x \approx 0$ one produces:

- a ν_1 with probability $\cos^2 \theta$ (later detected as a ν_μ with probability $\sin^2 \theta$, or as a ν_e with probability $\cos^2 \theta$), and
- a ν_2 with probability $\sin^2 \theta$ (later detected as a ν_μ with probability $\cos^2 \theta$, or as a ν_e with probability $\sin^2 \theta$).

Therefore one obtains the same result as in (3.4)

$$P(\nu_e \rightarrow \nu_\mu) = 2 \sin^2 \theta \cos^2 \theta, \quad P(\nu_e \rightarrow \nu_e) = \sin^4 \theta + \cos^4 \theta.$$

We now discuss in more detail how the averaging over the energy spectrum transforms coherent oscillations into an incoherent process.

This discussion implies that experimental bounds on oscillations can be approximatively summarized by reporting two numbers: the upper bound on Δm^2 assuming maximal mixing, and the upper bound on θ assuming large Δm^2 . If some effect is discovered, one can test if it is due to oscillations (and eventually measure oscillation parameters) by studying how it depends on the neutrino energy and path-length. The most characteristic phenomenon appears in the intermediate region.

B The intermediate region. Due to the uncertainty ΔE on the energy E (and possibly on the path-length L), coherence gets lost when neutrinos of different energy have too different oscillation phases $\phi \sim \Delta m^2 L/E$, i.e. when

$$\Delta\phi \approx \frac{\Delta E}{E} \phi \gtrsim 1 \quad (3.5)$$

Therefore one can see $n \sim E/\Delta E$ oscillations before they average out. So far, no experiment could clearly observe an oscillation dip. The energy resolution of the experiment often gives the dominant contribution to the total ΔE .

Before concluding, we discuss in greater detail how the formalism here employed automatically takes into account loss of coherence. In the alternative wave-packet formalism, coherence is lost when the wave-packets corresponding to different mass eigenstates (that move at different velocities $\Delta v \sim \Delta m^2/E^2$) no longer overlap. This happens when

$$\Delta v \cdot t \gtrsim \Delta x \quad (3.6)$$

where Δx is the size of the wave-packet.

In the stationary case that we are considering, this phenomenon is accounted by the energy average over the minimal ΔE demanded by quantum mechanics, approximatively equal to $\Delta E \approx 1/\Delta x$, as dictated by the uncertainty relation $\Delta x \cdot \Delta p \gtrsim \hbar$. In fact, one can verify that eq. (3.5) and (3.6) are equivalent. This point is pictorially illustrated in fig. 3.1: computing the Fourier transform of a sequence of wave-packets (case 3) one finds a broader energy spectrum than in case 1.

A numerical example shows that this phenomenon is hardly relevant. A supernova could emit a pulse of neutrinos as short as $\Delta t \sim 0.1$ s (case 2). The corresponding quantum uncertainty on their energy is $\Delta E \sim 1/\Delta t \sim 10^{-5}$ eV, which is much smaller than their typical energy, $E \sim 100$ MeV, and therefore becomes important only after $\Delta E/E \sim 10^{13}$ oscillations i.e. after oscillating for cosmological distances with wavelength $\lambda = 4\pi E/\Delta m^2$. This same estimate can be reobtained computing the separation between neutrino wave-packets

$$\Delta v \cdot t \approx L \frac{\Delta m^2}{E^2} \approx 0.1 \text{ s} \frac{L}{10^{25} \text{ m}} \frac{\Delta m^2}{3 \cdot 10^{-3} \text{ eV}^2} \left(\frac{100 \text{ MeV}}{E} \right)^2$$

and comparing it with the length of the wave-packet, $\Delta x \sim c\Delta t \sim 0.1$ s.

3.1.3 Vacuum oscillations of n neutrinos

Some results follow from general arguments:

- *Conservation of probability* implies

$$\sum_{\ell'} P(\nu_{\ell} \rightarrow \nu_{\ell'}) = \sum_{\ell'} P(\bar{\nu}_{\ell} \rightarrow \bar{\nu}_{\ell'}) = 1$$

- CPT *invariance* implies

$$P(\nu_{\ell} \rightarrow \nu_{\ell'}) = P(\bar{\nu}_{\ell'} \rightarrow \bar{\nu}_{\ell})$$

- In many situations CP *invariance* approximately holds and implies

$$P(\nu_{\ell} \rightarrow \nu_{\ell'}) = P(\bar{\nu}_{\ell} \rightarrow \bar{\nu}_{\ell'})$$

Together with CPT-invariance, CP-invariance is equivalent to T *invariance*

$$P(\nu_{\ell} \rightarrow \nu_{\ell'}) = P(\nu_{\ell'} \rightarrow \nu_{\ell})$$

Therefore T-conserving (breaking) contributions are even (odd) in the base-line L .

Up to an irrelevant overall phase, the transition amplitude is

$$A(\nu_\ell \rightarrow \nu_{\ell'}) = \langle \nu_{\ell'} | \nu_\ell(L) \rangle = \langle \nu_{\ell'} | U(L) | \nu_\ell \rangle = \sum_i V_{\ell'i} V_{\ell'i}^* e^{2i\varphi_i}, \quad U(L) = \exp \left(-i \frac{m \cdot m^\dagger L}{2E} \right) \quad (3.7)$$

where $\varphi_i \equiv -m_i^2 L / 4E$. We see that Majorana phases do not affect oscillations. In the short baseline limit, approximating $\exp i\epsilon t \simeq \mathbb{1} + i\epsilon t + \mathcal{O}(t^2)$ (here ϵ is a flavour matrix), the oscillation probability reduces to first-order perturbations $P(\nu_\ell \rightarrow \nu_{\ell'}) = |\epsilon_{\ell\ell'}|^2$ for $\ell \neq \ell'$.

Eq. (3.7) can be used in numerical computations. However when $|\varphi_i| \gg 1$ the result rapidly oscillates and it is cumbersome to compute numerically its mean value, that usually determines what can be measured. In the simple case of vacuum oscillations it is possible and convenient to rewrite eq. (3.7) in a longer but more useful form. Using $e^{2i\varphi} = 1 - 2\sin^2 \varphi + i \sin 2\varphi$, from eq. (3.7) we get

$$\begin{aligned} P(\nu_\ell \rightarrow \nu_{\ell'}) &= |A(\nu_\ell \rightarrow \nu_{\ell'})|^2 = \sum_{ij} J_{ij}^{\ell\ell'} (1 - 2\sin^2 \varphi_{ij} + i \sin 2\varphi_{ij}) \\ &= \underbrace{\delta_{\ell\ell'} - \sum_{i < j} 4\text{Re} J_{ij}^{\ell\ell'} \sin^2 \varphi_{ij}}_{\text{CP-conserving}} - \underbrace{\sum_{i < j} 2\text{Im} J_{ij}^{\ell\ell'} \sin 2\varphi_{ij}}_{\text{CP-violating}}. \end{aligned} \quad (3.8)$$

where

$$\varphi_{ij} \equiv \varphi_i - \varphi_j = \frac{\Delta m_{ij}^2 L}{4E}, \quad \Delta m_{ij}^2 \equiv m_j^2 - m_i^2, \quad J_{ii'}^{\ell\ell'} = V_{\ell i}^* V_{\ell' i'}^* V_{\ell' i} V_{\ell i'}. \quad (3.9)$$

$\text{Im} J_{ij}^{\ell\ell'}$ is a rephasing-invariant measure of CP violation, because it arises from a product of elements of V where any flavour and any mass-eigenstate ν_ℓ and ν_i enters twice, once with a complex conjugation, once without. The corresponding formulæ for antineutrinos are obtained by exchanging $V \leftrightarrow V^*$, so that in the final formula only the sign of the CP-violating term changes. In the limit of averaged oscillations $\langle \sin^2 \varphi_{ij} \rangle = 1/2$ and $\langle \sin 2\varphi_{ij} \rangle = 0$ one can reobtain the oscillation probabilities by combining probabilities (rather than quantum amplitudes):

$$P(\nu_\ell \rightarrow \nu_{\ell'}) = P(\bar{\nu}_\ell \rightarrow \bar{\nu}_{\ell'}) = \sum_i |\langle \nu_i | \nu_\ell \rangle|^2 = \sum_i |V_{\ell i} V_{\ell' i}|^2 \quad (3.10)$$

which in general depends on the CP-violating phases that affect $|V_{\ell i}|$.

3.1.4 Vacuum oscillations of 3 neutrinos

Specializing to the case of 3 neutrinos one gets

$$P(\bar{\nu}_\ell \rightarrow \bar{\nu}_{\ell'}) = \delta_{\ell\ell'} + p_{\ell\ell'}^{12} \sin^2 \varphi_{12} + p_{\ell\ell'}^{13} \sin^2 \varphi_{13} + p_{\ell\ell'}^{23} \sin^2 \varphi_{23} \pm 8J \sin \varphi_{12} \sin \varphi_{13} \sin \varphi_{23} \sum_{\ell''} \epsilon_{\ell\ell'\ell''} \quad (3.11)$$

where the $-$ sign holds for neutrinos, the $+$ sign for anti-neutrinos, ϵ is the permutation tensor ($\epsilon_{123} = +1$), and

$$S_{ij} = \sin^2 \varphi_{ij}, \quad p_{ii'}^{\ell\ell'} = -4\text{Re} V_{\ell i} V_{\ell' i'} V_{\ell' i}^* V_{\ell i'}^*, \quad \text{and in particular} \quad p_{ii'}^{\ell\ell} = -4|V_{\ell i} V_{\ell i'}|^2$$

The CP-violating term is simpler than in eq. (3.8) because, with only 3 neutrinos oscillations depend only on one CP-violating phase and

$$\text{Im } J_{ii'}^{\ell\ell'} = J \sum_{i'',\ell''} \epsilon_{ii'i''} \epsilon_{\ell\ell'\ell''} \quad \text{where} \quad 8J \equiv \cos \theta_{13} \sin 2\theta_{13} \sin 2\theta_{12} \sin 2\theta_{23} \cdot \sin \phi. \quad (3.12)$$

Up to a sign J equals to twice the area of the ‘unitarity triangle’ with sides $V_{\ell i} V_{\ell i}^*$ and $V_{\ell' i'} V_{\ell' i'}^*$. Eq. (3.12) tells that all such triangles have the same area. The maximal value $|J| = 1/6\sqrt{3}$ is obtained in the case known as ‘trimaximal mixing’: for $\phi = \pi/2$, $\theta_{12} = \theta_{23} = \pi/4$ and $\cos^2 \theta_{13} = 2/3$ all elements of V have the same modulus $|V_{\ell i}| = 1/\sqrt{3}$, and oscillation probabilities can reach the borders of the allowed range $0 \leq P \leq 1$. (This case is not realized in nature).

We have simplified the CP-violating contribution to $P(\nu_\ell \rightarrow \nu_{\ell'})$ using the trigonometrical identity

$$\sin 2\varphi_{12} + \sin 2\varphi_{23} + \sin 2\varphi_{31} = 4 \sin \varphi_{12} \sin \varphi_{23} \sin \varphi_{13}.$$

As expected the CP-violating contribution vanishes if $\ell = \ell'$ and is odd in L . In the small L limit, it is proportional to L^3 . It is small when any mixing angle θ_{ij} or any oscillation phase φ_{ij} is small; it averages to zero when some $\varphi_{ij} \gg 1$. These properties explain why it is difficult to observe CP-violation.

As anticipated in section 1.2, data indicate that

$$|\Delta m_{13}^2| \approx |\Delta m_{23}^2| = \Delta m_{\text{atm}}^2 \approx 3 \cdot 10^{-3} \text{ eV}^2, \quad \Delta m_{12}^2 = \Delta m_{\text{sun}}^2 \approx 10^{-4} \text{ eV}^2.$$

Therefore it is interesting to consider the limit $|\Delta m_{23}^2| \gg \Delta m_{12}^2$, i.e. $S_{13} \approx S_{23}$ so that we can simplify

$$p_{\ell\ell'}^{13} + p_{\ell\ell'}^{23} = -4 \text{Re } w_3^{\ell\ell'} (w_1^{\ell\ell'*} + w_2^{\ell\ell'*}) = -4 \text{Re } w_{\ell\ell'}^3 (\delta_{\ell\ell'} - w_3^{\ell\ell'*}).$$

getting

$$P(\overline{\nu}_\ell \rightarrow \overline{\nu}_{\ell'}) \simeq \begin{cases} 1 - 4|V_{\ell 1}^2 V_{\ell 2}^2| S_{12} - 4|V_{\ell 3}^2|(1 - |V_{\ell 3}^2|) S_{23} & \text{for } \ell = \ell' \\ -4|V_{\ell 1} V_{\ell 2} V_{\ell' 1} V_{\ell' 2}| S_{12} + 4|V_{\ell 3}^2 V_{\ell' 3}^2| S_{23} \mp P_{\text{CP}} & \text{for } \ell \neq \ell' \end{cases} \quad (3.13)$$

where the CP-violating terms becomes $P_{\text{CP}} = 8J \sin^2 \varphi_{13} \sin \varphi_{12}$. In this limit vacuum oscillations no longer depend on the sign of Δm_{23}^2 , which controls if neutrinos have ‘normal’ or ‘inverted’ hierarchy. Inserting the explicit parametrization of V in eq. (2.12) gives

$$P(\nu_e \rightarrow \nu_\mu) = s_{23}^2 \sin^2 2\theta_{13} S_{23} + c_{23}^2 \sin^2 2\theta_{12} \underline{S}_{12} + P_{\text{CP}}, \quad (3.14a)$$

$$P(\nu_e \rightarrow \nu_\tau) = c_{23}^2 \sin^2 2\theta_{13} S_{23} + s_{23}^2 \sin^2 2\theta_{12} \underline{S}_{12} - P_{\text{CP}}, \quad (3.14b)$$

$$P(\nu_\mu \rightarrow \nu_\tau) = c_{13}^4 \sin^2 2\theta_{23} S_{23} - s_{23}^2 c_{23}^2 \sin^2 2\theta_{12} \underline{S}_{12} + P_{\text{CP}}, \quad (3.14c)$$

and

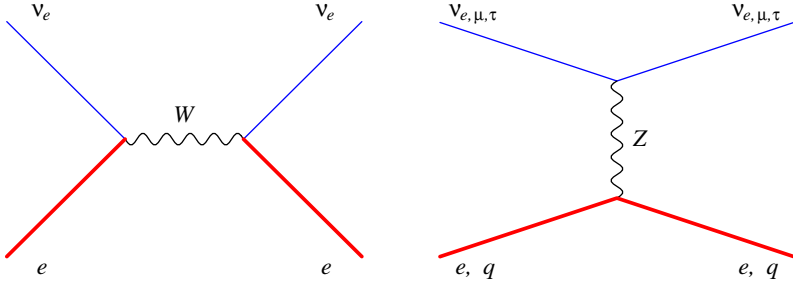
$$P(\nu_e \rightarrow \nu_e) = 1 - \sin^2 2\theta_{13} S_{23} - c_{13}^2 \sin^2 2\theta_{12} S_{12}, \quad (3.14d)$$

$$P(\nu_\mu \rightarrow \nu_\mu) = 1 - 4c_{13}^2 s_{23}^2 (1 - c_{13}^2 s_{23}^2) S_{23} - c_{23}^4 \sin^2 2\theta_{12} \underline{S}_{12}, \quad (3.14e)$$

$$P(\nu_\tau \rightarrow \nu_\tau) = 1 - 4c_{13}^2 c_{23}^2 (1 - c_{13}^2 c_{23}^2) S_{23} - s_{23}^4 \sin^2 2\theta_{12} \underline{S}_{12}. \quad (3.14f)$$

For simplicity we set $\theta_{13} = 0$ in the coefficients of the underlined \underline{S}_{12} terms. Special interesting limiting cases are:

- $S_{12} \approx 0$ (the baseline is so short that solar oscillations cannot be seen);

Figure 3.3: *Interactions of neutrinos with electrons and quarks.*

- $\langle S_{23} \rangle \approx 1/2$ (the baseline is so long that atmospheric oscillations are averaged);
- $\langle S_{12} \rangle = \langle S_{23} \rangle = 1/2$ (the baseline is so long that both solar and atmospheric oscillations are averaged). The survival probabilities are given by eq. (3.10) and depend on the CP-phase ϕ .

3.2 Oscillations in normal matter

The probability that a neutrino of energy $E \sim \text{MeV}$ gets scattered while crossing the earth is $\sim 10^{-12}$ (section 4). Neutrinos of ordinary energies cross the earth or the sun without being significantly absorbed. Still, the presence of matter can significantly affect neutrino propagation [28]. This apparently unusual phenomenon has a well known optical analogue. A transparent medium like air or water negligibly absorbs light, but still significantly reduces its speed: $v_{\text{phase}} = c/n$, where n is the ‘refraction index’. In some materials or in presence of an external magnetic field n is different for different polarizations of light, giving rise to characteristic effects, such as birefringence. The same thing happens for neutrinos. Since matter is composed by electrons (rather than by μ and τ), ν_e interact differently than $\nu_{\mu,\tau}$, giving rise to a flavour-dependent refraction index. We now compute it and study how oscillations are affected.

Forward scattering of neutrinos interferes with free neutrino propagation, giving rise to refraction. Scattering of ν_ℓ on electrons and quarks mediated by the Z boson (fig. 3.3b) is the same for all flavours $\ell = \{e, \mu, \tau\}$, and therefore does not affect flavour transitions between active neutrinos. The interesting effect is due to $\nu_e e$ scattering mediated by the W boson (fig. 3.3a), that is described at low energy by the effective Hamiltonian (its sign is predicted by the SM)

$$\mathcal{H}_{\text{eff}} = \frac{4G_F}{\sqrt{2}} (\bar{\nu}_e \gamma_\mu P_L \nu_e) (\bar{e} \gamma^\mu P_L e).$$

In a background composed by non-relativistic and non-polarized electrons and no positrons (e.g. the earth, and to excellent approximation the sun) one has

$$\langle \bar{e} \gamma_\mu \frac{1 - \gamma_5}{2} e \rangle = \frac{N_e}{2} (1, 0, 0, 0)_\mu \quad \text{and therefore} \quad \langle \mathcal{H}_{\text{eff}} \rangle = \sqrt{2} G_F N_e (\bar{\nu}_e \gamma_0 P_L \nu_e)$$

medium	A_{CC} for $\nu_e, \bar{\nu}_e$ only	A_{NC} for $\nu_{e,\mu,\tau}, \bar{\nu}_{e,\mu,\tau}$
e, \bar{e}	$\pm\sqrt{2}G_F(N_e - N_{\bar{e}})$	$\mp\sqrt{2}G_F(N_e - N_{\bar{e}})(1 - 4s_W^2)/2$
p, \bar{p}	0	$\pm\sqrt{2}G_F(N_p - N_{\bar{p}})(1 - 4s_W^2)/2$
n, \bar{n}	0	$\mp\sqrt{2}G_F(N_n - N_{\bar{n}})/2$
ordinary matter	$\pm\sqrt{2}G_F N_e$	$\mp\sqrt{2}G_F N_n/2$

Table 3.1: *Matter potentials for ν (upper sign) and $\bar{\nu}$ (lower sign).* We assumed a non-relativistic and non-polarized background medium, so that these formulae do not apply to a background of neutrinos.

where N_e is the electron number density. Including also the Z -contribution⁴, the effective matter Hamiltonian density in ordinary matter is

$$\langle \mathcal{H}_{\text{eff}} \rangle = \bar{\nu}_\ell A \gamma_0 P_L \nu_\ell \quad \text{where} \quad A = \sqrt{2}G_F \left[N_e \text{diag}(1, 0, 0) - \frac{N_n}{2} \text{diag}(1, 1, 1) \right] \quad (3.15)$$

is named ‘matter potential’ and is a 3×3 flavour matrix. If extra sterile neutrinos exist, A becomes a bigger diagonal matrix and all its ‘sterile’ elements vanish.

In table 3.1 we show the separate contributions to A generated by matter eventually containing anti-particles. In order to study neutrino oscillations in the early universe one more ingredient is needed, as discussed in section 3.6.

Adding the matter correction to the Hamiltonian density describing free propagation of an ultra-relativistic neutrino, one obtains a modified relation between energy and momentum, as we will now discuss. In ordinary circumstances the neutrino index of refraction n is so close to one, $n-1 \simeq A/E_\nu \ll 1$, that optical effects like neutrino lensing are negligible. On the contrary matter effects significantly affect oscillations, since $A/(\Delta m^2/E_\nu)$ can be comparable or larger than one.

3.2.1 Majorana vs Dirac neutrinos

It is easy to see that pure Majorana neutrinos oscillate in vacuum in the same way as pure Dirac neutrinos. Looking only at vacuum oscillations it is not possible to experimentally discriminate the two cases. The additional CP-violating phases present in the Majorana case do not affect oscillations.

It is less easy to realize that, in the realistic case of ultrarelativistic neutrinos, this unpleasant result continues to hold also for oscillations in matter. The equations for the neutrino wavefunctions in the two cases are

⁴One needs to evaluate quark currents $\bar{q}\gamma_\mu q$ over a background of normal matter. The result is shown in table 3.1. Non obvious but well known properties of the quark currents guarantee that the proton electric charge is $2q_u + q_d$. Similarly, one correctly evaluates the average value of the quark currents in terms of proton and neutron number densities N_p and N_n by simply using $p = uud$ and $n = udd$. ‘Ordinary matter’ is composed by electrons, protons, neutrons with $N_p = N_e$ (no net electric charge) and $N_n \approx N_p$. The mass density is $\rho \approx m_p N_p + m_n N_n$. At tree level matter effects do not distinguish ν_μ from ν_τ ; loop effects generate a small difference of order $(m_\tau/M_W)^2 \sim 10^{-5}$ [28].

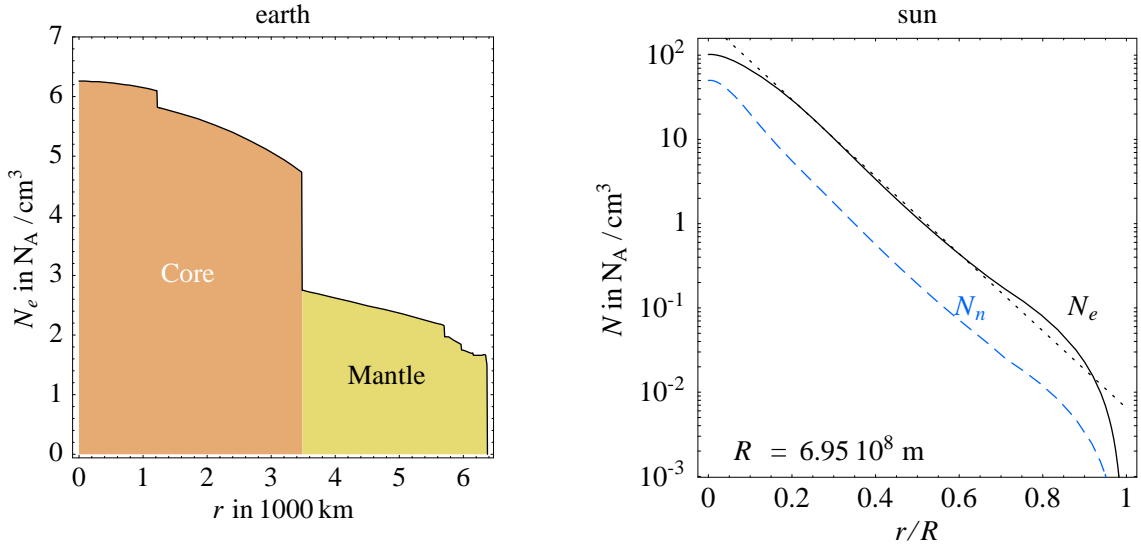


Figure 3.4: Density profile of (a) the earth (b) the sun.

Majorana. Neutrinos have only a left-handed component, and are described by a single Weyl field ν_L . Adding the matter term the equation of motion for the neutrino wavefunction is

$$(i\partial - A\gamma_0)\nu_L = m\bar{\nu}_L$$

where m is the symmetric Majorana mass matrix. Squaring, in the ultrarelativistic limit one obtains the dispersion relation

$$(E - A)^2 - p^2 \simeq mm^\dagger$$

i.e.

$$p \simeq E - \left(\frac{mm^\dagger}{2E} + A \right).$$

Dirac. Neutrinos have both a left and a right-handed component. Their equation of motion is

$$\begin{cases} i\partial\nu_L = m\bar{\nu}_R + A\gamma_0\nu_L \\ i\partial\bar{\nu}_R = m^\dagger\nu_L \end{cases}$$

where m is the Dirac mass matrix. Eliminating ν_R and assuming that A is constant one gets

$$[\partial^2 + mm^\dagger + A i\partial\gamma_0]\nu_L = 0.$$

In the ultrarelativistic limit $i\partial\gamma_0\nu_L \simeq 2i\partial_0\nu_L$, giving the dispersion relation

$$p \simeq E - \left(\frac{mm^\dagger}{2E} + A \right).$$

The density of ordinary matter negligibly changes on a length scale $\sim 1/E$ (which is even typically smaller than an atom) so that the gradient of A can indeed be neglected.

Summarizing, oscillations in matter of ultrarelativistic neutrinos are described by the equation

$$i\frac{d}{dx}\nu = H\nu, \quad \text{where} \quad H = \frac{m \cdot m^\dagger}{2E} + A, \quad \nu = \begin{pmatrix} \nu_e \\ \nu_\mu \\ \nu_\tau \end{pmatrix}, \quad (3.16)$$

that can be solved starting from the production point knowing which flavour is there produced. A is given in eq. (3.15) and $mm^\dagger = V^* \cdot \text{diag}(m_1^2, m_2^2, m_3^2) \cdot V^T$ where V is the neutrino mixing matrix and $m_{1,2,3} \geq 0$ are the neutrino mass eigenvalues. For anti-neutrinos one needs to change $m \rightarrow m^*$ (such that $m \cdot m^\dagger$ gets replaced by $m^\dagger \cdot m = m^\dagger m = V \cdot \text{diag}(m_1^2, m_2^2, m_3^2) \cdot V^\dagger$; this induces genuine CP-violating effects) and $A \rightarrow -A$ (the background of ordinary matter breaks CP). In the case of Majorana neutrinos the mass matrix m is symmetric, so that $m^* = m^\dagger$.

3.2.2 Matter oscillations of two neutrinos

The matter density can depend on both time and position, but usually it depends only on the position (e.g. in the sun). Sometimes it is roughly constant (e.g. in the earth mantle⁵) and it is convenient to define effective energy-dependent neutrino mass eigenvalues m_m^2 , eigenvectors ν_m and mixing angles θ_m in matter by diagonalizing H . These effective oscillation parameters depend on the neutrino energy, and of course on the matter density. In the simple case with only the ν_e and ν_μ flavours and a mixing angle θ

$$mm^\dagger = \frac{m_1^2 + m_2^2}{2} \begin{pmatrix} 1 & 0 \\ 0 & 1 \end{pmatrix} + \frac{\Delta m^2}{2} \begin{pmatrix} -\cos 2\theta & \sin 2\theta \\ \sin 2\theta & \cos 2\theta \end{pmatrix}$$

where $\Delta m^2 = m_2^2 - m_1^2$ so that the oscillation parameters in matter are

$$\tan 2\theta_m = \frac{S}{C}, \quad \Delta m_m^2 = \sqrt{S^2 + C^2}, \quad \text{where} \quad \begin{aligned} S &\equiv \Delta m^2 \sin 2\theta, \\ C &\equiv \Delta m^2 \cos 2\theta \mp 2\sqrt{2}G_F N_e E \end{aligned} \quad (3.17)$$

and θ and Δm^2 are the oscillation parameters in vacuum. The $-$ $(+)$ sign holds for ν ($\bar{\nu}$) and

$$V = \begin{pmatrix} \cos \theta & \sin \theta \\ -\sin \theta & \cos \theta \end{pmatrix}, \quad V_m = \begin{pmatrix} \cos \theta_m & \sin \theta_m \\ -\sin \theta_m & \cos \theta_m \end{pmatrix}$$

Fig. 3.5 shows a numerical example. The most noticeable features are:

- Unlike vacuum oscillations, **matter oscillations distinguish θ from $\pi/2 - \theta$** . Consequently $\sin^2 2\theta$ (used in fig. 3.2a) is no longer a good variable; it is customary to use $\tan^2 \theta$ in log-scale plots (because $\tan^2 \theta \rightarrow 1/\tan^2 \theta$ under a reflection $\theta \rightarrow \pi/2 - \theta$) and $\sin^2 \theta$ in linear-scale plots (because, under the same reflection, $\sin^2 \theta \rightarrow 1 - \sin^2 \theta$). Not caring of the sign of $\theta_m - \pi/4$, eq. (3.17) can be rewritten as

$$\sin^2 2\theta_m = \frac{\sin^2 2\theta}{\lambda^2}, \quad \Delta m_m^2 = \lambda \cdot \Delta m^2, \quad \lambda = \sqrt{\sin^2 2\theta + \left(\cos^2 2\theta \mp \frac{2\sqrt{2}G_F N_e E}{\Delta m^2} \right)^2}.$$

⁵The density profile of the earth, shown in fig. 3.4a, has a few sub-structures [29]. The continental crust is rigid and has a thickness that varies between 20 to 70 km, and is made primarily of light elements like potassium, sodium, silicon, calcium, aluminium silicates. The mantle is liquid and has a depth of about 2900 km, and is made primarily of iron and magnesium silicates. Density discontinuities of about 6% and 10% are expected to occur in few-km thick layers at depths of about 400 km and 670 km. The core is generally believed to be made primarily of iron, solid in the inner core and liquid in the outer core. The deepest hole which has ever been dug is only ~ 10 km deep. The above expectations are mostly based on seismological data (earthquakes or man-made explosions), interpreted at the light of our knowledge of physical properties of materials.

To a good approximation one can compute neutrino oscillations by considering only the two main structures (the mantle and the core) provided that one employs their average density over the path followed by the neutrino. Precise values of the local densities have been computed and are needed for long-baseline neutrino experiments that hope to discover subtle effects, such as CP-violation in neutrino oscillations.

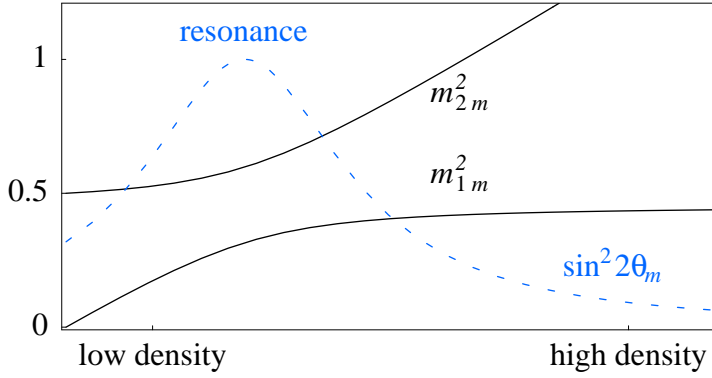


Figure 3.5: *Effective masses and mixing angle in matter for two neutrino flavours as a function of the density. We take $\theta = 0.3$, $\Delta m^2 = 1/2$ (arbitrary units).*

- **Resonance.** If $\Delta m^2 \cos 2\theta > 0$ (< 0) the matter contribution can render equal the diagonal elements of the effective neutrino (anti-neutrino) mass matrix, so that θ_m can be maximal, $\theta_m = \pi/4$, even if $\theta \ll 1$. At the resonance $\Delta m_m^2 = \Delta m^2 \sin 2\theta$. Matter effects resonate at

$$E \sim \frac{\Delta m^2}{2\sqrt{2}G_F N_e} = 3 \text{ GeV} \frac{\Delta m^2}{10^{-3} \text{ eV}^2} \frac{1.5 \text{ g/cm}^3}{\rho Y_e}. \quad (3.18)$$

Numerically the matter potential equals

$$\sqrt{2}G_F N_e = 0.76 \cdot 10^{-7} \frac{\text{eV}^2}{\text{MeV}} \frac{N_e}{N_A/\text{cm}^3} = 0.76 \cdot 10^{-7} \frac{\text{eV}^2}{\text{MeV}} \frac{Y_e \rho}{\text{g/cm}^3}. \quad (3.19)$$

The typical electron number density of ordinary matter is $N_e \sim 1/\text{\AA}^3$. For example, the density of the mantle of the earth is $\rho \approx 3 \text{ g/cm}^3$ and therefore $N_e = \rho Y_e / m_N \approx 1.5 N_A / \text{cm}^3$, where $N_A = 6.022 \cdot 10^{23}$ is the Avogadro number, m_N is the nucleon mass and $Y_e \equiv N_e / (N_n + N_p) \approx 0.5$ the electron fraction. Other characteristic densities are $\rho \sim 6 \text{ g/cm}^3$ in the earth core, $\rho \sim 100 \text{ g/cm}^3$ in the solar core, and $\rho \sim m_n^4 \sim 10^{14} \text{ g/cm}^3$ in the core of a type II supernova. The density profiles of the earth and of the sun are plotted in fig. 3.4.

- **Matter-dominated oscillations.** When neutrinos have high enough energy the matter term dominates: being flavour-diagonal it suppresses oscillations. In this situation, neutrinos oscillate in matter with an energy-independent wave-length $\lambda = \pi / \sqrt{2}G_F N_e$. In the earth mantle $\lambda \sim 3000 \text{ km}$, comparable to the size of the earth.

The modified relation between energy and momentum can be presented as a ‘neutrino refraction index’ $n = 1 + A/E$. While in principle the well known optical phenomena (like refraction, focussing, ...) also occur with neutrino rays, $n - 1 \sim 10^{-10}$ is too small for giving significant effects.

Let us show the relevance of earth matter effects in a case of practical interest. Neutrinos produced by distant sources (e.g. the sun, supernovæ, ...) reach the earth as an incoherent mixture of mass eigenstates, because oscillations average to zero the coherency among different flavors. These neutrinos can be detected after having crossed the earth (indeed in various circumstances only upward-going neutrinos can be detected, because the background of cosmic rays prevents

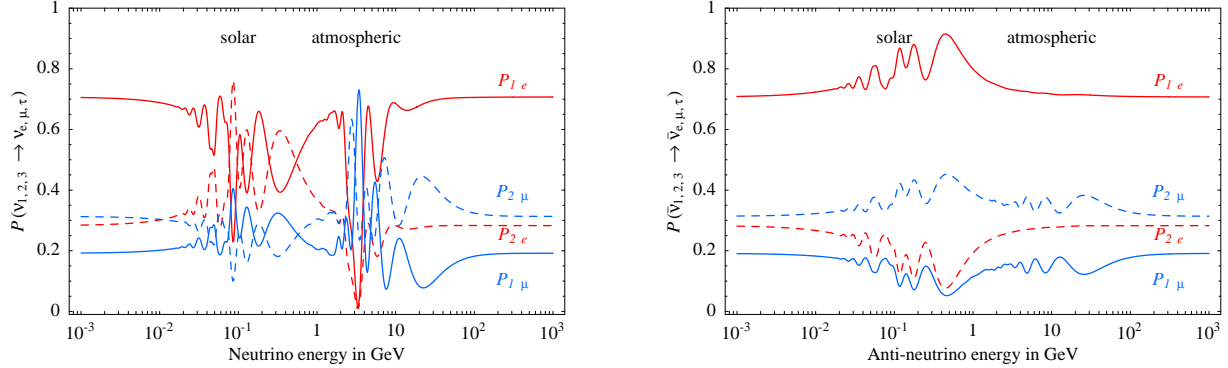


Figure 3.6: *How a neutrino mass eigenstate that crosses all earth is affected by earth matter effects. We assumed $\theta_{13} = 0.1$, no CP-violation, normal hierarchy and best-fit solar and atmospheric parameters. Choosing a much smaller θ_{13} the ‘atmospheric’ effects around $E_\nu = 10$ disappear.*

detection of downward-going neutrinos). Fig. 3.6 shows how earth matter affects a neutrino mass eigenstate that crosses the center of the earth. The two structures peaked around $E_\nu \sim 100$ MeV and around $E_\nu \sim 10$ GeV are respectively due to solar and atmospheric oscillations. Atmospheric effects are present only if $\theta_{13} > 0$.

3.3 Oscillations in a varying density

In order to study solar and supernova neutrinos it is useful to develop an approximation for the oscillation probabilities for neutrinos produced in the core of the star (where matter effects are important), that escape into the vacuum (where matter effects are negligible). At some intermediate point matter effects can be resonant.

Here, we discuss the case of two neutrino generations in the sun; later it will be easy to generalize the discussion. Briefly, solar neutrinos behave as follows.

1. ν_e are produced in the core of the sun, $r \approx 0$. The probability of ν_e being $\nu_{1m}(r \approx 0)$ or $\nu_{2m}(r \approx 0)$ are $\cos^2 \theta_m$ and $\sin^2 \theta_m$ respectively. When matter effects are dominant $\nu_e \simeq \nu_{2m}$ (i.e. $\sin^2 \theta_m = 1$).
2. The oscillation wave-length λ is much smaller than the solar radius R . Therefore neutrinos propagate for many oscillation wave-lengths: the phase averages out so that we have to combine probabilities instead of amplitudes. If the density changes very slowly (‘adiabatic approximation’, see below) each neutrino mass eigenstate will remain the same. Otherwise neutrinos will flip to the other mass eigenstate with some level-crossing probability P_C that we will later compute:

$$\nu_{2m}(r \approx 0) \text{ evolves to } \begin{cases} \nu_{2m}(r \approx R) = \nu_2 \text{ with probability } 1 - P_C \\ \nu_{1m}(r \approx R) = \nu_1 \text{ with probability } P_C \end{cases}$$

(and similarly for $1 \leftrightarrow 2$).

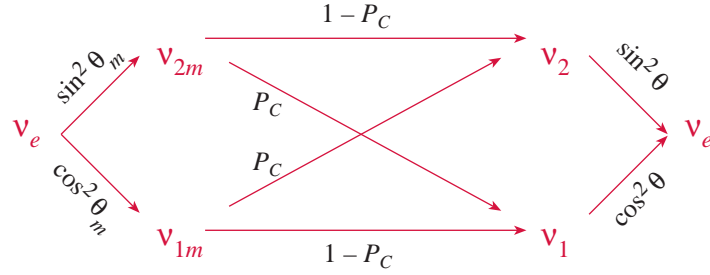


Figure 3.7: *Propagation of a neutrino from the sun to the earth, that leads to eq. (3.20). See the text.*

3. Neutrinos propagate from the sun to the earth, and eventually inside the earth before reaching the detector. For simplicity we start ignoring earth matter effects. The complete 3-neutrino analysis including earth matter effects is presented in section 3.4.
4. Finally, the ν_1 (ν_2) is detected as ν_e with probability $\cos^2 \theta$ ($\sin^2 \theta$).

Combining all these probabilities, as summarized in fig. 3.7, one gets

$$P(\nu_e \rightarrow \nu_e) = \frac{1}{2} + \left(\frac{1}{2} - P_C\right) \cos 2\theta \cos 2\theta_m \quad (3.20)$$

where θ_m is the effective mixing angle at the production point. It is instructive to specialize eq. (3.20) to a few limiting cases:

- a) $P(\nu_e \rightarrow \nu_e) = 1 - \frac{1}{2} \sin^2 2\theta$ (averaged vacuum oscillations) when matter effects are negligible: $\theta_m = \theta$ and $P_C = 0$. This case seem realized for solar neutrinos at lower energies.
- b) $P(\nu_e \rightarrow \nu_e) = P_C$ when $\cos 2\theta_{2m} = -1$ (i.e. matter effects dominate so that the heavier effective neutrino mass eigenstate is $\nu_{2m}(0) \simeq \nu_e$) and $\theta \ll 1$.
- c) $P(\nu_e \rightarrow \nu_e) = \sin^2 \theta$ when $\cos 2\theta_{2m} = -1$ and neutrinos propagate adiabatically ($P_C = 0$). This case seem realized for solar neutrinos at higher energies.
- d) $P(\nu_e \rightarrow \nu_e) = 1 - \frac{1}{2} \sin^2 2\theta$ when $\cos 2\theta_m = -1$ and in the extreme non-adiabatic limit ($P_C = \cos^2 \theta$). This value of P_C can be computed by considering very dense matter that abruptly terminates in vacuum. The produced neutrino $\nu_e \simeq \nu_{2m}$ does not change flavour at the transition region, since it is negligibly short. Therefore $P_C = |\langle \nu_e | \nu_1 \rangle|^2 = \cos^2 \theta$.

To see why $P(\nu_e \rightarrow \nu_e)$ is equal to averaged vacuum oscillations let us follow the neutrino path: matter effects are very large and block oscillations around and after the production point, until they become suddenly negligible.

In the next section we compute P_C . The main result should be intuitively clear to physicists and pickpockets: $P_C = 0$ when the variation of the matter density is smooth enough. We will see that this is the case for solar neutrinos, and that the general discussion in the next section might be necessary in the case of supernova neutrinos, if $\theta_{13} \sim$ few degrees.

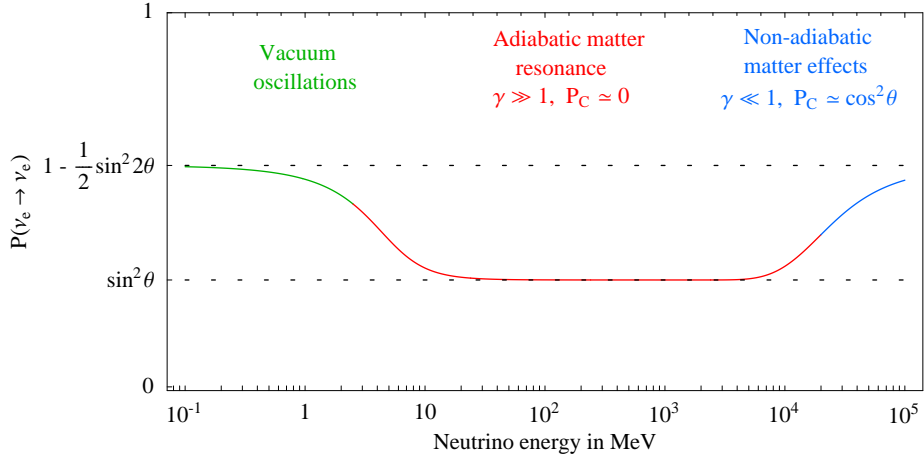


Figure 3.8: Behavior of $P(\nu_e \rightarrow \nu_e)$ that illustrates the limiting regimes a, c, d discussed at page 33. a) At lower energies matter effects are negligible. c) At intermediate energies matter effects are dominant and adiabatic. d) At higher energies the MSW resonance is no longer adiabatic. The numerical example corresponds to solar oscillations. Absorption is neglected.

3.3.1 Adiabaticity

We rewrite the evolution equation $i d\nu/dx = H(x)\nu$ in the new basis of instantaneous matter mass eigenstates ν_m , related to the flavour basis by

$$\nu = V_m(x)\nu_m, \quad V_m = \begin{pmatrix} \cos \theta_m & \sin \theta_m \\ -\sin \theta_m & \cos \theta_m \end{pmatrix}. \quad (3.21)$$

In this new basis the effective Hamiltonian is diagonal, $H_m = V_m^{-1}H V_m = \text{diag}(m_{1m}^2, m_{2m}^2)/2E$. However the wave equation contains an additional term due to the fact that the new basis is position-dependent:

$$i \frac{d\nu_m}{dx} = \left(H_m - i V_m^{-1} \frac{dV_m}{dx} \right) \nu_m = \begin{pmatrix} m_{1m}^2/2E_\nu & -i d\theta_m/dx \\ i d\theta_m/dx & m_{2m}^2/2E_\nu \end{pmatrix} \nu_m. \quad (3.22)$$

This basis is convenient for analytic computations because the off-diagonal term can be relevant only in the (possibly narrow) interval of r where level crossing occurs. In the extreme adiabatic limit where the density gradient is small enough that we can always neglect $d\theta_m/dx$, the level-crossing probability is $P_C = 0$. A resonance is adiabatic if the ratio between the difference in the diagonal elements and the off-diagonal element of (3.22) is always much larger than one. Therefore one usually defines

$$\gamma \equiv \min_x \left| \frac{\Delta m_m^2/4E_\nu}{d\theta_m/dx} \right|. \quad (3.23)$$

In general the position of the minimum depends on the detailed form of the matter potential A . Whenever the resonance is sharp enough that, around it, A can be approximated with a linear function of x , eq. (3.17) shows that the minimum occurs at the resonance point (e.g. in the case of a $\nu_e/\nu_{\mu,\tau}$ resonance in normal matter, the resonance condition is $2E_\nu \sqrt{2}G_F N_e(r) = \Delta m^2 \cos 2\theta$)

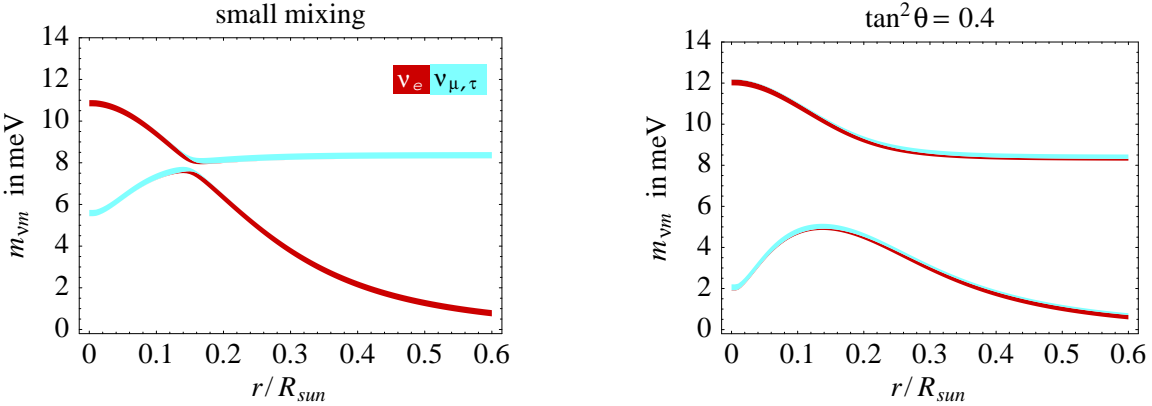


Figure 3.9: Variation of the matter neutrino eigenstates inside the sun for $E_\nu = 10$ MeV, $\Delta m^2 = 7 \cdot 10^{-5}$ eV 2 and $m_1 = 0$ (i.e. $m_2 \approx 8$ meV). Dark red (light blue) denotes the ν_e ($\nu_{\mu,\tau}$) flavour component.

and γ equals

$$\gamma = \left| \frac{2H_{12}}{\frac{1}{2H_{12}} \frac{d(H_{22} - H_{11})}{dx}} \right|_{\text{res}} = \tilde{\gamma} \cdot \frac{\sin^2 2\theta}{2\pi \cos 2\theta}, \quad \tilde{\gamma} = \frac{\pi \Delta m^2 / E_\nu}{|d \ln A / dx|_{\text{res}}}. \quad (3.24)$$

where the second analytic expression holds for a two neutrino system, and the first expression, written in terms of the ‘crossing elements’ of the effective Hamiltonian H in the flavour basis, is useful in numerical computations in generic cases with many neutrinos.

A resonance is adiabatic if $\gamma \sim \tilde{\gamma}\theta^2 \gg 1$. Physically $\tilde{\gamma}$ is the number of vacuum oscillations (wave length $\lambda_0 = 4\pi E_\nu / \Delta m^2$) present in the typical length-scale where the matter potential changes ($r_0 = |d \ln A / dr|_{\text{res}}^{-1}$). In the sun

$$\tilde{\gamma} \approx \frac{\Delta m^2 / E_\nu}{10^{-9} \text{ eV}^2 / \text{MeV}}$$

having used the approximate density $N_e(r) = 245 N_A / \text{cm}^3 \times \exp(-10.54 r/R)$ (dashed line in fig. 3.4b).⁶ The solar neutrino anomaly seems due to oscillations with large mixing angle and $\Delta m^2 \approx 7 \cdot 10^{-5}$ eV 2 . The level crossing scheme is shown in fig. 3.9b and corresponds to a broad adiabatic resonance: at $E_\nu \sim 10$ MeV one has $\gamma \gg 1$ and consequently $P_C = 0$. The resonance ceases to be adiabatic at $E_\nu \gtrsim 10$ GeV, much higher than the maximal solar neutrino energy. Fig. 3.8 illustrates the behavior of $P(\nu_e \rightarrow \nu_e)$.

3.3.2 Analytic approximation for the crossing probability

P_C can be accurately approximated as follows [30]. When the mixing angle is small there is a narrow resonance (such as the one shown in fig. 3.9a) and one can approximate any smooth

⁶We are using the average density. The transition becomes less adiabatic if N_e fluctuates on scales comparable to the neutrino oscillation wavelength. This effect seems negligible in the sun, where the amplitude of helioseismic fluctuations should be too small.

density profile (e.g. fig. 3.4 show the solar density) with a simple function, such that the wave equation (3.22) can be solved analytically. By choosing an appropriate simple function that resembles the true one, this procedure can be applied even to the broader resonances generated by large mixing angles $\theta \sim \pi/4$ (when $\theta > \pi/4$ there is no resonance point, but adiabaticity is still dominantly violated only in the restricted region where $A(r) \simeq \Delta m^2/2E_\nu$). Approximating A with an exponential, $A \propto e^{-r/r_0}$, and solving (3.22) by brute force, one obtains

$$P_C = \frac{e^{\tilde{\gamma} \cos^2 \theta} - 1}{e^{\tilde{\gamma}} - 1}, \quad \tilde{\gamma} = \frac{\pi r_0 \Delta m^2}{E_\nu} \quad (3.25)$$

This expression was used in analyses of solar neutrinos. When $\gamma \gg 1$ we go back to the adiabatic approximation, $P_C = 0$. In the non-adiabatic limit, $\gamma \ll 1$, one gets $P_C = \cos^2 \theta$ as expected. If the density profile $A(r)$ is not exactly exponential, a good approximation is often obtained by inserting in (3.25) the gradient $1/r_0 = |d \ln A/dr|$ evaluated at the point $r = r_*$ where $A(r_*) = \Delta m^2/2E_\nu$.

Exact solutions are available also for a few other density distributions. For $A \propto r^n$ and any n P_C can be written in ‘double exponential’ form

$$P_C = \frac{\exp \left[-\pi \gamma F/2 \right] - \exp \left[-\pi \gamma F/2 \sin^2 \theta \right]}{1 - \exp \left[-\pi \gamma F/2 \sin^2 \theta \right]} \quad (3.26)$$

where the function $F(\theta)$ has a simple expression for $n = 1$ ($F = 1$), for $n = -1$ ($F = (1 - \tan^2 \theta)^2/(1 + \tan^2 \theta)$) and for $n = -\infty$, which is again the exponential case ($F = 1 - \tan^2 \theta$ and eq. (3.26) simplifies to (3.25)). The profile of a supernova is maybe well approximated by $n \approx 3$.

When the resonance is narrow, $\theta \ll 1$ as in fig. 3.9a, all above solutions reduce to the LSZ approximation: $P_C \simeq e^{-\pi \gamma/2}$, derived using a technique essentially similar to the WKB approximation, developed in quantum mechanics to compute reflection probabilities. Basically, it employs the adiabatic approximation and avoids the resonance region (where it is not valid) by making a mathematical excursion in the complex x plane. When the resonance is not narrow the LSZ technique gives $P_C \simeq e^{-\pi \gamma F/2}$. The function $F(\theta)$ is expressed as an integral, that can be evaluated numerically for arbitrary density profiles, and analytically for various simple profiles. In this way the functions F in eq. (3.26) can be computed systematically. However, the LSZ approximation fails in the extreme non-adiabatic limit ($\gamma \ll 1$) giving $P_C = 1$ rather than $\cos^2 \theta$. Usually one improves the LSZ approximation by replacing it with the ‘double exponential’ form of eq. (3.26), because this turned out to be the exact solution in all cases where it was computed.

For anti-neutrinos in normal matter, the matter potential has the opposite sign. If one also changes the sign of Δm^2 the oscillation probabilities remain the same. Therefore the $\bar{\nu}$ oscillation probabilities are obtained from the above formulæ valid for neutrinos by replacing $\theta \leftrightarrow \pi/2 - \theta$.

3.4 The density matrix and solar oscillations

In order to make physics as transparent as possible, so far we studied the simplest situations using the simplest formalism. Such simple computations can also be done using the neutrino density matrix, which becomes necessary in more complicated situations and is often convenient even in the simplest situations, when physics is more conveniently described by mixed rather than by pure quantum states.

In fact, in various circumstances of experimental interest neutrinos are detected after many oscillations. The neutrino mass eigenstates ν_i develop large phase differences $\varphi_i - \varphi_j$ which depend on neutrino energy. As a result the flavour composition of $\nu(E_\nu) \equiv \sum_{i=1}^3 \rho_{ii}(E_\nu) e^{i\varphi_i(E_\nu)} \nu_i$ depends so strongly on neutrino energy that only its average value is measured. However at each E_ν the pure state $\nu(E_\nu)$ has a well defined flavour, that is not measured. The average flavour can be computed performing the appropriate average over E_ν : however doing numerically averages of rapidly oscillating functions is a time-consuming task. It is more convenient to employ the density matrix formalism that directly describes the ‘average’ neutrino which is observed.

Of course, in simple situations the average is easily performed analytically. In the case of vacuum oscillations the regime of ‘averaged oscillations’ was discussed at page 23, and generalized in eq. (3.14). In the case of matter oscillations eq. (3.20) contains such average. The density matrix becomes really useful in more difficult situations with multiple Δm^2 (e.g. when ‘atmospheric’ oscillations are averaged, while ‘solar’ ones are not).

Furthermore, in sections 3.5 and 3.6 we will consider cases where neutrino scatterings are not negligible and break the coherence among neutrino mass eigenstates, so that propagation of neutrinos must be described in terms of a neutrino density matrix.

The evolution equation for ρ_E , the 3×3 density matrix of neutrinos with energy E , is

$$\frac{d\rho_E}{dx} = -i[H, \rho_E] \quad (3.27)$$

where H is given in eq. (3.16). The explicit solution is $\rho(L) = e^{-iHL} \rho(0) e^{iHL}$. In vacuum the solution becomes

$$\rho_{ij}^m(L) = \rho_{ij}^m(0) \exp \left[-i(E_i - E_j)L \right] \quad \text{and in particular} \quad \rho_{ii}^m(L) = \rho_{ii}^m(0). \quad (3.28)$$

The superscript ‘ m ’ denotes that we used the basis of neutrino mass eigenstates. Eq. (3.28) also holds in uniform matter, in the basis of matter eigenstates. The mass matrix in the flavour basis is obtained as $\rho = V^m \rho^m V^{m\dagger}$.

3.4.1 Fast average over fast oscillations

Since too rapid oscillations cannot be observed, and since computing numerically the relevant energy-averaged oscillation probabilities is time-consuming, one often likes to replace the exact oscillation formula adding something that damps oscillations in the long-baseline limit. In the simplest case of vacuum oscillations of two neutrinos one can use

$$P(\nu_e \rightarrow \nu_\mu) = \sin^2 2\theta \frac{1 - e^{-\epsilon L \Delta m^4 / 4E_\nu^2} \cos(\Delta m^2 L / 2E_\nu)}{2}$$

with small ϵ , e.g. $\epsilon = 0.01L$. We here show how to correctly extend this approximation to a generic three-neutrino case, possibly with matter effects. It is convenient to consider the evolution of the density matrix in the basis of matter eigenstates. Its diagonal elements remain constant, while the phases of off-diagonal elements oscillate. The correct approximation is

$$\rho_{ij}^m(E_\nu, L) = \rho_{ij}^m(E_\nu, 0) \exp \left[-i(H_i - H_j)L - \epsilon(H_i - H_j)^2 L \right] \quad \text{for } i \neq j \quad (3.29)$$

where H_i are the Hamiltonian eigenvalues. Off-diagonal entries get suppressed after many oscillations, as desired. The density profile of the earth is approximatively piecewise constant, such that the above formula can be applied in each piece. For a generic density profile the same average is performed by adding an appropriate coherency-breaking term to the evolution equation:

$$\frac{d\rho}{dx} = -i[H, \rho] - \epsilon[H, [H, \rho]]. \quad (3.30)$$

One can verify that the extra term suppresses $\text{Tr}(\rho^2)$, thereby transforming a pure state into a mixed state, and that when H is constant acts like in (3.29). Eq. (3.30) can be obtained by considering two energies E_1 and E_2 and suitably approximating the equation for the average $\rho = (\rho_{E_1} + \rho_{E_2})/2$.

Some theorists speculate that, at some fundamental level (quantum gravity?), quantum mechanics might have to be modified adding de-coherence terms. Possible decoherence terms are restricted by consistency considerations [31], which suggest the general form

$$\dot{\rho} = -i[H, \rho] - [D, [D, \rho]] \quad \text{with} \quad [D, H] = 0$$

where D is an arbitrary operator. Our approximation in eq. (3.30) corresponds to $D \propto H$. Regarding such term not as a computational trick but as a real physical effect, we notice that the simplest choice $D \propto H$ is poorly probed by neutrino oscillations, because they are a low-energy phenomenon. Claims that neutrino oscillations allow sensitive tests of de-coherence are based on appropriate non-minimal choices of D .

3.4.2 Solar oscillations of three neutrinos

We here extend the solar oscillation formula, eq. (3.20), to 3 neutrinos. Analytical expressions that describe the full evolution are conveniently obtained using the density matrix formalism. Such expressions clarify the physics, but are not needed in numerical computations. Indeed a simple and systematic way of performing any computation consists in evolving the density matrix step-by-step, starting from its initial value.

ν_e are produced around the center of sun where matter eigenstates are given by $\nu_i^m = V_{\ell i}^m \nu_\ell$. The initial density matrix in the matter eigenstate basis is $\rho^m = V^m \Pi_e V^m$ where $\Pi_e = \text{diag}(1, 0, 0)$ is the projector over ν_e . In adiabatic approximation the diagonal elements of ρ^m remain constant, while the flavor of matter eigenstates evolves. The off-diagonal elements acquire oscillation phases. In many relevant cases phases differences are large and therefore amount to average to zero the off-diagonal elements, resulting in $\rho^m = \text{diag}(|V_{e1}^m|^2, |V_{e2}^m|^2, |V_{e3}^m|^2)$. In this limit quantum amplitudes reduce to classical probabilities, fully described by the diagonal elements of ρ^m .

We must take into account that adiabaticity can be violated at level crossings. Solar neutrinos undergo one ν_1^m/ν_2^m level crossing and exit from the sun as

$$\begin{aligned} \rho_S^m &= \text{diag} \begin{pmatrix} 1 - P_C & P_C & 0 \\ P_C & 1 - P_C & 0 \\ 0 & 0 & 1 \end{pmatrix} \cdot \begin{pmatrix} |V_{e1}^m|^2 \\ |V_{e2}^m|^2 \\ |V_{e3}^m|^2 \end{pmatrix} \\ &= \text{diag} \left(\cos^2 \theta_{13} \left[\frac{1}{2} + \left(\frac{1}{2} - P_C \right) \cos 2\theta_{12}^m \right], \cos^2 \theta_{13} \left[\frac{1}{2} - \left(\frac{1}{2} - P_C \right) \cos 2\theta_{12}^m \right], \sin^2 \theta_{13} \right). \end{aligned} \quad (3.31)$$

This holds in vacuum where matter eigenstates coincide with vacuum eigenstates. In the last equation we approximated $\theta_{13}^m \simeq \theta_{13}$ because matter effects negligibly affect the ‘atmospheric’ θ_{13} mixing. Solar neutrinos detected during the day do not cross the earth: therefore the oscillation probability is

$$P(\nu_e \rightarrow \nu_e, \text{ day}) = \text{Tr} [\Pi_e \rho_S] = (\rho_S)_{ee} = \sin^4 \theta_{13} + \cos^4 \theta_{13} \left[\frac{1}{2} + \left(\frac{1}{2} - P_C \right) \cos 2\theta_{12} \cos 2\theta_{12}^m \right] \quad (3.32)$$

that generalizes eq. (3.20) to $\theta_{13} \neq 0$.

3.4.3 Earth regeneration

Neutrinos that reach the earth with density matrix ρ_E can be detected after crossing the earth: the density matrix at detector becomes $\rho_E = U \rho_S U^\dagger$ where U is the unitary matrix describing evolution inside the earth, computed solving eq. (3.16). It is often convenient to compute the evolution numerically performing the average described in section 3.4.1. The computation is easily done in mantle/core approximation. Eq. (3.29) tells how ρ^m evolves in a medium with constant density. At the sharp air/mantle and mantle/core transitions one simply has to rotate ρ^m from the old to the new basis of matter eigenstates: when passing from medium A to medium B one has $\rho_B^m = P \rho_A^m P^\dagger$. Notice that the factor $P = V_B^{m\dagger} V_A^m$ can be interpreted as a non-adiabaticity factor, fully analogous to the one introduced in eq. (3.31) to account for the possibly non-adiabatic MSW resonance. Indeed, when levels i and j cross, P is a rotation in the (ij) plane with angle α given by $\tan^2 \alpha = P_C / (1 - P_C)$, where P_C is the level-crossing probability. When level crossing is adiabatic $P_C = 0$, $\alpha = 0$ and $P = \mathbb{1}$. When level crossing is fully non-adiabatic $P_C = 1$, $\alpha = \pi/2$ and the matrix P is given by $P = V_B^{m\dagger} V_A^m$. When the off-diagonal elements of ρ^m can be neglected this procedure reduces to combining classical probabilities as in eq. (3.31).

In the case of solar neutrinos, earth matter affects neutrinos detected during the night and one is interested in the oscillation probability

$$P(\nu_e \rightarrow \nu_e, \text{ night}) = (\rho_E)_{ee} = \sum_{i=1}^3 P_{ie} \cdot (\rho_S)_{ii}, \quad P_{ie} = |\langle \nu_e | U | \nu_i \rangle|^2.$$

At solar neutrino energies $E_\nu \lesssim 10$ MeV earth matter effects negligibly affect the most splitted neutrino ν_3 , so that $P_{3e} \approx |\langle \nu_e | \nu_3 \rangle|^2 = \sin^2 \theta_{13}$. Eliminating $P_{1e} = 1 - P_{3e} - P_{2e}$ gives

$$P(\nu_e \rightarrow \nu_e, \text{ night}) = P(\nu_e \rightarrow \nu_e, \text{ day}) + \frac{P_{2e} - c_{13}^2 s_{12}^2}{c_{13}^2 \cos 2\theta_{12}} (1 - 2P(\nu_e \rightarrow \nu_e, \text{ day}) - 2s_{13}^2 + 3s_{13}^4). \quad (3.33)$$

This formula describes the effect known as ‘earth regeneration’ of solar neutrinos. One needs to compute the function $P_{2e}(E_\nu)$ taking into account the path followed by the neutrino inside the earth. Neglecting earth matter effects one has $P_{2e} = c_{13}^2 s_{12}^2$ and the survival probability reduces to its ‘day’ value.

3.5 Oscillations and absorption

We study the combined effect of oscillations and absorption, starting from the simplest case: neutrinos propagate in normal matter that gets negligibly affected by neutrinos. So far this

case is not relevant for any experimental result: indeed absorption becomes relevant in the sun at $E_\nu \gtrsim 100$ GeV and in the earth at $E_\nu \gtrsim 10$ TeV. In the future it might become relevant for a) detection of up-going ultra-high energy neutrinos of cosmic origin. b) detection of neutrinos generated by annihilations of dark matter particles clustered around the center of the sun and/or of the earth.

As usual, we can neglect $\nu \leftrightarrow \bar{\nu}$ spin-flip reactions, suppressed by a factor $(m_\nu/E_\nu)^2$. Therefore the appropriate formalism consists in studying the spatial evolution of the $n \times n$ flavour *density matrices* of neutrinos, $\rho(E_\nu)$, and of anti-neutrinos, $\bar{\rho}(E_\nu)$ where $n = 3$ or greater if one considers extra sterile neutrinos. Matrix densities are necessary because scatterings damp coherencies, so that neutrinos are not in a pure state. The evolution equation is

$$\frac{d\rho}{dr} = -i[H, \rho] + \left. \frac{d\rho}{dr} \right|_{\text{CC}} + \left. \frac{d\rho}{dr} \right|_{\text{NC}} + \left. \frac{d\rho}{dr} \right|_{\text{in}} \quad (3.34)$$

with an analogous equation for $\bar{\rho}$. The first term describes oscillations in vacuum or in matter, and the Hamiltonian H is given in eq. (3.16). The last term represent the neutrino injection due e.g. to annihilations of DM particles. The second and the third term describe the absorption and re-emission due to CC and NC scatterings. Deep inelastic scatterings of $(\bar{\nu})$ on nucleons are the dominant processes at $E_\nu \gg$ GeV (see section 4.2.3).

NC scatterings $(\bar{\nu})N \leftrightarrow (\bar{\nu})N$ remove a neutrino from the flux and re-inject it with a lower energy. So they contribute to the evolution equation as:

$$\left. \frac{d\rho}{dr} \right|_{\text{NC}} = - \int_0^{E_\nu} dE'_\nu \frac{d\Gamma_{\text{NC}}}{dE'_\nu}(E_\nu, E'_\nu) \rho(E_\nu) + \int_{E_\nu}^\infty dE'_\nu \frac{d\Gamma_{\text{NC}}}{dE'_\nu}(E'_\nu, E_\nu) \rho(E'_\nu) \quad (3.35)$$

where

$$\Gamma_{\text{NC}}(E_\nu, E'_\nu) = N_p(r) \text{ diag } \sigma(\nu_\ell p \rightarrow \nu'_\ell X) + N_n(r) \text{ diag } \sigma(\nu_\ell n \rightarrow \nu'_\ell X) \quad (3.36)$$

and $N_{p,n}(r)$ are the proton and neutron profile densities⁷ The first term describes the absorption: the integral over E'_ν just gives the total NC cross section. The second term describes the reinjection of lower energy neutrinos.

CC scatterings remove a neutrino and produce a charged lepton together with hadrons: these particles can decay back to neutrinos. While μ^\pm are long-lived and hadrons have strong interactions, such they get stopped by ambient matter before decaying, τ^\pm can decay promptly re-injecting secondary fluxes of energetic neutrinos: this effect is known as $(\bar{\nu})_\tau$ regeneration [32]. A τ^- decays always into ν_τ and decays into $\bar{\nu}_\mu, \bar{\nu}_e$ with BR = 0.175, such that $(\bar{\nu})_\tau$ regeneration couples neutrinos with anti-neutrinos. It is relevant at energies E_ν GeV: we can assume that all particles are collinear. The CC contribution to the evolution equation of the density matrices is therefore

$$\begin{aligned} \left. \frac{d\rho}{dr} \right|_{\text{CC}} = & -\frac{\{\Gamma_{\text{CC}}, \rho\}}{2} + \int \frac{dE_\nu^{\text{in}}}{E_\nu^{\text{in}}} \left[\Pi_\tau \rho_{\tau\tau}(E_\nu^{\text{in}}) \Gamma_{\text{CC}}^\tau(E_\nu^{\text{in}}) f_{\tau \rightarrow \tau}(E_\nu^{\text{in}}, E_\nu) \right. \\ & \left. + \Pi_{e,\mu} \bar{\rho}_{\tau\tau}(E_\nu^{\text{in}}) \bar{\Gamma}_{\text{CC}}^\tau(E_\nu^{\text{in}}) f_{\bar{\tau} \rightarrow e,\mu}(E_\nu^{\text{in}}, E_\nu) \right]. \end{aligned} \quad (3.37)$$

⁷In the sun N_p/N_n varies from the BBN value, $N_p/N_n \sim 7$ present in the outer region $r/R_\odot \gtrsim 0.3$, down to $N_p/N_n \sim 2$ in the central region composed of burnt ${}^4\text{He}$. The earth is mostly composed by heavy nuclei, so that $N_p \approx N_n$.

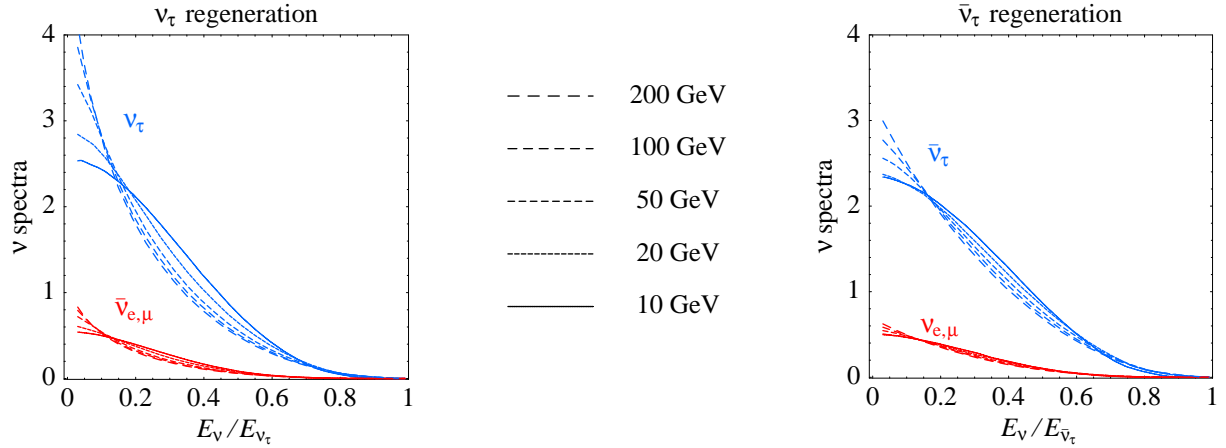


Figure 3.10: *Energy distributions of neutrinos regenerated by CC scatterings of a $(\bar{\nu})_\tau$ with given energy E_{ν_τ} , produced by one $(\bar{\nu})_\tau$ /nucleon scattering. The blue upper curves are $f_{\tau \rightarrow \tau}(E_{\nu_\tau}, E'_\nu)$, and the red lower curves are $f_{\tau \rightarrow e, \mu}(E_{\nu_\tau}, E'_\nu)$, plotted for several values of the incident ν_τ energy E_{ν_τ} .*

The first term describes the absorption; the anticommutator arises because loss terms correspond to an anti-hermitian effective Hamiltonian. The second term describes the ‘ ν_τ regeneration’. In the formulæ above, Π_ℓ are 3×3 matrices projecting on the flavor ν_ℓ . The Γ_{CC} , $\bar{\Gamma}_{\text{CC}}$ matrices express the rates of absorption due to the CC scatterings and are given by

$$\Gamma_{\text{CC}}(E_\nu) = \text{diag}(\Gamma_{\text{CC}}^e, \Gamma_{\text{CC}}^\mu, \Gamma_{\text{CC}}^\tau), \quad \Gamma_{\text{CC}}^\ell = N_p(r) \sigma(\nu_\ell p \rightarrow \ell X) + N_n(r) \sigma(\nu_\ell n \rightarrow \ell X), \quad (3.38)$$

Notice that $\Gamma_{\text{CC}}^\tau < \Gamma_{\text{CC}}^\mu = \Gamma_{\text{CC}}^e$ due to the kinematical effect of the τ mass. The functions $f(E_\nu, E'_\nu)$, plotted in fig. 3.10, are the energy distributions of secondary neutrinos produced by a CC scattering of an initial neutrino with energy E_{ν_τ} .

3.6 Oscillations in the early universe

When the universe was cooling down after the big-bang, weak interactions kept neutrinos in thermal equilibrium with other particles for about one second, down to temperatures of few MeV (see section 10). At these energies the observed solar and atmospheric oscillations are faster than the expansion rate of the universe, $H \sim T^2/M_{\text{Pl}} \sim 1/\text{s}$ and give minor corrections to big-bang nucleosynthesis. If extra sterile neutrinos exist, oscillations could thermalize them, giving significant observable effects.

The precise study of neutrino oscillations in the early universe involves new ingredients [33]: i) the background medium is expanding and contains a significant amount of neutrinos; ii) neutrino oscillations can modify the background; iii) new matter effects.

We assume that the medium is in thermal equilibrium and can be described by macroscopic parameters (such as temperature, densities of different particles, . . .). We neglect inhomogeneities. We want to study the time evolution of the the neutrino and anti-neutrino matrix densities ρ_p and $\bar{\rho}_p$, where p is the neutrino momentum.

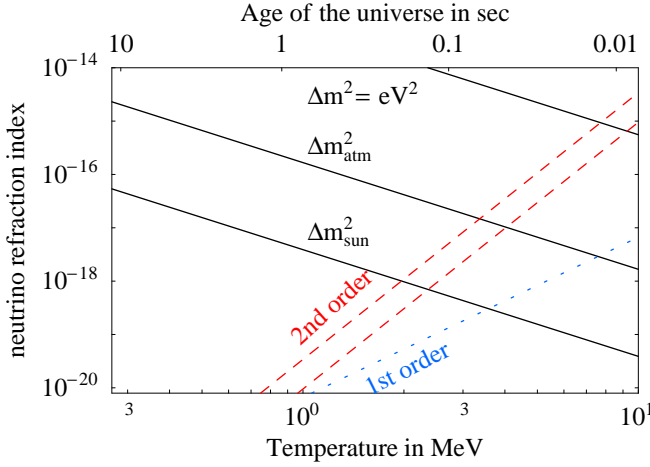


Figure 3.11: Contributions to the refraction index $n - 1$ from neutrino masses (continuous lines), matter effects at 2nd order in G_F (dashed lines, for ν_e and $\nu_{\mu,\tau}$). Matter effects at 1st order are suppressed by n_B/n_γ and therefore negligible.

The relevant interactions at $T \sim$ MeV are CC neutrino/matter scatterings, NC neutrino/matter scatterings and scatterings among 4 neutrinos. The amplitude of these weak interactions is proportional to the Fermi constant G_F . Up to second order in G_F the evolution equation of ρ_p can be found by computing and adding their separate contributions:

$$\dot{\rho}_p = -i[E_p^0, \rho_p] + (\dot{\rho}_p)_{\text{CC}} + (\dot{\rho}_p)_{\text{NC}} + (\dot{\rho}_p)_S \quad (3.39)$$

where $E_p^0 \simeq p + mm^\dagger/2p$ is the energy of a non-interacting ultrarelativistic neutrino with momentum p . We do not write the explicit but lengthy collision integrals. In practical applications the evolution equations are often approximately mimicked by

$$\dot{\rho}_p = -i[E_p^0 + A_p, \rho_p] - \{\Gamma, (\rho_p - \rho_p^{\text{eq}})\}. \quad (3.40)$$

- The $\Gamma = \text{diag}(\Gamma_{\nu_e}, \Gamma_{\nu_\mu}, \Gamma_{\nu_\tau})$ terms, describe neutrino production and absorption. The anti-commutator (that approximates a more complicated structure) describes how collisions tend to drive neutrino to their thermal equilibrium values, $\rho_p^{\text{eq}} = \text{diag}(n_{\nu_e}, n_{\nu_\mu}, n_{\nu_\tau})_p$. A detailed comparison with the full equations (3.39) reveals that they can be best approximated by inserting the following values of the damping coefficients:
 - In the equations for the off-diagonal components of ρ , insert the *total scattering rate* $\Gamma_{\text{tot}} \sim G_F^2 T^5$ because all scatterings damp the coherent interference between different flavours.
 - In the equations for the diagonal components of ρ , insert the *annihilation rate* $\Gamma_{\text{ann}} \sim \Gamma_{\text{tot}}/10$, since annihilations are needed to change the number of neutrinos.

(Unlike the exact equations, the simple approximated equations depend on the choice of flavour basis; when coherencies among ν_μ and ν_τ are important, one should use their mass eigenstate basis).

- The A_p terms describe the usual matter effects that arise at first order in G_F (to be computed taking into account that the background contains neutrinos) plus second order terms, which

turn out to be the dominant ones. In fact, when the universe had temperatures $T \gg m_e$ the thermal plasma contained large densities of electrons and positrons, but they were almost equal: $N_e \simeq N_{\bar{e}} \sim T^3$. Therefore the first-order matter effects almost cancel out, being proportional to $N_e - N_{\bar{e}}$.

The second order term in the low-energy expansion of the W, Z propagators,

$$1/(k^2 - M^2) \approx -1/M^2 - k^2/M^4 + \dots \text{ for } k \ll M,$$

induces a new contribution to the matter potential, $A \sim G_F(E^2/M^2)(n_e + n_{\bar{e}}) \sim G_F^2 T^5$, with the same sign for neutrinos and anti-neutrinos. In a plasma made of photons, electrons and neutrinos the second-order matter potential is (at $m_e \ll T \ll m_\mu$)

$$A_p \approx \frac{16\sqrt{2}G_F p}{3} \left[\frac{\langle E_\nu \rangle}{M_Z^2} \text{diag}(n_{\nu_e}, n_{\nu_\mu}, n_{\nu_\tau}) + \frac{\langle E_e \rangle}{M_W^2} \text{diag}(n_e, 0, 0) \right] \quad (3.41)$$

A further approximation allows to replace the equations for ρ_p with a single equation for the total matrix density. Oscillations tend to distort the energy distribution of neutrinos, while scatterings tend to thermalize it: we can neglecting spectral distortions and assume that neutrinos follow a Boltzmann distribution at temperature T_ν , possibly different from the γ, e, \bar{e} temperature T . Inserting $n_e = 2T^3/\pi^2$, $n_\nu = T_\nu^3/\pi^2$ and the average momentum $\langle p \rangle = 3T_\nu$ and energy $\langle E_e \rangle = 3T$ one gets, at $T \gg m_e$

$$A = -\frac{48\alpha_2 T_\nu}{\pi M_W^4} \left[T_\nu^4 \cos^2 \theta_W \text{diag}(1, 1, 1) + 2T_\nu^4 \text{diag}(1, 0, 0) \right], \quad (3.42)$$

$$\begin{aligned} \Gamma_{\text{tot}} &\approx 3.6 G_F^2 T^5 \quad \text{for } \nu_e, \bar{\nu}_e, & \Gamma_{\text{tot}} &\approx 2.5 G_F^2 T^5 \quad \text{for } \nu_{\mu,\tau}, \bar{\nu}_{\mu,\tau}, \\ \Gamma_{\text{ann}} &\approx 0.5 G_F^2 T^5 \quad \text{for } \nu_e, \bar{\nu}_e, & \Gamma_{\text{ann}} &\approx 0.3 G_F^2 T^5 \quad \text{for } \nu_{\mu,\tau}, \bar{\nu}_{\mu,\tau}. \end{aligned}$$

We neglected possible neutrino asymmetries, which could be important only if orders of magnitude larger than the baryon asymmetry. Otherwise, as illustrated in fig. 3.11, the normal matter effect becomes dominant only at lower temperatures, $T \lesssim m_e$, where scatterings become negligible. If extra sterile neutrinos exist, A and Γ become bigger matrices with vanishing ‘sterile’ entries. The tools here presented are applied to compute BBN bounds on extra sterile neutrinos (see section 10.1).

Chapter 4

Detecting neutrinos

Neutrinos only have weak interactions: at ordinary energies they cross the earth without being absorbed. Neutrinos can be detected if one has a intense enough flux of neutrinos and a big enough detector with low enough background (often achieved by going underground in order to suppress the cosmic-ray background). We now discuss what ‘enough’ means in practice.

4.1 Neutrino/electron scattering

According to the SM, the amplitude for scattering of neutrinos on electrons at rest is $\mathcal{M} \sim G_F m_e E_\nu$. The total cross section is $\sigma \sim |\mathcal{M}|^2/s$, where $s = (P_e + P_\nu)^2$ in terms of the quadr-momenta P . Electrons in atoms have a small velocity $v \sim \alpha_{\text{e.m.}}$ and can be considered at rest. If $E_\nu \ll m_e$ one has $s \sim m_e^2$ and so $\sigma \sim G_F^2 E_\nu^2$. If $E_\nu \gg m_e$ one has $s \sim m_e E_\nu$ and so $\sigma \sim G_F^2 m_e E_\nu$. In the energy range $m_e \ll E_\nu \ll M_Z^2/m_e$, the SM prediction at tree level is [34]

$$\sigma(\nu_\ell e \rightarrow \nu_\ell e) = \frac{2m_e E_\nu G_F^2}{\pi} (G_{L\ell}^2 + \frac{1}{3} G_{R\ell}^2), \quad \sigma(\bar{\nu}_\ell e \rightarrow \bar{\nu}_\ell e) = \frac{2m_e E_\nu G_F^2}{\pi} (G_{R\ell}^2 + \frac{1}{3} G_{L\ell}^2). \quad (4.1)$$

Only Z -exchange contributes to $\nu_{\mu,\tau}$ and $\bar{\nu}_{\mu,\tau}$ scattering on electrons (see fig. 3.3b). Therefore when $\ell = \{\mu, \tau\}$ the effective $G_{L,R\ell}$ are equal to the $\ell Z \ell$ couplings, named $g_{L,R\ell}$ and listed in table 4.1 in terms of the weak mixing angle $s_W^2 \approx 0.223$. On the contrary W boson exchange contributes to $\nu_e e \rightarrow \nu_e e$ and $\bar{\nu}_e e \rightarrow \bar{\nu}_e e$ scatterings (see fig. 3.3a): therefore $G_{Le} = +\frac{1}{2} + s_W^2 \neq g_{Le}$ and $G_{Re} = g_{Re}$, giving rise to a larger cross section.¹ Putting numbers

$$\sigma(\nu_e e) = 0.93\sigma_0, \quad \sigma(\nu_{\mu,\tau} e) = 0.16\sigma_0, \quad \sigma(\bar{\nu}_e e) = 0.39\sigma_0, \quad \sigma(\bar{\nu}_{\mu,\tau} e) = 0.13\sigma_0 \quad (4.2)$$

where $\sigma_0 = 10^{-44} \text{cm}^2 E_\nu/\text{MeV}$ and $E_\nu \gg m_e$.

SK detects solar neutrinos through νe scattering. With 10^{10} moles of electrons (20.000 ton of water), a flux of few $\times 10^6 \nu_e/\text{cm}^2 \text{s}$ with $E_\nu \sim 10 \text{ MeV}$ (the solar Boron neutrinos), and a 50% efficiency SK can detect about 10000 ν_e/yr (finding that about half of them oscillate away). SK and SNO can measure $T_e = E_e - m_e$, the kinetic energy of the recoiling electron. Its kinematically allowed range is $0 \leq T_e \leq E_\nu/(1 + m_e/2E_\nu)$. SK and SNO can only detect electrons with

¹The $\bar{\nu}_e e \rightarrow \bar{\nu}_e e$ process is resonantly enhanced at $s = M_W^2$ i.e., for electrons at rest, at $E_\nu = M_W^2/2m_e = 6.3 \times 10^6 \text{ GeV}$. W scattering also gives $\nu_\ell e \rightarrow \nu_\ell \ell$ with $\ell = \{\mu, \tau\}$ at $E_\nu \gtrsim m_\ell$, while $\bar{\nu}_\ell e \rightarrow \bar{\nu}_\ell \ell$ violates lepton flavour and does not occur.

SM fermion	$U(1)_Y$	$SU(2)_L$	$SU(3)_c$	Z couplings	g_L	g_R
$U = u_R$	$-\frac{2}{3}$	1	$\bar{3}$	ν_e, ν_μ, ν_τ	$\frac{1}{2}$	0
$D = d_R$	$\frac{1}{3}$	1	$\bar{3}$	e, μ, τ	$-\frac{1}{2} + s_W^2$	s_W^2
$E = e_R$	1	1	1	u, c, t	$\frac{1}{2} - \frac{2}{3}s_W^2$	$-\frac{2}{3}s_W^2$
$L = (\nu_L, e_L)$	$-\frac{1}{2}$	2	1	d, s, b	$-\frac{1}{2} + \frac{1}{3}s_W^2$	$\frac{1}{3}s_W^2$
$Q = (u_L, d_L)$	$\frac{1}{6}$	2	3			

Table 4.1: The SM fermions and their Z couplings.

$T_e \gtrsim 5$ MeV. The SM at tree level predicts the energy spectrum of recoil electrons as

$$\frac{d\sigma}{dT_e}(\nu_\ell e \rightarrow \nu_\ell e) = \frac{2G_F^2 m_e}{\pi} \left[G_{L\ell}^2 + G_{R\ell}^2 (1-y)^2 - G_{L\ell} G_{R\ell} \frac{m_e}{E_\nu} y \right] \quad \text{where} \quad y \equiv \frac{T_e}{E_\nu}. \quad (4.3)$$

The measurement of T_e alone does not allow to reconstruct E_ν , nor allows to discriminate ν_e from $\nu_{\mu,\tau}$. In principle, E_ν can be reconstructed by measuring T_e and the opening angle $\vartheta_{\nu e}$ between the incident neutrino and the scattered lepton. However, this angle is small, $\vartheta_{\nu e} \sim (m_e/E_\nu)^{1/2}$. When the position of the neutrino source is known (e.g. the sun) measuring $\vartheta_{\nu e}$ helps in discriminating the signal from the background; when it not known (e.g. a supernova) measuring the direction of the scattered e helps in locating the source.

4.2 Neutrino/nucleon scattering

4.2.1 Neutrino/nucleon scattering at $E_\nu \ll \text{GeV}$

Similarly, the SM amplitude for scattering of neutrinos on nucleons (i.e. protons or neutrons) at rest is $\mathcal{M} \sim G_F m_p E_\nu$. Therefore the total cross section is $\sigma \sim G_F^2 E_\nu^2$ for $E_\nu \ll m_p$ and $\sigma \sim G_F^2 m_p E_\nu$ for $E_\nu \gg m_p$. In this case neutrino scattering breaks the nucleon (giving pions and nucleons in the final state) and the cross section is obtained by summing the contributions of the individual neutrino/quark sub-processes. Since $m_p \gg m_e$ neutrino/nucleon has a larger cross-section than neutrino/electron scattering.

At $E_\nu \ll m_p$ (e.g. solar and reactor neutrinos), if one is interested only in CC processes (so that the neutrino is converted into a charged lepton, that can be detected) only the reactions $\bar{\nu}_e p \rightarrow e^+ n$ and $\nu_e n \rightarrow e p$ are possible ($\nu_e p \rightarrow e^\pm n$ violates either charge or lepton-number), and only the first one is of experimental interest, because it is not possible to build a target containing enough free neutrons, that would anyway decay. Enough free protons are obtained using targets made of water (H_2O), hydrocarbonic scintillators, etc.

The precise SM prediction is [35]

$$\sigma(\bar{\nu}_e p \rightarrow \bar{e} n) = \frac{G_F^2 \cos^2 \theta_C}{\pi} (1 + 3a^2) E_e p_{\bar{e}} = \frac{2\pi^2 E_{\bar{e}} p_{\bar{e}}}{f m_e^5 \tau_n} \approx 0.952 \cdot 10^{-43} \text{ cm}^2 \frac{E_e p_e}{\text{MeV}^2} \quad (4.4)$$

where $a = 1.26$ is the axial coupling of nucleon and $f = 1.715$ is a phase space factor. The second expression (obtained by relating σ to the neutron lifetime τ_n) is more accurate. This reaction has a relatively large cross section and allows to reconstruct the neutrino energy. When $E_\nu \ll m_p$

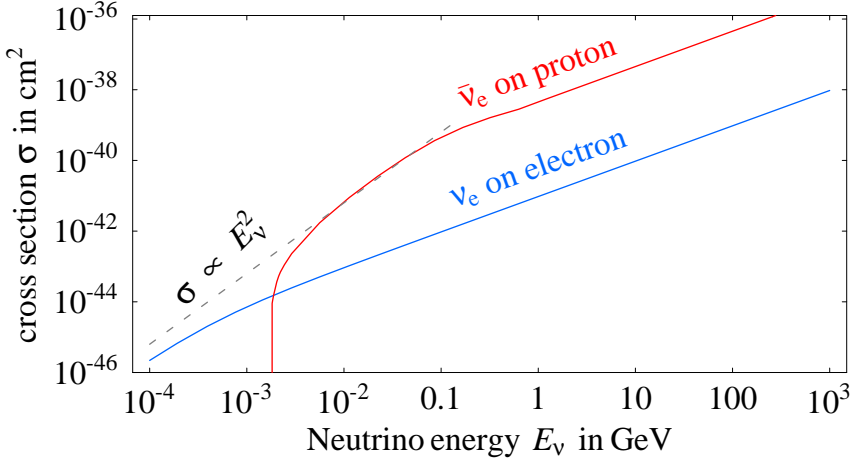


Figure 4.1: *Characteristic neutrino cross sections on target particles at rest with mass m : $\sigma \propto E_\nu^2$ at $E_\nu \lesssim m$ and $\sigma \propto E_\nu$ at $E \gtrsim m$.*

conservation of energy approximately means $E_\nu = E_{\bar{e}} + m_n - m_p = E_e + 1.293 \text{ MeV}$. Therefore the neutrino energy can be deduced by measuring $E_{\bar{e}}$ alone. Since $E_{\bar{e}} \geq m_e$ this reaction is only possible if $E_\nu \geq m_e + m_n - m_p = 1.804 \text{ MeV}$ (taking into account the recoil of the neutron, the energy threshold becomes 1.806 MeV). An analogous expression holds for $\bar{\nu}_\mu p \rightarrow \mu^+ n$ scattering, that needs $E_\nu > m_\mu$ — a too high threshold for reactor and supernova antineutrinos.

4.2.2 Neutrino/nucleon scattering at $E_\nu \sim \text{GeV}$

Neutrino/nucleon scatterings at energies comparable to the nucleon mass depends on the imprecisely known nucleon structure: as a consequence expressions for the cross sections are complicated, not very accurate and not reported here. One sums the elastic scatterings with a few dominant non-elastic channels, like one-pion production, computed according to models of form factors. Fig. 4.1 shows that the low- and the high-energy limits match reasonably well.

This energy range is relevant for experimental studies of neutrino oscillations, because recoiled particles are emitted at large angles: as described in section 5.5 this allows to reconstruct the neutrino energy if the direction of the incoming neutrino is known, e.g. in neutrino beam experiments. These experiments deal with unprecisely known cross sections by building also a detector near to the neutrino source, as similar as possible to the far detector used for oscillation studies.

4.2.3 Neutrino/nucleon scattering at $E_\nu \gg \text{GeV}$

At $E_\nu \gg \text{GeV}$ (e.g. atmospheric and accelerator neutrinos of higher energy) the dominant effect is neutrino/quark scattering. The fact that quarks are bound into a nucleon has no effect on the total ('inclusive') cross-section: the quark q^* that collides with neutrinos gets an energy much larger than the binding energy and unavoidably finds some way of escaping from the nucleon. Typically q^* hadronizes picking a $q\bar{q}$ pair from the vacuum, breaking the nucleon as $N = qqq^* \rightarrow [qqq][\bar{q}\bar{q}] = N\pi$, giving rise to processes like $\nu p \rightarrow \ell^+ n\pi^0$ o $\nu p \rightarrow \ell^+ p\pi^-$.

One has to sum over all quark sub-processes, taking into account the distribution of quarks in the nucleon (structure functions). Neutrino/quark scattering is similar to electron/quark, and

gives a cross section $\propto G_F E_\nu m_N$. The effective ν_ℓ -quark Lagrangian predicted by the SM at tree level is

$$\mathcal{L}_{\text{eff}} = -2\sqrt{2}G_F([\bar{\nu}_\ell \gamma_\alpha \ell_L][\bar{d}_L \gamma^\alpha u_L] + \text{h.c.}) - 2\sqrt{2}G_F \sum_{A,q} g_{Aq} [\bar{\nu}_\ell \gamma_\alpha \nu_\ell][\bar{q}_A \gamma^\alpha q_A] \quad (4.5)$$

where $A = \{L, R\}$, $\ell = \{e, \mu, \tau\}$, $q = \{u, d, s, \dots\}$ and the Z couplings g_{Aq} are given in table 4.1 in terms of the weak mixing angle $s_W \equiv \sin \theta_W$. Neutrino and CKM mixings appear in the first CC term, if one needs to rewrite it in terms of mass eigenstates.

The cross sections for the CC quark sub-processes are

$$\frac{d\hat{\sigma}}{dy}(\nu_\ell d \rightarrow \ell u) = \frac{d\hat{\sigma}}{dy}(\bar{\nu}_\ell \bar{d} \rightarrow \bar{\ell} \bar{u}) = \frac{2G_F^2 (p_\nu \cdot p_d)(p_\ell \cdot p_u)}{\pi (p_\nu \cdot p_d)} R_W \simeq \frac{G_F^2 \hat{s}}{\pi} R_W, \quad (4.6a)$$

$$\frac{d\hat{\sigma}}{dy}(\nu_\ell \bar{u} \rightarrow \ell \bar{d}) = \frac{d\hat{\sigma}}{dy}(\bar{\nu}_\ell u \rightarrow \bar{\ell} d) = \frac{2G_F^2 (p_\nu \cdot p_d)(p_\ell \cdot p_u)}{\pi (p_\nu \cdot p_u)} R_W \simeq \frac{G_F^2 \hat{s}}{\pi} (1-y)^2 R_W \quad (4.6b)$$

In the last terms scalar products among quadri-momenta have been evaluated assuming $E_\nu \gg m_N$ and thereby neglecting quark and lepton masses. In this limit the factor $y \equiv -\hat{t}/\hat{s}$ has kinematical range $0 \leq y \leq 1$. In the system where the nucleon is at rest $y = 1 - E'/E_\nu$ where E' is the energy of the scattered lepton.²

For NC scatterings at $E_\nu \gg m_N$ one has

$$\frac{d\hat{\sigma}}{dy}(\nu q \rightarrow \nu q') = \frac{d\hat{\sigma}}{dy}(\bar{\nu} \bar{q} \rightarrow \bar{\nu} \bar{q}') = \frac{G_F^2 \hat{s}}{\pi} [g_{Lq}^2 + g_{Rq}^2 (1-y)^2] R_Z, \quad (4.7a)$$

$$\frac{d\hat{\sigma}}{dy}(\bar{\nu} q \rightarrow \bar{\nu} q') = \frac{d\hat{\sigma}}{dy}(\nu \bar{q} \rightarrow \nu \bar{q}') = \frac{G_F^2 \hat{s}}{\pi} [g_{Rq}^2 + g_{Lq}^2 (1-y)^2] R_Z. \quad (4.7b)$$

We neglected quark and lepton masses. The factors $R_Z \equiv (1+Q^2/M_Z^2)^{-1}$, $R_W \equiv (1+Q^2/M_W^2)^{-1}$ equal to one when the transferred quadri-momentum $Q^2 = -\hat{t}$ is much smaller than the W, Z masses squared.

In the range $m_N \ll E_\nu \ll M_{W,Z}^2/m_N$ i.e. GeV $\ll E_\nu \ll 10$ TeV the total quark CC cross sections are

$$\hat{\sigma}(\nu_\ell d \rightarrow \ell u) = \hat{\sigma}(\bar{\nu}_\ell \bar{d} \rightarrow \bar{\ell} \bar{u}) = 3\hat{\sigma}(\bar{\nu}_\ell u \rightarrow \bar{\ell} d) = 3\hat{\sigma}(\nu_\ell \bar{u} \rightarrow \ell \bar{d}) = \frac{G_F^2 \hat{s}}{\pi}. \quad (4.8)$$

$\sqrt{\hat{s}}$ is the center-of-mass energy of the quark sub-processes. It is given by $\hat{s} = s x$, where x is the fraction of the total nucleon momentum P carried by a quark, $\hat{p} = x P$.

The neutrino/nucleon cross section are found integrating over the momentum distribution of the quarks, $q(x)$. The quantities $p_q = \int_0^1 dx x q(x)$ are the fraction of the total nucleon momentum carried by the quark. In the proton

$$\begin{aligned} p_u &\approx 25\%, & p_{\bar{u}} &\approx 4\%, \\ p_d &\approx 15\%, & p_{\bar{d}} &\approx 6\% \end{aligned} \quad (4.9)$$

²If E_ν is not much greater than m_N the above kinematical formulæ get generalized as follows. We define the “parton mass” as $m \equiv m_N x$ and assume that the final state lepton is not a τ^\pm , so that we neglect its mass. The factor $y \equiv -\hat{t}/\hat{s} = (1 - E'/E_\nu)/(1 + m/2E_\nu)$ ranges between $0 \leq y \leq (1 + m/2E_\nu)^{-2}$. The scattering angle ϑ of the final state lepton in the rest frame of the nucleon is given by $1 - \cos \vartheta = m(E_\nu - E')/E_\nu E'$ and ranges between $-1 \leq \cos \vartheta \leq 1$. Its typical value is $\vartheta \sim (m/E_\nu)^{1/2}$.

When the scattered lepton is a τ^\pm it is also necessary to take into account its polarization in order to compute its decay products [36].

where u (d) indicate that we summed over all types of up-type (down-type) quarks. We remind that nucleons contain valence quarks together with virtual $q\bar{q}$ pairs and gluons. Gluons carry about $1/2$ of the total proton momentum. Anti-quarks carry a fraction $\epsilon \approx 1/5$ of the momentum carried by quarks; this fraction increases at higher energy. Numbers in eq. (4.9) hold at $Q^2 \sim 10 \text{ GeV}^2$. The momentum distribution of the neutron is approximatively equal to the one of the proton, with up and down-type quarks exchanged. Consequently the total neutrino/nucleon CC cross sections at $s \simeq 2E_\nu m_N \gg \text{GeV}^2$ are

$$\begin{aligned}\sigma(\nu_\ell p \rightarrow \ell X) &\approx \frac{G_F^2 s}{\pi} (0.15 + \frac{1}{3} 0.04), & \sigma(\nu_\ell n \rightarrow \ell X) &\approx \frac{G_F^2 s}{\pi} (0.25 + \frac{1}{3} 0.06) \\ \sigma(\bar{\nu}_\ell n \rightarrow \bar{\ell} X) &\approx \frac{G_F^2 s}{\pi} (\frac{1}{3} 0.15 + 0.04), & \sigma(\bar{\nu}_\ell p \rightarrow \bar{\ell} X) &\approx \frac{G_F^2 s}{\pi} (\frac{1}{3} 0.25 + 0.06).\end{aligned}\quad (4.10)$$

Numerically $G_F^2 m_N^2 / \pi = 1.48 \cdot 10^{-38} \text{ cm}^2$.

4.2.4 Neutrino/nucleon scattering at ultra-high energies

At energies $E_\nu \gtrsim M_{W,Z}^2/m_N$ the transferred energy becomes comparable with $M_{W,Z}$ and one must take into account deviations of $R_{W,Z}$ from 1. The results simplifies again for $E_\nu \gg M_{W,Z}^2/m_N$ (at these high energy the SM predictions have not been tested: new physics could change the result) the total CC and NC partonic cross-sections approach constant values

$$\hat{\sigma}_{\text{CC}} \simeq \frac{G_F^2 M_W^2}{\pi} \approx 1.07 \cdot 10^{-33} \text{ cm}^2, \quad \hat{\sigma}_{\text{NC}} \simeq \frac{G_F^2 M_Z^2}{\pi} [g_{Lq}^2 + g_{Rq}^2]. \quad (4.11)$$

These cross sections are not suppressed by E_ν because they are soft i.e. dominated by small $Q \sim M_{W,Z}$. To compute the neutrino/nucleon cross section σ one has to integrate the partonic cross sections $\hat{\sigma}$ times the partonic distribution functions; in practice σ is given by $\hat{\sigma}$ times the number of quarks and anti-quarks that carry a fraction x of the nucleon momentum greater than $x \gtrsim M_{W,Z}^2/m_N E_\nu$. So far experiments only probed $x \gtrsim 10^{-4}$; HERA data and BFKL theoretical techniques suggest that parton distribution functions diverge at $x \rightarrow 0$ as $xq(x) \propto x^{-\beta}$ with $\beta \approx 0.5$. This results into a growth $\sigma \propto E_\nu^\beta$, which seems to violate perturbative unitarity. Ignoring this possible problem, the SM prediction is

$$\sigma_{\text{CC}}(\nu N) \simeq \sigma_{\text{CC}}(\bar{\nu} N) \approx 2.8 \cdot 10^{-32} \text{ cm}^2 \left(\frac{E_\nu}{10^{10} \text{ GeV}} \right)^{0.40}, \quad (4.12a)$$

$$\sigma_{\text{NC}}(\nu N) \simeq \sigma_{\text{NC}}(\bar{\nu} N) \approx 1.2 \cdot 10^{-32} \text{ cm}^2 \left(\frac{E_\nu}{10^{10} \text{ GeV}} \right)^{0.40}. \quad (4.12b)$$

up to a theoretical uncertainty of about a factor 2.

4.3 Neutrino/nucleus scattering

4.3.1 Neutrino/nucleus scattering at $E_\nu \gg \text{GeV}$

At neutrino energies larger than the nuclear binding energy neutrino/nucleus scattering reduces to a sum of neutrino/nucleon scatterings. We give cross-sections for scattering of neutrinos on a typical nucleus \mathcal{N} at rest which contains Z protons and approximatively Z neutrons. The CC cross sections are

$$\sigma(\nu_\ell \mathcal{N} \rightarrow \ell X) \approx \frac{2ZE_\nu}{\text{GeV}} \times 0.6 \cdot 10^{-38} \text{ cm}^2. \quad (4.13)$$

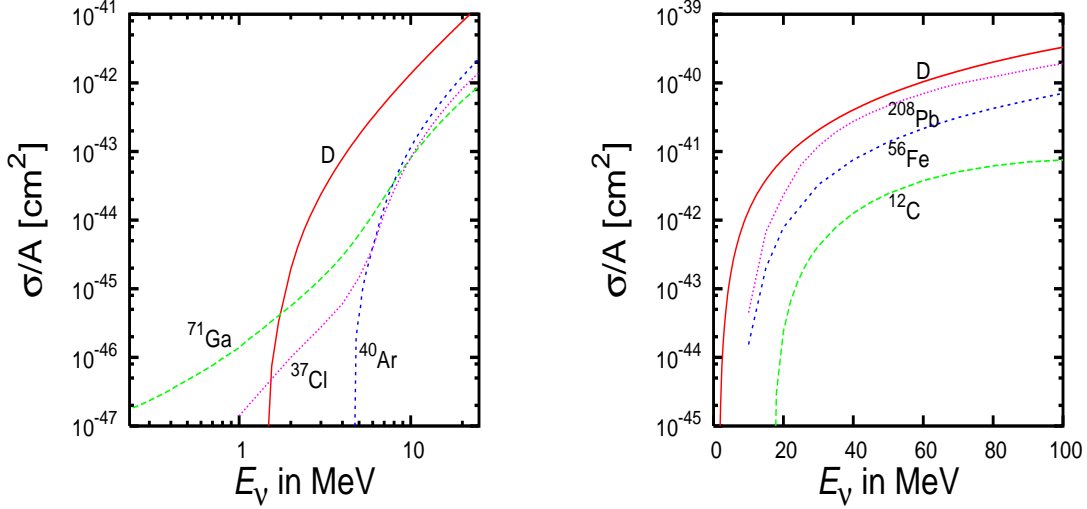


Figure 4.2: Some cross sections of ν_e with nuclei, normalized to their atomic number A .

and

$$r \equiv \frac{\sigma(\bar{\nu}_\ell \mathcal{N} \rightarrow \bar{\ell} X)}{\sigma(\nu_\ell \mathcal{N} \rightarrow \ell X)} = \frac{\epsilon + 1/3}{1 + \epsilon/3} \approx 0.5. \quad (4.14)$$

The average angle $\delta\theta$ between the direction of the lepton ℓ with respect to the direction of the neutrino is $\delta\theta \approx 0.3\sqrt{m_N/E_\nu}$. At $E_\nu \gtrsim M_{W,Z}^2/m_p \sim 10$ TeV the factors $R_{W,Z}$ start to deviate from unity and must be taken into account.

The NC cross sections are

$$R_\nu \equiv \frac{\sigma(\nu_\ell \mathcal{N} \rightarrow \nu_\ell X)}{\sigma(\nu_\ell \mathcal{N} \rightarrow \ell X)} = \frac{(g_L^2 + g_R^2/3) + \epsilon(g_R^2 + g_L^2/3)}{1 + \epsilon/3} = g_L^2 + r g_R^2 \quad (4.15)$$

$$R_{\bar{\nu}} \equiv \frac{\sigma(\bar{\nu}_\ell \mathcal{N} \rightarrow \bar{\nu}_\ell X)}{\sigma(\bar{\nu}_\ell \mathcal{N} \rightarrow \bar{\ell} X)} = \frac{(g_R^2 + g_L^2/3) + \epsilon(g_L^2 + g_R^2/3)}{1/3 + \epsilon} = g_L^2 + \frac{1}{r} g_R^2 \quad (4.16)$$

where $g_L^2 \equiv g_{Lu}^2 + g_{Ld}^2 = \frac{1}{2} - s_W^2 + \frac{5}{9}s_W^4 \approx 0.30$, $g_R^2 \equiv g_{Ru}^2 + g_{Rd}^2 = \frac{5}{9}s_W^4 \approx 0.03$.

4.3.2 Neutrino/nucleus scattering at low energy

The relevant reactions of a low energy neutrino with a nucleus (A, Z) are [37]

$$\bar{\nu}_e(A, Z) \rightarrow e^+(A, Z-1), \quad \nu_e(A, Z) \rightarrow e^-(A, Z+1), \quad \nu(A, Z) \rightarrow \nu(A, Z). \quad (4.17)$$

These processes are understood in the following way. Neutrino interactions excite various energy levels E_i with certain values of spin, isospin and parity, probing also continuum levels when above $E_\nu \gtrsim 50$ MeV. The energy thresholds can be easily computed from kinematical considerations, knowing the masses of the nuclei involved. While at high energies $E_\nu \gg m_p$ one has the forward-peaked incoherent scattering described in the previous section (cross section $\sigma \sim G_F^2 A m_p E_\nu$), at low energy the cross sections are only slightly directional and increase as $p_e E_e$ for any level. Beside the vectorial interactions, which are related by CVC to the electromagnetic currents and are accurately understood theoretically (Fermi transitions) there are the axial interactions that are less easily modeled (Gamow-Teller transitions) and have much larger theoretical uncertainties of the

order of 50% at least. Empirical information, isospin and crossing invariance can be occasionally used in order to constrain the transitions better, e.g., connecting the CC interaction $\nu_e \mathcal{N} \rightarrow \mathcal{N}' e$ with the β^+ decay $\mathcal{N}' \rightarrow \mathcal{N} \nu_e e^+$ (traditionally the latter information is presented as a $\log(ft)$ value, where f is the QED final state correction and $t = \ln 2/\Gamma$ is the half-life time). Deuterium and carbon interactions have been studied with artificial neutrino beams. Deuterium, chlorine and gallium nuclei permitted observations and measurements of solar neutrinos at relatively low energies. Other nuclei have been studied only theoretically. In the figures, we provide as an example a few CC ν_e interactions with nuclei in the energy regions relevant for solar neutrino detection (left) and for supernovæ (right). Although so far ν_e supernova events have not yet been observed, and inverse beta decay will allow to collect large samples of $\bar{\nu}_e$ events, weak interactions (CC and NC) of neutrinos with $E_\nu \lesssim 200$ MeV are important for the dynamics of core collapse supernovæ. We recall incidentally that the trapping of muon and tau neutrinos in supernovæ is due to neutral current reactions, that are large due to coherence (namely, they are proportional to A^2). Some reactions allow to detect NC events: e.g. $\nu D \rightarrow \nu p n$ (already used by SNO, see section 6.3.4) and $\nu^{12}C \rightarrow \nu^{12}C^*$ followed by $^{12}C^* \rightarrow ^{12}C \gamma$ (15.1 MeV) where the neutron and the photon allow to tag the event. At high energy, $E_\nu \gtrsim 50$ MeV, it is common practice to describe the nucleons in a nucleus adopting a Fermi gas model or simplified descriptions of the nuclear process.

4.4 Neutrino detectors

Ideally, one would like to detect neutrinos in real time measuring their energy, direction and flavour. We have seen how physics ultimately limits what can be done. We here discuss in a generic way the detection techniques that allow to approach these ultimate limits. We will give more precise descriptions of the main experiments that have been performed so far when we will discuss their results.

In practice, one has to find a compromise between the various and contrasting needs of an experiment, e.g. between the wish to have a very ‘granular’ detector to see all the details of the reaction, and the need to monitor a big amount of matter.

Muons are one of the particles possibly produced by neutrino interactions, and deserve a dedicated discussion, because μ^\pm can travel for distances bigger than the detector: their range roughly is $2.5 \text{ km} \cdot \text{eV} \cdot \ln(1 + 2E_\mu/\text{TeV})$. This long range is annoying when μ^\pm escape from the detector, and is advantageous because allows to see neutrino interactions originated in the material outside the detector: the event rate is proportional to the area of the detector, rather than to its volume. The loss of information on the event is compensated by a gain in the event rate. Similarly, at ultra-high neutrinos energies neutrinos could be detected using the Earth atmosphere as target and looking for the macroscopic quasi-horizontal air showers of particles produced by neutrino scatterings (no positive detection has been claimed so far).

4.4.1 Water Čerenkov

WC detectors consist of pure water surrounded by photomultipliers, that see in real time the Čerenkov light emitted by relativistic charged particles scattered by neutrinos. At neutrino energies less than about a GeV, neutrinos can only scatter e^\pm and μ^\pm . WC detectors can distinguish electrons from muons (because a scattered μ or $\bar{\mu}$ produces a clean Čerenkov ring, while an e^\pm produces a fuzzier ring) but cannot distinguish particles from anti-particles. τ leptons fastly decay

into hadrons, that cannot be easily studied. Furthermore, WČ detectors can see the γ emitted by nuclear de-excitations or particle decays, such as $\pi^0 \rightarrow 2\gamma$. The γ are seen as fuzzy rings, like electrons.

Measuring the Čerenkov light, WČ detectors allow to reconstruct the energy and the direction of the scattered charged particle(s).

At $E_\nu \sim \text{GeV}$ and if the position of the neutrino source is known (e.g. in neutrino beam experiments) one can combine these two pieces of information to reconstruct the neutrino energy. This becomes impossible at larger E_ν , where neutrino make inelastic scatterings producing unseen neutral particles. At $E_\nu \gg \text{GeV}$ scatterings are forward peaked, such that the direction of the scattered particle(s) are strongly correlated with the direction of incoming neutrino. Furthermore, μ^\pm have a long enough range in matter that the material below the detector (e.g. rock) acts as a target. If $E_\nu \ll \text{GeV}$, WČ can see electrons scattered by neutrinos via NC and CC: (anti)neutrinos with different flavors contribute to this single measurable rate as discussed in section 4. The WČ allowed to detect solar neutrinos down to $E_\nu \sim 5 \text{ MeV}$. In section 6.3.4 we describe how, replacing water with heavy water, allowed to discriminate ν_e from $\nu_{\mu,\tau}$.

Since water is cheap, the WČ technique allows to build the large detectors needed by neutrino physics. However, some signals (e.g. solar neutrinos, proton decay) can only be seen by placing the detector in underground caverns, in order to suppress the background due to cosmic rays: this is today the dominant limit on the target mass, that could reach a Mton in some future project.

A variant of the WČ technique (water replaced with heavy water) allows to observe NC events, as done by SNO and discussed in section 6.3.4. A variant of the WČ technique allows to reach km^3 volumes: strings of photo-multipliers are inserted in ice or sea-water. The transparency of the water or ice limits the distance among photo-multipliers, and a poorly granular detector anyway has a poor energy resolution and high energy threshold (because particles loose energy before reaching the first photo-multiplier). Experiments of this kind are being planned as telescopes for neutrinos with $E_\nu \gtrsim \text{TeV}$: they are mostly sensitive to $\bar{\nu}_\mu$ and allow to precisely reconstruct their direction.

4.4.2 Liquid scintillators

It is possible to build useful and relatively cheap neutrino detectors using liquid organic scintillators. The largest ones in operation are LVD (total mass: 1 kton, formed by 840 separate tanks) and KamLAND (a unique sphere), and there is a proposal to build a detector 30 times larger, LENA. The working principle is the collection of the light released by charged particles propagating in the scintillator, that is subsequently amplified by photomultipliers; these detectors can measure energy well but are not directly useful for particle identification.

Scintillators are adopted for two types of measurements involving neutrinos with $E_\nu \sim 10 \text{ MeV}$: the search of neutrinos from supernovæ, performed with relatively simple and stable detectors like BUST at Baksan in Ukraine and LVD in Gran Sasso; the study of neutrinos from pion decay at rest, done by Karmen, LSND and MiniBOONE. Scintillators perform well at low energy, and in fact, they are the only possible conventional detectors for the low energy neutrinos ($E_\nu \sim \text{MeV}$), such as (a) reactor neutrinos (the main experiments are KamLAND, CHOOZ, Bugey); (b) geo-neutrinos (first observation in KamLAND); (c) low energy solar neutrinos, which are the main goal of Borexino.

We now list the main low energy neutrino reactions [38]. (1) inverse beta decay $\bar{\nu}_e p \rightarrow ne^+$: a scintillator sees the e^+ and can also tag the neutron, because it produces a gamma-ray thanks to

the reaction $np \rightarrow D\gamma$ (it is possible to increase the energy of the nuclear gamma-ray by doping the scintillator with a suitable nucleus, like gadolinium). (2) Reactions with carbon e.g., the CC reaction $\nu_e {}^{12}\text{C} \rightarrow e^- {}^{12}\text{N}$, (3) Elastic scattering on electrons (that will be used to see beryllium solar neutrinos) and possibly (4) also on protons (that give sub-MeV events with supernova neutrinos). (5) A last important reaction is with the iron of the support structure.

4.4.3 Calorimeters

Calorimeters measure the total energy of charged and of strongly interacting particles produced by neutrino scatterings. By alternating layers of calorimeters to e.g. scintillators one gains information on the tracks of the charged particles. This allows to accurately discriminate CC events due to ν_μ : the muons produced by CC scatterings make longer tracks than electrons (that give e.m. showers) or the hadrons produced in CC or NC interactions. By magnetizing the calorimeter (that can be made e.g. by iron) one can also discriminate charged particles from their anti-particles. The NuTeV (section 9.3) and MINOS (section 5.6) detectors use this technology.

4.4.4 Radio chemical

This technique was used by the first solar neutrino experiments, and allows to reach the lowest neutrino energies so far. A sufficiently large mass of an appropriate target nucleus is put underground (in order to avoid backgrounds), such that neutrinos induce a nuclear reaction. The target nucleus is chosen such that the cross section is precisely computable and such that the produced nuclei can be later counted, e.g. because they decay back in the original nucleus. These experiments measured solar neutrino rates with $\approx 5\%$ accuracy: future improvements would need detector calibrations.

Chapter 5

The atmospheric evidence

The evidence for $\nu_\mu \rightarrow \nu_\tau$ oscillations is named ‘atmospheric’ because it was established by the SuperKamiokande experiment, studying atmospheric neutrinos. MACRO, IMB, SUDAN2 and MINOS performed similar measurements. The K2K and NuMi beam experiments confirm the effect. The CHOOZ experiment gives important bounds on alternative oscillation channels.

5.1 Atmospheric neutrinos

Atmospheric neutrinos are generated by collisions of primary cosmic rays (mainly composed by H and He nuclei, yielding respectively $\sim 82\%$ and $\sim 12\%$ of the nucleons. Heavier nuclei constitute the remaining fraction). The process can be schematized in 3 steps [39]:

1. Primary cosmic rays hit the nuclei of air in the upper part of the earth atmosphere, producing mostly pions (and some kaon).
2. Charged pions decay promptly generating muons and muonic neutrinos:

$$\pi^+ \rightarrow \mu^+ \nu_\mu, \quad \pi^- \rightarrow \mu^- \bar{\nu}_\mu$$

(the decay rate into electrons is suppressed by m_e^2/m_μ^2). The total flux of $\nu_\mu, \bar{\nu}_\mu$ neutrinos is about $0.1/\text{cm}^2\text{s}$ at $E_\nu \sim \text{GeV}$ with a $\sim 20\%$ error (mostly due to the uncertainty in the flux of cosmic rays and in their hadronic interactions). At higher energy the flux $d\Phi/d\ln E_\nu$ approximately decreases as $E_\nu^{-2\pm0.05}$. The few kaons decay like pions, except that $K \rightarrow \pi e^+ \nu_e$ decays are not entirely negligible.

3. The muons produced by π decays travel a distance

$$d \approx c\tau_\mu \gamma_\mu \approx 1 \text{ km} \frac{E_\mu}{0.3 \text{ GeV}}$$

where τ_μ is the muon life-time and $\gamma_\mu = E_\mu/m_\mu$ is the relativistic dilatation factor. If all muons could decay

$$\mu^- \rightarrow e^- \bar{\nu}_e \nu_\mu \quad \mu^+ \rightarrow e^+ \nu_e \bar{\nu}_\mu$$

one would obtain a flux of ν_μ and ν_e in proportion $2 : 1$, with comparable energy, larger than $\sim 100 \text{ MeV}$. However, muons with energy above few GeV typically collide with the earth before decaying, so that at higher energy the $\nu_\mu : \nu_e$ ratio is larger than 2.

The fluxes predicted by detailed computations is shown in fig. 5.1, at SK location, averaged over zenith angle and ignoring oscillations.

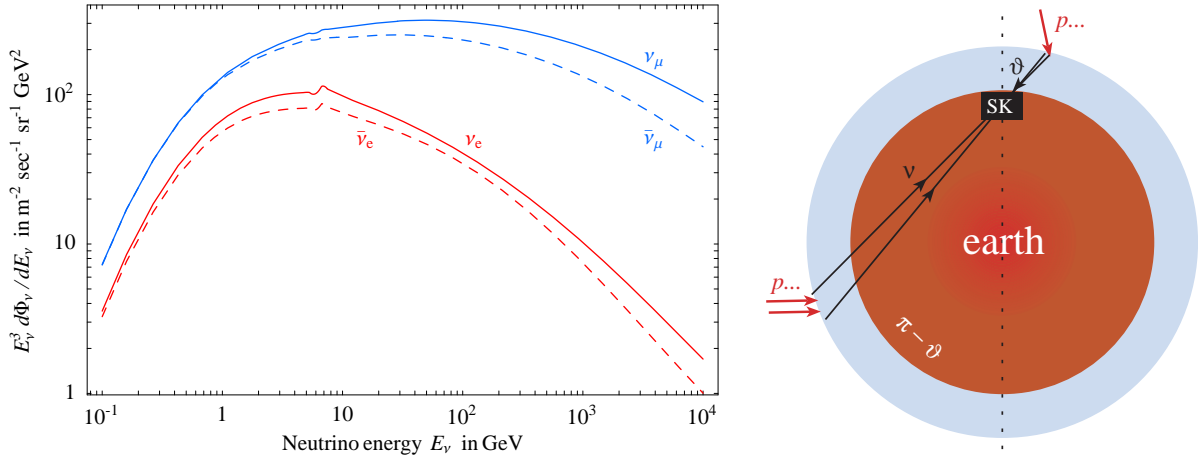


Figure 5.1: *Flux of atmospheric neutrinos in absence of oscillations, as predicted by FLUKA [39]. The cartoon at the right shows that, since the earth is spheric, without oscillations the flux of atmospheric neutrinos would be up/down symmetric.*

5.2 SuperKamiokande

SK [5] detects atmospheric neutrinos through CC scattering on nucleons, $\nu_\ell N \rightarrow \ell N'$. SK is a cylindrical tank containing 50000 ton of light water surrounded by photomultipliers, located underground in the Kamioka mine in Japan. A relativistic charged lepton ℓ traveling in water gives rise to a detectable Čerenkov ring (the scattered proton is not visible because its energy is typically below the WČ threshold). As discussed in section 4.4, SK can distinguish ν_μ from ν_e but cannot distinguish particles from anti-particles. The atmospheric fluxes contain a roughly equal number of ν and $\bar{\nu}$, and ν have roughly a two times larger cross section on nucleons than $\bar{\nu}$.

Measuring the Čerenkov light SK reconstructs the energy E_ℓ and the direction ϑ_ℓ of the scattered charged lepton. At high energy $E_\ell \gg m_N$ the scattered lepton roughly keeps the direction of the neutrino, whose zenith-angle ϑ_ν is related to the pathlength L by

$$L = \underbrace{\sqrt{h^2 + 2hr_E + r_E^2 \cos^2 \vartheta_\nu - r_E |\cos \vartheta_\nu|}}_{\text{in the atmosphere}} + \underbrace{2r_E |\cos \vartheta_\nu|}_{\text{in the earth, if } \cos \vartheta_\nu < 0} \quad (5.1)$$

where $r_E = 6371$ km is the radius of the earth and $h \sim (15 \div 20)$ km is the height of the atmosphere. Down-ward going neutrinos ($\cos \vartheta_\nu = 1$) travel $L \sim h$. Horizontal neutrinos ($\cos \vartheta_\nu = 0$) travel $L \sim \sqrt{2r_E h} \sim 500$ km. Up-ward neutrinos ($\cos \vartheta_\nu = -1$) travel $L = 2r_E$.

Measuring E_ℓ and ϑ_ℓ is not sufficient to reconstruct the neutrino energy, $E_\nu \gtrsim E_\ell$, since it is not known from which direction one atmospheric neutrino arrives. In practice SK can group their data into few big energy ‘bins’ defined according to the topology of the events:

1. **Fully-contained** electron or muon events: the scattered lepton starts and ends inside the detector, so that its energy can be measured. These events are conveniently sub-divided into

- **sub-GeV** events¹, with $E_\ell \lesssim 1.4$ GeV, and are produced by neutrinos with a typical

¹The cut is precisely defined in terms of the amount of Čerenkov light. It is chosen such that sub-GeV μ -like

energy of about a GeV. The average opening angle between the incoming neutrino and the detected charged lepton is $\vartheta_{\ell\nu} \sim 60^\circ$: the sub-GeV sample has a poor angular resolution: E_ν and L can only be estimated.

- **multi-GeV** events with $E_\ell \gtrsim 1.4$ GeV are produced by neutrinos with a typical energy of few GeV. The average opening angle between the incoming neutrino and the detected charged lepton is $\vartheta_{\ell\nu} \sim 15^\circ$ (decreasing at higher energy), allowing a reasonably precise measurement of L .

2. **Partially contained muons**: the muon is scattered inside the detector, but escapes from the detector, so that its energy cannot be measured. These events originate from neutrinos with a typical energy only slightly higher than those giving rise to multi-GeV muons. Therefore these two classes of events can be conveniently grouped together.
3. **Up-going stopping muons**: the scattered μ is produced in the rock below the detector (so that its energy cannot be measured) and stops inside the detector.² The typical energy of parent neutrinos is $E_\nu \sim 10$ GeV. This technique cannot be used for studying ν_e (because the scattered electrons shower before reaching the detector) nor for down-going ν_μ (due to the background of cosmic ray muons).
4. **Through-going up muons**: the μ is scattered in the rock below the detector and crosses the detector without stopping. MACRO is here competitive with SK because the important parameter is the surface of the detector, rather than its mass. These events are produced by neutrinos with a typical energy between 10 GeV and 10 TeV. Predictions and direct measurements of cosmic ray primaries at high energies are difficult [39].

In conclusion, atmospheric neutrinos cover a *wide energy range*, from less than a GeV to more than a TeV. Atmospheric neutrinos also allow to probe a *wide range of baselines*, between 10 and 10000 km. Therefore they are a good probe of oscillations (see fig. 1.1).

The SuperKamiokandeI data are shown in fig. 5.2 (1489 days of data taking, terminated by an accident. SK collected few thousands of events). The two histograms show the prediction assuming no oscillations, and the best $\nu_\mu \rightarrow \nu_\tau$ oscillation fit, for $\Delta m_{\text{atm}}^2 = 2.5 \cdot 10^{-3}$ eV² and $\sin^2 2\theta_{\text{atm}} = 1$. The atmospheric neutrino fluxes are varied, within their uncertainties, to their best-fit values independently in the two cases.

The “multi-GeV $\mu + PC$ ” data sample shows that a neutrino anomaly is present even without relying our knowledge of atmospheric neutrino fluxes. The crucial point is that since the Earth is a good sphere, in absence of oscillations the neutrino rate would be up/down symmetric, i.e. it depends only on $|\cos \vartheta|$.³ The $dN/d\cos \vartheta_\nu$ spectrum would be flat, if one could ignore that horizontal muons have more time for freely decaying before hitting the earth, while vertical muons cross the atmosphere along the shortest path. This effect produces the peak at $\cos \vartheta_\nu \sim 0$ visible in fig. 5.2b.

While the zenith-angle distribution of μ events is clearly asymmetric, e -like events show no asymmetry. The flux of up-ward going muons is about two times lower than the flux of down-ward

events are mostly fully contained: the scattered lepton is produced and remains inside the detector.

²This is the first method proposed for detecting atmospheric ν_μ [40].

³The mountain around the detector and especially the magnetic field of the earth break this symmetry. But they are minor effects at multi-GeV energy.

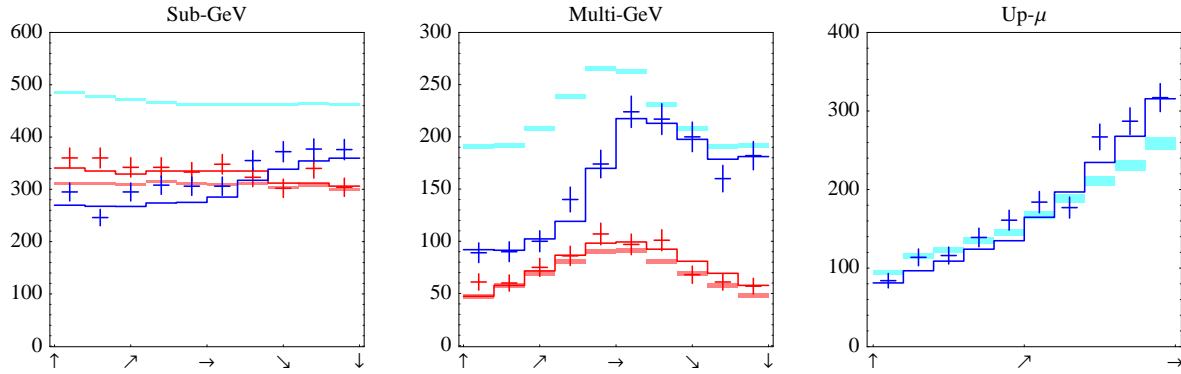


Figure 5.2: The main SK data: number of e^\pm (red) and of μ^\pm (blue) events as function of direction of scattered lepton. The horizontal axis is $\cos \vartheta$, the cosine of the zenith angle ranging between -1 (vertically up-going events) and $+1$ (vertically down-going events). Fig. 5.2c shows high-energy through-going muons, only measured in the up direction. The crosses are the data and their errors, the thin lines are the best-fit oscillation expectation, and thick lines are the no-oscillation expectation: these are roughly up/down symmetric. Data in the multi-GeV muon samples are very clearly asymmetric, while data in the electron samples (in red) are compatible with no oscillations.

muons. Therefore the data can be interpreted assuming that nothing happens to ν_e and that ν_μ oscillate into ν_τ (or into sterile ν_s). Neglecting earth matter corrections, we assume

$$P(\nu_e \rightarrow \nu_e) = 1 \quad P(\nu_e \leftrightarrow \nu_\mu) = 0 \quad P(\nu_\mu \rightarrow \nu_\mu) = 1 - \sin^2 2\theta_{\text{atm}} \sin^2 \frac{\Delta m_{\text{atm}}^2 L}{4E_\nu} \quad (5.2)$$

The main result can be approximately extracted from very simple considerations. Looking at the zenith-angle dependence we notice that down-ward going neutrinos (\downarrow) are almost unaffected by oscillations, while up-ward going neutrinos (\uparrow) feel almost averaged oscillations, and therefore their flux is reduced by a factor $1 - \frac{1}{2} \sin^2 2\theta_{\text{atm}}$. This must be equal to the up/down ratio $N_\uparrow/N_\downarrow = 0.5 \pm 0.05$, so that $\sin^2 2\theta_{\text{atm}} = 1 \pm 0.1$. Furthermore, multi-GeV neutrinos have energy $E_\nu \sim 3 \text{ GeV}$, and according to fig. 5.2b they begin to oscillate around the horizontal direction ($\cos \vartheta \sim 0$) i.e. at a pathlength of about $L \sim 1000 \text{ km}$. Therefore $\Delta m_{\text{atm}}^2 \sim E_\nu/L \sim 3 \cdot 10^{-3} \text{ eV}^2$.

A global fit (performed including also the less safe input from MonteCarlo predictions of neutrino fluxes) gives the best-fit values shown in fig. 5.3b. SK cannot precisely measure Δm_{atm}^2 because around the horizontal L depends strongly on ϑ_ν .

Historically, the measurement of a deficit in the ratio between μ -like and e -like events gave the first argument for an atmospheric neutrino anomaly. As explained in section 5.1, while the overall number of atmospheric ν_μ and of ν_e cannot be precisely predicted, their ratio is predicted to be close to 2 in absence of oscillations. The measurement of the double ratio $(N_\mu/N_e)_{\text{exp}}/(N_\mu/N_e)_{\text{MC}} \sim 0.65$ was considered as the main evidence; however $(N_\mu/N_e)_{\text{MC}}$ significantly deviates from the ideal value 2, due to the different ν_μ and ν_e energy spectra and experimental cuts. The main evidence for the atmospheric anomaly is provided by the zenith-angle dependence of N_μ discussed above.

5.3 Oscillations?

Here we discuss at which level SK probes if the atmospheric anomaly follows the specific energy and pathlength dependence of $P(\nu_\mu \rightarrow \nu_\mu)$ predicted by oscillations.

Energy dependence. Fig. 5.2 shows that the anomaly is visible not only in multi-GeV data, but also at lower energy in sub-GeV data and at higher energy in stopping and through-going muons. One can see that the anomaly decreases at higher energy and increases at lower energy, as predicted by $\nu_\mu \rightarrow \nu_\tau$ oscillations. One can be more quantitative: fitting the SK data assuming

$$P(\nu_\mu \rightarrow \nu_\mu) = 1 - \sin^2 2\theta \sin^2 \alpha L E^n$$

($n = -1$ is predicted by oscillations; $n = 0$ can be obtained from CPT-violating effects; $n = 1$ from violation of Lorentz invariance) gives $n = -1.03 \pm 0.13$ [5].

Path-length dependence. SK can see that $P(\nu_\mu \rightarrow \nu_\mu)$ decreases by 50% when going from short to long baselines. However it cannot observe the most characteristic feature of oscillations: the first oscillation dip. As illustrated in fig. 3.2b at page 22, this happens because SK cannot measure the neutrino energy: the oscillation pattern gets washed when averaging over too different neutrino energies. While neutrino decay $P(\nu_\mu \rightarrow \nu_\mu) = e^{-Lm_\nu/E_\nu \tau}$ cannot explain SK data, one might think that any function that interpolates

$$P(\nu_\mu \rightarrow \nu_\mu \text{ at short } L) = 1 \quad \text{with} \quad P(\nu_\mu \rightarrow \nu_\mu \text{ at long } L) \approx 1/2$$

provides an acceptable description of SK data. This is not the case: the dip-less SK data in fig. 5.2 are in excellent quantitative agreement with the oscillation prediction. Global fits of SK data disfavor at about 4σ alternative ν_μ disappearance mechanisms which do not give rise to a dip in $P(\nu_\mu \rightarrow \nu_\mu)$ [5]. Some concrete examples are

$$P(\nu_\mu \rightarrow \nu_\mu) \simeq \begin{cases} 1 - (\sin^2 \theta + \cos^2 \theta e^{-cL/E})^2 & \text{decay of mixed neutrinos [41]} \\ 1 - \frac{1}{2} \sin^2 2\theta (1 - e^{-cL/E^n}) & \text{decoherence [31]} \\ |\cos^2 \theta + \sin^2 \theta (1 - \text{erf} \sqrt{icL/E})|^2 & \text{oscillations into 5-dimensional } \nu \text{ [42]} \end{cases}$$

where c and n are arbitrary constants. The case $n = 1$ is the least disfavored [5]; the theoretical considerations of section 3.4 suggest $n = 2$.

SK reanalyzed their data selecting a sub-sample of ‘cleanest’ events, where the resolution in L/E_ν is good enough to see a hint of the first oscillation dip. This is roughly done by excluding events with energy $E_\mu \lesssim \text{GeV}$ (because at low energy the direction of the scattered muon is poorly correlated with the direction of the neutrino) and with reconstructed zenith-angle $|\cos \vartheta_\nu| \lesssim 0.2$ (around the horizontal it is difficult to measure the path-length, because it strongly depends on ϑ_ν , see eq. (5.1) and fig. 3.2b). In this way SK achieved a $\sim 50\%$ resolution in L/E_ν . By choosing L/E_ν bins smaller than the resolution, SK could produce plots where the first oscillation dip is visible to the naked eye [5]. This kind of analysis provides a better resolution in Δm_{atm}^2 at the expenses of a poorer resolution in θ_{atm} : the result is shown in fig. 5.3b.

In section 7 we will discuss which future experiments can more directly test these important issues.

5.4 $\nu_\mu \rightarrow \nu_\tau$ or $\nu_\mu \rightarrow \nu_s$?

Up to this point, the atmospheric anomaly could be explained by the $\nu_\mu \rightarrow \nu_\tau$ oscillations or by $\nu_\mu \rightarrow \nu_s$ oscillations, where ν_s is a speculative extra sterile neutrino, i.e. a fermion with no weak interactions. A closer analysis of SK data shows that three different kinds of data favor $\nu_\mu \rightarrow \nu_\tau$ and indicate that $\nu_\mu \rightarrow \nu_s$ can at most give a minor correction.

1. **Earth matter corrections** do not affect $\nu_\mu \rightarrow \nu_\tau$ oscillations but would affect $\nu_\mu \rightarrow \nu_s$ oscillations. Given the value of Δm_{atm}^2 this would be a significant effect, suppressing oscillations at high energy, after possibly having crossed a resonance (section 3.2).⁴ According to global fits, stopping and through-going up muons independently favor $\nu_\mu \rightarrow \nu_\tau$ at 3σ . Another 3σ hint comes from the analogous effect in through-going up muons detected by the MACRO experiment at Gran Sasso.
2. **Neutral-current rates.** ‘Multi-ring’ events (i.e. events with two or more separated Čerenkov rings which also satisfy certain other selection cuts) contain a significant fraction of NC-induced events, about 30% according to the SK MonteCarlo. The main NC processes which produce multi-ring events are $\nu N \rightarrow \nu N \pi\pi$ and $\nu N \rightarrow \nu N \pi^0 \rightarrow \nu N \gamma\gamma$. Multi-ring events are also produced by CC processes, such as $\nu_e N \rightarrow e N' \pi$. While $\nu_\mu \rightarrow \nu_\tau$ conversion would not affect NC rates, $\nu_\mu \rightarrow \nu_s$ oscillations would decrease the number of NC events in a zenith-angle dependent way. The total number of events does not allow to discriminate the two possibilities because the relevant cross-sections have not yet been precisely measured and cannot be precisely computed. The measured up/down asymmetry of multi-ring events is consistent with up/down symmetric NC events, and favors $\nu_\mu \rightarrow \nu_\tau$ with respect to $\nu_\mu \rightarrow \nu_s$ at about 3.5σ [5].⁵
3. **τ appearance.** The expected signal rate is about $1\tau/\text{kton} \cdot \text{yr}$. In SK it is difficult to experimentally discriminate τ events from hadronic events, which are expected to have a rate about two orders of magnitude larger. By imposing appropriate selection cuts, SK defines a class of τ -like events. The resulting sample is not clean: about 8% of them should be composed by τ produced by $\nu_\mu \rightarrow \nu_\tau$ oscillations. SK data show a zenith-angle dependent enhancement of τ -like events, giving a $\sim 2\sigma$ hint for ν_τ appearance.

Combining all these hints give a combined 7σ evidence for $\nu_\mu \rightarrow \nu_\tau$ versus $\nu_\mu \rightarrow \nu_s$. Fitting SK data in terms of mixed active/sterile oscillations $\nu_\mu \rightarrow \cos \xi \nu_\tau + \sin \xi \nu_s$ gives $\sin^2 \xi = 0 \pm 0.10$ [5].

In section 7 we will discuss which future experiments can more directly test this important issue.

5.5 K2K

An artificial long-baseline ν_μ pulsed beam is sent from KEK to the SK detector, located $L = 250$ km away in the Kamioka mine. Since the beam is pulsed, SK can discriminate atmospheric ν from KEK ν_μ , both detected using charged-current scattering on nucleons, as previously discussed. The neutrino beam was produced by colliding a total of $9 \cdot 10^{19}$ accelerated protons on a target.

⁴This is not generically true if one considers oscillations into many sterile ν_s — a possibility anyway disfavored by arguments 2. and 3.

⁵According to [43] this conclusion is doubtful because uncertainties on cross sections have been underestimated.

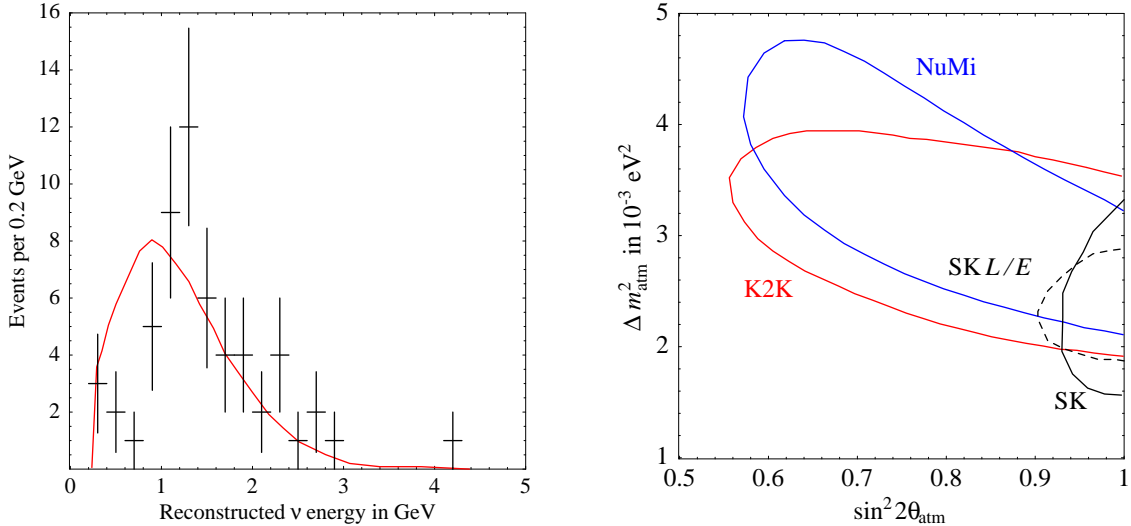


Figure 5.3: Fig. 5.3a shows the K2K data, and the expectation in absence of oscillations [6]. Fig. 5.3b shows the best-fit ranges at 90% CL from SK, K2K and NuMi.

A magnetic field is used to collect and focus the resulting π^+ , obtaining from their decays a 98% pure ν_μ beam with an average energy of $E_\nu \sim 1.3$ GeV. The base-line L and the energy E_ν have been chosen such that

1. $\Delta m_{\text{atm}}^2 L / E_\nu \sim 1$ in order to sit around the first oscillation dip;
2. $E_\nu \sim m_p$ in order to have large opening angles between the incoming neutrino and the scattered μ : $\vartheta_{\mu\nu} \sim 1$.

Since the direction of the incoming neutrino is known (unlike in the case of atmospheric neutrinos), measuring E_μ and $\vartheta_{\mu\nu}$ SK can reconstruct the neutrino energy

$$E_\nu = \frac{m_N E_\ell - m_\mu^2/2}{m_N - E_\ell + p_\ell \cos \vartheta_{\mu\nu}} \quad (5.3)$$

having assumed that $\nu_\mu n \rightarrow \mu p$ is the dominant reaction. Around $E_\nu \sim$ GeV pion production and deep-inelastic scattering give subleading ($\sim 10\%$) contributions. Since the neutrino flux and the $\nu_\mu N$ cross section are not precisely computable, small detectors (mainly a 1 kton WČ and fine-grained systems) have been built close to the neutrino source in KEK, so that oscillations can be seen by comparing SK data with near detectors. $\nu_\mu \rightarrow \nu_\tau$ oscillations at the atmospheric frequency should give an energy-dependent deficit of events in the far detector, according to eq. (5.2).

The latest K2K results presented in 2004 and shown in fig. 5.3 are consistent with the expectations based on SK atmospheric data and contain a 4σ indication for oscillations. Concerning the total rate, one expects in absence of oscillations 151 ± 12 fully contained events in the SK fiducial volume (the uncertainty is mainly due to the far/near extrapolation and to the error on the fiducial volume). SK detected 107 events of this kind. In view of the poorer statistics the atmospheric mixing angle is determined much more precisely by SK than by K2K.

The most important K2K result is the energy spectrum: K2K is competitive on the determination of Δm_{atm}^2 because, unlike SK, K2K can reconstruct the neutrino energy and data show a

Isotope	^{235}U	^{239}Pu	^{238}U	^{241}Pu
Typical relative abundance f_i	54%	33%	8%	5%
Energy per fission E_i in MeV	201.7	205.0	210.0	212.4
a_0	0.870	0.896	0.976	0.793
a_1	-0.160	-0.239	-0.162	-0.080
a_2	-0.091	-0.0981	-0.079	-0.1085

Table 5.1: *Parameters that describe reactor neutrinos.*

hint of the spectral distortion characteristic of oscillations. As a consequence K2K suggests a few different local best-fit values of Δm_{atm}^2 , and the global best fit lies in the region suggested by SK (fig. 5.3b).

5.6 NUMI

The running NUMI experiment [7] is similar to K2K: we emphasize their differences. A dominantly ν_μ pulsed beam is sent from FermiLab to the MINOS detector, located 735 km away (fig. 1.2). Thanks to the longer base-line, the NUMI neutrino beam has a larger mean energy (around a few GeV) than K2K. A near detector, functionally identical to the far detector, allows to predict the non-oscillation rate. Both detectors consist of magnetized steel plates alternated to scintillator strips. The far detector has a 5.4 kton mass and a magnetic field $B \sim 1.2$ Tesla: this allows to discriminate particles from anti-particles, and to discriminate NC from CC scatterings. CC events are selected with $\approx 87\%$ efficiency and $\approx 97\%$ purity. Backgrounds are suppressed down to a negligible level.

The NuMi beam has been produced so far using a total of about 10^{20} protons-on-target, like the K2K beam. 92 events have been observed at energies lower than 10 GeV, showing a 5σ deficit with respect to the number of events expected in absence of oscillations, 177 ± 11 . Like K2K data, NUMI data also contain a hint of the spectral distortion predicted by oscillations, and point to a best-fit region similar to the K2K best-fit region, see fig. 5.3b. First NuMi data (combined with the SK measurement of the atmospheric mixing angle) provide the best single measurement of the mass splitting, $\Delta m_{\text{atm}}^2 = (2.7 \pm 0.4) \cdot 10^{-3} \text{ eV}^2$. Future NUMI data should reduce the uncertainty on Δm_{atm}^2 by a factor of few, achieve a sensitivity to θ_{23} slightly worse than SK and a sensitivity to $\nu_\mu \rightarrow \nu_e$ slightly better than CHOOZ.

5.7 CHOOZ: $\nu_\mu \rightarrow \nu_e$?

The atmospheric anomaly cannot be due to $\nu_\mu \rightarrow \nu_e$ oscillations, since no ν_e appearance effect is observed by SK. However, once that the dominant $\nu_\mu \rightarrow \nu_\tau$ oscillations have transformed the initial flux $N_{\nu_e} : N_{\nu_\mu} : N_{\nu_\tau} \sim 1 : 2 : 0$ into $\sim 1 : 1 : 1$, this flavour-blind proportion is unaffected by possible further flavour conversions. Therefore SK cannot set a strong limit on subdominant $\nu_\mu \rightarrow \nu_e$ oscillations, such as those produced by solar oscillations (at the smaller solar frequency and with a large mixing angle, see section 6) or by a small mixing angle θ_{13} at the atmospheric frequency Δm_{atm}^2 . Detailed analyses confirm this qualitative argument.

While in principle both atmospheric and solar data are sensitive to θ_{13} , the dominant bound on θ_{13} is given by the CHOOZ experiment, which looked for disappearance of $\bar{\nu}_e$ emitted by nuclear

reactors. The data, shown in fig. 5.4a, are consistent with no effect.

Reactor $\bar{\nu}_e$ have an energy of few MeV and CHOOZ was located at a distance $L \approx 1$ km from two french reactors: therefore it is sensitive to Δm^2 down to 10^{-3} eV 2 , (see eq. (3.2)), probing all values of Δm^2 consistent with the atmospheric anomaly. Eq. (3.14d) shows how oscillations at the atmospheric frequency affect $P(\bar{\nu}_e \rightarrow \bar{\nu}_e)$; solar oscillations and earth matter corrections can be neglected. Taking into account statistical and systematic errors as described in [44], fig. 3.2a at page 22 shows the region of the $(\Delta m_{\text{atm}}^2, \sin^2 2\theta_{13})$ plane excluded at 90% CL (2 dof). CHOOZ could not see atmospheric oscillations because θ_{13} is too small. CHOOZ implies $\Delta m_{\text{atm}}^2 < 0.7 \cdot 10^{-3}$ eV 2 for $\theta_{13} = \pi/4$, and $\sin^2 2\theta_{13} < 0.10$ for large Δm_{atm}^2 . The CHOOZ bound on θ_{13} strongly depends on Δm_{atm}^2 . Combining its determination from SK and K2K with CHOOZ, using the statistical techniques described in appendix B, gives $\sin^2 2\theta_{13} = 0 \pm 0.05$.

Assuming $\theta_{13} = 0$, the CHOOZ bound of fig. 3.2a also applies to the $(\Delta m_{\text{sun}}^2, \sin^2 2\theta_{\text{sun}})$ plane: CHOOZ could not see solar oscillations because Δm_{sun}^2 is somewhat too small. We conclude this section with a detailed description of reactor experiments, as the next section starts discussing how KamLAND, another reactor experiment with longer base-line, confirms the solar anomaly.

5.8 Reactor experiments

Nuclear reactors use neutrons to break heavy nuclei. Each fission produces other neutrons that sustain the chain reaction, a few nuclear fragments that decay producing about 6 $\bar{\nu}_e$, and of course kinetic energy. The energy spectrum of $\bar{\nu}_e$ emitted by a nuclear reactor can be accurately approximated as

$$\frac{dn}{dE} = \frac{W}{\sum_j f_j E_j} \sum_i f_i \exp(a_{0i} + a_{1i}E + a_{2i}E^2)$$

where $E = E_\nu / \text{MeV}$. The sums run over the isotopes, $i, j = \{^{235}\text{U}, ^{239}\text{Pu}, ^{238}\text{U}, ^{241}\text{Pu}\}$, which fissions produce virtually all the total thermal power W . Their typical relative abundances f_i , and all numerical coefficients are listed in table 5.1, from [45]. A typical reactor produces a thermal power $W \sim \text{few GigaWatt (GW} = 6.24 \cdot 10^{21} \text{ MeV/s)}$ and neutrinos have a typical energy of about a MeV. Assuming no oscillations, the $\bar{\nu}_e$ flux at distance d from the reactor is $dn/dE/(4\pi d^2)$, and can be predicted with a few % error.

The CHOOZ experiment in France had $d \approx 1$ km, optimal for studying $\bar{\nu}_e$ disappearance induced by oscillations with $\Delta m^2 \approx 6 \cdot 10^{-3}$ eV 2 . The KamLAND experiment in Japan is located at distances ranging between 80 to few hundred km from several reactors. Most $\bar{\nu}_e$ come from reactors at $d \sim 200$ km, optimal for studying $\bar{\nu}_e$ disappearance induced by oscillations with $\Delta m^2 \approx 3 \cdot 10^{-5}$ eV 2 .

Neutrinos are detected using the gold-plated reaction $\bar{\nu}_e p \rightarrow e^+ n$, discussed in section 4.2, eq. (4.4). Using a scintillator it is possible to see both the γ ray emitted when the neutron n is captured and the two γ rays with energy $E_\gamma = m_e$ emitted by the positron e^+ as it moves and finally annihilates with an e^- . In KamLAND the n random walks for $\sim 200 \mu\text{s}$ before being captured by a proton giving a γ ray with $E_\gamma = 2.2 \text{ MeV}$. In order to maximize the n capture efficiency and to get more energetic γ , Gd was added to the scintillator used in CHOOZ. The delayed coincidence between the γ can be measurable by photomultipliers with good time and spatial resolution and allows to select $\bar{\nu}_e$ events from background. The total measured energy is $E_{\text{vis}} = E_{e^+} + m_e$, and E_{e^+} is related to the neutrino energy by the kinematical relation $E_\nu = E_{e^+} + m_n - m_p$ (neglecting the recoil of the neutron).

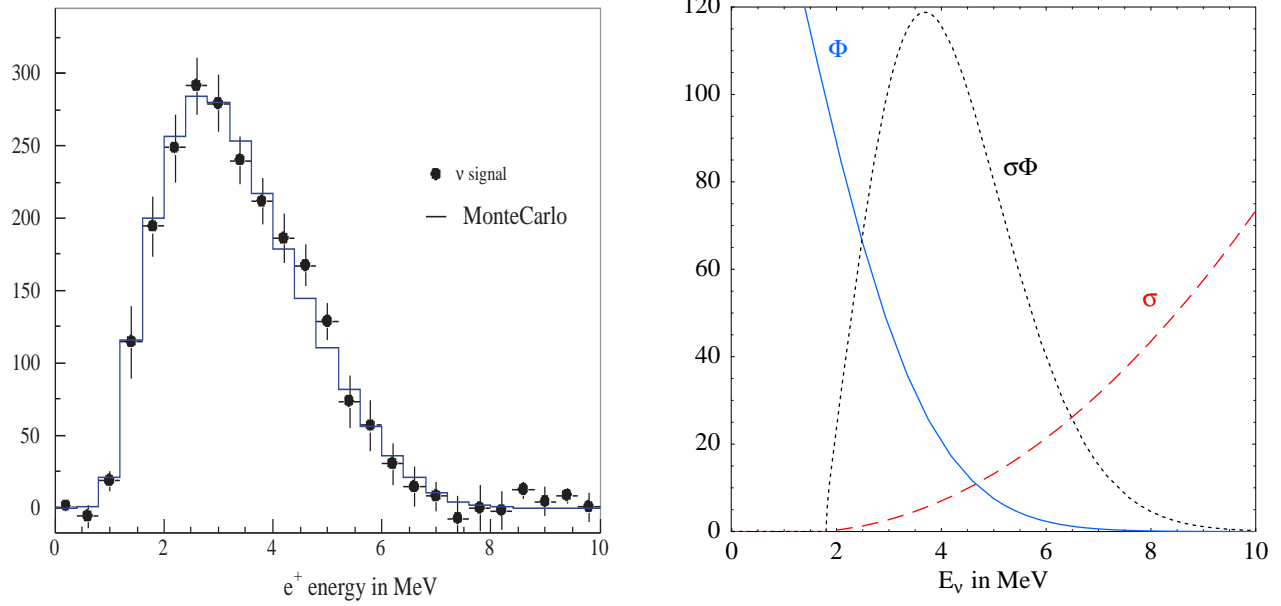


Figure 5.4: Fig. 5.4a shows the final data from CHOOZ [44]. Fig. 5.4b shows $\sigma(\bar{\nu}_e p \rightarrow n e^+)$ in 10^{-43} cm^2 (dashed line), the flux of $\bar{\nu}_e$ in $10^{14} / \text{cm}^2 \text{ yr MeV}$ at 1 km from a reactor with thermal power $W = 1 \text{ GW}$ (continuous line) and the resulting interaction rate in $1/\text{ton yr MeV}$ (dotted line).

Summing over all reactors r (that emit a power W_r from a distance d_r), the number of neutrino events with visible energy in any given range $E_{\text{vis}}^{\text{min}} < E_{\text{vis}} < E_{\text{vis}}^{\text{max}}$ is

$$N = \sum_r \int dE_\nu P_{ee}(d_r/E_\nu) \sigma(E_\nu) N_p \frac{dn_r/dE_\nu}{4\pi d_r^2} \int_{E_{\text{vis}}^{\text{min}}}^{E_{\text{vis}}^{\text{max}}} dE_{\text{vis}} \frac{e^{-(E_{\text{vis}} - E_\nu + 0.782 \text{ MeV})^2/2\sigma_E^2}}{\sqrt{2\pi}\sigma_E} \varepsilon(E_{\text{vis}})$$

where ε is the efficiency. Neglecting small differences between the energy spectra of different reactors (i.e. assuming that all reactors have the same relative isotope abundances f_i), the spectrum of detected neutrinos dN/dE_ν can be conveniently rewritten as

$$\frac{dN}{dE_\nu} = n_0 \langle P_{ee}(E_\nu) \rangle R(E_\nu)$$

where n_0 is the rate expected in absence of oscillations, $\langle P_{ee}(E_\nu) \rangle$ is the averaged survival probability

$$\langle P_{ee}(E_\nu) \rangle = \sum_r p_r P_{ee}(E_\nu/d_r) \quad p_r = \frac{W_r/d_r^2}{\sum_{r'} W_{r'}/d_{r'}^2}$$

and R is the *response function* (normalized such that $\int dE_\nu R = 1$). Assuming no oscillations, fig. 5.4b shows dN/dE_ν .

Chapter 6

The solar evidence

Disappearance of solar ν_e (and later appearance of $\nu_{\mu,\tau}$) gave the first signal of a neutrino anomaly, that was therefore named ‘solar anomaly’. Oscillations predicted that few different clean experimental signals could have been detectable, depending on the actual value of the oscillation parameters. In order to find the true one, all signals have been searched: therefore we have a large amount of data. Fits of solar data correctly indicate that the best-fit solution of the solar neutrino anomaly has a large mixing angle θ_{sun} and $\Delta m_{\text{sun}}^2 \sim 10^{-4} \text{ eV}^2$ (‘LMA’ solution) but, as shown in fig. 6.1a, do not fully exclude other disfavored solutions with much smaller Δm^2 . Finally, in 2002 the KamLAND experiment confirmed LMA oscillations by discovering disappearance of $\bar{\nu}_e$ generated by nuclear reactors. Fig. 6.1b shows a fit of reactor data. Fig. 6.1c shows a global fit of all solar ν and reactor $\bar{\nu}$ data. Reactor data can be understood in a simpler way and in the future should give the best measurements of Δm_{sun}^2 , and maybe of θ_{sun} . Therefore we start (contrarily to historical development) describing reactor data, and we later discuss solar data.

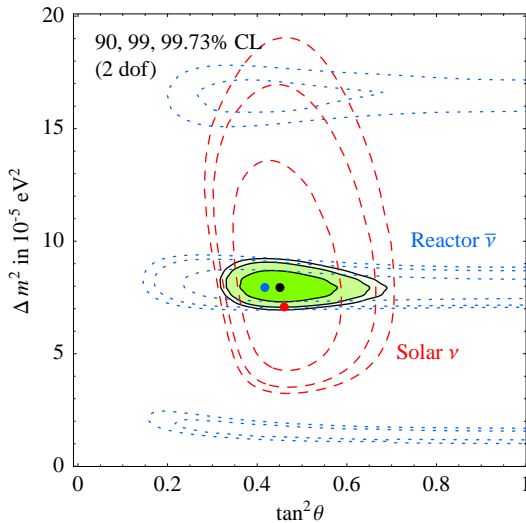


Figure 6.1: **Solar oscillation parameters.** Best-fit regions at 90, 99 and 99.73% CL obtained fitting solar ν data (red dashed contours); reactor $\bar{\nu}$ data that do not distinguish θ from $\pi/2 - \theta$ (blue dotted contours); all data (shaded region). Dots indicate the best fit points.

6.1 KamLAND

We presented reactor experiments in section 5.8. KamLAND [11] is a Čerenkov scintillator composed by 1 kton of a liquid scintillator (the number of protons, $8.6 \cdot 10^{31}$, is about 200 times larger than in CHOOZ) contained in a spherical balloon surrounded by inert oil that shields external radiation. KamLAND detects $\bar{\nu}_e$ emitted by terrestrial (mainly Japanese) reactors using the $\bar{\nu}_e p \rightarrow e^+ n$ reaction. The detector can see both the positron and the 2.2 MeV γ ray from neutron capture on proton. By requiring their delayed coincidence and being located underground and having achieved sufficient radio-purity, KamLAND reactor data are almost background-free. As illustrated in fig. 6.2a, KamLAND only analyzes $\bar{\nu}_e$ events with $E_{\text{vis}} = E_{e^+} + m_e > 2.6 \text{ MeV}$ (i.e. $E_\nu > 3.4 \text{ MeV}$) in order to avoid a poorly predictable background of $\bar{\nu}_e$ generated by radioactive elements inside the earth [46].¹ Above this energy threshold KamLAND should detect, in absence of oscillations, about 500 events per $\text{kton} \cdot \text{yr}$, depending on operating conditions of reactors.² Thanks to previous reactor experiments the unoscillated $\bar{\nu}_e$ flux is known with $\sim 3\%$ uncertainty. This expectation can be checked only partially: it is not possible to turn off reactors or built detectors close to each reactor.

The effect of oscillations is given by

$$P(\bar{\nu}_e \rightarrow \bar{\nu}_e) = 1 - \sin^2 2\theta_{\text{sun}} \sin^2 \frac{\Delta m_{\text{sun}}^2 L}{2E_\nu} \quad (6.1)$$

up to minor corrections due to earth matter effects and to the small θ_{13} atmospheric mixing angle.

The KamLAND efficiency is about 90%. Using as fiducial volume only an inner fraction of the detector (known with 4.7% uncertainty), the latest 2004 data (766.3 ton yr) showed 258 events instead of the 365 ± 24 events expected in absence of oscillations. This gives a 4σ evidence for a $68.6 \pm 4.4(\text{stat}) \pm 4.5(\text{syst})\%$ reduction in the $\bar{\nu}_e$ rate. As illustrated in fig. 6.2b, this is consistent with expectations from solar data. KamLAND receives $\bar{\nu}_e$ from many nuclear reactors located at different distances. However, most reactors are at $L \approx 180 \text{ km}$, because KamLAND is located in the Kamioka mine in a central region of Japan, while, in absence of big rivers, Japanese reactors are built around the coast.

More importantly, KamLAND data allow to test if the $\bar{\nu}_e$ survival probability depends on the neutrino energy as predicted by oscillations. In fact, KamLAND can measure the positron energy with a $\sigma_E/E = 7.5\%/\sqrt{E/\text{MeV}}$ error. The neutrino energy is directly linked to E_{e^+} as $E_{\bar{\nu}} \approx E_{e^+} + m_n - m_p$. Present KamLAND spectral data (fig. 6.2a) give a 3σ indication for oscillation dips: the first one at $E_{\text{vis}} \approx 7 \text{ MeV}$ (where statistics is poor) and the second one at $E_{\text{vis}} \approx 4 \text{ MeV}$. Taking into account the average baseline $L \approx 180 \text{ km}$, this second dip occurs at $L/E_{\bar{\nu}_e} \approx 45 \text{ km/MeV}$. This fixes $\Delta m_{\text{sun}}^2 = 6\pi E_{\bar{\nu}_e}/L|_{\text{2nd dip}} \approx 8 \cdot 10^{-5} \text{ eV}^2$. The global fit of fig. 6.1 shows that Δm_{sun}^2 is presently dominantly fixed by KamLAND data, which however still allow 3 different best-fit regions: the oscillation dip most likely identified as the second one could instead be the first or the third one. Solar data help in resolving this ambiguity and dominantly fix the

¹‘Geoneutrinos’ are generated by decays of uranium, thorium and potassium. These elements are located with comparable total abundances in continental crusts and in the mantle. While geo- $\bar{\nu}_e$ have geological interest, it seems not possible to use them for oscillation studies because their total flux can be predicted only up to a maybe 20% uncertainty. About 1/3 of them arrive from distances between 10 and 100 km, about 1/4 from 100 to 1000 km, and the remaining fraction from more than 1000 km.

²In 2003 reactors operated only at 50% of maximum due to safety lapses. A new reactor (‘Shika-II’) at 88 km from KamLAND might be operative since 2006.

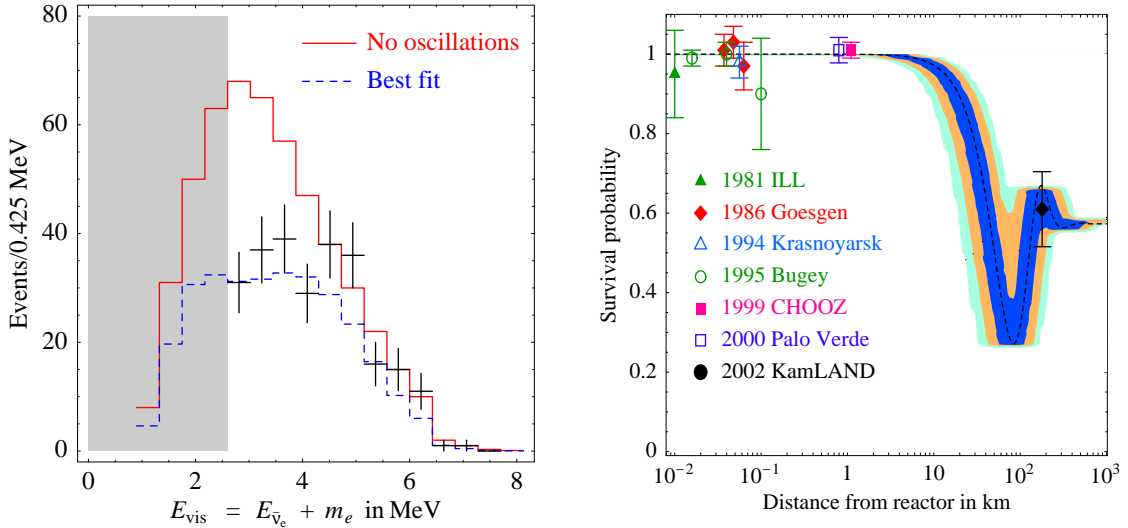


Figure 6.2: **KamLAND**. Fig. 6.2a: the $E_{\text{vis}} = E_{\bar{\nu}_e} + m_e$ energy spectrum measured by KamLAND. Fig. 6.2b: history of reactor experiments and reduction in the reactor $\bar{\nu}_e$ flux as predicted at 1, 2, 3 σ by a global oscillation fit of solar data.

solar mixing angle θ_{sun} . In the future the total KamLAND systematic error might be reduced from 6.4% down to (3 \div 4)%, allowing a competitive reactor measurement of θ_{sun} .

6.2 Solar neutrinos

How old is the earth? Around the end of 19th century, biologists and geologists (like Darwin) suggested that more than 300 Myr were necessary for natural selection and erosion. Physicists (like Kelvin) showed that the sun can shine for $(GM^2/R)/(d^2K_{\text{sun}}) \sim 30$ Myr at most, using gravitational energy to emit the flux of energy that, at distance d from the sun we receive at earth, $K_{\text{sun}} = 8.53 \cdot 10^{11} \text{ MeV cm}^{-2} \text{ s}^{-1}$. Theologians (like Lightfoot) believed that the earth was created on october 23, -4004, at nine o'clock in the morning.

Biologists and geologists were right. Physicists (like Aston, Eddington, Gamow, Bethe) later found the missing pieces of the puzzle: the sun shines thanks to nuclear fusion. Around the center of the sun, energy and neutrinos are produced essentially through the ${}^4\text{He}$ reaction

$$4p + 2e \rightarrow {}^4\text{He} + 2\nu_e \quad (Q = 26.7 \text{ MeV}). \quad (6.2)$$

The predicted ν_e spectrum [47], in absence of oscillations, is shown in fig. 6.3. The reason of such a complex spectrum is that the overall reaction (6.2), having 6 particles in the initial state, proceeds in a sequence of steps, following different routes. The main routes are summarized in fig. 6.5, and give rise to five main types of neutrinos.

1. pp neutrinos, generated in the first step $pp \rightarrow de^+\nu_e$, have a large and precisely predicted flux. However their maximal energy is only $0.42 \text{ MeV} \sim 2m_p - m_d - m_e$, so that it is difficult to detect pp neutrinos. Since the average solar neutrino energy is much smaller than Q , most of the energy is carried out from the sun by photons, that after random-walking in the solar interior for about 10^4 years, carry to the earth the well known flux of energy, K_{sun} .

Flux	Reaction	Φ_ν $10^{10}/\text{cm}^2\text{s}$	$\langle E_\nu \rangle$ MeV	E_ν^{max} MeV	Q MeV	Cl SNU	Ga SNU
<i>pp</i>	$pp \rightarrow {}^2\text{H} \bar{e} \nu_e$	$6.0 \pm 1\%$	0.267	0.423	13.10	0	70.3
<i>pep</i>	$pep \rightarrow {}^2\text{H} \nu_e$	$0.014 \pm 1\%$		1.445	11.92	0.22	2.8
<i>hep</i>	${}^3\text{He} p \rightarrow {}^4\text{He} \bar{e} \nu_e$	$\sim 10^{-6}$	9.628	18.8	3.737	0.04	0.1
Be	${}^7\text{Be} e \rightarrow {}^7\text{Li} \nu_e$	$0.477 \pm 9\%$	0.814	0.863	12.60	1.15	34.2
B	${}^8\text{B} \rightarrow {}^8\text{Be} \bar{e} \nu_e$	$0.00050 \pm 20\%$	6.735	16.3	6.630	5.76	12.1
N	${}^{13}\text{N} \rightarrow {}^{13}\text{C} \bar{e} \nu_e$	$0.033 \pm 20\%$	0.706	1.20	3.456	0.05	2.0
O	${}^{15}\text{O} \rightarrow {}^{15}\text{N} \bar{e} \nu_e$	$0.026 \pm 20\%$	0.996	1.73	21.57	0.18	2.9
all	$4p \ 2e \rightarrow {}^4\text{He} \ 2\nu_e$	—	—	—	26.7	7.4 ± 1.3	124 ± 9

Table 6.1: **Predicted solar neutrino fluxes in absence of oscillations.** Φ is the total ν_e flux at earth. $\langle E_\nu \rangle$ (E_ν^{max}) is the mean (maximal) neutrino energy. Q is the energy released in the reaction. The last two columns show the contributions to the total rate measured in Cl and Ga experiments. 89.7% (10.3%) of the ${}^7\text{Be}$ neutrinos are produced in ground state (excited state) capture and have energy 0.8631 MeV (0.386 MeV).

Therefore, the present total neutrino luminosity of the sun is $\Phi \sim 2K_{\text{sun}}/Q \sim 6.5 \cdot 10^{10}/\text{cm}^2\text{s}$. The precise solar model prediction is $\Phi_{pp} = 0.91 \cdot 2K_{\text{sun}}/Q$.

2. *pep* neutrinos, generated in $pep \rightarrow d\nu_e$ collisions, have a relatively small flux and low energy, $E \approx 2m_p + m_e - m_d = 1.445$ MeV, but are not totally negligible. The *pep* and Be neutrinos are almost monochromatic, because generated by electrons colliding on heavy particles at temperatures $T \ll m_e$.
3. Be neutrinos have a relatively well predicted and large flux and relatively high energy and are important for present experiments, as shown in fig. 6.4. They are of great interest for future experiments, mainly because they are almost monochromatic, $E_{\text{Be}} \approx m_{{}^7\text{Be}} - m_{{}^7\text{Li}} - m_e \approx 0.863$ MeV, allowing interesting measurements (see below). Thermal motions produce a small asymmetric broadening of the line (FWHM = 1.6 keV).
4. B neutrinos are a small fraction of all solar neutrinos, but can have a relatively large energy, up to $E \lesssim m_{{}^8\text{B}} - 2m_\alpha$. SK and SNO detect neutrinos with energy larger than about 6 MeV, and are consequently sensitive only to B and *hep* neutrinos.
5. *hep* neutrinos have the highest energy, but are too rare for having significant effects, given the accuracy of present experiments.

Solar models predict that in stars heavier than the sun most of the energy is produced by a different chain of reactions, named CNO cycle. In the sun, CNO neutrinos give a minor additional component of solar neutrinos (fig. 6.3).

The energy spectra of the single components are essentially determined by kinematics and do negligibly depend on details of the solar interior. *Solar models play a crucial rôle in predicting their total fluxes.* The flux of B neutrinos, produced by the terminal reaction of the chain, strongly depends on the the solar temperature and cannot be accurately predicted. Today the dominant uncertainties no longer come from solar parameters, but from nuclear physics inputs [48]: S_{17} (that parameterizes the ${}^7\text{Be} p \rightarrow {}^8\text{B} \gamma$ cross-section in fig. 6.5, thereby fixing the total flux of B

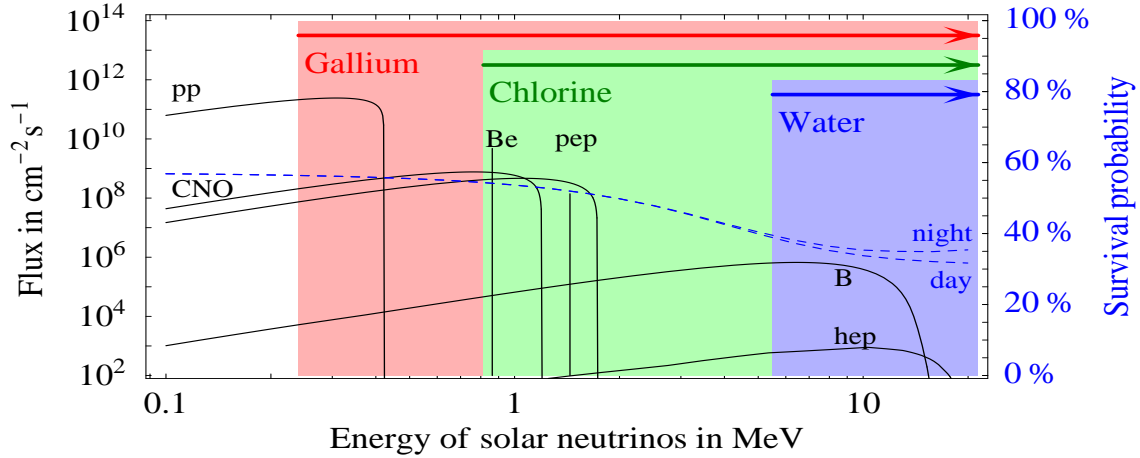


Figure 6.3: The predicted unoscillated spectrum $d\Phi/dE_\nu$ of solar neutrinos, together with the energy thresholds of the experiments performed so far and with the best-fit oscillation survival probability $P_{ee}(E_\nu)$ (dashed line).

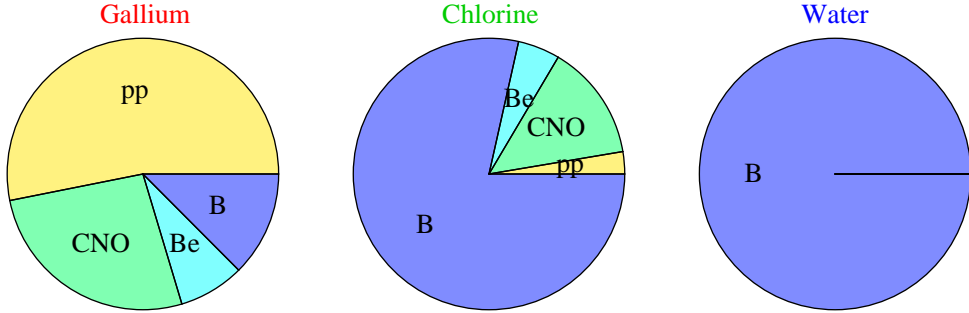


Figure 6.4: The predicted fractional contributions to the neutrino rates of present experiments, assuming energy-independent oscillations.

neutrinos. The ${}^7\text{Be}e$ cross section giving rise to Be neutrinos is larger and precisely known because not suppressed by the Coulomb barrier [49]) and S_{34} (that parameterizes the ${}^3\text{He}\alpha \rightarrow {}^7\text{Be}\gamma$ cross-section in fig. 6.5, thereby fixing the total flux of B plus Be neutrinos). This explains the uncertainties on the fluxes predicted in table 6.1 (fits of solar data take into account correlations among them, as discussed in subsection 6.4).

6.3 Solar neutrino experiments

We now discuss the main characteristics and results of all solar neutrino experiments, listed in table 6.2.

6.3.1 Chlorine

R. Davis leaded the first experiment which detected solar neutrinos and saw the first hint of a solar neutrino anomaly [4], using a radiochemical technique suggested by Pontecorvo. Solar ν_e

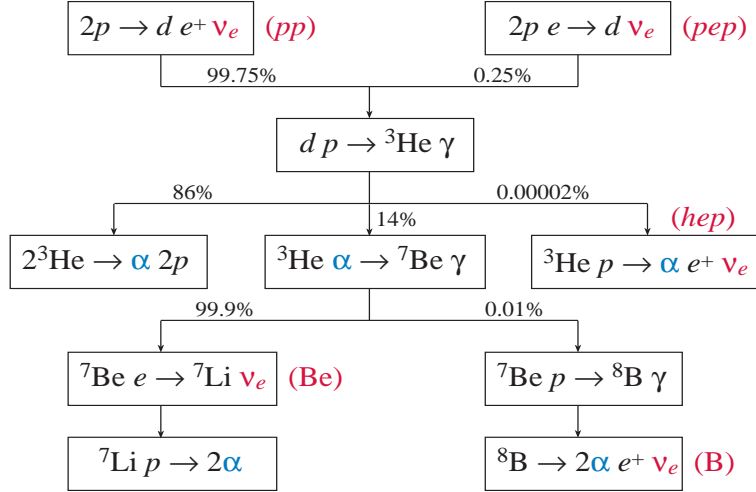


Figure 6.5: The $4p + 2e \rightarrow {}^4\text{He} + 2\nu_e$ chain.

induce the reaction $\nu_e {}^{37}\text{Cl} \rightarrow {}^{37}\text{Ar} e$, producing the isotope ${}^{37}\text{Ar}$. Such isotopes were separated using their different chemical behavior; by observing their later decays back to ${}^{37}\text{Cl}$ (the half-life is 35 days) it was possible to count a few atoms in a tank of few hundred tons.

The Cl reaction was employed because its cross section is precisely computable and its energy threshold, $E_{\nu_e} > 0.814$ MeV, is low enough that the Cl experiment is sensitive to Boron ν_e with some minor contribution from lower energy solar ν_e (see fig. 6.4 or table 6.1).

The measured Cl rate was found to be about 3 times lower than the predicted value, suggesting an intriguing discrepancy between a pioneering experiment and supposedly accurate enough solar models. In 1972 Pontecorvo commented “*It starts to be really interesting! It would be nice if all this will end with something unexpected from the point of view of particle physics. Unfortunately, it will not be easy to demonstrate this, even if nature works that way*”. About 15 years were necessary for a second experiment, and 30 for finally establishing solar oscillations.

6.3.2 Gallium experiments

The next radiochemical experiments, SAGE and GALLEX/GNO [8] (respectively located in the Baksan and Gran Sasso underground laboratories in Soviet Union and Italy) employed the reaction $\nu_e {}^{71}\text{Ga} \rightarrow {}^{71}\text{Ge} e$ which has the lowest threshold reached so far, $E_{\nu_e} > 0.233$ MeV. As a consequence more than half of the ν_e -induced events is generated by pp neutrinos, see fig. 6.4. Their total flux can be reliably approximated from the solar luminosity and can be predicted by solar models with 1% error. After a half-live of 16.5 days the inverse β -decay of ${}^{71}\text{Ge}$ produces observable Auger electrons and X -rays with the typical L -peak and K -peak energy distributions, giving two different signals used to infer the flux of solar ν_e . The rate measured in Gallium experiments is about 2 times lower than the predicted value. This result made harder to believe that the solar neutrino anomaly was due to wrong solar model predictions.

The reliability of the Gallium technique was tested using an artificial neutrino source. Gallium experiments improved with time, and both their central values decreased by about two standard deviations with respect to the first data.

Experiment	Reaction	E_{th} (MeV)	ν fluxes	Running time	R^{exp}	R^{BP00}
Homestake	$\nu_e {}^{37}\text{Cl} \rightarrow {}^{37}\text{Ar} e$	0.814	mainly ${}^8\text{B}$	1970 – 1994	2.56 ± 0.23	7.6 ± 1.3
SAGE				1990 – 2003	69.1 ± 5.7	
GALLEX	$\nu_e {}^{71}\text{Ga} \rightarrow {}^{71}\text{Ge} e$	0.233	all	1991 – 1997	77.5 ± 7.7	128 ± 9
GNO				1998 – 2003	62.9 ± 5.9	
Kamiokande		6.75		1987 – 1995	2.80 ± 0.36	
SK	$\nu e \rightarrow \nu e$	4.75		1996 – 2001	2.35 ± 0.06	
		5.2			2.31 ± 0.21	
SNO	$\nu_{e\bar{d}} \rightarrow p\bar{p}$	6.9		1999 – 2003	1.67 ± 0.08	
	$\nu d \rightarrow p\nu$	2.2			5.17 ± 0.38	5.05 ± 0.9
			${}^8\text{B}, \text{hep}$			

Table 6.2: *Solar neutrino experiments. Rates measured by radiochemical experiments are expressed in SNU $\equiv 10^{-36}$ interactions per target atom and per second, while SK and SNO report neutrino fluxes in $10^6 \text{ cm}^{-2}\text{s}^{-1}$.*

6.3.3 Kamiokande and SuperKamiokande

SK [9] is a 50 kton WČ detector with a 22.5 kton fiducial volume. The experiment stopped when an accident damaged its 11146 photomultipliers. During its 1496 live days, between 1996 and 2001, SK-I collected about 20000 solar neutrinos. Solar neutrinos are detected via scattering on electrons $\nu_{e,\mu,\tau}e \rightarrow \nu_{e,\mu,\tau}e$. SK can measure the kinetic energy T_e and the direction of the scattered electron. The dominant backgrounds to the solar neutrino signal are ${}^{222}\text{Rn}$ in the water, external γ rays and muon-induced spallation products. As a consequence only data above the cut $T_e > 5.5 \text{ MeV}$ are used. Since $T_e \gg m_e$ the electrons are scattered roughly along the direction of the solar neutrino: before Kamiokande radiochemical experiments could count neutrinos but could not verify that they come from the sun. The direction of the scattered electron allows SK to discriminate solar neutrino events from a comparable number of background events.

Although SK cannot distinguish ν_e from $\nu_{\mu,\tau}$, all active neutrinos contribute to the total SK solar neutrino rate. Oscillations suppress the Boron ν_e flux Φ_B generating fluxes of $\nu_{\mu,\tau}$ and possibly of sterile neutrinos. Their effect can be parameterized as:

$$\Phi_{\nu_e} = \Phi_B P_{ee}, \quad \Phi_{\nu_{\mu,\tau}} = \Phi_B (1 - P_{ee})(1 - \eta_s), \quad \Phi_{\nu_s} = \Phi_B (1 - P_{ee})\eta_s, \quad (6.3)$$

Neglecting the possible dependence of P_{ee} and η_s on the neutrino energy, the SK rate gets suppressed by $P_{ee} + 0.155(1 - P_{ee})(1 - \eta_s)$, where 0.155 is the value of $\sigma(\nu_{\mu,\tau}e)/\sigma(\nu_e e)$ at $E_\nu \sim 10 \text{ MeV}$ (see section 4). The measured rate reported in table 6.2 is not the main SK result. SK could search for various signals possibly generated by oscillations. Since none of them was found significant ranges of neutrino masses and mixings were excluded, and global analyses of solar data started favoring the active-only large mixing angle solution as the true one.

- The *electron energy spectrum* is consistent with an energy-independent reduction in the flux of B neutrinos. This excluded SMA and part of VO solutions, which predicted an energy-dependent survival probability P_{ee} . LMA oscillations predict a small slope comparable to the present experimental accuracy (see fig. 6.3).

Furthermore, SK is a real-time experiment: this allowed to search for seasonal and day/night variations in the neutrino rate.

- Vacuum oscillations with $\Delta m^2 \sim 10^{-10} \text{ eV}^2$ have a wave-length comparable to the distance d between the sun and the earth, and therefore should produce an anomalous seasonal variation of the solar neutrino flux (beyond the observed trivial variation due to the geometrical

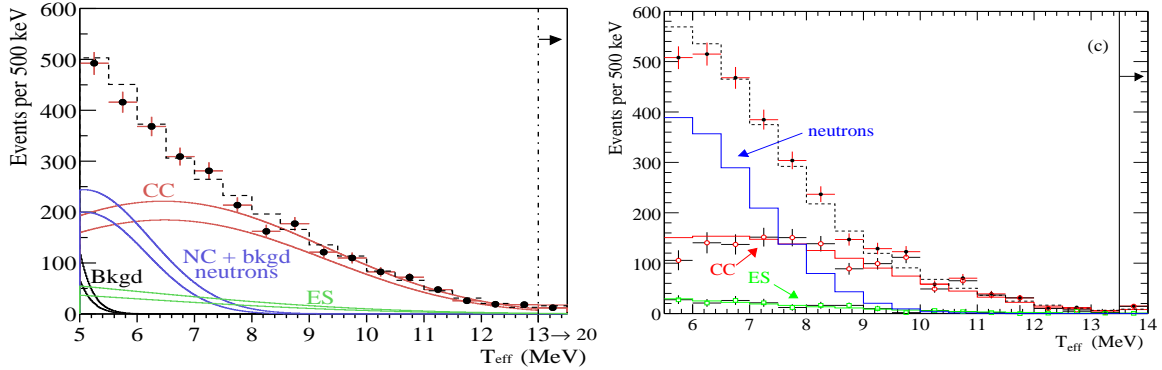


Figure 6.6: **SNO**. The left (right) figure shows the energy spectra in the second (third) phase of SNO, decomposed according to their components. From [10].

$1/d^2$ flux factor). The SK rate is consistent with no anomalous seasonal variation. Together with the absence of spectral distortions, this disfavored VO.

- During the night neutrinos cross the earth before being detected by SK. Earth-matter corrections significantly affect neutrinos with energy around the resonant energy of eq. (3.18):

$$E_\nu^{\text{res}} = \frac{\Delta m^2}{2\sqrt{2}G_F N_e^\oplus} \approx 200 \text{ MeV} \frac{\Delta m^2}{10^{-4} \text{ eV}^2}$$

where N_e^\oplus is the electron density of the earth mantle. The absence of a large day/night asymmetry at $E_\nu \sim 10 \text{ MeV}$

$$A_{\text{DN}}^{\text{SK}} \equiv 2 \frac{\text{night rate} - \text{day rate}}{\text{night rate} + \text{day rate}} = 1.8 \pm 1.6_{\text{stat}} \pm 1.3_{\text{syst}} \%$$
(6.4)

excluded oscillations with $\Delta m_{\text{sun}}^2 \sim 10^{-5 \div 7} \text{ eV}^2$ and $\theta_{\text{sun}} \sim 1$. LMA predicts a $\sim 2\%$ day/night asymmetry, with a specific energy and zenith-angle dependence.

Finally, SK puts interesting bounds on exotic processes, such as time variations of the solar neutrino rate [50] and conversion into $\bar{\nu}_e$. The KamLAND bound $P(\nu_e \rightarrow \bar{\nu}_e) < 2.8 \cdot 10^{-4}$ at 90% CL [11] is stronger than the SK bound, $P(\nu_e \rightarrow \bar{\nu}_e) < 0.8 \cdot 10^{-2}$ at 90% CL [9].

6.3.4 SNO

SNO [10] is a real-time WC experiment similar to SK and smaller than it. The crucial improvement is that SNO employs 1 kton of *salt heavy water* rather than water, so that neutrinos can interact in different ways, allowing to measure separately the ν_e and $\nu_{\mu,\tau}$ fluxes: SNO is the first solar neutrino *appearance* experiment.

ES Like in SK, $\nu_{e,\mu,\tau}$ can be detected (but not distinguished) thanks to CC and NC scattering on electrons: $\nu_{e,\mu,\tau} e \rightarrow \nu_{e,\mu,\tau} e$. This allows to measure $\Phi_{\nu_e} + 0.155\Phi_{\nu_{\mu,\tau}}$ and contrast it with the SSM prediction:

SNO events are mostly produced by two interactions not present in SK:

CC Only ν_e can produce $\nu_e d \rightarrow p p e$. SNO sees the scattered electron and measures its direction and energy.

NC All active neutrinos can break deuterons: $\nu_{e,\mu,\tau} d \rightarrow \nu_{e,\mu,\tau} p n$. The cross section is equal for all flavours and has a $E_\nu > 2.2$ MeV threshold. About one third of the neutrons are captured by deuterons and give a 6.25 MeV γ ray: observing the photo-peak SNO can detect n with $\sim 15\%$ efficiency. Adding salt allowed to tag the n with enhanced $\sim 45\%$ efficiency, because neutron capture by ^{35}Cl produces multiple γ rays.

Several handles allow to discriminate ES from CC from NC events. ES events are not much interesting and can be subtracted since, unlike CC and NC events, ES events are forward peaked. CC/NC discrimination was performed in different ways before (phase 2) and after (phase 3) adding salt to heavy water.

As illustrated in fig. 6.6a, in phase 2 SNO mostly discriminated CC from NC events from their energy spectra: NC events produce a γ ray of known average energy (almost always smaller than 9 MeV). The spectrum of CC events can be computed knowing the spectrum of ^8B neutrinos (oscillations only give a minor distortion). Phase 2 SNO data imply

$$\Phi_{\nu_e} = 1.76 \pm 0.06(\text{stat}) \pm 0.09(\text{syst}) \frac{10^6}{\text{cm}^2 \text{s}} \quad \Phi_{\nu_{e,\mu,\tau}} = 5.09 \pm 0.44(\text{stat}) \pm 0.46(\text{syst}) \frac{10^6}{\text{cm}^2 \text{s}} \quad (6.5)$$

(uncertainties are mildly anti-correlated). The total flux agrees with the value predicted by solar models, and the reduced ν_e flux gives a 5σ evidence for $\nu_e \rightarrow \nu_{\mu,\tau}$ transitions.

After adding salt, SNO could statistically discriminate events from the pattern of photomultiplier-tube hits: NC events produce multiple γ rays and consequently a more isotropic Čerenkov light than the single e produced in CC and ES scatterings. Phase 3 SNO data imply

$$\Phi_{\nu_e} = 1.59 \pm 0.08(\text{stat}) \pm 0.08(\text{syst}) \frac{10^6}{\text{cm}^2 \text{s}} \quad \Phi_{\nu_{e,\mu,\tau}} = 5.21 \pm 0.27(\text{stat}) \pm 0.38(\text{syst}) \frac{10^6}{\text{cm}^2 \text{s}} \quad (6.6)$$

giving a more accurate and independent measurement of total $\nu_{e,\mu,\tau}$ flux. SNO finds $\Phi_{\nu_e}/\Phi_{\nu_{e,\mu,\tau}} < 1/2$, that can be explained by oscillations enhanced by matter effects.

In a successive phase, by adding ^3He SNO will be able of tagging NC events on an event-by-event basis by detecting neutrons via the scattering $n \ ^3\text{He} \rightarrow p \ ^3\text{H}$: proportional counters allow to see both p and ^3H .

Like SK, SNO can also search for energy-dependent or time-dependent effects. The day/night asymmetry of the ν_e flux is found to be

$$A_{\text{DN}}^{\text{CC}} = 7.0 \pm 5.1\% \quad (6.7)$$

assuming zero day/night asymmetry in the $\nu_{e,\mu,\tau}$ flux (the direct measurement of this asymmetry is consistent with zero up to a $\sim 15\%$ uncertainty).

Since oscillations among active neutrinos do not affect the total $\nu_{e,\mu,\tau}$ flux, enhancing the NC rate makes the overall SNO energy spectrum of fig. 6.6b less sensitive to spectral distortions. At the moment SK is more sensitive than SNO to spectral distortions: SNO has much less statistics than SK, only partially compensated by the fact that the energy of electrons scattered in CC reactions is more strongly correlated with the parent neutrino energy than in ES (because $m_e \ll E_\nu \ll m_d$).

6.4 Implications of solar data

Oscillations can successfully explain all these data. No other proposed interpretation can simultaneously explain the solar ν data and the reactor $\bar{\nu}$ data. Although in figures we show results of global fits (performed as described at the end of this section), thanks to the recent clean SNO and KamLAND data, main results can now be extracted from simple arguments, that we discuss in the text.

6.4.1 Which oscillation parameters?

Atmospheric oscillations have a minor or negligible impact on solar neutrino and KamLAND data. Indeed, $\nu_\mu \leftrightarrow \nu_\tau$ oscillations have no effect (because ν_μ cannot be distinguished from ν_τ when their energy is so low that they only have NC interactions), and ν_e are at most marginally involved in atmospheric oscillations (the mixing angle θ_{13} is small, and it is not enhanced by matter effects because $G_F N_e^{\text{sun}} \ll \Delta m_{\text{atm}}^2 / E_\nu$). In conclusion, solar $\nu_e \leftrightarrow \nu_{\mu,\tau}$ oscillations depend on two oscillation parameters:

$$\Delta m_{\text{sun}}^2 \equiv \Delta m_{12}^2 \quad \text{and} \quad \theta_{\text{sun}} \equiv \theta_{12},$$

and effectively realize oscillations of two neutrinos. Things become more complicated if one adds extra sterile neutrinos.

6.4.2 The solar mass splitting

Δm_{sun}^2 is directly determined by the position of the oscillation dips at KamLAND, with negligible contribution from solar experiments. More precisely, this will be rigorously true in the future. For the moment solar data are needed to eliminate spurious solutions mildly disfavored by KamLAND data, as illustrated in fig. 6.1. KamLAND data also imply a large mixing angle, but its value is more precisely measured by SNO.

6.4.3 Prediction for $P(\nu_e \rightarrow \nu_e)$

This implies that oscillations in the sun are adiabatic to an excellent level of approximation³, that seasonal variations are negligible and earth matter corrections are small. The dashed line in fig. 6.3 shows the survival probability $P(\nu_e \rightarrow \nu_e, E_\nu)$ for best-fit values of Δm_{sun}^2 and θ_{sun} . Its main features can be understood as follows. Solar matter effects are negligible at neutrino energies much lower than

$$E_* \equiv \frac{\Delta m_{\text{sun}}^2}{2\sqrt{2}G_F N_e^{\text{sun}}} \approx 4 \text{ MeV} \frac{\Delta m_{\text{sun}}^2}{0.8 \cdot 10^{-4} \text{ eV}^2} \quad (6.8)$$

where N_e^{sun} is the electron density around the solar center. Therefore:

- Solar neutrinos with $E_\nu \ll E_*$ (so far probed only by Gallium experiments) experience averaged vacuum oscillations:

$$P(\nu_e \rightarrow \nu_e, \text{small } E_\nu) \simeq 1 - \frac{1}{2} \sin^2 2\theta_{\text{sun}} \geq 1/2. \quad (6.9)$$

³Some authors worry that this conclusion might be invalidated by unexpected inhomogeneities in the sun [51].

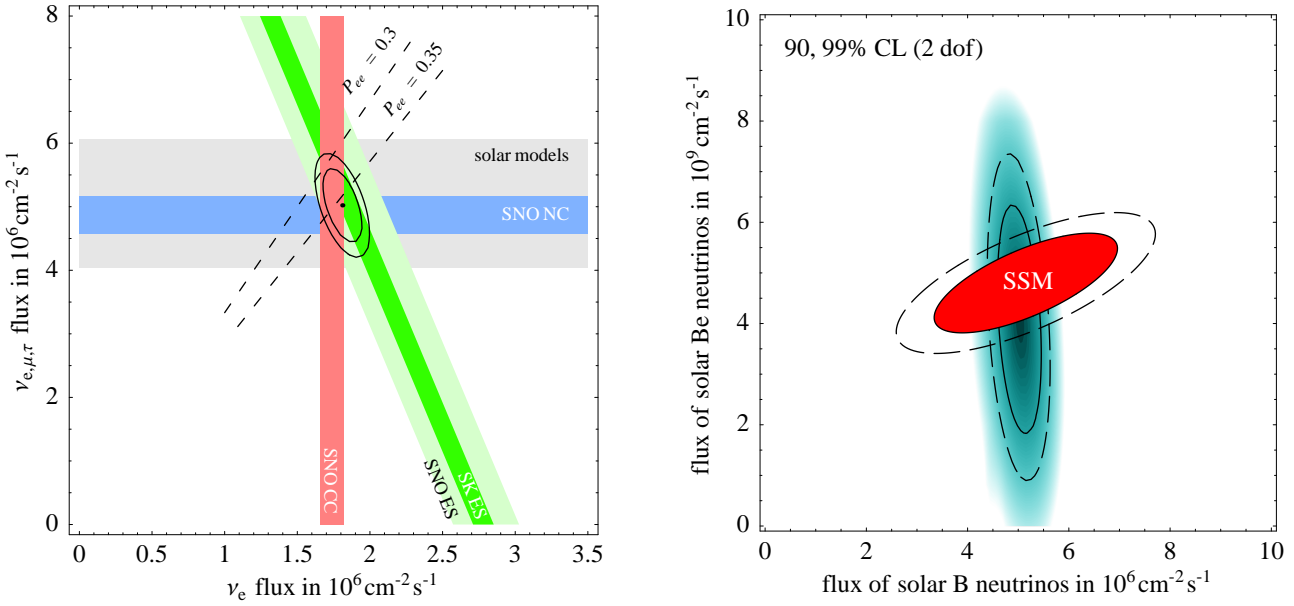


Figure 6.7: **Solar fluxes from solar neutrino experiments.** Fig. 6.7a: determinations of the oscillated fluxes of Boron neutrinos. Fig. 6.7b: unoscillated Boron and Beryllium fluxes, as determined by solar neutrino experiments without using standard solar model (SSM) predictions. Fig. 6.7b also applies to Boron and CNO fluxes. Contours are drawn at 90 and 99% CL (2 dof).

- Solar neutrinos with $E_\nu \gg E_*$ experience dominant and adiabatic solar matter effects that, as discussed in point b. of section 3.3, convert ν_e into ν_2 :

$$P(\nu_e \rightarrow \nu_e, \text{large } E_\nu) \simeq \sin^2 \theta_{\text{sun}}. \quad (6.10)$$

These limiting values of $P(\nu_e \rightarrow \nu_e)$ do not depend on Δm_{sun}^2 nor on the precise density profile of the sun, that instead determine the value of the transition energy E_* .

In view of this situation, present solar data do not precisely determine Δm_{sun}^2 . Nevertheless, it is interesting to point out that global fits of solar data alone, as shown in fig. 6.1, point to a Δm_{sun}^2 range compatible with KamLAND. This happens for the following reasons:

- Smaller values $\Delta m_{\text{sun}}^2 \sim 10^{-5} \text{ eV}^2$ are safely excluded because lead to large earth matter effects (such as day/night asymmetries) not seen by SK nor SNO.
- Larger value of Δm_{sun}^2 are excluded because E_* increases and it becomes impossible to get the SNO value of $P(\nu_e \rightarrow \nu_e)$, smaller than $1/2$ at 5σ .

6.4.4 The solar mixing angle

θ_{sun} is directly determined by SNO measurements of NC and CC solar Boron rates. Assuming flavour conversions among active neutrinos, SNO implies

$$\langle P(\nu_e \rightarrow \nu_e) \rangle \equiv \Phi(\nu_e) / \Phi(\nu_{e,\mu,\tau}) = 0.357 \pm 0.030. \quad (6.11)$$

where the average is performed around energies $E_\nu \sim 10$ MeV. Solar models and SK data provide extra less precise information on $\langle P(\nu_e \rightarrow \nu_e) \rangle$: fig. 6.7a illustrates the consistency of all these determinations.

Eq. (6.11) can be compared with the oscillation prediction for $\langle P(\nu_e \rightarrow \nu_e) \rangle$: at $E_\nu \sim 10$ MeV matter effects are not yet fully dominant, and there is a little deviation from the large-energy limit of eq. (6.10): one has

$$\langle P(\nu_e \rightarrow \nu_e) \rangle \approx 1.15 \sin^2 \theta_{12}. \quad (6.12)$$

Therefore, by combining eq.s (6.11) and (6.12), one infers

$$\tan^2 \theta_{12} = 0.45 \pm 0.05 \quad (6.13)$$

which agrees with the results of the global analysis in table 1.1, both in the central value and in its uncertainty. Notice that the only solar model input that enters our approximate determination of solar oscillation parameters is the solar density around the center of the sun, that controls the 15% correction to $\langle P(\nu_e \rightarrow \nu_e) \rangle$ in eq. (6.13). This correction factor is comparable to the 1σ uncertainty in $\langle P(\nu_e \rightarrow \nu_e) \rangle$: indeed the associated increase of $P(\nu_e \rightarrow \nu_e)$ at smaller E_ν (see fig. 6.3) is not visible in the energy spectra measured by SNO and SK.

6.4.5 Sterile neutrinos?

By adding to the data-set the extra input of the solar model prediction for the total Boron flux Φ_B one can extract from SNO measurements both the solar mixing angle and the parameter η_s (assumed to be energy-independent, and precisely defined by eq. (6.3)) that tells the fraction of solar neutrinos that possibly oscillate into sterile neutrinos. One finds

$$\eta_s \approx \frac{\Phi_B - \Phi_{\nu_{e,\mu,\tau}}}{\Phi_B - \Phi_{\nu_e}} \approx 0 \pm 0.2$$

i.e. data do not suggest extra sterile neutrinos. As discussed in section 13.2, η_s can be dramatically energy-dependent, and the above constraint applies to its value at $E_\nu \sim 10$ MeV Global fits find a somewhat stringent constraint $\eta_s = 0 \pm 0.10$, because to accommodate sterile effects one increases Φ_B and reduces θ_{sun} and this tends to give unseen spectral distortions.

6.4.6 Effects of a small θ_{13} .

The main effect of a non vanishing θ_{13} consists in changing the limiting values achieved by $P(\nu_e \rightarrow \nu_e)$ in the lower-energy regime and in the higher-energy regime as⁴

$$P(\nu_e \rightarrow \nu_e, \text{large } E_\nu) = \sin^4 \theta_{13} + \cos^4 \theta_{13} \sin^2 \theta_{12}, \quad (6.14a)$$

$$P(\nu_e \rightarrow \nu_e, \text{small } E_\nu) = \sum_i |V_{ei}|^4 = \sin^4 \theta_{13} + \cos^4 \theta_{13} \left[1 - \frac{1}{2} \sin^2 2\theta_{12} \right]. \quad (6.14b)$$

This means

$$P(\nu_e \rightarrow \nu_e, \text{small } E_\nu) \leq 1 - 2P(\nu_e \rightarrow \nu_e, \text{large } E_\nu) + 2P(\nu_e \rightarrow \nu_e, \text{large } E_\nu)^2. \quad (6.15)$$

⁴The transition between the two regimes happens at $E_\nu \sim$ few MeV, and the high-energy regime is approached for $E_\nu \gtrsim 20$ MeV.

where the equality applies for $\theta_{13} = 0$: low-energy solar data agree with this oscillation prediction for $P(\nu_e \rightarrow \nu_e, \text{small } E_\nu)$. This quantity is presently dominantly determined by Gallium data and its value can be extracted with a simple approximate argument. Subtracting from the total Gallium rate

$$(68.1 \pm 3.7) \text{ SNU} = R_{\text{Ga}} = R_{pp,pep}^{\text{Ga}} + R_{\text{CNO}}^{\text{Ga}} + R_{7\text{Be}}^{\text{Ga}} + R_{8\text{B}}^{\text{Ga}} \quad (6.16)$$

its ${}^8\text{B}$ contribution (as directly measured by SNO via CC, $R_{8\text{B}}^{\text{Ga}} = 4.3 \pm 1 \text{ SNU}$) and regarding all remaining fluxes as low energy ones, suppressed by $P(\nu_e \rightarrow \nu_e, \text{small } E_\nu)$, determines it to be 0.57 ± 0.03 . Alternatively, by subtracting also the intermediate-energy CNO and Beryllium fluxes, one gets $P(\nu_e \rightarrow \nu_e, \text{small } E_\nu) = 0.58 \pm 0.05$. We here included only the error on the Gallium rate, which is the dominant error. This rough analysis shows that the result only mildly depends on how one deals with intermediate energy neutrinos, and on model-dependent details of the intermediate region, thereby suggesting the following general result:

$$P(\nu_e \rightarrow \nu_e, \text{large } E_\nu) = 0.31 \pm 0.03, \quad P(\nu_e \rightarrow \nu_e, \text{small } E_\nu) = 0.58 \pm 0.04. \quad (6.17)$$

The resulting solar constraint on θ_{13} is weaker than the CHOOZ constraint.

6.4.7 Implications for solar fluxes

The initial goal of solar neutrino experiments that discovered neutrino oscillations was testing models of the sun. This can be done today that oscillations seem sufficiently well understood, and might lead to more unexpected discoveries. We here study how well present solar neutrino data determine solar neutrino fluxes [52, 53]. We recall that the energy spectrum of each single component is safely determined by simple physics, and we want to measure and test their total fluxes. Apparently a detailed global fit of solar neutrino data seems needed to address this issue, but — once again — main results follow from simple considerations:

1. Assuming the absence of short term (million year) variations of the solar energy release, the measured solar luminosity allows us to precisely predict the *pp* flux (directly related to the smaller *pep* flux). Indeed neutrino experiments tell that other fluxes are small enough that they negligibly contribute to the luminosity constraint, that therefore simply fixes the *pp* fluxes to their solar model value.
2. SNO measured the Boron flux.
3. Only two kind of experiments, Gallium and Chlorine, have measured low-energy neutrino fluxes. Therefore, the data constrain only two linear combinations of low-energy fluxes.
4. However, the Chlorine experiment has a poor sensitivity to low energy neutrinos. After subtracting the $\sim 80\%$ Boron contribution to the Chlorine rate, as directly measured by SNO via CC, the residual low-energy contributions to the Chlorine rate is just about 2σ above zero.

Therefore the Chlorine rate carries so little information on low energy fluxes, that our present knowledge on low-energy fluxes is well summarized by a single number: their contribution to the Gallium rate. Starting again from eq. (6.16), we now subtract from the total Gallium rate R_{Ga} its

^8B contribution and its pp , pep contributions (as predicted by solar models and LMA oscillations, see eq. (6.17): $R_{pp,pep}^{\text{Ga}} = 41.3 \pm 1.5$), obtaining

$$(22.5 \pm 4) \text{ SNU} = R_{\text{CNO}}^{\text{Ga}} + R_{^7\text{Be}}^{\text{Ga}} = \frac{4.0\Phi_{^7\text{Be}} + 4.6\Phi_{\text{CNO}}}{10^9/\text{cm}^2\text{s}} \text{ SNU.} \quad (6.18)$$

We have taken into account that, in the standard scenario, oscillations suppress both rates by about 0.55 ± 0.02 — a value negligibly different from the low-energy limit of $P(\nu_e \rightarrow \nu_e)$ of eq. (6.17). Eq. (6.18) means that present data cannot discriminate between Be and CNO, and (supplemented by $\Phi_{^7\text{Be}} > 0$) implies

$$\Phi_{\text{CNO}} < 6 \cdot 10^9/\text{cm}^2\text{s} \quad \text{at } 3\sigma \text{ (1 dof),} \quad (6.19)$$

which is one order of magnitude above solar model predictions. This bound means that the CNO cycle does not give the dominant contribution to the total solar luminosity L_\odot . Indeed by converting the neutrino flux Φ_{CNO} into the corresponding energy flux L_{CNO} , eq. (6.19) reads $L_{\text{CNO}} \lesssim 0.1 L_\odot$.

According to solar models, the oscillated CNO contribution to both the Cl and Ga rate is slightly smaller than the experimental error on these rates: solar neutrino experiments cannot confirm that the CNO cycle exist (other experiments can [52]). Setting the CNO flux to its standard value, eq. (6.18) reduces to $\Phi_{^7\text{Be}} = (4.9 \pm 1.1) \cdot 10^9/\text{cm}^2\text{s}$. This simplified result agrees with the result of a global analysis, shown in fig. 6.7b. The BOREXINO experiment [54] should significantly improve over the present determination of $\Phi_{^7\text{Be}}$.

6.4.8 Global fits

As previously discussed, thanks to SNO and KamLAND, global fits are no longer essential. (Various authors might disagree with this view). Fig. 6.1 shows the result of a global $\nu_e \leftrightarrow \nu_{\mu,\tau}$ oscillation fit of all available solar and reactor data. For completeness, we conclude by summarizing how a generic global fit are performed.

Assuming that the solar anomaly is due to oscillations, one needs to compute neutrino propagation in the sun, in the space and in the earth (for neutrinos arrived during the night), taking into account matter effects in the sun and in the earth, and seasonal effects due to the eccentricity of the earth orbit. One needs to average over the neutrino production point in the sun, as predicted by solar models, using the solar density profile predicted by solar models (and confirmed by helioseismology). Neutrinos produced around the center (on the opposite side) of the sun experience one (two) MSW resonances.

At this point, one can compute the rates measured by the various experiments, taking into account their cross sections, cuts and energy thresholds. To include earth matter effects one must know how much time the sun is seen at each zenith-angle from the sites of the various experiments (there are only minor differences between Homestake, Gran Sasso, Kamioka, Sudbury).

Finally, in order to extract the oscillation parameters from data, one forms a global χ^2 , taking into account the correlated uncertainties on the solar model predictions⁵, on the cross sections,

⁵Solar models predict the unoscillated ν_e fluxes Φ_k as function of 11 uncertain parameters

$$\lambda_i = \{S_{11}, S_{33}, S_{34}, S_{1,14}, S_{17}, \text{luminosity}, Z/X, \text{age}, \text{opacity}, \text{diffusion}, C_{\text{Be}}\}$$

measured to be $\lambda_i = \lambda_{i0}$ with uncorrelated one-sigma errors σ_{λ_i} . We write any quantity x as $x = x_0 + \delta x$, where

and the statistical and systematic experimental errors [55]. While all Gallium experiments can be condensed into a single rate, SK and SNO presented rates binned as function of energy and zenith-angle, forming a total data-set of almost 100 rates. Each predicted rate R can be computed as a function T of oscillation parameters, of solar fluxes Φ , and of various systematic parameters λ (that take into account uncertainties on the Boron energy spectrum, on energy scale, resolution in the solar experiments, . . .). Marginalizing the global

$$\chi_{\text{sun}}^2(\theta, \Delta m^2, \Phi, \lambda) = (R - T) \cdot (\sigma_R^2)^{-1} \cdot (R - T) + \chi_{\Phi}^2(\Phi) + \chi_{\lambda}^2(\lambda) \quad (6.20)$$

with respect to the nuisance parameters Φ and λ in Gaussian approximation (appendix B, eq. (B.8)) gives the $\chi_{\text{sun}}^2(\theta, \Delta m^2)$ plotted in fig. 6.1.

δx represents deviations from the central value x_0 . In Gaussian approximation solar model predictions can be written as $\Phi_k(\lambda) \simeq \Phi_{0k}(1 + M_{\Phi ki} \delta \lambda_i / \lambda_i)$ i.e. $\delta \ln \Phi = M_{\Phi} \cdot \delta \ln \lambda$. The numerical values of the central values and logarithmic shift coefficients M_{Φ} can be found in the literature [55]. As discussed in appendix B, eq. (B.8), the resulting matrix of correlated uncertainties on solar fluxes is

$$\sigma_{\Phi}^2 = \frac{1}{\Phi_0^T} \cdot M_{\Phi} \cdot \text{diag} \left(\frac{\sigma_{\lambda_i}^2}{\lambda_i^2} \right) \cdot M_{\Phi}^T \cdot \frac{1}{\Phi_0} \quad \text{so that} \quad \chi_{\Phi}^2(\Phi) = (\Phi - \Phi_0)^T \cdot (\sigma_{\Phi}^2)^{-1} \cdot (\Phi - \Phi_0).$$

For the purpose of fitting present data, this procedure mainly corrects the uncorrelated uncertainties of table 6.1 adding a strong correlation between N and O fluxes and some correlation with Be and B fluxes.

Chapter 7

Future oscillation experiments

7.1 The global oscillation picture?

We have discussed the established solar and atmospheric neutrino anomalies. Few other anomalies, discussed in section 9, could be confirmed or refuted by future experiments. For the moment we ignore them and discuss how the solar and atmospheric data can be jointly explained in terms of oscillations between the three SM neutrinos. The Δm^2 responsible of the atmospheric anomaly is larger than the one responsible of the solar anomaly. Therefore we identify (see fig. 2.3)

$$|\Delta m_{13}^2| \approx |\Delta m_{23}^2| = \Delta m_{\text{atm}}^2 \approx (2.5 \pm 0.2) 10^{-3} \text{ eV}^2, \quad \Delta m_{12}^2 = \Delta m_{\text{sun}}^2 \approx (8.0 \pm 0.3) 10^{-5} \text{ eV}^2.$$

A positive Δm_{23}^2 means that the neutrinos separated by the atmospheric mass splitting are heavier than those separated by the solar mass splitting (fig. 2.3a): this is usually named ‘normal hierarchy’. At the moment this cannot be distinguished from the opposite case (fig. 2.3b) usually named ‘inverted hierarchy’. As their names indicate, the ‘normal’ case is considered more plausible than the ‘inverted’ one.

As explained in section 2, the neutrino mixing matrix contains 3 mixing angles: two of them (θ_{23} and θ_{13}) produce oscillations at the larger atmospheric frequency, one of them (θ_{12}) gives rise to oscillations at the smaller solar frequency. Solar data want a large mixing angle. The CHOOZ constraint tells that ν_e are can only be slightly involved in atmospheric oscillations, and SK finds that atmospheric data can be explained by $\nu_\mu \rightarrow \nu_\tau$ oscillations with large mixing angle. These considerations single out the global solution

$$\theta_{23} = \theta_{\text{atm}} \sim 45^\circ \quad \theta_{12} = \theta_{\text{sun}} \sim 30^\circ, \quad \theta_{13} \lesssim 10^\circ, \quad \phi = \text{unknown}$$

more quantitatively summarized in table 1.1. Nothing is known on the CP-violating phase ϕ . If $\theta_{13} = 0$ the solar and atmospheric anomalies depend on different set of parameters; there is no interplay between them. A $\theta_{13} \neq 0$ would affect both solar and atmospheric data. Both data provide some upper bound on θ_{13} , preferring $\theta_{13} = 0$. The strongest bound on θ_{13} is directly provided by the CHOOZ experiment. In conclusion, all pieces of data point in the same direction, and, up to small corrections, can be analyzed without performing a 3 neutrino analysis. Present data can be interpreted in terms of oscillations among the three SM neutrinos with the oscillation parameters in table 1.1 (page 4). The corresponding neutrino mixing matrix is

$$|V| = \begin{pmatrix} \nu_1 & \nu_2 & \nu_3 \\ \nu_e & 0.84 \pm 0.01 & 0.54 \pm 0.02 & 0.05 \pm 0.05 \\ \nu_\mu & 0.38 \pm 0.06 & 0.60 \pm 0.06 & 0.70 \pm 0.06 \\ \nu_\tau & 0.38 \pm 0.06 & 0.60 \pm 0.06 & 0.70 \pm 0.06 \end{pmatrix} \quad (7.1)$$

as pictorially represented in fig. 2.3.

7.2 Known unknowns

We here *assume* that oscillations between the 3 SM neutrinos are the true global picture. Furthermore we assume that neutrino masses are of Majorana type. While plausible, this is only an assumption to be tested by future experiments, that could discover something more, or something different. If our assumption is true, the goal of future experiments is the reconstruction of the neutrino Majorana mass matrix: as discussed in subsection 2.4 we have to measure 9 real parameters: 3 mass eigenvalues, 3 mixing angles and 3 CP-phases. Two 2 squared mass differences and 2 mixing angles are already partially known. The main steps of this program are:

1. Establishing that both the solar and atmospheric anomalies are really due to oscillations.
2. Measuring better and better the solar and atmospheric parameters. Discovering eventual deviations of θ_{23} from maximal mixing is an important but difficult issue. It is important because maximal mixing could be the result of a new symmetry. It is difficult because dominant $\nu_\mu \leftrightarrow \nu_\tau$ oscillations are controlled by $\sin^2 2\theta_{23} = 1 + 0\epsilon - 4\epsilon^2 + \dots$ where $\epsilon = \theta_{23} - \pi/4$. For example $\sin^2(2 \cdot 40^\circ) \approx 0.97$. Order ϵ corrections do not vanish in subdominant oscillations induced by Δm_{12}^2 or θ_{13} , see eq. (3.14).
3. **Discovering the last mixing angle**, θ_{13} that induces $\nu_\mu \leftrightarrow \nu_e$ oscillations at the atmospheric frequency.

If a non zero θ_{13} will be discovered...

4. Oscillations in matter allow to discriminate **the sign of Δm_{23}^2** (i.e. if the atmospheric anomaly is due to the lightest or heaviest neutrinos, see fig. 2.3). If $\Delta m_{23}^2 > 0$ (normal hierarchy) matter effects enhance $\nu_\mu \leftrightarrow \nu_e$ oscillations and suppress $\bar{\nu}_\mu \leftrightarrow \bar{\nu}_e$, while the opposite happens if $\Delta m_{23}^2 < 0$ (inverted hierarchy).
5. The **sign of $\theta_{23} - 45^\circ$** (which tells whether the neutrino state with mass m_3 contains more ν_τ or more ν_μ) can be measured from atmospheric oscillations by measuring e.g.

$$P(\nu_e \rightarrow \nu_e) = 1 - \sin^2 2\theta_{13} \sin^2 \frac{\Delta m_{23}^2 L}{4E_\nu} \quad \text{and} \quad P(\nu_\mu \rightarrow \nu_e) = \sin^2 \theta_{23} \cdot [1 - P(\nu_e \rightarrow \nu_e)]$$

Note that ν_μ disappearance experiments alone cannot distinguish θ_{23} from $90^\circ - \theta_{23}$, and that the present bound $\sin^2 2\theta_{23} \gtrsim 0.95$ allows the relatively loose range $1/3 \lesssim \sin^2 \theta_{23} \lesssim 2/3$.

Notice that, in line of principle, issues 4. and 5. are meaningful even if $\theta_{13} = 0$, in view of the presence of the small solar splitting: both θ_{13} and Δm_{12}^2 produce $\nu_\mu \leftrightarrow \nu_e$ oscillations. However in practice Δm_{12}^2 is so small that planned experiments can answer these issues only if θ_{13} is large enough. The following oscillation issue needs $\theta_{13} \neq 0$ both in practice and in principle:

6. The **CP-violating phase** ϕ can be measured in realistic long-baseline oscillation experiments.

As discussed at page 28, oscillation experiments cannot access the whole neutrino mass matrix and cannot tell if neutrinos have Majorana or Dirac masses. Oscillations are sensitive to squared neutrino mass differences, but not to the overall scale of neutrino masses. We have measured the charged lepton Dirac masses m_e , m_μ , m_τ . It would be unsatisfactory if instead we knew only the values of $m_\tau^2 - m_\mu^2$ and $m_\mu^2 - m_e^2$. In the Dirac case oscillation experiments miss only the overall neutrino mass scale. In the Majorana case they also miss two CP-violating phases, α and β .

7. In order to access to non oscillation parameters we need non oscillation experiments (section 8). Furthermore, neutrino-less-double-beta decay and cosmology are other realistic ways of clarifying the issue 4 (normal or inverted hierarchy?).

7.3 Atmospheric experiments

There are two possible directions for future improvements: bigger detectors, better detectors.

Muons are contained in a bigger detector up to higher energies. The ICECUBE detector [56] achieves a large km^3 volume at the price of a poor photo-multiplier granularity, such that it can only study atmospheric $\langle \bar{\nu}_\mu \rangle$ at high energy, $E_\nu \circ > \text{TeV}$, where atmospheric oscillations give small effects. It can collect about 80000 atmospheric events per year. A Mton-scale detector [57] (motivated by many other considerations) could repeat the atmospheric measurements performed by SK with much more statistics.

One possible goal is the search for sub-leading $\mu \leftrightarrow e$ transitions. In the standard oscillation scenario they can be generated by the θ_{13} mixing angle and by solar oscillations. In view of the different Δm^2 , solar oscillations dominantly affect the sub-GeV e -like angular rate and atmospheric θ_{13} oscillations would be most clearly seen in the multi-GeV e -like angular rate. However the impact of $\mu \leftrightarrow e$ transitions gets suppressed by a ‘screening factor’ $r(\cos^2 \theta_{\text{atm}} - 1)$, where r is the ratio between the unoscillated $\langle \bar{\nu}_\mu \rangle$ and $\langle \bar{\nu}_e \rangle$ atmospheric fluxes. At sub-GeV energies $r \approx 2$: if the atmospheric mixing angle is maximal the initial flavour ratio $\langle \bar{\nu}_e \rangle : \langle \bar{\nu}_\mu \rangle : \langle \bar{\nu}_\tau \rangle = 1 : 2 : 0$ gets converted by atmospheric oscillations into the flavour-blind ratio $\langle \bar{\nu}_e \rangle : \langle \bar{\nu}_\mu \rangle : \langle \bar{\nu}_\tau \rangle = 1 : 1 : 1$, that is not affected by further $\mu \leftrightarrow e$ transitions. This explains the origin of the ‘screening factor’: unless θ_{atm} is significantly non-maximal, atmospheric experiments are a poor probe of $\mu \leftrightarrow e$ transitions.

Alternatively, one can build a smaller (30 kton?) magnetized detector capable of distinguishing neutrinos from anti-neutrinos [58]. This detector could reconstruct the L/E of atmospheric (anti)neutrinos a few times better than SK, allowing to see the first ≈ 2 atmospheric oscillations. Furthermore, if θ_{13} is as large as possible, cleanly observing the oscillation pattern would help in determining the neutrino mass hierarchy.

7.4 Solar experiments

The main goals of future solar neutrino experiments seem [59]: 1) detecting some small effect characteristic of oscillations; 2) measuring better and better the oscillation parameters; 3) testing solar model predictions; 4) constraining and eventually discovering unexpected effects. Taking into account LMA predictions and experimental capabilities, concrete progress seem possible on the following points.

- LMA predicts that earth matter effects give a few % total **day/night asymmetry**, with a characteristic energy and zenith-angle dependence. For example, fig. 7.1 shows the expected

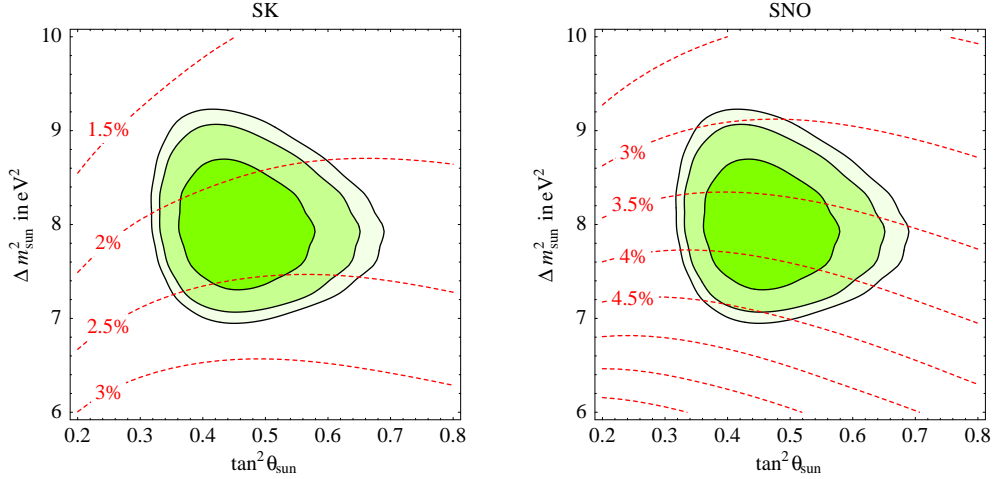


Figure 7.1: *Iso-contours of the expected day/night asymmetry in the total rate of solar neutrinos as measured via ES scatterings at SK and by CC scatterings at SNO. The green area is the best-fit region at 90, 99, 99.73% CL.*

day/night asymmetry in the total ES rate at SK and in the total CC rate at SNO. SK and SNO data show a 1σ hint for this effect, see eq. (6.4) and (6.7). Large neutrino energy and large statistics is needed to see it: these conditions could be realized by a future SK-like WC experiment with a Mton of water [57].

- No **other time variation** of solar neutrino fluxes is expected. Beryllium neutrinos, being almost monochromatic, are a much more sensitive probe than Boron neutrinos of effects, like seasonal variations, that depend on neutrino energy. The Borexino experiment (and maybe KamLAND) should measure the Beryllium flux with significant statistics. If an effect will be seen, it could be explained by invoking new physics, such as sterile neutrinos.
- LMA predicts that at lower energy the ν_e survival probability P_{ee} increases reaching

$$P_{ee} \simeq 1 - \frac{1}{2} \sin^2 2\theta_{\text{sun}} = 0.59 \pm 0.02 \quad \text{at } E_\nu \ll E_* \quad (7.2)$$

(where $E_* \sim 4$ MeV, see eq. (6.8)). Gallium experiments have seen this effect: global fits disfavor a fully energy-independent P_{ee} .

It is difficult to measure P_{ee} around $E_\nu \sim E_*$ because there are few solar neutrinos with these energies. Borexino should give another test of this effect at relatively low neutrino energy. In the future it might be possible to measure the spectrum of sub-MeV pp neutrinos. Since solar models can predict their flux with 1% uncertainty could be used for a **precise measurement of θ_{sun}** .

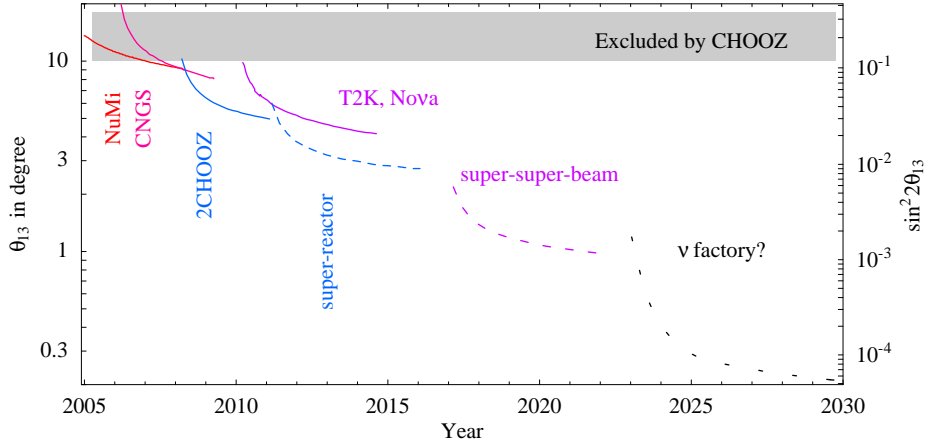


Figure 7.2: *Sensitivity to θ_{13} of planned (continuous lines) and possible (dashed lines) future experiments.*

7.5 Reactor experiments

Improved reactor experiments [45] are being planned with the main goal of searching for θ_{13} , that gives $\bar{\nu}_e$ disappearance effects well described by

$$P(\bar{\nu}_e \rightarrow \bar{\nu}_e) \simeq 1 - \sin^2 2\theta_{13} \sin^2 \frac{\Delta m_{13}^2 L}{4E_\nu}. \quad (7.3)$$

We can here neglect solar oscillations and earth matter effects. Sterile neutrinos could produce extra disappearance effects.

Several projects have been proposed [45], all based on the same concept: one near detector (needed in order to reduce systematic errors) and one far detector located at distance $L \approx (1 \div 2)$ km, in order to sit around the atmospheric oscillation dip. The statistical error then depends on the size of the far detector times the power of the nuclear reactor. Reducing systematic errors down to the 0.5% level is considered feasible by the proponents of these projects. If this goal will be achieved, the DOUBLECHOOZ proposal will provide an increase in the sensitivity to θ_{13} , illustrated in fig. 7.2, ‘cheaper and faster’ than the long-baseline experiments discussed in the next sections. On longer time-scales the KASKA and BRAIDWOOD proposals are considered as possible ‘ultimate’ reactor experiments, with costs of about 50 M€.

Future reactor experiments can also study other issues. If a θ_{13} signal is seen, a reactor experiment can measure $|\Delta m_{13}^2|$, while long-baseline ν_μ -beam experiments are dominantly sensitive to $|\Delta m_{23}^2|$: measuring both Δm^2 with uncertainty smaller than Δm_{sun}^2 would allow to discriminate direct from inverted neutrino mass hierarchy. Other techniques can achieve this goal in more realistic ways. Concerning the solar mixing angle θ_{12} , an improved KamLAND-like reactor experiment with base-line of about 50 km could measure it with 1σ accuracy comparable to future solar experiments.

7.6 Conventional neutrino beams

Neutrino beam experiments are considered the main next step of oscillation studies. K2K (in Japan), NUMI (in USA) and CNGS (in Europe) are the first long-baseline experiments. Table 7.1

Experiment	from	to	baseline	beam	ν energy in GeV	off-axis	start
K2K [6]	KEK	Kamioka	250 km	ν_μ	$\sim (0.5 \div 2)$	0	1999
NUMI [7]	FermiLab	Soudan	735 km	ν_μ	$\sim (2 \div 10)$	0	2005
CNGS [60]	CERN	Gran Sasso	730 km	ν_μ	$\sim (5 \div 30)$	0	2006
T2K [61]	JPARC	Kamioka	295 km	$\langle \bar{\nu} \rangle_\mu$	$\approx (0.3 \div 1.3)$	2°	2008
NO ν A [62]	FermiLab	Ash river	810 km	$\langle \bar{\nu} \rangle_\mu$	$\approx (1 \div 3)$	0.8°	2010
SPL [63]	CERN	Frejus	130 km	$\langle \bar{\nu} \rangle_\mu$	$\approx (0.1 \div 0.5)$?	?

Table 7.1: *Main characteristics of long-base-line conventional neutrino beams.*

summarizes their main properties. They all employ a ν_μ beam (preferred, at least initially, to a $\bar{\nu}_\mu$ beam because ν_μ detection cross sections are about two times higher) produced using the ‘conventional’ technique. A proton beam with energy $E_p \sim 20E_\nu$ is sent on a target; mesons with positive or negative charge are focused by magnetic horns; the decays of the resulting charged pions and Kaons produce the neutrino beam. Using positively charged mesons one gets a ν_μ beam, typically polluted by a few % of $\bar{\nu}_\mu$, $\sim 1\%$ of ν_e and a few per mille of $\bar{\nu}_e$.

It is difficult to discuss the rôle of these experiments, that had been planned when SK started, with the goals of confirming the atmospheric anomaly and exploring its main properties. SK already provided first answers to these issues, and future experiments are now being planned with new goals.

The K2K experiment [6] (already performed and discussed in section 5.5) indeed confirmed the atmospheric anomaly, finding a result consistent with its oscillation interpretation, and shown how accurately neutrino beam experiments could measure Δm_{atm}^2 , if sufficient statistics is accumulated. A measurement of Δm_{atm}^2 with 10% accuracy should be performed by the NUMI project [7] (already stated and discussed in section 5.6). K2K and NUMI have chosen the neutrino energy which allows to maximize the oscillation effect.

On the contrary, the CNGS project [60] employs a higher E_ν (at the price of a lower oscillation probability), somewhat above the $\nu_\tau \rightarrow \tau$ production threshold, with the goal of directly confirming the $\nu_\mu \rightarrow \nu_\tau$ character of atmospheric oscillations by detecting a few τ appearance events. The experimental signal of a ν_τ is a ‘kink’ i.e. two vertices separated by a distance comparable to $\tau_\tau = 0.086$ mm (long-lived particles like K and π produce a background), that could be directly seen with a fine-grained emulsion detector. In practice the detector OPERA is built by alternating emulsion with some cheaper material (lead), that constitutes most of the detector mass, such that in most events one infers the presence of two separated vertices from the observed tracks. In other detectors, one can select a class of τ -like events by appropriate cuts (‘statistical analysis’) analogously to what SK did for atmospheric neutrinos.

A long-baseline neutrino beam also allows to test if ν_μ travel at the speed of the light within $2 \cdot 10^{-6}$ accuracy, improving by a factor 20 on the previous constraint. However SN1987A data already constrain the $\bar{\nu}_e$ velocity with $2 \cdot 10^{-9}$ accuracy (at the light of oscillations this constraint should now be reinterpreted in terms of $\bar{\nu}_{1,2,3}$ velocities).

Discovering θ_{13} is today considered the main goal of future experiments. These first long-baseline beam projects can moderately improve on the present bound, as shown in fig. 7.2. However, these experiments cannot discriminate the neutrino mass hierarchy, and are not sensitive to CP-violation in neutrino oscillations. Therefore, an approximation for the $\nu_\mu \rightarrow \nu_e$ oscillation

probability enough accurate for these experiments can be obtained by neglecting the solar mass splitting in the vacuum oscillation formula of (3.14a), and by improving it taking into account that earth matter effects dominantly affect the frequency of $\nu_\mu \rightarrow \nu_e$ oscillations:

$$P(\nu_\mu \rightarrow \nu_e) \simeq \sin^2 2\theta_{13} \sin^2 \theta_{23} \frac{\sin^2((1-r)\delta)}{(1-r)^2}, \quad (7.4)$$

where $\delta = \Delta m_{13}^2 L / 4E_\nu$ is the atmospheric oscillation phase in vacuum and

$$r \equiv \frac{2\sqrt{2}G_F N_e E_\nu}{\Delta m_{13}^2} = \frac{N_e}{1.3 N_A / \text{cm}^3} \frac{E_\nu}{10 \text{ GeV}} \frac{2 \cdot 10^{-3} \text{ eV}^2}{\Delta m_{13}^2} \quad (7.5)$$

is an adimensional ratio that controls the relative importance of matter effects. Notice that $\Delta m_{13}^2 \equiv m_3^2 - m_1^2$, so that $\delta, r > 0$ ($\delta, r < 0$) if neutrinos have (normal) inverted mass hierarchy. $P(\bar{\nu}_\mu \rightarrow \bar{\nu}_e)$ is obtained from (7.4) by replacing $r \rightarrow -r$.

The goal of oscillation studies is not only θ_{13} but also determining the type of neutrino mass hierarchy, and possibly discovering CP-violation. To reach these extra goals, studying both ν_μ and $\bar{\nu}_\mu$ beams is essential. We now give an explicit approximate expression for the oscillation probability, and later discuss the experiments planned to address all these issues.

7.6.1 Approximating the oscillation probability

In all planned beam experiments neutrinos travel through a matter density which is constant to a good approximation: the maximal depth z reached by a beam with path-length L much smaller than the earth radius r_E is $z \simeq L^2/8r_E^2 \sim 20 \text{ km} (L/1000 \text{ km})^2$. The oscillation probabilities can be easily found by numerically computing the exponential of the 3×3 matrix H given in eq. (3.16): $P(\nu_i \rightarrow \nu_f) = \exp(-iLH)_{fi}$. One can derive a more explicit analytical approximation by splitting $H = H_0 + H_1$ where H_0 contains all ‘large’ effects: ($\theta_{\text{atm}}, \Delta m_{\text{atm}}^2$ in the μ/τ sector and earth matter effects) and H_1 contains the remaining ‘small’ effects (θ_{13} and solar oscillations). The formula

$$e^{-iL(H_0+H_1)} = e^{-iLH_0} + \int_0^1 dx e^{-iL(1-x)H_0} \cdot (-iLH_1) \cdot e^{-iLxH_0} + \mathcal{O}(H_1^2)$$

then allows to expand the survival probabilities in the small parameters

$$\varepsilon \equiv \Delta m_{12}^2 / \Delta m_{13}^2 \approx \pm 0.04 \quad \text{and} \quad \varepsilon' \equiv \sin 2\theta_{13} \lesssim 0.2.$$

The matrix H_0 is immediately exponentiated, because matter effects are diagonal in the μ/τ sector, and does not generate $(\bar{\nu})_e \leftrightarrow (\bar{\nu})_\mu$ oscillations. These oscillations are generated at first order by H_1 as

$$P(\nu_\mu \rightarrow \nu_e) \simeq \left| \varepsilon e^{i\phi} \cos \theta_{23} \sin 2\theta_{12} \frac{e^{-2ir\delta} - 1}{2r} + \varepsilon' \sin \theta_{23} \frac{e^{-2ir\delta} - e^{-2i\delta}}{2(1-r)} \right|^2. \quad (7.6)$$

where δ (the atmospheric oscillation phase in vacuum) and r (that controls matter effects) are defined in (7.5). In the limit $L \rightarrow 0$ eq. (7.6) reduces to the expected $P(\nu_e \rightarrow \nu_\mu) \simeq |H_{e\mu}|^2$. Converting the exponentials to trigonometrical functions gives

$$\begin{aligned} P(\nu_\mu \rightarrow \nu_e) \simeq & \varepsilon^2 \sin^2 2\theta_{12} \cos^2 \theta_{23} \frac{\sin^2(r\delta)}{r^2} + \varepsilon'^2 \sin^2 \theta_{23} \frac{\sin^2((1-r)\delta)}{(1-r)^2} + \\ & + \varepsilon \varepsilon' \sin(2\theta_{12}) \sin(2\theta_{23}) \frac{\sin(r\delta) \sin((1-r)\delta)}{r(1-r)} \cos(\delta + \phi) \end{aligned} \quad (7.7)$$

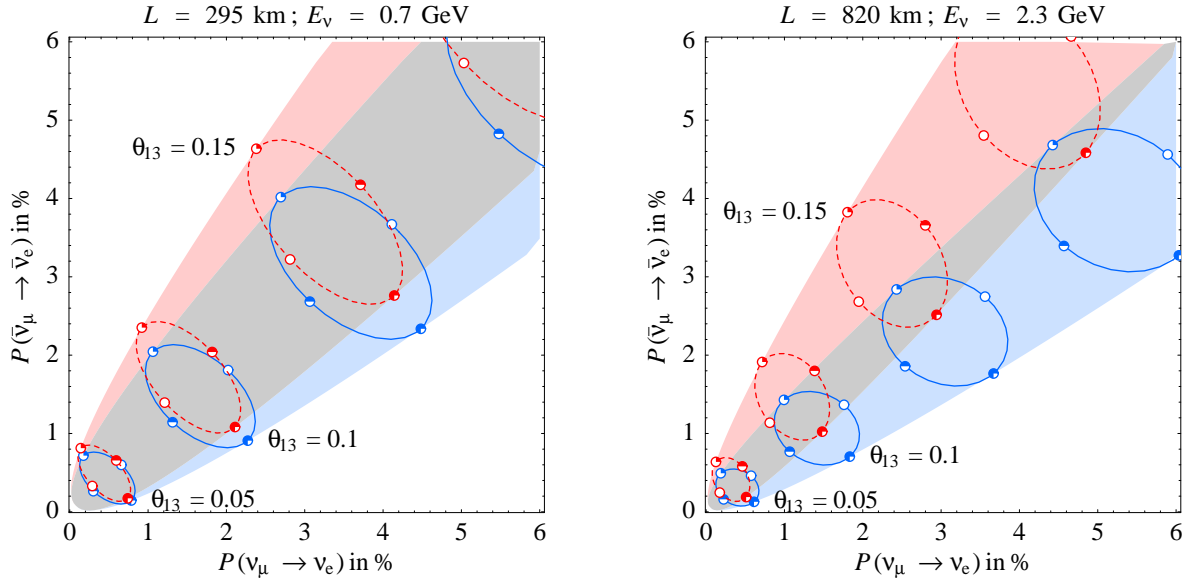


Figure 7.3: $\langle \bar{\nu} \rangle_\mu \rightarrow \langle \bar{\nu} \rangle_e$ oscillation probabilities for the present best-fit values of $|\Delta m_{13}^2|$, Δm_{12}^2 , θ_{12} , θ_{23} , for $\theta_{13} = \{0.05, 0.1, 0.15, 0.2\}$, $N_e = 1.5 \text{ moles/cm}^3$, and varying the CP-phase ϕ . The points correspond to $\phi = 0$ (empty circles), $\pi/2$ (1/4 filled circles), π (half filled circles), $3\pi/4$ (3/4 filled circles). The continuous blue (red dashed) lines correspond to normal (inverted) mass hierarchy. The left (right) plot shows a T2K-like (NO ν A-like) configuration.

$P(\bar{\nu}_\mu \rightarrow \bar{\nu}_e)$ is obtained by substituting $r \rightarrow -r$ in eq. (7.7). $P(\nu_e \rightarrow \nu_\mu)$ is obtained by substituting $\delta \rightarrow -\delta$. $P(\bar{\nu}_e \rightarrow \bar{\nu}_\mu)$ is obtained by substituting $\delta \rightarrow -\delta$ and $r \rightarrow -r$.

The above expressions confirm that, since the earth is not CP symmetric, matter effects create a fake CP asymmetry: $(P(\nu_e \rightarrow \nu_\mu) \neq P(\bar{\nu}_e \rightarrow \bar{\nu}_\mu))$ even if $\phi = 0$) and show that they do not create a fake T asymmetry ($P(\nu_e \rightarrow \nu_\mu) = P(\nu_\mu \rightarrow \nu_e)$ if $\phi = 0$). This happens because we here assumed a constant matter density: in general the matter density profile gets reversed creating also a fake T asymmetry. Experiments performed only with $(\bar{\nu})_\mu$ beams must subtract the fake CP asymmetry, but this is not a problem as earth matter effects are well known. Detailed experiment-dependent matter profiles can be obtained with the collaboration of geologists.

At least two measurements are necessary to reconstruct θ_{13} , ϕ and the neutrino mass hierarchy [64]. In fig. 7.3 we show how the two measurable $\nu_\mu \rightarrow \nu_e$ and $\bar{\nu}_\mu \rightarrow \bar{\nu}_e$ oscillation probabilities (computed for T2K-like and NO ν A-like choices of the neutrino path-length and energy) depend on θ_{13} and ϕ . In agreement with the approximate formula of eq. (7.7), varying ϕ at fixed θ_{13} approximatively give ellipses. Ellipses corresponding to normal mass hierarchy are partially shifted from ellipses corresponding to inverted mass hierarchy, because of earth matter effects. We see how the amount of overlap depends on θ_{13} and is smaller in the NO ν A-like configuration than in the T2K-like configuration. This means that, depending on the values of ϕ and of θ_{13} , a measurement of these two oscillation probabilities could be or could be not able of univocally determining θ_{13} and ϕ and the neutrino mass hierarchy. Having two different experimental configurations helps in measuring oscillation parameters without discrete ambiguities. Building one T2K detector in Korea (at $L \sim 1000$ km) would help even more.

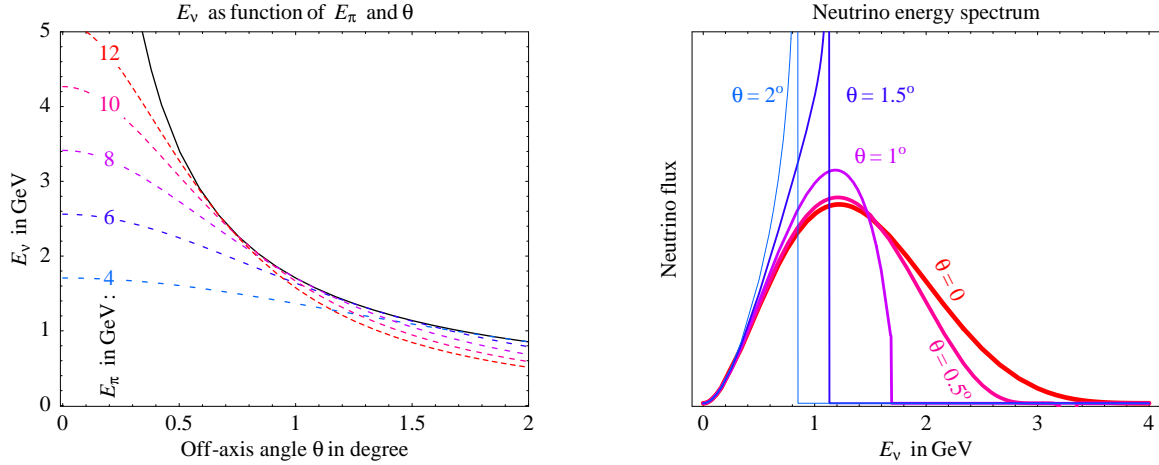


Figure 7.4: Fig. 7.4a: E_ν produced at angle θ with respect to the π momentum by the decay of a π with energy E_π . The continuous line shows the maximal E_ν . Fig. 7.4b: neutrino energy spectrum produced by π decays with a typical energy distribution as seen off-axis by an angle θ .

Many papers tried to discuss which configuration is the optimal one, but the result depends on the unknown parameters we would like to discover. Therefore experiments will likely be performed at baselines reasonably fixed by geopolitical considerations and with a beam energy chosen such that the atmospheric phase is large.

7.6.2 Off-axis super-beams

Improved experiments, still based on ‘conventional’ $\bar{\nu}_\mu$ beams, can make significant progress towards clarifying the known unknowns of neutrino oscillations. There are two projects in this direction: T2K [61] and NO ν A [62].

First of all, present experiments can be improved by building i.) more intense beams; ii.) bigger detectors. Although the figure of merit of a neutrino beam experiment is proportional to

$$(\text{intensity of the source}) \times (\text{size of the detector})$$

each one of the two factors is separately relevant for other experiments, such that one has to find the best distribution of resources for a whole set of experiments:

- i.) The factor that presently limits the beam intensity is the target used to convert protons into mesons, since it gets destroyed by a too intense proton beam. It seems possible to build proton drivers that can work up to a few MWatt power. An intense proton driver also produces muons and other particles, allowing to perform several ‘high intensity’ experiments other than neutrino oscillation studies: searches for rare or forbidden processes (e.g. $\mu \rightarrow e$ conversion, μ -EDM, etc.) and maybe for dark matter [65].
- ii.) It seems possible to build a Mton-scale neutrino detector [57]. A neutrino beam can be pulsed, allowing to relax the background requirements. However, suppressing the backgrounds would greatly increase the scientific interest of the project, allowing high-statistics

studies of solar neutrinos, atmospheric neutrinos supernova neutrinos and to search for proton decay.

The T2K project could hopefully culminate in having a Mton ‘HyperKamiokande’ WČ and a beam generated by a 4MW proton driver. Around this point systematic errors start to dominate over statistical errors, and further improvements would need new techniques, as discussed in the next sections. The NO ν A project can be competitive with T2K on the θ_{13} issue, but the detector will not be underground and can therefore be used almost only for the neutrino beam experiment.

Another improvement employed by both T2K and NO ν A consists in putting the detector off-axis (with respect to the center of the neutrino beam): in this way the neutrino beam acquires interesting features that make it more apt for oscillation studies (more restricted energy) and in particular for $\nu_\mu \rightarrow \nu_e$ searches (reduced ν_e contamination). To see this, we recall that the decaying pions have spin 0: therefore in their Center of Mass (CM) frame $\pi \rightarrow \mu\nu_\mu$ decays produce an isotropic distribution of ν_μ with fixed energy $E_\nu^{\text{CM}} = (m_\pi^2 - m_\mu^2)/2m_\pi \approx 30$ MeV. Then kinematics allows to compute the energy of neutrinos emitted with angle θ with respect to the momentum of π with energy $E_\pi \gg m_\pi$:

$$E_\nu = \frac{2E_\nu^{\text{CM}} E_\pi m_\pi}{m_\pi^2 + E_\pi^2 \tan^2 \theta}. \quad (7.8)$$

This function is plotted in fig. 7.4a: the upper bound $E_\nu < E_\nu^{\text{CM}} / \tan \theta$ (continuous line) is the most notable feature, that can be understood as

$$E_\nu \simeq p_\nu^\perp = \frac{p_\nu^\perp}{\tan \theta} = \frac{E_\nu^{\text{CM}} \sin \theta^{\text{CM}}}{\tan \theta} \leq \frac{E_\nu^{\text{CM}}}{\tan \theta}. \quad (7.9)$$

Therefore neutrinos emitted off-axis have a maximal energy E_{max} , and actually the off-axis neutrino beam has a more narrow energy distribution peaked just below this maximal energy. Fig. 7.4 shows sample energy spectra for a few off-axis angles, computed assuming a π beam with a typical energy distribution, $dN/dE_\pi \propto (1 - E_\pi/E_p)^5$ where $E_p = 10$ GeV is the energy of the proton beam used to produce π . (Full MonteCarlo computations take into account other mesons, and the spread in the meson directions). We see that going off-axis the flux decreases at higher energy and increases at lower energy. These features help oscillation experiments, because neutrinos of higher energy have higher cross-sections and lower oscillation probabilities. The narrower energy spectrum helps in avoiding that detailed oscillation features (such as CP-violation) get suppressed by the average over the energy spread.

Furthermore, going off-axis and selecting events with energy around the peak allows to reduce the ν_e background contamination of the beam from about 1% to about 0.2%, see e.g. section 3 of the JHF project [61]. Indeed this background is generated by two sources: by $K \rightarrow \pi e \bar{\nu}$ and by $\pi \rightarrow \mu \rightarrow \nu_e$ decays. and the first source becomes less relevant at the energy where π decays accumulate.

A different possible set-up sensitive to CP violation consists in sending a on-axis broad-band $\langle \bar{\nu}_\mu \rangle$ beam with $E_\nu \sim (1 \div 5)$ GeV to a big (\sim Mton) WČ detector located at distance $L \sim 2000$ km, able of measuring the energy of quasi-elastic events with 10% accuracy.

7.7 Neutrino factory

Technologies for producing a muon beam had been initially explored with the purpose of building a muon collider with TeV-scale energy. This seems impossible because muon decays would pro-

duce TeV-scale neutrinos with cross sections low enough that they cannot be shielded, but high enough to give unacceptable radiation hazards. Reducing the muon energy down to $E_\mu \sim 10$ GeV simplifies the technology, and muon decays can be used to obtain a neutrino beam. This machine, called ‘neutrino factory’ [66], is considered as feasible, on long time-scales (after 2020?) and probably with G€-scale costs.

The neutrino-factory beam is produced by circulating μ^- or μ^+ beams with energy E_μ in accumulators with km-scale straight sections. Conventional neutrino beams from π^- (or π^+) decays are dominantly composed by $\bar{\nu}_\mu$ (or ν_μ). On the contrary, a neutrino beam produced by decays of μ^- (or μ^+) consists of $\nu_\mu + \bar{\nu}_e$ (or $\bar{\nu}_\mu + \nu_e$). This makes easier to build big detectors dedicated to studies of $(\bar{\nu}_\mu \leftrightarrow \bar{\nu}_e)$ oscillations: with a conventional neutrino beam their signature is e^\pm appearance; with a neutrino factory beam their best signature becomes ‘wrong-sign’ μ^\pm appearance: e.g. μ^+ decays produce $\bar{\nu}_\mu$ (detected as μ^+) and ν_e (detected as e^-), that can oscillate into ν_μ (detected as μ^-). Big detectors with poor granularity are more sensitive to muons than to electrons, because muons have a much longer range in matter.

The energy and flavour spectra of a ν -factory beam is easily and accurately computed using the known formulæ that describe $\mu \rightarrow e\bar{\nu}_e\bar{\nu}_\mu$ decays. The resulting flux would be known at per-mille level. E.g. N_μ decays of unpolarized beamed μ^+ with energy $E_\mu \gg m_\mu$, produce the following neutrino fluxes along the beam axis and at distance L from the decay region:

$$\frac{dN_{\bar{\nu}_\mu}}{dx \, dS} = \frac{N_{\mu^+}}{\pi L^2} \left(\frac{E_\mu}{m_\mu} \right)^2 \cdot 2x^2(3 - 2x), \quad \frac{dN_{\nu_e}}{dx \, dS} = \frac{N_\mu}{\pi L^2} \left(\frac{E_\mu}{m_\mu} \right)^2 \cdot 12x^2(1 - x) \quad (7.10)$$

where $x = E_\nu/E_\mu$. These are wide-band spectra with average energies $\langle E_{\nu_\mu} \rangle = 7E_\mu/10$ and $\langle E_{\bar{\nu}_e} \rangle = 3E_\mu/5$. N_μ could be as high as 10^{21} per year. The flux increases with E_μ^2 because more energetic muons produce a more narrow neutrino beam, with opening angle $\theta \sim m_\mu/E_\mu$.

The following channels seem more promising:

1. ‘Golden channel’. $\nu_e \rightarrow \nu_\mu$ oscillations are signaled by μ^- appearance, best seen by WČ detectors or tracking calorimeters. Parameterizing the oscillation probability as $P(\nu_e \rightarrow \nu_\mu) \approx |\Delta m_{\text{eff}}^2(L, E) \cdot L/2E_\nu|^2$ the number of μ^- events is

$$N_{\mu^-} \approx \frac{N_{\mu^+} N_{\text{kt}} \epsilon}{10^{21}} \frac{E_\mu}{70 \text{ GeV}} \left| \frac{\Delta_{e\mu}^{\text{eff}}}{10^{-5} \text{ eV}^2} \right|^2 \quad (7.11)$$

where N_{kt} is the size of the detector in kilo·tons and ϵ is its efficiency. At short $L \lesssim 500$ km and large enough energy one simply has

$$\Delta m_{\text{eff}}^2 \simeq (m \cdot m^\dagger)_{e\mu} \simeq \Delta m_{\text{atm}}^2 \theta_{13} \sin \theta_{23} + e^{i\phi} \Delta m_{\text{sun}}^2 \cos \theta_{23} \sin \theta_{12} \cos \theta_{12}$$

and the generic approximation for the oscillation probability is given in eq. (7.6).

In anti-neutrinos, the related process $\bar{\nu}_e \rightarrow \bar{\nu}_\mu$ gives a μ^+ signal with a rate about 2 times lower than in neutrinos.

2. ‘Silver channel’. $\nu_e \rightarrow \nu_\tau$ oscillations are signaled by ν_τ appearance, that can be detected as described at page 83. Detecting both the ‘golden’ and the ‘silver’ channel would allow to test if CP violation is produced by a unique phase, as predicted in the standard neutrino scenario (where the two channels should have CP asymmetries with opposite sign).

3. ‘Bronze channel’. While $\nu_\mu \rightarrow \nu_e$ searches are considered as hopeless (because the signal would be e^- appearance), searches for the e^+ produced by $\bar{\nu}_\mu \rightarrow \bar{\nu}_e$ oscillations could be performed with a magnetized liquid argon TPC, which is maybe not too unrealistic.

Eq. (7.11) allows to estimate the sensitivity of a neutrino factory. The sensitivity to θ_{13} is illustrated in fig. 7.2, and is accompanied by an interesting sensitivity to CP-violation in neutrino oscillations and to their mass hierarchy. The relative merit of a neutrino factory versus a conventional neutrino beam is being actively studied: a neutrino factory seems to have a better sensitivity if θ_{13} is small, while, if $\theta_{13} \gtrsim 0.05$, systematic errors dominate and the situation is not yet fully clarified. Indeed, neutrino factory plans have been optimized for small values of θ_{13} ; while if θ_{13} is large a short baseline would be preferable to reduce earth matter uncertainties. The fact that no technology seems clearly preferable to the others possibly means that the choice is not much important.

Furthermore, it has been discussed which energy and baseline L allows the ‘best’ experiment. For example, by choosing $L = \sqrt{2\pi}/G_F N_e \approx 7400$ km (known as ‘magic baseline’ [66]) one has $\sin(r\delta) = 0$ such that oscillation probability in eq. (7.7) simplifies to its second term only, which no longer depends on ϕ allowing a direct measurement of θ_{13} . Such a long baseline would require building a long inclined and expensive decay tunnel for μ^+ ; furthermore uncertainties on the earth density profile might be a serious limitation.

7.8 Beta beams

The neutrino factory concept can be technologically simplified (although a km-scale decay ring is still needed) by replacing muons with a β -decaying ionized nucleus [67], allowing to produce intense, perfectly pure and (if desired) pulsed $\bar{\nu}_e$ or ν_e beams. Therefore one can perform $(\bar{\nu})_e \rightarrow (\bar{\nu})_\mu$ searches with a WČ detector, or with any other detector unable of identifying the μ^\pm charge,

One can choose a nucleus which has a conveniently long life-time (e.g. $\tau \sim \text{sec}$), which produces neutrinos with known energy spectrum (reconstructed from measurements of the e^\pm spectrum), and which can be easily produced (spallation neutrons allow to get up to $\sim 10^{13}$ nuclei/sec). By accelerating the ionized nucleus up to energy $E = \gamma m$ one can focus the neutrino beam into a cone with opening angle $\sim 1/\gamma$. In practice the neutrino rate might be too much limited because: (i) the number of ions that it is possible to collect limits the neutrino flux; (ii) ions have a lower q/m than protons or muons, such that, the resulting neutrino beta-beam reaches a lower energy than a conventional beam or a neutrino factory beam. Let us discuss two concrete proposals

- A $\bar{\nu}_e$ beam can be obtained collecting $\approx 5 \cdot 10^{13}$ ${}^6\text{He}^{++}$ nuclei/sec (this number might be too optimistic): their decay ${}^6\text{He}^{++} \rightarrow {}^6\text{Li}^{+++} e^- \bar{\nu}_e$, boosted at $\gamma \approx 150$ generates a $\bar{\nu}_e$ beam with energy around 0.5 GeV, that produces 70 events per year in a kton detector located $L \approx 130$ km away.
- A ν_e beam can be obtained collecting $\approx 10^{12}$ ${}^{18}\text{Ne}$ nuclei/sec: their decay ${}^{18}\text{Ne} \rightarrow {}^{18}\text{F} e^+ \nu_e$, boosted at $\gamma \approx 250$ generates a ν_e beam with energy around GeV, that produces 2 events per year in a kton detector located $L \approx 130$ km away.

Several variations are possible. The energies $E = \gamma/m$ quoted above can be reached with a small accelerator, such as the CERN SPS. Beta beams with higher energy, $E_\nu \sim \text{few GeV}$ need a larger accelerator, like TeVatron or even LHC, and allow detection after a longer baseline $L \sim$

1000 km (possibly using rock as target): earth matter effects become more important increasing the sensitivity to the neutrino mass hierarchy and reducing the sensitivity to CP violation.

Beta beams with lower energy, $E_\nu \sim 10$ MeV, allow nuclear experiments, that study e.g. νN interactions relevant for supernova physics. Furthermore, β -beam techniques also allow to obtain a *monochromatic* neutrino beam, by using a weak decay with an electron in the final state ('electron capture', e.g. $\text{C}^{11}e^- \rightarrow \text{B}^{11}\nu_e$), such that the final state involves only two particles (while β -decays have at least three particles in the final state, and therefore a continuous energy spectrum).

Finally, we mention the somewhat related possibility of using the reaction $A_{Z-1} \leftrightarrow A_Z \bar{\nu}_e e^-$ (where the two atoms A could be ^3H and ^3He) for emitting and resonantly detecting monochromatic $\bar{\nu}_e$ with energy $E_\nu = M(Z) - M(Z-1) \sim 20$ keV and $\Delta E_\nu/E_\nu \sim 10^{-17}$ [68]. If future experiments will be able of observing this process at baselines ~ 10 cm, one can use it for performing searches for θ_{13} at baselines ~ 10 m, and for testing gravitational red-shift of neutrinos.

Chapter 8

Non-oscillation experiments

Oscillation experiments are insensitive to the absolute neutrino mass scale (parameterized by the mass of the lightest neutrino) and to the 2 Majorana phases α and β . Other types of experiments can study some of these quantities and the nature of neutrino masses. They are:

- β -decay experiments, that to good approximation probe $m_{\nu_e}^2 \equiv (m \cdot m^\dagger)_{ee} = \sum_i |V_{ei}^2| m_i^2$;
- neutrino-less double-beta decay ($0\nu2\beta$) experiments, that probe the absolute value of the ee entry of the neutrino Majorana mass matrix m , $|m_{ee}| = |\sum_i V_{ei}^2 m_i|$;
- cosmological observations (Large Scale Structures and anisotropies in the Cosmic Microwave Background), that in good approximation probe the sum of neutrino masses, $m_{\text{cosmo}} \equiv m_1 + m_2 + m_3$

Only $0\nu2\beta$ probes the Majorana nature of the mass. The values $|m_{ee}|, m_{\nu_e}, m_{\text{cosmo}}$ are unknown, and can be partially inferred from oscillation data.

Ordering these probes according to their present sensitivities, the list is cosmology, $0\nu2\beta$ and finally β decay. Ordering them according to reliability would presumably result into the reverse list: cosmological results are based on plausible theoretical assumptions, and $0\nu2\beta$ suffers from severe uncertainties in the nuclear matrix elements.

Present data contain a few anomalies. There is a claim that the $0\nu2\beta$ transition has been detected [15] (see section 9.1), there is a persisting anomaly in TROIITSK β decay, and even in cosmology, there is one (weak) claim for a positive effect. None of these hints can be considered as a discovery of neutrino masses, but experiments seem not far from reaching the necessary sensitivity. Existing or planned experiments will lead to progress in a few years.

8.1 Cosmology

There is a non obvious link between cosmological data and neutrino masses, explained in section 10 (mainly in its subsection 10.2). Here we give a short summary of results.

Cosmological data roughly probe mostly the sum of neutrino masses: $m_{\text{cosmo}} = m_1 + m_2 + m_3$, that within standard cosmology controls the present energy fraction Ω_ν in non relativistic neutrinos as $\Omega_\nu h^2 = m_{\text{cosmo}}/93.5 \text{ eV}$, where as usual $h \approx 0.7$ parameterizes the present value of the Hubble constant as $h \equiv H_{\text{today}}/(100 \text{ km/s Mpc})$. Cosmology does not distinguish Majorana from Dirac neutrino masses.

non-oscillation parameter	probed by	experimental limit at 99% CL	99% CL range normal hierarchy	99% CL range inverted hierarchy
ee -entry of m	$0\nu2\beta$	$m_{ee} < 0.39 h$ eV	$(1.1 \div 4.5)$ meV	$(12 \div 57)$ meV
$(m^\dagger m)_{ee}^{1/2}$	β -decay	$m_{\nu_e} < 2.1$ eV	$(4.6 \div 10)$ meV	$(42 \div 57)$ meV
$m_1 + m_2 + m_3$	cosmology	$m_{\text{cosmo}} \lesssim 0.5$ eV	$(51 \div 66)$ meV	$(83 \div 114)$ meV

Table 8.1: *Summary of present constraints on non-oscillation neutrino mass parameters. Some $0\nu2\beta$ data are controversial, and $h \sim 1$ parameterizes uncertain nuclear matrix elements. The last two columns show the oscillation predictions assuming that the lightest neutrino is massless in the two cases of normal (i.e. $m_1 \ll m_2 \ll m_3$) and inverted (i.e. $m_3 \ll m_1 < m_2$) mass hierarchy. In the opposite limit neutrinos are quasi-degenerate and $|m_{ee}|, m_{\nu_e}, m_{\text{cosmo}}$ can be arbitrarily large.*

In order to convert CMB and LSS data into a constraint on neutrino masses one needs to assume a cosmological model. The cosmological constraint [69] assumes that the observed structures are generated by Gaussian adiabatic primordial scalar fluctuations with a constant spectral index n evolved in presence of the known SM particles, of cold dark matter and of a cosmological constant. This standard model of cosmology seems consistent with all observations. CMB data alone constrain $m_1 + m_2 + m_3 < 2.6$ eV at 99% C.L. LSS data are more strongly affected by neutrino masses, and give stronger constraints, after assuming that observed luminous matter tracks the dark matter density up to a bias factor. Neutrino masses have the largest impact at scales so small that nowadays inhomogeneities no longer are a minor correction to a uniform background, such that computations become difficult and theoretical uncertainties can become problematic. Lyman- α data probe inhomogeneities at such small scales and at earlier times, with imperfect agreement between different groups. The resulting cosmological constraint depends on how one deals with these difficulties: more risky approaches give stronger constraints. The value reported in table 8.1 is a reasonably conservative choice.

In the future the sensitivity to neutrino oscillations will improve thanks to better CMB data and to new LSS measurements less plagued by potential systematic effects. If cosmology were simple (e.g. a spectral index $n = 1$, no tensor fluctuations,...) then it seems possible to detect even neutrino masses as small as allowed by oscillation data [69]. The expected ranges of m_{cosmo} are reported in table 8.1 in the limiting case where the lightest neutrino is massless, and in fig. 8.5a in the general case. Within standard cosmology and standard neutrinos, a positive signal is guaranteed if a sensitivity down to $m_{\text{cosmo}} \sim 50$ meV is reached; furthermore a precise measurement could identify the kind of neutrino mass hierarchy.

8.2 Astrophysics

Time delays between supernova neutrinos allows to constrain neutrino masses [70]. We discuss this technique very briefly because it presently gives sub-dominant bounds, and is seems impossible to reach an interesting enough future sensitivity.

At the next gravitational collapse of a supernova, the general strategy will consist in identifying structures in the time and/or energy distributions of neutrinos sensitive to neutrino masses, as the neutronization peak, the rising (or falling) ramp of the cooling phase, a hypothetical sharp cutoff due to black hole formation. The sensitivity of these approaches has been quantified in

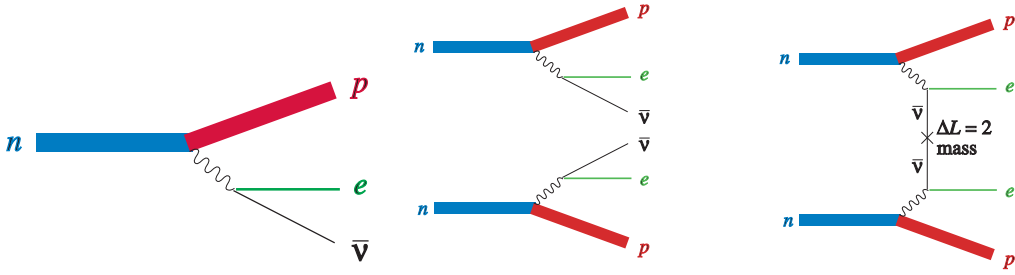


Figure 8.1: Feynman diagrams for β decay, double- β decay, and neutrino-less double- β decay.

several works, assuming the capabilities of present detectors (SuperKamiokande, SNO, LVD, . . .). The difference in time of flight between neutrinos and gravitons will only be sensitive to neutrinos heavier than about 1 eV, comparable to present β -decay bounds. The difference in time of flight between different neutrinos will only be sensitive to neutrino mass *differences* larger than few 10 eV. If neutrino emission were suddenly terminated by black hole formation, a measurement of the difference in time of flight between neutrinos of different energy will only be sensitive to neutrino masses larger than few eV.

8.3 β -decay

Neutrino masses distort the electron spectrum in the β -decay of a nucleus (i.e. $d \rightarrow ue\bar{\nu}_e$ at the quark level, and $n \rightarrow pe\bar{\nu}_e$ at the nucleon level, see fig. 8.1a). The most sensitive choice is tritium decay

$$^3\text{H} \rightarrow ^3\text{He } e \bar{\nu}_e \quad (Q = m_{^3\text{H}} - m_{^3\text{He}} = 18.6 \text{ keV}).$$

Energy conservation tells that $E_e \simeq Q - E_\nu$. The maximal electron energy is $Q - m_\nu$ (assuming that all neutrinos have a common mass m_ν). Around its end-point, the electron energy spectrum is essentially determined by the neutrino phase space factor $\propto E_\nu p_\nu$. So

$$\frac{dN_e}{dE_e} = F(E_e)(Q - E_e) \sqrt{(Q - E_e)^2 - m_\nu^2} \quad (8.1)$$

where $F(E_e)$ can be considered as a constant. The signal produced by m_ν is illustrated in fig. 8.2a.

The fraction of events in the end-point tail is $\propto (m_\nu/Q)^3$, so nuclear decays with a low Q (and a reasonable life-time) offer the best sensitivity. Older experiments found a fake 4.6σ evidence for a *negative* $m_{\nu_e}^2 = -96 \pm 21 \text{ eV}^2$, probably because the energy resolution was overestimated. This was not confirmed by the most recent experiments TROITSK and MAINZ, that find

$$m_{\nu_e}^2 = -0.6 \pm 2.2 \pm 2.1 \text{ eV}^2 \quad [71] \quad \text{and} \quad m_{\nu_e}^2 = -2.3 \pm 2.5 \pm 2.0 \text{ eV}^2 \quad [72]. \quad (8.2)$$

Their combined constraint is reported in table 8.1.

The approved experiment KATRIN should improve the sensitivity to m_{ν_e} by one order of magnitude down to about 0.3 eV [73]. New ideas are needed to plan a β -decay experiment able of reaching the neutrino mass scale suggested by oscillation data. In line of principle, a β -decay experiment is sensitive to neutrino masses m_i and mixings $|V_{ei}|$:

$$\frac{dN_e}{dE_e} = \sum_i |V_{ei}|^2 F(E_e)(Q - E_e) \sqrt{(Q - E_e)^2 - m_i^2}. \quad (8.3)$$

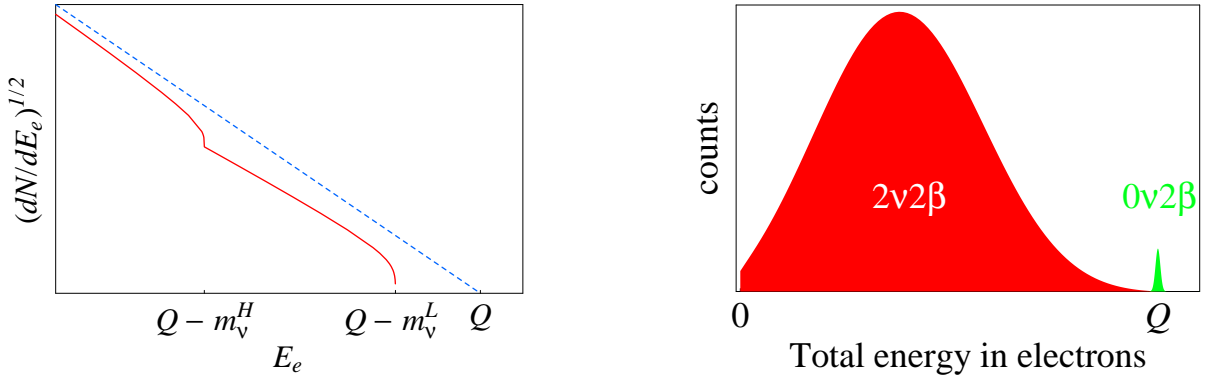


Figure 8.2: Fig. 8.2a: β -decay spectrum close to end-point for a massless (dotted) and massive (continuous line) neutrino. Fig. 8.2b: $2\nu 2\beta$ and $0\nu 2\beta$ spectra.

This is illustrated in fig. 8.2a, where we show the combined effect of a *Heavier* neutrino with little e component and of a *Lighter* neutrino with sizable e component. Following Kurie we plotted the square root of dN_e/dE_e , that in absence of neutrino masses is a linear function close to the end-point, assumed to be known with negligible error. In fig. 8.3 we show the predicted reduction of the β -decay rate around its end-point. The various curves are for different values of the lightest neutrino mass.

In practice the energy resolution is limited, and only broad features can be seen. If it is not possible to resolve the difference between neutrino masses, it is useful to approximate eq. (8.3) with (8.1) and present the experimental bound in terms of the single effective parameter

$$m_{\nu_e}^2 \equiv \sum_i |V_{ei}^2| m_i^2 = \cos^2 \theta_{13} (m_1^2 \cos^2 \theta_{12} + m_2^2 \sin^2 \theta_{12}) + m_3^2 \sin^2 \theta_{13}. \quad (8.4)$$

The last equality holds in the standard three-neutrino case. The expected ranges of m_{ν_e} are reported in table 8.1 in the limiting case where the lightest neutrino is massless. From this it is immediate to obtain the ranges corresponding to the generic case of a non vanishing lightest neutrino mass m_{lightest} : as clear from the definition $m_{\nu_e}^2 \equiv (m \cdot m^\dagger)_{ee}$ or from the more explicit expression in eq. (8.4) one just needs to add m_{lightest}^2 to $m_{\nu_e}^2$. The resulting bands at 99% CL are plotted in fig. 8.5b.

Searches for ν_μ and ν_τ masses have been performed by studying decays like $\pi \rightarrow \mu \bar{\nu}_\mu$. The resulting bounds, $m_{\nu_{\mu,\tau}} \lesssim \text{MeV}$ are very loose. Notice that β -decay experiments probe anti-neutrinos. If one does not trust CPT and allows neutrinos and anti-neutrinos to have different masses, the looser bound $m_{\nu_e} < 200 \text{ eV}$ applies to neutrinos.

8.4 Neutrino-less double β decay

A few nuclei can only decay through double- β decay, that at the nucleon level corresponds to two simultaneous $n \rightarrow p e \bar{\nu}_e$ decays, see fig. 8.1b). This is e.g. the case of $^{76}_{32}\text{Ge}$, that cannot β -decay to $^{76}_{33}\text{As}$ because it is heavier. It can only jump to the lighter $^{76}_{34}\text{Se}$:



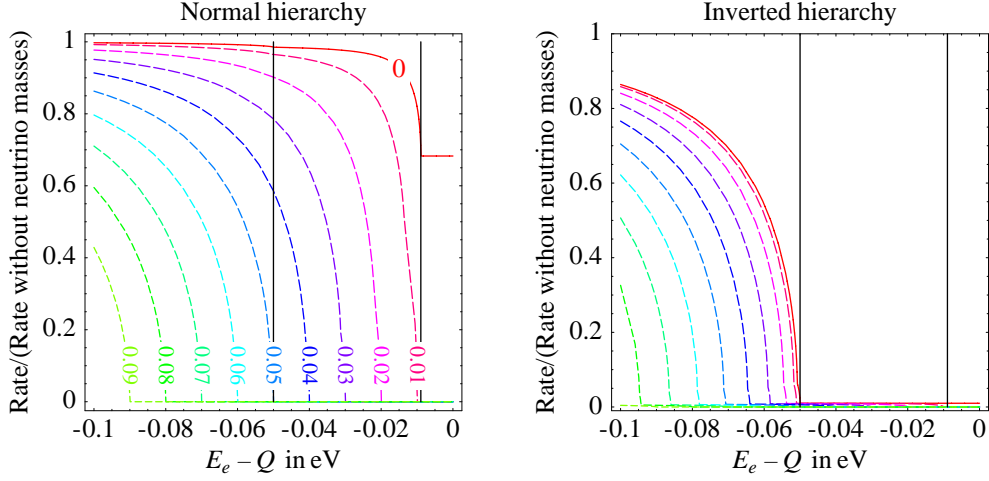


Figure 8.3: β -decay spectrum close to end-point predicted for best-fit values of oscillation parameters (we assumed $\theta_{13} = 0.1$; the difference with respect to $\theta_{13} = 0$ is hardly visible) and for different values of the lightest neutrino mass, indicated on each curve in the left plot. The vertical lines indicate the positions of $(\Delta m_{\text{sun,atm}}^2)^{1/2}$. Even without neutrino masses the phase space strongly suppresses the rate around the end-point.

Since it is a second order weak process, ${}^{76}\text{Ge}$ has a very long life-time, $\tau \sim 10^{21}$ yr. The measurement of the electron energy spectrum seems to provide the only direct confirmation of the fact that $\bar{\nu}_e$ obey the Pauli exclusion principle [74], as predicted by the only sensible theory.

If neutrinos have Majorana masses, the alternative neutrino-less double β decay ($0\nu2\beta$) decay ${}^{76}\text{Ge} \rightarrow {}^{76}\text{Se ee}$ is also possible. Fig. 8.1c shows the Feynman diagram for $0\nu2\beta$ at nuclear level. The clashing arrows reflect the insertion of a Majorana mass in the virtual neutrino line, that violates (electronic) lepton number by two unities, $\Delta L_e = 2$.

$0\nu2\beta$ can be distinguished from ordinary $2\nu2\beta$ decay relying on kinematics: as illustrated in fig. 8.2b $0\nu2\beta$ gives two electrons with total energy equal to Q , while $2\nu2\beta$ decay gives two electrons with a continuous spectrum that extends up to Q . In real life one has to fight with limited energy resolution and other backgrounds.

In general, double- β decay processes are:

$$(A, Z) \rightarrow (A, Z + 2) + 2 e^- + n \bar{\nu}_e, \quad n = 0, 2$$

The competing β decay is kinematically forbidden for some even-even nuclei (${}^{76}\text{Ge}$, ${}^{130}\text{Te}$, ${}^{100}\text{Mo}$, ...) that have ground levels arranged such that the levels (A, Z) and $(A, Z + 2)$ are below $(A, Z + 1)$. Other related processes, that involve absorption of atomic electrons and/or emission or positrons, do not seem appropriate for achieving a sufficient sensitivity to m_{ee} .

8.4.1 Connection between $0\nu2\beta$ and neutrino masses

Experiments can measure the $\Gamma_{0\nu2\beta}$ decay rate. Assuming that neutrino masses are much smaller than Q , the $0\nu2\beta$ decay amplitude is proportional to m_{ee} , the $\nu_{eL}\nu_{eL}$ element of the neutrino mass matrix. There seems to be no realistic way of probing other elements of the Majorana neutrino

mass matrix. Assuming three Majorana neutrinos, m_{ee} can be written in terms of the neutrino masses m_i , mixing angles θ_{ij} and Majorana CP-violating phases α, β as

$$m_{ee} = \sum_i V_{ei}^2 m_i = \cos^2 \theta_{13} (m_1 e^{2i\beta} \cos^2 \theta_{12} + m_2 e^{2i\alpha} \sin^2 \theta_{12}) + m_3 \sin^2 \theta_{13}. \quad (8.5)$$

$\Gamma_{0\nu2\beta}$ can be computed in terms of ν masses as

$$\Gamma_{0\nu2\beta} = G \cdot |\mathcal{M}^2| \cdot |m_{ee}|^2$$

where G is a known phase space factor and \mathcal{M} is the nuclear $0\nu2\beta$ matrix element, plagued by a sizable theoretical uncertainty.

Indeed different calculations find values of \mathcal{M} different by factors of $\mathcal{O}(\text{few})$. This probably over-estimates the theoretical uncertainty, as not all models are equally accurate. It would be useful if future calculations of matrix elements could provide error estimates. This can be done, within any single model, by comparing model predictions with data on $\Gamma_{2\nu2\beta}$, β -decay and β -capture, which are induced by operators similar to the one relevant for $0\nu2\beta$ decay. For definiteness we adopt the $0\nu2\beta$ nuclear matrix elements \mathcal{M}_0 computed in [75]. Assuming $m_{ee} = 1 \text{ eV}$, the lifetime for $0\nu2\beta$ decay of the most promising isotopes, ^{76}Ge , ^{82}Se , ^{100}Mo , ^{130}Te and ^{136}Xe , is 2.33, 0.60, 1.27, 0.49 and 2.21×10^{24} years respectively.

To use a different calculation with matrix element \mathcal{M} , just rescale by the factor $h = \mathcal{M}_0/\mathcal{M}$, which depends on the nucleus studied, obtaining

$$\Gamma_{0\nu2\beta} = G \cdot |\mathcal{M}_0|^2 \cdot |m_{ee}/h|^2 \quad (8.6)$$

We always explicit the factors h when quoting an experimental result on $0\nu2\beta$. For instance we consider ^{76}Ge and ^{130}Te that have been used by the most precise experiments. Different published computations find h in the following ranges

$$0.3 [76] < h(^{76}\text{Ge}) < 2.4 [77], \quad 0.4 [76] < h(^{130}\text{Te}) < 2.7 [78]. \quad (8.7)$$

The quantity $h(^{130}\text{Te})/h(^{76}\text{Ge})$ is also uncertain, spanning the following range:

$$0.3 [79] < h(^{130}\text{Te})/h(^{76}\text{Ge}) < 1.7 [78]. \quad (8.8)$$

8.4.2 Why improving on $0\nu2\beta$ is difficult

The number of $0\nu2\beta$ events that can be observed is given by

$$N_{\text{sig}} = \mathcal{T} \cdot \Gamma_{0\nu2\beta} \cdot f \cdot N \cdot \epsilon \quad (8.9)$$

where \mathcal{T} is the observation live-time; $\Gamma_{0\nu2\beta}$ is the $0\nu2\beta$ rate; $\epsilon \leq 1$ is the efficiency in the detection of electrons; N is the total number of nuclei; f is the isotopic fraction that contributes to $0\nu2\beta$ (e.g. the isotope ^{76}Ge is a fraction $f \sim 7\%$ of natural germanium).

From this formula, one might think that the sensitivity to $\Gamma_{0\nu2\beta}$ scales linearly with the mass of the detector and with the time \mathcal{T} . This is true only neglecting the background. Assuming that the background in the signal window ΔE scales in a similar way one gets¹

$$N_{\text{bkg}} = \mathcal{T} \Delta E \frac{d\Gamma_b}{dE} N$$

¹Other cases are possible: e.g. a surface contamination might exist and would not scale with N .

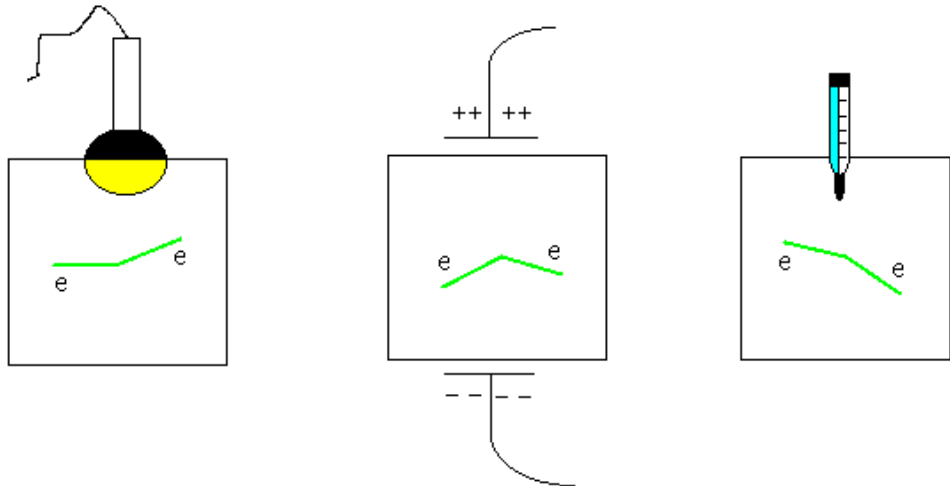


Figure 8.4: Sketch of various possibilities to measure the energy of 2β decays: (a) tracking-calorimetry, (b), charge-collection, (c) bolometric.

nucleus	Present bound on $ m_{ee} /h$ in eV	Sensitivity to $ m_{ee} /h$ in meV
^{76}Ge	0.35	25 GERDA
^{76}Ge	0.38	25 MAJORANA
^{130}Te	0.42	33 CUORE
^{100}Mo	1.7	52 EXO
^{136}Xe	2.2	55 SuperNEMO

Table 8.2: Left: present constraints at 90% CL. Right: future sensitivities. The factor $h \sim 1$ reminds that $0\nu2\beta$ elements are uncertain ($h = 1$ corresponds to the matrix elements of [75]).

(here, $d\Gamma_b/dE$ is the background rate per atom per energy interval and it is supposed to be a constant). To compare the performances of different detectors, we can introduce a figure of merit F , which has to be as large as possible. The simplest definition is the ratio between the number of events N_s with the Poisson fluctuation of the background $\sqrt{N_b}$:

$$F = \frac{N_{\text{sig}}}{\sqrt{N_{\text{bkg}}}} = \Gamma_{0\nu2\beta} \cdot f \cdot \epsilon \cdot \sqrt{\frac{N \cdot \mathcal{T}}{\Delta E \cdot d\Gamma_b/dE}}$$

The dependence on m_{ee} and on the nuclear matrix element is quadratic, while the dependence on the parameters we can control experimentally is milder: the isotopic fraction f and the efficiency enter linearly; the mass, \mathcal{T} and background rate only as a square root. In order to increase the sensitivity in m_{ee} by a factor 10 one needs to make the experiment 10^4 bigger, or to improve it.

As should be clear from the discussion above, we absolutely need to measure the energy well. The sketch in fig. 8.4 illustrates some basic concepts to achieve this goal.

- (a) The first concept, implemented by the NEMO3 collaboration, aims at tracking the single electrons well. It would allow a significant suppression of the background, but it did not yield (yet) very precise energy measurements: this is in practice its limitation. A positive signal would allow to check if the energy spectra of the single electrons are the ones characteristic of a light massive neutrino exchange, or of some other source of $0\nu2\beta$.

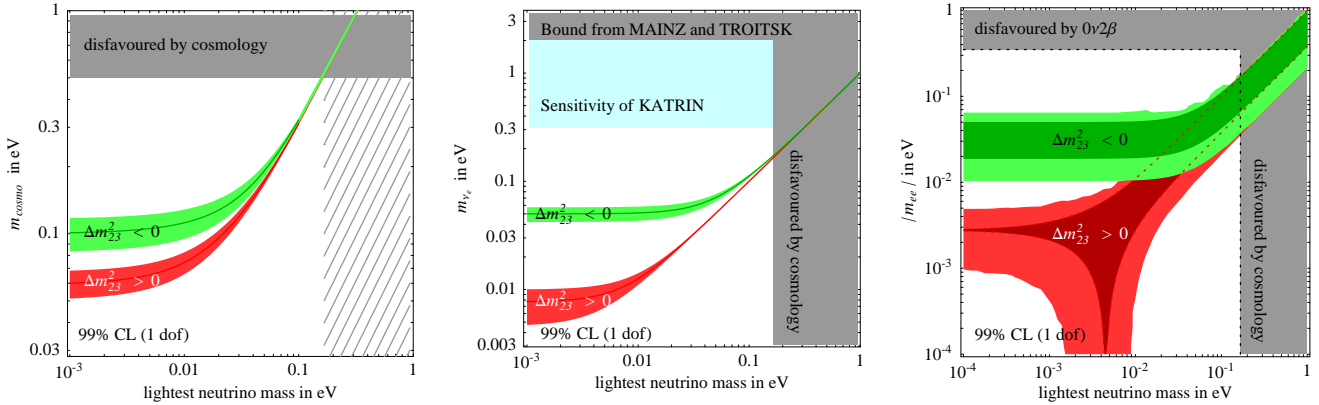


Figure 8.5: 99% CL expected ranges as function of the lightest neutrino mass for the parameters: $m_{\text{cosmo}} = m_1 + m_2 + m_3$ probed by cosmology (fig. 8.5a), $m_{\nu_e} \equiv (m \cdot m^\dagger)_{ee}^{1/2}$ probed by β -decay (fig. 8.5b), $|m_{ee}|$ probed by $0\nu2\beta$ (fig. 8.5c). $\Delta m_{23}^2 > 0$ corresponds to normal hierarchy ($m_{\text{lightest}} = m_1$) and $\Delta m_{23}^2 < 0$ corresponds to inverted hierarchy ($m_{\text{lightest}} = m_3$), see fig. 2.3. The darker regions show how the ranges would shrink if the present best-fit values of oscillation parameters were confirmed with negligible error.

(b) The second concept, proposed in 1967 by Fiorini *et al.* [16], aims at collecting the ionization charge produced by the electrons, with MeV-scale energy. Experiments using ^{76}Ge yield the best existing limit (from HM and IGEX [16]). This technique is seriously considered for future steps (GERDA, Majorana, GEM proposals).

(c) Fiorini et al. push the bolometer concept with tellurium: its isotope of interest has a large isotopic fraction in nature. This produced the next better result (from CUORICINO, to be enlarged to CUORE).

Many other experiments and proposals are based on (various combinations of) these concepts and other important considerations (background control, isotopic enrichment, double tag, etc.). The so called “pulse shape discrimination” is a good example of how the background can be reduced in ^{76}Ge detectors; in the terminology above, it might be classified as a rough “electron tracking”. E.g. background from γ radiation deposits monochromatic energy in the crystal, producing a line in the energy spectrum, at energies that can be dangerously close to the $0\nu2\beta$ line. However, the energy is deposited in a wider area (since the daughter γ from e^+ annihilation is able to spread the energy around), and the electric pulse from charge collection has on average a different time structure. In this way, HM reduced the background by a factor $\mathcal{O}(2)$ (IGEX also employs the same technique).

8.4.3 Present $0\nu2\beta$ experiments

As clear from table 8.2 the main present experiments are HM, IGEX and CUORICINO. Their main features can be summarized as follows.

	HM	IGEX	CUORICINO
Nucleus	^{76}Ge	^{76}Ge	^{130}Te
Q value of $0\nu2\beta$	2039 keV	2039 keV	2529 keV
Exposure in 10^{25} nuclei·yr	25	7	0.14
Isotopic fraction f	0.86	0.86	0.34
Efficiency ϵ	0.5	0.7	0.84
Energy resolution σ_E	1.6 keV	1.7 keV	3 keV
Total events n	21	9.6	24
Expected background b	20.4 ± 1.6	17.2 ± 2	35.2 ± 2
Predicted signal s	$76 m_{ee}/h\text{ eV} ^2$	$23.5 m_{ee}/h\text{ eV} ^2$	$21.5 m_{ee}/h\text{ eV} ^2$

We reported the number of events and expected background in a $\pm 3\sigma_E$ region around the Q value of the $0\nu2\beta$. The Poisson likelihood of having s signal events is $\mathcal{L}(s) \propto e^{-s}(b+s)^n$ and $\chi^2 = -2 \ln \mathcal{L}$. IGEX and CUORICINO observe a number of events slightly below the expected background, while the opposite happens for HM. This simple analysis gives the constraints reported in table 8.2, where $h = 1$ if one assumes the $0\nu2\beta$ nuclear matrix elements of [75]. One can do a more precise analysis of the energy spectrum. This will be discussed in section 9.1 in connection with the HM hint.

Assuming that neutrino masses are of Majorana type (Dirac neutrino masses would not induce the L -violating $0\nu2\beta$ decay) one can partially infer $|m_{ee}|$ from oscillation data [80]. Its explicit expression is given in eq. (8.5). Besides oscillation parameters, which have been partially measured, m_{ee} depends on the unknown Majorana phases α, β and on the absolute neutrino mass scale, conveniently parameterized by the lightest neutrino mass. Presently this is also unknown, but β -decay and cosmology can measure it. Fig. 8.5c shows the allowed range of $|m_{ee}|$.

In the simplest case of quasi-degenerate neutrinos with mass m_ν , the three non-oscillation parameters m_{ν_e} , m_{cosmo} and m_{ee} are given by

$$m_{\nu_e} = m_\nu, \quad m_{\text{cosmo}} = 3m_\nu, \quad 0.24m_\nu < |m_{ee}| < m_\nu \text{ at 99\% C.L.} \quad (8.10)$$

The lower bound on $|m_{ee}|$ holds thanks to the fact that solar data exclude a maximal solar mixing and that CHOOZ requires a small θ_{13} . Therefore the upper bound on $|m_{ee}|$ implies the constraint $m_\nu/h < 1.1$ eV at 99% C.L., with $h \sim 1$ defined in eq. (8.6).

Chapter 9

Unconfirmed anomalies

In this section we review anomalous experimental results that might be due to rare statistical fluctuations, or to mistakes, or be the first hints of new discoveries. Since this is not established physics we unavoidably touch controversial issues. Rather than presenting an acritical list of claims we emphasize the controversial points that must be clarified. Hopefully future work will lead to definite conclusions, maybe confirming one or more of these anomalies.

9.1 Heidelberg-Moscow

We recall basic facts about $0\nu2\beta$ signals in $^{76}_{32}\text{Ge}$ experiments, discussed in section 8.4. $0\nu2\beta$ gives two electrons with total kinetic energy equal to the Q value of the decay. The HM collaboration reports the event rate as function of the total electron energy looking for the following $0\nu2\beta$ signal:

a peak at $Q = 2038.6 \text{ keV}$ with known width, $\sigma_E \approx 1.6 \text{ keV}$ given by the energy resolution, emerging over the $\beta\beta$ and other backgrounds, which are not fully known.

While the HM collaboration used their data to set a bound on $|m_{ee}|$, some members of the HM collaboration reinterpreted the data as a 4.2σ evidence for $0\nu2\beta$ [15]. Indeed a hint of a $0\nu2\beta$ peak (indicated by the arrow) is visible in the most recent data plotted in fig. 9.1a. In these latest results the peak is more visible than in latest published HM data [16], partly thanks to higher statistics (increased from 53.9 to 71.7 kg yr) and partly thanks to an ‘improved analysis’).

This claim is controversial, mainly because one needs to fully understand the background before being confident that a signal has been seen. In order to allow a better focus on this key issue, we present fig. 9.1b, that should be uncontroversial. It shows the statistical significance of the $0\nu2\beta$ signal as function of b , the unknown *true* level of quasi-flat background around the Q -value of $0\nu2\beta$.

The crucial point under debate is: how large is b ? The HM collaboration earlier claimed [16] $b = (13.6 \pm 0.7) \text{ events}/(71.7 \text{ kg yr} \cdot \text{keV})$. In such a case the statistical significance of the signal would be less than 1σ , see fig. 9.1b. This can be considered as the upper bound on b computed assuming that all events in a wider range around Q come from a quasi-flat background.

A statistically significant hint for $0\nu2\beta$ is obtained if one can show that b is lower. The continuous line in fig. 9.1a shows a fit of HM data using a tentative model of the background, assumed to have a quasi-flat component (mainly due to ‘natural’ and ‘cosmogenic’ radioactivity) plus some peaks due to faint γ lines of ^{214}Bi , which is a radioactive impurity present in the

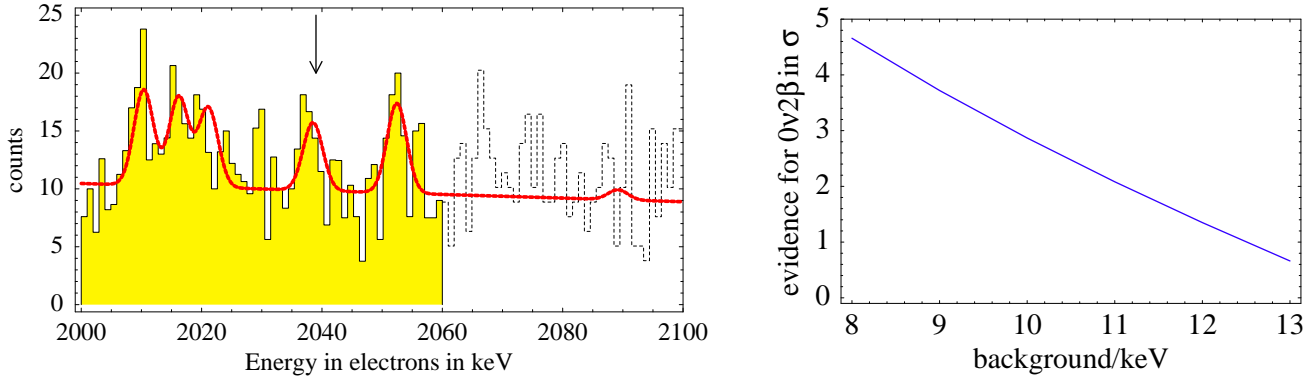


Figure 9.1: Fig. 9.1a: the latest HM data ($71.7 \text{ kg} \cdot \text{yr}$) used to claim a 4.2σ evidence for $0\nu2\beta$. Fig. 9.1b: the statistical significance of the $0\nu2\beta$ signal, as function of the assumed flat component of the background.

apparatus (from the ^{238}U decay chain). Their positions and intensities can be estimated from tables of nuclear decays; however they are modified by $\mathcal{O}(1)$ factors by detector-related effects which depend on the unknown localization of ^{214}Bi . The fit in fig. 9.1a is performed by allowing the intensity of each line to freely vary. In this way part of the background is interpreted as ^{214}Bi peaks, thereby reducing the quasi-flat component. We find that the statistical significance of the $0\nu2\beta$ signal is about 2.7σ .

Some details in its implementation prevent this analysis from fully reaching its goal, which is determining b from regions with no peaks. 1) the latest data have been published only below 2060 keV. (Above 2060 keV in fig. 9.1a we plotted HM data, artificially rescaled to account for the larger statistics. Including the old data above 2060 keV in the fit would reduce the significance of the signal down to about 2.2σ . 2) HM data contain hints of extra unidentified spurious peaks at specific energies (at 2030 keV and above 2060 keV). Fitting data assuming that these extra peaks can be present at arbitrary energies with arbitrary intensities reduces b and enhances the statistical significance of the signal.

Part of the background is due to single-particle events, while in $0\nu2\beta$ events the energy is deposited by two electrons. The HM collaboration [15] tried to exploit this difference to suppress the background ('pulse shape discrimination'). This can be done in more or less sophisticated ways; in the resulting spectrum the $0\nu2\beta$ peak becomes more clearly visible, but its statistical significance does not increase with respect to the analysis without pulse shape discrimination.

According to some members of the HM collaboration (paper by A.M. Bakalyarov et al. in [15])) some HM detectors find extra unidentified peaks in runs where pulses under discriminator threshold are included in the data-set: omitting these runs the hint for a $0\nu2\beta$ peak disappears. This claim is refuted by the members of the HM collaboration which claim a signal.

In conclusion, we think that the latest HM data (below 2060 keV) contain a 2.7σ hint for $0\nu2\beta$. Higher statistical significance can be obtained making different assumptions about the background. It is crucial to understand how large is its quasi-flat component around Q . The natural interpretation of the signal would be in terms of quasi-degenerate neutrino masses of $(0.1 \div 0.9) \text{ eV}$.

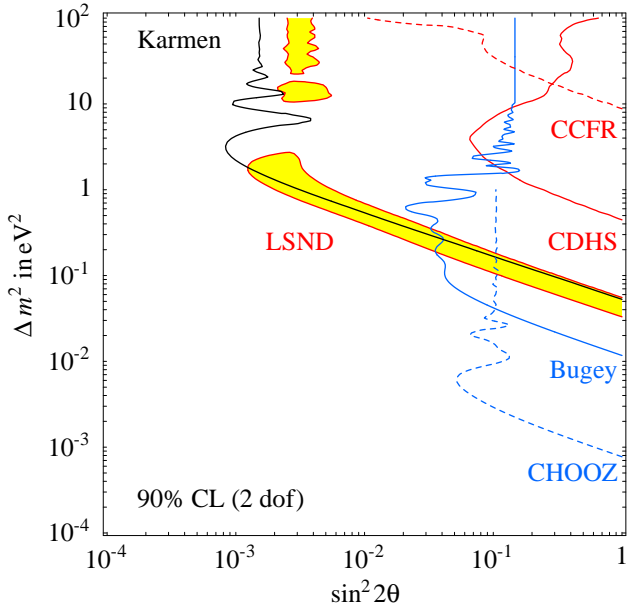


Figure 9.2: **Collection of data in the ν_e, ν_μ sector.** The mixing angle θ on the horizontal axis is different for the different experiments. Bound from KARMEN and LSND region (shaded) for $\nu_\mu \rightarrow \nu_e$. Bounds from BUGEY and CHOOZ ($\bar{\nu}_e$ disappearance), CDHS ($\bar{\nu}_\mu$ disappearance), CCFR (ν_μ disappearance). All at 90% CL (2 dof).

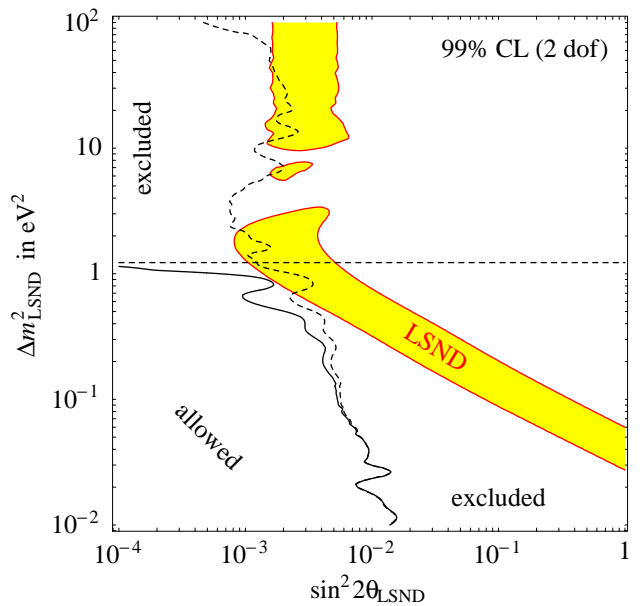


Figure 9.3: **3+1 oscillations.** The region of the $(\Delta m^2, \sin^2 2\theta_{e\mu})$ plane favored by LSND is compared with the combined constraint from cosmology and ν experiments (continuous lines). Dropping the cosmological bound on ν masses (horizontal line), the dashed line shows the constraints from the ν data in fig. 9.2 and SK. All at 99% CL (2 dof).

Various future experiments plan to test the claim of [15]. In our view, a discussion of what should be considered as a convincing evidence for $0\nu2\beta$, is useful, because any experiment (past and future) needs to confront with this issue. Observing $0\nu2\beta$ with different nuclei seems really advisable for two reasons: to be fully sure that the signal is not faked by a spurious line, and in view of theoretical uncertainties on $0\nu2\beta$ matrix elements.

9.2 LSND

In the LSND [12] and KARMEN [13] experiments, a proton beam is used to produce π^+ , that decay as

$$\pi^+ \rightarrow \mu^+ \nu_\mu, \quad \mu^+ \rightarrow e^+ \nu_e \bar{\nu}_\mu$$

generating $\bar{\nu}_\mu, \nu_\mu$ and ν_e neutrinos. The resulting neutrino beam also contains a small $\bar{\nu}_e$ contamination, about $\bar{\nu}_e/\bar{\nu}_\mu \lesssim 10^{-3}$. In KARMEN both π^+ and μ^+ decay at rest, so that the SM prediction for the neutrino energy spectra can be easily computed: ν_μ have an energy of 29.8 MeV, while ν_e and $\bar{\nu}_\mu$ have a continuous spectrum up to 52.8 MeV. In LSND π^+ and μ^+ decay at rest produce most of the neutrinos. Decay-in-flight of π^+ produce some flux of ν_μ with higher energy, that has been used for $\nu_\mu \rightarrow \nu_e$ searches.

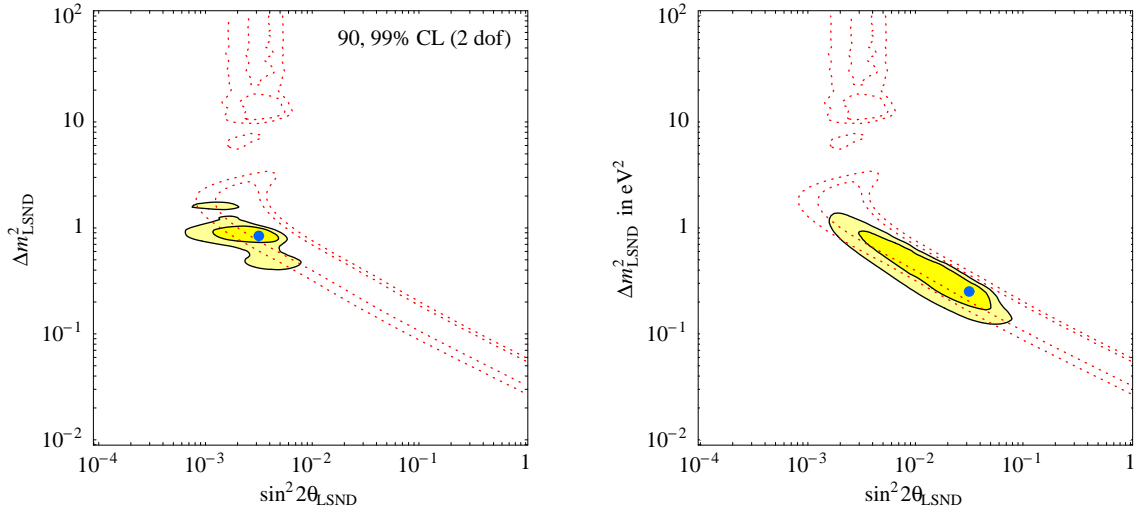


Figure 9.4: **Best-fit regions at 90% and 99% CL (2 d.o.f.) for the LSND parameters assuming oscillations.** Fig. 9.4a assumes that the LSND anomaly is generated through a sterile neutrino ('3+1' scheme). Fig. 9.4b assumes that the LSND anomaly is generated by active neutrinos, while something else generates either the atmospheric or the solar anomaly, without affecting LSND. The dotted lines show the regions suggested by only the LSND data. The dots show the best fit points.

The search for $\bar{\nu}_\mu \rightarrow \bar{\nu}_e$ is performed using the detection reaction $\bar{\nu}_e p \rightarrow n e^+$, that has a large cross section (section 4.2). The detector tries to identify both the e^+ and the n (via the 2.2 MeV γ line obtained when n is captured by a proton). The neutrinos have energy $E_\nu \sim (10 \div 50)$ MeV and travel for $L \approx 30$ m in LSND and $L \approx 17.5$ m in KARMEN. These experiments are more sensitive to oscillations than older experiments, that used higher neutrino energy.

LSND finds an evidence for $\bar{\nu}_\mu \rightarrow \bar{\nu}_e$, that ranges between 3 to 7σ depending on how data are analyzed. This happens because LSND has a poor signal/background ratio: choosing the selection cuts as in [81] the LSND sample contains 1000 background events and less than 100 signal events, distinguished only on a statistical basis. The statistical significance of the LSND signal depends on how cuts are chosen, and relies on the assumption that all sources of background have been correctly computed. The main backgrounds are cosmic rays and ν_e misidentification. The final LSND results for the average oscillation probabilities are

$$P(\bar{\nu}_\mu \rightarrow \bar{\nu}_e) = (2.6 \pm 0.8) 10^{-3}, \quad P(\nu_\mu \rightarrow \nu_e) = (1.0 \pm 1.6) 10^{-3}. \quad (9.1)$$

The LSND anomaly can be interpreted as due to oscillations. Fitting LSND data alone in a two-flavour context gives the best-fit regions shown in fig. 9.3a.

KARMEN finds 15 events versus an expected background of 15.8 events. KARMEN has a few times less statistics and shorter base-line than LSND, but is cleaner. The main reason is that the KARMEN beam is pulsed, allowing to reduce the cosmic ray background (KARMEN also has a better shield), and ν_e misidentification (due to a nuclear decay with a life-time different than the one characteristic of n capture). At the end, KARMEN excludes a significant part, but not all, of the $(\Delta m^2, \theta)$ range suggested by LSND, as shown in fig. 9.3a.

The LSND anomaly is being tested by the MiniBoone experiment [82], that will have more

model and number of free parameters	$\Delta\chi^2$	mainly incompatible with	main future test
ideal fit	0		?
3 + 1 : $\Delta m_{\text{sterile}}^2 = \Delta m_{\text{LSND}}^2$	9	6 + 9?	BUGEY + cosmology?
3 + 2 : $\Delta m_{\text{sterile}}^2 = \Delta m_{\text{LSND}}^2$	14	4 + 9+?	BUGEY + cosmology?
$\Delta L = 2$ decay $\bar{\mu} \rightarrow \bar{e}\bar{\nu}_\mu\bar{\nu}_e$	6	12 + 6	KARMEN + TWIST
3 ν and CPT (no $\Delta\bar{m}_{\text{atm}}^2$)	10	20	SK atmospheric
3 ν and CPT (no $\Delta\bar{m}_{\text{sun}}^2$)	10	25	KamLAND
normal 3 neutrinos	5	25	LSND
2 + 2 : $\Delta m_{\text{sterile}}^2 = \Delta m_{\text{sun}}^2$	9	40	SNO
2 + 2 : $\Delta m_{\text{sterile}}^2 = \Delta m_{\text{atm}}^2$	9	50	SK atmospheric
			$\bar{\nu}_\mu$ LBL?
			KamLAND
			MINIBOONE
			SNO
			ν_μ LBL

Table 9.1: *Interpretations of solar, atmospheric and LSND data, ordered according to the quality of their global fit. A $\Delta\chi^2 = n^2$ roughly signals an incompatibility at n standard deviations.*

statistics than LSND and a pulsed beam. Initially, MiniBoone will look for $\nu_\mu \rightarrow \nu_e$, at higher energy and longer base-line than LSND.

If confirmed, the LSND anomaly will require a significant revision of the standard picture. Oscillations between the three SM neutrinos are described by two independent squared neutrino mass differences, allowing to explain only two of the three atmospheric, solar and LSND neutrino anomalies as oscillations.

One possible global explanation of the three anomalies is that an extra sterile neutrino generates one of them. However, each anomaly, when fitted independently from the other ones, prefers active oscillations refusing the sterile neutrino. The relatively better global fit is obtained with a ‘3+1 spectrum’ (sterile LSND oscillations), rather than with a ‘2+2 spectrum’ (sterile solar or atmospheric oscillations). We now discuss these and other proposed interpretations of the LSND anomaly [83]. Many interpretations have been excluded by other experiments, as summarized in table 9.1. Only the most exotic interpretations can fully reconcile all data.

9.2.1 A sterile neutrinos with 3+1 spectrum

‘3+1’ indicates that the additional sterile neutrino is separated by the large LSND mass gap from the 3 active neutrinos, separated among them only by the small solar and atmospheric mass differences (see fig. 9.5a). Therefore within this scheme the sterile neutrino is directly employed to generate the LSND anomaly.

3+1 oscillations present a phenomenological problem, because predict that $\nu_\mu \rightarrow \nu_e$ oscillations at the LSND frequency proceed through $\nu_\mu \rightarrow \nu_s \rightarrow \nu_e$ and $\nu_{e,\mu} \rightarrow \nu_s$ are strongly constrained by disappearance experiments. Keeping only oscillations at the dominant LSND frequency

$$S \equiv \sin^2(\Delta m_{\text{LSND}}^2 L / 4E_\nu)$$

one has

$$P(\nu_e \rightarrow \nu_e) = 1 - S \sin^2 2\theta_{es} \quad P(\nu_\mu \rightarrow \nu_\mu) = 1 - S \sin^2 2\theta_{\mu s} \quad P(\nu_e \rightarrow \nu_\mu) = S \sin^2 2\theta_{\text{LSND}}$$

with $\theta_{\text{LSND}} \approx \theta_{es}\theta_{\mu s}$, or more precisely [83]

$$\sin^2 2\theta_{\text{LSND}} \simeq 4\theta_{\text{LSND}}^2 \simeq \frac{1}{4} \sin^2 2\theta_{es} \sin^2 2\theta_{\mu s}. \quad (9.2)$$

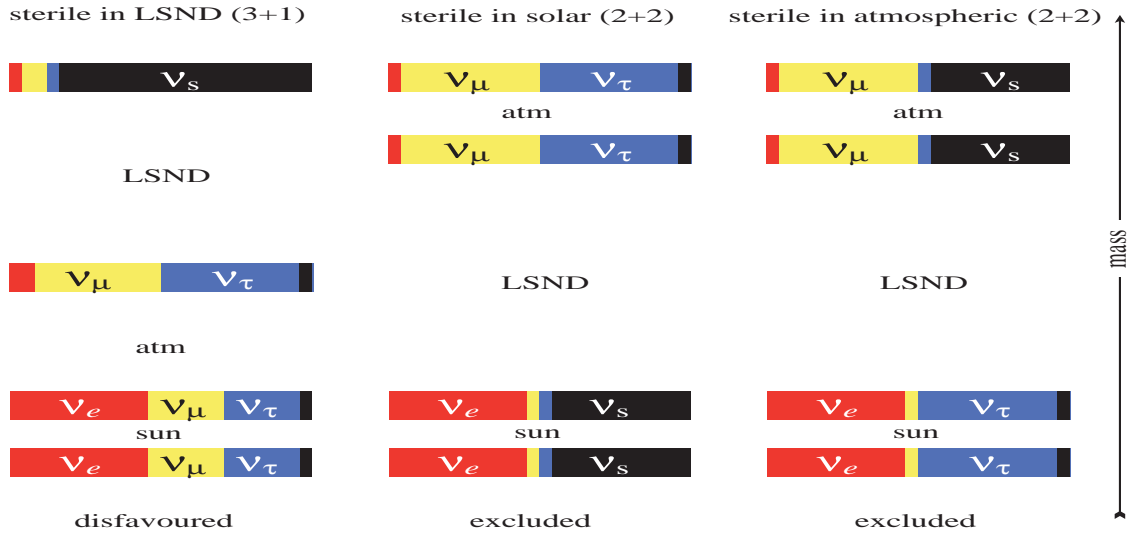


Figure 9.5: *Three different mass spectra that try to explain the solar, atmospheric and LSND anomalies adding one extra sterile neutrino.*

In view of present constraints on the θ_{es} and the $\theta_{\mu s}$ mixing angles, this ‘product rule’ prevents a clean explanation of the LSND anomaly. The θ_{es} mixing angle is constrained by BUGEY, CHOOZ, SK atmospheric data and the $\theta_{\mu s}$ mixing angle by SK, CDHS and CCFR [84]. These bounds are illustrated in fig. 9.2. Combining them also with the direct KARMEN bound gives the bound on the effective LSND mixing angle shown in fig. 9.3. In gaussian approximation, all 96% CL LSND confidence region is excluded at, at least, 96% CL level. Therefore 3+1 solutions do not give a good fit. One needs to invoke a statistical fluctuation with around % probability to explain why only LSND sees the sterile oscillations. Ignoring the poor quality of the fit, the best combined fit region for the LSND parameters is shown in fig. 9.4a. Since θ_{es} is strongly constrained by reactor data, the best fit is obtained for relatively large $\theta_{\mu s}$, which gives potentially observable ν_μ disappearance at the LSND frequency, $P(\nu_\mu \rightarrow \nu_\mu) \sim 0.8$.

Assuming standard cosmology, the extra sterile neutrino would be thermalized. Four thermalized neutrinos are mildly disfavored by BBN data. Furthermore, the global fit in fig. 9.4a shows that the sterile neutrino should have a mass of about 1 eV: this is disfavored by the cosmological limit on neutrino masses of eq. (10.8). Such cosmological constraints can be avoided by invoking appropriate non-standard cosmologies.

9.2.2 A sterile neutrino with 2+2 spectrum

‘2+2’ indicates 2 couples of neutrinos (one generates the solar anomaly, and the other one the atmospheric anomaly), separated by the large LSND mass gap. Within this scheme, the sterile neutrino is employed to generate the solar or atmospheric anomaly, see fig. 9.5b,c. Intermediated cases are also possible and can parameterized by a sterile mixing angle θ_s .¹ Experiments now tell that both the solar and atmospheric anomalies are generated by active neutrinos, and only a small sterile contribution is allowed. Quantitatively:

¹In general, mixing of one sterile neutrino is fully described by three mixing angles (section 13.2). In view of the large LSND mass gap two of these angles must be sufficiently close to zero that setting them to zero simplifies the discussion without affecting the conclusions.

- Interpreting solar data as $\nu_e \rightarrow \nu_{\mu,\tau} \cos \theta_s + \nu_s \sin \theta_{st}$ oscillations one gets

$$\sin^2 \theta_{st} = 0 \pm 0.10.$$

- Interpreting atmospheric data as $\nu_\mu \rightarrow -\nu_\tau \sin \theta_s + \nu_s \cos \theta_{st}$ oscillations one gets

$$\cos^2 \theta_{st} = 0 \pm 0.16.$$

Therefore data tell that the total ‘fraction of sterile in solar and atmospheric’ oscillations is less than $1 = \sin^2 \theta_s + \cos^2 \theta_s$, as would be implied by 2+2 oscillations, that are therefore ‘strongly disfavored’ or ‘excluded’ .

9.2.3 Sterile neutrinos with 3+2 spectrum

Generically one expects that replacing one sterile neutrino with n sterile neutrinos does not make LSND more compatible with disappearance experiments. In fact replacing the couple θ_{es} and $\theta_{\mu s}$ with a few couples of smaller mixings θ_{es_n} and $\theta_{\mu s_n}$ reduces the LSND transition probability (governed by $\theta_{LSND} \approx \sum_n \theta_{es_n} \theta_{\mu s_n}$) more than the disappearance probabilities $1 - 2 \sum_n \theta_{es_n}^2$. A detailed analysis performed with 2 sterile neutrinos [83] found some improvement in the LSND fits and in the fit of data from disappearance experiments (which contain some mild anomaly) but apparently not in their mutual compatibility.

Furthermore cosmological data indicate that standard BBN is not compatible with two extra thermalized sterile neutrinos. The values of their masses suggested by 3+2 fits are not compatible with standard cosmology, that implies the cosmological bound on neutrino masses of eq. (10.8). These conflicts can be avoided by invoking appropriate non-standard cosmologies.

9.2.4 CPT violation

Neutrinos might have different masses and mixings than anti-neutrinos. It was proposed that one mass splitting among anti-neutrinos might be in the range suggested by LSND. However newer data and more careful reanalyses showed that this is not possible because the solar and atmospheric anomalies are now seen also in anti-neutrinos, with mass splittings in agreement with CPT invariance. Indeed KamLAND confirmed the solar ν_e anomaly studying reactor $\bar{\nu}_e$. SK atmospheric data are more sensitive to ν_μ than to $\bar{\nu}_\mu$ (because $\sigma(\nu_\mu N) \sim 2\sigma(\bar{\nu}_\mu N)$, see eq. (4.14)), but anyhow imply a Δm^2 in the atmospheric range also in anti-neutrinos. A more direct test will be possible with the MINOS detector, that can study atmospheric neutrinos discriminating μ from $\bar{\mu}$.

9.2.5 A sterile neutrino plus CPT violation

A satisfactory global fit is possible by introducing one sterile neutrino and allowing neutrinos and anti-neutrinos to have different masses and mixings. One can fit the LSND anomaly in anti-neutrinos without introducing any effect in neutrinos and thereby avoiding constraints from experiments performed with neutrinos.

9.2.6 A decaying sterile neutrino

Alternatively, one can relax constraints from other experiments by assuming that the sterile neutrino decays back into active neutrinos.

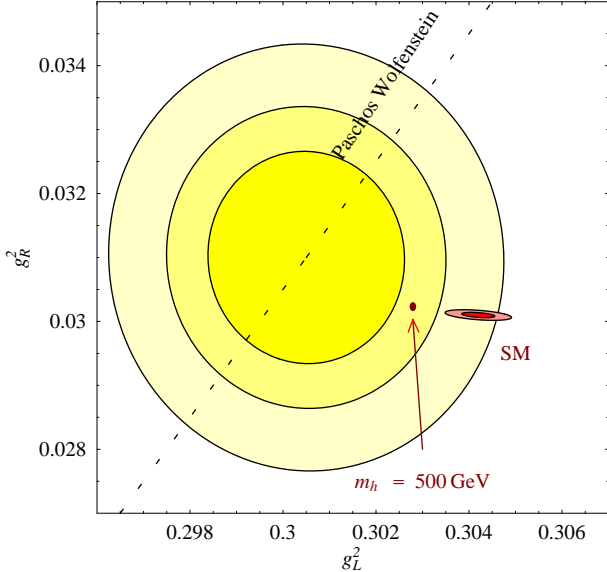


Figure 9.6: The SM prediction for (g_L^2, g_R^2) at 68, 99% CL and the NuTeV determination, at 68, 90, 99% CL. The NuTeV central value moves along the PW line using different sets of parton distribution functions that assume $s = \bar{s}$ and $u^p = d^n$.

9.2.7 Anomalous muon decay

The LSND anomaly might be due to a speculative anomalous muon decay channel of the type $\bar{\mu} \rightarrow \bar{e}\bar{\nu}_e(\bar{\nu})$, with branching ratio equal to the oscillation probability suggested by LSND, eq. (9.1), up to an $\mathcal{O}(1)$ factor that takes into account that the anomalous decay might give a $\bar{\nu}_e$ spectrum softer (harder) than the one from ordinary μ decay needs a higher (lower) branching ratio. Therefore the needed anomalous decay generically leads to deviations from the SM at the few 10^{-3} level in the μ life-time and in the energy spectrum of the emitted electrons. Both these effects are somewhat disfavored by data, Global fits of electroweak data [85] indicate that the μ life-time agrees with the SM at 10^{-3} level. The measured value of the Michel parameter ρ (that characterizes the electron spectrum) is $\rho = 3/4 + (0.8 \pm 1.0)10^{-3}$ [86], where $3/4$ is the SM prediction.

Furthermore the fact that LSND has a longer path-length than KARMEN plays no rôle according to this interpretation, that is therefore disfavored by KARMEN.

9.2.8 Anomalous neutrino couplings

It seems impossible to interpret the LSND anomaly as due to anomalous flavour-violating interactions of $\nu_{e,\mu}$ without generating too large corresponding effects among e, μ .

Furthermore the fact that LSND has a longer path-length than KARMEN plays no rôle according to this interpretation, that is therefore disfavored by KARMEN.

9.2.9 Mass-varying neutrinos

Neutrino masses might be controlled by the vacuum expectation value of some field that can depend on space, on time, on the local density of matter,... The fact that solar and reactor data give compatible determinations of Δm_{sun}^2 makes such models less appealing. However, thanks to its generality, this possibility allows to fit LSND data.

9.3 NuTeV

The NuTeV collaboration [14] reported a $\sim 3\sigma$ anomaly in the NC/CC ratio of deep-inelastic muon-neutrino/nucleon scattering. The effective ν_μ coupling to left-handed quarks is found to be about 1% lower than the best fit SM prediction. LEP experiments found that charged lepton couplings agree with SM predictions within *per-mille* accuracy. See [87] for other related experiments.

The NuTeV experiment sent both a ν_μ and a $\bar{\nu}_\mu$ beam (obtained from the FermiLab Tevatron) on an iron target. Neutrinos had energy $E_\nu \sim 100$ GeV and the average transferred momentum was $\langle q^2 \rangle \approx -20$ GeV². Events were detected by a calorimeter. The muon produced in CC events gives a long track, while the hadrons in NC events give a short track. In this way the NuTeV collaboration could statistically distinguish NC from CC events. The neutrino energy spectrum was computed by a MonteCarlo simulation. The ratios of neutral-current (NC) to charged-current (CC) deep-inelastic neutrino–nucleon scattering total cross–sections, R_ν and $R_{\bar{\nu}}$, are free from the uncertainties on the neutrino fluxes and contain the most interesting pieces of information. We recall the tree-level SM prediction for these quantities. The ν_μ -quark effective Lagrangian predicted by the SM at tree level is given by eq. (4.5) in terms of the Z couplings g_{Aq} ($q = \{u, d, s, \dots\}$, $A = \{L, R\}$) listed in table 4.1 at page 45. Including only first generation quarks, for an isoscalar target, and to leading order, R_ν and $R_{\bar{\nu}}$ are given by

$$R_\nu \equiv \frac{\sigma(\nu\mathcal{N} \rightarrow \nu X)}{\sigma(\nu\mathcal{N} \rightarrow \mu X)} = \frac{(3g_L^2 + g_R^2)q + (3g_R^2 + g_L^2)\bar{q}}{3q + \bar{q}} = g_L^2 + rg_R^2 \quad (9.3a)$$

$$R_{\bar{\nu}} \equiv \frac{\sigma(\bar{\nu}\mathcal{N} \rightarrow \bar{\nu} X)}{\sigma(\bar{\nu}\mathcal{N} \rightarrow \bar{\mu} X)} = \frac{(3g_R^2 + g_L^2)q + (3g_L^2 + g_R^2)\bar{q}}{q + 3\bar{q}} = g_L^2 + \frac{1}{r}g_R^2, \quad (9.3b)$$

where q and \bar{q} denote the fraction of the nucleon momentum carried by quarks and antiquarks, respectively. For an isoscalar target, $q = (u + d)/2$, and we have defined

$$r \equiv \frac{\sigma(\bar{\nu}\mathcal{N} \rightarrow \bar{\mu} X)}{\sigma(\nu\mathcal{N} \rightarrow \mu X)} = \frac{3\bar{q} + q}{3q + \bar{q}} \quad (9.4)$$

and

$$g_L^2 \equiv g_{Lu}^2 + g_{Ld}^2 = \frac{1}{2} - \sin^2 \theta_W + \frac{5}{9} \sin^4 \theta_W, \quad g_R^2 \equiv g_{Ru}^2 + g_{Rd}^2 = \frac{5}{9} \sin^4 \theta_W. \quad (9.5)$$

The observables R_ν^{exp} and $R_{\bar{\nu}}^{\text{exp}}$ measured at NuTeV differ from the ideal observables in eq. (9.3). Total cross–sections can only be determined up to experimental cuts and uncertainties, such as those related to the spectrum of the neutrino beam, the contamination of the ν_μ beam by electron neutrinos, and the efficiency of NC/CC discrimination. Once all these effects are taken into account, the NuTeV data can be presented as a measurement of

$$g_L^2 = 0.3005 \pm 0.0014 \quad \text{and} \quad g_R^2 = 0.0310 \pm 0.0011, \quad (9.6)$$

where errors include both statistical and systematic uncertainties. According to (9.6) g_L is $\sim 3\sigma$ below its SM prediction.

The difference of the effective couplings $g_L^2 - g_R^2$ (‘Paschos–Wolfenstein ratio’ [88]) is subject to smaller theoretical and systematic uncertainties than the individual couplings:

$$R_{\text{PW}} \equiv \frac{R_\nu - rR_{\bar{\nu}}}{1 - r} = \frac{\sigma(\nu\mathcal{N} \rightarrow \nu X) - \sigma(\bar{\nu}\mathcal{N} \rightarrow \bar{\nu} X)}{\sigma(\nu\mathcal{N} \rightarrow \ell X) - \sigma(\bar{\nu}\mathcal{N} \rightarrow \bar{\ell} X)} = g_L^2 - g_R^2 = \frac{1}{2} - \sin^2 \theta_W. \quad (9.7)$$

NuTeV is consistent with previous experiments, such as CCFR [89]. CCFR had a beam containing both ν_μ and $\bar{\nu}_\mu$, while NuTeV has two separate ν_μ and $\bar{\nu}_\mu$ beams. This is the main improvement because allows to get rid of the unprecisely known partonic structure of the nucleon using R_{PW} , which, under the above assumptions, is independent of q and \bar{q} . The NuTeV value of R_{PW} is $\sim 3\sigma$ below its SM prediction.

Doing precision physics with iron is a delicate task. One needs to carefully study if the apparent anomaly could be due to under-estimated errors, or to some neglected effect. Progress concerning the following points would be welcome

- **NLO QCD corrections** have been neglected in the NuTeV analysis, and cancel out in the ideal PW observable [90]. Probably this cancellation remains strong enough in the true PW-like observable.
- **QED** and electroweak loops give a few % correction to R_{PW} and cannot explain the anomaly if they have been included taking into account experimental cuts. Without knowing them, the impact of recent precise computations cannot be determined.
- **Nuclear effects** could affect R_ν and $R_{\bar{\nu}}$, but only at low momentum transfer and apparently not in a way that allows to reconcile NuTeV data with the SM [90]. These effects are partially automatically included in the NuTeV analysis, based on their own parton distributions obtained fitting only iron data.
- **Parton distributions:** $q(x)$ are extracted from global fits, usually performed under two simplifying assumptions: $s(x) = \bar{s}(x)$ and $u^p(x) = d^n(x)$. These approximations could be not accurate enough, at the level of precision reached by NuTeV. In presence of a momentum asymmetry $q^- = \int_0^1 x[q(x) - \bar{q}(x)]dx$ the ideal PW observable shifts as

$$R_{\text{PW}} = \frac{1}{2} - \sin^2 \theta_W + (\text{EW corrections}) + (1.3 + \text{QCD corrections})(u^- - d^- - s^-)$$

According to naïve estimates, $u^- - d^- \sim \max[(m_u - m_d)/\Lambda_{\text{QCD}}, \alpha_{\text{em}}]$ and $s^- \sim s, \bar{s}$, these effects could account for the NuTeV anomaly.

- Isospin is broken by quark masses and by electromagnetism. Electromagnetism gives an effect with the correct sign: $u^- - d^- < 0$ because u quarks have bigger charge than d quarks and therefore radiate more photons. Some detailed computations performed replacing QCD with more tractable phenomenological models suggest that, due to cancellations, isospin-violating effects are somewhat too small. It is not clear if a QCD computation would lead to the same conclusion. An **isospin-violating** interpretation of the NuTeV anomaly is compatible with other available data.
- Since a nucleon contains 3 quarks (rather than three antiquarks) one expects that s and \bar{s} carry comparable (but not equal) fractions of the total nucleon momentum. Non perturbative fluctuations like $p \leftrightarrow K\Lambda$ are expected to give s harder than \bar{s} since K is lighter than Λ . Indeed $s^- > 0$ could explain the NuTeV anomaly. Some model computations suggest that s^- is too small, but again it is not clear how reliable they are. The s^- issue can also be addressed relying on inclusive DIS data and on charm-production scattering data: after some controversy recent global fits find $-10^{-3} < s^- < 4 \cdot 10^{-3}$ giving a hint for a **strange momentum asymmetry** of the desired sign and magnitude.

In conclusion, testing and eventually excluding such SM ‘systematic effects’ which can produce the NuTeV anomaly seems to be a difficult job. Therefore, it is useful to speculate about possible new physics interpretations which might have cleaner signatures [90]. Unfortunately, no particularly compelling new physics with distinctive signatures has been found. The problem is that $\bar{\ell}Z\ell$ and $\bar{\ell}W\nu$ couplings (where ℓ denotes charged leptons) agree with the SM and have been measured about 10 times more accurately than $\bar{\nu}Z\nu$ couplings. Proposals which overcome this problem look exotic, while more plausible possibilities work only if one deals with constraints in a ‘generous’ way or introduces and fine-tunes enough free parameters.

For example, mixing the Z boson with an extra Z' boson modifies NC neutrino couplings, but also NC couplings of leptons (ℓ_L and ν are unified in the same $SU(2)_L$ doublet) conflicting with precision data. New physics that only affects the gauge boson propagators cannot fit the NuTeV anomaly due to the same constraints. Neutrino oscillations are not compatible with other experiments. A reduction of neutrino couplings due to a $\sim 1\%$ mixing with sterile singlets does not work, because CC neutrino couplings have been too precisely tested by μ decay together with precision data. Combinations of the above effects with enough unknown parameters can work². The NuTeV anomaly can be fitted by adding to the SM Lagrangian the specific $SU(2)_L$ invariant effective operator $-(0.024 \pm 0.009)2\sqrt{2}G_F[\bar{L}_2\gamma_\mu L_2][\bar{Q}_1\gamma^\mu Q_1]$ (1,2 are generation indexes). The new physics which could generate it can either be heavy with sizable couplings (so that future colliders should see it) or light with small couplings (e.g. a Z' with few GeV mass and negligible mixing with the Z).

On the experimental side [87] it is possible to measure alternative processes where the possible new physics behind the NuTeV anomaly could manifest. Facilities built for long-baseline neutrino experiments will allow to repeat the NuTeV experiment, possibly at larger neutrino energies. Future reactor experiments could measure $\bar{\nu}_e e$ couplings as accurately as NuTeV measured $\nu_\mu N$ couplings. The E158 experiment is measuring the weak angle θ_W in ee collisions, at energies even lower than NuTeV.

In conclusion, there are various possible SM and new physics interpretations of the NuTeV anomaly. More work is needed to identify the true one.

²For example, mixing with a sterile singlet together with a heavy higgs fits all data if one also assumes that some extra unspecified new physics affects M_W and therefore ignores this measurement [90]. A failure of the SM fit of electroweak data would support the case for new physics, but at the moment we do not see any convincing problem.

Chapter 10

Neutrinos in cosmology

In absence of new physics, neutrinos are light, weakly interacting and essentially stable so that relic big bang neutrinos ('CMB neutrinos') must still exist today and be, after photons, the most abundant particle species in the universe. Cosmology allows to count CMB neutrinos and to study some of their properties because neutrinos significantly influenced observed relics of the past evolution of the universe. We will discuss stages where this happened, presenting the predictions of standard cosmology

- *Big Bang Nucleosynthesis* (section 10.1). The relative number of protons and neutrons (and of few other light nuclei) has been fixed by weak interactions involving neutrinos, that decoupled below temperatures $T \sim \text{MeV}$ (about one minute after the big-bang). Controversial measurements of their primordial abundances are consistent with SM predictions (3 neutrinos in thermal equilibrium at $T \sim \text{MeV}$).
- *Cosmic Microwave Background* (section 10.2). Photons decoupled at $T \sim 0.3 \text{ eV}$ (about 0.3 Myr later) when electrons and protons formed neutral hydrogen. Measurements of anisotropies in photon CMB are now testing many aspects of cosmology, including neutrinos. Present data indicate that CMB neutrinos were present at $T \sim 0.3 \text{ eV}$.
- *Large Scale Structures* (section 10.2). Gravity tends to cluster non relativistic particles (normal matter and cold dark matter), while relativistic non-interacting particles suppress this process. Massive neutrinos became non relativistic when $E_\nu \sim T \lesssim m_\nu \sim 300 \text{ K}$, leaving a small imprint in the measurable amount of clustering of galaxies. Present data give bounds on m_ν competitive with laboratory experiments.
- *Thermal Leptogenesis* (section 10.3). The tiny excess of matter over anti-matter [69]

$$\eta \equiv \frac{n_B - n_{\bar{B}}}{n_\gamma} = \frac{n_B}{n_\gamma} = (6.15 \pm 0.25) 10^{-10} \quad (10.1)$$

might have been generated in decays of right-handed neutrinos with mass maybe around 10^{10} GeV . We do not know how to test this speculative mechanism.

The hottest relics observed so far were produced only at $T \lesssim \text{MeV}$ — an energy region explored with cosmic rays and colliders more than 50 years ago. However cosmology is sensitive to kinds of new physics which cannot be probed by such experiments. So far cosmological data are consistent with the SM, but significant progress is expected in the near future.

10.1 Big-bang nucleosynthesis

We discuss the reasonable agreement with data of the standard BBN scenario, and the consequent bounds on non-standard neutrino properties. Detailed discussions can be found in the relevant literature [91, 92, 93].

Big-bang nucleosynthesis is the theory of abundances of light nuclei. We start presenting the predictions of standard cosmology. The early universe at temperatures $m_e \ll T \ll m_p$ contained $\gamma, e, \bar{e}, \nu_{e,\mu,\tau}, \bar{\nu}_{e,\mu,\tau}$ plus a minor component of protons and neutrons. Reacting species were in quasi-homogeneous phase (as suggested by simplest inflationary scenarios and supported by CMB data), with the 3 light neutrinos in thermal equilibrium. Abundances have been determined by different processes, all happened around $T \sim \text{MeV}$, because MeV is

1. the typical binding energy of light nuclei (e.g. $m_n - m_p = 1.293 \text{ MeV}$).
2. the temperature at which electrons become non-relativistic. This event indirectly affected BBN.
3. the neutrino decoupling temperature. In fact, the neutrino interaction rate (i.e. the number of collisions experienced by a neutrino per unit time) was $\Gamma_\nu \sim \sigma(\nu e) \cdot n_\nu \sim G_F^2 T^2 \cdot T^3$. Comparing it with the expansion rate $H \sim T^2/M_{\text{Pl}}$ gives $\Gamma_\nu/H \sim (T/T_\nu^{\text{dec}})^3$: neutrinos decoupled below $T_\nu^{\text{dec}} \sim g^{1/6} (G_F^2 M_{\text{Pl}})^{-1/3} \sim \text{MeV}^1$.

Weak scatterings involving ν_e ($\nu_e n \leftrightarrow e p$ and $\bar{\nu}_e p \leftrightarrow \bar{e} n$) kept the number ratio between protons and neutrons in thermal equilibrium, $n_n(T)/n_p(T) = e^{-(m_n - m_p)/T}$. Neutrinos decoupled about one second after the big-bang, freezing $n_n/n_p \sim e^{-(m_n - m_p)/T_\nu^{\text{dec}}} \sim 1/6$. Therefore $e\bar{e} \rightarrow \gamma$ annihilations at $T \sim m_e$ heated photons but not neutrinos.

Neutrons are still free and can decay: n_n/n_p decreases down to about 1/7 when, at $T \approx 0.07 \text{ MeV}$ (see fig. 10.1b) the universe is sufficiently cold that neutrons get bound in nuclei. Almost all neutrons form ${}^4\text{He}$ because it is the light nucleus with the largest binding energy ($B = 28.3 \text{ MeV}$), and production of heavier nuclei (like ${}^7\text{Li}$, there are no stable isotopes with 5, 6, 7 or 8 nucleons) is strongly suppressed by Coulombian repulsion. Therefore the prediction for the ${}^4\text{He}$ mass fraction is² $Y_p \approx 2n_n/(n_n + n_p) \approx 1/4$. Around the central values of n_B and N_ν one has

$$Y_p = 0.248 + 0.0096 \ln \frac{n_B/n_\gamma}{6 \cdot 10^{-10}} + 0.013(N_\nu^{{}^4\text{He}} - 3). \quad (10.2)$$

Numerical factors follow from our semi-quantitative arguments. We reported the precise values obtained from public codes that describe the nuclear network, giving predictions accurate at the per-mille level. The apix ‘ ${}^4\text{He}$ ’ on N_ν is present because we want to consider generic kinds of new physics that modify Y_p (e.g. a sterile neutrino that thermalizes during BBN): we parameterize their correction to Y_p in terms of an observable ‘effective numbers of neutrinos’, $N_\nu^{{}^4\text{He}}$, univocally

¹The precise value of H depends on the number of neutrinos N_ν as follows: $H = (8\pi\rho/3)^{1/2}/M_{\text{Pl}} = 1.66g^{1/2}T^2/M_{\text{Pl}}$ where $\rho = g\pi^2 T^4/30$ is the energy density and $g = 2 + \frac{7}{8}(4 + 2N_\nu)$ is the number of SM spin degrees of freedom at $T \gg m_e$.

²An important detail. Let us consider e.g. deuterium, the lightest nucleus produced by $pn \leftrightarrow D\gamma$ reactions. Since $\eta = n_B/n_\gamma \ll 1$ deuterium is formed not at $T \sim B$ ($B = 2.22 \text{ MeV}$ is the small binding energy of deuterium) but at $T \sim B/\ln(n_\gamma/n_B) \sim 0.1 \text{ MeV}$. Time in seconds and temperature in MeV are related by $t \sim 1/T^2$. Y_p depends slightly on n_B/n_γ because its smallness delays nucleosynthesis, giving more time to neutrons to decay.

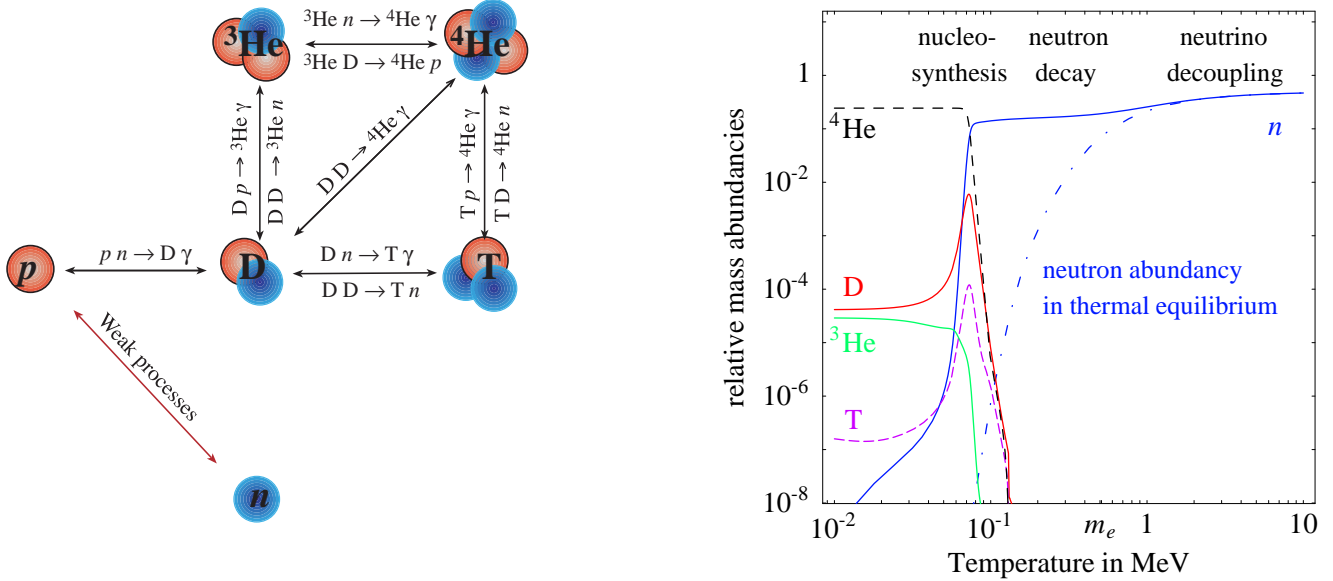


Figure 10.1: Left: main reactions relevant for BBN. Right: evolution of the main nuclear components.

defined by the inversion of eq. (10.2). We will define in an analogous way a few other cosmological observables.

All other nuclei have small abundances, that depend on powers of $\eta \equiv n_B/n_\gamma$ and on N_ν essentially through the combination $\eta/\sqrt{g_*}$, where $g_* = 4 + (7/4)(11/3)^{4/3}N_\nu$ is the number of relativistic dof after $e\bar{e}$ annihilations. Of particular importance is the deuterium abundance, predicted to be

$$\frac{Y_D}{Y_H} \approx (2.75 \pm 0.13) 10^{-5} \frac{1 + 0.11 (N_\nu^D - 3)}{(\eta/6.15 10^{-10})^{1.6}} \quad (10.3)$$

with an uncertainty mainly induced from nuclear cross-sections. The observed abundances of ^4He , deuterium, ^7Li can all be reproduced for $\eta \sim \text{few} \cdot 10^{-10}$. CMB and LSS data presently give an independent measurement of η , reported in eq. (10.1), which is consistent with (and more precise than) BBN, if we assume that the present standard cosmological model (flat Λ CDM, ...) is correct.

We are here interested in testing the expansion rate, parameterized in eq.s (10.2), (10.3) by $N_\nu - 3$, the number of extra relativistic species in thermal equilibrium at $T \sim \text{MeV}$. The (conservative) observational values for the ^4He and D abundance imply [92]

$$\begin{aligned} Y_p &= 0.25 \pm 0.01 & : & N_\nu^{^4\text{He}} &= 3 \pm 0.7 \\ Y_D/Y_H &= (2.8 \pm 0.5) 10^{-5} & : & N_\nu^D &\approx 3 \pm 2 \end{aligned} \quad (10.4)$$

In order to discriminate $N_\nu = 3$ from $N_\nu = 4$ it is necessary to either *i*) somewhat improve the determination of Y_p , or to *ii*) improve on Y_D , somewhat improve on η and on the theoretical uncertainty on Y_D .

Today the error budget is dominated by the observational uncertainties. Measurements of the primordial abundances Y_d and Y_D are difficult and controversial. One of the problems is that, after BBN, nuclear abundances have been modified by stars and other astrophysical processes.

Helium-4 Since stars produce ${}^4\text{He}$ together with heavier elements ('metals') one reconstructs the primordial ${}^4\text{He}$ abundance by measuring it in differently contaminated environments and extrapolating to zero metallicity. Of particular importance are the metal-poor HII regions: gas clouds ionized by young stars. Measuring de-excitation light spectra one deduces the relative abundance of ionized and doubly ionized ${}^4\text{He}$ with respect to ionized hydrogen. In order to reconstruct the ${}^4\text{He}/\text{H}$ relative abundance one needs stellar population models able of controlling systematic corrections due to stellar absorption, to different ionization regions for H and ${}^4\text{He}$, to Balmer lines excited by collisional processes and to temperature fluctuations. We think that our eq. (10.4) correctly summarizes the present situation. Adding more digits would suggest that Y_p has an established central value and uncertainty. Unfortunately this is not the case: it is difficult to quantify the above systematical uncertainties. Some authors report smaller errors or smaller central values, such that $N_\nu^{{}^4\text{He}} = 4$ looks already excluded. According to some authors, future improvements are possible.

Deuterium Alternatively, future measurements of the deuterium abundance might give the most stringent test of the number of neutrinos during BBN. Deuterium has different and apparently less problematic systematic uncertainties: it is not produced but only destroyed by stars, and can be partly hidden in HD molecules. It is measured from quasar absorption line systems at high redshift, which are presumably not contaminated by stars. Several groups quote $\sim 10\%$ uncertainties but obtain $\sim 50\%$ discrepancies among their central values. Finding and studying well-suited high-redshift systems might result in precise determinations of the D abundance.

Other nuclei Tritium decays. The ${}^7\text{Li}$ abundance seems to be 3 times lower than the value $Y_{7\text{Li}} \approx 4 \cdot 10^{-10}$ predicted by BBN assuming eq. (10.1). This might be due to systematic uncertainties. Other primordial abundance (${}^3\text{He}, \dots$) are poorly determined.

The message is that present data seem to agree in a satisfactory way with standard BBN predictions, but are not yet accurate enough to discriminate $N_\nu = 3$ (SM) from $N_\nu = 4$ (SM plus one extra thermalized fermion) or from $N_\nu = 3 + 4/7$ (SM plus one extra thermalized scalar). This could be done by future measurements of the ${}^4\text{He}$ or deuterium abundances: we subscribe the conclusion of Sarkar's review in [94] "... measurements [of abundances] ought to constitute a *key* programme for cosmology, with the same priority as, say, the measurements H_0 or Λ ".

It is important to emphasize that one should not say ' $N_\nu = 5$ is excluded' but rather ' $N_\nu = 5$ is not compatible with standard cosmology'. Standard cosmology has not been tested, and many more or less motivated non-standard BBN scenarios have been proposed. There could be further reprocessing of nuclear elements, e.g. by a very early population of stars; neutrinos could have a non thermal distribution (e.g. in scenarios with very low reheating temperature) or carry leptonic asymmetries; the distribution of light nuclear species (or even, the baryon number distribution itself) might be non-homogeneous; late decaying particles can modify the cosmological scenario where BBN takes place; large magnetic fields might exist during nucleosynthesis; fundamental constants may vary; neutrinos might have non standard properties; other light species might populate the Universe; etc.

In view of this situation it is important to test if $N_\nu = 3$ with as many observables as possible. We now discuss what we can learn from CMB anisotropies.

10.2 Cosmic microwave background and large-scale structures

Photons decoupled from matter when the universe cooled enough that electrons and protons formed neutral hydrogen. The last scattering occurred when the universe had temperature $T \approx 0.3 \text{ eV}$, age $\approx 2 \cdot 10^5 \text{ yr}$ and was about $1 + z \sim 1000$ times smaller than today. Namely, the observable horizon had a size of about a $\text{Mpc} \equiv 3.26 \cdot 10^6 \text{ ly}$, comparable to the typical distance between galaxies today. Measuring the fossil CMB radiation teaches a lot of things about the early universe. In particular, the pattern of observed small anisotropies in the CMB temperature, $\delta T/T \sim 10^{-5}$, depends on primordial fluctuations (possibly produced during a period of inflation), on photon/baryon ‘acoustic’ oscillations occurred around CMB decoupling, and on the later evolution of the universe. Although one has to study all these effects in order to disentangle them, we here concentrate on the rôle played by neutrinos.

As discussed in section 10.1, neutrinos decoupled at a temperature $T \sim \text{few} \cdot m_e$. Therefore electron/positron annihilations that occurred at $T \lesssim m_e$ transferred their energy into photons but negligibly to neutrinos. As a consequence the temperature of CMB neutrinos is predicted to be $T_\nu = (4/11)^{1/3} T$ where T is the CMB photon temperature.³ Today $T = 2.73^\circ\text{K}$ so that $T_\nu = 1.96^\circ\text{K} = 0.17 \text{ meV}$, which corresponds to a present neutrino number density $n_{\nu_i} = n_{\bar{\nu}_i} = 3n_\gamma/22 = 56/\text{cm}^3$. Since T_ν is smaller than the neutrino mass scale suggested by solar and atmospheric oscillations, CMB neutrinos are today mostly non-relativistic. Their present contribution to the total energy density is

$$\Omega_\nu \equiv \frac{\rho_\nu}{\rho_{\text{critical}}} = \frac{\sum_i m_{\nu_i} n_{\nu_i}}{3H^2/8\pi G_N} = \frac{10^{-3}}{h^2} \frac{\sum_i m_{\nu_i}}{0.1 \text{ eV}} \quad (10.5)$$

where, as usual, the present Hubble constant is written as $H = 100h \text{ km/s Mpc}$ with $h \approx 0.7$. Neutrino masses have a minor effect (not yet observed), so that it is convenient, in first approximation, to consider neutrinos as massless.

In this approximation the total energy density in relativistic particles (‘radiation’) around recombination, $T \sim 0.3 \text{ eV}$, is predicted to be

$$\rho_{\text{rad}} = \rho_\gamma + \rho_\nu = \left[1 + \frac{7}{8} \left(\frac{4}{11} \right)^{4/3} N_\nu^{\text{CMB}} \right] \rho_\gamma \quad (10.6)$$

with $N_\nu^{\text{CMB}} = 3$ (small corrections from the approximation above give $N_\nu^{\text{CMB}} = 3.04$). In presence of new physics the SM formula eq. (10.6) is no longer true, but still used as the definition of the effective parameter N_ν^{CMB} .

We recall that the total energy density $\rho = \rho_\Lambda + \rho_{\text{CDM}} + \rho_\gamma + \rho_\nu + \rho_{\text{baryons}} + \dots$ started being dominated by non-relativistic matter rather than by relativistic radiation at $T \sim \text{eV}$, slightly

³We present the computation. After neutrino decoupling, the neutrino temperature decreases as $T_\nu \propto 1/R$. Since electron/positron annihilations proceed in thermal equilibrium with photons, their total entropy $(s_e + s_\gamma)R^3$ remains constant. Consequently $(T_\nu/T)^3 = (2 + 4s_e(T)/s_\gamma(T))/(2 + 4 \cdot 7/8)$. At temperatures above m_e $T_\nu = T$ and the total energy density is $\rho = g\pi^2 T^4/30$ with $g = 43/4$. At temperatures below m_e we can neglect s_e so that $T_\nu = T(4/1)^{1/3}$ and $g = 2 + \frac{7}{8}2 \cdot 3 \cdot (\frac{4}{11})^{4/3} = 3.36$. More precise computation take into account that at $T \sim m_e$ neutrinos are not completely decoupled, especially the most energetic ones. As a consequence $e\bar{e}$ annihilations also generate a few additional ν_e (partially converted into $\nu_{\mu,\tau}$ by solar and atmospheric oscillations) distorting their energy spectrum.

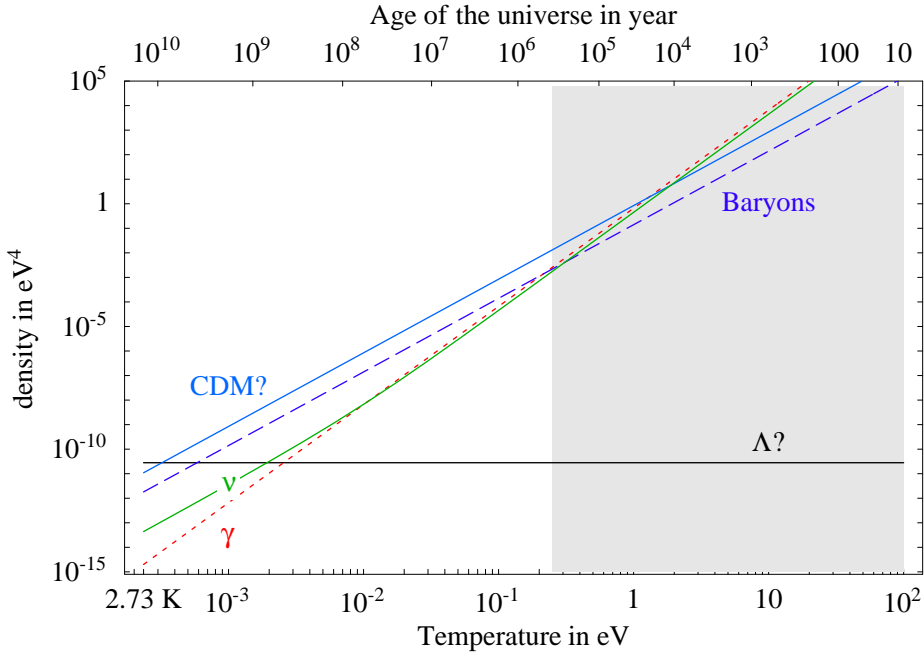


Figure 10.2: *Evolution of the average energy densities of photons, neutrinos, baryons, Cold Dark Matter and cosmological constant Λ .* We assumed that today $h \approx 0.7$, $\Omega_{\text{tot}} = 1$, $\Omega_{\Lambda} \approx 0.7$, $\Omega_{\text{CDM}} \approx 0.3$. Neutrinos are relativistic at $T \gg m_{\nu}$ ($\rho_{\nu} \approx T^4$), and non-relativistic at lower temperatures ($\rho_{\nu} \approx m_{\nu} T^3$). Shading covers the epoch before γ decoupling.

before recombination, see fig. 10.2. Measurements of CMB anisotropies allow to reconstruct N_{ν} in two different ways: a) from the total energy density in relativistic particles, ρ_{rad} , that significantly contributes to the measurable expansion rate around recombination, since recombination happened slightly later than the transition from a radiation to a matter-dominated; b) the energy density in freely moving relativistic particles (like neutrinos, and unlike photons) can be reconstructed, as they smooth out inhomogeneities, as discussed in the next section. These effects are shown in fig. 10.3 where we plot how CMB anisotropies change by varying, at fixed best-fit values of all other cosmological parameters, i) N_{ν} ; b) the fraction p of freely-moving neutrinos. The standard scenario predicts $N_{\nu} = 3$ and $p = 1$. Global fits take into account that a non-standard neutrino cosmology can be masked by variations of other cosmological parameters: one usually considers Λ CDM flat models. Data are reaching the necessary sensitivity; at the moment different analyses find somewhat contradictory results [69, 95, 96]: a reasonable summary probably is:

$$N_{\nu}^{\text{CMB}} \approx 3 \pm 0.5, \quad p \approx 1 \pm 0.3. \quad (10.7)$$

We remark that these cosmological data cannot measure the relative weight of each neutrino flavour, and cannot discriminate neutrinos from other speculative freely-moving relativistic particles.

10.2.1 Neutrino free-stream

We here describe how it is possible to test if the energy ρ_{ν} is carried by freely-moving relativistic particles. This allows to discriminate between massless vs massive and between free vs interacting neutrinos.

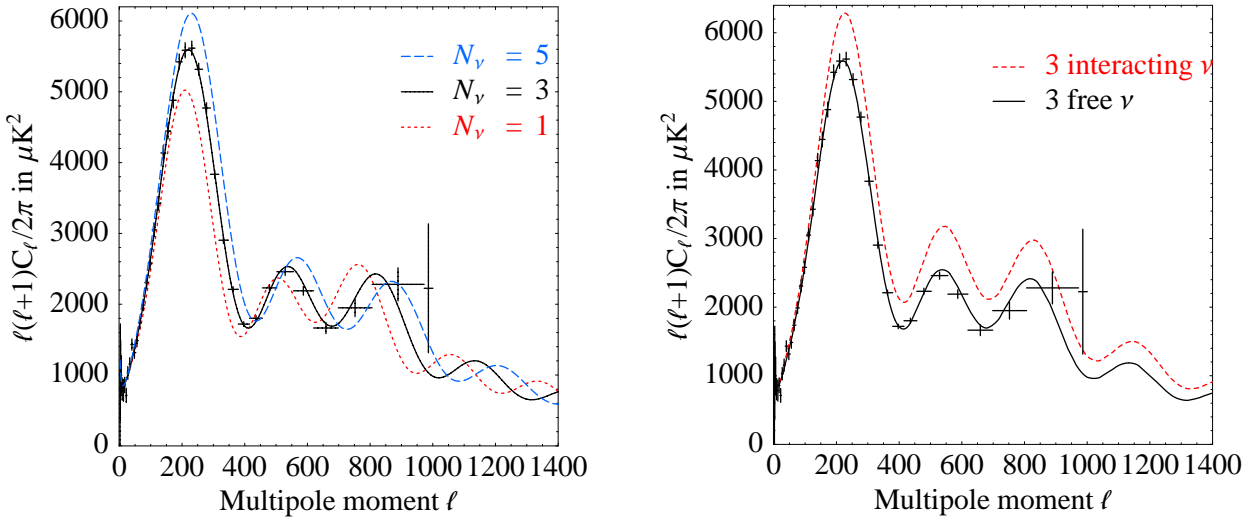


Figure 10.3: How CMB anisotropies (parameterized in terms of the conventional C_ℓ) depend, at fixed values of other cosmological parameters, on a) the energy density in relativistic free-streaming species (parameterized in terms of the conventional ‘number of neutrinos’ N_ν); b) the fraction of free vs interacting neutrinos. The crosses are the WMAP data.

Gravity tends to increase the initial fluctuations in the CDM density: this clustering process finally forms galaxies and the other structures we observe today. Relativistic particles with mean free path larger than the horizon (such as SM neutrinos) freely move (‘free stream’) and suppress this clustering process. In presence of new physics, neutrinos could instead interact among themselves or with new particles: in such a case neutrinos would tend to cluster in structures with size comparable to their Jeans length.

The presence or absence of neutrino free-streaming shifts the positions of the acoustic peaks of the CMB photon radiation. In this way it is possible to measure one more observable, N_ν^{FS} , which tests possible extra interactions among neutrinos. Present data mildly favor the standard scenario [95].

Neutrino free-stream is also prevented by neutrino masses: at $T \lesssim m_\nu$ neutrinos become non-relativistic and slow down so that in a Hubble time travel only in a fraction $\sim v/c$ of the horizon. Therefore massive neutrinos only reduce clustering at such small scales. Neutrino masses determine two different things: 1) the temperature at which neutrinos cease to be non-relativistic, which controls the length on which neutrinos travel reducing clustering; 2) the fraction of energy carried by neutrinos, see eq. (10.5), which controls how much neutrinos can smooth inhomogeneities.

Assuming standard cosmology LSS and CMB data imply an upper bound on Ω_ν , the energy density in neutrinos [96]:

$$\Omega_\nu h^2 \lesssim 0.6 \cdot 10^{-2} \quad \text{i.e.} \quad \sum m_{\nu_i} \lesssim 0.6 \text{ eV} \quad \text{at 99.9% C.L.} \quad (10.8)$$

which is the presently dominant upper bound on neutrino masses. CMB data alone give a bound on neutrino masses which is almost one order of magnitude weaker, and are mainly needed

to determine other cosmological parameters. We have chosen a large C.L. because presently statistical fluctuations (or systematic shifts?) make the constraint slightly stronger than the sensitivity. The precise final bound depends on how one deals with systematic uncertainties in LSS data: more aggressive strategies give stronger but less reliable bounds. In presence of extra sterile neutrinos the constraint depends on their abundances and can get slightly relaxed.

For the reader not satisfied by our short qualitative discussion we here re-discuss the above issues in a more quantitative way. A standard Newtonian computation shows that small fluctuations in the DM density $\delta_{\text{DM}}(x) = \delta\rho_{\text{DM}}(x)/\rho_{\text{DM}} \ll 1$ evolve according to [97]

$$\ddot{\delta}_{\text{DM}} + 2H\dot{\delta}_{\text{DM}} = 4\pi G_{\text{N}} \delta\rho \quad (10.9)$$

where the source term $\delta\rho$ is the fluctuation around the average *total* density ρ . For our purposes $\rho = \rho_{\text{DM}} + \rho_{\nu}$ and, as long as $T \gg m_{\nu}$, the relativistic motion of neutrinos basically prevents neutrino clustering: $\delta\rho_{\nu} = 0$. Therefore the evolution equation becomes

$$\ddot{\delta}_{\text{DM}} + 2H\dot{\delta}_{\text{DM}} = 4\pi G_{\text{N}}\rho(1 - f_{\nu})\delta_{\text{DM}} \quad (10.10)$$

where $f_{\nu} \equiv \rho_{\nu}/\rho_{\text{DM}}$. Our universe has critical density $\rho = 3H^2/8\pi G_{\text{N}}$ and during matter domination $H \simeq 2/3t$: for $f_{\nu} = 0$ one finds a growing solution $\delta_{\text{DM}} \propto t^{2/3} \propto a \propto T^{-1}$, where a is the expanding scale-factor of the universe (normalized to be $a = 1$ today). From matter domination to today primordial fluctuations increased by a factor $\text{eV}/T_{\text{now}} \sim 5000$ producing the observed LSS.

A $f_{\nu} > 0$ suppresses the growth of DM fluctuations: assuming e.g. a constant f_{ν} the solution is

$$\delta_{\text{DM}}(t) \propto a(t)^p \quad \text{with} \quad p = \frac{\sqrt{1 + 24(1 - f_{\nu})} - 1}{4}. \quad (10.11)$$

Fluctuations do not grow if $f_{\nu} = 1$ i.e. in a universe dominated by relativistic particles. This is why we only consider the matter-dominated era. We can also neglect the fact that during the latest stage of evolution the universe gets dominated by some form of vacuum energy (maybe a cosmological constant): it reduces the late-time growth of fluctuations by $\sim 25\%$ only.

Neutrinos started to be non relativistic after $a > a_{\text{NR}} \approx T_{\nu}^0/m_{\nu} = 1.6 \cdot 10^{-4} \text{ eV}/m_{\nu}$; in the phase with non relativistic neutrinos one has a constant $f_{\nu} = \Omega_{\nu}/\Omega_{\text{DM}} = \Omega_{\text{DM}}^{-1} \cdot \sum m_{\nu}/94 \text{ eV}$. Therefore neutrino masses reduce the power spectrum P (proportional to δ^2) by

$$\frac{P(m_{\nu})}{P(m_{\nu} = 0)} = a_{\text{NR}}^{2(1-p)} \approx e^{-8f_{\nu}}. \quad (10.12)$$

The last form is a simple numerical interpolation. This widely reported formula is the maximal effect, realized only on small scales (right side of fig. 10.4). To fully understand the effect of neutrino masses on different scales, we need two further steps inside cosmology.

- Fluctuations $\delta(t, x)$ are decomposed in Fourier components $\delta(t, k)$ (where the wavenumber k is a comoving scale, corresponding to the physical scale $k/a(t)$) and the scale-dependent power spectrum is $P(k) \propto \delta(k)^2$. We will not need the proportionality factor, defined such that the adimensional combination $\sqrt{k^3 P(k)/2\pi^2}$ is the relative inhomogeneity δ on scale k .

- Evolution of neutrino inhomogeneities δ_ν is described by an equation analogous to (10.9) with an extra pressure term:

$$\ddot{\delta}_\nu + 2H\dot{\delta}_\nu = 4\pi G_N \delta\rho - \left(\frac{kc_s}{a}\right)^2 \delta_\nu \quad (10.13)$$

where c_s is the average neutrino velocity (a precise computation must study the evolution of the neutrino angular and energy distribution). At $a \gtrsim a_{\text{NR}}$ neutrinos become non-relativistic and $c_s \approx T_\nu/m_\nu = T_\nu^0/m_\nu a$. We previously assumed that neutrinos do not cluster: this is true when k is so large than the pressure term dominates over the gravitational terms i.e. for $k > k_{\text{Jeans}}(a) \approx H_0 a^{1/2} m_\nu / T_\nu^0$.

Eq. (10.12) can now be generalized by repeating the previous arguments in the different clustering regimes. The result is

$$\frac{P(m_\nu, k)}{P(m_\nu = 0, k)} \approx \begin{cases} 1 & k \lesssim k_{\text{NR}} \\ (k_{\text{NR}}/k)^{4(1-p)} & k_{\text{NR}} \lesssim k \lesssim k_0 \\ (k_{\text{NR}}/k_0)^{4(1-p)} & k \gtrsim k_0 \end{cases} \quad (10.14)$$

and depends on two scales:

$$k_{\text{NR}} = k_{\text{Jeans}}(a = a_{\text{NR}}) \approx 60H_0 \sqrt{m_\nu / \text{eV}}, \quad k_0 \equiv k_{\text{Jeans}}(a = 1) \approx 5000H_0 (m_\nu / \text{eV}).$$

At $k \gtrsim k_0$ one recovers eq. (10.12).

Fig. 10.4 shows the result of a full numerical computation. Neutrino masses have a detectable effect if $m_\nu \gtrsim 0.1 \text{ eV}$; optimistically future cosmological measurements of $P(k)$ might be sensitive to the atmospheric mass splitting.

Neutrino masses have a minor impact on CMB anisotropies, basically because photons last scattered at $T \sim 0.3 \text{ eV}$, before that neutrino masses started to be an important factor.

10.2.2 Caveats

We explained the basic physics, but we could not here review the theoretical and the experimental techniques necessary to derive these results. However these results should not be accepted acritically: we now emphasize their main limitations.

On the theoretical side, global fits are usually performed assuming ‘minimal cosmology’: ΛCDM in presence of primordial adiabatic fluctuations with constant spectral index. Sometimes critical density and/or scale-invariant spectrum is also assumed. This model has only been partially tested and confirmed. Fig. 10.2 shows the evolution of the main contributions to the average density: a question mark is added on ‘ Λ ’ and ‘ CDM ’ because these components have not yet been directly tested. A kink in the spectral index could simulate or mask the small effect of neutrino masses. Minimal cosmology assumes no kink, but non-minimal models can easily produce it (e.g. adding a jump in the inflaton potential or in other more elegant ways). In conclusion, *results of precision analyses of CMB and LSS data do not follow only from data but also rely on theoretical assumptions*.

Furthermore, the evolution of fluctuations can be analytically computed until they are a small corrections to an homogeneous background, such as around photon decoupling. Today this is true only on large enough scales, $k \lesssim 0.3/\text{Mpc} \approx 1000H_0$, while on small scales there are large deviations from the smooth approximation (e.g. galaxies are $\sim 10^5$ more dense than the average

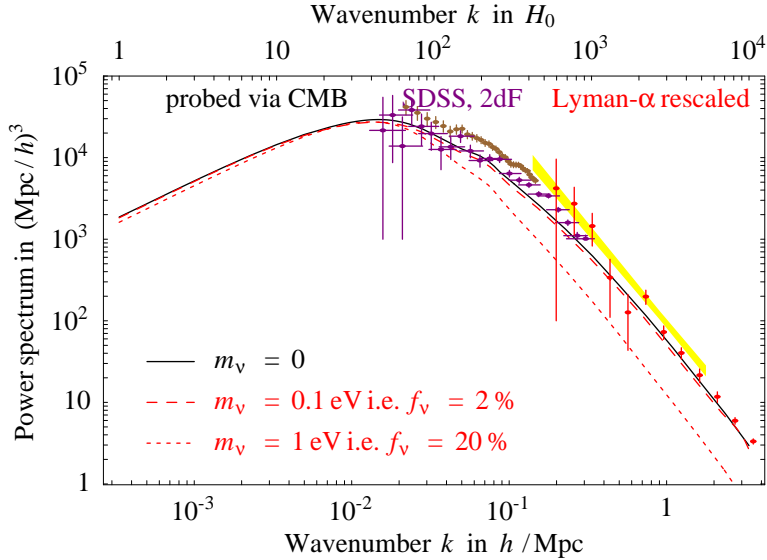


Figure 10.4: The matter power spectrum $P(k)$ predicted by the best-fit Λ CDM cosmological model (continuous curve) and how neutrino masses affect it (dashed curves). Measurements at different scales have been performed with different techniques, that slightly overlap. The data points do not show the overall uncertainty that plagues galaxy surveys (SDSS, 2dF) at intermediate scales and especially Lyman- α data at smaller scales i.e. at larger k .

universe). Numerical simulations or approximations are needed to study the non-linear evolution of sizable inhomogeneities. Due to this reason one sometimes prefers not to include the Lyman- α data in fig. 10.4, that probe the power spectrum on small scales dangerously close to the non-linear regime where the effects of neutrino masses are more sizable.

On the experimental side there are some problematic systematics. Presently we can only measure the density of luminous matter, and predict fluctuations in the total density. Most analyses are performed assuming that relative inhomogeneities in the density of galaxies are proportional (not necessarily equal) to relative inhomogeneities in the total energy density, with a scale-independent proportionality factor b ('bias'). Some analyses get stronger bounds by assuming models for the bias, that can be partially validated using the data. Future measurements of gravitational lensing of CMB light and/or of light generated by far galaxies should allow to directly measure the total density with greater accuracy. In this way, it might be possible to see the cosmological effects of neutrino masses, and measure them with an error a few times smaller than the atmospheric mass scale. This could allow to discriminate between normal and inverted neutrino mass hierarchy.

10.2.3 Direct detection of neutrino CMB

It would be interesting to directly test the background of relic CMB neutrinos. Extra light particles might distort it, giving neutrino decay, anomalous neutrino interactions, extra oscillation channels... Since relic neutrinos are today mostly non relativistic, their effects significantly depend on whether neutrinos have Majorana or Dirac masses. Furthermore massive neutrinos slower than the escape velocity cluster in galaxies. Locally $v_{\text{escape}} \approx 500 \text{ km/sec}$, which is comparable to the average neutrino velocity $\langle v_\nu \rangle \simeq (8T_\nu/\pi m_i)^{1/2} = (6200 \text{ km/sec})(\text{eV}/m_\nu)^{1/2}$. Gravitational forces

change the direction but not the spin of neutrinos, thereby populating the non-interacting helicity of Dirac neutrinos. Since neutrinos are fermions, local overdensities $n_{\nu_i}^{\text{local}}$ are severely limited by the Pauli exclusion principle (at most one neutrino in the phase-space volume $\Delta x \Delta p \sim \hbar$). In fact, assuming that all levels get occupied up to $p \sim m_\nu v_{\text{escape}}$ ⁴ one has

$$n_{\nu_i}^{\text{local}} - n_{\nu_i} \lesssim \frac{(m_{\nu_i} v_{\text{escape}})^3}{12\pi^2} = \frac{5000}{\text{cm}^3} \left(\frac{m_{\nu_i}}{\text{eV}} \frac{v_{\text{escape}}}{500 \text{ km}} \right)^3 \quad (10.15)$$

where we inserted order one factors [98]. Precise simulations find an over-density of 50% for $m_{\nu_i} = 0.15 \text{ eV}$.

The detection of CMB neutrinos is a very challenging goal, because their interaction rates are much below present experimental capabilities. Some possibilities might become realistic in the future [98]:

- *Coherent scattering.* The neutrino-nucleus cross section is so small, $\sigma \sim G_F^2 \max(E_\nu, m_\nu)^2 / \pi$, that CMB neutrinos give something like one event per year in a detector with mass 10^{16} kg .

A better signal is obtained exploiting the fact that CMB neutrinos have a macroscopic de Broglie wavelength, $\lambda = 1/p = (0.02 \text{ cm}) \text{meV}/p$. Therefore one can envisage elastic cross sections enhanced by the square of the number N of nucleons in a volume of size $R \lesssim \lambda/2\pi$. Coherence on even larger scales can be achieved using foam-like or laminated materials, or simply many grains of size R . Since each collision is accompanied by a momentum transfer $\Delta p = 2p$, a flux $\Phi_\nu \sim n_\nu^{\text{local}} v$ of non-relativistic neutrinos produces an acceleration

$$a \sim \Phi_\nu \sigma_{\nu N} \Delta p \frac{N^2}{M} \sim 10^{-28} \frac{\text{cm}^2}{\text{sec}} \frac{n_\nu^{\text{local}}}{10^3/\text{cm}^3} \frac{10^{-3}}{v} \frac{\rho}{\text{g/cm}^3} \left(\frac{R}{1/(m_\nu v)} \right)^3 \quad (10.16)$$

where $v = |\langle \vec{v}_\nu - \vec{v}_\oplus \rangle|$ is the mean relative velocity between CMB neutrinos and the target, ρ is density of the target and M is its mass. The minimal acceleration that can be detected at present is 10^{-13} cm/s^2 , orders of magnitude above the expected signal.

The estimate (10.16) is correct for Dirac neutrinos, that can have vectorial couplings. Majorana neutrinos only have axial couplings, that in the non-relativistic limit give effects suppressed by $v^2 \sim 10^{-6}$ for an unpolarized target, or by $v \sim 10^{-3}$ for a polarized target.

- *The Stodolski effect.* The energy of an electron receives an extra contribution (analogous to the MSW effect) $\delta E \sim G_F \vec{s} \cdot \vec{v} (n_\nu - n_{\bar{\nu}})$ that depends on the direction of its spin \vec{s} with respect to the neutrino wind \vec{v} . Notice that δE is linear in G_F but suppressed if the neutrino asymmetry $\eta_\nu = (n_\nu - n_{\bar{\nu}})/n_\gamma$ is small. We do not show the dependence on the Dirac or Majorana nature of neutrinos. The effect manifests as a torque $\tau \sim N_e \delta E$ acting on magnetized macroscopic object with N_e polarized electrons. Therefore an object with size R , one polarized electron per atom, atomic number A , mass $M \sim N_e m_e A$ feels a linear acceleration

$$a \sim \frac{\tau}{MR} \sim 10^{-28} \frac{\text{cm}}{\text{sec}^2} \frac{100}{A} \frac{\text{cm}}{R} \frac{v_\nu}{10^{-3}} \eta_\nu. \quad (10.17)$$

- *Scattering of ultra-high-energy cosmic rays (CR).* Cosmic rays with energy $E = M_Z^2/2m_{\nu_i} = 4 \cdot 10^{21} \text{ GeV} (\text{eV}/m_{\nu_i})$ scatter on relic neutrinos with cross section enhanced by the Z -peak

⁴For comparison, the Fermi-Dirac distribution roughly corresponds to having levels occupied up to $p \sim T_\nu$.

resonance, $\sigma \simeq 2\pi\sqrt{2}G_F$. Their mean free path $1/(n_\nu\sigma)$ is about two orders of magnitude larger than the Hubble distance. Therefore one can search for a few % absorption dip in the spectrum of UHE CR, and for the consequent scattering products (protons, photons,...). This process could produce cosmic rays above the GZK cut-off [18].

Scattering with relic neutrinos of particle beams produced in foreseeable future accelerators does not give interesting rates.

10.2.4 Neutrinos and the vacuum energy

Cosmological data suggest that some contribution ρ_{DE} to the total energy density ρ of the universe remains roughly constant and is becoming today the dominant contribution, see fig. 10.2. It is known as ‘Dark Energy’ (DE) because we do not know what it is. The DE might be a cosmological constant, $\rho_{\text{DE}} = \rho_\Lambda = (2.3 \text{ meV})^4$. This interpretation involves only one free parameter and is so far consistent with data. However it is puzzling that ρ_Λ is so much smaller than particle-physics energy scales that, according to theoretical prejudices, should contribute to it: e.g. $\rho_\Lambda \sim 10^{-35} \Lambda_{\text{QCD}}^4 \sim 10^{-50} v^4 \sim 10^{-120} M_{\text{Pl}}^4$. All theoretical attempts of understanding the smallness of ρ_Λ failed. This issue might be affected by anthropic selection: a ρ_Λ 100 times bigger would have prevented the formation of our galaxy.

Alternatively, one can imagine that due to some unknown reason the cosmological constant is zero, that DE is due to something else possibly related to particle physics. We here discuss neutrino masses, which are a good candidate because happen to be comparable to $\rho_\Lambda^{1/4}$.

‘Mass varying neutrinos’ [99] are the most direct possibility: in the non relativistic limit $\rho_\nu \sim m_\nu T^3$, so that a constant DE would be obtained if $m_\nu \propto 1/T^3$. Attempts of building models with this property assume that neutrino masses m_ν depend on the vev of a light scalar field ϕ that evolves such that the total energy density $\rho_\nu(\phi) + V(\phi)$ remains roughly constant. There is a generic problem: a scalar ϕ that evolves tracking the minimum of $\rho_\nu(\phi) + V(\phi)$ also generates a long-range force among neutrinos that causes their clustering, leaving a vanishing cosmological constant in the space outside of the neutrino clusters. Furthermore quantum corrections to the potential $V(\phi)$ are much larger than the needed $V(\phi)$. Without caring of such theoretical problems, one can even speculate that the LSND anomaly is due to the fact that neutrino masses in rock are larger than neutrino masses in air.

Alternatively, one can try to see what can be achieved in a self-consistent theoretical framework [99]. Pseudo-Goldstone scalars are naturally light: a scalar field with vev f that spontaneously breaks a global symmetry, also broken explicitly at a low energy M , gets a potential $V(\phi) \sim M^4 \cos(\phi/f) + \text{cte}$. If $M^4 \sim \rho_{\text{DE}}$ and $f \sim M_{\text{Pl}}$ the scalar is so light, $m_\phi \sim \rho_{\text{DE}}^{1/2}/M_{\text{Pl}} \sim 10^{-33} \text{ eV}$, that only today $H^{-1} \sim m_\phi$ and ϕ starts falling towards the minimum of its potential. Unfortunately it seems that ϕ cannot couple to SM particles, because such couplings would destroy its lightness and/or would lead to unobserved long range forces. Interestingly, it is possible to couple ϕ to *right-handed* neutrinos such that the identification $M \sim m_\nu$ has oscillation signatures. Models where Majorana masses of left-handed neutrinos depend on ϕ fail, because Majorana *LL* masses come either from a non renormalizable interaction or from exchange of heavy new particles (see section 2), resulting in either case in $M \gg m_\nu$. Successful models are obtained by assuming that only the Majorana *RR* mass M of light right-handed neutrino(s) depends on ϕ , because this is obtained from a renormalizable Yukawa interaction. A detailed analysis shows that neutrino masses can be obtained by adding *LR* Dirac masses but no *LL* Majorana masses, resulting in a particular sub-case of mixed Majorana/Dirac. (The opposite possibility is also trivially allowed,

but does not seem phenomenologically interesting).

Recently, possible space or time variations of fundamental constants attracted some interest. We remark that if the vacuum energy is small thanks to a fine-tuning done once and for all, detectable variations of e.g. α_{em} or m_e/m_p are not compatible with its observed smallness. The above discussion shows that neutrino masses are the only fundamental constants that can vary without generating a too large vacuum energy.

10.3 Baryogenesis through leptogenesis

The present baryon density of eq. (10.1)⁵ can be obtained from an hot big-bang as the result of a small excess of baryons over anti-baryons. We would like to understand why, when at $T \lesssim m_p$ matter almost completely annihilated with anti-matter, we survived thanks to the ‘almost’

$$n_B - n_{\bar{B}} \propto 1000000001 - 1000000000 = 1.$$

This might be the initial condition at the beginning of the big-bang, but it would a surprisingly small excess. In inflationary models it is regarded as a surprisingly large excess, since inflation erases initial conditions.

Assuming that the hot-big-bang started with zero baryon asymmetry at some temperature $T \gg m_p$, can the baryon asymmetry can be generated dynamically in the subsequent evolution? Once that one realizes that this is an interesting issue (this was done by Sakharov), the answer is almost obvious: yes, provided that at some stage [100]

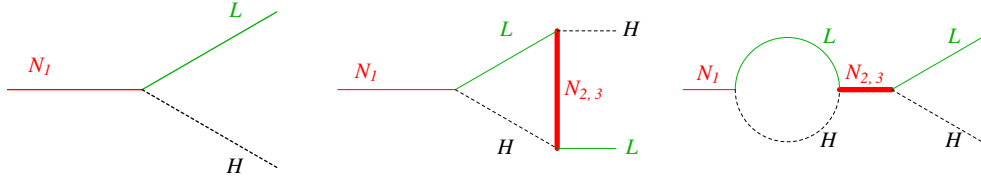
1. baryon number B is violated;
2. C and CP are violated (otherwise baryons and antibaryons are generated in the same rate);
3. the universe was not in thermal equilibrium (since we believe that CPT is conserved, particles and antiparticles have the same mass, and therefore in thermal equilibrium have the same abundance).

A large amount of theoretical and experimental work showed that *within the SM these conditions are not fulfilled*. At first sight one might guess that the only problem is 1.; in reality 2. and 3. are problematic.

1. Within the SM B is violated in a non trivial way [100], thanks to quantum anomalies combined with non-perturbative $SU(2)_L$ processes known as sphalerons⁶: the anomalous B and L symmetry are violated, while $B - L$ is a conserved anomaly-free symmetry. At temperatures $T \ll 100 \text{ GeV}$ sphaleron rates are negligible because suppressed by a tunneling

⁵We discuss how this number is measured. The photon density directly follows from the measurement of the temperature of the CMB. Measuring baryons is more difficult, because only a fraction of baryon formed stars and other luminous objects. As discussed in section 10.1, BBN predictions depend on n_B/n_γ . In particular the presence of many more photons than baryons delays big-bang nucleosynthesis (e.g. by enhancing the reaction $pn \leftrightarrow D\gamma$ in the \leftarrow direction) and therefore directly follows from the primordial helium-4 abundancy. The accurate determination in eq. (10.1) of n_B/n_γ follows from global fits of WMAP data about CMB anisotropies [69].

⁶We just state the result, because we are not able of providing an intuitive explanation of the basic physics, which needs a deep understanding of advanced quantum field theory. The η' mass is the only observed consequence of this sector, and it is due to the QCD analogous of electroweak sphalerons. Therefore there should be no doubt that sphalerons really exist, and this is almost all what one needs to know to understand leptogenesis quantitatively.

Figure 10.5: *CP-violating N_1 decay.*

factor $e^{-2\pi/\alpha_2}$: tritium decays at an unobservably slow rate.⁷ At $T \gtrsim 100$ GeV thermal tunneling gives fast $B+L$ -violating sphaleron processes: the space-time density of sphaleron interactions, $\gamma \sim \alpha_2^5 T^4$, is faster than the expansion rate of the universe up to temperatures of about $T \sim 10^{12}$ GeV [100].

3. SM baryogenesis is not possible due to the lack of out-of equilibrium conditions. The electroweak phase transition was regarded as a potential out-of equilibrium stage, but experiments now demand a higgs mass $m_h \gtrsim 115$ GeV [85], and SM computations of the Higgs thermal potential show that, for $m_h \gtrsim 70$ GeV, the higgs vev shifts smoothly from $\langle h \rangle = 0$ to $\langle h \rangle = v$ as long as the universe cools down below $T \sim m_h$.
2. In any case, the amount of CP violation provided by the CKM phase would have been too small for generating the observed baryon asymmetry.

Many extensions of the SM could generate the observed n_B . ‘Baryogenesis at the electroweak phase transition’ needs new particles coupled to the higgs in order to obtain a out-of-equilibrium phase transition and to provide extra sources of CP violation. This already disfavored possibility will be tested at future accelerators. ‘Baryogenesis from decays of GUT particles’ seems to conflict with non-observation of magnetic monopoles, at least in simplest models. Furthermore minimal GUT model do not violate $B - L$, so that sphaleron processes would later wash out the eventually generated baryon asymmetry.

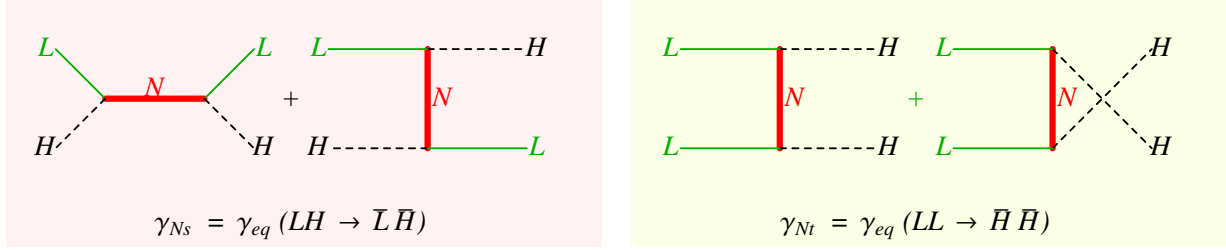
The existence of sphalerons changes the rules of the game and suggests *baryogenesis through leptogenesis*: lepton number might be violated by some non SM physics, giving rise to a lepton asymmetry, which is converted into the observed baryon asymmetry by sphalerons.

This scenario can be realized in many different ways [100]. Majorana neutrino masses violate lepton number and presumably CP, but do not provide enough out-of-equilibrium processes. The minimal successful implementation [19] needs just the minimal amount of new physics which can give the observed small neutrino masses via the see-saw mechanism: heavy right-handed neutrinos N with masses M . ‘*Baryogenesis via thermal leptogenesis*’ [19] proceeds at $T \sim M$, when out-of-equilibrium (condition 3) CP-violating (condition 2) decays of heavy right-handed neutrinos generate a lepton asymmetry, converted in baryon asymmetry by SM sphalerons (condition 1).

10.3.1 Thermal leptogenesis

We now discuss the basic physics, obtaining estimates for the main results. The SM is extended by adding the heavy right-handed neutrinos suggested by see-saw models. To get the essential

⁷Sphalerons do not induce proton decay, because there are 3 generations and all of them must be involved in sphaleron processes.

Figure 10.6: Wash-out $\Delta L = 2$ scatterings.

points, we consider a simplified model with one lepton doublet L and two right-handed neutrinos, that we name ‘ N_1 ’ and ‘ $N_{2,3}$ ’, with N_1 is lighter than $N_{2,3}$. The relevant Lagrangian is

$$\mathcal{L} = \mathcal{L}_{\text{SM}} + \bar{N}_{1,2,3} i \not{D} N_{1,2,3} + \lambda_1 N_1 H L + \lambda_{2,3} N_{2,3} H L + \frac{M_1}{2} N_1^2 + \frac{M_{2,3}}{2} N_{2,3}^2 + \text{h.c.}$$

By redefining the phases of the N_1 , $N_{2,3}$, L fields one can set M_1 , $M_{2,3}$, λ_1 real leaving an ineliminabile CP-violating phase in $\lambda_{2,3} = |\lambda_{2,3}|e^{-i\delta}$.

At tree-level, the decay width of N_1 is $\Gamma_1 = \lambda_1^2 M_1 / 8\pi$. The interference between tree and loop diagrams shown in fig. 10.5 renders N_1 decays CP-asymmetric:

$$\varepsilon_1 \equiv \frac{\Gamma(N_1 \rightarrow LH) - \Gamma(N_1 \rightarrow \bar{L}H^*)}{\Gamma(N_1 \rightarrow LH) + \Gamma(N_1 \rightarrow \bar{L}H^*)} \sim \frac{1}{4\pi} \frac{M_1}{M_{2,3}} \text{Im} \lambda_{2,3}^2$$

In fact

$$\Gamma(N_1 \rightarrow LH) \propto |\lambda_1 + A\lambda_1^* \lambda_{2,3}^2|^2, \quad \Gamma(N_1 \rightarrow \bar{L}H^*) \propto |\lambda_1^* + A\lambda_1 \lambda_{2,3}^{2*}|^2$$

where A is the complex CP-conserving loop factor. In the limit $M_{2,3} \gg M_1$ the sum of the two one loop diagrams reduces to an insertion of the $(LH)^2$ neutrino mass operator mediated by $N_{2,3}$: therefore A is suppressed by one power of $M_{2,3}$. The intermediate states in the loop diagrams in fig. 10.5 can be on shell; therefore the Cutkosky rule [101] guarantees that A has an imaginary part. Inserting the numerical factor valid for $M_{2,3} \gg M_1$ we can rewrite the CP-asymmetry as

$$\varepsilon_1 \simeq \frac{3}{16\pi} \frac{\tilde{m}_{2,3} M_1}{v^2} \sin \delta = 10^{-6} \frac{\tilde{m}_{2,3}}{0.05 \text{ eV}} \frac{M_1}{10^{10} \text{ GeV}} \sin \delta \quad (10.18)$$

where $\tilde{m}_{2,3} \equiv |\lambda_{2,3}^2| v^2 / M_{2,3}$ is the contribution to the light neutrino mass mediated by $N_{2,3}$.⁸

⁸In a generic see-saw model defined by the Lagrangian in eq. (2.6), the CP asymmetry in the decay of the lightest right-handed neutrino N_1 with mass $M_1 < M_2 < M_3$ can be written as the sum of a Vertex contribution and of a Self-energy contribution

$$\varepsilon_1 = - \sum_{j=2,3} \frac{M_1}{M_j} \frac{\Gamma_j}{M_j} \left(S_j + \frac{V_j}{2} \right) \frac{\text{Im} [Y_{1j}^2]}{|Y_{11}|Y_{jj}}, \quad (10.19)$$

where

$$\frac{\Gamma_j}{M_j} = \frac{|Y_{jj}|}{8\pi} \equiv \frac{\tilde{m}_j M_j}{8\pi v^2}, \quad S_j = \frac{M_j^2 \Delta M_{1j}^2}{(\Delta M_{1j}^2)^2 + M_1^2 \Gamma_j^2}, \quad V_j = 2 \frac{M_j^2}{M_1^2} \left[\left(1 + \frac{M_j^2}{M_1^2} \right) \log \left(1 + \frac{M_1^2}{M_j^2} \right) - 1 \right], \quad (10.20)$$

The final amount of baryon asymmetry can be written as

$$\frac{n_B}{n_\gamma} = -1.14 \frac{\varepsilon_1 \eta}{g_{\text{SM}}} \quad (10.22)$$

where $g_{\text{SM}} = 118$ is the number of spin-degrees of freedom of SM particles (present in the denominator of eq. (10.22) because only N_1 among the many other particles in the thermal bath generates the asymmetry) and η is an efficiency factor that depends on how much out-of-equilibrium N_1 -decays are. We now discuss this issue.⁹ If N_1 decays and annihilations are slow enough, the N_1 abundancy does not decrease according to the Boltzmann equilibrium statistics $\sim e^{-M_1/T}$ demanded by thermal equilibrium, so that out-of-equilibrium N_1 decays can generate a lepton asymmetry. Slow enough decay means $\Gamma_1 < H(T)$ at $T \sim M_1$, i.e. N_1 lifetime longer than the inverse expansion rate. Numerically

$$\gamma \equiv \frac{\Gamma_1}{H} \sim \frac{\tilde{m}_1}{\tilde{m}^*} \quad \text{where} \quad \tilde{m}^* \equiv \frac{256 \sqrt{g_{\text{SM}}} v^2}{3 M_{\text{Pl}}} = 2.3 \cdot 10^{-3} \text{ eV}$$

depends on cosmology.

All the dependence on the mass and Yukawa couplings of N_1 is incorporated in $\tilde{m}_1 \equiv \lambda_1^2 v^2 / M_1$, the contribution to the light neutrino mass mediated by N_1 . Unfortunately \tilde{m}_1 and $\tilde{m}_{2,3}$ are only related to the observed atmospheric and solar mass splittings in a model-dependent way. Unless neutrinos are almost degenerate (and unless there are cancellations) \tilde{m}_1 and $\tilde{m}_{2,3}$ are smaller than $m_{\text{atm}} \approx 0.05 \text{ eV}$.

If $\gamma \ll 1$ (i.e. N_1 decays strongly out-of-equilibrium) then $\eta = 1$. If instead $\gamma \gg 1$ the lepton asymmetry is suppressed by $\eta \sim 1/\gamma$. The reason is that $\Delta L = 1$ wash-out interactions (mainly N_1 decays and inverse-decays) have N_1 as an external state and therefore at low temperature $T < M_1$ their thermally-averaged rates are suppressed by a Boltzmann factor: $\gamma_{\Delta L=1}(T < M_1) \approx \gamma e^{-M_1/T}$. The N_1 quanta that decay when $\gamma_{\Delta L=1} < 1$, i.e. at $T < M_1 / \ln \gamma$, give rise to unwashed leptonic asymmetry. At this stage the N_1 abundancy is suppressed by the Boltzmann factor $e^{-M_1/T} = 1/\gamma$. In conclusion, the suppression factor is approximately given by

$$\eta \sim \min(1, \tilde{m}^* / \tilde{m}_1) \quad (\text{if } N_1 \text{ initially have thermal abundancy}).$$

Fig. 10.6 shows additional $\Delta L = 2$ washing interactions mediated by $N_{1,2,3}$. Dropping the contribution mediated by on-shell N_1 (already included as successive inverse decays and decays,

with $\Delta M_{ij}^2 \equiv M_j^2 - M_i^2$ and $Y \equiv \lambda_N \cdot \lambda_N^\dagger$. In the hierarchical limit $M_{2,3}/M_1 \rightarrow \infty$ one has $S_{2,3} = 1$ and $V_{2,3} = 1$. If N_1 and N_2 are almost degenerate the CP-asymmetry is enhanced by a new effect, CP violation in $N_1 N_2$ mixing, which can give $|\varepsilon_1| \sim 1$. This phenomenon is accounted by the factor S_j , which has a form well known from the analogous $K^0 \bar{K}^0$ system. Neglecting this potential effect, the CP-asymmetry can be rewritten in a way which emphasizes the flavour structure of the Yukawa couplings:

$$\varepsilon_1 = -\frac{1}{8\pi} \frac{\text{Im} (Y \cdot f(M_N/M_1) \cdot Y^*)_{11}}{Y_{11}} = \frac{1}{8\pi} \sum_{i>1} \frac{\text{Im} Y_{1i}^2}{Y_{11}} f\left(\frac{M_i}{M_1}\right) \quad (10.21)$$

In the SM

$$f(r) = r(1+r^2) \ln(1+r^{-2}) - r + r/(r^2-1) \simeq 3/2r \quad \text{for } r \gg 1$$

and in supersymmetric extensions of the SM $f(r) = r \ln(1+r^{-2}) + 2r/(r^2-1) \simeq 3/r$.

⁹A precise description can be achieved by solving the relevant set of Boltzmann equations, taking into account CP-violating N_1 decays and scatterings as well as their inverse processes, as described in the literature [19]. We here give exact numerical results, presenting a semi-quantitative explanation of the main features.

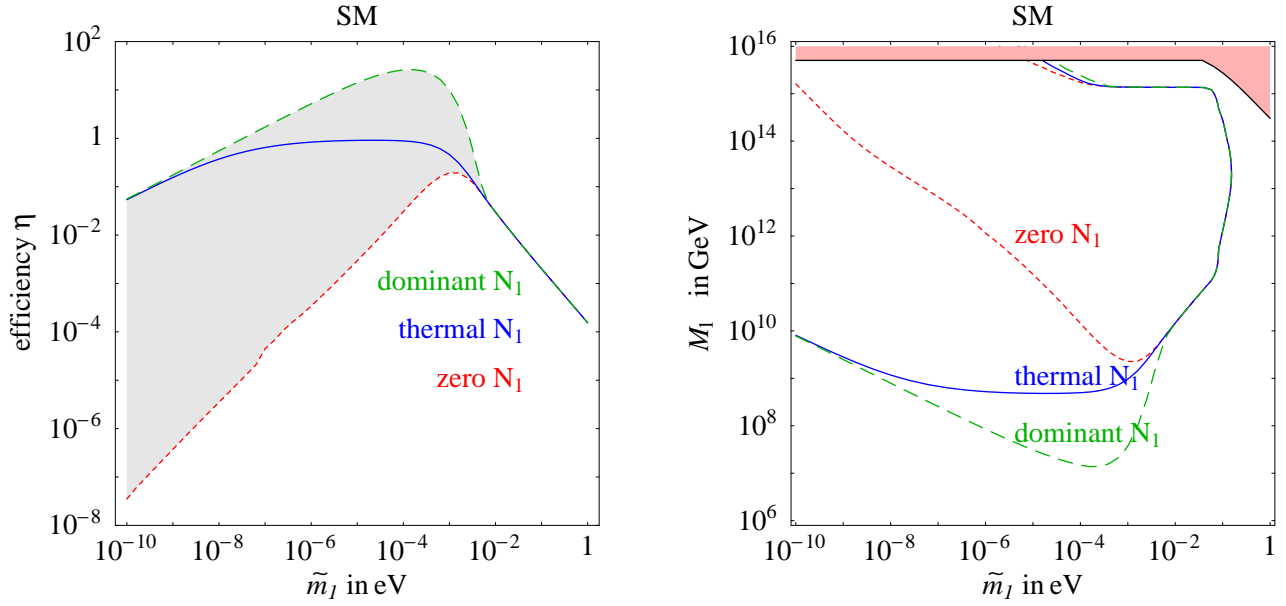


Figure 10.7: **Thermal leptogenesis.** *Fig. 10.7a:* efficiency η as function of \tilde{m}_1 for $M_1 = 10^{10}$ GeV and for different assumptions about the initial N_1 abundancy. *Fig. 10.7b:* the regions in the (\tilde{m}_1, M_1) plane inside the curves can lead to successful leptogenesis.

$H^* \bar{L} \leftrightarrow N_1 \leftrightarrow HL$) these scatterings are generated by the same dimension 5 operators that give rise to Majorana neutrino masses. Their thermally-averaged interaction rates are relevant only at $M_1 \gtrsim 10^{14}$ GeV, when neutrinos have $\mathcal{O}(1)$ Yukawa couplings. In such a case these interactions wash out the baryon asymmetry exponentially, because are not suppressed at $T \lesssim M_1$ by the small N_1 abundance.

So far we assumed that right-handed neutrinos have thermal abundance. If instead N_1 start with zero abundance and are generated only by the scattering processes previously discussed, at $T \sim M_1$ they reach thermal abundance only if $\gamma \gg 1$. Their abundance is otherwise suppressed by a γ factor. Therefore the efficiency factor is approximatively given by

$$\eta \sim \min(\tilde{m}_1/\tilde{m}^*, \tilde{m}^*/\tilde{m}_1) \quad (\text{if } N_1 \text{ initially have zero abundance}).$$

If instead N_1 dominate the energy density of the universe, the suppression factor $1/g_{\text{SM}}$ in eq. (10.22) no longer applies, and the efficiency factor can reach $\eta \sim g_{\text{SM}}$.

These estimates agree with the results of a detailed numerical computation¹⁰, shown in fig. 10.7a (for simplicity these computations are performed ignoring $\mathcal{O}(1)$ effects that depend

¹⁰The evolution of the total density of right-handed neutrinos, $Y_{N_1} \equiv n_{N_1}/s$ and of the lepton asymmetry, $Y_L \equiv (n_L - n_{\bar{L}})/s$ (measured in units of the total entropy density s) as function of $z \equiv M_{N_1}/T$ is described by the Boltzmann equations

$$zHs \frac{dY_{N_1}}{dz} = -\gamma_D \left(\frac{Y_{N_1}}{Y_{N_1}^{\text{eq}}} - 1 \right), \quad zHs \frac{dY_L}{dz} = \gamma_D \left[\varepsilon_1 \left(\frac{Y_{N_1}}{Y_{N_1}^{\text{eq}}} - 1 \right) - \frac{Y_L}{2Y_L^{\text{eq}}} \right] \quad (10.23)$$

where we kept only the dominant processes, $HL \leftrightarrow N_1 \leftrightarrow H^* \bar{L}$, with thermally averaged spacetime density γ_D . The suffix 'eq' denotes the values in thermal equilibrium. The first three factors in the equation for Y_L correspond to three Sacharov conditions: violation of lepton number (γ_D), of CP (ε_1), departure from thermal

on the unknown flavor of leptons produced by N_1 decays). If $\tilde{m} \gg \tilde{m}^*$ (in particular if $\tilde{m} = m_{\text{atm}}$ or m_{sun}) the efficiency does not depend on initial conditions because N is close to thermal equilibrium.

10.3.2 Leptogenesis constraints on neutrino masses

Assuming that the observed baryon asymmetry is due to thermal leptogenesis and that right-handed neutrinos are hierarchical, one can derive interesting constraints on the masses of left-handed and right-handed neutrinos. We remark that these results, discussed in the rest of this section, *hold only under these untested assumptions* and therefore are not true bounds.

Assuming $M_1 \ll M_{2,3}$ and neglecting terms suppressed by powers of $M_1/M_{2,3}$, the two one-loop diagrams in fig. 10.5 reduce to insertion of the neutrino mass operator $(LH)^2$. Therefore the CP-asymmetry ε_1 is directly related to neutrino masses, and e.g. ε_1 vanishes if neutrinos are degenerate. In fact, using the parametrization in eq. (2.16)

$$\varepsilon_1 = \frac{3}{16\pi} \frac{M_1}{v^2} \frac{\text{Im}(\lambda_N \cdot m_\nu^* \cdot \lambda_N^T)_{11}}{(\lambda_N \lambda_N^\dagger)_{11}} = \frac{3}{16\pi} \frac{M_1}{v^2} \frac{\sum_i m_{\nu_i}^2 \text{Im} R_{1i}^2}{\sum_i m_{\nu_i} |R_{1i}|^2}$$

gives an upper bound on the CP-asymmetry in N_1 decays [102]:

$$|\varepsilon_1| \leq \frac{3}{16\pi} \frac{M_1}{v^2} (m_{\nu_3} - m_{\nu_1}). \quad (10.24)$$

Here m_{ν_3} (m_{ν_1}) denotes the mass of the heaviest (lightest) neutrino. In the limit $m_{\nu_1} \ll m_{\nu_3}$ the bound is trivial and holds when the CP asymmetry is controlled by the neutrino mass operator, independently of the specific source that generates it (this implicitly means that the contribution to neutrino masses non mediated by N_1 is mediated by something much heavier than N_1). The factor $m_{\nu_3} - m_{\nu_1}$ is non-trivial and specific to the see-saw model with 3 right-handed neutrinos. It can be intuitively understood as follows: 3 right-handed neutrinos can produce the limiting case of degenerate neutrinos $m_{\nu_1} = m_{\nu_2} = m_{\nu_3} = m_\nu$ only in the following way: each N_i gives mass m_ν to one neutrino mass eigenstate. Since they are orthogonal in flavour space, the CP-asymmetry of eq. (10.24) vanishes due to flavour orthogonality: this is the origin of the $m_{\nu_3} - m_{\nu_1}$ suppression factor.

The bound (10.24) becomes more stringent if right-handed neutrinos are light. Combined with a precise SM computation of thermal leptogenesis (performing neglecting flavour issues) and with the measured values of the baryon asymmetry and of the neutrino masses it implies that

$$M_1 > \begin{cases} 2.4 \times 10^9 \text{ GeV} & \text{if } N_1 \text{ has zero} \\ 4.9 \times 10^8 \text{ GeV} & \text{if } N_1 \text{ has thermal initial abundancy at } T \gg M_1. \\ 1.7 \times 10^7 \text{ GeV} & \text{if } N_1 \text{ has dominant} \end{cases} \quad (10.25)$$

However, the CP asymmetry can be much larger than in eq. (10.24) if right-handed neutrinos are either not much hierarchical ($M_1/M_{2,3} \sim 0.01$ is enough) or quasi-degenerate. In both cases M_1

equilibrium ($Y_{N_1} \neq Y_{N_1}^{\text{eq}}$). An important subtlety: decays and inverse-decays $N_1 \leftrightarrow HL, H^* \bar{L}$ alone generate a lepton asymmetry even in thermal equilibrium: if N_1 decays preferentially produce leptons, then CPT-invariance implies that inverse decay preferentially destroy anti-leptons. Boltzmann equations that respect the Sacharov conditions are obtained after including the non-resonant part of $\Delta L = 2$ scatterings $HL \leftrightarrow H^* \bar{L}$.

State-of-the-art computations include various, but not all, subdominant effects.

can be lighter than in eq. (10.25); one can even have leptogenesis at the TeV scale. Unfortunately not even this case can be tested at accelerators because right-handed neutrinos are too weakly coupled, and the amount of baryon asymmetry depends on their tiny mass difference.

The bound (10.24) becomes more stringent if neutrinos are quasi-degenerate, and implies that neutrinos must be lighter than about 0.2 eV. Since thermal leptogenesis depends on $\tilde{m} \equiv (\lambda_N \lambda_N^\dagger)_{11} v^2 / M_1 = \sum_i m_{\nu_i} |R_{1i}|^2$, this bound can be improved by computing the upper bound on ε_1 at given \tilde{m} [102] and maximizing n_B with respect to \tilde{m} . The final bound is $m_{\nu_3} < 0.15$ eV combining experimental uncertainties at 3σ .

However, this constraint holds under the dubious assumption that hierarchical right-handed neutrinos give quasi-degenerate left-handed neutrinos. Good taste suggests that quasi-degenerate neutrinos are more naturally produced by quasi-degenerate right-handed neutrinos. In such a case the constraint on neutrino masses gets relaxed because ε_1 can be resonantly enhanced, and because ε_1 no longer need to vanish when neutrinos are degenerate. The result depends on possible reasons that naturally give rise to quasi-degenerate left-handed neutrinos. With conservative assumptions, a $\sim 10\%$ quasi-degeneracy among $N_{1,2,3}$ allows neutrinos heavier than an eV compatibly with leptogenesis. A constraint $m_{\nu_3} \lesssim 0.5$ eV arises instead if some flavour symmetry (e.g. SO(3)) keeps right-handed neutrinos as degenerate as left-handed neutrinos.

10.3.3 Leptogenesis in alternative models of neutrino masses

Adding *supersymmetry* does not significantly affect leptogenesis [103]:

- If $M_1 \gg m_{\text{SUSY}}$ one can ignore SUSY breaking effects; right-handed neutrinos and sneutrinos have equal masses, equal decay rates and equal CP-asymmetries: both Γ_1 and ε_1 become 2 times larger, because there are new decay channels. Eq. (10.22) remains almost unchanged, because adding spartners roughly doubles both the number of particles that produce the baryon asymmetry and the number of particles that share it. As a consequence of more CP-asymmetry compensated by more wash-out, the constraints on right-handed and left-handed neutrino masses discussed in the non-supersymmetric case remain essentially unchanged.
- If instead M_1 is not much larger than the scale of SUSY-breaking (presumed to be below 1 TeV), complex soft terms give new contributions to the CP-asymmetry. Being related to supersymmetry breaking rather than to neutrino masses, the bound on the CP-asymmetry of eq. (10.24) no longer holds and M_1 lighter than in eq. (10.25) is allowed. This scenario is named ‘*soft leptogenesis*’: At larger M_1 soft terms can still be relevant, but only in a fine-tuned range of parameters with an anomalously small B -term associated to the N_1 mass, by generating a mixing between the CP-odd and the CP-even component of the lightest right-handed sneutrino.

Alternatively, leptogenesis is typically produced by decays of the lightest particle that violates lepton number: it might not be a right-handed neutrinos. As discussed in section 2, two other particles can mediate Majorana neutrino masses at tree level: fermion $SU(2)_L$ triplets and scalar $SU(2)_L$ triplets. Unlike in the singlet case, these particles have gauge interactions that keep their abundancy close to thermal equilibrium (potentially conflicting with the 3rd Sakharov condition) such that their efficiency is univocally predicted and a quantitative analyses have shown that it can large enough [103].

- *Leptogenesis from decays of a fermion triplet.* Three fermion triplets $N_{1,2,3}$ is the only possibility which, with as few parameters as the singlet model, can lead to successful leptogenesis. If N_1 decays are slower than $N_1 N_1$ annihilations, one can approximate leptogenesis in three steps: 1) At $T \gg M_1$ gauge interactions thermalize the triplet abundance. 2) At $T \sim M_1$ gauge scatterings partially annihilate triplets. A standard freeze-out estimate (see e.g. [97]) shows that a fraction $\eta \sim M_1/10^{12} \text{ GeV}$ survives to gauge annihilations. 3) At $T \ll M_1$ triplets freely decay generating a lepton asymmetry. If instead decays are sufficiently fast that compete with annihilations, the efficiency of thermal leptogenesis is comparable to the one of the right-handed neutrino case, even at small values of $M_1 \sim \text{TeV}$. In conclusion, the efficiency is approximatively given by

$$\eta(\text{fermion triplet}) \approx \min \left[1, \frac{H}{\Gamma}, \frac{M}{10^{12} \text{ GeV}} \max(1, \frac{\Gamma}{H}) \right]. \quad (10.26)$$

- *Leptogenesis from decays of a scalar triplet.* One scalar triplet with mass M_T is the extension of the SM that can mediate generic neutrino masses having the minimal number of beyond-the-SM parameters; however it does not lead to a large enough CP asymmetry. Successful leptogenesis from scalar triplet decays is possible in presence of other sources of CP violation, that, in the simplest scenario, might be contributions to neutrino masses mediated by heavier particles. Writing the neutrino mass matrix \mathbf{m}_ν as the sum of the triplet contribution \mathbf{m}_T , plus an extra contribution \mathbf{m}_H mediated by other much heavier particles: $\mathbf{m}_\nu = \mathbf{m}_T + \mathbf{m}_H$, the lepton asymmetry produced per decay is:

$$\varepsilon_L \equiv \frac{\Gamma(\bar{T} \rightarrow LL) - \Gamma(T \rightarrow \bar{L}\bar{L})}{\Gamma_T} = \frac{1}{4\pi} \frac{M_T}{v^2} \sqrt{B_L B_H} \frac{\text{Im} \text{Tr} \mathbf{m}_T^\dagger \mathbf{m}_H}{\tilde{m}_T} \quad (10.27)$$

where $\tilde{m}_T^2 \equiv \text{Tr} \mathbf{m}_T^\dagger \mathbf{m}_T$. One can derive an upper bound on $|\varepsilon_L|$ noticing that the last factor is less than $\sqrt{\sum_i m_{\nu_i}^2}$. In terms of the parameters of eq. (2.8), the decay widths are

$$\Gamma(T \rightarrow LL) = \frac{M_T}{16\pi} \text{Tr} \mathbf{\lambda}_L \mathbf{\lambda}_L^\dagger = B_L \Gamma_T, \quad \Gamma(T \rightarrow \bar{H}\bar{H}) = \frac{M_T}{16\pi} \lambda_H \lambda_H^\dagger = B_H \Gamma_T, \quad (10.28)$$

The efficiency can be estimated similarly to the fermion triplet case:

$$\eta(\text{scalar triplet}) \approx \min \left[1, \frac{H}{\min(\Gamma_L, \Gamma_H)}, \frac{M_T}{10^{12} \text{ GeV}} \max(1, \frac{\Gamma_L + \Gamma_H}{H}) \right]. \quad (10.29)$$

Notice that despite the presence of gauge interactions, that tend to maintain the triplet abundance very close to thermal equilibrium, one can have even maximal efficiency, $\eta \sim 1$ for any M_T if i) one of the two decay rates ($T \rightarrow \bar{L}\bar{L}$ or $T \rightarrow HH$) is faster than the annihilation rate; ii) the other one is slower than the expansion rate. Thanks to i) annihilations are ineffective: triplets decay before annihilating. Thanks to ii) fast decays do not produce a strong washout of the lepton asymmetry (and consequently a small efficiency η), because lepton number is violated only by the contemporaneous presence of the two $T \rightarrow \bar{L}\bar{L}$ and $T \rightarrow HH$ processes.

Finally, if neutrinos have *Dirac masses*, one can invent models where the neutrino Yukawa coupling are mediated by tree level exchange of some extra particle, whose L -conserving decays produce leptogenesis, by generating equal and opposite lepton asymmetries in right-handed neutrino and in left-handed leptons [103].

10.3.4 Testing leptogenesis?

At the moment nobody knows how to test if leptogenesis produced the baryon asymmetry. Direct tests seem impossible; indirect tests seem unlikely, because there are too many unknown high energy parameters and only one observable.¹¹ One can hope of obtaining more concrete results within restrictive flavour models (see section 12.4.1). For example, the minimal see-saw model with 2 right-handed neutrinos described by eq. (12.14) [104] has only one CP-violating phase and apparently allows to relate CP-violation in neutrino oscillations (ϕ) to CP-violation in leptogenesis. Unfortunately not even the sign of ϕ can be predicted since CP-violation in leptogenesis (including its sign) depends on the unknown ratio between the two right-handed neutrino masses. As discussed in section 13.5, we can hope that quantum corrections imprint high-energy neutrino Yukawa couplings into measurable slepton masses. In this case the minimal see-saw model would be testable. However, in general, these extra observables are not enough for a full reconstruction and test of the high-energy model of neutrino masses.

Maybe future experiments will discover supersymmetry, LFV in charged leptons, and will confirm that neutrino masses violate lepton number and CP, and we will be able to convincingly argue that this can be considered as circumstantial evidence for see-saw and thermal leptogenesis. Archeology is not an exact science.

¹¹In principle we could also measure the three lepton flavour asymmetries. But in practice we are not even able of detecting CMB neutrinos.

Chapter 11

Neutrinos in astrophysics

This section discusses neutrinos from astrophysical sources, and the effects due to oscillations. The most interesting possibilities, putting aside those discussed previously, are (1) the ~ 10 MeV supernova neutrinos, (2) the $1 \div 100$ TeV neutrinos from galactic sources, like young supernova remnants, and (3) the ultra-high energy neutrinos from AGN, GRB or other unknown sources. These correspond to different techniques of detection, namely (1) underground detectors as those used to study solar neutrinos or proton decay; (2) dedicated underwater or under-ice observatories, possibly as big as a cubic km in size; (3) observatories of extensive air showers. The field of neutrino astronomy has been pioneered by the 20 events from SN1987A [105], and these are the only observations of this type we have so far. These observations were preceded by a few inspired theoretical works and stimulated a considerable number of papers; here we quote just a review and a book [106]. They certainly did renew the tight link among astronomy, astrophysics, nuclear and particle physics.

It can be said in general that there are no solid expectations for the fluxes of the neutrinos we consider in this section. Moreover, we should be ready for surprises, as always when opening a new window on the cosmos. Thus, without denying the important rôle of the various effects due to neutrino masses and mixing, the primary goal of present (experimental and theoretical) investigations are just the astrophysical sources of neutrinos. Keeping these considerations in mind, we begin by describing the possible goals of ‘neutrino astronomy’ and giving an overview of the expectations in section 11.1, postponing an extensive discussion of supernova neutrinos to section 11.2. We continue by outlining how neutrino masses and mixing can play a rôle in section 11.3, and conclude with section 11.4 underscoring neutrinos from core collapse supernovæ and supernova remnants. We hope that it will be needed to update or enlarge this section soon.

11.1 Neutrino sources

In this section we recall the connection of neutrino and photon astronomy and give a list of possible neutrino sources.

11.1.1 Multi-messenger astronomy

We can study astrophysical sources by detecting the different kinds of particles that they emit, at different energies. Let us compare neutrinos to other messenger particles. Since neutrinos are neutral and stable they are not deflected by magnetic fields. Thus they point to the astrophysical

site of production, just as the photons do.¹ Actually, this is the most important signal to identify high energy neutrinos.

The method used for low-energy supernova neutrinos is the self-trigger of a large number of events (let us recall that some low-energy neutrino reactions, like $\nu e \rightarrow \nu e$, are mildly directional, giving us a chance to identify the direction of the supernova).

Neutrinos can be used to probe astrophysical sources and to obtain information complementary to the one from light. E.g., around the sources of galactic or extragalactic cosmic rays (CR) π^\pm, π^0 are formed; their decay yields γ and neutrinos in comparable amounts. Neutrinos are much more difficult to observe than photons, especially at low energy, but for the same reason they are not easily reprocessed at sources or absorbed during the propagation. We recall in particular that (a) the γ radiation from core collapse of a supernova is not *directly* related to the neutrino radiation, it is produced in later phases and it is consequently much smaller; (b) it is difficult to identify the γ 's from π^0 decays, and to distinguish them from those of electromagnetic origin; (c) finally, photons with energies above 100 TeV originated outside our galaxy do not reach us, due to $\gamma\gamma \rightarrow e^+e^-$ scatterings on background IR photons.

11.1.2 A list of the main possibilities

Solar neutrinos (already observed and here discussed in section 6) are ν_e at production, and have energy $E_\nu = (0.1 \div 20) \text{ MeV}$. There is little doubt that this is ‘ ν -astronomy’. Low energy ν experiments Gallex/GNO and SAGE proofed that the *pp*-chain is the main energy source and discovered $\nu_e \rightarrow \nu_{\mu,\tau}$ oscillations, thanks also to the important rôle of some theorists, like J.N. Bahcall, and G.T. Zatsepin and V.A. Kuzmin, who advocated solar neutrino astronomy. The physics at the center of the sun (density, temperature) has been probed, with results consistent with the more precise helioseismological probes. The agreement of present data with expectations is excellent, but future precise studies of pp-neutrinos could teach us new surprising lessons on astrophysics or in particle physics. This will be done in existing experiments as Borexino, KamLAND, SAGE, and future projects aiming at (real time) detection of low energy neutrinos.

Atmospheric neutrinos (already observed and here discussed in section 5) are electron and muon (anti)neutrinos and have energy $E_\nu \sim (0.05 \div 1000) \text{ GeV}$. The study of atmospheric neutrinos originates as a branch of cosmic rays studies. The investigation of CR secondaries, like γ , muons and ν , permits us to understand CR spectra and their interactions with the earth atmosphere (which is not that different from possible sites of production of CR). The main existing experiment for atmospheric neutrinos is Super-Kamiokande, which will be hopefully followed by new larger experiment. It is a bit puzzling that the most recent calculations of neutrino fluxes [107] suggest that some features of the observations (like the total $\langle \bar{\nu}_e \rangle$ flux) are not perfectly accounted for, even including oscillations. New measurements of CR fluxes (possibly with new techniques) and of the relevant hadronic cross sections (HARP experiment) are in this connection rather important. Atmospheric muons and neutrinos are the most important background for neutrino astronomy.

¹Another interesting probe are very high energy neutrons coming from the galactic center, that reach us thanks to relativistic time dilatation: $c \cdot \tau = 8.5 \text{ kpc} \cdot E / 10^{18} \text{ eV}$. At even higher energies, protons are no longer significantly deflected by galactic magnetic fields and keep memory of their sources as can be seen from the Larmor radius $R_L = 3 \text{ kpc} \cdot E / 10^{19} \text{ eV} \cdot B / 3 \mu\text{G}$ in a typical galactic magnetic field (the extragalactic fields are unknown, but expected to be on nG scale).

Geoneutrinos (first hints, target of future investigations) have energy $E_\nu \sim \text{MeV}$. They originate from radioactive decays of uranium, thorium and potassium, that are expected to accumulate in the continental crust: their total abundance in the mantle is expected to be only comparable to the total abundance in the continental crust. According to earth models [29, 46] radioactivity produces a large fraction of heat released by the Earth, and initially melted iron, that started falling to the center getting much more heated by gravitational energy. The information carried by neutrinos is not accessible to geological investigations and allows to test the above part of the Earth model. The $\bar{\nu}_e$ from uranium and thorium decay can be seen with IBD; the $\bar{\nu}_e$ (and a few ν_e) from ^{40}K cannot, due to their low energy (although they are presumed to be the main part of neutrino radiation). The accumulation of several kton \times years of exposure will permit a significant test of the current theoretical predictions. Geoneutrinos can be investigated at KamLAND [46], that obtained a hint of 9 ± 6 events, and Borexino [54].

Neutrinos from DM annihilation (searched) might exists with energy below 10 GeV to 1 TeV [108]. DM might be a thermal relic of WIMP with mass $m_{\text{DM}} \sim (T_{\text{now}} \cdot M_{\text{Pl}})^{1/2} \sim 100 \text{ GeV}$. DM particles accumulate around the center of the earth and of the sun, and important over-densities can also arise in central regions of the galactic halo or around the galactic black hole. Their annihilation products involve neutrinos with energy below m_{DM} , that can be dominantly observed as up-going muons induced by $\langle \bar{\nu}_\mu \rangle$. Baksan, Baikal, SK, MACRO, AMANDA have produced upper limits [109]. These search will be continued with the future detectors mentioned in the next items, and will be ultimately limited by the atmospheric neutrino background.

Neutrinos from galactic sources (“knee-neutrinos”) (very actively searched) with energies around $1 \div 100 \text{ TeV}$ [110]. This is an interesting window for observation of cosmic sources, since the atmospheric neutrino background (from ν_μ and $\bar{\nu}_\mu$) is overwhelming at lower energies, while above several 100 TeV the Earth becomes opaque to neutrinos. The observation of point or diffuse sources is a very important goal: e.g. ν and γ astronomy at these high energies can shed light on the origin of CR around the knee and below, that is known to be of galactic origin. Among the most promising galactic point sources are the young supernovae or young supernova remnants and other objects as miniquasars. Some confidence in this search comes from the argument of Ginzburg and Syrovatskii, that the kinetic energy stored in supernova remnants is likely to be the origin of CR of the Milky Way. Therefore, possible interactions of CR with matter in the surrounding environment would produce pions, that decay generating high energy ν and γ . Further hope of success is given by the fact that the atmospheric neutrino background decreases more rapidly than the spectrum of γ rays till observed $\sim 10 \text{ TeV}$. We cannot exclude the possibility of other intense sources of neutrinos but not of photons, generically denoted as “hidden sources” (e.g., a micro-quasar, or a black hole inside a star which screens the electromagnetic radiation) or even extragalactic sources. The existing limits come from MACRO, Super-Kamiokande, KGF, Soudan, Baikal, AMANDA. There are plans to build km^3 detectors in the Antarctica (IceCUBE), in the lake Baikal and also in the Mediterranean sea, where the Antares, NEMO, NESTOR collaborations are at present operating, and could result in one future large installation, named KM3NeT. A neutrino telescope in the northern hemisphere can ‘see’ the galactic center.

GZK and other UHE neutrinos (hopes for close future) till $\sim 10^{20} \text{ eV}$, that is nowadays the last frontier in energy (see again [110]). Neutrinos of ultra-high energy are known to exist: these are sometimes called ‘GZK neutrinos’, and are due to the existing UHE-CR that occasionally

interact and produce π 's. However the question is whether there are sources intense enough to be detectable, without contradicting what we know from observed electromagnetic radiation and CR (this is not a trivial requirement). AGN and GRB have been considered as possible astrophysical sources of CR with energies at the 'ankle' and below. Other sources of neutrinos discussed in the literature include decay of superheavy quasi-stable particles, topological defects, and other [111]. UHE particles are detected looking at the air showers that they produce. Neutrinos have smaller cross sections, and therefore dominantly manifest as quasi-horizontal air showers², searched for by AGASA, Hi-Res, EAS-TOP, and other experiments [113], producing limits. A big step forward on the question of UHE neutrinos is expected to come from the results of AUGER [114] and ANITA [115]. There are also attempts of detection using acoustic detectors or by monitoring the atmosphere from a satellite. More possibilities for observations arise by the production of τ leptons [116].

Supernova neutrinos (observed in one occasion) have energy $E_\nu \lesssim 100$ MeV, include neutrinos of all types and will be discussed in more details in the next section. This type of search promises big dividends in astro/physics currency: core collapse SN are a possible source of infrared, visible, X , and γ radiation, and possibly of gravitational waves; they are of key importance for origin of galactic CR, galactic reprocessing of elements; etc. Many operating neutrino detectors like SK, SNO, LVD, KamLAND, Baksan, MiniBOONE, AMANDA/IceCUBE could be blessed by the next galactic supernova and other detectors like Borexino or ICARUS could contribute to galactic supernovæ monitoring in the future. Experiments almost have the sensitivity that seems necessary to observe relic $\bar{\nu}_e$ emitted by past supernova collapses [117].

11.2 Core collapse supernovæ

In this section, we discuss neutrinos from supernovæ. More precisely, we will always be concerned with *core collapse* supernovæ, and we focus mostly on galactic events. In section 11.2.1 we present the possible type of observable events, the expected SN rate and other general astronomical facts. In section 11.2.2 we describe the theoretical scenario for the gravitational collapse and explosion, concentrating mostly on the 'delayed scenario'. In section 11.2.3 we summarize the expectations for the neutrino fluxes.

11.2.1 General considerations

Galactic, extragalactic, and relic supernovæ Let us begin by discussing the various types of supernovæ that can lead to an observable signal in existing and future detectors.

²Let us give some useful numbers. The density of the atmosphere decreases roughly as $e^{-h/8.4\text{ km}}$, and 99% of the atmosphere mass lies in its lower 30 km. The depth of the atmosphere is $L_\downarrow = 0.01033\text{ kmwe}$ when crossed vertically, and $L_\rightarrow = 0.36\text{ kmwe}$ when crossed horizontally; the depth of the Earth and Sun crossed along a diameter is $L_\oplus = 1.1 \cdot 10^5\text{ kmwe}$ and $L_\odot = 3 \cdot 10^7\text{ kmwe}$ respectively. The interaction length of a particle with cross section σ on nucleons is $L = 1.7 \cdot 10^7\text{ kmwe} (\text{pb}/\sigma)$. Protons have $\sigma \approx 0.15\text{ b}$ and thereby interact in the upper atmosphere. According to the SM, UHE neutrinos have a much smaller $\sigma \approx 10^4\text{ pb} \cdot (E_\nu/10^{18}\text{ eV})^{0.4}$, such that their interaction length is a few orders of magnitude bigger than the atmosphere depth, and smaller than the Earth depth. Detection of UHE neutrinos would allow to measure their cross-section [112] and many authors studied how exotic new physics (such as extra dimensions and TeV-scale quantum gravity) could affect this cross section.

- (1) The hope of existing neutrino telescopes is the explosion of a galactic supernova, for the simple fact that the $1/D^2$ scaling of the flux is severe. For reference, in water or scintillator detectors one expects roughly 300 ν -events per kton for a distance $D = 10$ kpc.³
- (2) Extragalactic neutrino astronomy begun several years ago with SN1987A. In principle, one could profit of the wealth of galaxies around us (say, those in the ‘local group’) to get events at human-scale pace. In practice, this is difficult, because core collapse SN takes place only in spiral or irregular galaxies, and not in elliptical ones.⁴ The only other large spiral galaxy of the local group is Andromeda (M31) but its mass is presumably only half of our galaxy and its distance is about 700 kpc. In the previous example, one would get 60 events in a future Mton WČ detector, assuming 100% efficiency. Perhaps, the best chance would be another ‘big’ SN from the Large Magellanic cloud (an irregular galaxy) but the odds for such an event are not high.
- (3) Another interesting possibility is the search for relic neutrinos emitted by past supernovæ. The practical method is to select an energy window around $20 \div 40$ MeV, where atmospheric and other neutrino backgrounds are small, and searching for an accumulation of neutrino events with more-or-less known energy distribution. The best limit has been obtained by SK [117], and the sensitivity is approaching the signal suggested by astrophysical models. In principle, one can suppress the main background (muons produced below the Čerenkov threshold) by identifying the neutron from inverse beta decay. This could be possible by loading the water with an appropriate nucleus [118], that should absorb the neutron and yield visible γ eventually.⁵

Astronomical and other observations Supernovæ (SN) are divided in two classes according to their light spectra: the first class comprises SN Ia that have very regular light curves (among the best ‘standard candles’ for cosmology); the second comprises the rest (SN II, Ib and Ic, depending on the presence of H and He lines in the spectra) with a wide variety of light curves (e.g., the observed optical luminosities vary by at least three orders of magnitudes). We are interested in the second class of objects, that are thought to originate from the gravitational collapse of a very massive star, $M > (6 \div 10) M_\odot$, that possibly leads to the formation of neutron stars and black holes.

About 2000 supernovæ have been observed [119], and their frequency depending on the type of galaxy has been studied on statistical basis. This makes it possible to predict the rate of occurrence of core-collapse supernovæ in our Galaxy:

$$R_{\text{SN}} = 1/(30 \div 70 \text{ yr}). \quad (11.1)$$

The main uncertainty is that the galactic type of the Milky Way (Sb or Sbc) is not firmly known. Numbers in the range 1 SN in 10 to 100 years have been also deduced on other basis, e.g. from the

³We recall that pc = 3.26 light-year and that our galaxy has a size of some 15 kpc, and we are located at 8.5 kpc from its center. One could expect that the chances of getting a supernova where matter is more abundant are higher (the galactic center), but one can also object that younger matter, conducive to SN formation, lies elsewhere (in the spiral arms). However, we are unaware of the existence of a ‘catalog of explosive stars of our galaxy’, or of calculations of weighted matter distributions of our galaxy.

⁴Their stellar population is older, and star forming regions are absent or very rare; in a sense, the stars of 10-40 solar masses are a problem of youth.

⁵Neutron identification by $p + n \rightarrow D + \gamma(2.2 \text{ MeV})$ was proved in scintillators (furthermore, no Čerenkov threshold impedes); however no existing or planned scintillator has a mass larger than 1 kton.

pulsar formation rate or from theoretical estimations of stellar lifetime *plus* stellar statistics, but they do not seem to be very reliable at present. A lower limit on occurrence of SN in the Milky Way can be put from the fact that no ν -telescope observe any event yet. The oldest telescope with galactic reach is Baksan [120], working since 30 June 1980 with 90% live-time. If we assume that since 1980 there was no main holes in time coverage, we arrive at a total live-time of about $T = 25$ yr in which no galactic SN has been seen. Poisson statistics implies

$$\exp(-TR_{\text{SN}}) > 1 - \text{C.L.} \quad \text{i.e.} \quad R_{\text{SN}} < \frac{1}{11\text{yr}} \text{ at 90\% C.L.} \quad (11.2)$$

Often, one recalls the possibility that SN events take place in optically obscured regions of our galaxy; however, one should also recall that, beside ν s, there are other manners to investigate the occurrence of such a phenomenon, e.g. from the released infrared radiation.

The large radiation in neutrinos in a stellar collapse is expected to be accompanied by other observable phenomena, such as gravitational waves (if the collapse deviates enough from spherical symmetry) and of course light (after that the shock wave emerges from the stellar mantle), γ radiation (after that the radioactive elements emerge from the core), etc. Gravitational radiation, is an important goal of future observations, and could indicate the beginning of the gravitational collapse.

11.2.2 Gravitational collapse and the explosion

We here present the expectations on the gravitational collapse and discuss the unclear points of the general picture we have of this phenomenon. For what regards astrophysics, the most puzzling aspect is certainly that the current simulations miss to reproduce the explosion.

Before summarizing precise results we explain the basic physics. In order to have a discussion as simple as possible we drop factors of order unity. We explicitly include \hbar , c and order one factors when this makes the physics more transparent. We find it convenient to use standard symbols for a star with mass M and radius R , volume $V \sim R^3$, composed by $N = M/m_n \sim 10^{57} M/M_\odot$ nucleons (with mass m_n) and $\sim N$ electrons (with mass m_e), with density $\rho \sim M/R^3$ and number density $n = N/V$. A single particle occupies an average volume $v \sim R^3/N \sim 1/n$ and has energy u . For the latest stage of the life of a massive star, it is important to recall that localized fermions are subject to Fermi motion: due to the Pauli indetermination relation $\Delta x \Delta p = 2\pi\hbar$, N fermions at zero temperature fill all states till the Fermi momentum

$$p_F = \hbar(3\pi^2 N/V)^{1/3} \sim \hbar n^{1/3}, \text{ where } n = \frac{N}{V}. \quad (11.3)$$

This motion originates a pressure (known as ‘degeneracy’ or ‘quantum pressure’)

$$P \sim \frac{1}{v} \cdot u(p_F) = n \cdot (\sqrt{(m_e c^2)^2 + (cp_F)^2} - m_e c^2) = \begin{cases} n^{5/3} \frac{\hbar^2}{m_e} & \text{non-relativistic} \\ n^{4/3} \hbar c & \text{relativistic} \end{cases} \quad (11.4)$$

that increases with the increasing density $\rho = m_n \cdot n$.

Stellar evolution and structure of the presupernova Stars form because a large enough cloud of particles is unstable under gravity. The cloud contracts and the gravitational potential energy gets converted into kinetic energy, $N \cdot u = GM^2/R$, heating the gas. When the gas becomes

hot enough, the nuclear reaction (6.2) begins to burn hydrogen into helium. The nuclear energy stops the contraction: one gets a star that shines in a quasi-equilibrium state between gravity and nuclear forces. When all the hydrogen in the core has been burned, the star contracts and, if enough massive, becomes enough hot to burn helium into carbon. After few of such steps (that are increasingly rapid and violent) very massive stars form an inert iron core, that cannot burn any more because ^{56}Fe is the most stable of all nuclei (this is the true ground state of QCD!). The core is surrounded by shells of unburned lighter nuclei. Occasionally this configuration is referred as ‘onion layers’ structure. However one should realize that the innermost layers can be quite ‘rough’ (due for instance to the presence of explosive nuclear reactions that occur in the latest stages of the life of the star) and the outermost ones can be expelled by intense stellar winds (actually, it is thought that SN Ib and Ic are such a type of objects).

Leaving for a moment the star and thinking about neutrinos, in order to compute matter effects one needs to know the profile density of the precursor of the supernova (‘pre-supernova’ star). This requires a good modelization of the electronic density $\rho_e(x) = \rho(x)Y_e(x)$ of the pre-supernova, especially at densities around $(10 \div 100) \text{ g/cm}^3$ (MSW ‘solar’ resonance) and $(500 \div 2000) \text{ g/cm}^3$ (MSW ‘atmospheric’ resonance). For orientation, a pre-supernova mantle density $\rho \sim 4 \cdot 10^4 (r_0/r)^3 \text{ g/cm}^3$ with $r_0 = 10^4 \text{ km}$ and $Y_e \sim 1/2$ can be used. If extra ‘sterile’ neutrinos exist, one needs to know the two functions $\rho(x)$ and $Y_e(x)$ separately, and recall that in the deleptonized core, Y_e can be rather small; this can give rise to additional MSW effects.

Gravitational instability of large mass stars The star remains stable if the force due to pressure ($F \sim P \cdot R^2$) compensates the attractive force due to gravity ($F \sim GM^2/R^2$) i.e. if $P = P_{\text{gravity}} \approx GM^2/R^4$. Assuming an equation of state $P(\rho)$ of the form $p = K\rho^\gamma$ it is possible to reach a stable configuration at a certain radius when $\gamma > 4/3$. We now show that: 1) for relatively small stars the quantum pressure due to non-relativistic electrons has $\gamma = 5/3$ and therefore supports the stars; 2) if the mass of the star is $M > (6 \div 10)M_\odot$, the iron core can become hot enough that electrons attain relativistic velocities, which reduces $\gamma = 4/3$ and originates a gravitational instability.

- 1) For non-relativistic electrons $u = p_F^2/2m_e \sim n^{2/3}\hbar^2/m_e$. Therefore the quantum pressure of electrons is

$$P \sim K\rho^\gamma \quad \text{where} \quad K \sim \frac{\hbar^2}{m_e m_n^{5/3}} \quad \text{and} \quad \gamma = \frac{5}{3}. \quad (11.5)$$

The above estimation also shows that the quantum pressure of the other heavier fermions (that instead dominate the mass density) is negligible. In conclusion, if the electrons are non-relativistic, quantum pressure compensates gravitational compression, and give rise to a stable configuration, a ‘white dwarf’ (equating P to P_{gravity} one realizes a characteristic feature of degenerate stars: the radius decreases with the mass as $R \propto M^{-1/3}$).

- 2) However, the Fermi momentum increases with the mass of the star, until electrons become relativistic, $u \gtrsim m_e c^2$. The energy of relativistic electrons is $u \sim cp_F \sim n^{1/3}\hbar$ so that the quantum pressure becomes

$$P \sim K\rho^\gamma \quad \text{where} \quad K = \frac{\hbar c}{m_n^{4/3}} \quad \text{and} \quad \gamma = \frac{4}{3}. \quad (11.6)$$

Thus, the quantum pressure P scales with $1/R^4$ just as the gravitational pressure; but while the first increases as $M^{4/3}$, the second increases faster, as M^2 . This implies that there

is a limiting mass, the Chandrasekhar mass $M \gtrsim M_{\text{Ch}} \sim (\hbar c/G)^{3/2}/m_n^2$ ($M_{\text{Ch}} = 1.4M_{\odot}$ including order one factors) above which the quasi-free electrons are unable to produce a stable configuration, and the star collapses under its weight.

Let us consider the situation when the inert iron core reaches a mass $M \sim M_{\text{Ch}}$, with radius $\sim 8 \cdot 10^3$ km. The collapse begins because at a certain point an increase of the temperature leads to a *decrease* of the pressure: the loss of kinetic energy is due to the onset of iron photodissociation reaction and of electron neutrino production, $ep \rightarrow n\nu_e$. The latter reaction gives rise to an initial burst of electron neutrinos, and this is occasionally referred as the ‘*infall phase*’. During this stage ν_e carry away some small fraction of the total energy (simulations suggest a fraction of % at most) and a part of the stored leptonic (electron) number. After some 100 ms, the inner part of the core (‘inner core’) contains mostly neutrons plus a soup of particle/antiparticle with an increasing temperature $T \gg m_e$. The particles lighter than T are photons, electrons, perhaps muons, and $\nu_{e,\mu,\tau}$. With increasing density, even neutrinos are momentarily trapped in the collapsing star.

Rebounce (and explosion?) When the inner part of the core (about $0.6 M_{\odot}$ according to simulations) reaches nuclear density, the collapse gets halted by the quantum pressure of neutrons (and remaining protons) that are non relativistic and therefore have $\gamma = 5/3$. An enormous amount of gravitational binding energy gets converted into kinetic energy. The radius of the core is about $R \sim \text{Fermi } N^{1/3} \sim (10 \div 20)$ km (1 Fermi = 10^{-13} cm). The rebounce of the inner core generates an outward-going shock wave, but at this point existing simulations meet a serious difficulty. In fact, the simulated shock wave loses energy due to iron dissociation on the way through the ‘outer core’, it slows down, and eventually stalls. Said in simpler terms, in practically all simulations the rebounce is too weak to generate the explosion we see. A popular working hypothesis is that the shock wave is rejuvenated by the outflowing neutrinos, which comprise the bulk of the kinetic energy. Indeed, the neutrinos trapped in the inner core will diffuse out; they hit and push the stalling matter from below in a way probably crucial for finally getting an explosion. This is called the ‘*delayed explosion*’ scenario. In some computer simulations, the delayed explosion happens in a fraction of a second, during the so called ‘*accretion phase*’. A successful explosion requires that at least about 10% of the energy emitted in neutrinos is transferred to the shock wave. The ‘*delayed explosion*’ is regarded by many as the most promising scenario to obtain a successful understanding of the explosion, but it is fair to recall that *ab initio* simulations are still unable to obtain explosions. In summary, we have not a ‘standard SN model’ yet. This could be due to a very complex dynamics; it could indicate that some ingredient is missing (such as an essential rôle of asphericity, of rotation, of magnetic fields, etc), or that there is nothing like a ‘*standard explosion*’; or perhaps it could be a hint that several core collapse do not lead to an optical burst (and explosion); or even it might be a hint for new physics.

Cooling The first second after the core collapse is probably of key importance to understand supernova explosion. However, the main part of the emission of neutrinos is supposed to take place later, in the ‘*cooling phase*’ (or ‘*thermal*’, or ‘*Kelvin-Helmotz*’ phase). In this phase, the proto-neutron star cools and contracts in a quasi equilibrium state.⁶ We begin the description of this phase by evaluating the total energy radiated in neutrinos (based on macroscopic arguments) and

⁶In other words, we do not know yet the details of explosion but we can argue that we do not need to know them to describe the bulk neutrino emission.

conclude estimating the luminosity, temperature, and time of the collapse based on simple minded microscopic arguments. A detailed discussion of expected neutrino fluxes is left to section 11.2.3.

The core is so dense and hot that neutrinos are efficiently produced and partly trapped. Other SM particles are much more strongly trapped, while gravitons are so weakly coupled that are neither trapped nor significantly produced. As a result neutrinos are able to carry away the energy. The stellar collapse is supposed to possibly lead to the formation of a neutron star, occasionally seen as a pulsar with mass $M_{\text{NS}} = (1 \div 2) M_{\odot}$, and radius $R_{\text{NS}} \approx 15 \text{ km}$ $(M_{\odot}/M_{\text{NS}})^{1/3}$ (the scaling is due to the degenerate character of the equation of state, as for white dwarfs). Including a factor of order one from the expected distribution of the nuclear matter, we come to the following estimation of the released binding energy:

$$\mathcal{E}_B \approx \frac{3M_{\text{NS}}^2}{7R_{\text{NS}}} = (1 \div 5) \cdot 10^{53} \text{ erg.}$$

One expects that the overwhelming part of \mathcal{E}_B is carried away by neutrinos.⁷ Neutrinos are produced with energy comparable to the temperature of the environment, $u = \mathcal{E}_B/N \sim 100 \text{ MeV}$: neutrinos thermalize by random walking in the interior. because their mean free path is $\ell \sim 1/n\sigma \sim 1/(G_F^2 T^5) \sim 10 \text{ km}$ $(10 \text{ MeV}/T)^5$ is smaller than the core.

Neutrinos around the outer and cooler part of the supernova, named ‘neutrinosphere’, escape cooling the neutron star. Therefore in thermal approximation only the temperature and density profile of the outer part of the SN are needed to compute neutrino fluxes. Simple estimations indicate that neutrinos exit with temperature $T \sim 10 \text{ MeV}$. The instantaneous luminosity is $\mathcal{L} \sim R^2 T^4 \sim 10^{52} \text{ erg/sec}$, thus the six types of neutrinos need about 10 seconds to carry out all energy. In the next section we present results of precise studies of neutrino interactions.

Let us finally comment on the possibility of producing a black hole. If also neutrons become ultra-relativistic, $T \gg m_n$, their equation of state is the standard one of massless quarks, $P = \rho/3$ (since we are not able of solving non perturbative QCD, we do not precisely know what happens when $T \sim m_n$, but we know that at $T \gg m_n$ the relevant degrees of freedom are quarks. The exponent $\gamma = 1$ in $P \propto \rho^\gamma$ can also be derived adapting the estimation done for electrons, taking into account that now $\rho = un$, rather than $\rho = m_n n$), such that gravity wins over pressure and the ultra-relativistic neutrons collapse into a black hole. This might abruptly terminate neutrino emission.

11.2.3 Neutrinos from core collapse supernovae

General properties of emitted neutrinos In the delayed scenario the collapse has four main phases. Correspondingly, we distinguish between two early neutrino emissions, named “infall” (or deleptonization, or early neutronization) and “flash” and the two late phases of “accretion” and “cooling”, as summarized in table 11.1. The most uncertain phase is certainly the one of “accretion”, that, together with “cooling”, accounts for most of the energetics. Perhaps, a fair estimation of uncertainties is around 100%. In support of this (apparently too conservative)

⁷Let us compare \mathcal{E}_B with other relevant energies. This is much bigger than the observed kinetic energy of the ejecta, $E_{\text{kin}} \sim 10^{51} \text{ erg}$ (a typical velocity of the shock wave is $v \sim 5000 \text{ km/s}$). It is also much bigger than the energy needed to dissociate the outer iron core $\sim 2.2 \text{ MeV} \cdot 0.6 M_{\odot}/m_n = 2 \cdot 10^{51} \text{ erg}$ (the mass of ^{56}Fe is 123 MeV smaller than $13m_{\alpha} + 4m_n$). The energy seen in photons is very small, $E_{\text{lum}} \approx 10^{49} \text{ erg} \approx 10^{-4} \mathcal{E}_B$ (sufficient to outshine the host galaxy though!). The energy emitted in gravitational waves depends on the detailed dynamics of the collapse. A naïve guess is $G_N(M_{\text{core}}v^2/2)^2/R \sim (v/c)^4 \cdot \mathcal{E}_B \ll \mathcal{E}_B$.

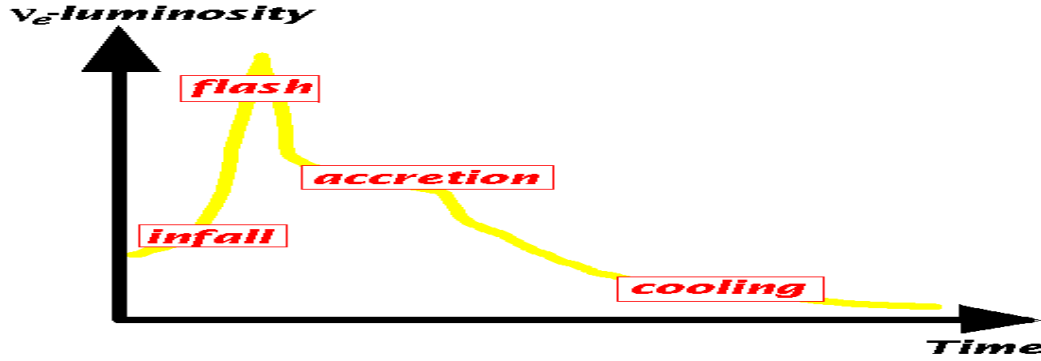


Figure 11.1: Sketchy plot of the behavior of the ν_e luminosity, for the delayed scenario.

statement, we recall that we have no *ab initio* calculations of these fluxes, and alternative scenarios have been proposed. Furthermore, the calculations that tried to estimate the effect of rotation [121] found very different fluxes, and in particular a severe suppression of muon and tau neutrinos.

We now describe detailed expectations for SN neutrinos. First we discuss the general characteristics and present a phenomenological survey, and in next paragraph we discuss how their luminosity, energy spectrum, and possible non-thermal effects can be parameterized. We can distinguish are 3 types of neutrinos:

$$\nu_e, \quad \bar{\nu}_e \quad \text{and} \quad \nu_x \equiv \nu_\mu, \bar{\nu}_\mu, \nu_\tau, \bar{\nu}_\tau$$

Indeed ν_μ , $\bar{\nu}_\mu$, ν_τ and $\bar{\nu}_\tau$ should have a very similar distribution because ν_μ and ν_τ are produced by NC in the same manner (muons are expected to be present only in the innermost core), and $\nu_{\mu,\tau}$ and $\bar{\nu}_{\mu,\tau}$ have similar properties. Different numerical calculations find values for the ‘average’ neutrino energies $\langle E_\nu \rangle$ and total emitted energy \mathcal{E}_ν in the following ranges:

$$\begin{aligned} \langle E_{\nu_e} \rangle &= 10 \div 12 \text{ MeV}, & \mathcal{E}_{\nu_e} &= 10 \div 30 \% \mathcal{E}_B, \\ \langle E_{\bar{\nu}_e} \rangle &= 12 \div 18 \text{ MeV}, & \mathcal{E}_{\bar{\nu}_e} &= 10 \div 30 \% \mathcal{E}_B, \\ \langle E_{\nu_x} \rangle &= 15 \div 28 \text{ MeV}, & \mathcal{E}_{\nu_x} &= 20 \div 10 \% \mathcal{E}_B. \end{aligned} \quad (11.7)$$

The general reason of the hierarchy in the average energies is that neutrinos that interact more decouple in more external regions of the star. The approximate equality between the energy radiated in the various neutrino types found in several numerical calculations has been named ‘equipartition’, but in our understanding, there is no profound reason behind this result. It is important to recall that till recently it was commonly assumed a rather strict equipartition and a large hierarchy of average energies between the various neutrinos, while recent calculations suggest that the hierarchy of average energies is modest, and the equipartition is satisfied only up to factor of 2.

This is important for oscillations signals: oscillation play an important rôle only if $\langle \bar{\nu}_e \rangle$ fluxes are different from $\langle \bar{\nu}_x \rangle$ fluxes: if instead the energy distribution is the same and equipartition is exact, there is no oscillation effect.

Phase	Neutrinos	Description	Duration	% of \mathcal{E}_B
infall	ν_e	Collapse. $ep \rightarrow \nu_e n$. ν -trapping increases.	~ 100 msec	< 1%
flash	ν_e	$t \equiv 0$. Bounce. Flash when ν -sphere is reached.	few msec	$\sim 1\%$
accretion	all	Stall. $e^+e^- \rightarrow \nu_x \bar{\nu}_x$. Explosion resumed (by neutrino heating?).	\lesssim sec	$(10 \div 20)\%$
cooling	all	Proto neutron-star cools and contracts.	$(10 \div 100)$ sec	$(80 \div 90)\%$

Table 11.1: *Brief description of the phases for neutrino emission in the delayed scenario for the explosion of core collapse SN. ν_x indicates non-electron ν a $\bar{\nu}$.*

Parameterized fluxes Let us begin recalling some definitions:

$$\begin{aligned} \text{flux} &= F = dN/dt dS dE, \\ \text{fluence} &= \Phi = dN/dS dE = \int F dt \\ \text{luminosity} &= \mathcal{L} = d\mathcal{E}/dt = \int E F dS dE. \end{aligned}$$

Assuming that the emission is isotropic (which should be true up to $\sim 10\%$ corrections, or presumably less during cooling phase), we can describe the flux at earth as:

$$F = \frac{\mathcal{L}}{4\pi D^2} \times \frac{n(E/T, \xi)}{T^2} \quad (11.8)$$

where T is the temperature, ξ one (or more) parameter(s) that describes the deviations from exact thermal distribution, and D the distance from the SN. The most common choices for the energy distributions are:

$$n(x, \xi) \propto \begin{cases} x^2/(1 + e^{x-\eta}) & \xi = \eta \neq 0, \\ x^2 e^{-(x/x_0)^2}/(1 + e^x) & \xi = x_0 \neq \infty, \\ x^\alpha \cdot e^{-x} & \xi = \alpha \neq 2. \end{cases} \quad (11.9)$$

namely, modified Fermi-Dirac or Maxwell-Boltzmann distributions. The normalization is $\int x \cdot n(x, \xi) dx = 1$, that implies that the instantaneous luminosity is \mathcal{L} as it should be. In these terms, we can formulate the (non-trivial) goal of reconstructing experimentally (or to calculate) three functions of time for each type of neutrino: \mathcal{L}, T, ξ . The total energy radiated \mathcal{E} is often used in place of the luminosity \mathcal{L} .

From now on for definiteness we assume the Fermi-Dirac distribution. In a simplified description, the full distributions can be characterized by a few parameters. The most important ones are

- \mathcal{E}_B , the total energy radiated (binding energy);
- $T_{\bar{e}}$, the temperature of antineutrinos, which can be easily measured;
- $\kappa \equiv T_x/T_{\bar{e}}$;
- $f = f_e = f_{\bar{e}}$, the energy fraction in electron (anti)neutrinos. One has $f_x = (1 - 2f)/4$, with $f = 1/6$ in the special case of ‘equipartition’.

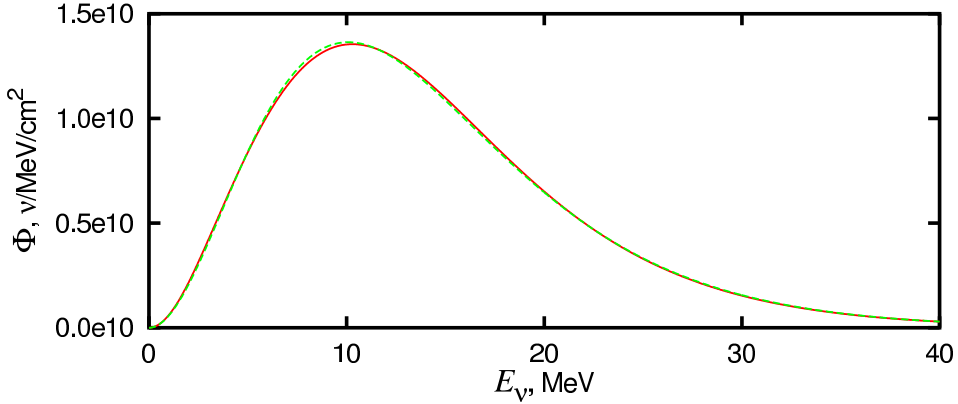


Figure 11.2: Comparison of the fluence obtained integrating the neutrino flux in time (red line) with an effective fluence described by appropriately chosen average (time independent) parameters (green line); see text for an accurate description. The agreement between the two curves is at the % level.

- an effective ‘pinching’ parameter η equal for all types of neutrinos (that is not expected to be accurate, but could be adequate).

Usually T_e is a less important parameter to describe the neutrino signal, and can be estimated from the above parameters by assigning a ‘reasonable’ condition on the emitted lepton number $N_e - N_{\bar{e}}$. In formulae,

$$T_e = T_{\bar{e}}/[1 + (N_e - N_{\bar{e}})(T_{\bar{e}}F_3(\eta)/F_2(\eta)) / (f\mathcal{E}_B)]. \quad (11.10)$$

where $F_n(\eta) \equiv \int_0^\infty dx x^n / (1 + e^{x-\eta})$.

At a further level of refinement, we describe time dependent features distinguishing between ‘cooling’ and ‘accretion’ neutrinos. The time dependence of the temperatures and luminosities can be approximated as

$$T_i(t) = T_i(0)/(1 + t/\tau_c)^{\beta_c}, \quad \mathcal{L}_i \propto T_i^4 \quad (11.11)$$

with $\tau_c \sim (10 \div 100)$ sec and the exponent β_c have to be extracted from the data or computed.

On top of that, we can model an hypothetical accretion phase with duration τ_a , adding, for $t < \tau_a$, another rather luminous phase, presumably with a marked non-thermal behavior ($\eta \neq 0$) and with its own effective temperature. Since the efficiency of energy transfer to matter is not large, $\langle \bar{\nu} \rangle_e$ should carry a sizable fraction of energy; ν_x are of little use to revive the shock, but presumably, only few of them are produced in this phase.

A simple model for the cooling employs the concept of ‘neutrino-spheres’ with radii R_i . Black-body emission gives:

$$\mathcal{L}_i = \frac{F_3(\eta_i)}{2\pi} \cdot R_i^2(t) \cdot T_i^4(t) \sim 5.2 \times 10^{51} \frac{\text{erg}}{\text{sec}} \left(\frac{R_i}{15 \text{ km}} \right)^2 \left(\frac{T_i}{4.5 \text{ MeV}} \right)^4 \quad (11.12)$$

for $i = e, \bar{e}, \mu \dots$ ($\hbar = c = k = 1$ here). The numerical value of the luminosity, obtained assuming $\eta = 0$, leads to an energy $\sim 5 \times 10^{52}$ erg radiated in 10 seconds, when we use reasonable values of the radius and temperature. Similarly, one can model the accretion phase by suggesting that the

non-thermal neutrino production is from e^\pm interactions with the accreting matter [122]. This implies that the fluxes are proportional to the cross sections: thus, their scaling with energy should be more similar to E_ν^4 than to E_ν^2 , namely the deviation from a thermal spectrum should be larger during accretion.

In order to show the use of these formulae, we conclude with a numerical example. Let us consider a time dependent flux, with temperature and radius of ‘neutrino-sphere’ starting from the values $T(0) = 5$ MeV and $R(0) = 10$ km and diminishing with time as in eq. (11.11) with $\tau_c = 10$ s and $\beta_c = 3/4$; non-thermal effects are described by assigning $\eta = 2$. We can readily calculate the energy radiated, about 6×10^{52} erg and the average neutrino energy, around 14.2 MeV, which are both reasonable values. The fluence that we obtain integrating the flux in time can be parameterized by a distribution with ‘average’ parameters $T \sim 4.45$ MeV and $\eta \sim 0.24$ (that give the right values of $\langle E_\nu \rangle$ and $\langle E_\nu^2 \rangle$). The good agreement between the two descriptions is illustrated in fig. 11.2.

11.3 Effects of neutrino oscillations

At first sight, astrophysical sites offer ideal conditions to study how neutrinos propagate. We have enormous distances (e.g., the distance of the galactic center is about 2.5×10^{20} m), a wide variety of energies (just think to the extension in energy of the cosmic ray spectrum), magnetic fields of huge intensity (e.g., 10^{12} G on the surface of a neutron star) or of wide extension (e.g., intergalactic fields), etc. This allows to probe oscillations, matter effects, and possibly magnetic moment and finite lifetime. However, these propagation effects have to be disentangled from the properties of the neutrino source (for instance supernovæ are discussed in section 11.1.2), that are plagued by sizeable astrophysical uncertainties.

We here mostly focus on the scenario suggested by solar and atmospheric data: oscillations of 3 neutrinos. These ‘active’ oscillations do not affect the total rate of NC events (as well known after SNO solar neutrino results [10]): the total fluxes $F_e^0 + F_\mu^0 + F_\tau^0$ and $F_{\bar{e}}^0 + F_{\bar{\mu}}^0 + F_{\bar{\tau}}^0$ remain unaffected. In this section we study neutrinos with energy $(1 \div 100)$ MeV produced in high density environments, such as in core collapse supernovæ, in neutron star mergers, or in accretion processes on a black hole. For concreteness we specifically consider the case of supernova neutrinos, but our considerations have more general validity.

11.3.1 Oscillation of supernova neutrinos

Oscillations in the star Since the μ and τ fluxes at production are supposed to be identical, two functions are needed to describe how oscillations affect CC rates: $P_{ee}(E_\nu)$ and $P_{\bar{e}\bar{e}}(E_\nu)$, the electron neutrino/antineutrino survival probabilities. This can be seen by rewriting the general expression $F_e = P_{ee}F_e^0 + P_{\mu e}F_\mu^0 + P_{\tau e}F_\tau^0$ as $F_e = P_{ee}F_e^0 + (P_{\mu e} + P_{\tau e})F_{\mu,\tau}^0$ and recalling that $1 = P_{ee} + P_{\mu e} + P_{\tau e}$. In order to calculate P_{ee} , one has to solve the evolution equation of eq. (3.16). Inserting numbers, the effective hamiltonian is

$$H = 2.534 \cdot V \frac{\text{diag}(m_i^2)}{E_\nu} V^\dagger \pm 3.868 \cdot 10^{-7} \rho Y_e \cdot \text{diag}(1, 0, 0) \quad (11.13)$$

where the sign $+$ holds for neutrinos and $-$ for $\bar{\nu}$. Neutrino masses m_i are in eV, the neutrino energy E_ν in MeV, the density ρ in g/cm³ and the effective hamiltonian is in 1/m. The supernova density ρ and the electron fraction $Y_e = N_p/(N_p + N_n)$ must be taken from some pre-supernova

model, including the modifications due to the shock wave when needed. Neutrinos are produced in the region where the matter term dominates and can encounter two MSW resonances: the ‘solar resonance’ (described by the oscillation parameters Δm_{12}^2 and θ_{12}) is very much likely to be adiabatic, like in the solar case; the ‘atmospheric resonance’ (described by Δm_{13}^2 and θ_{13}) is adiabatic if θ_{13} is large enough. More quantitatively, assuming a typical pre-supernova profile $\rho \sim 2 \cdot 10^4 (10^4 \text{km}/r)^3 \text{g/cm}^3$ and $Y \sim 1/2$ and using the adiabaticity condition described in section 3.3, the atmospheric resonance is adiabatic ($P_C \simeq 0$) if $\theta_{13} \gg \sqrt{E_\nu/\Delta m_{\text{atm}}^2} \text{ km} \sim 1^\circ$ and is non adiabatic ($P_C \simeq 1$) if $\theta_{13} \ll 0.1^\circ$. Taking into account that neutrinos experience the solar resonance, and that neutrinos (anti-neutrinos) experience the atmospheric resonance if neutrinos have normal (inverted) hierarchy, we get:

	normal hierarchy	inverted hierarchy	(11.14)
$P_{\bar{e}\bar{e}}$	V_{e1}^2	$(1 - P_C)V_{e3}^2 + P_C V_{e1}^2$	
P_{ee}	$(1 - P_C)V_{e3}^2 + P_C V_{e2}^2$	V_{e2}^2	

This leads to the following limiting possibilities:

A) If θ_{13} is small enough that $P_C \simeq 1$ one has, for normal and inverted hierarchy:

$$F_{\bar{e}} = F_{\bar{e}}^0 \cos^2 \theta_{12} + F_{\bar{\mu},\bar{\tau}}^0 \sin^2 \theta_{12} \quad F_e = F_e^0 \sin^2 \theta_{12} + F_{\mu,\tau}^0 \cos^2 \theta_{12}.$$

B) If θ_{13} is large enough that $P_C \simeq 0$ and neutrinos have normal hierarchy one has:

$$F_{\bar{e}} \text{ as in A}), \quad F_e = F_{\mu,\tau}^0.$$

C) If θ_{13} is large enough that $P_C \simeq 0$ and neutrinos have inverted hierarchy one has:

$$F_e \text{ as in A}), \quad F_{\bar{e}} = F_{\bar{\mu},\bar{\tau}}^0.$$

The case of inverted hierarchy gives rise to a more sizable variation with θ_{13} , and this variation takes place in anti-neutrinos, that can be better observed thanks to IBD.

Shock wave An interesting possibility is that P_C could be time dependent, because the shock wave can cross the layer where the MSW resonance takes place, increasing the density gradient: depending on θ_{13} and to the type of neutrino mass hierarchy this effect possibly leads to observable signals in future large neutrino detectors.

Earth matter effect If (anti)neutrinos cross the Earth before hitting the detector, new oscillations occur and previous expressions are slightly modified. To understand the features of these oscillations we consider a constant density, say, the Earth mantle. Earth matter effects can be accounted by performing the following replacements in eq. (11.14)

$$V_{e2}^2 \rightarrow V_{e2}^2 + \delta P, \quad \text{and} \quad V_{e1}^2 \rightarrow V_{e1}^2 - \delta P \quad (11.15)$$

such that Earth matter effects are sensitive to θ_{13} and to the type of neutrino mass hierarchy. By explicitly solving the evolution equation one finds

$$\delta P = \varepsilon \cdot \frac{\sin^2(\Delta m_{12}^2 L / 4E_\nu) \sqrt{(1 + \varepsilon)^2 - 4\varepsilon \cos^2 \theta_{12}}}{(1 + \varepsilon)^2 - 4\varepsilon \cos^2 \theta_{12}} \sin^2 2\theta_{12} \quad (11.16)$$

Case	Hierarchy	$\sin^2 \theta_{13}$	Earth	Shock	ν_e burst
A)	Any	$\lesssim 10^{-5}$	Yes	No	Yes
B)	Normal	$\gtrsim 10^{-3}$	Yes	No	No
C)	Inverted	$\gtrsim 10^{-3}$	No	Yes	Yes

Table 11.2: *Presence or absence of Earth-matter and shock wave effects in the $\bar{\nu}_e$ spectra and of the ν_e burst for different neutrino mixing scenarios.*

This δP holds for neutrinos; for anti-neutrinos one must replace $\theta_{12} \rightarrow \pi/2 - \theta_{12}$. The quantity ε is

$$\varepsilon = \frac{\sqrt{2}G_F N_e}{\Delta m_{\text{sun}}^2/2E_\nu} \approx 5.5\% \frac{E_\nu}{20 \text{ MeV}} \frac{\rho}{3 \text{ g/cm}^3} \quad (11.17)$$

having assumed $Y_e = 1/2$ and the measured Δm_{sun}^2 . This effect is small for solar neutrinos, that have $E_\nu < 20 \text{ MeV}$. Supernova neutrinos are expected to reach larger energies, and earth matter effect can become detectably large. At first order in ε we can approximate the fraction with \sin^2 (vacuum oscillation phase). The typical oscillation length is (see eq. (3.3)) $\lambda \approx 600 \text{ km}$, somewhat smaller than the radius of the earth. In conclusion, earth matter effects are best seen at higher E_ν and if the supernova is seen just below the horizon.

Summary of oscillation effects Table 11.2 summarizes the discussion: the first columns define the three scenarios that we emphasized, and the subsequent three columns the possible signatures: the Earth matter effect for $\bar{\nu}_e$ (detectable via IBD); the presence of modifications due to the shock wave for $\bar{\nu}_e$ (detectable via IBD); the absence of a neutronization ν_e burst (detectable via a reaction with a suitable nucleus or via ES). In order to make quantitative statements one would need a definite theory of neutrino emission: the first two signals disappear if all antineutrinos are emitted with similar distributions; even the latter signal could be modified if rotation has an important role in the collapse.

Other possible effects Let us recall for completeness some possible extra effects. In presence of a polarized (magnetized) underlying medium, the MSW term in eq. (3.16) is different (it does not reduce to the average weak charge). Suitable neutrino magnetic moment can permit transitions from neutrino to antineutrino states. If extra sterile neutrinos with keV-scale masses exist, they can encounter MSW resonances in the inner region where neutrinos are trapped: this result into a complicated (and not yet fully understood) dynamics because neutrinos themselves contribute to matter potential resulting into non-linear evolution equations [123]. Lighter sterile neutrinos give rise to extra MSW resonances in the outer region.

11.3.2 Oscillations from cosmic sources

High-energy neutrinos are expected to be produced in diffuse media, such that matter corrections to oscillations are negligible; if these neutrinos cross the Earth, matter effects suppress oscillations and absorption can be relevant. The path-length is so large that vacuum oscillations are in the averaged regime, where oscillation probabilities are described by eq. (3.10): inserting the observed

mixing angles one finds

$$P_{\ell\ell'} = \sum_{i=1}^3 |V_{\ell i} V_{\ell' i}|^2 \approx \begin{pmatrix} 0.6 & 0.2 & 0.2 \\ 0.2 & 0.4 & 0.4 \\ 0.2 & 0.4 & 0.4 \end{pmatrix}. \quad (11.18)$$

Since $\theta_{23} \approx \pi/4$ the muon and tau fluxes become almost equal at the detector. In the typical situation of the π decay chain, the initial flavor ratio is $e : \mu : \tau = 1 : 2 : 0$ and becomes 1:1:1.

The observation of neutrinos from cosmological distances, if possible, could allow us to search for new effects possibly produced by neutrino decay (see section 13.3), or by slow neutrino oscillations into extra sterile neutrinos (see section 13.2).

11.3.3 Oscillations and interactions for neutrinos from DM annihilations

Annihilations of DM particles accumulated around the core of the earth and of the sun can produce detectable fluxes of neutrinos [108] with energy below m_{DM} , here called $\text{DM}\nu$. Assuming that DM arises as thermal relict of a weakly interacting massive particle points to the mass range $m_{\text{DM}} \sim 10 \text{ GeV} \div 10 \text{ TeV}$, and detectably large fluxes can be obtained. In a given model, astrophysical uncertainties (mainly on the local distribution of DM particles) make the total flux uncertain by about one order of magnitude. Solar fluxes can be comparable to terrestrial fluxes, since the sun is bigger but the earth core is closer. Furthermore, the DM capture rate in the earth is enhanced if m_{DM} is comparable to the mass of some heavy element in the earth, while this is not possible in the sun that is dominantly composed of H and He. In the sun the capture rate is typically in equilibrium with the annihilation rate, while this is not the case for the earth: the present annihilation rate depends on past history.

Captured DM particles must have negligible velocity, below the escape velocity (at most 11 km/sec in the earth, and at most 620 km/sec in the sun). The density distribution of DM particles within the sun or the earth is approximatively given by [108]

$$n(r) = n_0 \exp(-r^2/R_{\text{DM}}^2) \quad R_{\text{DM}} = \frac{R}{\sqrt{\beta m_{\text{DM}}}} \quad (11.19)$$

where r is the radial coordinate, $\beta = 2\pi G_F \rho_0 R^2 / 3T_0$, ρ_0 and T_0 are the central density and temperature of the body (sun or earth) and R is its radius. Numerically $\beta = 1.76/\text{GeV}$ for the earth and $\beta = 98.3/\text{GeV}$ for the sun.

The energy and flavour spectrum of $\text{DM}\nu$ depends on the possible DM annihilation channels. The main possibilities (including only known particles) are $\nu\bar{\nu}$, $\tau\bar{\tau}$, bb , W^+W^- , ZZ , $t\bar{t}$. The last three channels are kinematically allowed only if $m_{\text{DM}} > M_W, M_Z, m_t$ respectively. Decays into too long lived or too strongly interacting particles (such as e, μ, π), that thereby get stopped by interactions with matter before decaying, do not produce energetic neutrinos. Interactions with matter are not important for W, Z, t , that directly decay into ‘prompt’ neutrinos as well as into b, τ , etc, whose decays produce more neutrinos. In order to compute the flux of neutrinos produced by decays of b, τ one must take into account that they loose some energy before decaying due to interactions with surrounding matter.

If the DM particle is a Majorana fermion, like the neutralino in SUSY models, its annihilation rate in a fermion/anti-fermion pair with mass m_f is suppressed by an helicity factor m_f^2/m_{DM}^2 .

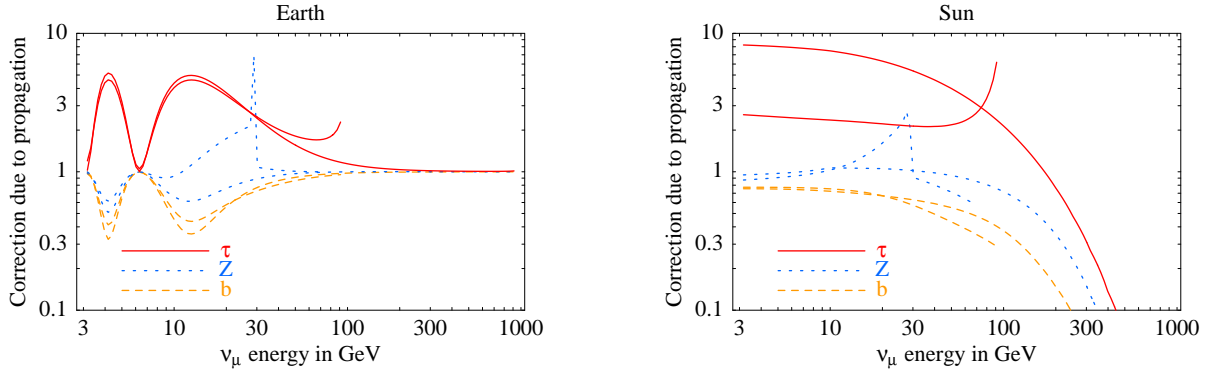


Figure 11.3: *Modifications of neutrino fluxes from DM annihilations due to propagation.* The figures show the ratio of ν_μ fluxes ‘with’ over ‘without’ the effects of neutrino propagation (oscillations, absorptions, regeneration). The lines refer to neutrinos from DM annihilations into $\tau\bar{\tau}$ (continuous line), ZZ (dotted) and $b\bar{b}$ (dashed), for $m_{\text{DM}} = \{100, 1000\} \text{ GeV}$ (distinguishable by the corresponding maximum neutrino energy).

This means that $b\bar{b}$ and $\tau\bar{\tau}$ channels are relevant only for $m_{\text{DM}} < M_W$, and that annihilation into $\nu\bar{\nu}$ is negligible. This is not the case if the DM particle has instead spin 1: annihilations into two neutrinos with energy m_{DM} can have significant branching ratio.

Different DM annihilation channels result in $\text{DM}\nu$ with a characteristic energy spectrum and typical energy $E_\nu \sim m_{\text{DM}}/(2 \text{ or } 3)$. One expects $F_e = F_\mu = F_{\bar{e}} = F_{\bar{\mu}} \neq F_\tau = F_{\bar{\tau}}$. The energy and flavour spectra can be significantly affected by oscillations: e.g. τ decays dominantly produce ν_τ , which are converted into ν_μ by atmospheric oscillations. Absorption is relevant for neutrinos produced around the center of the sun with energy above 100 GeV (and above $\sim 10^5$ GeV in the earth). NC processes reduce the energy but not the number of $(\bar{\nu})_{e,\mu,\tau}$. CC processes have cross sections a few times higher than NC processes, and do not directly produce a flux of secondary neutrinos. This happens indirectly only in the case of $(\bar{\nu})_\tau$, that generate τ^\pm with left polarization, that decay back mainly into $(\bar{\nu})_\tau$ with lower energy. Section 3.5 presented the formalism appropriate for computing the combined effect of oscillations and absorption, that amounts to a $\mathcal{O}(0.1 \div 10)$ correction, as illustrated in fig. 11.3. The main effects are

- ⊕ DM ν from the Earth are affected by atmospheric $(\bar{\nu})_\mu \leftrightarrow (\bar{\nu})_\tau$ oscillations at energies $E_\nu \lesssim 100 \text{ GeV}$, and by absorption at $E_\nu \gtrsim 10 \text{ TeV}$.
- ⊙ DM ν from the Sun of any flavor and any energy are affected by averaged ‘solar’ and ‘atmospheric’ oscillations. Furthermore, absorption suppresses neutrinos with $E_\nu \gtrsim 100 \text{ GeV}$, that are partially converted (by NC and by $(\bar{\nu})_\tau$ regeneration) into lower energy neutrinos. Neutrinos with energy $E_\nu \gg 100 \text{ GeV}$ approach a well-defined limit spectrum.

So far no DM ν have been seen, and atmospheric neutrinos are the main background. (A less important background is similarly produced in the ‘atmosphere’ of the sun). Therefore one needs big experiments with good angular resolution, such that one can point to the known source of DM ν . Experiments can achieve a resolution of few degrees and be ultimately limited by the typical scattering angle $\sim (m_N/E_\nu)^{1/2}$ of $\nu N \rightarrow \ell N'$ processes. In the case of DM ν from the earth, the size of the production region results in a comparable angular spread. Therefore experiments give stronger constraints on the DM ν fluxes for larger m_{DM} .

Detectors with surface and volume bigger than SK are built by inserting strings of photo-multipliers in the sea water or ice, used as target material. To perform a Čerenkov experiment a transparent enough medium is needed, and one has to cope with luminescent fishes in water and bubbles of air in ice. IceCUBE [109] should reach a km^3 volume, but with poor granularity: a bigger experiment has a lower density of photo-multipliers so that particles scattered by neutrinos can only be seen above the energy threshold of few tenths of GeV, their energy can be measured only up to a $\gtrsim 30\%$ uncertainty, and there are only two classes of events: 1) μ^\pm that produce a long track; 2) showers' originated by hadrons, τ^\pm, e^\pm, \dots

11.4 Observations of neutrinos from cosmic sources

In section 11.4.1 we discuss the neutrino observations from SN1987A. Targets of future supernova observations are discussed in section 11.4.2. Section 11.4.3 reviews the expectations for high energy neutrinos from shell-type, galactic supernova remnants.

11.4.1 SN1987A

Galactic neutrino astronomy is still to begin, whereas, curiously enough, extragalactic neutrino astronomy has already begun. At 7:36 (UT) of 23 february 1987, a number of experiments detected a neutrino signal from an atypically energetic stellar collapse occurred 170000 years ago in the Large Magellanic Cloud. These experiments are: KamiokandeII (12 events), IMB (8 events), possibly Baksan (6 events) and perhaps LSD [105].

SN1987A neutrinos were not particularly useful to learn on oscillations, due to poor statistics and to astrophysical uncertainties. The most reasonable hypothesis is that the ~ 20 neutrinos observed are due to $\bar{\nu}_e$ [106]. In fact, $\sigma(\bar{\nu}_e p \rightarrow ne^+)$ is two orders of magnitude larger than the cross sections of the other ν and $\bar{\nu}$, and it gives e^+ with almost isotropic angular distribution (while scattering on electrons gives a forward-peaked e). There is a reasonable agreement with expectations. This is true in particular for the duration of the emission, for the total amount of energy released in $\bar{\nu}_e$, and for their mean energy.⁸ Poor statistics does now allow to discriminate well the temperature from the total energy: a reduction in temperature can be compensated by an increase in flux.

Attempts of extracting as much information as possible by performing event-by-event fits are also limited by the fact that, at a closer sight, a number of puzzling features appear. We here recall those pertinent to neutrinos: the agreement between IMB and KII data is less than perfect; the average energy is on the low side of theoretical expectations; the temporal sequence of KII events is rather non-uniform and the first event recorded at KII seem to point back to the source (which would suggest a unexpected identification of a ν_e); the LSD detector at Mont Blanc recorded other 5 neutrinos but some five hours before the main signal. The latter point is probably the most troublesome. Together with a hint for gravitational radiation obtained at Geograv, it could be interpreted as a manifestation of collapse in 2 stages, see [124].

An analysis of KII, IMB and Baksan data yielded some support not only for a ‘standard’ collapse, but also of a luminous accretion-like phase in the first half-a-second of the neutrino emission [122].

⁸The light yield, the observations of γ radiation from radioactive species and the astronomical properties of the precursor do not contradict the general theoretical picture, even though all of these show rather peculiar features.

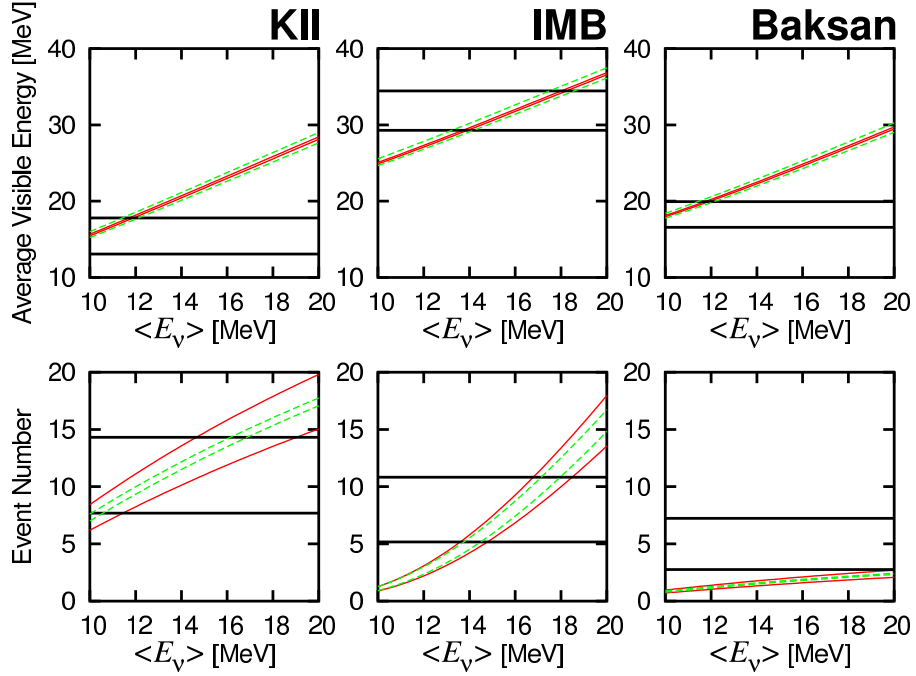


Figure 11.4: Comparison of observations (horizontal strips) and expectations calculated in the IBD hypothesis [127]. The 3 upper panels show the average visible energy, the lower panels show the number of events, assuming $\mathcal{E}_{\bar{e}} = 4 \cdot 10^{52}$ erg. In each panel we show 4 expectations: the continuous red lines correspond to a variation of the energy \mathcal{E}_x radiated in $\bar{\nu}_{\mu,\tau}$ parameter in the range $(2 \div 6) \cdot 10^{52}$ erg. The dashed green lines correspond to a variation of the average energy $\langle E_x \rangle$ in the range $(1 \div 1.2) \cdot \langle E_{\bar{e}} \rangle$.

The low average energy of KII and Baksan events lead many people to remark that the inclusion of solar oscillations with large mixing angle transforms some hotter $\bar{\nu}_{\mu,\tau}$ into $\bar{\nu}_e$ thereby increasing their expected average energy and worsening the agreement with data [125]. This argument weakens if the hierarchy of temperatures is modest [126] or if the originally produced flux of $\bar{\nu}_{\mu,\tau}$ is small.

However, the most common view is to neglect these discrepancies and puzzles in consideration of the small number of neutrino events at our disposal, interpret all events as $\bar{\nu}_e$, and draw no firm conclusion on the impact of oscillations on SN1987A events. In figure 11.4, we show that in this assumption there is a reasonable agreement between expectations and the observations, for certain values of the astrophysical parameters that describe neutrino emission that fall in the expected range given in eq. 11.7.

11.4.2 Future observations of supernova neutrinos

The galactic supernova rate is at best comparable to the inverse lifetime of a physicist, see eq. (11.1). A duty time of a minute per century makes difficult to build dedicated detectors, but allows to detect SN neutrinos using other neutrino experiments. Presently, at least one adequate neutrino experiment is kept running at any moment. With several detectors located in different parts of the world, some of them could receive the next SN explosion during night, allowing to probe also earth matter effects.

By measuring neutrinos emitted at the next supernova explosions, we will probably learn more

on oscillations and test non standard neutrino properties, especially if we will have an accurate theory of supernova explosions. Surely, the next supernova neutrino burst will lead great advances in the astrophysics of the core collapse.

What we would like to know from next galactic supernova? It is not difficult to compile a list of wishes: we would like to have detailed information on *time* and *energy* distributions, and study the signal in all possible *flavors*. In practice, we can measure the spectrum of $\bar{\nu}_e$ very well; the spectrum of electrons scattered by $\nu_e e$; the total neutrino rate by neutral current.⁹ The possible goals are a detailed picture of the various phases of the collapse and of the explosion; in particular the study of the first second (accretion?) seems to be of tremendous interest for astrophysics. Furthermore, it would be important to test the flavor distributions of the emitted neutrinos (e.g. the amount of ν_e and $\bar{\nu}_e$ during accretion).

11.4.3 Remarks on supernova remnants as neutrino sources

As recalled previously, high energy neutrinos are an uncharted territory. We discuss supernova remnants (SNR) as sources of neutrinos above the TeV in some more detail, and begin by recalling the main theoretical reason why these are considered as possible sources of neutrinos. A crucial part of the argument is the identification of SNR as CR sources. Indeed, the Milky Way radiates CR at a rate $\mathcal{L}_{\text{CR}} = V_{\text{CR}} \rho_{\text{CR}} / \tau_{\text{CR}} \sim 10^{41}$ erg/s (where the volume, the lifetime and the average density of CR are all rather uncertain) which can be compensated if any 30 year a new supernova remnant (of any type) is able to convert 10% of its kinetic energy (of the order of 1 foe = 10^{51} erg) into CR. Furthermore, a theoretical mechanism called ‘diffusive shock acceleration’ supports this argument, There is little doubt that a maximum energy $E_{\text{max}} = 0.1$ PeV can be achieved, and there are active discussions on whether it is possible to reach energies comparable to the energy of the knee (around 3 PeV).

Let us come to the present observations and expectations. The observation of the Southern sky with gamma rays at the TeV and above revealed two bright SNR, RX J1713.7-3946 and RX J0852.0-4622, and the observed spectra below 10 TeV look to be power laws with hard spectral indices $\Gamma \sim 2$. Since these sources are expected to be transparent to γ radiation, a tentative identification of these γ as ‘hadronic’ (i.e. coming from CR interactions) implies that we should expect neutrinos (up-going muons) in Northern hemisphere. Extrapolating the γ spectra till several hundred TeV suggests signals of about $10 \div 15$ induced-muon events per km^2 per year. However, this should be reduced by about 50% if the neutrino spectrum drops below the assumed power law around 10 TeV (which would be consistent with the present expectations on E_{max} , since the expected neutrino energy is 1/20 the energy of primary CR) and by a similar factor to account for finite detection efficiency. Thus, we are lead to expect that we need a rather effective rejection of the background and a large exposure in order to see these sources.

These considerations are not meant to be in any manner conclusive, but rather to illustrate the possible relevance of theoretical expectations and (in the case of SNR) of γ ray observations. Indeed, there is no doubt that TeV neutrino astronomy is in the phase of discovery and we should be ready to surprises, but this is just the stage when it is important to prepare and refine the theoretical tools. (Furthermore, we should not forget that more surprises and discoveries could come from other observations that are now in progress).

⁹All reactions of practical use do not allow to measure the energy of individual neutral current events, but only their total number and time distribution. A possible exception is $\nu p \rightarrow \nu p$ [128], that could be studied by scintillators with very low threshold like Borexino [54].

Chapter 12

Understanding neutrino masses

Most of the fundamental parameters known so far are fermion masses, or in other words *flavor parameters*. We measure quark, lepton and neutrino masses and mixings with the hope of understanding (sooner or later) why they are what they are. This is the flavour problem.

Let us describe the content of this section. We begin (section 12.1) with a discussion of the present obstructions and difficulties towards a theory of flavor. In sections 12.2 we describe the two extremal patterns that could emerge from the observed ν masses and mixings. Section 12.3 offers a brief review of existing approaches to the ‘flavor problem’, focussing on the concrete results relevant for neutrinos (we show how a typical flavour model looks like, and discuss how flavour models can be tested). The well-motivated approaches based on grand unification are discussed in section 12.3.2 and their successes, strictures and failures are outlined. Finally, we review in section 12.4.1 tentative predictions for θ_{13} , mostly based on the assumptions that neutrino mass matrices have texture zeroes.

12.1 The problem of the flavour problem

Here, we try to diagnosis the difficulties that are blocking our theoretical and experimental attempts of understanding flavour. On the theoretical side, understanding the values of the fundamental parameters in QFT is particularly difficult because they receive ultraviolet divergent quantum correction. Without knowing which high-energy theory provides the physical cut-off (possibly related to quantum gravity), the practicable way to get some control over the parameters is recognizing possible symmetries that relate different parameters. Examples of very concrete progress achieved thanks to this approach are well known:

- Around 1970, thanks to **gauge invariance**, theorists have been very useful in understanding experiments and in establishing the SM along the following road:

$$\text{photon} \rightarrow \text{gauge invariance} \rightarrow \text{gluons, } Z, W.$$

The most generic gauge invariant renormalizable Lagrangian that can be written with the SM fields contains 18 apparently fundamental parameters; 13 of them describe flavour.¹

¹The cosmological constant and the QCD θ parameter are two extra parameters, not included in the above counting. The first parameter is apparently crucial to understand the expansion of the Universe. The QCD θ parameter gives rise to unobserved CP-violating effects: present bounds on the neutron EDM imply $\theta \lesssim 10^{-9}$, while one would naively expect $\theta \sim 1$. Although this issue might have some connection with the flavour problem, we will not consider it here.

Further success along this line could be obtained by assuming that the SM is the low-energy limit of a ‘unification’ theory, with gauge group $SU(5)$ or $SO(10)$ broken at large energy $M_{\text{GUT}} \sim 10^{16} \text{ GeV}$.

- **Supersymmetry** could become another predictive symmetry. Although all searches for supersymmetric signals gave so far null results, weak-scale supersymmetry remains one possible interpretation to the Higgs mass hierarchy problem.² (It should be added for fairness that supersymmetry introduces new flavor problems).

However, lepton and quark masses and mixings show no clear pattern that indicates the eventual symmetry behind them, and in the SM are simply described by a list of 13 mysterious numbers.

It is hard to obtain predictions in the flavour sector, because flavour extensions of the SM often involve many more unknown parameters than the SM. Neglecting neutrino masses, the lepton kinetic terms and Yukawa couplings are described by three 3×3 matrices which contain 36 real parameters; but only 3 of them are measurable at low energy: m_e , m_μ and m_τ . Similarly SM quarks are described by 63 real parameter; but only 10 of them are measurable at low energy (6 masses, 3 mixings, 1 CP-violating phase). Since $3 \ll 36$ and $10 \ll 63$, only very restrictive symmetries or assumptions give testable predictions.

By postulating properly broken flavour symmetries (possibly in a context where quarks and leptons are unified) one can ‘explain’ the hierarchy $m_e \ll m_\mu \ll m_\tau$ and the similar one in quarks, in terms of few small symmetry-breaking parameter and dozens of unknown order-one parameters. See [129] for the first attempts. Unfortunately it is possible to achieve the same in many different ways, and these efforts resulted in thousands of papers (one every few days since many years) with no observable consequence, up to rare exceptions.

This situation is reminiscent of the outcome of another possible approach: although quantum gravity likely gives effects too small to be observed, it has been theoretically investigated hoping that it leads to a unique ‘theory of everything’, or at least to a predictive theory. String/ M theory seemed a promising attempt, that apparently leads to one simple theory in 11 dimensions. Unfortunately, SM physics is neither simple nor 11 dimensional, and there are so many different ways of getting rid of the extra dimensions (e.g. there are 5 string models in 10 dimensions) that after reaching 4 dimensions one has $10^{O(500)}$ string models and predictivity is lost. Indeed in these string models the complicated physics that we see at low energy arises mostly thanks to a complicated higher dimensional geography.

The pattern of SM fundamental parameters suggests one deeper reason behind the apparently uselessly vast ‘landscape’ of flavour models and of string models. The SM allows the existence of many stable nuclei, but this richness arises because (relevant combinations of) α_{em} , Λ_{QCD} and of the electron, up- and down-quark masses happen to have special values. Different values would not lead to the complex chemistry that allows our existence. This and analogous considerations concerning the cosmological constant lead to speculate about *anthropic selection* [130]: some apparently fundamental parameters could (in some way) take many different values, and we happen to observe one atypical set of values that allows for the existence of observers. Like geography, flavour would not be a fundamental issue and the key point that we should understand

²Weak-scale supersymmetry is also motivated by gauge unification. Non super-symmetric $SU(5)$ makes one wrong prediction for the SM gauge couplings. A successful prediction is obtained assuming MSSM supersymmetric particles at the weak-scale. The probability that this agreement happens accidentally is $\sim \%$ according to ‘reasonable’ estimates of theoretical uncertainties.

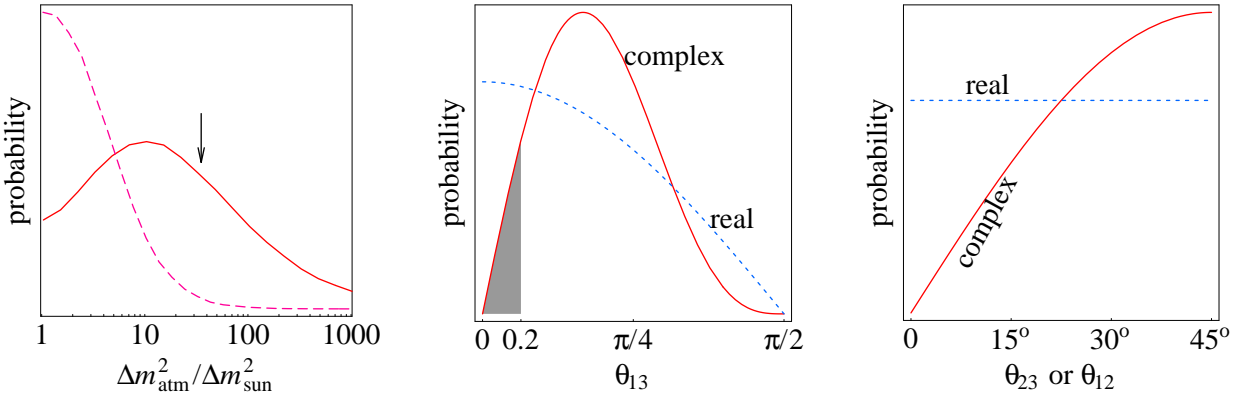


Figure 12.1: **Oscillation parameters expected from a structureless neutrino mass matrix.** Fig. 12.1a: see-saw (solid line), non see-saw (dashed) with complex couplings. Fig. 12.1b,c: complex couplings (solid), real couplings (dashed).

would be: in which way fundamental parameters can take different set of values? The simplest way consists in writing models where the potential has many different local minima, by e.g. employing many heavy scalar fields (that in string models parameterize the unknown higher-dimensional geography). Other ways (e.g. employing light scalars with position-dependent vevs) might lead to observable signals.

Maybe these speculations will lead to results that will be summarized in future reviews. We here review standard approaches, focussing on simple models of neutrino masses and mixings. Since neutrinos masses (as well as quark and lepton masses of second and third generation) do not seem to be too much anthropically relevant, one can hope that they reflect some property of the high energy theory.

12.2 In the search for a pattern

Before writing flavour models that can explain the pattern of fermion masses, one must qualitatively interpret how this pattern looks like. Charged leptons and quarks clearly exhibit large mass hierarchies and small mixing angles. Neutrinos show a qualitatively different pattern, but the situation is not yet clear. In this section we present two plausible extremal interpretations; the true pattern probably lies somewhere in between.

12.2.1 A structure-less mass matrix?

The obvious starting question is: is there any structure in the neutrino mass matrix suggested by experiments? A neutrino mass matrix with generic $\mathcal{O}(0.03)$ eV entries would give all mixing angles of $\mathcal{O}(1)$ and all $\Delta m^2 \sim 10^{-3}$ eV². The experimental signals typical of this minimal case were studied in [131], and have been not observed. As a result, experiments now require relatively small values of

$$\theta_{13} < \theta_{13\max} \approx 0.15 \quad \text{and of} \quad R = \Delta m_{\text{sun}}^2 / \Delta m_{\text{atm}}^2 = (0.030 \pm 0.005). \quad (12.1)$$

How likely these two small numbers are accidentally produced by a structure-less (or ‘anarchical’) mass matrix?

Some authors tried to estimate such probability in two different ways [132]: i) by generating many random matrices and counting how frequently they satisfy the bounds of eq. (12.1); ii) by computing the analogous frequency as function of some parameter ϵ (such that $\epsilon \ll 1$ generates the small R and θ_{13} measured by experiments) and testing if a small ϵ works better than $\epsilon = 1$. In Bayesian language (see appendix B) these are two MonteCarlo procedures that compute two probabilities; in both cases $\mathcal{O}(1)$ factors depend on the assumed arbitrary prior. They are different because answer to two different questions: i) has the meaning of a gof test and ii) tests at which $CL \epsilon = 1$ is in the best-fit range of ϵ . As usual (see appendix B) ii) is more reliable — less arbitrary factors affect a relative probability than an absolute probability. This kind of studies suggests that the observed pattern of neutrino masses and mixings contains some kind of structure with $\sim 90\%$ probability: a structure-less mass matrix is disfavored but not excluded. More precisely, assuming that the modulus of each matrix element has flat probability in some interval, in fig. 12.1 we show the probability distribution of R , of θ_{13} and of $\theta_{12,23}$. We can understand analytically why the probability scales in a non-trivial way with R and with θ_{13} .

- *Scaling with R .* As expected, anarchical neutrino mass matrices give a small R with small probability $p \propto R^{1/2}$ (solid line of fig. 12.1a). A larger probability $p \propto R^{1/4}$ (dashed line) is obtained in see-saw models, i.e. by assuming that neutrino masses are mediated by virtual exchange of heavy right-handed neutrinos with anarchical Yukawa couplings and masses.
- *Scaling with θ_{13} .* It is reasonable to assume that the probability distribution of the mixing angles is given by the Haar measure of the $U(3)$ flavour group (or $SO(3)$ if one assumes that CP is conserved)³ [132]:

$$dp \propto \begin{cases} d \cos^4 \theta_{13} d \sin^2 \theta_{12} d \sin^2 \theta_{23} d\phi & \text{complex couplings,} \\ d \sin \theta_{13} d\theta_{12} d\theta_{23} & \text{real couplings.} \end{cases} \quad (12.2)$$

Assuming complex couplings, small values of θ_{13} have a non trivially small probability: $p(\theta_{13} < \theta_{13\max}) = 1 - \cos^4 \theta_{13\max} \simeq 2\theta_{13\max}^2$. The quadratic dependence on $\theta_{13\max}$ is related to the fact that the CP-phase ϕ becomes non physical at $\theta_{13} = 0$. The probability that a random θ_{13} is accidentally compatible with the CHOOZ upper bound is $\int e^{-\chi^2(\theta_{13})/2} d \cos^4 \theta_{13} = 5\%$. Assuming real couplings gives a weaker linear dependence of p on $\theta_{13\max}$. These results agree with the numerical scan of fig. 12.1b.

Anarchy suggests that θ_{13} should be not much below its present experimental upper bound. If this is the case, we will remain in an ambiguous situation: measured masses and mixings disfavor anarchy but do not clearly indicate the presence of some structure. From a theoretical point of view, anarchy trivially arises from flavour models where lepton doublets are not charged under any flavour symmetry. Within the SM and within $SU(5)$ unified models, this is consistent with the non-anarchical pattern clearly present in charged lepton and quark masses and mixing. For

³Since this result might seem obscure, it is useful to remind that analogous non trivial trigonometric factors arise in a well known case, where their geometrical origin is more transparent. Analyses of solar and atmospheric neutrino data use the well known fact that a isotropic background is flat in $d\Omega = d \cos \vartheta_{\text{zenith}} d\varphi$, where $\vartheta_{\text{zenith}}$ and φ are the usual polar coordinates. The Haar measure analogously describes the ‘solid angle’ on a (complex) hyper-sphere.

example, a $U(1)$ flavour symmetry with charges $q_{5_i} = \{0, 0, 0\}$ and $q_{10_i} = \{2, 1, 0\}$ gives

$$m_\nu \propto \mathcal{O} \begin{pmatrix} 1 & 1 & 1 \\ 1 & 1 & 1 \\ 1 & 1 & 1 \end{pmatrix}, \quad m_E \sim m_D^T \propto \mathcal{O} \begin{pmatrix} \epsilon^2 & \epsilon^2 & \epsilon^2 \\ \epsilon & \epsilon & \epsilon \\ 1 & 1 & 1 \end{pmatrix}, \quad m_U \propto \mathcal{O} \begin{pmatrix} \epsilon^4 & \epsilon^3 & \epsilon^2 \\ \epsilon^3 & \epsilon^2 & \epsilon \\ \epsilon^2 & \epsilon & 1 \end{pmatrix}$$

which reproduces reasonably well the order of magnitude of all observed masses and mixings. If this is the case, long-baseline and $0\nu 2\beta$ experiments will easily measure more neutrino parameters, but we will not understand what they mean, until models will be able of predicting $\mathcal{O}(1)$ factors.

12.2.1.1 Mass hierarchy between largely mixed states?

We have seen that neutrino masses and mixings show two potentially small numbers (θ_{13} and $R = \Delta m_{\text{sun}}^2 / \Delta m_{\text{atm}}^2$) that one might want to explain by inventing appropriate flavour models. While a small θ_{13} can be explained in many different ways, a small R (together with $\theta_{\text{atm}} \sim 1$) is a very characteristic feature. If not due to an accident, it is a strong indication because, while it is easy to write matrices that give hierarchical masses with small mixing, or large mixing without mass hierarchies, only few Majorana neutrino mass matrices give both. Indeed a large atmospheric mixing angle between the *most splitted* neutrino states ($\Delta m_{\text{atm}}^2 \gg \Delta m_{\text{sun}}^2$) is naturally produced by two plausible peculiar structures for the Majorana neutrino mass matrix \mathbf{m}_ν . We write them in the limit $\Delta m_{\text{sun}}^2 = 0$ and $\theta_{13} = 0$ and working in the mass eigenstate basis of charged leptons.

(h) If $\Delta m_{\text{atm}}^2 > 0$ (i.e. neutrinos have a **hierarchical** spectrum) one needs the rank one matrix [133]

$$\mathbf{m}_\nu(\text{h}) \propto \begin{pmatrix} 0 & 0 & 0 \\ 0 & s^2 & sc \\ 0 & sc & c^2 \end{pmatrix}. \quad (12.3)$$

The see-saw mechanism can naturally generate such a rank 1 mass matrix: if only one right-handed neutrino exists, it gives mass to only one left-handed neutrino, leaving the other two massless. Therefore the matrix (h) is obtained when one right-handed neutrino, coupled mostly to L_μ and L_τ ,

$$\lambda N(sL_\mu + cL_\tau)H_u + \frac{M}{2}N^2, \quad (12.4)$$

gives the dominant contribution to the light neutrino masses.

(i) If $\Delta m_{\text{atm}}^2 < 0$ (i.e. neutrinos have an **inverted** spectrum) one needs to justify why two of them are almost degenerate. A rank two pseudo-Dirac matrix does the job [134]:

$$\mathbf{m}_\nu(\text{i}) \propto \begin{pmatrix} 0 & s & c \\ s & 0 & 0 \\ c & 0 & 0 \end{pmatrix}. \quad (12.5)$$

The eigenvalues of this matrix are proportional to $0, 1, -1$: massive degenerate neutrinos have opposite CP-parity. Other choices of the relative phase between the two massive state do not suggest to a ‘natural’ form for \mathbf{m}_ν .

The matrix (i) can be justified by imposing a $L_e - L_\mu - L_\tau$ $U(1)$ flavour symmetry, that in the unbroken limit automatically implies $\Delta m_{\text{sun}}^2 = 0$, $\theta_{13} = 0$ and $\theta_{12} = \pi/4$. This last prediction

U(1) charges	no structure	small θ_{13}	normal hierarchy	inverted hierarchy
$q_{Q_i} = q_{U_i} = q_{E_i}$	3, 2, 0	2, 1, 0	3, 2, 0	3, 2, 0
$q_{L_i} = q_{D_i}$	0, 0, 0	1, 0, 0	2, 0, 0	1, -1, -1
q_{N_i}	0, 0, 0	2, 1, 0	1, -1, 0	-1, 1, 0
q_{H_u}, q_{H_d}	0, 0	0, 0	0, 0	0, 0
$R = \Delta m_{\text{sun}}^2 / \Delta m_{\text{atm}}^2$	$\mathcal{O}(1)$	$\mathcal{O}(1)$	$\mathcal{O}(\lambda^4)$	$\mathcal{O}(\lambda^2)$
θ_{13}	$\mathcal{O}(1)$	$\mathcal{O}(\lambda)$	$\mathcal{O}(\lambda^2)$	$\mathcal{O}(1)$
θ_{12}	$\mathcal{O}(1)$	$\mathcal{O}(\lambda)$	$\mathcal{O}(1)$	$\mathcal{O}(1)$
θ_{23}	$\mathcal{O}(1)$	$\mathcal{O}(1)$	$\mathcal{O}(1)$	$\mathcal{O}(1)$

Table 12.1: *Sample of SU(5)-unified see-saw models with realistic U(1) flavour symmetries. We here aim at simplicity, rather than at fully reproducing quark and lepton masses and mixings up to $\mathcal{O}(1)$ uncertainties. Although in the second model θ_{12} is typically small, the same accident that gives $R \ll 1$ can also give $\theta_{12} \sim 1$.*

is incompatible with data, that demand a large but not maximal $\theta_{12}, \theta_{12} + \theta_{13} < \pi/4$. Although can find specific sources of breaking of $L_e - L_\mu - L_\tau$ that give a large correction only to $\theta_{12} - \pi/4$ [134], models for inverted hierarchy (that typically use $L_e - L_\mu - L_\tau$ as ingredient) seem now less appealing. One can assume that $\mathbf{m}_\nu(i)$ holds in a basis where the charged lepton mass matrix has non diagonal elements, that provide extra sources for mixing angles and reduce predictivity.

In the see-saw context $\mathbf{m}_\nu(i)$ can be generated by exchanging a pseudo-Dirac couple of right-handed neutrinos, N and N' . By appropriately extending the $L_e - L_\mu - L_\tau$ symmetry to N and N' one can justify the following see-saw model:

$$\lambda N(sL_\mu + cL_\tau)H_U + \lambda' N'L_eH_U + MNN'. \quad (12.6)$$

(d) Neutrinos could also have a **quasi-degenerate** spectrum, but we know no simple way of justifying why this should be the case. Various constructions have been discussed, mostly based on an SO(3) flavor symmetry.

12.3 Flavor symmetries

In this section we describe how typical flavour models look like, and discuss in section 12.4 the difficulties of the experimental approach to flavour. (We warn the reader that the issues here discussed are often simply ignored).

12.3.1 Writing flavour models

The SM Lagrangian has a $U(3)^5$ flavour symmetry (rotations of the E, L, U, D, Q families) explicitly broken by the Yukawa couplings. This structure implies a peculiar strong suppression of CP-violating effects in K mixing and decay, a very strong suppression of e, n electric dipoles, and no flavour-violating processes like $\mu \rightarrow e\gamma$ in leptons. Present data agree with SM predictions, disfavoring different flavour structures (e.g. things would be different if two Higgs doublets would give comparable contributions to fermion masses).

One can try to understand flavour by assuming that some subgroup of $U(3)^5$ is an exact flavour symmetry, spontaneously broken by the vev of some scalar ϕ named ‘flavon’. The flavour symmetry could be global, or gauged, or some theoretically more fashionable variant. All them work in almost the same way.

The minimal choice of the flavour symmetry is an $U(1)_F$ subgroup of $U(3)^5$. One proceeds by assigning arbitrary $U(1)_F$ charges q_F to the various fields F . Without loss of generality, we can assume that the flavon ϕ has $U(1)_F$ charge $+1$ (so that ϕ^* has charge -1). We assume that ϕ is neutral under the SM gauge group G_{SM} , since we want to break G_{SM} only by an ordinary Higgs field.⁴

In the non-renormalizable effective theory valid below some cut-off Λ describing the SM fields plus the flavon ϕ , an operator \mathcal{O} containing SM fields with total $U(1)_F$ charge $q_{\mathcal{O}}$ (for example $\mathcal{O} = UQH$ has $q_{UQH} = q_U + q_Q + q_H$) typically appears with coefficient of order $|\phi/\Lambda|^{q_{\mathcal{O}}}$. All small numbers are expected to arise from the smallness of $\lambda \equiv \phi/\Lambda$. One can write explicit renormalizable models containing many new particles with mass $\sim \Lambda$ that mediate all the couplings [21]. Since many models exist, each with many free parameters, it is often convenient to focus of how the flavour symmetry restricts the low-energy effective theory. Of course, one can invent specific examples of a full theory that gives atypical outcomes (e.g. some operator could be absent).

Restricting to the sub-case of integer charges, the Yukawa couplings are expected to be of order

$$\lambda_U^{ij} \sim \lambda^{|q_{U_i} + q_{Q_j} + q_H|}, \quad \lambda_D^{ij} \sim \lambda^{|q_{D_i} + q_{Q_j} - q_H|}, \quad \lambda_E^{ij} \sim \lambda^{|q_{E_i} + q_{L_j} - q_H|}. \quad (12.7)$$

The rules of the game become a bit different in **supersymmetric** extensions of the SM: the flavon ϕ has a fermionic partner $\tilde{\phi}$: consequently it is no longer possible to generate a flavon of charge -1 by complex conjugation. The precise statement is: the superpotential \mathcal{W} is a holomorphic function of the superfields. When building a supersymmetric extension of the SM, due to this fact one introduces two Higgs doublets with opposite hypercharge: H_U coupled to up-quarks, and H_D , coupled to down-quarks and leptons. The MSSM superpotential then contains all needed couplings

$$\mathcal{W} = \lambda_E E L H_D + \lambda_D D Q H_D + \lambda_U U Q H_U + \mu H_U H_D.$$

One can similarly introduce two flavons with opposite flavour charge, φ_+ and φ_- . In general they have different vev. Writing and minimizing explicit supersymmetric potentials, one can see that often one of the two flavons gets negligible vev. This means that (12.7) has to be modified allowing for $\lambda_+ \neq \lambda_-$: the sign of $q_{\mathcal{O}}$ becomes important.

A $U(1)$ example One can easily invent assignments of flavour charges under an $U(1)_F$ flavour group that qualitatively reproduce all masses and mixings of charged leptons and quarks. A typical choice (compatible with $SU(5)$ unification) is

$$q_{Q_i} = q_{U_i} = q_{E_i} = \{4, 2, 0\}, \quad q_{L_i} = q_{D_i} = \{4, 3, 2\}, \quad q_H = 0, \quad \lambda \sim 0.2 \quad (12.8)$$

and gives

$$|\lambda_U| \sim \mathcal{O} \begin{pmatrix} \lambda^8 & \lambda^6 & \lambda^4 \\ \lambda^6 & \lambda^4 & \lambda^2 \\ \lambda^4 & \lambda^2 & 1 \end{pmatrix}, \quad |\lambda_D^T| \sim |\lambda_E| \sim \mathcal{O} \begin{pmatrix} \lambda^8 & \lambda^7 & \lambda^6 \\ \lambda^6 & \lambda^5 & \lambda^4 \\ \lambda^4 & \lambda^3 & \lambda^2 \end{pmatrix}$$

⁴One could instead employ some discrete subgroup of $U(1)_F$, or some larger non-abelian group, such as an $U(2)$. Other approaches do not employ a flavour group: for example, assuming that the SM fermions are localized in different places in hypothetical extra dimensions, small fermion masses could be due to a small overlap between fermion wave-functions [135].

in order-of-magnitude agreement with measured values. Table 12.1 exemplifies U(1) flavour models that roughly reproduce neutrino patterns suggested by present data.

A U(2) example By considering non-abelian flavor symmetries the transformation properties of fields F become less arbitrary, but non-abelian groups need a more complicated pattern of symmetry breaking. We give an example of a predictive model. By postulating a U(2) flavour symmetry [136] acting on the first two generations, the only allowed Yukawa couplings are λ^{33} and $|\lambda^{21}| = |\lambda^{12}|$. U(2) can be spontaneously broken in such a way that Yukawa matrices get the following form:

$$\left| \frac{\lambda_D}{\lambda_D^{33}} \right| = \begin{pmatrix} 0 & \epsilon'_D & 0 \\ \epsilon'_D & \epsilon_D & \sim \epsilon_D \\ 0 & \sim \epsilon_D & 1 \end{pmatrix}, \quad \left| \frac{\lambda_U}{\lambda_U^{33}} \right| = \begin{pmatrix} 0 & \epsilon'_U & 0 \\ \epsilon'_U & \epsilon_U & \sim \epsilon_U \\ 0 & \sim \epsilon_U & 1 \end{pmatrix}. \quad (12.9)$$

The texture (12.9) implies three *predictions* in the quark sector. At dominant order in small ratios between quark masses they are

$$\left| \frac{V_{ub}}{V_{cb}} \right| = \sqrt{\frac{m_u}{m_c}}, \quad \left| \frac{V_{td}}{V_{ts}} \right| = \sqrt{\frac{m_d}{m_s}}, \quad |V_{us}| = \left| \sqrt{\frac{m_d}{m_s}} + e^{i\phi} \sqrt{\frac{m_u}{m_c}} \right|. \quad (12.10)$$

where ϕ is the CKM phase. The first prediction in (12.10) is no longer compatible with present data [136]. By relaxing some assumptions one can easily avoid making predictions.

By adding right-handed neutrinos with GUT-scale masses, one can extend this kind of flavour models to neutrinos. It is useful to start recalling that typical expectations for neutrino masses made before experiments have been contradicted by data:

- **The expectation.** As suggested by quark-lepton unification, neutrino masses arise from the see-saw mechanism, with neutrino Yukawa couplings comparable to the other Yukawa couplings. Therefore neutrinos have small mixing angles. In analogy to (12.10) one expects $\theta_{e\mu} \sim (m_e/m_\mu)^{1/2}$: the deficit of solar ν_e can be produced by a small mixing angle (SMA) resonantly enhanced by MSW effects. See-saw models naturally give small hierarchical neutrino masses roughly proportional to squared quark (or lepton) masses: $m_{\nu_\ell} \propto m_\ell^2$. Since $m_{\nu_\mu}^2 = \Delta m_{\text{sun}}^2$, τ -neutrinos have eV masses, providing the hot dark matter suggested by cosmology. Kamiokande was designed to look for proton decay, as predicted by GUT ('nde' = nucleon decay experiment at the Kamioka mine).
- **The data.** Facts contradicted speculations. NOMAD and CHORUS (built for looking for $\nu_\mu \leftrightarrow \nu_\tau$ oscillations with large Δm^2 and small mixing angle) found nothing, and cosmology now needs cold dark matter. (Super)Kamiokande discovered atmospheric $\nu_\mu \leftrightarrow \nu_\tau$ oscillations with large mixing angle and small Δm^2 ('ande' = atmospheric neutrino detector experiment). Solar experiments established large mixing angle oscillations.

12.3.2 Unified flavour models and neutrino masses

Gauge-unified extensions of the SM are considered more appealing and potentially more predictive also in the flavour sector. One can say that the indication that neutrinos are massive is one of the successes of SO(10) [137] and other GUTs. In certain models, the scale of right handed neutrinos

is connected to the unification scale, and the texture of neutrino masses to the texture of charged fermion masses. Right-handed neutrinos (or scalar triplets) permit to implement leptogenesis (section 10.3) and, in supersymmetric GUT, leptonic flavor transition such as $\mu \rightarrow e\gamma$ can be detectably large (section 13.5).

We concentrate the discussion on a few selected points: in section 12.3.3 we outline features the SM that permit to appreciate GUT better. SU(5) models are discussed in section 12.3.4. In section 12.3.5 we concentrate on SO(10): we describe the situation of a simple model and offer a brief overview of other models.

12.3.3 SM and GUTs: common aspects and differences

It is natural to consider the SM as the prototype gauge theory from where we can start to give a meaning to fermion masses. The features of the SM that are relevant to the present discussion are:

1. In the SM there is only one massive parameter, the scale of $SU(2)_L \otimes U(1)_Y$ symmetry breaking; the masses of all particles (gauge bosons, higgs particle, quarks and leptons) are proportional to this unique scale.

This first property is lost when the SM is extended adding right-handed neutrinos (or the other non-chiral particles, that can mediate tree-level neutrino masses). While the same situation holds in SU(5)-unified extensions of the SM, in other cases the high scale behind neutrino masses is related to a gauge scale. For example, the mass of right-handed neutrinos breaks the $U(1)_{B-L}$ and/or $SU(2)_R$ symmetries contained in Left-Right, Pati-Salam or SO(10) models:

$$SU(3)_c \otimes SU(2)_L \otimes SU(2)_R \otimes U(1)_{B-L} \subset SU(4)_c \otimes SU(2)_L \otimes SU(2)_R \subset SO(10).$$

In these models all quark, lepton and neutrino masses can be controlled by gauge-symmetry breaking scales.

2. The SM contains are 3 replicæ of the 5 types of fermions Q, U, D, L, E that form a family. The kinetic terms of the fermions have a global symmetry $U(3)^5$, called the *flavor group*.

The structure of the flavour group simplifies in unified models. For instance, the existence of right handed neutrino in a family becomes a necessity in SO(10) where all fermions of a family (including ν_R) fit in the 16-dimensional spinorial representation. The flavor group of SO(10) is just $U(3)$.

3. In the SM fermion masses break explicitly the $U(3)^5$ flavour group, but some $U(1)$ subgroups remain unbroken: lepton flavour L_e, L_μ, L_τ and $B - L$.

Both neutrino masses and gauge unification break lepton flavour.

12.3.4 SU(5) and fermion masses

In SU(5) models, the SM fermions are unified in $\bar{5}_i = D_i \oplus L_i$ and $10_i = Q_i \oplus U_i \oplus E_i$ SU(5) multiplets, while right-handed neutrinos remain gauge singlets. Therefore L and D have the same $U(1)_F$ charge, at least in simpler models; in general, $U(1)_F$ charges can be shifted by SU(5)-breaking effects. Extra assumptions are needed to get results. E.g. assuming that Higgs doublets

lie in a 5 representation, in the limit of unbroken $SU(5)$ one gets $\lambda_D = \lambda_E^T$, which roughly resembles the observed pattern. Among the consequent predictions for the Yukawa couplings renormalized at the GUT scale

$$\lambda_\tau = \lambda_b, \quad \lambda_\mu = \lambda_s, \quad \lambda_e = \lambda_d$$

the first one can be acceptable in supersymmetric $SU(5)$, while the lighter fermion masses rather satisfy $\lambda_\mu \approx 3\lambda_s$ and $\lambda_e \approx \lambda_d/3$. These two 3 factors can be nicely justified in non minimal $SU(5)$ models [138] built in such a way that (i) $\lambda_D^{11} = \lambda_E^{11} = 0$; (ii) $SU(5)$ -breaking effects generate $\lambda_D^{22} = -N_C \lambda_E^{22}$ (where $N_C = 3$ is the number of colors). The 12 element of λ_D gives a contribution $\sqrt{m_d/m_s}$ to the Cabibbo angle, which happens to be close to the measured value. We can therefore expect that the corresponding 12 element in λ_E is diagonalized by a 12 rotation with angle

$$\Delta\theta_{12} = \sqrt{m_e/m_\mu}. \quad (12.11)$$

Combined with the (unknown) matrix that diagonalizes the neutrino mass matrix, this often results into a contribution to the physical θ_{13} mixing angle.

Let us now discuss the compatibility of neutrino masses and mixings with $SU(5)$ unification. It is difficult to invent flavour models compatible with $SU(5)$, if one thinks that a flavour model should explain the smallness of θ_{13} , $R = \Delta m_{\text{sun}}^2 / \Delta m_{\text{atm}}^2$. The reason is that R, θ_{13} are much larger than analogous mass ratios and mixing angles in quarks and leptons. Table 12.1 shows a few examples. If instead one thinks that the smallness of θ_{13} and R does not require a dedicated interpretation and accepts a ‘anarchical’ neutrino mass matrix, this is immediately married with $SU(5)$: one just assumes that the flavour symmetry acts equally on $\bar{5}_{1,2,3}$ and assigns appropriate flavour charges to $10_{1,2,3}$. The first column of table 12.1 shows one example. A qualitative pattern emerges: no mass hierarchy among neutrinos and a strong mass hierarchy among up-quarks implies (in agreement with data) an intermediate mass hierarchy among down-quarks and among charged leptons and relatively small quark mixing angles.

In conclusion, $SU(5)$ looks easily compatible with neutrino data but does not suggest precise predictions. Roughly the opposite happens in the $SO(10)$ case.

12.3.5 $SO(10)$ and fermion masses

Right-handed neutrinos become massive after that $SO(10)$ (and in particular its subgroups $U(1)_{B-L}$ and $SU(2)_R$) break down to the SM gauge group. The right-handed neutrino mass operator has the form $16 \ 16 \ \langle \overline{126} \rangle$, where the $\overline{126}$ could be either an elementary Higgs or a composite field (e.g. the product of two $\overline{16}$).

The simplest $SO(10)$ models, with the Higgs entirely contained in the minimal 10 representation, predict $\lambda_N = \lambda_E = \lambda_D = \lambda_U$ and symmetric Yukawa matrices, in qualitative contrast with the observed data: up-quarks exhibit a stronger mass hierarchy than leptons and down-quarks, neutrinos have large mixing angles while quarks have small mixings.

This unwanted prediction can be avoided by assuming that Yukawas arise from effective higher dimensional operators containing $SO(10)$ -breaking vevs [139], but going in this direction does not make full use of $SO(10)$. A $SU(3)$ flavour model based on rank-1 matrices has been proposed and studied in detail in the last paper of [139]. These models tend to give relatively small values of θ_{13} .

An alternative road, that exploits the $SO(10)$ symmetry, consists in assigning the Higgs doublet to non-minimal $SO(10)$ representations [140]: 10 and $\overline{126}$. One often prefers to build a

supersymmetric model, such that also a 126 is needed.⁵ Restricting to renormalizable couplings only the superpotential contains two Yukawa matrices

$$\mathcal{W} = \lambda_{ij}^{10} 16_i 16_j 10 + \lambda_{ij}^{126} 16_i 16_j \overline{126}$$

that generate the quark and lepton Yukawa matrices as

$$\begin{aligned} \lambda_U &= \lambda^{10} \cos \alpha_U + \lambda^{126} \sin \alpha_U & \lambda_D &= \lambda^{10} \cos \alpha_D + \lambda^{126} \sin \alpha_D \\ \lambda_E &= \lambda^{10} \cos \alpha_D - 3\lambda^{126} \sin \alpha_D & \lambda_N &= \lambda^{10} \cos \alpha_U - 3\lambda^{126} \sin \alpha_U \end{aligned} \quad (12.12)$$

where α_D, α_U are complex angles that parametrize how the light Higgs is contained in the 10, 126 representations. Right-handed neutrino masses are proportional to λ_{ij}^{126} and to $\langle \overline{126} \rangle$, such that all flavour matrixes are predicted in terms of two flavour matrices and a few other parameters.

The couplings to the 10 lead to the adequate expectation of b/τ unification, the couplings to the $\overline{126}$ permit to give large Majorana neutrino masses to the right handed neutrinos and to correct for the strict $\lambda_D = \lambda_E^T$ equality for all 3 families. This model offers the hope to reproduce the observed fermion masses and mixing. All existing fits based on such a model agree to predict that θ_{13} should be rather large. However, at this stage, the model is not complete, since the $\overline{126}$ Higgs can spontaneously break SO(10) only down to SU(5). Adding just another higgs field (the 210) allows to break SO(10) to the SM gauge group and to produce the desired mixed composition of the MSSM higgs fields (i.e. $\alpha_{U,D} \neq 0$).⁶ The existing fits of fermion masses have been performed allowing complete freedom in the choice of higgs composition and of the neutrino mass scale. However, it seems that this freedom does not exist in the full model with the 210. More specifically, it seems possible to have the neutrinos with masses larger than v^2/M_{GUT} only in certain points of the parameter space where: 1) charged fermion masses cannot be reproduced; 2) supersymmetric unification of gauge couplings fails. Even if deeper investigations will confirm that this is real conclusion, this model remains an example of how SO(10) allows to obtain predictions.

12.4 Testing flavour models

The true problem is how to test speculations about flavour symmetries. There are two possibilities:

- 1) **Direct tests:** the model predicts some new physical process. However flavour data agree with SM predictions, pushing the flavour scale Λ to so large energies that direct tests seem not feasible. In fact, $U(1)_F$ flavour symmetries allow operators like

$$\frac{c_1}{\Lambda^2} |D_1 Q_1|^2 + \frac{c_2}{\Lambda^2} |D_2 Q_2|^2$$

⁵The $\overline{126}$ has other advantages. Its vev directly controls right-handed neutrino masses, and preserves the matter parity, often introduced in supersymmetric models to avoid unseen effects.

⁶This concludes the definition of the model, that has been termed ‘minimal’ due to the small number of higgs fields and of free supersymmetric parameters (26). The less appealing points of this model are the fact that non-renormalizable terms are ignored; the scale where non-perturbativity is lost is rather close to the grand unification scale; simplicity (and simple string models) prefer smaller SO(10) representations; no special mechanism explains the lightness of the higgs doublet (apart from a suitable fine-tuning of parameters); some fine-tunings among λ^{10} and λ^{126} are needed to reproduced fermion masses. None of these objections seems to point to a real contradiction, and in our view they are to a certain extent counterbalanced by the fact that this model does not need any flavour symmetry, is predictive for proton decay, leptogenesis and lepton flavor violation as well.

that therefore are expected to appear with coefficients $c_i \sim 1$. Rotating the Q, D fields by an angle $\theta_C \sim 0.2$ one reaches the mass eigenstate basis, where the above operators contains a term $\sim \theta_C^2 (c_1 - c_2) |s d|^2 / \Lambda^2$ that contributes to mixing and CP-violation in the $K^0 \bar{K}^0$ system, such that $\Lambda \gtrsim 10^3$ TeV. Appropriate unbroken non-abelian symmetries like $U(2)$ could force $c_1 = c_2$, avoiding this unseen new-physics effect. However:

- a) flavour symmetries must be broken; spontaneous breaking generates light Goldstone bosons (that become longitudinal polarizations of massive gauge bosons, in case the flavour symmetry is gauged) that in the non-abelian case mediate unseen flavour-changing processes.
- b) no flavour symmetry compatible with the electron mass term $m_e E L H^*$ can forbid the operator $c \cdot m_e (E \gamma_{\mu\nu} F_{\mu\nu} L) H^* / \Lambda^2$ that would induce an unobserved electric dipole for the electron. This implies $\Lambda \gtrsim 10^2$ TeV, and an analogous constraints comes from the neutron electric dipole. (Of course the situation can be better in specific models, e.g. if CP is broken in some appropriate way such that c is real).

In many models the flavour scale Λ is identified with the unification or Planck scales.

2) **Indirect tests:** the model predicts a relation between the SM parameters. The predictive power of a model can be naïvely estimated as

$$\text{number of predictions} \approx \text{number of SM parameters} - \text{number of parameters}$$

and is usually negative. This estimate is sometimes too pessimistic: some parameters of the model could be irrelevant because small (e.g. 13 entries of Yukawa matrices), or could not affect all observables (e.g. lepton and quark mass matrices could be two separate sectors).

We conclude listing predictions for neutrino physics.

12.4.1 Predictions for θ_{13} and texture zeroes

There are two qualitative reasons to expect that θ_{13} is detectably large. First, adding to the hierarchical texture (12.3) small perturbations that generate the solar $\nu_e/\nu_{\mu,\tau}$ mixing and mass typically generates also a contribution to θ_{13} of order

$$\theta_{13} \sim \theta_{\text{sun}} \sqrt{R} \sim 0.1 \quad \text{where} \quad R \equiv \frac{\Delta m_{\text{sun}}^2}{\Delta m_{\text{atm}}^2}. \quad (12.13)$$

Of course the most generic perturbation gives the most generic hierarchical mass matrix, such that there are no generic predictions for θ_{13} . However a θ_{13} much smaller than 0.1 needs a cancellation, which should be considered as unlikely unless it follows from some underlying symmetry reason.

Second, SU(5) unification suggests that λ_E is non diagonal, and possibly leads to the Cabibbo-like e/μ angle in eq. (12.11). Combined with the roughly maximal ν_μ/ν_τ atmospheric mixing, it induces a contribution to θ_{13} of order [138]

$$\theta_{13} \approx \sqrt{\frac{m_e}{2m_\mu}} \approx 0.05.$$

Since qualitative predictions are not constraining enough, in order to make real progress we need testable quantitative *predictions*.

Except in neutrinos, all SM flavour parameters have already been measured. We do not expect a significant reduction of the experimental errors in the near future. Future models will make *postdictions*, that unlike predictions are never badly wrong. Although this is not common practice we here ignore postdictions.⁷

Concerning θ_{12} , many models predicted a maximal θ_{12} . When experiments showed that it was less than maximal, it was possible to construct models that predict $\tan^2 \theta_{12} = 1/2$. Later, data favored a lower value, which can be neatly predicted as $\theta_{12} = \pi/4 - \theta_C$ [141], after discussing why the Cabibbo angle θ_C has something to do with neutrino physics. Future measurements can reduce the uncertainty on θ_{12} , but it seems too late for predicting it. Even in the 23 sector the sum of the (small) quark mixing plus the atmospheric mixing can be maximal.

We now review concrete predictions for the not yet measured quantities: θ_{13} , $|m_{ee}|$, deviations of θ_{23} from $\pi/4$, and the CP-violating phase ϕ . Since it seems likely that only θ_{13} will be precisely measured in the close future, we focus on models that make *quantitative predictions* for θ_{13} .

- We ignore predictions up to unknown $\mathcal{O}(1)$ factors. We ignore predictions already disfavored by data. We ignore models that predict some combination of θ_{13} and of CP-violating phases, since it is not of immediate experimental interest.

Predictive models need bold assumptions. Most models are based on ‘texture zeros’ i.e. they assume that only a few elements of the lepton mass matrices are non vanishing. These attempts could lead us to recognize that some elements might really be negligibly small; this would constitute a valuable step towards a theory of flavour. However, estimates of the future experimental accuracy and of the number of possible textures show that too many different predictions are possible: whatever will be the true value of θ_{13} , few textures will probably be able of predicting it. Therefore, in order to get some useful result that experiments can disproof we need to be more selective.

- We focus on predictive models which look more attractive, either because ‘theoretically motivated’ or because explain the observed smallness of θ_{13} and of $R = \Delta m_{\text{sun}}^2 / \Delta m_{\text{atm}}^2$ in a ‘natural’ way, without a fine-tuning of the parameters.

This last criterium could be misleading and is certainly subjective, but we do not know any better attempt. Here is a list of attempts that satisfy to these requirements. In almost all cases analogous predictions with $\theta_{23} \rightarrow \pi/2 - \theta_{23}$ are obtained by building analogous models with $\mu \leftrightarrow \tau$ replaced. For the moment the atmospheric mixing is consistent with maximal and the two kind of possibilities cannot be distinguished.⁸ We follow the notations of section 2: λ_N (λ_E) is the matrix of neutrino (charged lepton) Yukawa couplings of see-saw models, m_ν (M_N) the symmetric mass matrix of left-handed (right-handed) neutrinos.

1. Assuming

$$\lambda_E = \begin{pmatrix} * & 0 & 0 \\ 0 & * & 0 \\ 0 & 0 & * \end{pmatrix} \quad \text{and} \quad m_\nu = \begin{pmatrix} 0 & 0 & * \\ 0 & * & * \\ * & * & * \end{pmatrix}$$

⁷We recall that many models that now ‘naturally reproduce all observed data’, previously reproduced the ‘Small Mixing Angle’ solution to the solar neutrino problem when it seemed favored. Similarly, all competitors of the SM were able of postdicting the photon; what made the difference is that the SM correctly predicted the Z boson.

⁸The predictions quoted in this section have been computed applying standard propagation of errors to the simplified data in table 1.1 (in order to avoid singular Jacobians we use with $\theta_{23} = \pi/4 \pm 0.06$ in place of $\sin^2 2\theta_{23}$). Within a factor of 2 this fast approximation agrees with a careful marginalization of the joint probability density.

(where ‘0’ denotes a vanishing entry and ‘*’ a generic non-vanishing entry) gives [142].

$$\theta_{13} \simeq \frac{\tan 2\theta_{12}}{2} \tan \theta_{23} (R \cos 2\theta_{12})^{1/2} = 0.12 \pm 0.02. \quad (12.14)$$

Such pattern does not need an underlying see-saw model, but can be realized from the following see-saw texture:

$$\lambda_N = \begin{pmatrix} * & 0 & 0 \\ 0 & * & 0 \\ 0 & 0 & * \end{pmatrix}, \quad M_N = \begin{pmatrix} * & * & * \\ * & * & 0 \\ * & 0 & 0 \end{pmatrix}.$$

2. Assuming

$$m_\nu = \begin{pmatrix} 0 & * & 0 \\ * & 0 & * \\ 0 & * & * \end{pmatrix}, \quad \lambda_E = \begin{pmatrix} * & 0 & 0 \\ 0 & * & * \\ 0 & 0 & * \end{pmatrix}$$

gives

$$\theta_{13} \simeq \frac{\tan 2\theta_{12}}{2} (R \cos 2\theta_{12})^{3/4} = 0.038 \pm 0.005. \quad (12.15)$$

This can be realized as a see-saw texture:

$$\lambda_N = \begin{pmatrix} * & 0 & * \\ 0 & * & 0 \\ 0 & 0 & * \end{pmatrix}, \quad M_N = \begin{pmatrix} 0 & * & 0 \\ * & 0 & 0 \\ 0 & 0 & * \end{pmatrix}.$$

3. There is one very simple see-saw texture not reducible to a texture for m_ν . Assuming two right-handed neutrinos with

$$\lambda_N = \begin{pmatrix} * & * & 0 \\ 0 & * & * \end{pmatrix}, \quad M_N = \begin{pmatrix} * & 0 \\ 0 & * \end{pmatrix}, \quad \lambda_E = \begin{pmatrix} * & 0 & 0 \\ 0 & * & 0 \\ 0 & 0 & * \end{pmatrix}$$

gives [104]:

$$\theta_{13} \simeq \frac{\sqrt{R}}{2} \sin 2\theta_{12} \tan \theta_{23} = 0.075 \pm 0.011, \quad m_{ee} = m_{\text{sun}} \sin^2 \theta_{12}, \quad (12.16)$$

4. A different prediction is obtained by assuming an alternative form for the right-handed neutrino mass matrix [143]:

$$M_N = \begin{pmatrix} * & * \\ * & 0 \end{pmatrix} \quad \text{gives} \quad \theta_{13} \simeq R^{1/4} \sin \theta_{12} = 0.224 \pm 0.013. \quad (12.17)$$

This prediction can be alternatively obtained from a M_N with vanishing diagonal entries, combined with a non diagonal λ_E .

5. One can easily invent simple neutrino mass matrices diagonalized by $R_{23}(\theta_{23})R_{12}(\pi/4)$, see e.g. eq. (12.5). Since experiments excluded maximal solar mixing, this cannot be the only contribution to the neutrino mixing matrix. Diagonalization of the charged lepton mass matrix generically gives another contribution. Assuming that it only gives a 12 rotation, with angle $\Delta\theta_{12}$ results into $V = R_{12}(\Delta\theta_{12}) \cdot R_{23}(\theta_{23})R_{12}(\pi/4)$. When rewritten in the standard parametrization (2.11), such V corresponds to having $\theta_{13} \neq \pi/4$ and $\theta_{13} \neq 0$ related by [144]

$$\sin \theta_{13} = \tan \theta_{23} \cdot \tan(\theta_{12} - \pi/4) = 0.20 \pm 0.04. \quad (12.18)$$

6. A texture that assumes some texture zeroes and some strict equalities among non vanishing entries predicts [145]

$$\sin \theta_{13} = \sqrt{2R/3} = 0.153 \pm 0.15. \quad (12.19)$$

7. Assuming that the product of the neutrino mixing matrix times the quark mixing matrix has a zero in the 13 entry implies $\theta_{13} = 9^\circ \text{arc} \pm 2^\circ$ [141].

We now list predictions for θ_{13} coming from models or textures based on SO(10). These models typically can reproduce all quarks and lepton masses and mixings in terms of a restricted set of parameters, that often need to be fine-tuned. The predictions are $\theta_{13} \simeq 0.037$ [146], $\theta_{13} \simeq 0.014$ [147], $\theta_{13} \simeq 0.138$ [148], $\theta_{13} \simeq m_e m_\mu / \sqrt{2} m_\tau^2 = 1.1 \cdot 10^{-5}$ [149], $\theta_{13} \simeq \theta_C / 3\sqrt{2} = 0.053$ [150].

To conclude we mention the traditional approach, that consists in identifying a symmetry that in the some limit predicts the rough features of neutrino masses and mixings. Symmetry breaking terms are responsible of the finer structure: unless they are theoretically predicted one gets back to the generic mass matrix. Various authors explored the following symmetries: $L_e - L_\mu - L_\tau$ [134], SO(3) (assuming quasi-degenerate neutrinos), $\mu \leftrightarrow \tau$ permutations⁹, S_3 $e \leftrightarrow \mu \leftrightarrow \tau$ permutations, ‘quark-lepton complementarity’ [141], and the discrete tetrahedral A_4 symmetry [151]: it has representations with dimensions 1, 2 and 3. A_4 can be broken in a way that naturally implies ‘tri-bi-maximal mixing’ ($\theta_{13} = 0$, $\theta_{23} = \pi/4$, $\tan^2 \theta_{12} = 1/2$) in some leading-order approximations. Deviations that lead to $\theta_{13} \neq 0$ are not predicted, unless one assumes that some particular source dominates: one possible expectation is e.g. $\theta_{13} = 0.03 \div 0.07$ [151].

⁹A neutrino mass matrix m symmetric under $\mu \leftrightarrow \tau$ commutes with the permutation matrix

$$P = \begin{pmatrix} 1 & 0 & 0 \\ 0 & 0 & 1 \\ 0 & 1 & 0 \end{pmatrix}.$$

Therefore, the eigenstates of m coincide with the eigenstates of P , implying maximal θ_{23} and $\theta_{13} = 0$. In charged leptons, the $\mu \leftrightarrow \tau$ symmetry is of course badly broken by $m_\tau \gg m_\mu$.

Chapter 13

Behind neutrino masses?

We here discuss possible speculative new phenomena suggested or possibly related to neutrino masses. Observing extra phenomena might allow us to identify which new physics generates the observed neutrino masses. Effective-Lagrangian arguments suggested that the main low-energy manifestation of heavy new physics that violates lepton number is the Majorana neutrino mass operator: neutrinos become massive and other neutrino properties are negligibly affected. Experiments are now confirming this view, by indicating that the new physics responsible of the solar (section 6) and atmospheric (section 5) anomalies is neutrino oscillations. New particles lighter than about a TeV can evade the above expectation giving rise to new phenomena.

- In section 13.1 we discuss the phenomenology of the main subleading effective operator: *neutrino magnetic moments*.

Some specific kinds of new particles can be so light that direct searches are possible. Studying the behavior of the existing light particles (photons, gravitons and neutrinos) allows to probe the possible existence of new light particles. We here review what can be done with neutrinos. They are sensitive to:

- New *light neutral fermions* can naturally interact only with neutrinos, behaving as ‘sterile neutrinos’, and giving extra oscillation effects as discussed in section 13.2.
- New *light neutral scalars* can interact with neutrinos, provided that new light neutral fermions also exist. As discussed in section 13.3 the main signals are a modified neutrino cosmology, neutrino decay, new matter effects.

Furthermore, we discuss two specific possibilities of new physics motivated by solutions to the hierarchy problem:

- In *supersymmetric see-saw models* quantum corrections induced by neutrino Yukawa couplings affect slepton masses and might result in detectably large rates for $\mu \rightarrow e\gamma$ or other lepton-flavour-violating processes (section 13.5). In section 13.4 we discuss quantum corrections to neutrino masses.
- In section 13.6 we discuss how (after forbidding in some way Majorana masses) *neutrinos in extra dimensions* can get small Dirac masses with potentially unusual phenomenology.

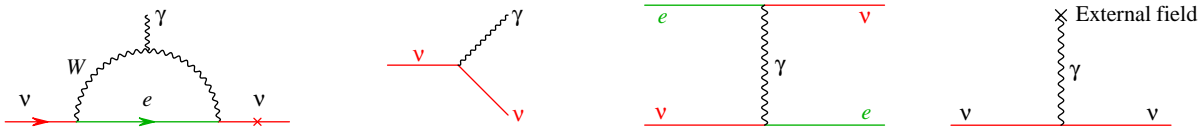


Figure 13.1: (a) Neutrino masses induce a magnetic moment. (b) Neutrino decay. (c) Neutrino/electron scattering. (d) Interaction with an external magnetic field.

13.1 Neutrino electro-magnetic dipoles

As discussed in section 2, neutrinos might have Majorana and/or Dirac masses. An analogous distinction arises for their electro-magnetic moments. In general, neutral fermions ψ_i can interact with photons via electro-magnetic moments μ_{ij} , described by the following dimension 5 Lagrangian operator

$$\sum_{ij} \mu_{ij} [\psi_i \gamma_{\mu\nu} \psi_j] F^{\mu\nu} + \text{h.c.} \quad (13.1)$$

where ψ_i are Weyl fermions and $\mu_{ij} = -\mu_{ji}$ has dimensions mass $^{-1}$. For $i = j$ one has $\mu_{ii} = 0$.

- Neutrinos might have only left-handed polarizations. In such a case neutrinos can only have $\Delta L = 2$ Majorana masses (section 2.4). Analogously, neutrinos can only have $\Delta L = 2$ ‘Majorana-like’ flavour-violating electro-magnetic dipoles $\mu_{e\mu}$, $\mu_{e\tau}$, $\mu_{\mu\tau}$, as can be seen inserting $\psi_i = \{\nu_e, \nu_\mu, \nu_\tau\}$ in eq. (13.1).
- Neutrinos might have both left and right-handed components. In such a case neutrinos can have $\Delta L = 2$ Majorana masses of *LL* type, $\Delta L = 2$ Majorana masses of *RR* type, and $\Delta L = 0$ Dirac masses of *LR* type. Only Dirac masses are allowed if lepton number is imposed (section 2.5).

Analogously, there can be *LL*, *RR* and *LR* electro-magnetic dipoles. Indeed the 6×6 asymmetric matrix μ_{ij} can be decomposed into three 3×3 sub-matrices as

$$\mu_{ij} = \begin{pmatrix} \mu_{\ell\ell}^{LL} & \mu_{\ell\ell}^{LR} \\ -\mu_{\ell\ell}^{LR} & \mu_{\ell\ell}^{RR} \end{pmatrix} \quad \text{in the basis} \quad \psi_i = \{\nu_\ell^L, \nu_\ell^R\}, \quad \ell = \{e, \mu, \tau\}. \quad (13.2)$$

If lepton number is imposed only the *LR* dipoles are allowed. Their flavour-diagonal components μ_{ii}^{LR} do not need to vanish and can be decomposed into the CP-conserving magnetic dipole $\text{Re } \mu_{ii}^{LR}$ and the CP-violating electric dipole $\text{Im } \mu_{ii}^{LR}$.

In both cases neutrino masses m_ν , together with electro-weak interactions produce tiny electro-magnetic dipoles (fig. 13.1a) [152]:

$$\mu_\nu \sim \frac{3eG_F}{8\sqrt{2}\pi^2} m_\nu = 3 \cdot 10^{-20} \mu_B \frac{m_\nu}{0.1 \text{ eV}} \quad (13.3)$$

where $\mu_B = e\hbar/2m_e c$ is the Bohr magneton. The expected dipoles are about 9 orders of magnitude below the present bounds discussed below, but new physics can give much larger dipoles.

Neutrino electro-magnetic dipoles can produce a variety of processes:

1. Neutrino decay (fig. 13.1b), $\Gamma_\nu(\nu \rightarrow \nu' \gamma) \sim m_\nu^3 \mu_\nu^2$.

2. Scattering on electrons (fig. 13.1c), with differential cross section [152]

$$\frac{d\sigma}{dT}(\bar{\nu}e \rightarrow \bar{\nu}e) = \frac{\pi \alpha_{\text{em}}^2 |\mu_\nu^2|}{\mu_B^2 m_e^2} \left(\frac{1}{T} - \frac{1}{E_\nu} \right). \quad (13.4)$$

The enhancement at small electron recoil energy T is limited by the detection threshold and ultimately by the presence of atomic energy levels. Experiments have been performed with atmospheric, reactor and solar neutrinos. Dipoles that involve ν_e are more strongly constrained: $\mu_\nu < 0.7 \cdot 10^{-10} \mu_B$ at 90% C.L. [152]. The next round of experiments might improve the sensitivity down to $10^{-12} \mu_B$.

3. If neutrinos have a right-handed component, it can get populated due to precession of the neutrino spin in an external magnetic field (fig. 13.1d). The consequent cooling of supernovæ and of red-giant stars allows to set the bound $\mu_\nu \lesssim 10^{-12} \mu_B$, subject to sizable astrophysical uncertainties [152].
4. Similarly, the combined effect of neutrino masses and of the interaction with the magnetic fields of the sun can convert solar ν_e into anti-neutrinos. Global fits of solar neutrino data, supplemented with models of the solar magnetic field, suggest $\mu_\nu \lesssim 10^{-10 \pm 12} \mu_B$ [152].

13.2 Neutrinos and light fermions

The SM contains fermions (e, ν, u, d, \dots) variously charged under electric, weak, strong interactions: fermions ν_R neutral under all SM gauge interactions might exist without giving any observable effect in collider experiments. The relevant terms in the $SU(2)_L$ -invariant effective Lagrangian that describes active neutrinos ν together with extra light ‘sterile neutrinos’ ν_R are

$$\frac{m_{LL}}{2} \frac{(LH)^2}{v^2} + \frac{m_{RR}}{2} \nu_R^2 + m_{LR} \nu_R L \frac{H}{v} + \text{h.c.} \quad (13.5)$$

H is the higgs doublet with vacuum expectation value $(0, v)$. The first dimension-5 operator gives Majorana ν masses m_{LL} and is naturally small if lepton number is broken at a high-energy scale. The second term gives Majorana ν_R masses m_{RR} , and the third term Dirac $\nu_L \nu_R$ masses m_{LR} : one needs to understand why m_{LR} and m_{RR} are small [153].

13.2.1 Motivations

A new light particle would probably be a discovery of fundamental importance, because its lightness is likely related to some fundamental principle, as it is the case for the known light particles, the photon, the neutrinos and the graviton. Attempts of guessing physics beyond the SM from first principles motivate a number of fermions which might have $\text{TeV}^2/M_{\text{Pl}}$ masses and behave as sterile neutrinos. A few candidates are axino, branino, dilatino, familino, Goldstino, Majorino, modulino, radino. These ambitious approaches so far do not give useful predictions on the flavour parameters in the effective Lagrangian of eq. (13.5).

More specific models can be more predictive. Unification of matter fermions into $\text{SO}(10)$ 16 or E_6 27 representations predicts extra singlets, which however generically receive GUT-scale masses. It is easy to invent ad-hoc discrete or continuous symmetries that keep a fermion light. One can use only ingredients already present in the SM. For example, the extra fermions can be

forced to be light assuming that they are chiral under some extra gauge symmetry (that could possibly become non perturbative at some QCD-like scale, and give composite sterile neutrinos). Alternatively, the extra fermions may be light for the same reason why neutrinos are light in the SM. Following this point of view up to its extreme, one can add to the SM a set of ‘mirror particles’, obtaining 3 sterile neutrinos.

A few theoretically favored patterns emerge from rather general naturalness considerations. We consider the most generic mass matrix with LL , RR and LR mass terms. If m_{LL} dominates one obtains light sterile neutrinos with mass $m_s \ll m_a$ and active/sterile mixings $\theta_s^2 \sim m_s/m_a$. If m_{RR} dominates, sterile neutrinos are heavy with $\theta_s^2 \sim m_a/m_s$. If m_{LR} dominates one obtains quasi-Dirac neutrinos that split into couples.

From a phenomenological point of view, sterile neutrinos have been the standard ‘emergence exit’ that allowed to fit many puzzling results in particle physics, astronomy, cosmology. We list some open questions; most (maybe all) of them will likely be sooner or later understood without invoking new physics. Sterile neutrinos could be the physics behind the LSND anomaly (section 9.2), the NuTeV anomaly (section 9.3), behave as dark matter (see in [154]), their decays could generate the diffuse ionization of our galaxy, can revive the shock wave that finally manifests as SN fireworks (section 11.2), can help r-process nucleosynthesis by reducing Y_e in presence of magnetic fields can generate the observed pulsar motion, can generate anomalous time modulations in solar neutrino rates [50].

13.2.2 Active/sterile mixings

We now review the most promising ways to probe the existence of eV-scale sterile neutrinos. Most probes are based on a careful study of natural sources of neutrinos (the universe, the sun, supernovæ, cosmic rays,...) which have their own peculiar capabilities and limitations. The sensitivity of some of these probes is enhanced by MSW resonances [28]. In cosmology, active ν and $\bar{\nu}$ encounter a MSW resonance with sterile neutrinos lighter than active ones. Roughly the same happens to supernova $\bar{\nu}_e$. On the contrary, solar ν_e encounter a MSW resonance with sterile neutrinos heavier than active neutrinos. The present constraints are compared in figures 13.2, where we assumed normal hierarchy of active neutrinos, a negligibly small θ_{13} , and added one extra sterile neutrino with arbitrary mass m_4 . We focus on the following six mixing patterns which cover the qualitatively different possibilities:

$$\nu_s/\nu_e, \quad \nu_s/\nu_\mu, \quad \nu_s/\nu_\tau, \quad \nu_s/\nu_1, \quad \nu_s/\nu_2 \quad \text{and} \quad \nu_s/\nu_3$$

where $\nu_{1,2,3}$ are the mass eigenstates in absence of sterile mixing. We remark one qualitative difference among the two classes of mixings:

- *Mixing with a flavour eigenstate* (depicted in fig. 13.3a): ν_s/ν_ℓ ($\ell = e$ or μ or τ). The sterile neutrino oscillates into a well defined flavour at 3 different $\Delta m^2 = m_4^2 - m_{1,2,3}^2$ (which cannot all be smaller than the observed splittings $\Delta m_{\text{sun,atm}}^2$).
- *Mixing with a mass eigenstate* (depicted in fig. 13.3b): ν_s/ν_i ($i = 1$ or 2 or 3). The sterile neutrino oscillates into a neutrino of mixed flavour at a single $\Delta m^2 = m_4^2 - m_i^2$, which can be arbitrarily small.

We now summarize the main constraints and the most promising signals.

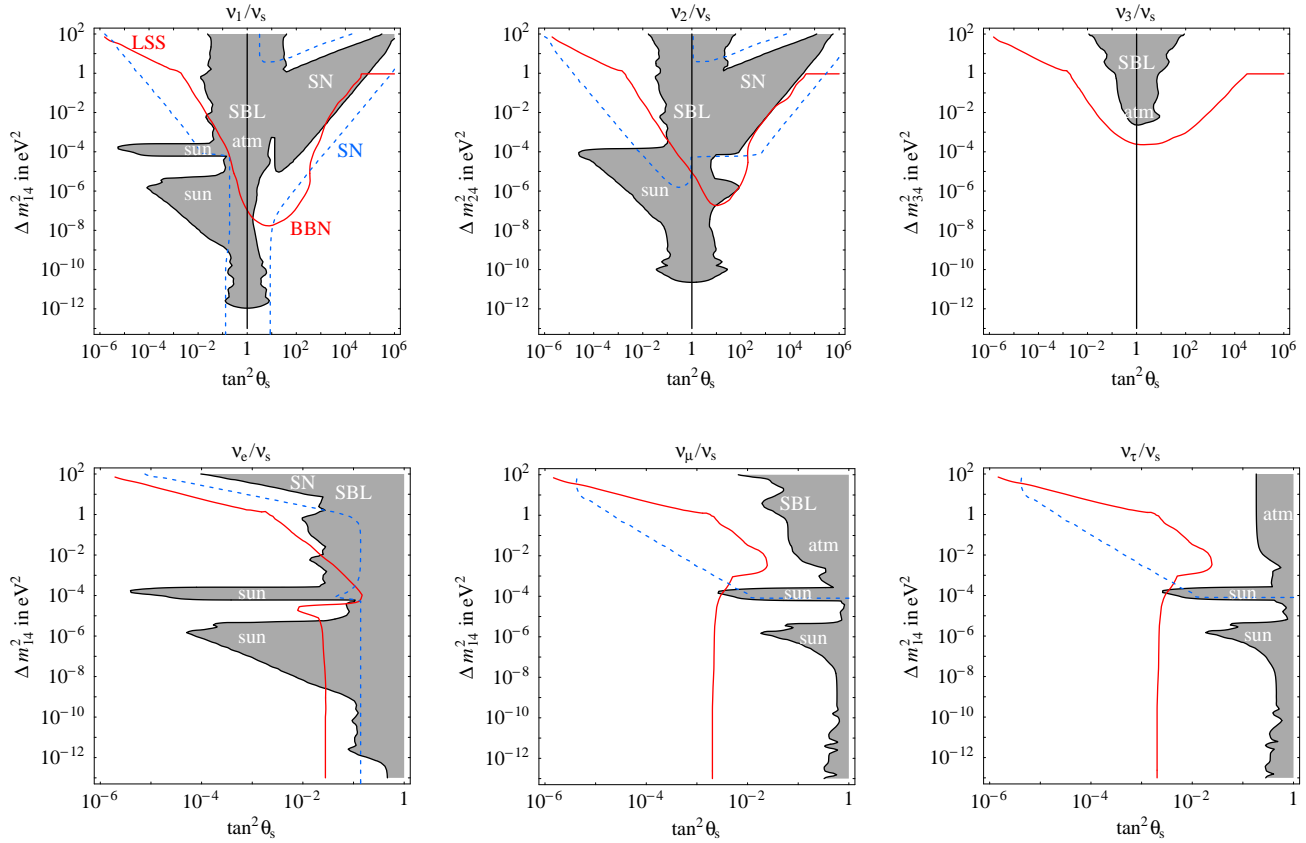


Figure 13.2: **Summary of sterile neutrino effects.** The shaded region is excluded at 99% C.L. (2 dof) by solar or atmospheric or reactor or short base-line experiments. We shaded also regions where sterile neutrinos suppress the SN1987A $\bar{\nu}_e$ rate by more than 70%. This rate is suppressed by more than 20% inside the dashed blue line, that can be explored at the next SN explosion if it will be possible to understand the collapse well enough. Within standard cosmology, the region above the red continuous line is disfavored (maybe already excluded) by BBN and LSS.

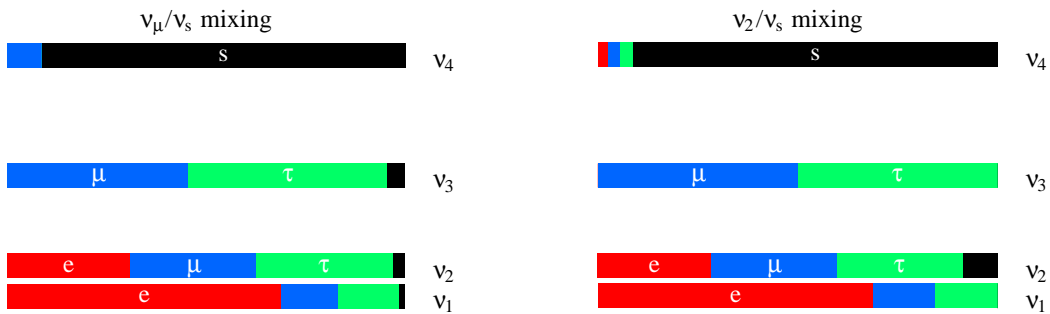


Figure 13.3: **Basic kinds of four neutrino mass spectra.** Left: sterile mixing with a flavour eigenstate (ν_μ in the picture). Right: sterile mixing with a mass eigenstate (ν_2 in the picture).

13.2.3 Cosmology

Compatibility with **standard BBN** constrains oscillations into sterile neutrinos dominantly occurred at temperatures $T \gtrsim 0.1$ MeV. The main observable is the *helium-4* primordial abundance, that we parameterize in terms of an effective number of neutrinos $N_\nu^{4\text{He}}$, see eq. (10.2). As discussed in section 10.1, present data do not exclude the presence of one extra thermalized neutrino, $N_\nu^{4\text{He}} = 4$. The helium-4 abundance is sensitive to two different sterile effects: i.) increase of the total neutrino density; ii.) depletion of electron-neutrinos. Section 3.6 presented the formalism appropriate for precisely computing these effects, that we now discuss in a semi-quantitative way.

i.) Sterile neutrinos thermalize via averaged oscillations (regime C of section 3.1.2). The sterile interaction rate at temperature T is given by $\Gamma_s \sim (\theta_s^m)^2 \Gamma_\nu$, where Γ_ν is the interaction rate of an active neutrino, and $\theta_s^m(T) \ll 1$ is the active/sterile mixing angle in matter at temperature T :

$$\frac{\Gamma_s}{H} \approx (\theta_s^m)^2 \left(\frac{T}{4 \text{ MeV}} \right)^3 \quad \theta_s^m \approx \frac{\theta_s}{1 + T^6 G_F^2 / \alpha \Delta m^2}. \quad (13.6)$$

Γ_s/H is maximal at $T_* \approx 10 \text{ MeV} (\Delta m^2 / \text{eV}^2)^{1/6}$ and the amount of thermalized sterile is

$$\Delta N_\nu \approx \frac{\Gamma_s}{H} \Big|_{\text{max}} \approx 10^3 \theta_s^2 \left(\frac{\Delta m^2}{\text{eV}^2} \right)^{1/2}. \quad (13.7)$$

The effect has a minor dependence on the flavour of the active neutrino involved in active/sterile mixing and becomes negligible at $\Delta m^2 \lesssim 10^{-5} \text{ eV}^2$. Our estimate does not take into account the possibility of resonant enhancement of active/sterile mixing, possible only if $\Delta m^2 < 0$ i.e. if the ‘mostly sterile’ neutrino is lighter than some ‘mostly active’ neutrino.

ii.) The second effect makes BBN sensitive to active/sterile oscillations down to $\Delta m^2 \sim 10^{-8} \text{ eV}^2$. If T_* is smaller than the neutrino decoupling temperature, sterile neutrinos are produced by depleting active neutrinos with the total neutrino density remaining constant. Since there are many more neutrinos than nucleons, decoupled neutrinos (i.e. interaction rate of neutrinos with nucleons smaller than the expansion rate) still play an active rôle (i.e. interaction rate of nucleons with neutrinos larger than the expansion rate): the p/n ratio is determined by $\nu_e n \leftrightarrow e p$ and $\bar{\nu}_e p \leftrightarrow \bar{e} n$ scatterings. A reduced $\langle \bar{\nu}_e \rangle$ number density affects BBN increasing the effective $N_\nu^{4\text{He}}$ parameter.

However, if BBN were non-standard, a modified density of electron neutrinos could compensate the sterile corrections to $N_\nu^{4\text{He}}$: for example helium-4 constraints on sterile oscillations can be evaded by allowing a large neutrino asymmetry.

For all these reasons it is important to measure a second BBN effect. Measurements of the *deuterium* primordial abundance are less affected by systematic uncertainties: in the future it might be possible to improve its measurement obtaining an uncertainty on the effective parameter N_ν^D (precisely defined in eq. (10.3)) significantly below 1, possibly making deuterium the most significant BBN probe. However, the deuterium abundance is less sensitive than the helium-4 abundance to ν_e depletion and therefore to values of Δm^2 below 10^{-5} eV^2 .

Future studies of CMB acoustic oscillations should allow to precisely measure the total neutrino density N_ν^{CMB} at recombination ($T \sim \text{eV}$) with ± 0.2 (PLANCK) or maybe ± 0.05 (CMBPOL) error [69]. Sterile neutrinos affect N_ν^{CMB} only if $\Delta m^2 \gtrsim 10^{-5} \text{ eV}^2$; in such a case $N_\nu^{\text{CMB}} \approx N_\nu^{4\text{He}} \approx N_\nu^D$.

As discussed in section 10.2.1, Large Scale Structure data are sensitive to neutrino masses. From a cosmological point of view, the main parameter that controls this kind of effects is the energy density in (massive) neutrinos, Ω_ν . Present data demand $\Omega_\nu \lesssim 0.01$ [69]. Sterile neutrinos contribute to Ω_ν .¹ For small active/sterile mixing LSS constrains sterile oscillations more strongly than BBN (fig. 10.1).

13.2.4 Solar neutrinos

Solar ν_e experiments have explored sterile oscillations not testable by cosmology, thanks to two different effects. (1) MSW resonances make solar ν_e sensitive to small active/sterile mixing and $\Delta m^2 \gtrsim 10^{-8} \text{ eV}^2$. (2) With large mixing, solar ν_e are sensitive down to $\Delta m^2 \sim 10^{-12} \text{ eV}^2$. Future experiments will explore new aspects of the solar neutrino anomaly, allowing to measure in a redundant way the active oscillation parameters or to discover a new anomaly. We emphasize one qualitative point. Due to LMA oscillations, neutrinos exit from the sun as almost pure ν_2 at energies $E_\nu \gtrsim$ few MeV (section 6). Neutrinos with these energies have been precisely studied by SNO and SK, but are not affected by sterile oscillations if they mostly involve ν_1 . This can happen either because ν_s mixes with ν_1 or because it is quasi-degenerate to it. Therefore there is a whole class of sterile effects which manifest only at $E_\nu \lesssim$ few MeV — an energy range explored so far only by Gallium experiments [8]. Future precise measurement of solar ν_e at sub-MeV energies will allow to significantly extend searches for active/sterile effects. Part of these extended region will be tested by Borexino [54], where a sterile neutrino can manifest as day/night variations, or as seasonal variations, or even by reducing the total rate.

13.2.5 Supernovæ

Supernova neutrinos will be good probes of sterile oscillations because have a different pattern of MSW resonances and a longer base-line than solar ν_e . Consequently supernova $\bar{\nu}_e$ are more sensitive than solar ν_e in two main cases: (a) small $\Delta m^2 \gtrsim 10^{-18} \text{ eV}^2$ with large θ_s ; (b) ν_s lighter than ν_1 with small mixing. Oscillations into one sterile neutrino can reduce the $\bar{\nu}_e$ rate by up to 80% and, in a more restricted range of oscillation parameters, vary the average $\bar{\nu}_e$ energy by 30%. SN1987A data agreed with expectations. Future SN experiments can perform quantitative tests, but it is not clear how to deal with theoretical uncertainties. Neutrinos emitted by past supernovæ, or by other extragalactic sources, do not seem to allow more sensitive searches for sterile neutrinos [117].

13.2.6 Atmospheric neutrinos

Atmospheric experiments (SK, MACRO, K2K) indirectly exclude active/sterile oscillations with $\Delta m^2 \gtrsim 10^{-3 \div 4} \text{ eV}^2$ and $\tan^2 \theta_s \gtrsim 0.1 \div 0.2$. Up to minor differences, this applies to all flavours. Terrestrial experiments that mainly probed disappearance of $\bar{\nu}_e$ and ν_μ (CHOOZ, CDHS, ...) exclude active/sterile mixings with these flavours for $\tan^2 \theta_s \gtrsim 0.03$ and $\Delta m^2 \gtrsim 10^{-3} \text{ eV}^2$. Therefore future short-baseline experiments can search for sterile effects with smaller θ_s . Possible signals

¹This parameter alone does not fully encode all relevant physics: e.g. a smaller non-thermal population of heavier sterile neutrinos behaves differently than a larger population of lighter sterile neutrinos. Heavy enough sterile neutrinos are a possible DM candidate, although present data only allow a small window around sterile masses of a few keV [154].

are $\bar{\nu}_e$ disappearance in reactor experiments, a deficit of NC events or ν_τ appearance in beam experiments. Within standard cosmology these effects can be probed by CMB and BBN, which already disfavor them.

13.3 Neutrinos and light scalars

Electromagnetic gauge invariance and Lorenz invariance allow Yukawa couplings g_{ij} between neutrinos and a hypothetical light scalar X , $g_{ij} \nu_i \nu_j X/2 + \text{h.c.}$ The electroweak invariant version of this operator has dimension 6: $X(LH)^2$, such that electroweak gauge invariance suppresses g_{ij} down to negligibly small values, unless g_{ij} are mediated by a particle lighter than the weak scale. Apparently, the only possibility that can lead to sizable g_{ij} consists in having also light sterile neutrino(s) ν_R . Indeed sterile neutrinos can have a Yukawa coupling g_{RR} to X not suppressed by electroweak gauge invariance, and the interactions

$$\frac{\nu_R^2}{2}(m_{RR} + g_{RR}X) + m_{LR} \frac{LH}{v} \nu_R + m_{LL} \frac{(LH)^2}{2v^2} + \text{h.c.} \quad (13.8)$$

generate the Yukawa coupling $g = g_{RR} m_{LR}^2 / 2m_{RR}^2$ between neutrinos and X after integrating out $\nu_R = -m_{LR}\nu / (m_{RR} + g_{RR}X)$. Introducing more than one sterile neutrino, one can similarly generate a Yukawa coupling between active neutrinos, sterile neutrinos and X . Although a sizable g needs light sterile neutrinos, we here study the phenomenology of the Yukawa couplings g in isolation from sterile neutrinos.

Another theoretical issue is: why X is light? One plausible sub-class of models provides a neat answer and implies a special phenomenology. The scalar X might be light because it is a (pseudo)-Goldstone boson if its vev spontaneously breaks a global lepton number symmetry; if neutrino masses $m_{ij} = g_{ij}\langle X \rangle$ arise only from the coupling $g_{ij}\nu_i \nu_j X/2$, X couples to neutrino mass eigenstates such that there is no neutrino decay in vacuum. Neutrino decay in matter is possible, because matter effects lead to couplings between different mass eigenstates.

Different areas of physics allows to test g_{ij} couplings. We start from the simplest and less sensitive probes, moving to the more sensitive and subtle probes.

13.3.1 Rare decays

Emission of X scalars would affect decays of π and K into $e\bar{\nu}_e$ or $\mu\bar{\nu}_\mu$, resulting in the constraint $|g_{ij}| \lesssim 10^{-2}$ for all $ij \neq \tau\tau$ [41]. These decays should likely be studied in the full theory, rather than using the effective g_{ij} couplings. $0\nu2\beta$ gives a stronger constraint on $|g_{ee}| \lesssim 10^{-4}$.

13.3.2 Neutrino decay

A minimal source of neutrino decay is provided by neutrino masses, together with one loop SM effects. However, estimates show that the resulting life-time is so long that neutrinos are practically stable even on astrophysical and cosmological time-scales:

$$\Gamma(\nu_i \rightarrow \gamma \nu_j) \sim \frac{e^2 g_2^4}{(4\pi)^5} \frac{m_i^5 m_\tau^2}{M_W^6} \sim \frac{1}{10^{40} \text{yr}} \left(\frac{m_i}{0.1 \text{eV}} \right)^5. \quad (13.9)$$

In the limit $m_i \gg m_j$ neutrinos with Majorana masses decay two times faster than Dirac neutrinos [41].

Therefore an eventual observation of neutrino decay would imply physics beyond the SM, and more specifically a coupling to some new very light or massless particle X . Assuming that X has spin 0, the Lagrangian coupling $g_{ij} \nu_i \nu_j X/2 + \text{h.c.}$ (where g_{ij} is a symmetric flavour matrix, here written in the basis of neutrino mass eigenstates ν_i) gives

$$\Gamma(\nu_i \rightarrow X \nu_j) = \Gamma(\nu_i \rightarrow X \bar{\nu}_j) = \frac{g_{ij}^2}{32\pi} m_i = \frac{g_{ij}^2}{0.40 \text{ mm}} \frac{m_i}{0.05 \text{ eV}} \quad (13.10)$$

for $m_i \gg m_j$. Taking into account Lorentz dilatation, the life-time of an ultrarelativistic neutrino is

$$\tau = \frac{E_\nu}{m_i} \Gamma = \frac{8000 \text{ km}}{g_{ij}^2} \frac{E_\nu}{\text{GeV}} \frac{2.5 \cdot 10^{-3} \text{ eV}^2}{m_i^2}$$

i.e. relativity tells that sensitive probes of neutrino decay must have a large L/E_ν , like in the case of oscillations. Neutrinos have been observed at the following values of L/E_ν :

$$\begin{aligned} \text{atmospheric: } 10^4 \text{ km}/300 \text{ MeV} &\sim 10^{-10} \text{ s/eV}, \\ \text{solar: } 500 \text{ sec}/5 \text{ MeV} &\sim 10^{-4} \text{ s/eV}, \\ \text{supernova: } 10 \text{ kpc}/10 \text{ MeV} &\sim 10^5 \text{ s/eV}. \end{aligned}$$

Present supernova data are not conclusive enough to derive constraints. Atmospheric data only imply $|g_{ij}| \lesssim 4\pi$, which is anyhow required by perturbativity. Solar data suggest $|g_{12}| \lesssim 10^{-3}$.

13.3.3 CMB and interacting neutrinos

As discussed in section 10.2.1 the presence of freely-moving relativistic neutrinos suppresses CMB anisotropies. The situation changes if the interaction rate Γ of neutrinos with scalars X is faster than H , the expansion rate at recombination ($T_{\text{rec}} \sim 0.3 \text{ eV}$). While a detailed analysis is needed to study the case $\Gamma \sim H$, if $\Gamma \gg H$ neutrinos and scalars form an interacting ν/X fluid and damp CMB anisotropies less effectively [95].

The evolution of its inhomogeneities can be precisely described by an equation somewhat analogous to eq. (10.9), that applies to DM inhomogeneities. The main differences are that the ν/X fluid would be relativistic ($w = 1/3$) and with a non-vanishing sound speed, $c_s^2 = 1/3$. The total energy density of the ν/X fluid is parameterized, in the standard cosmological language, in terms of an ‘effective number of neutrinos’ N_ν^I , where I stands for *Interacting*. N_ν^I can be bigger than 3 if the scalar(s) X carry some energy, and smaller than 3 if less neutrinos significantly interact with X ; the remaining neutrinos behave normally. These are the minimal parameters that characterize the cosmological behavior of the system. Neutrino masses and the X mass(es) can be additional parameters, and lead to time-dependent $N_\nu^I u, w, c_s^2$.

Present global fits of cosmological data indicate a $(3 \div 4)\sigma$ preference for the standard scenario of freely moving neutrinos [95], and future data should settle the issue. This effect can give the most sensitive probe to the g_{ij} couplings. Indeed the $\nu_j \nu_j \leftrightarrow XX$ processes have a rate $\Gamma \sim g_{ij}^4 T$ comparable to the expansion rate $H \sim T^2/M_{\text{Pl}}$ for $g_{ij} \lesssim (T_{\text{rec}} M_{\text{Pl}})^{1/4} \sim 10^{-6}$. If neutrino decay $\nu_i \rightarrow \nu_j X$ ($i \neq j$) is kinematically allowed because X is light enough, its rate $\Gamma \sim g_{ij}^2 m_i$ is comparable to the universe expansion rate at recombination for $g_{ij} \lesssim (T_{\text{rec}} M_{\text{Pl}})^{1/2} \sim 10^{-12}$, allowing to probe very small values of the off-diagonal couplings g_{ij} .

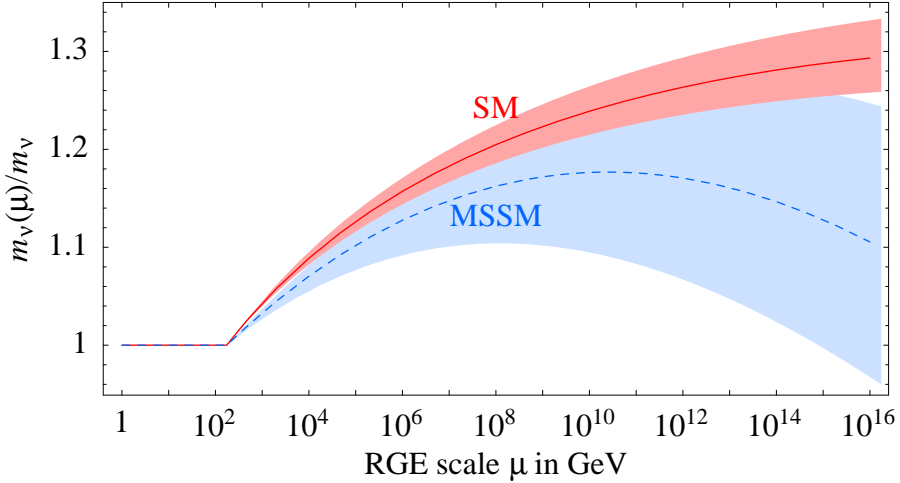


Figure 13.4: *Universal running of m_ν in the SM and in the MSSM. The bands indicate the present uncertainty.*

13.4 Quantum corrections to neutrino masses

Quantum corrections shift the coefficient κ of the dimension-5 effective operator

$$\frac{\kappa_{ij}}{4}(L_i H)(L_j H) \quad (13.11)$$

that induces Majorana neutrino masses $m_{ij} = \kappa_{ij}v^2/2$ with $v = \langle H \rangle = 174$ GeV. We now compute these quantum effects.

13.4.1 MSSM

We start from the MSSM where the computation can be easily performed since superpotential interactions (like the operator in (13.11)) do not receive direct quantum corrections [155]. The kinetic term of a generic chiral superfield Φ (with Yukawa interactions λ and gauge interactions g) receive quantum corrections that correct it into

$$\mathcal{L}_{\text{kin}} = Z_\Phi^2(\Phi^\dagger \Phi) \quad \text{where} \quad Z_\Phi = 1 + (g_I^2 c_I^\Phi - \lambda^2)t + \mathcal{O}(g^2 t)^2, \quad t \equiv \frac{\ln \mu/\Lambda}{(4\pi)^2}.$$

$\Lambda(\mu)$ is a supersymmetric UV (IR) cutoff and c_I^Φ are Casimir factors ($c_2^{L,H} = 3/2$ and $c_Y^{L,H} = 1/2$ for Higgs and lepton doublets). Rewriting the Lagrangian in terms of renormalized fields with standard kinetic terms, $\Phi \rightarrow \Phi/Z_\Phi$, the coupling κ gets corrected into

$$\kappa(\mu) = \kappa(\Lambda)/Z_L^2 Z_H^2. \quad (13.12)$$

These expressions are accurate only if $g^2 t \ll 1$. When $\mu \sim M_Z$ and $\Lambda \sim M_{\text{Pl}}$ this condition is violated by too large logarithms $\ln \Lambda/\mu$. An accurate expression can be obtained by resumming all quantum corrections of $\mathcal{O}(g^2 t)^n$. This is accomplished using renormalization group techniques, by transforming (13.12) into the differential RGE equation

$$\frac{d\kappa}{dt} = \kappa(-2g_Y^2 - 6g_2^2 + 6\lambda_t^2) + \kappa \cdot (\lambda_E^\dagger \cdot \lambda_E)^T + (\lambda_E^\dagger \cdot \lambda_E) \cdot \kappa + \mathcal{O}\left(\frac{g^4}{(4\pi)^2}\right) \quad (\text{MSSM}). \quad (13.13)$$

13.4.2 SM

In the SM, RGE equations maintain the same structure with different numerical factors [156]:

$$\frac{d\kappa}{dt} = \kappa(\lambda - 3g_2^2 + 6\lambda_t^2) - \frac{3}{2} \left[\kappa \cdot (\lambda_E^\dagger \cdot \lambda_E)^T + (\lambda_E^\dagger \cdot \lambda_E) \cdot \kappa \right] + \mathcal{O}\left(\frac{g^4}{(4\pi)^2}\right) \quad (\text{SM}) \quad (13.14)$$

The lepton and higgs couplings λ_E and λ are defined in (2.1). In both the SM and MSSM cases the first terms give an overall rescaling: its effect is plotted in fig. 13.4 where we have assumed $\alpha_3(M_Z) = 0.118$, a pole top mass of 175 GeV, $m_h = 115$ GeV in the SM and moderately large $\tan\beta$ in the MSSM. Neutrino masses increase by a few 10% when renormalizing up to high energy scales.

The second term is flavour dependent and renormalizes neutrino masses and mixing angles.² It is numerically negligible, with the exception of two special circumstances: i) $\tan\beta$ is so large than $\lambda_\tau \sim 1$. ii) One considers fine-tuned neutrino mass matrices, unstable under these small RGE corrections. For example, if one puts by hand large equal masses to all neutrinos, small RGE corrections can generate a sizable mass splitting.

13.4.3 See-saw models

See-saw contain extra renormalization effects at energies above the masses of right-handed neutrinos, generated by the neutrino Yukawa couplings λ_N . The technique described above would allow to easily compute these effects in supersymmetric see-saw models, taking into account that the quantum corrections Z_N (renormalizations of kinetic terms of heavy right-handed neutrinos) do not affect light neutrinos. In practice λ_N are unknown so that we do not learn much by studying their effects. For example, some neutrino Yukawa couplings could be large enough that the solar mixing angle, renormalized at the unification scale, becomes maximal or achieves any other value.

In the next section we study a different class of quantum corrections present in supersymmetric see-saw models, that can have detectable effects.

13.5 Lepton-flavour violation and supersymmetry

An unpleasant feature of the see-saw mechanism is that we do not see how it can be realistically tested, i.e. how it could became true physics rather than remaining a plausible speculation.

In general, if the observed solar and atmospheric anomalies are due to neutrino masses, lepton-flavour-violating (LFV) decays such as $\mu \rightarrow e\gamma$ and $\tau \rightarrow \mu\gamma$ must be present at some level. However, if the effective theory at energies below the new physics that generates neutrino masses is the SM, then lepton flavour is violated only by non-renormalizable interactions and the resulting rates are of order $\text{BR}(\mu \rightarrow e\gamma) \sim (m_\mu m_{e\mu}/m_W^2)^2 \sim 10^{-50}$ where $m_{e\mu}$ is the $e\mu$ element of the neutrino mass matrix. This would be hopelessly below the present experimental bound $\text{BR}(\mu \rightarrow e\gamma) \lesssim 10^{-11}$ and below any possible future improvement, as summarized in table 13.1. See-saw models give a concrete example of this general fact: one can precisely compute the $\mu \rightarrow e\gamma$

²One can write RGE equations for neutrino masses and mixings, however they have a structure much more complicated than RGE equations for the neutrino mass matrix. The ‘run-and-diagonalize’ approach (i.e. solve the above RGE equations and at the end diagonalize the neutrino mass matrix) is usually much more convenient than the ‘diagonalize-and-run’ approach, not discussed here.

present bound		future?		present bound		future?	
d_N	$< 3.0 \cdot 10^{-26} e \text{ cm}$	[157]	$10^{-27} e \text{ cm}$	$\text{BR}(\tau \rightarrow \mu\gamma)$	$< 0.7 \cdot 10^{-7}$	[158]	10^{-9}
d_e	$< 1.5 \cdot 10^{-27} e \text{ cm}$	[159]	$10^{-29} e \text{ cm}$	$\text{BR}(\mu \rightarrow e\gamma)$	$< 1.2 \cdot 10^{-11}$	[17]	10^{-14}
$d_{^{199}\text{Hg}}$	$< 1.8 \cdot 10^{-28} e \text{ cm}$	[160]		$\text{BR}(\mu \rightarrow e\bar{e}e)$	$< 1.0 \cdot 10^{-12}$	[161]	10^{-16}
d_μ	$< 1.0 \cdot 10^{-18} e \text{ cm}$	[162]	$10^{-25} e \text{ cm}$	$\text{CR}(\mu \rightarrow e \text{ in Ti})$	$< 6.1 \cdot 10^{-13}$	[163]	10^{-18}

Table 13.1: *Compilation of 90% CL bounds on CP-violating and lepton-flavor violating processes.*

decay amplitude, confirming that it is unobservably small because proportional to $\lambda_N^2/M_N \propto m_\nu$. Furthermore, the smallness of the observed neutrino masses, $m_\nu \sim \lambda_N^2 v^2/M_N$, suggests that directly observing the right-handed neutrinos is also impossible, either because M_N is too heavy, or because λ_N is too small.

If supersymmetric particles exists at the weak scale, things can be very different [164]. In the context of the Minimal Supersymmetric Standard Model (MSSM) radiative corrections induced by λ_N affect supersymmetry-breaking slepton mass terms, if they are already present in the Lagrangian at energies above M_N (alternatively supersymmetry-breaking could instead be transmitted to MSSM particles at energies below M_N , where right-handed neutrinos no longer exists). The crucial difference between the SM and the MSSM is that the SM remembers of the existence of very heavy right-handed neutrinos only trough non-renormalizable operators like $(LH)^2/\Lambda$ (that give rise to neutrino masses). The MSSM contains more renormalizable terms, like slepton masses $\mathbf{m}_L^2 \tilde{L}^* \tilde{L}$, where right-handed neutrinos can leave their imprint. For example, the correction to the 3×3 mass matrix of left-handed sleptons is

$$\mathbf{m}_L^2 = m_0^2 \mathbb{I} - \frac{3m_0^2}{(4\pi)^2} \mathbf{Y}_N + \dots \quad \text{where} \quad \mathbf{Y}_N \equiv \boldsymbol{\lambda}_N^\dagger \ln\left(\frac{M_{\text{GUT}}^2}{\mathbf{M} \mathbf{M}^\dagger}\right) \boldsymbol{\lambda}_N \quad (13.15)$$

having neglected A -terms and $\mathcal{O}(\lambda_N^4)$ effects and assumed universal soft terms at M_{GUT} ³. In this approximation, the experimental bounds from $\ell_i \rightarrow \ell_j \gamma$ decays are saturated for

$$[\mathbf{Y}_N]_{\tau\mu}, [\mathbf{Y}_N]_{\tau e} \sim 10^{1\pm 1}, \quad [\mathbf{Y}_N]_{\mu e} \sim 10^{-1\pm 1}. \quad (13.16)$$

The precise value depends on the so far unknown masses of supersymmetric particles. Large neutrino couplings (e.g. $\lambda_N \sim \lambda_t$) could give $\mu \rightarrow e\gamma$ or $\tau \rightarrow \mu\gamma$ just below their experimental bounds, while smaller neutrino couplings (e.g. $\lambda_\nu \sim \lambda_\tau$) would give no significant effect. However, we have no idea of which value $Y_N \sim \lambda_N^2$ should have (neutrino masses only tell us the value of λ_N^2/M_N), so that *see-saw models make no testable prediction*. In fact, the \mathbf{M}_N , $\boldsymbol{\lambda}_N$ and $\boldsymbol{\lambda}_E$ matrices that describe the supersymmetric see-saw contain 15 real parameters and 6 CP-violating phases. At low energy, in the mass eigenstate basis of the leptons, 3 real parameters describe the lepton masses, and both the neutrino and the left-handed slepton mass matrices are described by 6 real parameters and 3 CP-violating phases. Since $(15 + 6) = (3 + 0) + (6 + 3) + (6 + 3)$ we see that the generic see-saw mechanism has too many free parameters to allow predictions: any

³In the MSSM lepton flavour is not an accidental symmetry as in the SM, and some unknown mechanism must suppress lepton/slepton mixing down to an acceptable level. This problem motivates the assumption of universal soft-terms at M_{GUT} , although nothing guarantees it. Rather, in GUT models the unified top quark Yukawa coupling distorts universal soft terms, giving rise to other LFV effects related to GUT physics rather than to neutrino physics.

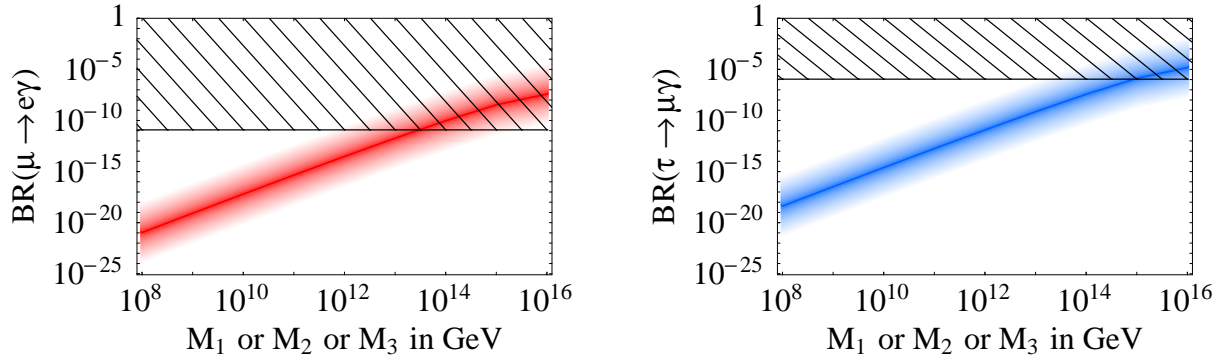


Figure 13.5: *Predictions for $\mu \rightarrow e\gamma$ and $\tau \rightarrow \mu\gamma$ rates induced by Yukawa neutrinos and supersymmetry under assumptions discussed in the text. The masses of right-handed neutrinos are unknown; leptogenesis suggests $M_1 \sim 10^9$ GeV.*

pattern of lepton and neutrino masses is compatible with any pattern of radiatively-generated flavor violations in left-handed slepton masses.

In order to get more concrete results, we assume that the Yukawa couplings of the neutrinos follow the same pattern observed in their masses: large μ/τ mixing in the ‘atmospheric’ sector and large $e/\mu/\tau$ mixing in the ‘solar’ sector. This is not demanded by data and plausible counterexamples exist [165]. Having fixed the mixing angles with this arbitrary assumption, we can plot in fig. 13.5 the predicted $\mu \rightarrow e\gamma$ and $\tau \rightarrow \mu\gamma$ rates as function of the remaining unknown parameters, the right-handed neutrino masses M_i . Leptogenesis suggests that the lightest ν_R has a mass around 10⁹ GeV (see section 10.3). Our present ignorance of sparticle masses induces an additional subdominant uncertainty of about 5 orders of magnitude, represented in fig. 13.5 by the thickness of the lines.

At low energy, lepton-flavour violation is transmitted from SUSY sparticles to SM particles mostly as an effective dipole operator. This implies characteristic correlations between $\mu \rightarrow e\gamma$, $\mu \rightarrow e\bar{e}e$, $\mu \rightarrow e$ rates.

In conclusion, in supersymmetric see-saw models large neutrino Yukawa *couplings* (e.g. $\lambda_N \sim \lambda_t$) can generate sizable $\mu \rightarrow e\gamma$ and $\tau \rightarrow \mu\gamma$ rates. These effects cannot be predicted in terms of measured neutrino *masses*. This means that, if these effects will be measured and if one can get convinced that they are generated only by neutrino Yukawa couplings, we would learn some information about neutrino Yukawa couplings. We cannot realistically hope that in this way it will be possible to experimentally reconstruct all see-saw parameters; a realistic summary of prospects is:

m_1, m_2, m_3	Two Δm^2 already measured; m_1 measurable only if large.
$\theta_{12}, \theta_{23}, \theta_{13}$	θ_{12} and θ_{23} already measured, θ_{13} measurable.
ϕ, α, β	ϕ measurable from oscillations; one combination of α, β affects $0\nu2\beta$.
$[Y_N]_{ee, \mu\mu, \tau\tau}$	Two measurable from slepton mass splittings.
$ Y_N _{e\mu, \mu\tau, e\tau}$	All measurable from LFV rates.
$\arg [Y_N]_{e\mu, \mu\tau, e\tau}$	One combination from electron electric dipole?

Measuring CP-violating phases is particularly important if one hopes to test whether leptogenesis

generated the observed baryon asymmetry. However various cancellations make the computation of electric dipoles induced by neutrino Yukawas tricky, and its result small. The reason behind these cancellations is that the Lagrangian has a $U(3)_L \otimes U(3)_E \otimes U(3)_N$ flavour symmetry, broken explicitly by the Yukawa couplings and right-handed neutrino masses. This restricts the way in which Yukawa couplings can combine to give a 3×3 flavour matrix of EDMs, that transforms in the $(3, 3, 1)$ representation. Detailed computations find that a detectable d_e can only arise if Y_N has large, order one, entries and if $\tan \beta$ is large.

In SUSY models LFV rates, and in particular the small electric dipoles, can receive other contributions not related to neutrino Yukawa couplings: this would complicate the situation.

13.6 Neutrinos in extra dimensions

The electric force between an electron and a proton is about 30 orders of magnitude stronger than their gravitational force. Supersymmetry can explain this huge number by relating the Fermi scale to the scale of supersymmetry breaking, that can naturally be much smaller than the Planck mass.

Different interpretations exist. If gravity propagates in d flat extra dimensions of radius R , while SM particles are confined on a 3+1 dimensional (mem)brane, the Newton force at $r \ll R$ is proportional to $1/r^{2+d}$. Depending on R and d , gravity can become strong at values of $1/r \sim M_D$ below the Planck scale. Choosing $M_D \sim \text{TeV}$ — the lowest value allowed by collider experiments — one could try to address the Higgs mass hierarchy problem in this context. The experimental success of the SM disfavors this drastic possibility, but only experiments that will start in ~ 2008 can exclude it. In the meantime, many authors explore its various phenomenological consequences. We review the ones concerning neutrinos.

Extra dimensions suggest a non-standard scenario for neutrinos. If right-handed neutrinos propagate in the extra dimensions, their Yukawa couplings to SM neutrinos are suppressed by M_D/M_{Pl} , like gravitational couplings. If one also assumes that Majorana neutrino masses are negligible (for example by imposing conservation of lepton number, that is no longer a good accidental symmetry as in the SM), this scenario gives small Dirac neutrino masses $m_\nu \sim v M_D/M_{\text{Pl}}$, somewhat smaller than what suggested by neutrino data. In non minimal models (e.g. with right-handed neutrinos propagating in $\delta < d$ extra dimensions, or with warped extra dimensions) the clean connection with gravity is lost and one can get any desired m_ν . For concreteness, we consider $4 + \delta$ -dimensional massless fermions $\Psi_i(x_\mu, y)$ which, inside their components, contain the “right-handed neutrinos” ν_{Ri} ($i = 1, 2, 3$ is the generation index). The fermions Ψ_i interact in our brane located at $y = 0$, through their components ν_{Ri} , with the lepton doublet L_i in a way that conserves total lepton number.

$$\mathcal{L} = [\mathcal{L}_{\text{SM}} - L_i \lambda_{ij} \nu_{Rj} H + \text{h.c.}] \delta(y) + \bar{\Psi}_i i \mathcal{D} \Psi_i \quad (13.17)$$

where $i \mathcal{D}$ is a $4 + \delta$ dimensional Dirac operator, H is the SM Higgs doublet and λ is a matrix of Yukawa couplings with dimensions $(\text{mass})^{-\delta/2}$. As manifest from (13.17), λ can be made diagonal without loss of generality at the price of introducing the usual unitary neutrino mixing matrix V . Using the KK decomposition

$$\Psi_i(x, \vec{y}) = \frac{1}{\sqrt{V}} \sum_{\vec{n}} \Psi_{\vec{n}i}(x) \exp\left(\frac{i \vec{n} \cdot \vec{y}}{R}\right), \quad (13.18)$$

where $V \equiv (2\pi R)^\delta$ is the volume of the extra dimensions, and performing the $d^\delta y$ integration, eq. (13.17) yields the 4-dimensional neutrino Lagrangian

$$\mathcal{L}_\nu = \bar{L}_i i\partial^\mu L_i + \sum_{\vec{n}} \bar{\Psi}_{\vec{n}i} \left(i\partial^\mu - \frac{\vec{n} \cdot \vec{\gamma}}{R} \right) \Psi_{\vec{n}i} - \left[\frac{\lambda_{ij}}{\sqrt{V}} L_i \nu_{R\vec{n}j} H + \text{h.c.} \right], \quad (13.19)$$

where $\vec{\gamma}$ are the extra-dimensional Dirac matrices. After electroweak symmetry breaking, neutrinos obtain a Dirac mass matrix $m_\nu = \lambda v / \sqrt{V}$, which are small if extra dimensions have a large volume. More interestingly, the above Lagrangian also describes the KK excitations ν_{Rn} ($n = 1, 2, 3, \dots$) of the right-handed neutrinos, which behave as a tower of sterile neutrinos with masses $m_n \sim n/R$ and mixing angles $\theta_n \sim m_\nu / m_n$ with the active ones. For simplicity we wrote explicit formulæ in the case of the simplest extra dimension, a δ -dimensional torus with equal radii R , but the phenomenon is quite general.

13.6.1 Oscillation signals of extra-dimensional neutrinos

If at least one extra dimension is large enough, some KK excitations can be light enough, to give detectable effects in neutrino oscillation experiments: $m_n \lesssim \text{eV}$. Since KK neutrinos are a particular form of sterile neutrinos, experimental data tell that they cannot be the source of the solar or atmospheric anomalies. One could try to use KK's to fit the LSND anomaly by choosing $1/R \sim \text{eV}$. In such a case the lightest KK ν_{1R} gives the dominant effect obtaining a scheme qualitatively similar to the ‘3+1’ scheme (see section 9.2). However: 1) the ‘3+1’ scheme has some tension with disappearance experiments and cosmology: these problems become slightly more serious in the ‘3+KK’ scheme. 2) unlike in the ‘3+1’ model, the minimal ‘3+KK’ model *predicts* the mixing angle between ν_{1R} and the SM neutrinos ν_ℓ to be $\pi V_{\ell 3} m_{\text{atm}} R / \sqrt{3}$ (assuming a hierarchical spectrum of active neutrinos; the other spectra are more problematic), which is too small in view of the CHOOZ bound on V_{e3} . 3) As discussed in the next section, $1/R \sim \text{eV}$ is not compatible with the observed SN1987A neutrino burst.

These problems can be alleviated by inventing less predictive non minimal models, obtained e.g. by adding 5-dimensional neutrino mass terms μ . At the end, one can introduce extra unknown parameters μ, μ' that modify the predictions for the masses of the KK into $m_n^2 \sim \mu^2 + (n/R)^2$ or into $m_n \sim \mu + n/R$ and the predictions for the mixing angles into $\theta_n \sim \mu' / m_n$, such that they are no longer related to neutrino masses.

In conclusion, oscillations into KK cannot be the source of observed oscillations, and do not give new appealing interpretations to existing anomalous results. If $1/R \gg \text{eV}$ the KK neutrinos have too small mixing angles to give detectable effects in future neutrino oscillation experiments. Still, there are two places where their effects could be seen.

13.6.2 Supernova signals of extra-dimensional neutrinos

The SN1987A observation puts severe constraints on extra dimensional right-handed neutrinos. This is because KK neutrinos can carry away from the supernova too much energy in invisible channels, thus weakening the observed neutrino burst in an unacceptable way. The energy loss rate in invisible channels, W_{inv} , must be less than about $10^{19} \text{ erg/gr} \cdot \text{sec}$ for typical average conditions of a SN core with a density $\rho \approx 3 \cdot 10^{14} \text{ gr/cm}^3$ and a temperature $T \approx 30 \text{ MeV}$ (see section 11.2). KK neutrinos can be produced both by incoherent scatterings and by coherent oscillations.

The rate of *incoherent production* of a single KK state is $\Gamma_{\text{inc}} \sim (m_\nu/E_\nu)^2 \Gamma_\nu$, where m_ν is the largest neutrino mass, $E_\nu \sim 3T \sim 100$ MeV is a typical neutrino energy and $\Gamma_\nu \approx G_F^2 n_N E^2$ is the collision rate of a standard neutrino in the supernova core, in terms of the nucleon density n_N . Multiplying for the number of KK states, approximately $(RE)^\delta$, the corresponding energy loss rate can be estimated as $W_{\text{inv}} \approx (m/E)^2 (RE)^\delta \cdot W_\nu$, where $W_\nu \approx 10^{27} \text{ erg/gr} \cdot \text{sec}$ is the energy loss rate produced by Γ_ν if the standard neutrinos were not trapped. Requiring $W_{\text{inv}}/W_\nu \lesssim 10^{-8}$ gives

$$R < 0.2 \text{ mm} \cdot 10^{-11(1-1/\delta)} \left(\frac{m^2}{10^{-3} \text{ eV}^2} \right)^{-1/\delta}. \quad (13.20)$$

Only in the case of a single large extra dimension, $\delta = 1$, the KK can be light enough to directly affect neutrino physics.

We now consider the effect of *coherent oscillations* of the active neutrino state associated with the mass m_ν into its KK tower. Depending on the sign of the matter potential $A \sim 10 \text{ eV}$ in the supernova core, MSW resonant oscillations will take place either in the neutrino or in the antineutrino channel, but not in both. KK states lighter than $m_n \approx n/R \approx (AE_\nu)^{1/2} \approx 10^4 \text{ eV}$ are involved in resonant transitions. The effect of these oscillations can be reliably estimated for small $\xi = m_\nu R$, because due to the small vacuum mixing angle between the n -th KK state and the standard neutrino, $\theta_n \approx \xi/n$, the width of the n -th resonance is smaller than the separation between two contiguous resonances. As a consequence, the survival probability for a standard neutrino (or antineutrino) produced in the core can be computed as the product of the survival probabilities in each resonance crossed during a mean free path, $P_{\nu\nu} \approx \prod_n P_n$. The survival probability at each level crossing is given by the Landau-Zener approximation (section 3.3), $P_n \approx e^{-\pi\gamma_n/2}$, where

$$\gamma_n \approx \frac{4\xi^2}{R^2 E} \frac{V}{dV/dr} \Big|_{\text{res}}$$

is the adiabaticity parameter at the n -th resonance crossing. Approximating $V/(dV/dr)$ with the radius of the core, $r_{\text{core}} \approx 10 \text{ km}$, γ_n is of order $m_\nu^2/(10^{-3} \text{ eV}^2)$ and is approximately n -independent. Hence the individual P_n are expected to deviate sensibly from unity. The condition $P_{\nu\nu} \lesssim 10^{-8}$ can be satisfied only if all KK are heavy enough that no resonance is crossed, $R \lesssim \text{Å}$.

If this condition is violated the SN gets strongly modified, possibly in an interesting and still allowed way. Depending on the sign of V (which can be different in different regions of the SN) either ν or $\bar{\nu}$ (but not both) promptly get converted into KK which escape from the SN. This process varies the chemical composition of the SN, and therefore the matter potential V . This fast loss of energy stops either when $V = 0$ is reached (if ν_e are involved) or due to Pauli blocking (when roughly all $\nu_{\mu,\tau}$ or all $\bar{\nu}_{\mu,\tau}$ have escaped). In this way about one half of the SN energy gets lost in KK. The remaining half is emitted in neutrinos, with non standard flavour ratios (typically more ν than $\bar{\nu}$). The constraint on the radius of the extra dimension gets relaxed at least down to $R \lesssim 10 \text{ Å}$: at larger R non-resonant oscillations produce too many KK. Detailed predictions have been computed only in non-minimal models, where R can be significantly larger.

13.6.3 Virtual signals of extra-dimensional neutrinos

Virtual exchange of extra-dimensional right-handed neutrinos at tree level gives the dimension-six operator (see fig. 13.6a)

$$\mathcal{L}_{\text{tree}} = \epsilon_{ij} 2\sqrt{2} G_F (H^\dagger \bar{L}_i) i\cancel{d} (H L_j), \quad (13.21)$$



Figure 13.6: *Tree-level and one-loop virtual effects of extra-dimensional right-handed neutrinos.*

where $\epsilon_{ij} = \epsilon_{ji}^*$ are dimensionless couplings. The hierarchy problem motivates TeV-scale quantum gravity, suggesting $\epsilon_{ij} \sim (v/\text{TeV})^2 \sim 10^{-\text{few}}$. In the minimal model of eq. (13.17) $\epsilon_{ij} \propto (m_\nu m_\nu^\dagger)_{ij}$, with an ultraviolet divergent proportionality factor, that can be only estimated by introducing some arbitrary cut-off. Exploiting the predicted flavour structure, the six ϵ_{ij} parameters can be expressed in terms of a single unknown ϵ as

$$\begin{aligned} \epsilon_{\tau\tau} \approx \epsilon_{\mu\mu} \approx \epsilon_{\mu\tau} \approx \frac{\epsilon}{2}, & \quad \epsilon_{ee} \approx \left(|V_{e3}|^2 + \frac{\Delta m_{\text{sun}}^2}{3\Delta m_{\text{atm}}^2} \right) \epsilon, \\ \epsilon_{e\mu} \approx \left(\frac{|V_{e3}|}{\sqrt{2}} + \frac{e^{-i\phi} \Delta m_{\text{sun}}^2}{3\Delta m_{\text{atm}}^2} \right) \epsilon, & \quad \epsilon_{e\tau} \approx \left(\frac{|V_{e3}|}{\sqrt{2}} - \frac{e^{-i\phi} \Delta m_{\text{sun}}^2}{3\Delta m_{\text{atm}}^2} \right) \epsilon, \end{aligned} \quad (13.22)$$

where we assumed normal hierarchy, maximal atmospheric mixing and $\tan^2 \theta_{12} = 1/2$.

The operators in eq. (13.21) induce potentially large flavour transitions $P(\nu_i \rightarrow \nu_j) \sim |\epsilon_{ij}^2|$ at $\mathcal{O}(L^0)$ (i.e. at very short baselines $L \ll E_\nu/\Delta m^2$), and CP-violating effects at $\mathcal{O}(L^1)$ (rather than at $\mathcal{O}(L^2)$ and $\mathcal{O}(L^3)$ as in ordinary oscillations). At one-loop level, other operators are generated, giving rise to rare muon and tau processes that violate lepton flavour (see fig. 13.6b). Again, the coefficients of these operators are cut-off dependent and can only be estimated; they are roughly suppressed by a four-dimensional loop factor $\sim \alpha/4\pi$ with respect to the tree level operator in (13.21). Their flavour structure is again dictated by the ϵ_{ij} parameters. Effects in charged leptons are suppressed by a one loop factor with respect to effects in neutrinos:

$$P(\nu_i \rightarrow \nu_j; L \approx 0) \sim |\epsilon_{ij}^2|, \quad \text{BR}(\ell_i \rightarrow \ell_j \gamma) \sim |e\epsilon_{ij}/4\pi|^2, \quad (i \neq j). \quad (13.23)$$

Present bounds from neutrino experiments and from charged lepton processes are summarized in table 1. Due to the loop factor, detectable neutrino effects are compatible with lepton flavour violating bounds.⁴ Values of $\epsilon_{ij} \gtrsim 10^{-4}$ (including possible CP-violating phases) will be probed

⁴SU(2)_L-invariant non renormalizable operators parameterize the low-energy effects of generic new physics too heavy for being directly probed. Various papers [166] studied how generic NRO could affect future neutrino experiments. However, a typical NRO affects both neutrinos and charged leptons at tree level (since they are unified into lepton doublets L). In such a case, present bounds on charged leptons prevent detectable effects in future neutrino experiments, except maybe in $\nu_\mu \leftrightarrow \nu_\tau$ transitions. The operator of eq. (13.21) is the simplest exception. Therefore it is interesting to study more generally which kind of new physics can induce it. It arises if lepton doublets mix at the TeV scale with ‘‘right-handed neutrinos’’. In four dimensions such models are not motivated by neutrino masses; conservation of lepton number (or something equivalent) must be imposed to avoid too large neutrino masses (see in [22]). Models with right-handed neutrinos in a warped extra dimension [22] also induce the operator in (13.21), but the connection between neutrino masses and ϵ_{ij} is extremely model dependent.

	present bounds from experiments with		future sensitivity from experiments with	
	neutrinos	charged leptons	neutrinos	charged leptons
$ \epsilon_{e\mu} $	< 0.05 (KARMEN)	$\lesssim 10^{-4}$ ($\mu \rightarrow e\gamma$)	$\sim 10^{-4}$ (ν factory)	$\sim 10^{-5 \div 6}$ (μ decays)
$ \epsilon_{e\tau} $	< 0.09 (NOMAD)	$\lesssim 10^{-1}$ ($\tau \rightarrow e\gamma$)	$\sim 10^{-4}$ (ν factory)	$\sim 10^{-1 \div 2}$ ($\tau \rightarrow e\gamma$)
$ \epsilon_{\mu\tau} $	< 0.013 (NOMAD)	$\lesssim 10^{-1}$ ($\tau \rightarrow \mu\gamma$)	$\sim 10^{-4}$ (ν factory)	$\sim 10^{-1 \div 2}$ ($\tau \rightarrow \mu\gamma$)
ϵ_{ee}	< 0.025 (reactors)	$\lesssim 10^{-3}$ (Z data)	$\sim 10^{-3}$ (ν factory)	$\sim 10^{-3 \div 4}$ (Z data)
$\epsilon_{\mu\mu}$	—	$\lesssim 10^{-3}$ (Z data)	$\sim 10^{-3}$ (ν factory)	$\sim 10^{-3 \div 4}$ (Z data)
$\epsilon_{\tau\tau}$	—	$\lesssim 10^{-2}$ ($Z \rightarrow \nu\bar{\nu}$)	—	$\sim 10^{-3}$ ($Z \rightarrow \nu\bar{\nu}$)

Table 13.2: *Bounds and future sensitivity reaches for the ϵ_{ij} coefficients defined by eq. (13.21).*

by future neutrino experiments. In the minimal model, μ, τ, π decays and precision LEP data imply $\epsilon \lesssim 0.004$.

Notice that the same low-energy physics can be obtained without extra dimensions, by mixing SM neutrinos with sterile neutrinos with TeV-scale pseudo-Dirac masses. The particular form of their mass matrix guarantees that lepton number is conserved, avoiding too large neutrino masses. In such renormalizable 4-dimensional models the estimates of eq. (13.23) can be replaced by precise results, which depend on the Yukawa couplings.

Chapter 14

Applications

Techniques developed for high-energy physics resulted into practical applications, but it seems hard to find practical applications for particles that decay in 10^{-20} sec. From this point of view, neutrinos might be an exception: unlike other particles not present in everyday life (such as muons, Z , W , etc...) neutrinos are light and stable. Furthermore, neutrinos can do things that ordinary particles present in everyday life (γ, e, p, n) cannot do: neutrinos can cross the earth or the sun without being absorbed. For practical purposes neutrinos have too much of this property: neutrino interaction rate are so small that neutrino detectors are big and expensive. Interaction rates grow with energy, but neutrino sources are more easily found at lower energies. Thanks to developments of detection techniques, neutrino physics already started to be relevant outside fundamental physics, and some more or less practical applications have been proposed [167]. Although short, this section exists.

Detectors such as CHOOZ and KamLAND have monitored the activity of nuclear reactors. A web of Mton-size $\bar{\nu}_e$ detectors could be used to discover and locate hidden nuclear reactors (as well as producing interesting physics): its cost is not out-of-scale if seen as a military project rather than as an experiment. KamLAND observed $\bar{\nu}_e$ emitted by radioactive material inside the earth [46], with results that agree with earth models. Neutrinos can be used to measure the density of the earth core. Solar experiments confirmed predictions of solar models, in particular the temperature around the center of the sun. Future experiments can test the expected low-energy features of the solar neutrino spectrum and search for eventual time variations of the solar neutrino rate. SK and SNO can see where the sun is during the night.

More importantly, earth matter effects are predicted to increase by a few % the rate of solar neutrinos detected during the night. Future big experiments could see this effect; furthermore matter inhomogeneities (e.g. oil instead of rock) located below the detector give rise to extra matter effects: a huge neutrino detector (installed e.g. in a submarine) has been discussed as a technique for searching oil.

Even more unrealistically, a neutrino beam with energy of about 1000 TeV has been discussed as a tool for destroying nuclear weapons.

Neutrinos also have unwanted effects. A circular $\mu^-\mu^+$ collider would allow higher energies than circular e^-e^+ colliders, because energy losses due to photon radiation get suppressed by a $(m_e/m_\mu)^4$ factor. However μ^\pm decay into e^\pm and $\langle\bar{\nu}\rangle$, giving rise to technical problems that can possibly be solved, but also to high-energy neutrino radiation which cannot be shielded and which would be too dangerous.

Appendix A

Acronyms

For clarity, we list many TAA (Technical Acronyms and Abbreviations) employed in neutrino physics and in our review.

$0\nu2\beta$	Neutrino-less double beta (decay).	GRB	Gamma Ray Burst.
AGN	Active Galactic Nucleus.	GUT	Grand Unified Theory.
BR	Branching Ratio.	IBD	Inverse Beta Decay, $\bar{\nu}_e p \rightarrow e^+ n$.
CMB	Cosmic Microwave Background.	KamLAND	Kamioka Liquid scintillator Anti-Neutrino Detector.
CC	Charged Current: scattering that transforms ν into charged leptons.	K2K	KEK to Kamioka long-baseline experiment.
CL	Confidence Level.	LEP	the most recent $e\bar{e}$ collider at CERN.
CNGS	CERN to Gran Sasso long baseline experiment.	LFV	Lepton Flavour Violation.
CP	Charge Conjugation times Parity.	LHC	Large (or Last) Hadron Collider.
CPT	CP times Time reversal.	LMA	Large Mixing Angle: the solution to the solar neutrino anomaly.
CR	Cosmic Rays.	LOW	a solution of the solar neutrino anomaly excluded by data.
DIS	Deep Inelastic Scattering.	LSND	A reactor experiment that claims $\bar{\nu}_\mu \rightarrow \bar{\nu}_e$ oscillations.
DM	Dark Matter.	LSZ	Landau-Stückelberg-Zener level crossing probability.
$DM\nu$	Neutrinos from DM annihilations.	MINOS	FermiLab to Homestake long-baseline experiment.
dof	degree of freedom.	MSSM	Minimal Supersymmetric Standard Model.
EDM	Electric Dipole Moment.	MSW	Matter corrections to neutrino oscillations.
ES	Electron Scattering (of neutrinos).	Mton	10^9 kg.
FWHM	Full Width at Half Maximum (of a bell).	NC	Neutral Current: scattering that does not transform ν into charged leptons.
FS	Free Streaming.		
GNO	Gallium Neutrino Observatory: a solar neutrino experiment.		

NRO	Non Renormalizable Operator.	SNR	SuperNova Remnant.
NS	Neutron Star.	SSM	Standard Solar Model.
PDF	Parton Distribution Function.	SUSY	SUperSYmmetry.
PDF	Portable Document Format.	T2K	Tokai to Kamioka: Japanese super-beam experiment.
PDF	Probability Distribution Function.	tof	time of flight.
pot	protons on target.	UHE	Ultra High Energy.
QFT	(Relativistic) Quantum Field Theory.	UNO	Underground Nucelon/Neutrino Observatory: project for a Mton detector.
QVO	Quasi-Vacuum Oscillations: a solution of the solar neutrino anomaly excluded by data.	vev	vacuum expectation value.
SK	SuperKamiokande: japanese experiment.	VO	Vacuum Oscillations: a solution to the solar neutrino anomaly excluded by data.
SM	Standard Model of particles.	WČ	Water Čerenkov: experimental technique.
SMA	Small Mixing Angle: a solution to the solar neutrino anomaly excluded by data.	WMAP	Wilkinson Microwave Anisotropy Probe.
SN	Supernova.	WKB	Wentzel-Kramers-Brillouin semiclassical approximation.
SNO	Sudbury Neutrino Observatory: a solar experiment.		

Appendix B

Statistics

The physics that we would like to learn is indirectly contained in some set of data. Since experiments need years and money, it is important to extract as much as information as possible with a correct and efficient use of statistics. Usually, this issue is crucial when new discoveries start emerging from experiments, and becomes less relevant after that data become so good that they speak by themselves.

According to a diffuse wrong impression, statistics is some difficult mathematics proofed centuries ago, so that a physicist interested in physics can apply it without understanding what he is doing. In real analyses, where non-standard situations occur, such attitude leads to violations of common sense at a numerically significant level. While experimental results are usually presented in a way which looks and is correct, reanalyses sometimes treat statistics in bizarre or inefficient ways. Statistical inference indeed is a delicate subject. Various subtle points lead to interesting philosophical discussions with no fully satisfactory solution. All details are carefully discussed in standard presentations, at the price of obscuring the numerically important part. We explain only the simple main tools, skipping all subtle points that are numerically irrelevant in most practical circumstances. In order to be concrete, we use a terminology specific of reanalyses of neutrino data — but the following discussions have a more general validity. We address the two following topics:

1. In section B.1 we explain how, given any theory, data can be used to infer the values of its free parameters.
2. Once 1. is done, we want to know if the theory describes data in a satisfactory way, or if the data contain an indication for some generic new physics. This issue is discussed in section B.2.

B.1 Statistical inference

We proceed in 3 steps. Readers who consider step 2 unsatisfactory can read step 2'.

1. Likelihood. We define the conditional probability $p(A|B)$ as the probability of A assuming that B is true. The starting point of any analysis is that we know $p(\text{data}|\text{theory})$: i.e. we can predict the probability distribution of observables assuming any given theory. This function is named ‘likelihood’ and describes what the experiment is doing. Experimental results should be reported in a way that allows to compute it. A typical example is $p(\text{data}|\text{theory}) = p(R|\Delta m^2, \theta)$

where $\Delta m^2, \theta$ are neutrino oscillation parameters that we want to infer from n measured neutrino rates R . It is convenient to write p in terms of a ‘chi-square’ χ^2 because in many cases it is a simple quadratic function of R

$$p(\text{data}|\text{theory}) = p(R|\Delta m^2, \theta) = \frac{\exp[-\chi^2/2]}{(2\pi)^{n/2} \sqrt{\det \sigma^2}} \quad \chi^2 = (R - T) \cdot \frac{1}{\sigma^2} \cdot (R - T) \quad (\text{B.1})$$

where $T(\Delta m^2, \theta)$ are the predicted rates and $\sigma^2(T)$ is the $n \times n$ error matrix.

We now discuss in which cases the likelihood is gaussian as function of R , so that we can use (B.1). The ‘central limit theorem’ shows that a random variable subject to many comparable statistical fluctuations follows a gaussian distribution. In some cases other distributions are appropriate (Poissonian for low counting rates, etc.). Often one does not know which bell to use. This is the case of ‘theoretical errors’ that arise e.g. when predictions can only be computed with a limited accuracy. It is pointless to debate if these errors should be described by a gaussian or by a flat distribution with the same standard deviation σ . The real issue is honestly *estimating* σ : doubling or halving the error is sometimes a matter of opinion. In such cases we choose a Gaussian because working with other shapes would be harder: approximating any bell with a Gaussian leads to important simple analytical results. This approximation may give an unrealistically low probability of many- σ fluctuations; however we do not really need to carefully distinguish a 10σ from a 20σ evidence: both are well established.

2. Bayesian inference. We have $p(\text{data}|\text{theory})$ and we want $p(\text{theory}|\text{data})$, i.e. we want to know the probability distribution that describes our knowledge of $\Delta m^2, \theta$, assuming that the data are true. Once we have $p(\Delta m^2, \theta|R)$ it is obvious how to use it: for example the 90% CL region is the set of θ and Δm^2 values with higher relative probability that encloses 90% of the total probability.

Up to a normalization factor $p(\text{theory}|\text{data})$ is given by the ‘Bayes theorem’ [168]

$$p(\text{theory}|\text{data}) \propto p(\text{data}|\text{theory})p(\text{theory}) \quad (\text{B.2})$$

easily demonstrated using elementary properties of probability:

$$p(A \text{ and } B) = p(A|B)p(B) = p(B|A)p(A).$$

Eq. (B.2) dictates how the information on the theory is updated from $p(\text{theory})$ to $p(\text{theory}|\text{data})$ when new experimental information $p(\text{data}|\text{theory})$ becomes available. In order to employ (B.2) for the first time, one needs to assume some arbitrary *a priori* probability distribution $p(\text{theory})$, called ‘prior’. There is no way of choosing a non-informative prior. For example a prior density probability flat in $\tan^2 \theta$ is different from a prior flat in $\sin^2 2\theta$, since the Jacobian relating these two variables is not constant (and divergent when $\theta \rightarrow \pi/4$). When data get so accurate that a ‘small’ θ range is selected, the initial arbitrariness becomes numerically irrelevant, since any reasonable prior is roughly constant in a small θ range.

3. Gaussian approximation. When data get accurate, the χ^2 can be well approximated, around its minimum, with a quadratic function of the theoretical parameters. In gaussian approximation the 90% CL region (2 dof) is the ellipse

$$\Delta\chi^2(\Delta m^2, \theta) < 4.61 \quad \text{where} \quad \Delta\chi^2(\Delta m^2, \theta) \equiv \chi^2(\Delta m^2, \theta) - \chi^2_{\min}.$$

In general, with N theoretical parameters θ_i one can analytically integrate their probability distribution over the $N - 1$ ‘angular’ combinations: the probability density of $z = \Delta\chi^2$ is

$$p_N(z) = \frac{2^{-N/2}}{\Gamma(N/2)} z^{N/2-1} e^{-z/2} \quad (\text{B.3})$$

To get the cut on $\Delta\chi^2$ corresponding to any desired CL, one has to perform the last integral in dz numerically, or read it from ‘tables of the χ^2 with N dof’. Here are some frequently used values:

	68.3%	90%	95%	99%	99.73%
1 dof	1	2.71	3.84	6.63	9
2 dof	2.30	4.61	5.99	9.21	11.8
3 dof	3.53	6.25	7.81	11.3	14.2

(B.4)

In general the PDF of θ_i has a non-Gaussian shape, maybe with few local minima (e.g. different solutions to the solar neutrino anomaly). Nevertheless a cut on the $\Delta\chi^2$ at the value that would be appropriate in the gaussian limit is usually an excellent approximation. Deviations from the gaussian approximation depend on the choice of the prior. Locally, one can always choose $p(\text{theory})$ to enforce this gaussian approximation.

We have discussed all essential points. In various circumstances one likes to perform some extra standard manipulations, that we now describe.

- Sometimes predictions depend on many unknown parameters, and one is interested in only a few of them. However a global fit gives a joint PDF for all parameters. For example one wants to extract from solar data the 2 oscillation parameters θ , Δm^2 . Solar fits involve other $k = N - 2$ parameters λ that describe the sun (e.g. the predicted neutrino rates depend on the flux of Boron neutrinos) and the response of the experimental apparatus. To focus on $\theta, \Delta m^2$ one considers the probability marginalized with respect to the ‘nuisance’ parameters λ :

$$p(\theta, \Delta m^2 | \text{data}) = \int d^k \lambda \, p(\theta, \Delta m^2, \lambda | \text{data}) \quad (\text{B.5})$$

In Gaussian approximation this reduces to

$$\chi^2(\theta, \Delta m^2) = \min_{\lambda} \chi^2(\theta, \Delta m^2, \lambda) \quad (\text{B.6})$$

and best fit regions are found cutting $\Delta\chi^2(\theta, \Delta m^2)$ at the $\Delta\chi^2$ value appropriate for 2 dof (Δm^2 and θ), not N dof. In fact, we now show how minimization over Gaussian nuisance parameters can be done analytically, and the result is equivalent to adding errors in quadrature. It is convenient to parameterize the χ^2 as follows. The k nuisance parameters λ shift the predictions T for the n observables as $T = T_0 + M \cdot \lambda$ where M is an $n \times k$ matrix. Forming the differences $\Delta = R - T = \Delta_0 - M \cdot \lambda$ between the measured and predicted values, one gets a χ^2 of the form

$$\chi^2 = \Delta^T \cdot V_0 \cdot \Delta + \lambda^T \cdot v \cdot \lambda \quad (\text{B.7})$$

where the symmetric matrices V_0 and v describe uncertainties on Δ and on λ . The χ^2 is minimized for

$$\lambda = \lambda_{\min} = (v + M^T \cdot V_0 \cdot M)^{-1} \cdot M^T \cdot V_0 \cdot \Delta_0$$

so that

$$\min_{\lambda} \chi^2 = \Delta_0^T \cdot V_0 \cdot \Delta_0 - \lambda_{\min}^T (v + M^T \cdot V_0 \cdot M) \lambda_{\min} = \Delta_0^T \cdot V \cdot \Delta_0$$

with

$$V = V_0 - V_0 \cdot M \cdot \frac{1}{v + M^T \cdot V_0 \cdot M} \cdot M^T \cdot V_0 = \left(\frac{1}{V_0} + M \cdot \frac{1}{v} \cdot M^T \right)^{-1}. \quad (\text{B.8})$$

The last expression for V is well known: Gaussian uncertainties can be combined by summing in quadrature individual contributions, and finally inverting the resulting $n \times n$ covariance matrix (where n is the number of data points). The first expression for V , or eq. (B.6), shows how the same result can be obtained by inverting a $k \times k$ matrix (where k is the number of individual sources of uncertainty). When k or n are large one approach (or a combination of the two) might be significantly simpler than the other one.

- Sometimes one is interested in all N parameters, but a function of $N > 2$ variables cannot be published on a 2-dimensional sheet of paper. Again, it is convenient to report marginalized probabilities. For example one can extract from solar data $p(\theta, \Delta m^2, \eta_s | R)$ (where η_s is the sterile neutrino fraction) and report $p(\theta, \Delta m^2 | R)$ and $p(\eta_s | R)$. In gaussian approximation, the 68% CL regions are obtained by cutting the $\Delta\chi^2$ at the appropriate values: $\Delta\chi^2(\theta, \Delta m^2) < 2.30$ (2 dof) $\Delta\chi^2(\eta_s) < 1$ (1 dof). Using $\Delta\chi^2 < 3.53$ (3 dof) is wrong, as pictorially illustrated in fig. B.1.
- Sometimes one wants to know one specific function $f(\theta)$ of the parameters θ extracted from a fit. Its PDF is

$$\begin{aligned} p(f) &= \int d^N \theta \, p(\theta | R) \, \delta(f(\theta) - f) && \text{Bayesian result} \\ \chi^2(f) &= \min_{\theta: f(\theta)=f} \chi^2(\theta) && \text{Gaussian approximation (1 dof)} \end{aligned} \quad (\text{B.9})$$

Two comments are in order. 1) When some of the parameters θ have a ‘large’ uncertainty the Bayesian analysis (assuming any reasonable prior) automatically disfavors values of f that require a fine-tuning of the unknown parameters. On the contrary the gaussian approximation does not introduce fine-tuning constraints. 2) When $f(\theta)$ is not a simple function, the minimization demanded by gaussian approximation can be conveniently performed using a Lagrange multiplier. In practice one builds $\chi^2(\theta) + \lambda f(\theta)$ and computes the location of its minimum $\theta(\lambda)$ as function of λ . By interpolating several points $(\chi^2(\theta(\lambda)), f(\lambda))$ one gets the desired $\chi^2(f)$.

One concrete problem where these two comments are useful is computing the range of the $0\nu2\beta$ observable $f = |m_{ee}|$ preferred by oscillation data.

2'. Neyman inference. Unlike steps 1 and 3, step 2 is not fully satisfactory because introduces the arbitrary prior. Various physicists prefer an alternative approach, suggested by Neyman [168].¹ It is useful and practicable only in special cases. In Gaussian approximation,

¹This is sometimes named *frequentist* approach, in order to emphasize that it only needs a restrictive definition of probability (based on the limiting frequency of repeated experiments) in place of the more flexible definition implicit in the Bayesian approach. A frequentistic definition of probability is adequate for e.g. uncertainties due to quantum fluctuations, but does not allow to include theoretical and systematic uncertainties (e.g. higher order QCD corrections do not fluctuate when the experiment is repeated). We use the name ‘Neyman inference’ because even with a Bayesian definition of probability the Neyman construction can be applied (as an alternative to the Bayes theorem) to build confidence regions.

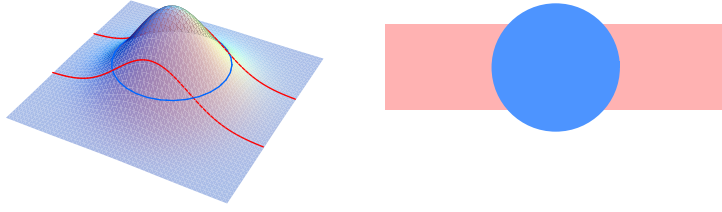


Figure B.1: *Two dimensional Gaussian: both the circle and the rectangle enclose 68% of the total probability. The diameter is larger than the height of the rectangle. Due to this trivial geometric effect, the $\Delta\chi^2$ depends on the number of dof, as exemplified in eq. (B.4).*

a proper Neyman construction gives the same results of the much simpler Bayesian approach. Therefore we just outline the basic points, without proving them.

Knowing the likelihood $p(\text{data}|\text{theory}) = p(R|\theta)$, for each value of θ one can build a range of R that contains 90% of the probability. If it contains the measured data point, that value of θ is accepted at 90% CL, because 90% of the families of ranges built in this way by repeating the same experiment contain the unknown true value. Even the Neyman inference contains an arbitrary choice: one can build a 90% range of R in many different ways. The simplest prescription is: build the range including first values of R with the highest $p(R|\theta)$ (Crow-Gardner ordering [168]). This is inefficient and unstable: in Gaussian approximation it reduces to a cut on the total χ^2 with $n - N$ dof (rather than on the $\Delta\chi^2$ with N dof).

A better prescription is: build the range including first values of R with the highest

$$p(R|\theta)/p(R|\theta_{\text{best}}(R)) \quad (\text{B.10})$$

(named by physicists as Feldman-Cousins [168] (FC) ordering, although it was already described e.g. on the book by Kendall-Stuart) where $\theta_{\text{best}}(R)$ is the best-fit value of the theoretical parameters as function of the possible experimental outcome R . In (B.10) the likelihood p is divided by the maximal value that p can get within the given theoretical model. Assuming that the theory is right, when we get an experimental outcome that is unlikely for all possible values of θ , we know that a statistical fluctuation occurred and we can correct for it. In this way the FC ordering recognizes and eliminates the statistical fluctuations that have nothing to do with the determination of the parameters. In Gaussian approximation it reduces to the cut on the $\Delta\chi^2$ discussed at point 3. If irrelevant data are included in the data-set, they contribute to the total χ^2 but cancel out when computing the $\Delta\chi^2$.

In special situations the FC regions can appreciably differ from their gaussian approximation. For example, when fitting oscillation data at values of Δm^2 so large that the oscillation probability practically depends only on the mixing angle θ (i.e. in region C of fig. 3.2) this technique recognizes that Δm^2 is no longer a relevant parameter and gives allowed regions that correspond to a cut on the $\Delta\chi^2$ with only 1 dof, rather than with 2 dof. When $n \gtrsim 10$ (i.e. there are more than ~ 10 data R), computing the FC regions exceeds the numerical capabilities of present computers, unless it is possible to reliably perform the necessary multi-dimensional integrations with MonteCarlo techniques. The FC construction looks intuitively obvious, when presented as a MonteCarlo procedure. The CL at which any given value of θ is accepted can be computed as follows:

- a) Compute the value of $r_{\text{exp}} = p(R|\theta)/p(R|\theta_{\text{best}}(R))$ (the $\Delta\chi^2$, in gaussian approximation), where R is the experimental result.
- b) Assuming the desired value of θ , generate a large enough sample of simulated experimental results R . For each R compute its value of r .
- c) Compute how frequently one obtains $r > r_{\text{exp}}$. This is the CL.

The extra manipulations described at point 3 can be performed by inventing appropriate non-standard ordering prescription or by adopting semi-Bayesian methods (e.g. marginalizing the likelihood). In gaussian approximation the final FC results agree with the much simpler Bayesian results previously discussed.

B.2 Goodness-of-fit

In the previous section we discussed how to use data to infer unknown theoretical parameters, assuming that the theory is true. We now discuss *how to test if the theory describes data in a good way?* This is a more difficult question that does not have a fully satisfactory answer nor a fully precise meaning. But of course this is what we want to know.

The true answer is: *look carefully at data searching for possible problems*. This seems ‘artificial’, but we do not know any ‘scientific’ statistical test that can be blindly applied giving efficient answers in the general case.

We first describe the frequently used Pearson χ^2 test, that provides one ‘objective’ answer. Let us consider $z = \min \chi^2$, the value of the total χ^2 evaluated at the best-fit point. If the theory and the data are correct, one expects that eq. (B.3) gives its probability distribution $p_N(z)$ where N is the total number of degrees of freedom:

$$N = \text{number of data points} - \text{number of unknown parameters}.$$

One usually reports the goodness-of-fit (gof), defined as the probability of having a z larger than the measured value. Gof values can be read, as function of z , from tables or computer codes.

For $N \gg 1$ p_N can be approximated by a Gaussian with mean $\mu_N = N$ and standard deviation $\sigma_N = \sqrt{2N}$: one expects $\min \chi^2 = N \pm \sqrt{2N}$. σ_N grows with N because when $N \gg 1$ one should expect some rare statistical fluctuation in the data-set: e.g. it is not unlikely to find a 4σ anomaly in a set of 100 data. If the anomaly is there because the theory makes a 4σ wrong prediction, the χ^2 test is not good enough to recognize that the theory is wrong. A practical example: the solar neutrino data-set has $N \sim 100$ observables and, according to the χ^2 test, some excluded solutions still have an acceptable gof.

A fit can be bad for different reasons. Depending on the specific case, it can be easy to perform an alternative more efficient test. In a real analysis one often encounters a mix of the following typical situations.

- a) A simple recipe allows to improve the efficiency of the Pearson χ^2 test while maintaining its general validity. *Perform the standard Pearson χ^2 test including only the data that really test the theory.* The improvement can be significant because data-sets are often chosen in the opposite way, including even irrelevant data. Authors like to claim “we perform a complete analysis” and feel not politically correct to drop results given by less accurate

experiments. Indeed, fitting all data is the right way to get the best possible inferences on unknown parameters: the tools discussed in the previous section automatically ignore statistical fluctuation unrelated to determination of parameters. But putting all together is not the right way of checking if some gof problem is present. For example, using many energy bins with width smaller than the energy resolution does not affect best-fit regions, but affects the total χ^2 deteriorating its efficiency.

b) *In some cases the fit is bad because different pieces of data are mutually incompatible*, in any ‘reasonable’ theory. For example let us suppose that an experiment receives a flux of neutrinos, known to be time-independent, finding $100 \pm \sqrt{100}$ events during the first year and $200 \pm \sqrt{200}$ in the second year. While a naïve Pearson χ^2 test would tell that any theory is disfavored, a ‘reasonable’ result is obtained by fitting the total number of events, as suggested in a).

It is interesting to notice that the rate per year is of course given by $\frac{1}{2}(300 \pm \sqrt{300})$, equal to the weighted average of the two annual rates. This shows that, if the discrepancy between 100 and 200 is due to a statistical fluctuation, it is wrong to enlarge the error on the average rate (possibly following one of the proposed recipes). Errors should be enlarged only if one thinks that there is something wrong in the experiment.

c) *In some cases the fit is bad because different pieces of data are mutually incompatible within the assumed theory*. In these cases one can perform a dedicated test. For example, the SMA solution to the solar neutrino problem was first excluded because it can not suppress the rates without also giving unseen spectral distortions. Splitting the data into 2 sets (rates and spectra) and fitting them separately, the SK collaboration obtained two disjoint best-fit regions, thereby showing that SMA oscillations allowed by rates were not allowed by spectral data.

Since there are many ways of splitting data into different sets, with this procedure one may obtain artificially low gof values by choosing a particular splitting after having seen the data. This is a well known practical problem of various statistical analyses. Therefore the splitting should be justified by honest physical motivations.

Acknowledgments We would like to thank our numerous collaborators; some of our recent papers arose as pieces of this review that needed original work. Special thanks to E. Bellotti, R. Bernabei, A. Bettini, C. Bucci, C. Cattadori, F. Cavanna, O. Cremonesi, S. Dugad, W. Fulgione, P.L. Ghia, A. Giuliani, W. Hofmann, H.V. Klapdor-Kleingrothaus, G. Mills, O. Palamara, G. Riccobene for the help with experimental data and interpretations; to F. Aharonian, J.F. Beacom, C. Distefano, G. Fiorentini, N. Fornengo, V.S. Imshennik, M. Kachelrieß, P. Lipari, T. Montaruli, D.K. Nadyozhin, G. Navarra, O. Ryazhskaya, K. Sato, M. Selvi for discussions and explanations regarding astrophysics/astroparticle physics; to R. Barbieri, G. Battistoni, Z. Berezhiani, W. Buchmuller, A. Butkevich, M. Chen, M. Cirelli, G. Co, S. Davidson, T. Hambye, F. Feruglio, K. Kar, A. Ianni, R.N. Mohapatra, B. Mukhopadhyaya, M. Nishimura, E. Paschos, N. Paver, S. Petcov, M. Picariello, M. Raidal, A. Romanino, R. Rattazzi, S. Rigolin, E. Roulet, R. Thorne, P. Vogel, T. Yanagida for help with various theoretical aspects. F.V. is particularly grateful to V.S. Berezinsky, S. Bertolini, M.L. Costantini, F. Nesti, G. Senjanović, A.Yu. Smirnov.

Preliminary versions of this review have been available since 2002 at www.cern.ch/astrumia/review.html, presented at the XI Seminario Nazionale di Fisica Teorica, Parma 2002, lost in a disk crash in 2003, eaten by S. Strumia in 2004, stolen in Madrid metro in 2005.

Bibliography

[1] **First papers about neutrinos.** W. Pauli, letter to “radioactive ladies and gentlemen” at the Tübingen conference, 4 dec. 1930. Effective theory of weak interactions: E. Fermi, “Tentativo di una teoria dei raggi β ”, *Nuovo Cim.* 11 (1934) 1. E. Fermi, “Versuch einer Theorie der β -Strahlen”, *Zeitschrift für Physik* 88 (1934) 161. Neutrinos seen: F. Reines, C.L. Cowan, *Phys. Rev.* 92 (830) 1953. C.L. Cowan, F. Reines, F.B. Harrison, H.W. Kruse, A.D. McGuire, *Science* 124 (1956) 123. Neutrinos are left-handed: M. Goldhaber, L. Grodzins, A.W. Sunyar, *Phys. Rev.* 109 (1958) 1015.

[2] **Oscillations.** $\nu \leftrightarrow \bar{\nu}$ transitions were discussed in B. Pontecorvo, *J. Exp. Theor. Phys.* 33 (1957) 549. B. Pontecorvo, *J. Exp. Theor. Phys.* 34 (1958) 247. It is now clear that the $\nu \leftrightarrow \bar{\nu}$ amplitude is negligible because suppressed by m_ν/E_ν . A derivation of the flavour vacuum oscillation formula was given (with a wrong factor 2 in the oscillation phase) in V. Gribov, B. Pontecorvo, *Phys. Lett.* B28 (1969) 493. See also B. Pontecorvo, *Sov. Phys. JETP* 26 (1967) 984.

[3] **Neutrino mixing matrix.** The commonly cited reference is: Z. Maki, M. Nakagawa, S. Sakata, *Prog. Theor. Phys.* 28 (1962) 870. The same group later discussed flavour mixing related to neutrino masses (rather than to a hypothetical lepton-hadron unification), see M. Nakagawa, H. Okonogi, S. Sakata, A. Toyoda, *Prog. Theor. Phys.* 30 (1963) 727. Mixed neutrinos had been previously discussed in Y. Katayama, K. Matumoto, S. Tanaka, E. Yamada, *Prog. Theor. Phys.* 28 (1962) 675. None of these authors mentioned neutrino oscillations, proposing instead $\mu \rightarrow e\gamma$ and related processes as experimental signals of lepton flavour violation. These kinds of flavour transitions have been instead observed in hadrons. The CKM matrix describing flavour mixing among hadrons (and later quarks) has been introduced later, see N. Cabibbo, *Phys. Rev. Lett.* 10 (1963) 531. M. Kobayashi, T. Maskawa, *Prog. Theor. Phys.* 49 (1973) 652.

[4] **Chlorine experiment.** The experimental technique was suggested in B. Pontecorvo, Chalk River Lab. PD-205 report (1946). See also L.W. Alvarez, UCRL-328 report (1949). First results were announced in R. Davis, *Phys. Rev. Lett.* 12 (1964) 302. R. Davis et al., *Phys. Rev. Lett.* 20 (1968) 1205. The final results of the Homestake experiment are reported in B.T. Cleveland et al., *Astrophys. J.* 496 (1998) 505.

[5] **Atmospheric data.** First hints of the atmospheric anomaly were presented in: Kamiokande collaboration, *Phys. Lett.* B205 (1988) 416. The first convincing evidence was presented in SuperKamiokande collaboration, *Phys. Rev. Lett.* 81 (1998) 1562. $\nu_\mu \rightarrow \nu_\tau$ versus $\nu_\mu \rightarrow \nu_s$: SuperKamiokande collaboration, *Phys. Rev. Lett.* 85 (2000) 3999 ([hep-ex/0009001](#)). Latest data: SuperKamiokande collaboration, *Phys. Rev.* D71 (2005) 112005 ([hep-ex/0501064](#)). SuperKamiokande collaboration, [hep-ex/0604011](#). Comparison with alternative non-oscillatory models: talk by K. Okumura at the workshop “Neutrino oscillations in Venice”, 2003. See also talks at the Neutrino 2004 conference, web site [neutrino2004.in2p3.fr](#). Hint for an oscillation dip: SuperKamiokande collaboration, *Phys. Rev. Lett.* 93 (2004) 101801 ([hep-ex/0404034](#)). (See however N. Takahashi, A. Misaki, [hep-ex/0505020](#)). The energy dependence of the atmospheric anomaly was analyzed in G. Fogli, E. Lisi, A. Marrone, *Phys. Rev.* D64 (2001) 093005 ([hep-ph/0105139](#)). M. Gonzalez-Garcia, M. Maltoni, *Phys. Rev.* D70 (2004) 033010 ([hep-ph/0404085](#)).

MACRO performed competitive measurements of through-going up muons: MACRO collaboration, *Phys. Lett.* B517 (2001) 59 ([hep-ex/0106049](#)). MACRO collaboration, *Phys. Lett.* B566 (2003) 35 ([hep-ex/0304037](#)). For a recent analysis of SOUDAN-2 data see SOUDAN-2 collaboration, *Phys. Rev.* D72 (2005) 052005 ([hep-ex/0507068](#)). MINOS data about atmospheric neutrinos: MINOS collaboration, *Phys. Rev.* D73 (2006) 072002 ([hep-ex/0512036](#)).

[6] **K2K.** K2K and SK collaborations, *ECONF* C020805 (2002) TTH02 ([hep-ex/0212035](#)). K2K collaboration, *Phys. Rev. Lett.* 90 (2003) 041801 ([hep-ex/0212007](#)). K2K collaboration, *Phys. Rev. Lett.* 94 (2005) 081802 ([hep-ex/0411038](#)). Talk by L. Ludovici at the NuFact 2005 conference, web site [www.lngs.infn.it/conference/2005/nufact05](#). K2K gives a bound on θ_{13} , subdominant with respect to the CHOOZ bound: K2K collab-

oration, *Phys. Rev. Lett.* 96 (2006) 181801 ([hep-ex/0603004](#)).

[7] **NuMi**. The first results, presented at the Joint Theoretical Experimental Seminar, Fermilab, 30/3/2006, are available from the web site: www-numi.fnal.gov. See also MINOS collaboration, [hep-ex/0605058](#).

[8] **Gallium experiments**. GALLEX collaboration, *Phys. Lett.* B447 (1999) 127. SAGE collaboration, *Phys. Rev.* C60 (1999) 055801. Calibration of the GALLEX experiment: GALLEX collaboration, *Phys. Lett.* B342 (1995) 440. Calibration of the SAGE experiment: SAGE collaboration, *Phys. Rev.* C73 (2006) 045805 ([nucl-ex/0512041](#)) and refs therein. Time dependence of the solar ν_e rate: SAGE collaboration, *J. Exp. Theor. Phys.* 95 (2002) 181 ([astro-ph/0204245](#)). Final GNO results: GNO collaboration, *Phys. Lett.* B616 (2005) 174 ([hep-ex/0504037](#)). Latest GALLEX, GNO and SAGE data have been presented in a talk by C. Cattadori at the ‘Neutrino 2004’ conference (Paris, 14-19 June), web site neutrino2004.in2p3.fr.

[9] **SK solar results**. Kamiokande final results: Kamiokande collaboration, *Phys. Rev. Lett.* 77 (1996) 1683. Super-Kamiokande final results: Super-Kamiokande collaboration, [hep-ex/0508053](#). Constraint on $\nu_e \rightarrow \bar{\nu}_e$: SuperKamiokande collaboration, *Phys. Rev. Lett.* 90 (2003) 171302 ([hep-ex/0212067](#)). Day night asymmetry: SuperKamiokande collaboration, *Phys. Rev.* D69 (2004) 011104 ([hep-ex/0309011](#)). Recent detailed results can be found in the theses listed by the SK web page: www-sk.icrr.u-tokyo.ac.jp/doc/sk/pub.

[10] **SNO**. First phase: SNO collaboration, *Phys. Rev. Lett.* 87 (2001) 071301 ([nucl-ex/0106015](#)). Second phase: SNO collaboration, *Phys. Rev. Lett.* 89 (2002) 011301 ([nucl-ex/0204008](#)). SNO collaboration, *Phys. Rev. Lett.* 89 (2002) 011302 ([nucl-ex/0204009](#)). More details are provided in SNO collaboration, *ECONF* C020805 (2002) TTH01 ([hep-ex/0211013](#)). Third phase: SNO collaboration, *Phys. Rev. Lett.* 92 (2004) 181301 ([nucl-ex/0309004](#)). See also the SNO web site www.sno.phy.queensu.ca.

[11] **KamLAND**. KamLAND collaboration, *Phys. Rev. Lett.* 90 (2003) 021802 ([hep-ex/0212021](#)). KamLAND collaboration, *Phys. Rev. Lett.* 94 (2005) 081801 ([hep-ex/0406035](#)). Web page: www.awa.tohoku.ac.jp/html/KamLAND.

[12] **LSND**. LSND collaboration, *Phys. Rev. Lett.* 81 (1998) 1774. LSND collaboration, *Phys. Rev.* D64 (2001) 112007 ([hep-ex/0104049](#)).

[13] **Karmen**. KARMEN collaboration, *Phys. Rev.* D65 (2002) 112001 ([hep-ex/0203021](#)).

[14] **NuTeV**. NuTeV collaboration, *Phys. Rev. Lett.* 88 (2002) 091802 ([hep-ex/0110059](#)).

[15] **Evidence for $0\nu2\beta$?** First claim: H.V. Klapdor-Kleingrothaus et al., *Mod. Phys. Lett.* A16 (2001) 2409. Problematic aspects of the claim were discussed by various authors. Appendix A of F. Feruglio, A. Strumia, F. Vissani, *Nucl. Phys.* B637 (2002) 345 ([hep-ph/0201291](#)). C.E. Aalseth et al., *Mod. Phys. Lett.* A17 (2002) 1475 ([hep-ex/0202018](#)). A. Ianni, LNGS/EXP-01/03 preprint. Y.G. Zdesenko, F.A. Danevic, V.I. Tretyak, *Phys. Lett.* B546 (2002) 206. H.L. Harney, *Mod. Phys. Lett.* A16 (2001) 2409. A.M. Bakalyarov et al., *Phys. Part. Nucl. Lett.* 2 (2005) 77 ([hep-ex/0309016](#)). The claim was strongly defended in: H.V. Klapdor-Kleingrothaus, [hep-ph/0205228](#). H.V. Klapdor-Kleingrothaus, *Found. of Phys.* 32 (2002) 1181. Recent measurement of ^{214}Bi spectrum: H.V. Klapdor-Kleingrothaus et al., *Nucl. Instrum. Meth.* A511 (2003) 335 ([hep-ph/0309157](#)). H.V. Klapdor-Kleingrothaus et al., *Phys. Lett.* B578 (2004) 54 ([hep-ph/0312171](#)). Latest data (with $\sim 30\%$ additional statistics): H.V. Klapdor-Kleingrothaus et al., [hep-ph/0404062](#).

[16] **$0\nu2\beta$ experiments**. The Germanium technique was proposed in E. Fiorini, A. Pullia, G. Bertolini, F. Cappellani, G. Restelli, *Phys. Lett.* B25 (1967) 602. Recent data: HEIDELBERG–Moscow collaboration, *Eur. Phys. J.* A12 (2001) 147 ([hep-ph/0103062](#)). IGEX collaboration, *Phys. Rev.* C65 (2002) 092007 ([hep-ex/0202026](#)).

CUORICINO collaboration, [hep-ex/0501034](#) and [hep-ex/0505045](#). NEMO3 collaboration, [hep-ex/0605104](#). Future experiments: MAJORANA collaboration, [nucl-ex/03011013](#). CUORE collaboration, [hep-ex/0501010](#). Alternatives to $0\nu2\beta$? See M. Ikeda et al., [hep-ph/0506062](#).

[17] **$\mu \rightarrow e\gamma$** . R. Bolton et al., *Phys. Rev.* D38 (1988) 2077. MEGA collaboration, *Phys. Rev. Lett.* 83 (1999) 1521. The next future experiment seems MEG at PSI, web page meg.web.psi.ch.

[18] **The GZK cut-off**. The GZK cut-off was first discussed in: K. Greisen, *Phys. Rev. Lett.* 16 (1966) 748. Recent experimental data: AGASA collaboration, *Astropart. Phys.* 19 (2003) 447 ([astro-ph/0209422](#)). HiRes collaboration, *Astropart. Phys.* 23 (2005) 157 ([astro-ph/0208301](#)).

Z-burst mechanism: T. Weiler, *Phys. Rev. Lett.* 49 (1982) 234 and erratum *ibidem* 12 (2000) 379. E. Roulet, *Phys. Rev.* D47 (1993) 5247. S. Yoshida et al., *Astrophys. J.* 479 (1997) 547. O.E. Kalashev et al., *Phys. Rev.* D65 (2002) 103003 ([hep-ph/0112351](#)). For a recent review see e.g. A. Ringwald, [hep-ph/0111112](#). Constraints from observed γ radiation: GLUE experiment: P. Gorham et al., *Phys. Rev. Lett.* 93 (2004) 041101. FORTE experiment: N. Lehtinen et al., *Phys. Rev.* D69 (2004) 013008.

[19] **Thermal leptogenesis.** M. Fukugita, T. Yanagida, *Phys. Lett.* B174 (1986) 45. The CP-asymmetry has been computed in E. Roulet, L. Covi, F. Vissani, *Phys. Lett.* B424 (1998) 101 ([hep-ph/9712468](#)). W. Buchmüller, M. Plümacher, *Phys. Lett.* B431 (1998) 354 ([hep-ph/9710460 version 2](#)). M. Flanz, E.A. Paschos, *Phys. Rev.* D58 (1998) 11309 ([hep-ph/9805427](#)). A. Pilaftsis, *Int. J. Mod. Phys.* A14 (1999) 1811 ([hep-ph/9812256](#)) (and references therein). For earlier attempts see e.g. A. Yu. Ignatiev, V. A. Kuzmin, M. E. Shaposhnikov, *JETP Lett.* 30 (1979) 688. F. J. Botella, J. Roldan, *Phys. Rev.* D44 (1991) 966. J. Liu, G. Segré, *Phys. Rev.* D48 (1993) 4609. B. A. Campbell, S. Davidson, K. A. Olive, *Nucl. Phys.* B399 (1993) 111. M. Flanz, E.A. Paschos, U. Sarkar, *Phys. Lett.* B345 (1995) 248. L. Covi et al., *Phys. Rev.* D57 (1998) 93 ([hep-ph/9704366](#)). First attempts of solving Boltzmann equations: M.A. Luty, *Phys. Rev.* D45 (1992) 455. M. Plümacher, *Z. Phys.* C74 (1997) 549 ([hep-ph/9604229](#)). Resonant processes: see the discussion in E.W. Kolb, S. Wolfram, *Nucl. Phys.* B172 (1980) 224, erratum *ibid.* B195 (1982) 542. Thermal and RGE corrections, correct subtraction of resonant processes, reheating effects have been included in G.F. Giudice, A. Notari, M. Raidal, A. Riotto, A. Strumia, *Nucl. Phys.* B685 (2004) 89 ([hep-ph/0310123](#)) that also contains a review of the basic formalism. Flavour effects have been included in R. Barbieri, P. Creminelli, N. Tetradis, A. Strumia, *Nucl. Phys.* B575 (2000) 61 ([hep-ph/9911315](#)). A. Abada, S. Davidson, F. Josse-Michaux, M. Losada, A. Riotto, *JCAP* 0604 (2006) 004 ([hep-ph/0601083](#)). E. Nardi, Y. Nir, E. Roulet, J. Racker, *JHEP* 01 (2006) 164 ([hep-ph/0601084](#)). A. Abada, S. Davidson, F. Josse-Michaux, M. Losada, A. Riotto, [hep-ph/0605281](#). One can approximate flavored Boltzmann equations with unflavored equations, provided that their parameters are chosen in a suitable way.

[20] www.ippp.dur.ac.uk/pre-SUSY05/seminars/haber.pdf

[21] The **see-saw** is such a natural extension of the SM that does not have a clear father. In our opinion the original reference should be P. Minkowski, *Phys. Lett.* B 67 (1977) 421. However the usually quoted references are M. Gell-Mann, P. Ramond and R. Slansky, proceedings of the supergravity Stony Brook workshop, New York, 1979 (ed.s P. Van Nieuwenhuizen and D. Freedman, North-Holland, Amsterdam). T. Yanagida, proceedings of the workshop on unified theories and baryon number in the universe, Tsukuba, Japan 1979 (ed.s O. Sawada and A. Sugamoto, KEK Report No. 79-18, Tsukuba). S.L. Glashow in “Quarks and Leptons”, Cargése, 1979 (ed.s M. Lévy et al., North Holland 1980, Amsterdam). R.N. Mohapatra, G. Senjanović, *Phys. Rev. Lett.* 44 (1980) 912.

In any case the general idea of generating effective operators by exchanging heavy particles was already known (e.g. from unification models): see e.g. H. Georgi, S.L. Glashow, *Phys. Rev. Lett.* 32 (1974) 438; The paper by Froggatt and Nielsen in [169]; S. Weinberg, *Phys. Rev. Lett.* 43 (1979) 1566.

[22] **Alternative sources of neutrino masses.** Exchange of a fermion $SU(2)_L$ triplet instead of a fermion singlet was discussed in R. Foot, H. Lew, X.-G. He, G. C. Joshi, *Z. Phys.* C44 (1989) 441. Exchange of a scalar triplet was discussed in G. B. Gelmini, M. Roncadelli, *Phys. Lett.* 99B (1981) 411. Neutrino mass could also arise from loop diagrams, exchanging various possible kinds of particles: E. Ma, *Phys. Rev. Lett.* 81 (1998) 1171 ([hep-ph/9805219](#)). E. Ma, [hep-ph/0605180](#). TeV-scale see-saw: J. Bernabéu et al., *Phys. Lett.* B187 (1987) 303. G.C. Branco, D. Delépine, B.M. Nobre, J. Santiago, *Nucl. Phys.* B657 (2003) 355 ([hep-ph/0209263](#)). Neutrino masses from SUSY breaking: N. Arkani-Hamed, L. Hall, H. Murayama, D. Smith, N. Weiner, *Phys. Rev.* D64 (2001) 115011 ([hep-ph/0006312](#)). F. Borzumati, Y. Nomura, *Phys. Rev.* D64 (2001) 053005 ([hep-ph/0007018](#)). From R -parity violation: see e.g. E.J. Chun, S.K. Kang, C.W. Kim, U.W. Lee, *Nucl. Phys.* B544 (1999) 89 ([hep-ph/9807327](#)). O.C.W. Kong, *Mod. Phys. Lett.* A14 (1999) 903 ([hep-ph/9808304](#)). S. Rakshit, G. Bhattacharyya, A. Raychaudhuri, *Phys. Rev.* D59 (1999) 091701 ([hep-ph/9811500](#)). B.C. Allanach, A. Dedes, H.K. Dreiner, *Phys. Rev.* D60 (1999) 075014 ([hep-ph/9906209](#)). E.J. Chun, S.K. Kang, *Phys. Rev.* D61 (2000) 075012 ([hep-ph/9909429](#)). S. Davidson, M. Losada, *JHEP* 005 (2000) 021 ([hep-ph/0005080](#)). S. Davidson, M. Losada, *Phys. Rev.* D65 (2002) 075025 ([hep-ph/0010325](#)). A.

Abada, G. Moreeau, [hep-ph/0604216](#). Small neutrino masses from supersymmetric couplings arise more naturally if supersymmetric particles have masses much above the weak scale. One can even build a minimal predictive model where supersymmetry unifies neutrino masses with charged lepton masses: a detailed computation shows that predictions are wrong.

Neutrino masses from warped extra dimensions: Y. Grossman, M. Neubert, *Phys. Lett.* B474 (2000) 361 ([hep-ph/9912408](#)). Neutrino masses from low-energy breaking of discrete symmetries: H. Davoudiasl, R. Kitano, G.D. Kribs, H. Murayama, *Phys. Rev.* D71 (2005) 113004 ([hep-ph/0502176](#)). Neutrino masses from ‘very special relativity’: A.G. Cohen, S.L. Glashow, [hep-ph/0605036](#).

[23] **Majorana phases.** Although the existence of additional (Majorana) phases was perhaps known even before, they were not discussed until S.M. Bilenkii, J. Hosek, S.T. Petcov, *Phys. Lett.* B94 (1980) 495. P. Langacker, S.T. Petcov, G. Steigman, S. Toshev, *Nucl. Phys.* B282 (1987) 589. J. Schechter, J.W. Valle, *Phys. Rev.* D22 (1980) 2227. Their observability in $0\nu2\beta$ decay was first remarked in M. Doi, T. Kotani, H. Nishiura, K. Okuda, E. Takasugi, *Phys. Lett.* B102 (1981) 323.

[24] J.A. Casas, A. Ibarra, *Nucl. Phys.* B618 (2001) 171 ([hep-ph/0103065](#)).

[25] We only list few instructive cases. S. Mohanty, [hep-ph/9702428](#) suggested that neutrinos emitted in decays of particles with life-time τ already oscillated for a time $\sim \tau$. A.H. Guth, L. Randall, M. Serna, JHEP 9908 (1999) 018 ([hep-ph/9903464](#)) rediscussed solar oscillations with $\theta = \pi/4$. A. de Gouvea, A. Friedland, H. Murayama, *Phys. Lett.* B490 (2000) 125 ([hep-ph/0002064](#)) rediscussed solar oscillations with $\theta > \pi/4$. S. De Leo, G. Ducati, P. Rotelli, *Mod. Phys. Lett.* A15 (2000) 2057 ([hep-ph/9906460](#)) emphasizes ambiguous factors of 2 in the oscillation phase. M. Blasone, G. Vitiello, *Phys. Rev.* D60 (1999) 111302 ([hep-ph/9907382](#)) presents a clean approach based on free fields, building a neutrino Fock space based on a coherent vacuum state. However the vacuum state in which we live is different, because gauge interactions exist and erase the coherences. K. Fujii, C. Habe, T. Yabuki, *Phys. Rev.* D64 (2001) 013011 ([hep-ph/0102001](#)). K.C. Hannabuss, D.C. Latimer, *J. Phys.* A36 (2003) 69 ([hep-th/0207268](#)). S. De Leo, C.C.Nishi, P.P.Rotelli, [hep-ph/0208086](#) and [hep-ph/0208086](#). J.H. Field, [hep-ph/0110064](#). L. B. Okun, M. G. Schepkin, I. S. Tsukerman, *Nucl. Phys.* B650 (2003) 443 ([hep-ph/0211241](#)). C.J. Horowitz, [hep-ph/0212012](#). S. De Leo, C.C. Nishi, P. Rotelli, [hep-ph/0303224](#). C. Giunti, [hep-ph/0302045](#) and [hep-ph/0312180](#) presents a theory of neutrino oscillations criticized in L.B. Okun et al., [hep-ph/0312280](#) and [hep-ph/0312151](#) and H.J. Lipkin, [hep-ph/0312292](#). Kh. M. Beshoev, [hep-ph/0304157](#). A. Friedland, C. Lumnardini, *JHEP* 10 (2003) 043 ([hep-ph/0307140](#)). V. Pazma, J. Vanko, [hep-ph/0311090](#).

[26] **Vacuum oscillations.** L. Stodolsky, *Phys. Rev.* D58 (1998) 036006 ([hep-ph/9802387](#)). H.J. Lipkin, [hep-ph/9901399](#). A. De Rujula, lessons at CERN.

[27] **Neutrino wave-packets.** See e.g. B. Kayser, *Phys. Rev.* D24 (1981) 110. C. Giunti, C.W. Kim, *Phys. Rev.* D58 (1998) 017301 ([hep-ph/9711363](#)). J.T. Peltoniemi and V. Sipilainen, *JHEP* 0006 (2000) 011 ([hep-ph/0004162](#)). Y Takeuchi et al., *Prog. Theor. Phys.* 105 (2001) 471 ([hep-ph/0006334](#)). M. Beuthe, *Phys. Rep.* 375 (2003) 105 ([hep-ph/0109119](#)).

[28] **Matter effects in neutrino oscillations.** L. Wolfenstein, *Phys. Rev.* D17 (1978) 2369. S.P. Mikheyev, A. Yu Smirnov, *Sov. J. Nucl. Phys.* 42 (1986) 913. Due to problems with referees, the same paper was published in S.P. Mikheyev, A. Yu Smirnov, *Nuovo Cim.* C9 (1986) 17. The small difference between ν_μ and ν_τ was computed in F.J. Botella, C.S. Lim, W.J. Marciano, *Phys. Rev.* D35 (1987) 896. Matter potential in polarized matter: H. Nunokawa, V. Semikoz, A. Smirnov, J. Valle, *Nucl. Phys.* B501 (1997) 17 ([hep-ph/9701420](#)).

[29] **Earth model.** A.M. Dziewonski, D.L. Anderson, *Phys. Earth Planet. Interior* 25 (1981) 297. See also mahi.ucsd.edu/gabi/rem.html.

[30] **Neutrino propagation in a varying density.** First analytical formulae were obtained in S. Parke, *Phys. Rev. Lett.* 57 (1986) 1275. P. Pizzochero, *Phys. Rev.* D36 (1987) 2293. Eq. (3.25) was found in S.T. Petcov, *Phys. Lett.* B200 (1988) 373. The LSZ approximation is discussed in T.K. Kuo, J. Pantaleone, *Phys. Rev.* D39 (1989) 1930. It was derived in L. Landau, *Phys. Z. Sowjetunion* 2 (1932) 46. E.C.G. Stückelberg, *Helv. Phys. Acta* 5 (1932) 369. C. Zener, *Proc. Roy. Soc. Lond.* A137 (1932) 696. For a review see T.K. Kuo, J. Pantaleone, *Rev. Mod. Phys.* 61 (1989) 937. For recent useful studies see G.L. Fogli, E. Lisi, D. Montanino, A. Palazzo, *Phys. Rev.* D62 (2000) 113004 ([hep-ph/0005261](#)). E. Lisi, A. Marrone, D. Montanino, A. Palazzo, S.T. Petcov, *Phys.*

Rev. D63 (2001) 93002 ([hep-ph/0011306](#)). Approximations specific for superovæ are discussed in M. Kachelriess et al., *Phys. Rev.* D65 (2002) 73016 ([hep-ph/0108100](#)). G.L. Fogli, E. Lisi, D. Montanino, A. Palazzo, *Phys. Rev.* D65 (2002) 073008 ([hep-ph/0111199](#)). For an analytical discussion of earth matter effects see A. N. Ioannisian, N. A. Kazarian, A. Y. Smirnov, D. Wyler, *Phys. Rev.* D71 (2005) 033006 ([hep-ph/0407138](#)). Effects of fluctuations in the average density have been considered in A. B. Balantekin, J.M. Fetter, F.N. Loret, *Phys. Rev.* D54 (1996) 3941 ([astro-ph/9604061](#)). H. Nunokawa, A. Rossi, V.B. Semikoz, J.W. Valle, *Nucl. Phys.* B472 (1996) 495. M. Koike, J. Sato, *Mod. Phys. Lett.* A14 (1999) 1297. T. Ota, J. Sato, *Phys. Rev.* D63 (2001) 093004. Fluctuations in the solar density seem negligible, see P. Bamert, C. P. Burgess, D. Michaud, *Nucl. Phys.* B513 (1998) 319. C.P. Burgess et al., *Mon. Not. Roy. Astron. Soc.* 348 (2004) 609 ([astro-ph/0304462](#)). Fluctuations in the earth density have been discussed in T. Miura, T. Shindou, E. Takasugi, M. Yoshimura, *Phys. Rev.* D64 (2001) 073017 ([hep-ph/0106086](#)).

[31] **Decoherence.** For theoretical considerations see G. Lindblad, *Commun. Math. Phys.* 48 (1976) 119. T. Banks, L. Susskind, M.E. Peskin, *Nucl. Phys.* B244 (1984) 125. F. Benatti, H. Narnhofer, *Lett. Math. Phys.* 15 (1988) 325. The case of neutrino oscillations is discussed in C.H. Chang et al., *Phys. Rev.* D60 (1999) 033006. S. Adler, *Phys. Rev.* D62 (2000) 117901 ([hep-ph/0005220](#)). For a recent comparison with atmospheric data see G.L. Fogli, E. Lisi, A. Marrone, D. Montanino, *Phys. Rev.* D67 (2003) 093006 ([hep-ph/0303064](#)).

[32] **ν_τ regeneration.** F. Halzen, D. Salzberg, *Phys. Rev. Lett.* 81 (1998) 4305. S.I. Dutta, M.H. Reno, I. Sarcevic, *Phys. Rev.* D62 (2000) 123001. F. Beccattini, S. Bottai, *Astropart. Phys.* 15 (2001) 323. E. Bugaev, T. Montaruli, Y. Shlepin, I. Sokalski, *Astropart. Phys.* 21 (2004) 491. D. Fargion, *Astrophys. J.* 570 (2002) 909 ([astro-ph/9704205](#)). J. F. Beacom, P. Crotty and E. W. Kolb, *Phys. Rev.* D66 (2002) 021302 ([astro-ph/0111482](#)).

[33] **Neutrino oscillations in the early universe.** A. Dolgov, *Sov. J. Nucl. Phys.* 33 (1981) 700. L. Stodolsky, *Phys. Rev.* D36 (1987) 2273. A. Manohar, *Phys. Lett.* B186 (1987) 370. M.J. Thomson, B.H.J. McKellar, *Phys. Lett.* B259 (1991) 113. J. Pantaleone, *Phys. Lett.* B287 (1992) 128. A. Friedland, C. Lunardini, *Phys. Rev.* D68 (2003) 013007 ([hep-ph/0304055](#)). The formalism is clearly summarized in G. Sigl, G. Raffelt, *Nucl. Phys.* B406 (1993) 423. The dominant contribution to the refraction index was discussed in D. Nötzold, G. Raffelt, *Nucl. Phys.* B307 (1988) 924.

[34] **Neutrino/electron scattering.** Radiative corrections are computed in S. Sarantakos, A. Sirlin, W. Marciano, *Nucl. Phys.* B217 (1983) 84. J.N. Bahcall, M. Kamionkowski, A. Sirlin, *Phys. Rev.* D51 (1995) 6146 ([astro-ph/9502003](#)). M. Passera, *Phys. Rev.* D64 (2001) 113002 ([hep-ph/0011190](#)). W.J. Marciano, Z. Parsa, *J. Phys.* G29 (2003) 2629 ([hep-ph/0403168](#)).

[35] **Neutrino/nucleon scattering.** C.H. Llewellyn-Smith, *Phys. Rept.* 3 (1972) 261. P. Vogel, J.F. Beacom, *Phys. Rev.* D60 (1999) 053003 ([hep-ph/9903554](#)). A. Strumia, F. Vissani, *Phys. Lett.* B564 (2003) 42 ([astro-ph/0302055](#)). Measurements of nuclear form factors have been recently discussed in H. Budd, A. Bodek, J. Arrington, *Nucl. Phys. Proc. Suppl.* 139 (2005) 90 ([hep-ex/0410055](#)). At intermediate energies $E_\nu \sim$ GeV neither the quasi-elastic neither the DIS approximations are valid, and one can try to take into account production of specific hadron resonances, computed in G. L. Fogli, G. Nardulli, *Nucl. Phys.* B160 (1979) 116. G. L. Fogli, G. Nardulli, *Nucl. Phys.* B165 (1980) 162. D. Rein, L. M. Sehgal, *Annals Phys.* 133 (1981) 79. For a recent discussion see K.S. Kuzmin, V.V. Lyubushkin, V.A. Naumov, [hep-ph/0511308](#). M. Valverde, J.E. Amaro, J. Nieves, [hep-ph/0604042](#). At ultra-high energies $E_\nu \gg 10^4$ GeV R. Gandhi, C. Quigg, M. Reno, I. Sarcevic, *Phys. Rev.* D58 (1998) 093009 ([hep-ph/9807264](#)). See however D. Dicus, S. Kretzer, W. Repko, C. Schmidt, *Phys. Lett.* B514 (2001) 103 ([hep-ph/0103207](#)) and the subsequent literature.

[36] **$\nu_\tau N$ scattering.** The cross sections for $\nu_\tau N \rightarrow \tau X$ have been computed in S. Kretzer, M.H. Reno, *Phys. Rev.* D66 (2002) 113007. K. Hagiwara, K. Mawatari, H. Yokoya, *Nucl. Phys.* B668 (2003) 364 ([hep-ph/0305324](#)). K.M. Graczyk, *Nucl. Phys.* A748 (2005) 313 ([hep-ph/0407275](#)). K.M. Graczyk, *Nucl. Phys. Proc. Suppl.* 139 (2005) 150 ([hep-ph/0407283](#)). For a simple summary of results see J.M. Lévy, [hep-ph/0407371](#). Spectra of τ decay products are reviewed in A. Stahl, *Physics with τ leptons* (2000) Heidelberg, Springer Verlag.

[37] J. N. Bahcall, *Neutrino astrophysics*, Cambridge University Press, 1989; M. Fukugita, T. Yanagida, *Physics of neutrinos and applications to astrophysics*, Springer-Verlag, 2003. Theoretical approaches to matrix element calculation are reviewed in K. Kubodera, S. Nozawa, *Int. J. Mod.*

Phys. E3 (1994) 101. For updates, see the proceedings of the NUINT workshops.

[38] Detection of the IBD neutron: A.E. Chudakov, O.G. Ryazhskaya, G. Zatsepin, Proc. of 13th ICRC Denver, 3 (1973) 2007; detection of the proton in $\nu p \rightarrow \nu p$: J. Beacom, S. Palomares-Ruiz, *Phys. Rev.* D67 (2003) 093001 ([hep-ph/0301060](#)). Use of gadolinium: [118]. The importance of the reactions with iron is remarked in: V. Imshennik, O. Ryazhskaya, *Astron. Lett.* 30 (2004) 14 ([astro-ph/0401613](#)). For reviews, see F. Cei, *Int. J. Mod. Phys.* A17 (2002) 1765 ([hep-ex/0202043](#)); M. Selvi, *Nucl. Phys. Proc. Suppl.* 145 (2005) 339.

[39] **Atmospheric neutrinos.** First computation: J.L. Osborne, S.S. Said, A.W. Wolfendale, *Proc. Phys. Soc.* 86 (1965) 93. For a review see T.K. Gaisser, M. Honda, *Ann. Rev. Nucl. Part. Sci.* 52 (2002) 153 ([hep-ph/0203272](#)). For recent works see V. Agrawal et al., BARTOL group, *Phys. Rev.* D53 (1996) 1314. P. Lipari, [hep-ph/002282](#). FLUKA group, *Astropart. Phys.* 19 (2003) 269 ([hep-ph/0207035](#)). FLUKA group, [hep-ph/0305208](#).

[40] **Through-going muons.** This technique was proposed in M.A. Markov, I.M. Zheleznykh, *Nucl. Phys.* 27 (1961) 385. K. Greisen, *Ann. Rev. Nucl. Sci.* 10 (1960) 63. The first atmospheric neutrinos were detected in mid sixties, see M.R. Krishnaswamy et al., KGF collaboration, *Proc. R. Soc.* A323 (1971) 511. M.F. Crouch et al., CWI collaboration, *Phys. Rev.* D18 (1978) 2239.

[41] **Neutrino decay.** Computations of lifetimes of Majorana or Dirac neutrinos: S.T. Petcov, *Sov. J. Nucl. Phys.* 25 (1977) 340. P.B. Pal, L. Wolfenstein, *Phys. Rev.* D25 (1982) 766. R. Shrock, *Nucl. Phys.* B206 (1982) 359. J.F. Nieves, *Phys. Rev.* D28 (1983) 1664. Neutrino decay in matter: C. Giunti et al., *PR* D45 (1992) 1557. J.F. Nieves, P.B. Pal, *Phys. Rev.* D56 (1987) 365 ([hep-ph/9702283](#)). Models that added extra light particles to get faster neutrino decays: Y. Chikashige, R.N. Mohapatra, R.D. Peccei, *Phys. Lett.* 98 (1981) 265. G.B. Gelmini, M. Roncadelli, *Phys. Lett.* B99 (1981) 411. Constraints from π, K decays: V.D. Barger, W.Y. Keung, S. Pakvasa, *Phys. Rev.* D25 (1982) 907. D.I. Britton et al., *Phys. Rev.* D49 (1994) 28. Constraints from $0\nu 2\beta$: K. Zuber, *Phys. Rept.* 305 (1998) 295. For non-obsolete phenomenological discussions see: P. Lipari, M. Lusignoli, *Phys. Rev.* D60 (1999) 013003 ([hep-ph/9901350](#)). G.L. Fogli et al., *Phys. Rev.* D59 (1999) 117303 ([hep-ph/9902267](#)). V.D. Barger et al., *Phys. Lett.* B462 (1999) 102 ([hep-ph/9907421](#)). J.F. Beacom, N.F. Bell, *Phys. Rev.* D65 (2002) 113009 ([hep-ph/0204111](#)). S. Ando, *Phys. Lett.* B570 (2003) 11 ([hep-ph/0307169](#)). G. L. Fogli, E. Lisi, A. Mirizzi, D. Montanino, *Phys. Rev.* D70 (2004) 013001 ([hep-ph/0401227](#)).

[42] **Neutrinos in extra dimensions.** S. Dimopoulos, talk given at the SUSY 1998 conference; K.R. Dienes, E. Dudas, T. Gherghetta, *Nucl. Phys.* B557 (1999) 25 ([hep-ph/9811428](#)). N. Arkani-Hamed, S. Dimopoulos, G. Dvali, J. March-Russell, *Phys. Rev.* D65 (2002) 024032 ([hep-ph/9811448](#)). A.E. Faraggi, M. Pospelov, *Phys. Lett.* B458 (1999) 237 ([hep-ph/9901299](#)). G.R. Dvali, A.Y. Smirnov, *Nucl. Phys.* B563 (1999) 63 ([hep-ph/9904211](#)). R. Barbieri, P. Creminelli, A. Strumia, *Nucl. Phys.* B585 (2000) 28 ([hep-ph/0002199](#)). A. Ioannian, A. Pilaftsis, *Phys. Rev.* D62 (2000) 066001 ([hep-ph/9907522](#)). R. Kitano, *Phys. Lett.* B481 (2000) 39 ([hep-ph/0002279](#)). R.N. Mohapatra and A. Perez-Lorenzana, *Nucl. Phys.* B593 (2001) 451 ([hep-ph/0006278](#)). A. Lukas, P. Ramond, A. Romanino, G.G. Ross, *Phys. Lett.* B495 (2000) 126 ([hep-ph/0008049](#)). D. O. Caldwell, R. N. Mohapatra, S. J. Yellin, *Phys. Rev. Lett.* 87 (2001) 041601 ([hep-ph/0010353](#)). A. Lukas, P. Ramond, A. Romanino, G.G. Ross, *JHEP* 0104 (2001) 010 ([hep-ph/0011295](#)). T.P. Cheng, L. Li, *Phys. Lett.* B502 (2001) 152 ([hep-ph/0101068](#)). A. De Gouvea, G.F. Giudice, A. Strumia, K. Tobe, *Nucl. Phys.* B623 (2002) 295 ([hep-ph/0107156](#)). H. Davoudiasl, P. Langacker, M. Perelstein, *Phys. Rev.* D65 (2002) 105015 ([hep-ph/0201128](#)). G. Cacciapaglia, M. Cirelli, Y. Lin, A. Romanino, *Phys. Rev.* D67 (2003) 053001 ([hep-ph/0209063](#)). G. Bhattacharyya, H.V. Klapdor-Kleingrothaus, H. Paes, A. Pilaftsis, *Phys. Rev.* D67 (2003) 113001 ([hep-ph/0212169](#)). G. Cacciapaglia, M. Cirelli, A. Romanino, *Phys. Rev.* D68 (2003) 033013 ([hep-ph/0302246](#)). Neutrinos in supersymmetric extra-dimensions have been explored in J. Matias, C.P. Burgess, *JHEP* 09 (2005) 052 ([hep-ph/0508156](#)).

[43] R. Foot, [hep-ph/0303005](#).

[44] **Recent short-baseline reactor experiments.** The BUGEY collaboration, *Nucl. Phys.* B434 (1995) 503. CHOOZ collaboration, *Phys. Lett.* B466 (1999) 415 ([hep-ex/9907037](#)). PALO VERDE collaboration, *Phys. Rev. Lett.* 84 (2000) 3764 ([hep-ex/9912050](#)). CHOOZ collaboration, *Eur. Phys. J.* C27 (2003) 331 ([hep-ex/0301017](#)).

[45] **Reactor neutrinos.** The $\bar{\nu}_e$ spectra have been reconstructed from measured ^{241}Pu , ^{239}Pu and ^{235}U

β decay spectra in K. Schreckenbach et al., *Phys. Lett.* B160 (1985) 325. A.A. Hahn et al., *Phys. Lett.* B218 (1989) 365. It has not yet been possible to measure $\bar{\nu}_e$ spectra from ^{238}U , which give a $\sim 10\%$ contribution to reactor $\bar{\nu}_e$. This is not a problem because, although heavy radioactive elements have many decay channels, theory can predict their $\bar{\nu}_e$ spectra with $\sim 10\%$ uncertainty. The BUGEY3 collaboration performed a dedicated study of $\bar{\nu}_e$ from reactors with a nearby detector, B. Achkar et al., *Phys. Lett.* B374 (1996) 243. Data about reactor spectra are collected in P. Vogel, J. Engel, *Phys. Rev.* D39 (1989) 3378. For a review, see C. Bemporad, G. Gratta, P. Vogel, *Rev. Mod. Phys.* 74 (2002) 297 ([hep-ph/0107277](#)).

Discussions about future reactor experiments: V. Kopeikin, L. Mikaelyan, V. Sinev, [hep-ph/0310246](#). J. Bernabéu, S. Palomar-Ruiz, *JHEP* 02 (2004) 068 ([hep-ph/0311354](#)). Double-CHOOZ letter of intent, [hep-ex/0405032](#). Q. Liu, J. Deng, B. Chen, P. Yang, *JHEP* 12 (2004) 066 ([hep-ph/0409155](#)). V. Kopelin, L. Mikaelyan, V. Sinev, [hep-ph/0412044](#). ANGRA project, *Nucl. Phys. Proc. Suppl.* 155 (2006) 231 ([hep-ex/0511059](#)). See also www.hep.anl.gov/ndk/hypertext/white.html. DAYA BAY project: dayawane.ihep.ac.cn. BRAIDWOOD project: mwtheta13.uchicago.edu. A measurement of θ_{13} is proposed in: KASKA collaboration, *Nucl. Phys. Proc. Suppl.* 149 (2005) 160 ([hep-ex/0502002](#)). Measurements of θ_{12} at a reactor experiment are discussed in H. Minakata et al., *Phys. Rev.* D71 (2005) 013005 ([hep-ph/0407326](#)). H. Minakata et al., *Nucl. Phys. Proc. Suppl.* 145 (2005) 45 ([hep-ph/0501250](#)).

[46] **Terrestrial neutrinos.** G. Eder, *Nucl. Phys.* 78 (1966) 657. Review: L. M. Krauss, S. L. Glashow, D. N. Schramm, *Nature* 310 (1984) 191. Experimental proposals: R.S. Raghavan et al., *Phys. Rev. Lett.* 80 (1998) 635. C.G. Rothschild et al., *Geophys. Research Lett.* 25 (1998) 1083 ([nucl-ex/9710001](#)). Recent works: G. Fiorentini et al., *Phys. Lett.* B557 (2003) 139 ([nucl-ex/0212008](#)). G. Fiorentini et al., *Phys. Lett.* B558 (2003) 15 ([hep-ph/0301042](#)). H. Nunokawa, W. J. Teves, R. Z. Funchal, *JHEP* 11 (2003) 020 ([hep-ph/0308175](#)). F. Mantovani, L. Carmignani, G. Fiorentini, M. Lissia, *Phys. Rev.* D69 (2004) 013001 ([hep-ph/0309013](#)). G. Fiorentini et al., *Phys. Lett.* B557 (2003) 129 ([nucl-ex/0312008](#)). G. Fiorentini et al., [hep-ph/0401085](#). G. Dombogatski, V. Kopeikin, L. Mikaelyan, V. Sinev, *Phys. Atom. Nucl.* 68 (2005) 69 ([hep-ph/0401221](#)). G.L. Fogli et al., [hep-ph/0405139](#). B.D. Fields, K.A. Hochmuth, [hep-ph/0406001](#). G. Fiorentini, M. Lissia, F. Mantovani, R. Vannucci, *Phys. Rev.* D72 (2005) 033017 ([hep-ph/0501111](#)). J.M. Herndon, D.A. Edgerley, [hep-ph/0501216](#). For a short review see G. Fiorentini, M. Lissia, F. Mantovani, R. Vannucci, *Nucl. Phys. Proc. Suppl.* 143 (2005) 53 ([hep-ph/0409152](#)).

KamLAND data: KamLAND collaboration, *Nature* 436 (2005) 499. For related work see G. Fiorentini, M. Lissia, F. Mantovani, B. Ricci, *Phys. Lett.* B629 (2005) 77 ([hep-ph/0508048](#)). S. Enomoto, E. Ohtani, K. Inoue, A. Suzuki, [hep-ph/0508049](#). LENA proposal: K.A. Hochmuth et al., [hep-ph/0509136](#).

[47] **Solar neutrino fluxes.** For an early attempt of predicting solar neutrino fluxes see J.N. Bahcall et al., *The Astrophys. J.* 137 (1963) 344. The standard solar model computed by J.N. Bahcall and collaborators is widely used in the neutrino community. BP00 model: J.N. Bahcall, S. Basu, M.H. Pinsonneault, *Astrophys. J.* 555 (2001) 990 ([astro-ph/0010346](#)). J.N. Bahcall, *Phys. Rev.* C65 (2002) 025801 ([hep-ph/0108148](#)). Recent computation of the width of the Be 'line': J.N. Bahcall, *Phys. Rev.* D49 (1994) 3923 ([astro-ph/9401024](#)). Recent computation of the spectrum of B neutrinos: J.N. Bahcall et al., *Phys. Rev.* C54 (1996) 411 ([nucl-th/9601044](#)). Recent measurements of nuclear cross sections: [49]. LUNA collaboration, *Phys. Lett.* B591 (2004) 61 ([nucl-ex/0312015](#)). Fluxes with updated nuclear cross sections: S. Degl'Innocenti et al., *Phys. Lett.* B590 (2004) 13 ([astro-ph/0312559](#)). See also www.sns.ias.edu/~jnb. Recent discussion of the *hep* flux: K. Kubodera, T. Park, *Ann. Rev. Nucl. Part. Sci.* 54 (2004) 19 ([nucl-th/0402008](#)).

[48] E.G. Adelberger et al., *Rev. Mod. Phys.* 70 (1998) 1265 ([astro-ph/9805121](#)).

[49] **Measurements of $S_{17}(0)$.** For a review see E.G. Adelberger et al., *Rev. of Modern Phys.* 70 (1998) 1265. Recent measurements: N. Iwasa et al., *Phys. Rev. Lett.* 83 (1999) 2910. B. Davids et al., *Phys. Rev. Lett.* 86 (2001) 2750. F. Hammache et al., *Phys. Rev. Lett.* 86 (2001) 3985. F. Strieder et al., *Nucl. Phys.* A696 (2001) 219. ISOLDE collaboration, *Phys. Rev. C* 67 (2003) 065805 ([nucl-ex/0212011](#)). A.R. Junghans et al., *Phys. Rev. C* 68 (2003) 065803 ([nucl-ex/0308003](#)). K.A. Snover et al., [nucl-ex/0311012](#). F. Schumann et al., *Phys. Rev. Lett.* 90 (2003) 232501. For a recent summary see M. Gai, [nucl-ex/0510081](#).

[50] **Time variations of solar neutrino fluxes?** Various positive claims have been made by some authors. P.A. Sturrock, G. Walther, M. S. Wheatland, *Astrophys. J.* 491 (1997) 409. A.

Milsztajn, [hep-ph/0301252](#). P.A. Sturrock, D.O. Caldwell, J.D. Scargle, M.S. Wheatland, *Phys. Rev.* D72 (2005) 113004 ([hep-ph/0501205](#)). G. Ranucci, [hep-ph/0511026](#). R.N. Ikhsanov, Yu.N. Gnedin, E.V. Miletsky, [hep-ph/0512094](#). P.A. Sturrock, [hep-ph/0601251](#). K. Ghosh, P. Raychaudhuri, [hep-ph/0605043](#). No statistically significant time variation is found in analyses performed by experimental collaborations: J. Yoo et al., SK collaboration, *Phys. Rev.* D68 (2003) 092002 ([hep-ex/0307070](#)). L. Pandola (GNO collaboration), *Astropart. Phys.* 22 (2004) 219 ([hep-ph/0406248](#)). SNO collaboration, *Phys. Rev.* D72 (2005) 052010 ([hep-ex/0507079](#)).

[51] **Effects of inhomogeneities in the sun?** For recent works see M. Guzzo, P. de Holanda, N. Reggiani, *Phys. Lett.* B569 (2003) 45 ([hep-ph/0303203](#)). C. Burgess et al., *JCAP* 0401 (2004) 007 ([hep-ph/0310366](#)).

[52] **Implications of solar data for solar fluxes.** Obsolete interesting analyses: N. Hata, P. Langacker, *Phys. Rev.* D52 (1995) 420 ([hep-ph/9409372](#)). P.I. Krastev, S.T. Petcov, *Phys. Lett.* B395 (1997) 69 ([hep-ph/9612243](#)). Recent analyses: R. Barbieri, A. Strumia, *JHEP* 0012 (016) 2000 ([hep-ph/0011307](#)) and updates. This paper contains a bound on the CNO flux, rederived in J.N. Bahcall et al., *Astrophys. J.* 586 (2003) 268 ([astro-ph/0212233](#)). Confirmation of the existence of the CNO cycle: M. Mozina, H. Ratcliffe, O. Manuel, [astro-ph/0512633](#). Implications for the solar metallicity: G. Gonzalez, [astro-ph/06056147](#).

[53] **Global fits of solar and/or atmospheric data.** For recent analyses see A. Bandyopadhyay, S. Choubey, S. Goswami, S. Petcov, D. Roy, *Phys. Lett.* B608 (2005) 115 ([hep-ph/0406328](#)). A. Strumia, F. Vissani, *Nucl. Phys.* B726 (2005) 294 ([hep-ph/0503246](#)). G.L. Fogli, E. Lisi, A. Marrone, A. Palazzo, [hep-ph/0506083](#). P. Aliani, V. Antonelli, M. Picariello, E. Torrente-Lujan, [hep-ph/0511071](#). B.L. Chen, H.L. Ge, C. Giunti, Q.Y. Liu, [hep-ph/0605195](#).

[54] **Borexino.** See [borex.lngs.infn.it](#).

[55] **Fitting solar data.** We list papers dedicated to developing a χ^2 for solar data; more material can be found in papers that performed solar analyses, listed in [53]. G.L. Fogli, E. Lisi, *Astropart. Phys.* 3 (1995) 185. J.N. Bahcall, E. Lisi, *Phys. Rev.* D54 (1996) 5417. M.C. Gonzales-Garcia et al., *Phys. Rev.* D63 (2001) 033005 ([hep-ph/0009350](#)) (see also M.V. Garzelli, C. Giunti, *Phys. Lett.* B488 (2000) 339 ([hep-ph/0006026](#))). G.L. Fogli et al., *Phys. Rev.* D66 (2002) 053010 ([hep-ph/0206162](#)).

[56] **IceCube** First results: IceCube collaboration, [astro-ph/0601269](#)

[57] **Mton WČ detectors.** For a summary of the HYPER-KAMIOKANDE ('HK') proposal see K. Nakamura, *Int. J. Mod. Phys.* A18 (2003) 4053. The UNO whitepaper is available at [ale.physics.Sunysb.edu/uno](#). See also C. K. Jung, *AIP Conf. Proc.* 533 (2000) 29 ([hep-ex/0005046](#)). The MEMPHYS project and other set-ups are discussed in: [nnn05.in2p3.fr/schedule.html](#). M3 preliminary proposal, M.V. Diwan et al, [hep-ex/0306053](#). See also A. Rubbia, [hep-ph/0407297](#).

[58] **Future atmospheric experiments** Capabilities of a magnetized detector have been discussed in Monolith project, *Nucl. Phys. Proc. Suppl.* 100 (2001) 142 ([hep-ex/0101040](#)). INO project: G. Rajasekaran, *AIP Conf. Proc.* 721 (2004) 243 ([hep-ph/0402246](#)). S.T. Petcov, T. Schwetz, *Nucl. Phys.* B740 (2006) 1 ([hep-ph/0511277](#)).

[59] **Future solar experiments.** KamLAND and SNO data changed the focus, making obsolete previous discussions like e.g. J.N. Bahcall, [hep-ex/0106086](#). One main goal of future experiments are precision measurement of oscillation parameters, as discussed in A. Strumia, F. Vissani, *JHEP* 048 (2001) 0111 ([hep-ph/0109172](#)). J.N. Bahcall, C. Peña-Garay, *JHEP* 004 (2003) 0311. A. Bandyopadhyay, S. Choubey, S. Goswami, S.T. Petcov, *Phys. Rev.* D72 (2005) 033013 ([hep-ph/0410283](#)).

Experimental proposals of future low-energy solar neutrino experiments have been presented at the dedicated 'LowNu' conferences: Tokyo, Dec 2000, [www-sk.icrr.u-tokyo.ac.jp/lownu](#); Heidelberg, May 2002, [www.mpi-hd.mpg.de/nubis/www_lownu2002](#); Paris, May 2003, [cdfinfo.in2p3.fr/LowNu2003](#).

[60] **CNGS** web site: [proj-cngs.web.cern.ch/proj-cngs](#). The planned energy spectrum is described at [www.mi.infn.it/~psala/Icarus/cngs.html](#). The sensitivity to θ_{13} is discussed in A. Ferrari, A. Guglielmi, P. Sala, *Nucl. Phys. Proc. Suppl.* 145 (2005) 93 ([hep-ph/0501283](#)).

[61] **T2K:** JHF-Kamioka neutrino project, [hep-ex/0106019](#). See also the web page [neutrino.kek.jp/jhfnu](#). A related 'T2KK' proposal: M. Ishitsuka, T. Kajita, H. Minakata, H. Nunokawa, *Phys. Rev.* D72 (2005) 033003 ([hep-ph/0504026](#)). K. Hagiwara, N. Okamura, K. Senda, [hep-ph/0504061](#).

[62] **NO ν A**: Proposal of the NO ν A collaboration, [hep-ex/0503053](#). A related proposal: ‘Super-Nova’: O. Mena Requejo, S. Palomares-Ruiz, S. Pascoli, *Phys. Rev.* D72 (2005) 053002 ([hep-ph/0504015](#)).

[63] **SPL**. CERN working group on Super Beams collaboration, [hep-ph/0105297](#). J. Campagne, A. Cazes, *Eur. Phys. J.* C45 (2006) 643 ([hep-ex/0411062](#)). J.E. Campagne, M. Maltoni, M. Mezzetto, T. Schwetz, [hep-ph/0603172](#).

[64] **Capabilities of neutrino beam experiments**. The combined capability of NuMi and CNGS was studied in V. Barger et al., *Phys. Rev.* D65 (2002) 053016 ([hep-ph/0110393](#)). The capabilities of conventional neutrino beams have been emphasized in B. Richter, [hep-ph/0008222](#). This issue has been discussed in many theoretical papers. E.g. W.J. Marciano, [hep-ph/0108181](#). V. Barger, D. Marfatia, K. Whisnant, *Phys. Lett.* B560 (2003) 75 ([hep-ph/0210428](#)). For a recent analysis see A. Donini, E. Fernández-Martínez, D. Meloni, S. Rigolin, [hep-ph/0512038](#). Plots of $P(\nu_\mu \rightarrow \nu_e)$ versus $P(\bar{\nu}_\mu \rightarrow \bar{\nu}_e)$ have been introduced in H. Minakata, H. Nunokawa, *JHEP* 10 (2001) 001 ([hep-ph/0108085](#)). T-violation has been studied in E. Akhmedov, P. Huber, M. Lindner, T. Ohlsson, *Nucl. Phys.* B608 (2001) 394 ([hep-ph/0105029](#)). Discrete ambiguities have been emphasized in V. Barger, D. Marfatia, K. Whisnant, *Phys. Rev.* D65 (2002) 073023 ([hep-ph/0112119](#)). The case $\theta_{13} = 0$ is studied in A. de Gouvea, W. Winter, *Phys. Rev.* D73 (2006) 033003 ([hep-ph/0509359](#)). Capabilities of a wide-band beam are studied in M. Diwan et al., BNL report, [hep-ex/0305105](#). For analytical approximations to oscillation probabilities see M. Honda et al., [hep-ph/0602115](#) and references therein.

[65] **Beam searches for dark matter**. A high intensity beam might allow to search for collisions with the ambient background of dark matter, see J. Hisano, M. Nagai, M. Nojiri, M. Senami, *AIP Conf. Proc.* 805 (2006) 423 ([hep-ph/0504068](#)). M. Cirelli, N. Fornengo, A. Strumia, [hep-ph/0512090](#). A dedicated study of the background is necessary to know if this kind of experiment is viable. The main background seems gas in the beam pipe generated by acceleration byproducts.

[66] **Neutrino factory**. The concept was proposed in S. Geer, *Phys. Rev.* D57 (1989) 6989 and revived by the neutrino group of the prospective study on $\mu^+\mu^-$ colliders (B. Autin et al.), CERN-SPSC-98-30. A. Bueno, M. Campanelli, A. Rubbia, [hep-ph/9808485](#). A. De Rujula, M. Gavela, P. Hernandez, *Nucl. Phys.* B547 (1999) 21 ([hep-ph/9811390](#)). V. Barger, S. Geer, K. Whisnant, *Phys. Rev.* D61 (2000) 053004 ([hep-ph/9906487](#)). Neutrino factory sensitivity to CP-violation have been studied in A. Donini, M. Gavela, P. Hernandez, S. Rigolin, *Nucl. Phys.* B574 (2000) 23 ([hep-ph/9909254](#)). A. Romanino, *Nucl. Phys.* B574 (2000) 675 ([hep-ph/9909425](#)). V. Barger, S. Geer, R. Raja, K. Whisnant, *Phys. Rev.* D62 (2000) 013004 ([hep-ph/9911524](#)). M. Freund, M. Lindner, S. Petcov, A. Romanino, *Nucl. Phys.* B578 (2000) 27 ([hep-ph/9912457](#)). A. Cervera et al., *Nucl. Phys.* B579 (2000) 17 ([hep-ph/0002108](#)) and erratum *ibid.* B593 (2001) 731. M. Freund, P. Huber, M. Lindner, *Nucl. Phys.* B585 (2000) 105 ([hep-ph/0004085](#)). The ‘silver’ channel: A. Donini, D. Meloni, P. Migliozzi, *Nucl. Phys.* B646 (2002) 321 ([hep-ph/0206034](#)). D. Autiero et al., *Eur. Phys. J.* C33 (2004) 243 ([hep-ph/0305185](#)). Some proposals: C. Albright et al., FermiLab report, [hep-ex/0008064](#). Muon Collider/Neutrino Factory collaboration, *Phys. Rev. ST Accel. Beams* 6 (2003) 081001 ([hep-ex/0207031](#)). M. Apollonio et al., CERN report, [hep-ph/0210192](#). The ‘magic baseline’ was discussed in: P. Lipari, *Phys. Rev.* D61 (2000) 113004 ([hep-ph/9903481](#)). P. Huber, W. Winter, *Phys. Rev.* D68 (2003) 037301 ([hep-ph/0301257](#)).

[67] **Beta beams**: P. Zucchelli, *Phys. Lett.* B532 (2002) 166. M. Mezzetto, *J. Phys. G* 29 (2003) 1771 ([hep-ex/0302007](#)). Low energy β -beam: C. Volpe, *J. Phys. G* 30 (2004) L1-L6 ([hep-ph/0303222](#)). High-energy β -beam: J. Burguet-Castell, D. Casper, J. Gomez-Cadenas, P. Hernandez, F. Sanchez, *Nucl. Phys.* B695 (2004) 217 ([hep-ph/0312068](#)). F. Terranova, A. Marotta, P. Migliozzi, M. Spinetti, *Eur. Phys. J.* C38 (2004) 69 ([hep-ph/0405081](#)). Monochromatic β -beam: J. Bernabeu, J. Burguet-Castell, C. Espinoza, M. Lindroos, *JHEP* 12 (2005) 014 ([hep-ph/0505054](#)). Sensitivity to oscillations: A. Donini, E. Fernandez-Martinez, P. Migliozzi, S. Rigolin, L. Scotto Lavina, *Nucl. Phys.* B710 (2005) 402 ([hep-ph/0406132](#)). A. Donini, E. Fernandez-Martinez, S. Rigolin, *Phys. Lett.* B621 (2005) 276 ([hep-ph/0411402](#)). P. Huber, M. Lindner, M. Rolinec, W. Winter, *Phys. Rev.* D73 (2006) 053002 ([hep-ph/0506237](#)). For a review see C. Volpe, [hep-ph/0605033](#).

[68] R.S. Raghavan, [hep-ph/0601079](#). H. Minakata, S. Uchinami, [hep-ph/0602046](#).

[69] **CMB and LSS**. WMAP data: WMAP collaboration, [astro-ph/0603451](#). Other CMB experiments: ACBAR collaboration, *Astrophys. J.* 600 (2004) 32 ([astro-ph/0212289](#)), web page cosmology.berkeley.edu/group/swlh/acbar.

CBI collaboration, *Astrophys. J.* 609 (2004) 498 ([astro-ph/0402359](#)) *Astrophys. J.* 609 4982004, web page www.astro.caltech.edu/~tjp/CBI. BOOMERANG collaboration, [astro-ph/0507494](#), web page cmb.phys.cwru.edu/boomerang. The future CMB experiment PLANCK is described at www.rssd.esa.int/Planck. The CMBPOL proposal is available at www.mssl.ucl.ac.uk/www_astro/submm/CMBpol1.html. Measurements of the power spectrum in Large Scale Structures. SDSS collaboration, *Astrophys. J.* 606 (2004) 702 ([astro-ph/0310725](#)), web page www.sdss.org. The 2dFGRS Collaboration, *Mon. Not. Roy. Astron. Soc.* 362 (2005) 505 ([astro-ph/0501174](#)), web page www.mso.anu.edu.au/2dFGRS. Lyman- α data: R.A.C. Croft et al., *Astrophys. J.* 581 (2002) 20 ([astro-ph/0012324](#)). P. McDonald et al., SDSS collaboration, *Astrophys. J. Suppl.* 163 (2006) 80 ([astro-ph/0405013](#)). P. McDonald et al., SDSS collaboration, *Astrophys. J.* 635 (2005) 761 ([astro-ph/0407377](#)). Codes for CMB computations are freely available, see e.g. U. Seljak, M. Zaldarriaga, *Astrophys. J.* 469 (1996) 437 (in Fortran) and lambda.gsfc.nasa.gov/toolbox/tb_camb_form.cfm (web form). Results presented in this review have been computed with a CMB code written by one of the authors: M. Cirelli, A. Strumia, to appear. This guarantees that we really understand what we wrote about neutrino cosmology.

[70] **Time delay between massive supernova neutrinos.** For a review see e.g. G.G. Raffelt., *Nucl. Phys. Proc. Suppl.* 110 (2002) 254 ([hep-ph/0201099](#)).
D. Fargion, *Lett. Nuovo Cim.* 31 (1981) 499 ([hep-ph/0110061](#)); N.Arnaud et al., *Phys. Rev.* D65 (2002) 033010 ([hep-ph/0109027](#)). O.G. Ryazhskaya, V.G. Ryasny, O. Saavedra, *Nuovo Cim.* A106 (1993) 257. J.F. Beacom, P. Vogel, *Phys. Rev.* D58 (1998) 93012 ([hep-ph/9806311](#)); J. F. Beacom, R. N. Boyd and A. Mezzacappa, *Phys. Rev.* D63 (2001) 73011 ([astro-ph/0010398](#)). E. Nardi, J.I. Zuluaga, *Phys. Rev.* D69 (2004) 103002 ([astro-ph/0306384](#)). J.I. Zuluaga, [astro-ph/0511771](#).

[71] MAINZ collaboration, *Eur. Phys. J.* C40 (2005) 447 ([hep-ex/0412056](#)).

[72] TROITSK collaboration, *Nucl. Phys. Proc. Suppl.* 91 (2001) 280. The latest results have been presented in a talk by V. Lobashev at the XI International Workshop on “Neutrino Telescopes” (Venezia, Feb. 22–25 2005).

[73] KATRIN web site: www-ik1.fzk.de/tritium.

[74] **Bosonic neutrinos?** A.D. Dolgov, A. Yu Smirnov, *Phys. Lett.* B621 (2005) 1 ([hep-ph/0501066](#)). A.D. Dolgov, S.H. Hansen, A. Yu Smirnov, *JCAP* 0506 (2005) 004 ([astro-ph/0503612](#)). A. Yu Ignatiev, V.A. Kuzmin, [hep-ph/0510209](#). S. Choubey, K. Kar, *Phys. Lett.* B634 (2006) 14 ([hep-ph/0510261](#)).

[75] **Nuclear matrix elements for $0\nu2\beta$.** A. Staudt et al., *Europ. Lett.* 13 (1990) 31.

[76] A. Staudt et al., *Phys. Rev.* C46 (1992) 871.

[77] E. Caurier, *Phys. Rev. Lett.* 77 (1996) 1954.

[78] V.A. Rodin et al., *Phys. Rev.* C68 (2003) 044302.

[79] J. Engel et al., *Phys. Rev.* C37 (1988) 871.

[80] **Connection between oscillations and $0\nu2\beta$.** S.T. Petcov, A.Y. Smirnov, *Phys. Lett.* B322 (1994) 109 ([hep-ph/9311204](#)). S.M. Bilenky, A. Bottino, C. Giunti, C.W. Kim, *Phys. Rev.* D54 (1996) 1881 ([hep-ph/9602216](#)). S.M. Bilenky, C. Giunti, C.W. Kim, S.T. Petcov, *Phys. Rev.* D54 (1996) 4432 ([hep-ph/9604364](#)). F. Vissani, *JHEP* 9906 (1999) 22 ([hep-ph/9906525](#)). T. Fukuyama, K. Matsuda, H. Nishiura, *Phys. Rev.* D57 (1998) 5884 ([hep-ph/9711415](#)). V.D. Barger, K. Whisnant, *Phys. Lett.* B456 (1999) 194 ([hep-ph/9904281](#)). F. Vissani, [hep-ph/9904349](#). C. Giunti, *Phys. Rev.* D61 (2000) 036002 ([hep-ph/9906275](#)). M. Czakon, J. Gluza, M. Zralek, *Phys. Lett.* B465 (1999) 211 ([hep-ph/9906381](#)). S.M. Bilenky, C. Giunti, W. Grimus, B. Kayser, S. T. Petcov, *Phys. Lett.* B465 (1999) 193 ([hep-ph/9907234](#)). H.V. Klapdor-Kleingrothaus, H. Pas, A.Y. Smirnov, *Phys. Rev.* D63 (2001) 73005 ([hep-ph/0003219](#)). W. Rodejohann, *Nucl. Phys.* B597 (2001) 110 ([hep-ph/0008044](#)). K. Matsuda, N. Takeda, T. Fukuyama, H. Nishiura, *Phys. Rev.* D64 (2001) 13001 ([hep-ph/0012357](#)). D. Falcone, F. Tramontano, *Phys. Rev.* D64 (2001) 077302 ([hep-ph/0102136](#)). S.M. Bilenky, S. Pascoli, S.T. Petcov, *Phys. Rev.* D64 (2001) 53010 ([hep-ph/0102265](#)). S.M. Bilenky, S. Pascoli, S.T. Petcov, *Phys. Rev.* D64 (2001) 113003 ([hep-ph/0104218](#)). P. Osland, G. Vigdor, *Phys. Lett.* B520 (2001) 143 ([hep-ph/0107161](#)). S. Pascoli, S.T. Petcov, L. Wolfenstein, *Phys. Lett.* B524 (2002) 319 ([hep-ph/0110287](#)). S. Pascoli, S.T. Petcov, *Phys. Lett.* B544 (2002) 239 ([hep-ph/0205022](#)). Recent precise analyses: paper by F. Feruglio et al. in [15]. J.N. Bahcall, H. Murayama, C. Peña-Garay, *Phys. Rev.* D70 (2004) 033012 ([hep-ph/0403167](#)). S. Pascoli, S.T. Petcov, T. Schwetz, *Nucl. Phys.* B734 (2006) 24

([hep-ph/0505226](#)). S. Choubey, W. Rodejohann, *Phys. Rev.* D72 (2005) 033016 ([hep-ph/0506102](#)). A. de Gouvea, J. Jenkins, [hep-ph/0507021](#).

[81] G. J. Drexlin, *Prog. Part. Nucl. Phys.* 48 (2002) 73. E.D. Church et al., *Phys. Rev.* D66 (2002) 013001 ([hep-ex/0203023](#)).

[82] The **MiniBoone** experiment is described at www-boone.fnal.gov.

[83] **Interpretations of the LSND anomaly.** Papers discussing mostly sterile neutrinos: N. Okada, O. Yasuda, *Int. J. Mod. Phys.* A12 (1997) 3669 ([hep-ph/9606411](#)). S.M. Bilenky, C. Giunti, W. Grimus, *Eur. Phys. J.* C1 (1998) 247 ([hep-ph/9607372](#)). V.D. Barger et al., *Phys. Lett.* B489 (2000) 345 ([hep-ph/0008019](#)). C. Giunti, M. Laveder, *JHEP* 102 (2001) 1 ([hep-ph/0010009](#)). O.L.G. Peres, A.Yu. Smirnov, *Nucl. Phys.* B599 (2001) 3 ([hep-ph/0011054](#)). W. Grimus, T. Schwetz, *Eur. Phys. J.* C20 (2001) 1 ([hep-ph/0102252](#)). M. Maltoni, T. Schwetz, J.W. Valle, *Phys. Lett.* B518 (2001) 252 ([hep-ph/0107150](#)). A. Strumia, *Phys. Lett.* B539 (2002) 91 ([hep-ph/0201134](#)). M. Maltoni, T. Schwetz, M.A. Tortola, J.W.F. Valle, *Nucl. Phys.* B643 (2002) 321 ([hep-ph/0207157](#)). R. Foot, *Mod. Phys. Lett.* A18 (2003) 2079 ([hep-ph/0210393](#)). H. Pas, L.G. Song, T.J. Weiler, *Phys. Rev.* D67 (2003) 073019 ([hep-ph/0209373](#)). H. Nunokawa, O. L. Peres, R. Zukanovich Funchal, *Phys. Lett.* B562 (2003) 279 ([hep-ph/0302039](#)).

Papers discussing only CPT-violating solutions: H. Murayama, T. Yanagida, *Phys. Lett.* B520 (2001) 263 ([hep-ph/0010178](#)). G. Barenboim, L. Borissov, J. Lykken, A. Smirnov, *JHEP* 10 (2002) 001 ([hep-ph/0108199](#)). S. Skadhauge, *Nucl. Phys.* B639 (2002) 281 ([hep-ph/0112189](#)). G. Barenboim, L. Borissov, J. Lykken, *Phys. Lett.* B534 (2002) 106 ([hep-ph/0201080](#)). A. de Gouvea, *Phys. Rev.* D66 (2002) 076005 ([hep-ph/0204077](#)). G. Barenboim, L. Borissov, J. Lykken., [hep-ph/0212116](#). M.C. Gonzalez-Garcia, M. Maltoni, T. Schwetz, *Phys. Rev.* D68 (2003) 053007 ([hep-ph/0306226](#)).

Papers dicussing only anomalous μ -decay: K.S. Babu, S. Pakvasa, [hep-ph/0204236](#). KARMEN collaboration, *Phys. Rev. Lett.* 90 (2003) 181804 ([hep-ex/0302017](#)). Anomalous neutrino couplings are partially discussed in S. Bergmann and Y. Grossman, *Phys. Rev.* D59 (1999) 093005. Two sterile neutrinos: M. Sorel, J. Conrad, M. Shaevitz, *Phys. Rev.* D70 (2004) 073004 ([hep-ph/0305255](#)). Sterile neutrino plus CPT-violation: V. Barger, D. Marfatia, K. Whisnant, *Phys. Lett.* B576 (2003) 303 ([hep-ph/0308299](#)).

Decaying sterile neutrinos: S. Palomares-Ruiz, S. Pascoli, T. Schwetz, *JHEP* 09 (2005) 048 ([hep-ph/0505216](#)) (it is difficult to obtain this scenario from a $SU(2)_L$ -invariant high energy theory). Mass-varying neutrinos: see e.g. S. Barshay, G. Kreyerhoff, *Astropart. Phys.* 10 (1999) 107; D.B. Kaplan, A.E. Nelson, N. Weiner, *Phys. Rev. Lett.* 93 (2004) 091801 ([hep-ph/0401099](#)). Mass-varying sterile neutrinos: V. Barger, D. Marfatia, K. Whisnant, *Phys. Rev.* D73 (2006) 013005 ([hep-ph/0509163](#)). Peculiar Lorentz violation: A. de Gouvea, Y. Grossman, [hep-ph/0602237](#).

[84] F. Dydak et al., the CDHS collaboration, *Phys. Lett.* 134B (1984) 281; I.E. Stockdale, the CCFR collaboration, *Phys. Rev. Lett.* 52 (1984) 1384.

[85] ALEPH, DELPHI, L3, OPAL collaborations and LEP, SLD electroweak working groups, [hep-ex/0312023](#). See also the LEP electroweak working group, web page www.web.cern.ch/LEPEWWG.

[86] TWIST collaboration, *Phys. Rev. Lett.* 94 (2005) 101805 ([hep-ex/0409063](#)). TWIST collaboration, *Phys. Rev.* D71 (2005) 071101 ([hep-ex/0410045](#)).

[87] **Possible tests of the NuTeV anomaly.** Møller scattering: E158 collaboration, *ECONF* C0307282 (2003) TTH04 ([hep-ex/0403010](#)). Reactor experiment: J.M. Conrad, J.M. Link, M.H. Shaevitz, *Phys. Rev.* D71 (2005) 073013 ([hep-ex/0403048](#)).

[88] E.A. Paschos, L. Wolfenstein, *Phys. Rev.* D7 (1973) 91.

[89] **CCFR.** CCFR collaboration, *Eur. Phys. J.* C1 (1998) 509 ([hep-ex/9701010](#)).

[90] **Interpretations of the NuTeV anomaly.** Various new and old-physics interpretations have been discussed in S. Davidson et al., *JHEP* 0202 (2002) 037 ([hep-ph/0112302](#)). For more recent summaries see A. Strumia, [hep-ex/0304039](#); J.T. Londergan, *Nucl. Phys. Proc. Suppl.* 141 (2005) 68 ([hep-ph/0408243](#)).

Isospin-breaking effects. Recent global fit: A.D. Martin, R.G. Roberts, W.J. Stirling, R.S. Thorne, *Eur. Phys. J.* C35 (2004) 325 ([hep-ph/0308087](#)). K. J. Eskola, H. Paukkunen, [hep-ph/0603155](#). For model computations see J. T. Londergan, A. W. Thomas, [hep-ph/0301147](#) and [hep-ph/0303155](#). M. Hirai, S. Kumano, T.H. Nagai, *Phys. Rev.* D71 (2005) 113007 ([hep-ph/0412284](#)). Y. Ding, R.G. Xu, B.Q. Ma, *Phys. Rev.* D71 (2005) 094014 ([hep-ph/0505153](#)).

Strange momentum asymmetry. First attempt of extracting it from DIS data: V. Barone, C. Pascaud, F. Zomer, *Eur. Phys. J.* C12 (2000) 243

([hep-ph/9907512](#)). Recent global fit (including dimuon data): S. Kretzer, F. Olness, J. Pumplin, M.H. Reno, D. Stump, W.K. Tung, *Phys. Rev. Lett.* 93 (2004) 041802 ([hep-ph/0312322](#)). F. Olness et al., *Phys. Rev. Lett.* 93 (2004) 041802 ([hep-ph/0312323](#)). NuTeV collaboration, *hep-ex/0405037*. For model computations see S.J. Brodsky, B.Q. Ma, *Phys. Lett.* B381 (1996) 317. H. Holtmann, A. Szczurek, J. Speth, *Phys. A*569 (1996) 631. F.G. Cao, A.I. Signal, *Phys. Lett.* B559 (2003) 229 ([hep-ph/0302206](#)). Y. Ding, B.Q. Ma, *Phys. Lett.* B590 (2004) 216 ([hep-ph/0405178](#)). J. Alwall, G. Ingelman, *Phys. Rev.* D70 (2004) 111505 ([hep-ph/0407364](#)). Y. Ding, R.G. Xu, B.Q. Ma, *Phys. Lett.* B607 (2005) 101 ([hep-ph/0408292](#)). M. Wakamatsu, *Phys. Rev.* D71 (2005) 057504 ([hep-ph/0411203](#)). hepart[hep-ph/0602241]Y. Ding, B.-Q. Ma.

Nuclear effects: G. A. Miller, A. W. Thomas, *Int. J. Mod. Phys.* A20 (2005) 95 ([hep-ex/0204007](#)). S. Kovalenko, I. Schmidt, J.-J. Yang, *Phys. Lett.* B546 (2002) 68. S. Kumano, *Phys. Rev.* D66 (2002) 111301 ([hep-ph/0209200](#)). S.A. Kulagin, *Phys. Rev.* D67 (2003) 091301 ([hep-ph/0301045](#)). W. Melnitchouk, A. W. Thomas, *Phys. Rev.* C67 (2003) 038201. S.J. Brodsky, I. Schmidt, J.J. Yang, *Phys. Rev.* D70 (2004) 116003 ([hep-ph/0409279](#)).

New physics: SUSY with violation of R parity: A. Kurylov et al., *Nucl. Phys.* B667 (2003) 321 ([hep-ph/0301208](#)). ν_e oscillations: C. Giunti, M. Laveder, [hep-ph/0202152](#). Mixing with a sterile ν : K.S. Babu, J.C. Pati, [hep-ph/0203029](#). W. Loinaz, N. Okamura, T. Takeuchi, L.C. Wijewardhana, *Phys. Rev.* D67 (2003) 073012 ([hep-ph/0210193](#)). Light Z' boson: C. Boehm, *Phys. Rev.* D70 (2004) 055007 ([hep-ph/0405240](#)).

NLO QCD corrections: S. Kretzer, M.H. Reno, *Phys. Rev.* D69 (2004) 034002 ([hep-ph/0307023](#)). B.A. Dobrescu, R. K. Ellis, *Phys. Rev.* D69 (2004) 114014 ([hep-ph/0310154](#)).

QED corrections: K. Diener, S. Dittmaier, W. Hollik, *Phys. Rev.* D69 (2004) 073005 ([hep-ph/0310364](#)).

[91] **BBN.** Original papers: C. Hayashi, *Prog. Theo. Phys.* 5 (1950) 224. R.A. Alpher, R.C. Herman, *Rev. Mod. Phys.* 22 (1950) 153. F. Hoyle, R.J. Tayler, *Nature* 203 (1964) 1108. P.J.E. Peebles, *Phys. Rev. Lett.* 16 (1966) 411.

Analytical approximations: J. Bernstein et al., *Rev. Mod. Phys.* 61 (1989) 25. R. Esmailzadeh, G.D. Starkman, S. Dimopoulos, *Astrophysical Journal* 378 (1991) 504.

Precision computations: Radiative and thermal corrections have been included in D.A. Dicus et al., *Phys. Rev.* D26 (1982) 2694. Neutrino reheating in A. Dolgov, M. Fukugita, *Phys. Rev.* D46 (1992) 5378. Effects of observed oscillations have been computed in S. Hannestad, *Phys. Rev.* D65 (2002) 083006 ([astro-ph/0111423](#)). For recent full computations see R.E. Lopez, M.S. Turner, *Phys. Rev.* D59 (1999) 103502. S. Esposito, G. Mangano, G. Miele, O. Pisanti, *Nucl. Phys.* B568 (2000) 421. G. Mangano, G. Miele, S. Pastor, M. Peloso, *Phys. Lett.* B534 (2002) 8 ([astro-ph/0111408](#)). S. Esposito et al., *Phys. Rev.* D63 (2001) 043004 ([astro-ph/0007419](#)).

Recent analyses: P. Di Bari, *Phys. Rev. D* 65 (2002) 043509 and addendum: P. Di Bari, *Phys. Rev. D* 67 (2003) 127301. R. H. Cyburt, B. D. Fields, K. A. Olive, *Phys. Lett. B* 567 (2003) 227. S. Hannestad as cited in [96]. V. Barger et al., *Phys. Lett.* B566 (2003) 8 ([hep-ph/0305075](#)). G. Mangano et al., *Nucl. Phys.* B729 (2005) 221 ([hep-ph/0506164](#)).

[92] **Recent measurements of the helium-4 primordial abundance.** A. Peimbert, M. Peimbert, V. Luridiana, *Astrophys. J.* 565 (2002) 668. Y.I. Izotov, T.X. Thuan, *Astrophys. J.* 602 (2004) 200 ([astro-ph/0310421](#)). K.A. Olive, E.D. Skillman, *Astrophys. J.* 617 (2004) 29 ([astro-ph/0405588](#)). M. Fukugita, M. Kawasaki, [astro-ph/0603334](#).

Recent measurements of the deuterium primordial abundance. D. Kirkman, D. Tytler, S. Burles, D. Lubin, J.M. O'Meara, *Astrophys. J.* 529 (2000) 665. J. M. O'Meara, D. Tytler, D. Kirkman, N. Suzuki, J.X. Prochaska, D. Lubin, A.M. Wolfe, *Astrophys. J.* 552 (2001) 718. D. Kirkman, D. Tytler, N. Suzuki, J.M. O'Meara, D. Lubin, *Astrophys. J. Suppl.* 149 (2003) 1 ([astro-ph/0302006](#)). M. Pettini, D.V. Bowen, *Astrophys. J.* 560 (2001) 41. S. D'Odorico, M. Dessauges-Zavadsky, P. Molaro, *Astronomy and Astrophysics* 368 (2001) L21. S.A. Levshakov, P. Molaro, M. Dessauges-Zavadsky, S. D'Odorico, *Astrophys. J.* 565 (2002) 696.

[93] **Sterile/active oscillations and BBN.** D. Kirilova, Dubna preprint JINR E2-88-301. R. Barbieri, A. Dolgov, *Phys. Lett.* B237 (1990) 440. K. Enqvist et al., *Phys. Lett.* B249 (1990) 531. K. Kainulainen, *Phys. Lett.* B244 (1990) 191. R. Barbieri, A. Dolgov, *Nucl. Phys.* B349 (1991) 743. K. Enqvist et al., *Nucl. Phys.* B373 (1992) 498. J.M. Cline, *Phys. Rev. Lett.* 68 (1992) 3137. X. Shi, D.N. Schramm, B.D. Fields, *Phys. Rev.* D48 (1993) 2563. R. Foot, M.J. Thomson, R.R. Volkas, *Phys. Rev.* D53 (1996) 5349. E. Lisi, S. Sarkar, F.L. Villante, *Phys. Rev.* D59

(1999) 123520 ([hep-ph/9901404](#)). D.P. Kirilova, M.V. Chizhov, *Phys. Rev.* D58 (1998) 073004 ([hep-ph/9707282](#)). D.P. Kirilova, M.V. Chizhov, *Nucl. Phys.* B591 (2000) 457 ([hep-ph/9909408](#)). A.D. Dolgov et al., *Nucl. Phys.* B632 (2002) 363. H.N. Abazajian, *Astropart. Phys.* 19 (2003) 303 ([astro-ph/0205238](#)). Sterile neutrinos and inhomogeneities: K. Abazajian, *Phys. Rev.* D73 (2006) 063506 ([astro-ph/0511630](#)).

[94] **Reviews, books.** Neutrinos: M.C. Gonzalez-Garcia, Y. Nir, *Rev. Mod. Phys.* 75 (2003) 345 ([hep-ph/0202058](#)). Some more recent mini reviews on neutrinos: W.M. Alberico, S.M. Bilenky, *Phys. Part. Nucl.* 35 (2004) 297 ([hep-ph/0306239](#)). W. Grimus, *Lect. Notes Phys.* 629 (2004) 169 ([hep-ph/0307149](#)). Z. Xing, *Int. J. Mod. Phys.* A19 (2004) 1 ([hep-ph/0307359](#)). V. Barger, D. Marfatia, K. Whisnant, *Int. J. Mod. Phys.* E12 (2003) 569 ([hep-ph/0308123](#)). C. Giunti, M. Laveder, [hep-ph/0310238](#). The basic formalism: B. Kayser, [hep-ph/0211134](#). The basic formalism, with an extensive discussion of alternatives to oscillations: S. Pakvasa, J.W.F. Valle, *Proc. Indian Natl. Sci. Acad.* 70A (2004) 189 ([hep-ph/0301061](#)). Non oscillation experiments: S.M. Bilenky et al., *Phys. Rept.* 379 (2003) 69 ([hep-ph/0211462](#)). Majorana neutrino masses: S.M. Bilenky, *J. Phys.* G32 (2006) R127 ([hep-ph/0511227](#)). Charm physics with neutrinos: G. de Lellis, P. Migliozzi, P. Santorelli, *Phys. Rep.* 399 (2004) 227. Solar neutrino physics: L. Miramonti, F. Reseghetti, *Riv. Nuovo Cim.* 25N7 (2002) 1 ([hep-ex/0302035](#)). Solar neutrino experiments: A. Bellerive, *Int. J. Mod. Phys.* A19 (2004) 1167 ([hep-ex/0312045](#)). Double β decay: S.R. Elliott, P. Vogel, *Ann. Rev. Nucl. Part. Sci.* 52 (2002) 115 ([hep-ph/0202264](#)). Neutrino astronomy: F. Halzen, D. Hooper, *Rept. Prog. Phys.* 65 (2002) 1025 ([astro-ph/0204527](#)). Physics of neutrinos and applications to astrophysics, M. Fukugita, T. Yanagida, *Physics of neutrinos and applications to astrophysics* (2003) Berlin, Springer. Neutrinos and cosmology: A.D. Dolgov, *Phys. Rept.* 370 (2002) 333 ([hep-ph/0202122](#)). R.R. Volkas, *AIP Conf. Proc.* 655 (2003) 220 ([hep-ph/0211309](#)). Big bang nucleosynthesis: P.J.E. Peebles, *Physical Cosmology* (1971) Princeton University Press, Princeton. S. Weinberg, *Gravitation and Cosmology* (1972) Basic Books, New York. S. Sarkar, *Rep. on Prog. in Phys.* 59 (1996) 1493 ([hep-ph/9602260](#)). Sphalerons: V.A. Rubakov, M.E. Shaposhnikov, *Phys. Usp.* 39 (1996) 461 ([hep-ph/9603208](#)). Baryogenesis: A. Riotto, M. Trodden, *Ann. Rev. Nucl. Part. Sci.* 49 (1999) 35 ([hep-ph/9901362](#)).

Realizations of baryogenesis through leptogenesis: K. Hamaguchi, [hep-ph/0212305](#). W. Buchmuller, P. Di Bari, M. Plumacher, *Ann. Phys.* 315 (2005) 305 ([hep-ph/0401240](#)). T. Hambye, [hep-ph/0412053](#). W. Buchmuller, R.D. Peccei, T. Yanagida, *Ann. Rev. Nucl. Part. Sci.* 55 (2005) 311 ([hep-ph/0502169](#)). Neutrinos from supernovæ: K. Kotake, K. Sato, K. Takanashi, [astro-ph/0509046](#). S. Woosley, H.T. Janka, [astro-ph/0601261](#).

Flavour models: G. Altarelli, F. Feruglio, *Phys. Rept.* 320 (1999) 295. G. Altarelli, F. Feruglio, *Springer Tracts Mod. Phys.* 190 (2003) 169 ([hep-ph/0206077](#)). R.N. Mohapatra, [hep-ph/0211252](#). S. King, *Rept. Prog. Phys.* 67 (2004) 107 ([hep-ph/0310204](#)). A.S. Joshipura, [hep-ph/0411154](#). Neutrinos and CMB: S. Bashinsky, U. Seljak, *Phys. Rev.* D69 (2004) 083002 ([astro-ph/0310198](#)). Neutrino experiments: R.D. McKeown, P. Vogel, *Phys. Rept.* 394 (2004) 315 ([hep-ph/0402025](#)). For a full list of recent references see www.nu.to.infn.it.

[95] **Interacting neutrinos and CMB.** Present data have been analyzed in the following works, finding somewhat different results. S. Hannestad, *JCAP* 0502 (2005) 011 ([astro-ph/0411475](#)). S. Hannestad, G. Raffelt, *Phys. Rev.* D72 (2005) 103514 ([hep-ph/0509278](#)). N. Bell, E. Pierpaoli, K. Sigurdson, *Phys. Rev.* D73 (2006) 063523 ([astro-ph/0511410](#)).

[96] **Cosmological bounds on neutrino cosmology.** For a review see J. Lesgourges, S. Pastor, [astro-ph/0603494](#). Cosmological signals of neutrino masses were explored in J.R. Bond, A. Szalay, *ApJ* 276 (1983) 443. C.P. Ma, E. Bertschinger, *ApJ* 455 (1985) 7. S. Dodelson, E. Gates, A. Stebbins, *Astrophys. J.* 467 (1996) 10 ([astro-ph/9509147](#)). For a recent global fits see D.N. Spergel et al., [astro-ph/0603449](#) U. Seljak, A. Slosar, P. McDonald, [astro-ph/0604335](#). Using only CMB: M. Fukugita et al., [astro-ph/0605362](#). Previous analyses found similar (sometimes weaker) bounds: S. Hannestad, *JCAP* 0305 (2003) 004 ([astro-ph/0303076](#)), S.W. Allen, R.W. Schmidt, S.L. Bridle, *Mon. Not. Roy. Astron. Soc.* 346 (2003) 593 ([astro-ph/0306386](#)), SDSS collaboration, *Phys. Rev.* D69 (2004) 103501 ([astro-ph/0310723](#)). The robustness of the bound in presence of non-adiabatic incoherent fluctuations was studied in R.H. Brandenberger, A. Mazumdar, M. Yamaguchi, *Phys. Rev.* D69 (2004) 081301 ([hep-ph/0401239](#)). In the future, significant improvements can be obtained by measuring gravitational lens-

ing produced by LSS. See e.g. L. Wan Waerbeke, Y. Mellier, [astro-ph/0305089](#). A. Refregier, *Ann. Rev. Astron. Astrophys.* 41 (2003) 645 ([astro-ph/0307212](#)). The impact of future data on neutrino masses searches is discussed in S. Wang et al., *Phys. Rev. Lett.* 95 (2005) 011302 ([astro-ph/0505390](#)). J. Lesgourges, L. Perotto, S. Pastor, M. Piat, *Phys. Rev.* D73 (2006) 045021 ([astro-ph/0511735](#)).

[97] **Cosmology.** See e.g. E.W. Kolb, M. S. Turner, *The Early Universe* (1989) frontiers in physics, Addison-Wesley. A.R. Liddle, D.H. Lyth, *Cosmological Inflation and Large-Scale Structure* (2000) Cambridge University Press, UK.

[98] **Detection of relic neutrinos.** Coherent scattering: Y. Zeldovich and M. Khlopov, *Sov. Phys. Usp.* 24 (1981) 755; P. Smith and J. Lewin, *Phys. Lett.* 127B (1983) 185; I. Ferreras and I. Wasserman, *Phys. Rev.* D52 (1995) 5459. Stodolsky effect: L. Stodolsky, *Phys. Rev. Lett.* 34 (1975) 110 erratum-ibid. 34 (1975) 508; N. Cabibbo, L. Maiani, *Phys. Lett.* B114 (1982) 115. P. Langacker, J.P. Leveille, and J. Sheiman, *Phys. Rev.* D27 (1983) 1228. We omitted papers with erroneous results.

For recent discussion see G. Duda, G. Gelmini and S. Nussinov, *Phys. Rev.* D64 (2001) 122001 ([hep-ph/0107027](#)); A. Ringwald, [hep-ph/0301157](#). Experimental prospects: C. Hagmann, [astro-ph/9905258](#); P.F. Smith, *Phil. Trans. Roy. Soc. Lond.* A361 (2003) 2591. P. Barbeau, J. Collar, J. Miyamoto, I. Shipsey, *IEEE Trans. Nucl. Sci.* 50 (2003) 1285 ([hep-ex/0212034](#)).

Scatterings of relic neutrinos with cosmic rays: T.J. Weiler, *Astrophys. J.* 285 (1984) 495; D. Faragon, B. Mele and A. Salis, *Astrophys. J.* 517 (1999) 725 ([astro-ph/9710029](#)); T. J. Weiler, *Astropart. Phys.* 11 (1999) 303 ([hep-ph/9710431](#)); S. Yoshida, G. Sigl, S. J. Lee, *Phys. Rev. Lett.* 81 (1998) 5505 ([hep-ph/9808324](#)); Z. Fodor, S. D. Katz and A. Ringwald, *JHEP* 0206 (2002) 046 ([hep-ph/0203198](#)); B. Eberle, A. Ringwald, L. Song and T. J. Weiler, *Phys. Rev.* D70 (2004) 023007 ([hep-ph/0401203](#)).

The local density of CMB neutrinos has been studied in S. Singh and C. P. Ma, *Phys. Rev.* D67 (2003) 023506 ([astro-ph/0208419](#)); A. Ringwald, Y.Y.Y. Wong, *JCAP* 0412 (2004) 005 ([hep-ph/0408241](#)). For general constraints following from the Pauli principle see D. Lynden-Bell, *Mon. Not. Roy. Astron. Soc.* 136 (1967) 101; S. Tremaine, J.E. Gunn, *Phys. Rev. Lett.* 42 (1979) 407; A. Kull, R. A. Treumann, H. Böhringer, *Astrophys. J.* 466 (1996) L1 ([astro-ph/9606057](#)). See also pag. 373 of the book by Kolb and Turner in [97].

[99] **Neutrinos and dark energy.** Mass-varying neutrinos were proposed in R. Fardon, A. E. Nelson, N. Weiner, *JCAP* 0410 (2004) 005 ([astro-ph/0309800](#)). Tentative models were built in R. Takanashi, M. Tanimoto, *Phys. Lett.* B633 (2006) 675 ([hep-ph/0507142](#)). R. Fardon, A. E. Nelson, N. Weiner, *JHEP* 03 (2006) 042 ([hep-ph/0507235](#)). However mass-varying neutrinos fail in reproducing dark energy as soon as CMB neutrinos become non relativistic, see M. Afshordi, M. Zaldarriaga, K. Kohri, *Phys. Rev.* D72 (2005) 065024 ([astro-ph/0506663](#)).

A different possible connection between neutrino masses and dark energy was discussed in R. Barbieri, L. Hall, S. Oliver, A. Strumia, *Phys. Lett.* B625 (2005) 189 ([hep-ph/0505124](#)).

[100] **Baryogenesis.** Sakharov conditions: A.D. Sakharov, *JETP Lett.* 91B (1967) 24. Anomalies: G. 't Hooft, *Phys. Rev. Lett.* 37 (1976) 37. G. 't Hooft, *Phys. Rev.* D14 (1976) 3432. Sphalerons: N.S. Manton, *Phys. Rev.* D28 (1983) 2019. V. Kuzmin, V.A. Rubakov and M.E. Shaposhnikov, *Phys. Lett.* 155B (1985) 36. J. Ambj?rn, T. Askgaard, H. Porter and M.E. Shaposhnikov, *Nucl. Phys.* B353 (1991) 346. P. Arnold, D. Son and L.G. Yaffe, *Phys. Rev.* D55 (1997) 6264 ([hep-ph/9609481](#)) pointed out that sphaleron rates are suppressed by an extra factor α_2 with respect to a 'classical' estimate. The sphaleron rate at TeV-scale temperature is summarized in Y. Burnier, M. Laine, M. Shaposhnikov, *JCAP* 0602 (2006) 007 ([hep-ph/0511246](#)).

See also among the reviews in [94].

[101] See e.g. in G.'t Hooft, M. Veltman, *Diagrammar* (1973) CERN yellow report, available from cds.cern.ch.

[102] **Constraints from leptogenesis.** The maximal CP asymmetry ϵ_1 of eq. (10.24) was derived in S. Davidson, A. Ibarra, *Phys. Lett.* B535 (2002) 25 ([hep-ph/0202239](#)). The bound on ϵ_1 at fixed \tilde{m} was derived in W. Buchmuller, P. Di Bari, M. Plümacher, *Nucl. Phys.* B665 (2003) 445 ([hep-ph/0302092](#)) and revised in T. Hambye et al., *Nucl. Phys.* B695 (2004) 169 ([hep-ph/0312203](#)). Mildly hierarchical right-handed neutrinos allow a much larger ϵ_1 , as discussed in S. Davidson, R. Kitano, *JHEP* 0403 (2004) 020 ([hep-ph/0312007](#)); M. Raidal, A. Strumia, K. Turzynski, *Phys. Lett.* B609 (2005) 351 ([hep-ph/0408015](#)).

For recent studies, mostly trying to find links with flavour models, see e.g. W. Buchmuller, D. Wyler, *Phys. Lett.* B521 (2001) 291 ([hep-ph/0108216](#)).

G.C. Branco et al., *Phys. Rev.* D67 (2003) 073025 ([hep-ph/0211001](#)). S. Davidson, *JHEP* 03 (2003) 037 ([hep-ph/0302075](#)). E. Kh. Akhmedov, M. Frigerio, A. Yu. Smirnov, *JHEP* 09 (2003) 021 ([hep-ph/0305322](#)). Connections with gravitinos is discussed in M. Fuji, T. Yanagida, *Phys. Lett.* B549 (2003) 273 ([hep-ph/0208191](#)). R. Allahverdi et al., [hep-ph/0504102](#)

[103] **Leptogenesis in non-minimal models.** Supersymmetric leptogenesis has been first studied in M. Plümacher, *Nucl. Phys.* B530 (1998) 207 ([hep-ph/9704231](#)). M. Plümacher, [hep-ph/9807557](#). Contributions from supersymmetry-breaking to the CP-asymmetry ('soft leptogenesis'): L. Boubekeur, [hep-ph/0208003](#). Y. Grossman, T. Kashti, Y. Nir, E. Roulet, *Phys. Rev. Lett.* 91 (2003) 251801 ([hep-ph/0307081](#)). First precise results (in a particular limit): G. D'Ambrosio, G. F. Giudice, M. Raidal, *Phys. Lett.* B575 (2003) 75 ([hep-ph/0308031](#)). First systematic analysis: Y. Grossman, T. Kashti, Y. Nir, E. Roulet, *JHEP* 11 (2004) 080 ([hep-ph/0407063](#)). G. D'Ambrosio et al., *Phys. Lett.* B604 (2004) 199 ([hep-ph/0407312](#)). T. Kashti, *Phys. Rev.* D71 (2005) 013008 ([hep-ph/0410319](#)). J. Ellis, S.K. Kang, [hep-ph/0505162](#). Contributions to the CP-asymmetry from R -parity violating NH_uH_d couplings: Y. Farzan, J.W.F. Valle, *Phys. Rev. Lett.* 96 (2006) 011601 ([hep-ph/0509280](#)).

Leptogenesis in left/right symmetric models: K.S. Babu, A. Bachri, H. Aissaoui, *Nucl. Phys.* B738 (2006) 76 ([hep-ph/0509091](#)). M. Frigerio, T. Hambye, E. Ma, [hep-ph/0603123](#). Effects of an enlarged gauge group at the leptogenesis scale have been studied in N. Cosme, *JHEP* 08 (2004) 027 ([hep-ph/0403209](#)). P.Q. Hung, [hep-ph/0604063](#). Effects of a modified expansion rate: N. Okada, O. Seto, *Phys. Rev.* D73 (2006) 063505 ([hep-ph/0507279](#)). Leptogenesis in brane-world cosmology: M. Bento, R. Gonzalez Felipe, N. Santos, *Phys. Rev.* D73 (2006) 023506 ([hep-ph/0508213](#)). Leptogenesis with quasi-degenerate right-handed neutrinos: M. Flanz, E.A. Paschos, U. Sarkar and J. Weiss, *Phys. Lett.* B389 (1996) 693. L. Covi, E. Roulet, *Phys. Lett.* B399 (1997) 113. A. Pilaftsis, *Phys. Rev.* D56 (1997) 5431 ([hep-ph/9707235](#)). A. Pilaftsis, T. Underwood, *Nucl. Phys.* B692 (2004) 303 ([hep-ph/0309342](#)). G. Branco, R. Gonzalez Felipe, F. Joaquim, B. Nobre, *Phys. Lett.* B633 (2006) 336 ([hep-ph/0507092](#)). A. Anisimov, A. Broncano, M. Plumacher, *Nucl. Phys.* B737 (2006) 176 ([hep-ph/0511248](#)). Leptogenesis from scalar triplets: T. Hambye, E. Ma, U. Sarkar, *Nucl. Phys.* B602 (2001) 23. T. Hambye, G. Senjanovic, *Phys. Lett.* B582 (2004) 73. S. Antusch, S.F. King, *Phys. Lett.* B597 (2004) 199. The efficiency and maximal CP asymmetry is computed in T. Hambye, M. Raidal, A. Strumia, *Phys. Lett.* B632 (2006) 667 ([hep-ph/0510008](#)).

Dirac leptogenesis: K. Dick, M. Lindner, M. Ratz, D. Wright, *Phys. Rev. Lett.* 84 (2000) 4039 ([hep-ph/9907562](#)). H. Murayama, A. Pierce, *Phys. Rev. Lett.* 89 (2002) 271601 ([hep-ph/0206177](#)).

[104] **Minimal see-saw texture.** A minimal predictive texture was presented in: P.H. Frampton, S.L. Glashow, T. Yanagida, *Phys. Lett.* B548 (2002) 119 ([hep-ph/0208157](#)). Its predictions have been discussed in: M. Raidal, A. Strumia, *Phys. Lett.* B553 (2003) 72 ([hep-ph/0210021](#)). S. Raby, *Phys. Lett.* B561 (2003) 119 ([hep-ph/0302027](#)). Models with two right-handed neutrinos have been discussed in S.F. King, *Phys. Rev.* D67 (2003) 113010 ([hep-ph/0211228](#)). V. Barger, D.A. Dicus, H.-J. He, T.-J. Li, *Phys. Lett.* B583 (2004) 173 ([hep-ph/0310278](#)). A. Ibarra, G.G. Ross, *Phys. Lett.* B591 (2004) 285 ([hep-ph/0312138](#)). J.-W. Mei, Z.-Z. Xing, *Phys. Rev.* D69 (2004) 073003 ([hep-ph/0312167](#)).

[105] **SN 1987A data.** The Kamiokande II collaboration, *Phys. Rev. Lett.* 58 (1987) 1490. The Kamiokande II collaboration, *Phys. Rev.* D38 (1988) 448. The IMB collaboration, *Phys. Rev. Lett.* 58 (1987) 1494. The IMB collaboration, *Phys. Rev.* D37 (1988) 3361. The BUST collaboration, *JETP Lett.* 45 (1987) 589. The BUST collaboration, *Phys. Lett.* B205 (1988) 209. The LSD collaboration, *JETP Lett.* 45 (1987) 593.

[106] V.L. Dadykin, G.T. Zatsepin, O.G. Ryazhskaya, *Sov. Phys. Usp.* 32(5) (1989) 459 and chapter 15 of J.N. Bahcall, "Neutrino astrophysics", Cambridge, UK: Univ. Pr. (1989).

[107] See e.g. the FLUKA calculation G. Battistoni et al., *Astropart. Phys.* 19 (2003) 269 and www.mi.infn.it/~battist/neutrino.html.

[108] **ν from DM annihilations.** J. Silk, K. A. Olive and M. Srednicki, *Phys. Rev. Lett.* 55 (1985) 257. M. Srednicki, K. A. Olive and J. Silk, *Nucl. Phys.* B279 (1987) 804. L.M. Krauss, K. Freese, D.N. Spergel, W.H. Press, *Astrophys. J.* 299 (1985) 1001. K. Freese, *Phys. Lett.* B167 (1986) 295. L. M. Krauss, M. Srednicki and F. Wilczek, *Phys. Rev.* D33 (1986) 2079. T. K. Gaisser, G. Steigman and S. Tilav, *Phys. Rev.* D34 (1986) 2206. G. B. Gelmini, P. Gondolo and E. Roulet, *Nucl. Phys.* B351 (1991) 623. M. Kamionkowski, *Phys. Rev.* D44 (1991) 3021. F. Halzen, T. Stelzer and M. Kamionkowski, *Phys. Rev.* D45 (1992)

4439. A. Bottino, V. de Alfaro, N. Fornengo, G. Mignola and M. Pignone, *Phys. Lett.* B265 (1991) 57. V. Berezinsky, A. Bottino, J. R. Ellis, N. Fornengo, G. Mignola and S. Scopel, *Astropart. Phys.* 5 (1996) 333 ([hep-ph/9603342](#)). L. Bergstrom, J. Edsjo and P. Gondolo, *Phys. Rev.* D55 (1997) 1765 ([hep-ph/9607237](#)). L. Bergstrom, J. Edsjo and M. Kamionkowski, *Astropart. Phys.* 7 (1997) 147 ([astro-ph/9702037](#)). L. Bergstrom, J. Edsjo and P. Gondolo, *Phys. Rev.* D58 (1998) 103519 ([hep-ph/9806293](#)). A. Bottino, F. Donato, N. Fornengo and S. Scopel, *Astropart. Phys.* 10 (1999) 203 ([hep-ph/9809239](#)). J. L. Feng, K. T. Matchev and F. Wilczek, *Phys. Rev.* D63 (2001) 045024 ([astro-ph/0008115](#)). V. D. Barger, F. Halzen, D. Hooper and C. Kao, *Phys. Rev.* D65 (2002) 075022 ([hep-ph/0105182](#)). V. Bertin, E. Nezri and J. Orloff, *Eur. Phys. J.* C26 (2002) 111 ([hep-ph/0204135](#)). V. Bertin, E. Nezri and J. Orloff, *JHEP* 0302 (2003) 046 ([hep-ph/0210034](#)). H. Baer, A. Belyaev, T. Krupovnickas and J. O'Farrill, *JCAP* 0408 (2004) 005 ([hep-ph/0405210](#)). K. M. Belotsky, M. Y. Khlopov, K. I. Shibaev, *Phys. Atom. Nucl.* 65 (2002) 382. K. M. Belotsky, T. Damour, M. Y. Khlopov, *Phys. Lett.* B529 (2002) 10 ([astro-ph/0201314](#)). D. Fargion et al., *Mod. Phys. Lett.* A11 (1996) 1363. A. E. Faraggi, K. A. Olive, M. Pospelov, *Astropart. Phys.* 13 (2000) 31 ([hep-ph/9906345](#)). I. F. M. Albuquerque, L. Hui and E. W. Kolb, *Phys. Rev.* D64 (2001) 083504 ([hep-ph/0009017](#)). The angular distribution of terrestrial ν DM is studied in J. Edsjo, P. Gondolo, *Phys. Lett.* B357 (1995) 595 ([hep-ph/9504283](#)). The impact of oscillations has also been discussed in: E. Roulet, *Phys. Lett.* B356 (1995) 264 ([hep-ph/9506221](#)); N. Fornengo, [hep-ph/9904351](#); M. Kovalski, *Phys. Lett.* B511 (2001) 119 ([hep-ph/0009183](#)); A. de Gouvea, *Phys. Rev.* D63 (2001) 093003 ([hep-ph/0006157](#)). The effect of neutrino interactions has been discussed in G. Jungman and M. Kamionkowski, *Phys. Rev.* D51 (1985) 328 ([hep-ph/9407351](#)). J. Edsjo, *Nucl. Phys. Proc. Suppl.* 43 (1995) 265 ([hep-ph/9504205](#)). The combined effect of oscillations and interactions has been discussed in P. R. Crotty, *Phys. Rev.* D66 (2002) 063504 ([hep-ph/0205116](#)). M. Cirelli et al., *Nucl. Phys.* B727 (2005) 99 ([hep-ph/0506298](#)). Background of solar corona neutrinos: G. Ingelman, M. Thunman, *Phys. Rev.* D54 (1996) 4385 ([hep-ph/9604288](#)).

[109] **Experimental constraints on ν DM.** BAKSAN collaboration (M. M. Boliev et al.), *Proc. of Int. Workshop on Aspects of Dark Matter in Astrophysics and Particle Physics*, Heidelberg, Germany, 16-20 Sep 1996. Published in *Heidelberg 1996, Dark matter in astro- and particle physics*, 711. BAIKAL collaboration, *Nucl. Phys. Proc. Suppl.* 143 (2005) 335-342. AMANDA collaboration, *Phys. Rev.* D66 (2002) 032006 ([astro-ph/0202370](#)); see also AMANDA collaboration, *Astropart. Phys.* 24 (2006) 459 ([astro-ph/0508518](#)) SK collaboration, *Phys. Rev.* D70 (2004) 083523 ([hep-ex/0404025](#)) and erratum: *ibid.* D70, 109901 (2004). MACRO collaboration, *Phys. Rev.* D60 (1999) 082002 ([hep-ex/9812020](#)).

Future proposals: ANTARES collaboration, “Prospects for dark matter searches with the ANTARES neutrino telescope”, prepared ofr the 4th International Workshop on the Identification of Dark Matter (IDM 2002), York, England, 2-6 Sep 2002. ICECUBE collaboration], *Astropart. Phys.* 20 (2004) 507 ([astro-ph/0305196](#)). NEMO collaboration, *Nucl. Phys. Proc. Suppl.* 138 (2005) 191 and web page [NEMOweb.lns.infn.it](#). NESTOR collaboration, web page [www.nestor.org.gr](#). See also [57].

[110] V.L. Ginzburg, S.I. Syrovatskii, “The origin of cosmic rays”, *Oxford, UK: Pergamon press (1964)*; V. Berezinsky et al., “Astrophysics of cosmic rays”, *Amsterdam, Netherlands: North-Holland (1990)* (Russian Ed. 1984). T.K. Gaisser, “Cosmic rays and particle physics”, *Cambridge, UK: Univ. Pr. (1990)*. For an updated discussion of galactic (resp. extragalactic) sources see W. Bednarek, G. F. Burgio, T. Montaruli, *New Astron. Rev.* 49 (2005) 1 (resp., F. Halzen, D. Hooper, *Rept. Prog. Phys.* 65 (2002) 1025). P. Lipari, [astro-ph/0605535](#)

[111] V. Berezinsky, M. Kachelriess, A. Vilenkin, *Phys. Rev. Lett.* 79 (1997) 4302. V. Berezinsky, A. Vilenkin, *Phys. Rev.* D62 (2000) 083512 ([hep-ph/9908257](#)).

[112] **Testing UHE neutrino cross sections.** A. Kusenko, T. Weiler, *Phys. Rev. Lett.* 88 (2002) 161101 ([hep-ph/0106071](#)). For extra-dimensional speculations see e.g. J. Feng, A. Shapere, *Phys. Rev. Lett.* 88 (2002) 021303 ([hep-ph/0109106](#)). R. Emparan, M. Masip, R. Rattazzi, *Phys. Rev.* D65 (2002) 064023 ([hep-ph/0109287](#)).

[113] AGASA Collaboration, *Nucl. Phys. Proc. Suppl.* 151 (2006) 3. HiRes collaboration, PoS HEP2005 (2006) 026. EAS-TOP collaboration, [SPIRES entry](#) prepared for the International Workshop on Frontier Science: Physics and Astrophysics in Space, Frascati and Rome, 14-19 June 2004.

[114] **AUGER**. Web page: www.auger.org. P. Billoir, *The highest energy neutrinos and the AUGER observatory*, talk given at NO-VE, Venice, Feb. 2006.

[115] **ANITA**. Web page: www.ps.uci.edu/~anita. ANITA collaboration, *Phys. Rev. Lett.* 96 (2006) 171101 ([astro-ph/0512265](http://arxiv.org/abs/astro-ph/0512265))

[116] D. Fargion, *Astroph. J.* 570 (2002) 909 ([astro-ph/0002453](http://arxiv.org/abs/astro-ph/0002453)).

[117] **Neutrinos from relic supernovæ**. Experimental constraints: Super-Kamiokande collaboration, *Phys. Rev. Lett.* 90 (2003) 061101 ([hep-ex/0209028](http://arxiv.org/abs/hep-ex/0209028)). KamLAND collaboration, *Phys. Rev. Lett.* 92 (2004) 071301 ([hep-ex/0310047](http://arxiv.org/abs/hep-ex/0310047)). Theoretical predictions: for recent works and references see C. Lunardini, [astro-ph/0509233](http://arxiv.org/abs/astro-ph/0509233). F. Daigne, K. Olive, P. Sandick, E. Vangioni, *Phys. Rev.* D72 (2005) 103007 ([astro-ph/0509404](http://arxiv.org/abs/astro-ph/0509404)).

[118] J.F. Beacom, M.R. Vagins, *Phys. Rev. Lett.* 93 (2004) 171101 ([hep-ph/0309300](http://arxiv.org/abs/hep-ph/0309300)). For theoretical considerations see S. Choubey, S. Petcov, *Phys. Lett.* B594 (2004) 333 ([hep-ph/0404103](http://arxiv.org/abs/hep-ph/0404103)).

[119] E. Cappellaro, R. Barbon, M. Turatto, [astro-ph/0310859](http://arxiv.org/abs/astro-ph/0310859) see also the web page of the Padova-Asiago Supernova Group www.pd.astro.it/supern.

[120] E.N. Alekseev, L.N. Alekseeva, *J. Exp. Theor. Phys.* 95 (2002) 5.

[121] V.S. Imshennik, *Astron. Lett.* 18 (1992) 489; C.L. Fryer and A. Heger, *Astrophys. J.* 541 (2000) 1033; T. Thompson, E. Quataert, A. Burrows, *Astrophys. J.* 620 (2005) 861 ([astro-ph/0403224](http://arxiv.org/abs/astro-ph/0403224)).

[122] T.J. Lamb, D.Q. Loredo, *Phys. Rev.* D65 (2002) 063002.

[123] Y.Z. Qian, G.M. Fuller, *Phys. Rev.* D51 (1995) 1479, K. Abazajian, G.M. Fuller, M. Patel, *Phys. Rev.* D64 (2001) 023501.

[124] A. De Rujula, *Phys. Lett.* B193 (1987) 514; V.S. Berezinsky et al., *Nuovo Cim.* 11C (1988) 287; V.S. Imshennik, O.G. Ryazhskaya, *Astron. Lett.* 30 (2004) 14;

[125] **Neutrino oscillations in supernovæ**. S.P. Mikheev, A.Yu. Smirnov, *Sov. Phys. JETP* 64 (1986) 4. Effects of solar oscillations: A.Y. Smirnov, D.N. Spergel, J.N. Bahcall, *Phys. Rev.* D49 (1994) 1389 ([hep-ph/9305204](http://arxiv.org/abs/hep-ph/9305204)). B. Jegerlehner, F. Neubig, G. Raffelt, *Phys. Rev.* D54 (1996) 1194. C. Lunardini, A. Yu. Smirnov, *Phys. Rev.* D63 (2001) 073009. Dependence on the initial temperatures has been studied in M. Kachelriess et al., *JHEP* 0101 (2001) 030. Effects of atmospheric θ_{13} oscillations:], *A. S. Dighe, A. Y. Smirnov* —PR (033007) D62 ([hep-ph/9907423](http://arxiv.org/abs/hep-ph/9907423))2000. V. Barger, P. Huber, D. Marfatia, *Phys. Lett.* B617 (2005) 167 ([hep-ph/0501184](http://arxiv.org/abs/hep-ph/0501184)). S.-H. Chiu, T.K. Kuo, [hep-ph/0511345](http://arxiv.org/abs/hep-ph/0511345). Their comparison with SN1987A data has been debated in H. Minakata, H. Nunokawa, *Phys. Lett.* B504 (2001) 301. V. Barger, D. Marfatia, B.P. Wood, *Phys. Lett.* B532 (2002) 19 ([hep-ph/0202158](http://arxiv.org/abs/hep-ph/0202158)). Effects of possible differences between ν_μ and ν_τ fluxes: E. K. Akhmedov, C. Lunardini, A. Y. Smirnov, *Nucl. Phys.* B643 (2002) 339 ([hep-ph/0204091](http://arxiv.org/abs/hep-ph/0204091)). Recent discussions of earth matter effects: C. Lunardini and A. Y. Smirnov, *Nucl. Phys.* B616 (307) 2001 ([hep-ph/0106149](http://arxiv.org/abs/hep-ph/0106149)). S. Dighe, M. Kachelriess, G. G. Raffelt, R. Tomas, *JCAP* 0401 (2004) 004 ([hep-ph/0311172](http://arxiv.org/abs/hep-ph/0311172)).

Bounds on sterile oscillations from the SN 1987A rate were discussed in S.P. Mikheev, A.Yu. Smirnov, *JETP Lett.* 46 (1987) 10. X. Shi, G. Sigl, *Phys. Lett.* B323 (1994) 360 ([hep-ph/9312247](http://arxiv.org/abs/hep-ph/9312247)). A. D. Dolgov, S. H. Hansen, G. Raffelt, D. V. Semikoz, *Nucl. Phys.* B590 (2000) 562 ([hep-ph/0008138](http://arxiv.org/abs/hep-ph/0008138)). P. Keranen, J. Maalampi, M. Myyryläinen, J. Riittinen, *Phys. Lett.* B597 (2004) 374 ([hep-ph/0401082](http://arxiv.org/abs/hep-ph/0401082)). H. Nunokawa, J. T. Peltoniemi, A. Rossi, J. W. F. Valle, *Phys. Rev.* D56 (1997) 1704 ([hep-ph/9702372](http://arxiv.org/abs/hep-ph/9702372)). Neutrinos and the r-process: G.C. McLaughlin, J.M. Fetter, A.B. Balantekin, G.M. Fuller, *Phys. Rev.* C59 (1999) 2873 ([astro-ph/9902106](http://arxiv.org/abs/astro-ph/9902106)). D. O. Caldwell, G. M. Fuller, Y. Z. Qian, *Phys. Rev.* D61 (2000) 123005 ([astro-ph/9910175](http://arxiv.org/abs/astro-ph/9910175)). J. Fetter, G. C. McLaughlin, A. B. Balantekin, G. M. Fuller, *Astropart. Phys.* 18 (2003) 433 ([hep-ph/0205029](http://arxiv.org/abs/hep-ph/0205029)).

[126] The newest evaluation of the temperatures, including a comparison with previous results is given in M.T. Keil et al., *Astrophys. J.* 590 (2003) 971.

[127] M. Costantini, A. Ianni, F. Vissani, *Phys. Rev.* D70 (2004) 043006 ([astro-ph/0403436](http://arxiv.org/abs/astro-ph/0403436))

[128] J.F. Beacom, S. Palomarez-Ruiz, *Phys. Rev.* D67 (2003) 093001.

[129] **First attempts of understanding flavour**. See e.g. R. Gatto, G. Sartori, M. Tonin, *Phys. Lett.* B28 (1968) 128. S. Weinberg, *Trans. New York Acad. Sci.* 38 (1977) 185. F. Wilczek, A. Zee, *Phys. Lett.* B70 (1977) 418 and erratum *ibidem* 72B (1978) 504. H. Fritzsch, *Phys. Lett.* B70 (1977) 436.

[130] **Anthropic selection?** Anthropic selection suggests a cosmological constant only one or two orders of magnitude larger than the value suggested by present data: S. Weinberg, *Phys. Rev. Lett.* 59 (1987) 2607. Different ways of arguing allow to straighten or to weaken the anthropic upper limit on the cosmological constant: A. Vilenkin, *Phys. Rev. Lett.* 74 (1995) 846. M. Tegmark, M.J. Rees, *Astrophys. J.* 499 (1998) 526. Anthropic selection and fermion masses: V. Agrawal, S. M. Barr, J. F. Donoghue and D. Seckel, *Phys. Rev.* D57 (1998) 5480 ([hep-ph/9707380](#)). C. Hogan, *Rev. Mod. Phys.* 72 (2000) 1149 ([astro-ph/0407086](#)). See also F. Hoyle, *ApJS* 1 (1954) 121. Anthropic expectation for neutrino masses (?): M. Tegmark, A. Vilenkin, L. Pogosian, *Phys. Rev.* D71 (2005) 103523 ([astro-ph/0304536](#)).

[131] A. Strumia, *JHEP* 04 (1999) 026 ([hep-ph/9904245](#)).

[132] **Anarchy or hierarchy?** L.J. Hall, H. Murayama, N. Weiner, *Phys. Rev. Lett.* 84 (2000) 2572 ([hep-ph/9911341](#)). N. Haba, H. Murayama, *Phys. Rev.* D63 (2001) 053010 ([hep-ph/0009174](#)). F. Vissani, *Phys. Lett.* B508 (2001) 79 ([hep-ph/0102236](#)). V. Antonelli, F. Caravaglios, R. Ferrar, M. Picariello, *Phys. Lett.* B549 (2002) 325 ([hep-ph/0207347](#)). G. Altarelli, F. Feruglio, I. Masina, *JHEP* 0301 (2003) 035 ([hep-ph/0210342](#)). A. de Gouvea, H. Murayama, *Phys. Lett.* B573 (2003) 94 ([hep-ph/0301050](#)). J.R. Espinosa, [hep-ph/0306019](#). A. de Gouvea, *Phys. Rev.* D69 (2004) 093007 ([hep-ph/0401220](#)).

[133] **Models for normal hierarchy: dominant singlet.** For a general analysis, see: A.Y. Smirnov, *Phys. Rev.* D48 (1993) 3264 ([hep-ph/9304205](#)). For more focussed discussions, stimulated by data see: S.F. King, *Phys. Lett.* B439 (1998) 350 ([hep-ph/9806440](#)). R. Barbieri et al., *JHEP* 9812 (1998) 017 ([hep-ph/9807235](#)). S.F. King, *Nucl. Phys.* B562 (1999) 57 ([hep-ph/9904210](#)).

[134] **Models for inverted hierarchy.** For a classification of zeroth-order textures see R. Barbieri et al., *Phys. Lett.* B445 (1999) 407 ([hep-ph/9808333](#)), that also presented a concrete realization based on a $L_e - L_\mu - L_\tau$ symmetry. (Analogous symmetries have been considered much earlier: for a two-generation example ($L_e - L_\mu$) see Ya. B. Zeldovich, *Dok. Akad. Nauk. CCCP* 86 (1952) 505. E.J. Konopinsky, H. Mahmoud, *Phys. Rev.* 92 (1953) 1045. For a three-generation example ($L_e - L_\mu + L_\tau$) see e.g. S. Petcov, *Phys. Lett.* B100 (1982) 245 and G.C. Branco, W. Grimus, L.avoura, *Nucl. Phys.* B312 (1989) 492). The zeroth-order pseudo-Dirac mass matrix suggested by present data can be obtained within the model in A. Zee, *Phys. Lett.* B93 (1980) 389, if supplemented by the extra assumption that $m_{\mu\tau}$ is small. Finally, $L_e - L_\mu - L_\tau$ -breaking effects were considered e.g. in: A.S. Joshipura, S.D. Rindani, *Eur. Phys. J.* C14 (2000) 85 ([hep-ph/9811252](#)). R.N. Mohapatra et al., *Phys. Lett.* B474 (2000) 355 ([hep-ph/9911395](#)). Q. Shafi, Z. Tavartkiladze, *Phys. Lett.* B482 (2000) 145 ([hep-ph/0002150](#)). Q. Shafi, Z. Tavartkiladze, [hep-ph/0101350](#). K.S. Babu, R.N. Mohapatra, *Phys. Lett.* B532 (2002) 77 ([hep-ph/0201176](#)). Ways to avoid the $\theta_{12} = \pi/4$ have been best discussed in: W. Grimus, L. Lavoura, *J. Phys.* G31 (2005) 683 ([hep-ph/0410279](#)); G. Altarelli, R. Franceschini, *JHEP* 03 (2006) 047 ([hep-ph/0512202](#)).

[135] See e.g. chapter 16 of M. B. Green, J. H. Schwarz, E. Witten, “*Superstring theory*”. Vol. 2 (Cambridge Monographs On Mathematical Physics). For a field-theory implementation see e.g. N. Arkani-Hamed, M. Schmaltz, *Phys. Rev.* D61 (2000) 033005 ([hep-ph/9903417](#)).

[136] **U(2) flavour models.** R. Barbieri, G. Dvali, L. Hall, *Phys. Lett.* B377 (1996) 76 ([hep-ph/9512388](#)). Extension to neutrinos: R. Barbieri, P. Creminelli, A. Romanino, *Nucl. Phys.* B559 (1999) 17 ([hep-ph/9903460](#)). Problems with data: R.G. Roberts, A. Romanino, G.G. Ross, L. Velasco-Sevilla, *Nucl. Phys.* B615 (2001) 358 ([hep-ph/0104088](#)).

[137] **SO(10) unification.** H. Fritzsch, P. Minkowski, *Annals Phys.* 93 (1973) 1975, H. Georgi, in *Coral Gables 1979 Proceedings, Theory and experiments in high energy physics* New York 1975, 329.

[138] H. Georgi, C. Jarlskog, *Phys. Lett.* B86 (1979) 297. For recent discussions of the relation $\theta_{13} \sim \sqrt{m_e/2m_\mu}$ see e.g. G. Altarelli, F. Feruglio, I. Masina, *Nucl. Phys.* B689 (2004) 157 ([hep-ph/0402155](#)). A. Romanino, *Phys. Rev.* D70 (2004) 013003. J. Ferrandis, S. Pakvasa, *Phys. Lett.* B603 (2004) 184 ([hep-ph/0409204](#)).

[139] **SO(10) models for fermion masses.** Several models and general principles are considered and reviewed in M.-C. Chen, K.T. Mahanthappa, *Int. J. Mod. Phys.* A18 (5819) 2003, G. Senjanovic, [hep-ph/0501244](#) and R.N. Mohapatra et al., [hep-ph/0510213](#). A non-supersymmetric SO(10) model is discussed in B. Bajc, A. Melfo, G. Senjanovic, F. Vissani, *Phys. Rev.* D73 (2006) 055001 ([hep-ph/0510139](#)) while the $S_0(10) \otimes SU(3)$ model briefly discussed in the text, has been recently proposed in Z. Berezhiani, F. Nesti, *JHEP* 03 (2006) 041 ([hep-ph/0510011](#)).

[140] **The ‘minimal’ $SO(10)$ model for fermion masses.** The model has been proposed independently in T.E. Clark, T.K. Kuo, N. Nakagawa, *Phys. Lett.* B115 (26) 1982 and C.S. Aulakh and R.N. Mohapatra, *Phys. Rev.* D28 (217) 1982 and was reconsidered in D.-G. Lee, *Phys. Rev.* D49 (1994) 1417 and more recently in C.S. Aulakh, B. Bajc, A. Melfo, G. Senjanović, F. Vissani, *Phys. Lett.* B588 (2004) 196. The expectations for fermion masses have been discussed in K.S. Babu, R. Mohapatra, *Phys. Rev. Lett.* 70 (1993) 2845 (seesaw of type I) and in B. Bajc, G. Senjanovic, F. Vissani, *Phys. Rev. Lett.* 90 (2003) 051802 (seesaw of type II). There are several fits of fermion masses made within the limitations discussed in the text, namely letting free the higgs composition and neutrino mass scale. Among the most recent ones are, Bertolini, *Phys. Rev.* D72 (2005) 055021 and K.S. Babu, C. Macesanu, *Phys. Rev.* D72 (2005) 115003. The “heavy” mass spectrum of the theory has been calculated in: C.S. Aulakh, A. Girdhar, *Int. J. Mod. Phys.* A20 (2005) 865, T. Fukuyama, A. Ilakovac, T. Kikuchi, S. Meljanac, N. Okada, *Eur. Phys. J.* C42 (2005) 191, C.S. Aulakh, *Phys. Rev.* D72 (2005) 051702 and B. Bajc, A. Melfo, G. Senjanovic, F. Vissani, *Phys. Rev.* D70 (2004) 035007. The last paper derives the composition of the light higgs, subsequently used in B. Bajc, A. Melfo, G. Senjanovic, F. Vissani, *Phys. Lett.* B634 (2006) 272 ([hep-ph/0511352](#)) to claim for possible difficulties with fermion mass fitting; compare also with C.S. Aulakh, [hep-ph/0506291](#) and C.S. Aulakh, S.K. Garg, [hep-ph/0512224](#). The pessimistic conclusion is apparently supported by the first detailed numerical analysis of the issue: S. Bertolini, T. Schwetz, M. Malinsky, [hep-ph/0605006](#).

[141] **Quark/lepton complementarity?** S.T. Petcov, A.Y. Smirnov in [80]. M. Raidal, *Phys. Rev. Lett.* 93 (2004) 161801 ([hep-ph/0404046](#)). H. Minakata, A.Y. Smirnov, *Phys. Rev.* D70 (2004) 073009 ([hep-ph/0405088](#)). S. Kang, C. Kim, J. Lee, *Phys. Lett.* B619 (2005) 129 ([hep-ph/0501029](#)). J. Harada, [hep-ph/0512294](#). A. Dighe, S. Goswami, P. Roy, *Phys. Rev.* D73 (2006) 071301 ([hep-ph/0602062](#)). For a healthy criticism see C. Jarlskog, *Phys. Lett.* B625 (2005) 63 ([hep-ph/0507212](#)). Prediction for θ_{13} : B.C. Chuhan et al., [hep-ph/0605032](#).

[142] **Minimal texture of the neutrino mass matrix.** M.C. Chen, K.T. Mahanthappa, *Phys. Rev.* D62 (2002) 113007 ([hep-ph/0005292](#)) discussed a specific $SO(10)$ model with $U(2)$ flavour symmetry, later generalized in M.C. Chen, K.T. Mahanthappa, *Phys. Rev.* D68 (2003) 017301 ([hep-ph/0212375](#)). For a general discussion see P.H. Frampton, S.L. Glashow, D. Marfatia, *Phys. Lett.* B536 (2002) 79. Z.-Z. Xing, *Phys. Lett.* B530 (2002) 159. B.R. Desai, D.P. Roy, A.R. Vaucher, *Mod. Phys. Lett.* A18 (2003) 1355. Q. Shafi and Z. Tavartkitadze, *Phys. Lett.* B594 (2004) 177 ([hep-ph/0401235](#)).

[143] Predictive minimal textures that can reproduce data without fine-tunings have been classified in R. Barbieri, A. Romanino, T. Hambye, *JHEP* 0303 (2003) 017 ([hep-ph/0302118](#)).

[144] A specific case, no longer compatible with data, was discussed in M. Jezanek, Y. Sumino, *Phys. Lett.* B457 (1999) 139 ([hep-ph/9904382](#)). Eq. (12.18) was presented in a footnote of R. Barbieri, G.G. Ross, A. Strumia, *JHEP* 10 (1999) 020 ([hep-ph/9906470](#)). For recent discussions see: C. Giunti, M. Tanimoto, *Phys. Rev.* D66 (2002) 053013. P.H. Frampton, S.T. Petcov, W. Rodejohann, *Nucl. Phys.* B687 (2004) 31 ([hep-ph/0401206](#)). A.S. Joshipura, S. Mohanty, *Phys. Rev.* D67 (2003) 091302. S.T. Petcov, W. Rodejohann, *Phys. Rev.* D71 (2005) 073002 ([hep-ph/0409135](#)).

[145] P.F. Harrison, W.G. Scott, *Phys. Lett.* B594 (2004) 324 ([hep-ph/0403278](#)).

[146] M. Bando, M. Obara, [hep-ph/0212242](#).

[147] C.H. Albright, S.M. Barr, *Phys. Rev.* D64 (2001) 073010 ([hep-ph/0104294](#)).

[148] Xiandong Ji, Yinghuan Li, R.N. Mohapatra, *Phys. Lett.* B633 (2006) 755 ([hep-ph/0510353](#)).

[149] K. Matsuda, H. Nishiura, *Phys. Rev.* D72 (2005) 033011 ([hep-ph/0506192](#)).

[150] S. King, *JHEP* 08 (2005) 105 ([hep-ph/0506297](#)).

[151] **A_4 as a flavour symmetry.** E. Ma, G. Rajasekaran, *Phys. Rev.* D64 (2001) 113012 ([hep-ph/0106291](#)). K. Babu, E. Ma, J. Valle, *Phys. Lett.* B552 (2003) 207 ([hep-ph/0206292](#)). G. Altarelli, F. Feruglio, *Nucl. Phys.* B741 (2006) 215 ([hep-ph/0512103](#)). Predictive sub-model: B. Adhikary, B. Brahmachari, A. Ghosal, E. Ma, M. Parida, [hep-ph/0603059](#). For a recent discussion of tri-bi-maximal mixing see P. Harrison, D. Perkins, W. Scott, *Phys. Lett.* B530 (2002) 167 ([hep-ph/0202074](#)).

[152] **Neutrino magnetic moment.** Magnetic moment induced by neutrino masses: K. Fujikawa and R. Shrock, *Phys. Rev. Lett.* 45 (1980) 963. Neutrino/electron scattering: see e.g. P. Vogel, J. Engel, *Phys. Rev.* D39 (1989) 3378. A.S. Joshipura, S. Mohanty, *Phys. Rev.* D66 (2002)

012003 ([hep-ph/0204305](#)). W. Grimus et al., *Nucl. Phys.* B648 (2003) 376 ([hep-ph/0208132](#)). The effect of atomic levels is discussed in V.I. Kopeikin et al., *Phys. Atom. Nucl.* 60 (1997) 2032. Experimental data: V.I. Kopeikin et al., *Phys. Atom. Nucl.* 63 (2000) 1012. MUNU collaboration, *Nucl. Phys. Proc. Suppl.* 100 (2001) 167. LSND collaboration, *Phys. Rev.* D63 (2001) 112001. TEXONO collaboration, [hep-ex/0605006](#). Neutrino decay: G.G. Raffelt, *Phys. Rev.* D39 (1989) 2066. Spin precession: K. Fujikawa, R. Shrock, *Phys. Rev. Lett.* 45 (1963) 1980. Spin-flavour precession: J. Schechter, J.W.F. Valle, *Phys. Rev.* D24 (1983) 1981. L.B. Okun, M.B. Voloshin, M.I. Vysotsky, *Sov. Phys. JETP* 64 (1986) 446. Resonant enhancement and $\nu \rightarrow \bar{\nu}$ conversions: C.S. Lim, W.J. Marciano, *Phys. Rev.* D37 (1988) 1368. E. Kh Akhmedov, *Sov. J. Nucl. Phys.* 48 (1988) 382. E. Kh Akhmedov, *Sov. J. Nucl. Phys.* 68 (1989) 690. E. Kh Akhmedov, S.T. Petcov, A. Yu Smirnov, *Phys. Lett.* B309 (1993) 95. For recent fits of solar data see E.Kh Akhmedov, J. Pulido, *Phys. Lett.* B553 (2003) 7 ([hep-ph/0209192](#)). O.G. Miranda, T.I. Rashba, A.I. Rez, J.W.F. Valle, *Phys. Rev. Lett.* 93 (2004) 051304 ([hep-ph/0311014](#)). Sin Kyu Kang, C.S. Kim, *Phys. Lett.* B584 (2004) 98. Astrophysical bounds: see G.G. Raffelt, *Phys. Rept.* 320 (1999) 319. For a recent summary see H.T. Wong, *Nucl. Phys. Proc. Suppl.* 143 (2005) 205 ([hep-ex/0409003](#)). If models that generate both neutrino masses and magnetic moments naturalness considerations suggest $|\mu| \lesssim 10^{-15} \mu_B$, see N. Bell, V. Cirigliano, M. Ramsey-Musolf, P. Vogel, M. Wise, *Phys. Rev. Lett.* 95 (2005) 151802 ([hep-ph/0504134](#)).

[153] **Models with sterile neutrinos.** Light fermions from a discrete symmetry: E. Ma, P. Roy, *Phys. Rev.* D52 (1995) 4780. R. Mohapatra, S. Nasri, H. Yu, *Phys. Rev.* D72 (2005) 033007 ([hep-ph/0505021](#)). From a continuos symmetry: E. Ma, *Mod. Phys. Lett.* A11 (1996) 1893. J. Sayre, S. Wiesenfeldt, S. Willenbrock, *Phys. Rev.* D72 (2005) 015001 ([hep-ph/0504198](#)). From a 27 of E_6 : E. Ma, *Phys. Lett.* B380 (1996) 286. From a supersymmetric R -symmetry: E.J. Chun, A.S. Joshipura, A.Yu. Smirnov, *Phys. Lett.* B357 (1995) 608. As Goldstone particles: E.J. Chun, A.S. Joshipura, A.Yu. Smirnov, *Phys. Rev.* D54 (1996) 4654. As modulinos: K. Benakli, A.Yu. Smirnov, *Phys. Rev. Lett.* 79 (1997) 4314. From a mirror world: S.I. Blinikov, M. Yu Khlopov, *Sov. Astron.* 27 (1983) 371. Z. Silagadze, *Phys. Atom. Nucl.* 60 (1997) 272 ([hep-ph/9503481](#)). R. Foot, R. Volkas, *Phys. Rev.* D52 (1995) 6595 ([hep-ph/9505359](#)).

Z.G. Berezhiani, R.N. Mohapatra, *Phys. Rev.* D52 (1995) 6607 ([hep-ph/9505385](#)). V. Berezinsky, M. Narayan, F. Vissani, *Nucl. Phys.* B658 (2003) 254 ([hep-ph/0210204](#)). From compositeness: N. Arkani-Hamed, Y. Grossman, *Phys. Lett.* B459 (1999) 179 ([hep-ph/9806223](#)). From warped extra dimensions or compositeness: T. Gherghetta, *Phys. Rev. Lett.* 92 (2004) 161601 ([hep-ph/0312392](#)). From mirror fermions: M. Bando, K. Yoshioka, *Prog. Theor. Phys.* 100 (1998) 1239 ([hep-ph/9806400](#)). From chiral representations of other gauge groups: K.S. Babu, G. Seidl, *Phys. Rev.* D70 (2004) 113014 ([hep-ph/0405197](#)). From supersymmetry: J. Kang, T. Li, [hep-ph/0501101](#). From supersymmetry breaking: K.S. Babu, T. Yanagida, *Phys. Lett.* B491 (2000) 148 ([hep-ph/0008110](#)). F. Borzumati, K. Hamaguchi, T. Yanagida, *Phys. Lett.* B497 (2001) 259 ([hep-ph/0011141](#)). Small sterile masses from supersymmetric flat directions: P. Langacker, *Phys. Rev.* D58 (1998) 093017 ([hep-ph/9805281](#)). From a $SU(3)_x \otimes SU(3)_L \otimes U(1)_X$ gauge group at the TeV scale: A.G. Dias et al., *Phys. Lett.* B628 (2005) 85 ([hep-ph/0508186](#)). C. Csaki et al., [hep-ph/0510293](#). A. Abada, G. Bhattacharyya, M. Losada, *Phys. Rev.* D73 (2006) 033006 ([hep-ph/0511275](#)). Models with 2 sterile neutrinos: W. Krolkowski, *Acta Phys. Polon.* B35 (2004) 1675 ([hep-ph/0402183](#)).

[154] Sterile neutrinos have been used to fit various neutrino anomalies. See e.g. S.L. Glashow, *Phys. Lett.* B256 (1991) 255. J.T. Peltoniemi, D. Tommasini, J. W. F. Valle, *Phys. Lett.* B298 (1993) 383. J. T. Peltoniemi, [hep-ph/9506228](#). J.F. Beacom, N.F. Bell, D. Hooper, J.G. Learned, S. Pakvasa, T.J. Weiler, *Phys. Rev. Lett.* 92 (2004) 011101 ([hep-ph/0307151](#)).

keV sterile neutrinos as dark matter: T. Asaka, S. Blanchet, M. Shaposhnikov, *Phys. Lett.* B631 (2005) 151 ([hep-ph/0503065](#)). K. Abazajian, S.M. Koushiappas, [astro-ph/0605271](#). keV sterile neutrino and ‘early’ reionization: P. Biermann, A. Kusenko, *Phys. Rev. Lett.* 96 (2006) 091301 ([astro-ph/0601004](#)).

Low energy see-saw and LSND: A. de Gouvea, *Phys. Rev.* D72 (2005) 033005 ([hep-ph/0501039](#)). W.-S. Hou, A. Soddu, [hep-ph/0512278](#). Yi Liao, [hep-ph/0604016](#).

[155] See e.g. J. Wess, J. Bagger, *Supersymmetry and Supergravity* (1992), Princeton Univeristy Press.

[156] **RGE equations for neutrino masses.** P.H. Chankowski, Z. Pluciennik, *Phys. Lett.* B316 (1993) 312 ([hep-ph/9306333](#)). K.S. Babu, C.N. Leung, J. Pantaleone, *Phys. Lett.* B319

(1993) 191 ([hep-ph/9309223](#)). An error has been corrected in S. Antusch, M. Drees, J. Kersten, M. Lindner, M. Ratz, *Phys. Lett.* B519 (2001) 238 ([hep-ph/0108005](#)). In the MSSM RGE equations have been computed up to two loops: S. Antusch, M. Ratz, *JHEP* 0207 (2002) 059 ([hep-ph/0203027](#)). Results are summarized in S. Antusch, J. Kersten, M. Lindner, M. Ratz, M.A. Schmidt, *JHEP* 03 (2005) 024 ([hep-ph/0501272](#)). J. Mei, *Phys. Rev.* D71 (2005) 073012 ([hep-ph/0502015](#)). RGE for Dirac neutrinos are discussed in M. Lindner, M. Ratz, M. Schmidt, *JHEP* 09 (2005) 081 ([hep-ph/0506280](#)). Effects of RGE corrections in neutrinos are discussed in: J. Ellis, S. Lola, *Phys. Lett.* B458 (1999) 310 ([hep-ph/9904279](#)). J.A. Casas, J.R. Espinosa, A. Ibarra, I. Navarro, *Nucl. Phys.* B556 (1999) 3 ([hep-ph/9904395](#)) and [hep-ph/9905381](#) and [hep-ph/9906281](#). Y-L. Wu, [hep-ph/9905222](#). P. H. Chankowski, W. Królikowski, S. Pokorski, *Phys. Lett.* B473 (2000) 109 ([hep-ph/9910231](#)). F. Vissani, M. Narayan, V. Berezinsky, *Phys. Lett.* B571 (2003) 209 ([hep-ph/0305233](#)). S. Antusch, J. Kersten, M. Lindner, M. Ratz, *Nucl. Phys.* B674 (2003) 401 ([hep-ph/0305273](#)).

[157] **Neutron EDM.** I.S. Altarev et al., *Phys. Lett.* B276 (1992) 242. P.G. Harris et al., *Phys. Rev. Lett.* 82 (1999) 904. C.A. Baker et al., [hep-ex/0602020](#).

[158] **$\tau \rightarrow \mu\gamma$.** CLEO collaboration, *Phys. Rev.* D61 (2001) 71101 ([hep-ex/9910060](#)). BELLE collaboration, *Phys. Rev. Lett.* 92 (2004) 171802 ([hep-ex/0310029](#)). BABAR collaboration, *Phys. Rev. Lett.* 95 (2005) 041802 ([hep-ex/0502032](#)). The future sensitivity indicated in the text would need a dedicated τ factory.
Constraints on $\text{BR}(\tau \rightarrow e\gamma)$: BELLE collaboration, [hep-ph/0501068](#). BABAR collaboration, *Phys. Rev.* D73 (2006) 031101 ([hep-ex/0508013](#)).

[159] **Electron EDM.** E.D. Commins, S.B. Ross, D. Demille, B.C. Regan, *Phys. Rev.* A50 (1994) 2960. E.D. Cummings, B.C. Regan as reported by E. Hinds at the KAON 2001 conference, Pisa (Italia) 12–17 June 2001.

[160] **Hg EDM.** M.V. Romalis, W.C. Griffith, E.N. Fortson, *Phys. Rev. Lett.* 86 (2001) 2505 ([hep-ex/0012001](#)).

[161] **$\mu \rightarrow e\bar{e}e$.** SINDRUM collaboration, *Nucl. Phys.* B299 (1988) 1.

[162] **Muon EDM.** CERN-Mainz-Daresbury collaboration, *Nucl. Phys.* B150 (1979) 1. J-PARC letter of intent L22, “Search for a permanent muon electric dipole moment at the $10^{-24} e\text{cm}$ level”, Y. Kuno, J.Miller, Y. Semertzidis spokespersons.

[163] **$\mu \rightarrow e$ conversion.** SINDRUM II collaboration, *Phys. Lett.* B422 (1998) 334. P. Wintz, *proceedings of the first international symposium on lepton and baryon number violation*, editors H.V. Klapdor-Kleingrothaus and I.V. Krivosheina, page 534. The next future experiment seems PRISM at JPARC.

[164] **Effects induced by neutrino Yukawa couplings in supersymmetric models.** F. Borzumati, A. Masiero, *Phys. Rev. Lett.* 57 (1986) 961. L.J. Hall, V.A. Kostelecky, S. Raby, *Nucl. Phys.* B267 (1986) 415. J. Hisano, T. Moroi, K. Tobe, M. Yamaguchi, T. Yanagida, *Phys. Lett.* B357 (1995) 579 ([hep-ph/9501407](#)). Such effects have been discussed with greater detail in many subsequent papers. We do not focus on this topic because $\text{BR}(\mu \rightarrow e\gamma)$ and related signals have not yet been seen and can be predicted in terms of neutrino masses only up to a factor proportional to the second power of the right-handed neutrino masses, which are and probably will remain unknown. In spite of this large uncertainty various authors agree on statements like “in a large class of see-saw models LFV rates are predicted to be within the reach of planned experiments”. Indeed future experiments should reach a sensitivity significantly below present bounds.

In our review we emphasized some problematic issues following S. Davidson, A. Ibarra, *JHEP* 09 (2001) 013 ([hep-ph/0104076](#)). S. Lavignac, I. Masina, C. A. Savoy, *Phys. Lett.* B520 (2001) 269 ([hep-ph/0106245](#)). A. Romanino, A. Strumia, *Nucl. Phys.* B622 (2002) 73 ([hep-ph/0108275](#)). This last reference estimated EDMs, explaining why they are small. For detailed computations of EDMs see I. Masina, *Nucl. Phys.* B671 (2003) 432 ([hep-ph/0304299](#)) and Y. Farzan, M. Peskin, *Phys. Rev.* D70 (2004) 095001 ([hep-ph/0405214](#)) and references therein.

[165] G. Altarelli, F. Feruglio, I. Masina, *Phys. Lett.* B472 (2000) 382 ([hep-ph/9907532](#)).

[166] **Neutrinos and NRO.** Y. Grossman, *Phys. Lett.* B359 (1995) 141 ([hep-ph/9507344](#)). M.C. Gonzalez-Garcia, Y. Grossman, A. Gusso, Y. Nir, *Phys. Rev.* D64 (2001) 096006 ([hep-ph/0105159](#)). S. Davidson, C. Pena-Garay, N. Rius, A. Santa-maria, *JHEP* 03 (2003) 011 ([hep-ph/0302093](#)) and references therein.

[167] **Applications.** Oil from oscillations: A.N. Ioanisian and A.Y. Smirnov, [hep-ph/0201012](#). Monitoring reactors: talk by J. Learned at Neutrino

2004, web page neutrino2004.in2p3.fr. Neutrinos against nuclear weapon proliferation: H. Sugawara, H. Hagura, T. Sanami, [hep-ph/0305062](https://arxiv.org/abs/hep-ph/0305062). ν geotomography: W. Winter, *Phys. Rev.* D72 (2005) 037302 ([hep-ph/0502097](https://arxiv.org/abs/hep-ph/0502097)). E. Akhmedov, M. Tortola, J. Valle, *JHEP* 06 (2005) 053 ([hep-ph/0502154](https://arxiv.org/abs/hep-ph/0502154)). Neutrino radiation from muon colliders: B.J. King, *AIP Conf. Proc.* 530 (2000) 165 ([hep-ex/0005006](https://arxiv.org/abs/hep-ex/0005006)).

[168] **Statistics.** Bayesian inference: T. Bayes, *Philos. Trans. Roy. Soc.* 53 (1763) 330. For a review see G. D'Agostini, *Bayesian reasoning in High Energy Physics — principles and applications* (1999) [169] C. D. Froggatt, H. B. Nielsen, *Nucl. Phys.* B147 (1979) 277. J. Bijnens, C. Wetterich, *Nucl. Phys.* B147 (1987) 292.

CERN ‘yellow’ report 1999-03, available from cds.cern.ch.

Neyman inference: J. Neyman, *Philos. Trans. R. Soc. London* A236 (1937) 333. E.L. Crow, R.S. Gardner, *Biometrika* 46 (1959) 441. See e.g. A. Stuart, J.K. Ord, Kendall's advanced theory of statistics, vol. 2, *Classical Inference and Relationship* 5th Ed. (Oxford University Press, New York, 1991); see also earlier editions by Kendall and Stuart, sec. 23.1. G.J. Feldman, R.D. Cousins, *Phys. Rev.* D57 (1998) 2873.

List of Tables

1.1	Experimental values of oscillation parameters	4
1.2	Main neutrino experiments	6
1.3	Neutrino sources	8
3.1	Matter potentials	28
4.1	Z couplings	45
5.1	Reactor neutrinos	60
6.1	Predicted total solar neutrino fluxes	66
6.2	Results of solar neutrino experiments	69
7.1	Long-base-line experiments	83
8.1	Non-oscillation data	92
8.2	$0\nu 2\beta$ experiments	97
9.1	LSND interpretations	104
11.1	Neutrinos from a supernova	142
11.2	Signals of oscillations of SN neutrinos	146
12.1	Sample of U(1) see-saw models	157
13.1	Experimental bounds on CP and lepton-flavor violating processes	178
13.2	Bounds and sensitivity to anomalous neutrino couplings	184

List of Figures

8.5	Expectations for non-oscillation experiments	98
9.1	HM data	101
9.2	Oscillation data in the ν_e, ν_μ sector	102
9.3	LSND fit	102
9.4	Oscillation interpretations of LSND	103
9.5	Mass spectra suggested by LSND	105
9.6	NuTeV data	107
10.1	BBN basics	113
10.2	Components of the early universe	116
10.3	Neutrinos and CMB	117
10.4	Matter power spectrum	120
10.5	CP violation in N_1 decays	124
10.6	$\Delta L = 2$ scatterings	125
10.7	Efficiency of leptogenesis	127
11.1	Luminosity of ν_e from supernova	141
11.2	Fluence of supernova neutrinos	143
11.3	Neutrinos from DM annihilations	148
11.4	SN1987A data	150
12.1	Expectations from anarchy	154
13.1	BSM neutrino effects	168
13.2	Summary of sterile neutrino effects	171
13.3	Basic four neutrino spectra	171
13.4	RGE running of neutrino masses	176
13.5	SUSY see-saw predictions for LFV	179
13.6	Effects of neutrinos in extra dimensions	183
B.1	χ^2 for different number of dof	192
1.1	Explored regions of the L/E plane	7
1.2	Location of neutrino experiments	7
2.1	Bounds on non renormalizable operators	10
2.2	Mediation of neutrino masses	12
2.3	Normal and inverted neutrino spectra	14
2.4	The flavour of neutrinos	16
3.1	Neutrino wave	20
3.2	Typical $(\Delta m^2, \sin^2 2\theta)$ plane	22
3.3	Matter effects	27
3.4	Density of the earth and of the sun	29
3.5	Mass and mixing in matter	31
3.6	Earth matter effects	32
3.7	Propagation steps	33
3.8	Example of oscillations	34
3.9	Example of matter effects	35
3.10	ν_τ regeneration	41
3.11	Matter effects in the early universe	42
4.1	Neutrino cross sections on p and e	46
4.2	Neutrino/nucleus cross section	49
5.1	Predicted flux of atmospheric neutrinos	54
5.2	SK atmospheric data	56
5.3	Fit of atmospheric data	59
5.4	CHOOZ data	62
6.1	Fit of solar oscillation parameters	63
6.2	KamLAND	65
6.3	Predicted solar neutrino spectra	67
6.4	Predicted solar neutrino rates	67
6.5	Nuclear reactions inside the sun	68
6.6	SNO	70
6.7	Fit of solar neutrino fluxes	73
7.1	Day/night asymmetry of solar neutrinos	81
7.2	Future sensitivity to θ_{13}	82
7.3	Sensitivity to CP violation	85
7.4	Off-axis	86
8.1	β , 2β and $0\nu2\beta$ decay	93
8.2	Spectra of β and $0\nu2\beta$ decay	94
8.3	End-point spectrum in β -decay	95
8.4	$0\nu2\beta$ techniques	97

Contents

1	Introduction	2	7	Future oscillation experiments	78																																																																																																																																																																																																						
1.1	Past	3	7.1	The global oscillation picture?	78																																																																																																																																																																																																						
1.2	Present	3	7.2	Known unknowns	79																																																																																																																																																																																																						
1.3	Future?	5	7.3	Atmospheric experiments	80																																																																																																																																																																																																						
2	Neutrino masses	9	7.4	Solar experiments	80																																																																																																																																																																																																						
2.1	Massless neutrinos in the SM	9	7.5	Reactor experiments	82																																																																																																																																																																																																						
2.2	Massive neutrinos beyond the SM	11	7.6	Conventional neutrino beams	82																																																																																																																																																																																																						
2.3	See-saw	12	7.7	Neutrino factory	87																																																																																																																																																																																																						
2.4	Pure Majorana neutrinos	15	7.8	Beta beams	89																																																																																																																																																																																																						
2.5	Pure Dirac neutrinos	16	8	Non-oscillation experiments	91																																																																																																																																																																																																						
2.6	Formalism	17	8.1	Cosmology	91	3	Oscillations	19	8.2	Astrophysics	92	3.1	Oscillations in vacuum	19	8.3	β -decay	93	3.2	Oscillations in normal matter	27	8.4	Neutrino-less double β decay	94	3.3	Oscillations in a varying density	32	9	Unconfirmed anomalies	100	3.4	The density matrix and solar oscillations .	36	9.1	Heidelberg-Moscow	100	3.5	Oscillations and absorption	39	9.2	LSND	102	3.6	Oscillations in the early universe	41	9.3	NuTeV	108	4	Detecting neutrinos	44	10	Neutrinos in cosmology	111	4.1	ν /electron scattering	44	10.1	Big-bang nucleosynthesis	112	4.2	ν /nucleon scattering	45	10.2	CMB and LSS	115	4.3	ν /nucleus scattering	48	10.3	Baryogenesis through leptogenesis	123	4.4	Neutrino detectors	50	11	Neutrinos in astrophysics	132	5	The atmospheric evidence	53	11.1	Neutrino sources	132	5.1	Atmospheric neutrinos	53	11.2	Core collapse supernovæ	135	5.2	SuperKamiokande	54	11.3	Effects of neutrino oscillations	144	5.3	Oscillations?	57	11.4	Observations of cosmic neutrinos	149	5.4	$\nu_\mu \rightarrow \nu_\tau$ or $\nu_\mu \rightarrow \nu_s$?	58	12	Understanding neutrino masses	152	5.5	K2K	58	12.1	The problem of the flavour problem	152	5.6	NuMI	60	12.2	In the search for a pattern	154	5.7	CHOOZ: $\nu_\mu \rightarrow \nu_e$?	60	12.3	Flavor symmetries	157	5.8	Reactor experiments	61	12.4	Testing flavour models	162	6	The solar evidence	63	13	Behind neutrino masses?	167	6.1	KamLAND	64	13.1	Neutrino electro-magnetic dipoles	168	6.2	Solar neutrinos	65	13.2	Neutrinos and light fermions	169	6.3	Solar neutrino experiments	67	13.3	Neutrinos and light scalars	174	6.4	Implications of solar data	72	13.4	Quantum corrections to neutrino masses .	176				13.5	Lepton-flavour violation and SUSY	177				13.6	Neutrinos in extra dimensions	180				14	Applications	185				A	Acronyms	186				B	Statistics	188				B.1	Statistical inference	188				B.2	Goodness-of-fit	193
8.1	Cosmology	91																																																																																																																																																																																																									
3	Oscillations	19	8.2	Astrophysics	92	3.1	Oscillations in vacuum	19	8.3	β -decay	93	3.2	Oscillations in normal matter	27	8.4	Neutrino-less double β decay	94	3.3	Oscillations in a varying density	32	9	Unconfirmed anomalies	100	3.4	The density matrix and solar oscillations .	36	9.1	Heidelberg-Moscow	100	3.5	Oscillations and absorption	39	9.2	LSND	102	3.6	Oscillations in the early universe	41	9.3	NuTeV	108	4	Detecting neutrinos	44	10	Neutrinos in cosmology	111	4.1	ν /electron scattering	44	10.1	Big-bang nucleosynthesis	112	4.2	ν /nucleon scattering	45	10.2	CMB and LSS	115	4.3	ν /nucleus scattering	48	10.3	Baryogenesis through leptogenesis	123	4.4	Neutrino detectors	50	11	Neutrinos in astrophysics	132	5	The atmospheric evidence	53	11.1	Neutrino sources	132	5.1	Atmospheric neutrinos	53	11.2	Core collapse supernovæ	135	5.2	SuperKamiokande	54	11.3	Effects of neutrino oscillations	144	5.3	Oscillations?	57	11.4	Observations of cosmic neutrinos	149	5.4	$\nu_\mu \rightarrow \nu_\tau$ or $\nu_\mu \rightarrow \nu_s$?	58	12	Understanding neutrino masses	152	5.5	K2K	58	12.1	The problem of the flavour problem	152	5.6	NuMI	60	12.2	In the search for a pattern	154	5.7	CHOOZ: $\nu_\mu \rightarrow \nu_e$?	60	12.3	Flavor symmetries	157	5.8	Reactor experiments	61	12.4	Testing flavour models	162	6	The solar evidence	63	13	Behind neutrino masses?	167	6.1	KamLAND	64	13.1	Neutrino electro-magnetic dipoles	168	6.2	Solar neutrinos	65	13.2	Neutrinos and light fermions	169	6.3	Solar neutrino experiments	67	13.3	Neutrinos and light scalars	174	6.4	Implications of solar data	72	13.4	Quantum corrections to neutrino masses .	176				13.5	Lepton-flavour violation and SUSY	177				13.6	Neutrinos in extra dimensions	180				14	Applications	185				A	Acronyms	186				B	Statistics	188				B.1	Statistical inference	188				B.2	Goodness-of-fit	193						
8.2	Astrophysics	92																																																																																																																																																																																																									
3.1	Oscillations in vacuum	19	8.3	β -decay	93	3.2	Oscillations in normal matter	27	8.4	Neutrino-less double β decay	94	3.3	Oscillations in a varying density	32	9	Unconfirmed anomalies	100	3.4	The density matrix and solar oscillations .	36	9.1	Heidelberg-Moscow	100	3.5	Oscillations and absorption	39	9.2	LSND	102	3.6	Oscillations in the early universe	41	9.3	NuTeV	108	4	Detecting neutrinos	44	10	Neutrinos in cosmology	111	4.1	ν /electron scattering	44	10.1	Big-bang nucleosynthesis	112	4.2	ν /nucleon scattering	45	10.2	CMB and LSS	115	4.3	ν /nucleus scattering	48	10.3	Baryogenesis through leptogenesis	123	4.4	Neutrino detectors	50	11	Neutrinos in astrophysics	132	5	The atmospheric evidence	53	11.1	Neutrino sources	132	5.1	Atmospheric neutrinos	53	11.2	Core collapse supernovæ	135	5.2	SuperKamiokande	54	11.3	Effects of neutrino oscillations	144	5.3	Oscillations?	57	11.4	Observations of cosmic neutrinos	149	5.4	$\nu_\mu \rightarrow \nu_\tau$ or $\nu_\mu \rightarrow \nu_s$?	58	12	Understanding neutrino masses	152	5.5	K2K	58	12.1	The problem of the flavour problem	152	5.6	NuMI	60	12.2	In the search for a pattern	154	5.7	CHOOZ: $\nu_\mu \rightarrow \nu_e$?	60	12.3	Flavor symmetries	157	5.8	Reactor experiments	61	12.4	Testing flavour models	162	6	The solar evidence	63	13	Behind neutrino masses?	167	6.1	KamLAND	64	13.1	Neutrino electro-magnetic dipoles	168	6.2	Solar neutrinos	65	13.2	Neutrinos and light fermions	169	6.3	Solar neutrino experiments	67	13.3	Neutrinos and light scalars	174	6.4	Implications of solar data	72	13.4	Quantum corrections to neutrino masses .	176				13.5	Lepton-flavour violation and SUSY	177				13.6	Neutrinos in extra dimensions	180				14	Applications	185				A	Acronyms	186				B	Statistics	188				B.1	Statistical inference	188				B.2	Goodness-of-fit	193												
8.3	β -decay	93																																																																																																																																																																																																									
3.2	Oscillations in normal matter	27	8.4	Neutrino-less double β decay	94	3.3	Oscillations in a varying density	32	9	Unconfirmed anomalies	100	3.4	The density matrix and solar oscillations .	36	9.1	Heidelberg-Moscow	100	3.5	Oscillations and absorption	39	9.2	LSND	102	3.6	Oscillations in the early universe	41	9.3	NuTeV	108	4	Detecting neutrinos	44	10	Neutrinos in cosmology	111	4.1	ν /electron scattering	44	10.1	Big-bang nucleosynthesis	112	4.2	ν /nucleon scattering	45	10.2	CMB and LSS	115	4.3	ν /nucleus scattering	48	10.3	Baryogenesis through leptogenesis	123	4.4	Neutrino detectors	50	11	Neutrinos in astrophysics	132	5	The atmospheric evidence	53	11.1	Neutrino sources	132	5.1	Atmospheric neutrinos	53	11.2	Core collapse supernovæ	135	5.2	SuperKamiokande	54	11.3	Effects of neutrino oscillations	144	5.3	Oscillations?	57	11.4	Observations of cosmic neutrinos	149	5.4	$\nu_\mu \rightarrow \nu_\tau$ or $\nu_\mu \rightarrow \nu_s$?	58	12	Understanding neutrino masses	152	5.5	K2K	58	12.1	The problem of the flavour problem	152	5.6	NuMI	60	12.2	In the search for a pattern	154	5.7	CHOOZ: $\nu_\mu \rightarrow \nu_e$?	60	12.3	Flavor symmetries	157	5.8	Reactor experiments	61	12.4	Testing flavour models	162	6	The solar evidence	63	13	Behind neutrino masses?	167	6.1	KamLAND	64	13.1	Neutrino electro-magnetic dipoles	168	6.2	Solar neutrinos	65	13.2	Neutrinos and light fermions	169	6.3	Solar neutrino experiments	67	13.3	Neutrinos and light scalars	174	6.4	Implications of solar data	72	13.4	Quantum corrections to neutrino masses .	176				13.5	Lepton-flavour violation and SUSY	177				13.6	Neutrinos in extra dimensions	180				14	Applications	185				A	Acronyms	186				B	Statistics	188				B.1	Statistical inference	188				B.2	Goodness-of-fit	193																		
8.4	Neutrino-less double β decay	94																																																																																																																																																																																																									
3.3	Oscillations in a varying density	32	9	Unconfirmed anomalies	100																																																																																																																																																																																																						
3.4	The density matrix and solar oscillations .	36	9.1	Heidelberg-Moscow	100	3.5	Oscillations and absorption	39	9.2	LSND	102	3.6	Oscillations in the early universe	41	9.3	NuTeV	108	4	Detecting neutrinos	44	10	Neutrinos in cosmology	111	4.1	ν /electron scattering	44	10.1	Big-bang nucleosynthesis	112	4.2	ν /nucleon scattering	45	10.2	CMB and LSS	115	4.3	ν /nucleus scattering	48	10.3	Baryogenesis through leptogenesis	123	4.4	Neutrino detectors	50	11	Neutrinos in astrophysics	132	5	The atmospheric evidence	53	11.1	Neutrino sources	132	5.1	Atmospheric neutrinos	53	11.2	Core collapse supernovæ	135	5.2	SuperKamiokande	54	11.3	Effects of neutrino oscillations	144	5.3	Oscillations?	57	11.4	Observations of cosmic neutrinos	149	5.4	$\nu_\mu \rightarrow \nu_\tau$ or $\nu_\mu \rightarrow \nu_s$?	58	12	Understanding neutrino masses	152	5.5	K2K	58	12.1	The problem of the flavour problem	152	5.6	NuMI	60	12.2	In the search for a pattern	154	5.7	CHOOZ: $\nu_\mu \rightarrow \nu_e$?	60	12.3	Flavor symmetries	157	5.8	Reactor experiments	61	12.4	Testing flavour models	162	6	The solar evidence	63	13	Behind neutrino masses?	167	6.1	KamLAND	64	13.1	Neutrino electro-magnetic dipoles	168	6.2	Solar neutrinos	65	13.2	Neutrinos and light fermions	169	6.3	Solar neutrino experiments	67	13.3	Neutrinos and light scalars	174	6.4	Implications of solar data	72	13.4	Quantum corrections to neutrino masses .	176				13.5	Lepton-flavour violation and SUSY	177				13.6	Neutrinos in extra dimensions	180				14	Applications	185				A	Acronyms	186				B	Statistics	188				B.1	Statistical inference	188				B.2	Goodness-of-fit	193																														
9.1	Heidelberg-Moscow	100																																																																																																																																																																																																									
3.5	Oscillations and absorption	39	9.2	LSND	102	3.6	Oscillations in the early universe	41	9.3	NuTeV	108	4	Detecting neutrinos	44	10	Neutrinos in cosmology	111	4.1	ν /electron scattering	44	10.1	Big-bang nucleosynthesis	112	4.2	ν /nucleon scattering	45	10.2	CMB and LSS	115	4.3	ν /nucleus scattering	48	10.3	Baryogenesis through leptogenesis	123	4.4	Neutrino detectors	50	11	Neutrinos in astrophysics	132	5	The atmospheric evidence	53	11.1	Neutrino sources	132	5.1	Atmospheric neutrinos	53	11.2	Core collapse supernovæ	135	5.2	SuperKamiokande	54	11.3	Effects of neutrino oscillations	144	5.3	Oscillations?	57	11.4	Observations of cosmic neutrinos	149	5.4	$\nu_\mu \rightarrow \nu_\tau$ or $\nu_\mu \rightarrow \nu_s$?	58	12	Understanding neutrino masses	152	5.5	K2K	58	12.1	The problem of the flavour problem	152	5.6	NuMI	60	12.2	In the search for a pattern	154	5.7	CHOOZ: $\nu_\mu \rightarrow \nu_e$?	60	12.3	Flavor symmetries	157	5.8	Reactor experiments	61	12.4	Testing flavour models	162	6	The solar evidence	63	13	Behind neutrino masses?	167	6.1	KamLAND	64	13.1	Neutrino electro-magnetic dipoles	168	6.2	Solar neutrinos	65	13.2	Neutrinos and light fermions	169	6.3	Solar neutrino experiments	67	13.3	Neutrinos and light scalars	174	6.4	Implications of solar data	72	13.4	Quantum corrections to neutrino masses .	176				13.5	Lepton-flavour violation and SUSY	177				13.6	Neutrinos in extra dimensions	180				14	Applications	185				A	Acronyms	186				B	Statistics	188				B.1	Statistical inference	188				B.2	Goodness-of-fit	193																																				
9.2	LSND	102																																																																																																																																																																																																									
3.6	Oscillations in the early universe	41	9.3	NuTeV	108	4	Detecting neutrinos	44	10	Neutrinos in cosmology	111	4.1	ν /electron scattering	44	10.1	Big-bang nucleosynthesis	112	4.2	ν /nucleon scattering	45	10.2	CMB and LSS	115	4.3	ν /nucleus scattering	48	10.3	Baryogenesis through leptogenesis	123	4.4	Neutrino detectors	50	11	Neutrinos in astrophysics	132	5	The atmospheric evidence	53	11.1	Neutrino sources	132	5.1	Atmospheric neutrinos	53	11.2	Core collapse supernovæ	135	5.2	SuperKamiokande	54	11.3	Effects of neutrino oscillations	144	5.3	Oscillations?	57	11.4	Observations of cosmic neutrinos	149	5.4	$\nu_\mu \rightarrow \nu_\tau$ or $\nu_\mu \rightarrow \nu_s$?	58	12	Understanding neutrino masses	152	5.5	K2K	58	12.1	The problem of the flavour problem	152	5.6	NuMI	60	12.2	In the search for a pattern	154	5.7	CHOOZ: $\nu_\mu \rightarrow \nu_e$?	60	12.3	Flavor symmetries	157	5.8	Reactor experiments	61	12.4	Testing flavour models	162	6	The solar evidence	63	13	Behind neutrino masses?	167	6.1	KamLAND	64	13.1	Neutrino electro-magnetic dipoles	168	6.2	Solar neutrinos	65	13.2	Neutrinos and light fermions	169	6.3	Solar neutrino experiments	67	13.3	Neutrinos and light scalars	174	6.4	Implications of solar data	72	13.4	Quantum corrections to neutrino masses .	176				13.5	Lepton-flavour violation and SUSY	177				13.6	Neutrinos in extra dimensions	180				14	Applications	185				A	Acronyms	186				B	Statistics	188				B.1	Statistical inference	188				B.2	Goodness-of-fit	193																																										
9.3	NuTeV	108																																																																																																																																																																																																									
4	Detecting neutrinos	44	10	Neutrinos in cosmology	111																																																																																																																																																																																																						
4.1	ν /electron scattering	44	10.1	Big-bang nucleosynthesis	112	4.2	ν /nucleon scattering	45	10.2	CMB and LSS	115	4.3	ν /nucleus scattering	48	10.3	Baryogenesis through leptogenesis	123	4.4	Neutrino detectors	50	11	Neutrinos in astrophysics	132	5	The atmospheric evidence	53	11.1	Neutrino sources	132	5.1	Atmospheric neutrinos	53	11.2	Core collapse supernovæ	135	5.2	SuperKamiokande	54	11.3	Effects of neutrino oscillations	144	5.3	Oscillations?	57	11.4	Observations of cosmic neutrinos	149	5.4	$\nu_\mu \rightarrow \nu_\tau$ or $\nu_\mu \rightarrow \nu_s$?	58	12	Understanding neutrino masses	152	5.5	K2K	58	12.1	The problem of the flavour problem	152	5.6	NuMI	60	12.2	In the search for a pattern	154	5.7	CHOOZ: $\nu_\mu \rightarrow \nu_e$?	60	12.3	Flavor symmetries	157	5.8	Reactor experiments	61	12.4	Testing flavour models	162	6	The solar evidence	63	13	Behind neutrino masses?	167	6.1	KamLAND	64	13.1	Neutrino electro-magnetic dipoles	168	6.2	Solar neutrinos	65	13.2	Neutrinos and light fermions	169	6.3	Solar neutrino experiments	67	13.3	Neutrinos and light scalars	174	6.4	Implications of solar data	72	13.4	Quantum corrections to neutrino masses .	176				13.5	Lepton-flavour violation and SUSY	177				13.6	Neutrinos in extra dimensions	180				14	Applications	185				A	Acronyms	186				B	Statistics	188				B.1	Statistical inference	188				B.2	Goodness-of-fit	193																																																						
10.1	Big-bang nucleosynthesis	112																																																																																																																																																																																																									
4.2	ν /nucleon scattering	45	10.2	CMB and LSS	115	4.3	ν /nucleus scattering	48	10.3	Baryogenesis through leptogenesis	123	4.4	Neutrino detectors	50	11	Neutrinos in astrophysics	132	5	The atmospheric evidence	53	11.1	Neutrino sources	132	5.1	Atmospheric neutrinos	53	11.2	Core collapse supernovæ	135	5.2	SuperKamiokande	54	11.3	Effects of neutrino oscillations	144	5.3	Oscillations?	57	11.4	Observations of cosmic neutrinos	149	5.4	$\nu_\mu \rightarrow \nu_\tau$ or $\nu_\mu \rightarrow \nu_s$?	58	12	Understanding neutrino masses	152	5.5	K2K	58	12.1	The problem of the flavour problem	152	5.6	NuMI	60	12.2	In the search for a pattern	154	5.7	CHOOZ: $\nu_\mu \rightarrow \nu_e$?	60	12.3	Flavor symmetries	157	5.8	Reactor experiments	61	12.4	Testing flavour models	162	6	The solar evidence	63	13	Behind neutrino masses?	167	6.1	KamLAND	64	13.1	Neutrino electro-magnetic dipoles	168	6.2	Solar neutrinos	65	13.2	Neutrinos and light fermions	169	6.3	Solar neutrino experiments	67	13.3	Neutrinos and light scalars	174	6.4	Implications of solar data	72	13.4	Quantum corrections to neutrino masses .	176				13.5	Lepton-flavour violation and SUSY	177				13.6	Neutrinos in extra dimensions	180				14	Applications	185				A	Acronyms	186				B	Statistics	188				B.1	Statistical inference	188				B.2	Goodness-of-fit	193																																																												
10.2	CMB and LSS	115																																																																																																																																																																																																									
4.3	ν /nucleus scattering	48	10.3	Baryogenesis through leptogenesis	123	4.4	Neutrino detectors	50	11	Neutrinos in astrophysics	132	5	The atmospheric evidence	53	11.1	Neutrino sources	132	5.1	Atmospheric neutrinos	53	11.2	Core collapse supernovæ	135	5.2	SuperKamiokande	54	11.3	Effects of neutrino oscillations	144	5.3	Oscillations?	57	11.4	Observations of cosmic neutrinos	149	5.4	$\nu_\mu \rightarrow \nu_\tau$ or $\nu_\mu \rightarrow \nu_s$?	58	12	Understanding neutrino masses	152	5.5	K2K	58	12.1	The problem of the flavour problem	152	5.6	NuMI	60	12.2	In the search for a pattern	154	5.7	CHOOZ: $\nu_\mu \rightarrow \nu_e$?	60	12.3	Flavor symmetries	157	5.8	Reactor experiments	61	12.4	Testing flavour models	162	6	The solar evidence	63	13	Behind neutrino masses?	167	6.1	KamLAND	64	13.1	Neutrino electro-magnetic dipoles	168	6.2	Solar neutrinos	65	13.2	Neutrinos and light fermions	169	6.3	Solar neutrino experiments	67	13.3	Neutrinos and light scalars	174	6.4	Implications of solar data	72	13.4	Quantum corrections to neutrino masses .	176				13.5	Lepton-flavour violation and SUSY	177				13.6	Neutrinos in extra dimensions	180				14	Applications	185				A	Acronyms	186				B	Statistics	188				B.1	Statistical inference	188				B.2	Goodness-of-fit	193																																																																		
10.3	Baryogenesis through leptogenesis	123																																																																																																																																																																																																									
4.4	Neutrino detectors	50	11	Neutrinos in astrophysics	132																																																																																																																																																																																																						
5	The atmospheric evidence	53	11.1	Neutrino sources	132	5.1	Atmospheric neutrinos	53	11.2	Core collapse supernovæ	135	5.2	SuperKamiokande	54	11.3	Effects of neutrino oscillations	144	5.3	Oscillations?	57	11.4	Observations of cosmic neutrinos	149	5.4	$\nu_\mu \rightarrow \nu_\tau$ or $\nu_\mu \rightarrow \nu_s$?	58	12	Understanding neutrino masses	152	5.5	K2K	58	12.1	The problem of the flavour problem	152	5.6	NuMI	60	12.2	In the search for a pattern	154	5.7	CHOOZ: $\nu_\mu \rightarrow \nu_e$?	60	12.3	Flavor symmetries	157	5.8	Reactor experiments	61	12.4	Testing flavour models	162	6	The solar evidence	63	13	Behind neutrino masses?	167	6.1	KamLAND	64	13.1	Neutrino electro-magnetic dipoles	168	6.2	Solar neutrinos	65	13.2	Neutrinos and light fermions	169	6.3	Solar neutrino experiments	67	13.3	Neutrinos and light scalars	174	6.4	Implications of solar data	72	13.4	Quantum corrections to neutrino masses .	176				13.5	Lepton-flavour violation and SUSY	177				13.6	Neutrinos in extra dimensions	180				14	Applications	185				A	Acronyms	186				B	Statistics	188				B.1	Statistical inference	188				B.2	Goodness-of-fit	193																																																																														
11.1	Neutrino sources	132																																																																																																																																																																																																									
5.1	Atmospheric neutrinos	53	11.2	Core collapse supernovæ	135	5.2	SuperKamiokande	54	11.3	Effects of neutrino oscillations	144	5.3	Oscillations?	57	11.4	Observations of cosmic neutrinos	149	5.4	$\nu_\mu \rightarrow \nu_\tau$ or $\nu_\mu \rightarrow \nu_s$?	58	12	Understanding neutrino masses	152	5.5	K2K	58	12.1	The problem of the flavour problem	152	5.6	NuMI	60	12.2	In the search for a pattern	154	5.7	CHOOZ: $\nu_\mu \rightarrow \nu_e$?	60	12.3	Flavor symmetries	157	5.8	Reactor experiments	61	12.4	Testing flavour models	162	6	The solar evidence	63	13	Behind neutrino masses?	167	6.1	KamLAND	64	13.1	Neutrino electro-magnetic dipoles	168	6.2	Solar neutrinos	65	13.2	Neutrinos and light fermions	169	6.3	Solar neutrino experiments	67	13.3	Neutrinos and light scalars	174	6.4	Implications of solar data	72	13.4	Quantum corrections to neutrino masses .	176				13.5	Lepton-flavour violation and SUSY	177				13.6	Neutrinos in extra dimensions	180				14	Applications	185				A	Acronyms	186				B	Statistics	188				B.1	Statistical inference	188				B.2	Goodness-of-fit	193																																																																																				
11.2	Core collapse supernovæ	135																																																																																																																																																																																																									
5.2	SuperKamiokande	54	11.3	Effects of neutrino oscillations	144	5.3	Oscillations?	57	11.4	Observations of cosmic neutrinos	149	5.4	$\nu_\mu \rightarrow \nu_\tau$ or $\nu_\mu \rightarrow \nu_s$?	58	12	Understanding neutrino masses	152	5.5	K2K	58	12.1	The problem of the flavour problem	152	5.6	NuMI	60	12.2	In the search for a pattern	154	5.7	CHOOZ: $\nu_\mu \rightarrow \nu_e$?	60	12.3	Flavor symmetries	157	5.8	Reactor experiments	61	12.4	Testing flavour models	162	6	The solar evidence	63	13	Behind neutrino masses?	167	6.1	KamLAND	64	13.1	Neutrino electro-magnetic dipoles	168	6.2	Solar neutrinos	65	13.2	Neutrinos and light fermions	169	6.3	Solar neutrino experiments	67	13.3	Neutrinos and light scalars	174	6.4	Implications of solar data	72	13.4	Quantum corrections to neutrino masses .	176				13.5	Lepton-flavour violation and SUSY	177				13.6	Neutrinos in extra dimensions	180				14	Applications	185				A	Acronyms	186				B	Statistics	188				B.1	Statistical inference	188				B.2	Goodness-of-fit	193																																																																																										
11.3	Effects of neutrino oscillations	144																																																																																																																																																																																																									
5.3	Oscillations?	57	11.4	Observations of cosmic neutrinos	149	5.4	$\nu_\mu \rightarrow \nu_\tau$ or $\nu_\mu \rightarrow \nu_s$?	58	12	Understanding neutrino masses	152	5.5	K2K	58	12.1	The problem of the flavour problem	152	5.6	NuMI	60	12.2	In the search for a pattern	154	5.7	CHOOZ: $\nu_\mu \rightarrow \nu_e$?	60	12.3	Flavor symmetries	157	5.8	Reactor experiments	61	12.4	Testing flavour models	162	6	The solar evidence	63	13	Behind neutrino masses?	167	6.1	KamLAND	64	13.1	Neutrino electro-magnetic dipoles	168	6.2	Solar neutrinos	65	13.2	Neutrinos and light fermions	169	6.3	Solar neutrino experiments	67	13.3	Neutrinos and light scalars	174	6.4	Implications of solar data	72	13.4	Quantum corrections to neutrino masses .	176				13.5	Lepton-flavour violation and SUSY	177				13.6	Neutrinos in extra dimensions	180				14	Applications	185				A	Acronyms	186				B	Statistics	188				B.1	Statistical inference	188				B.2	Goodness-of-fit	193																																																																																																
11.4	Observations of cosmic neutrinos	149																																																																																																																																																																																																									
5.4	$\nu_\mu \rightarrow \nu_\tau$ or $\nu_\mu \rightarrow \nu_s$?	58	12	Understanding neutrino masses	152																																																																																																																																																																																																						
5.5	K2K	58	12.1	The problem of the flavour problem	152	5.6	NuMI	60	12.2	In the search for a pattern	154	5.7	CHOOZ: $\nu_\mu \rightarrow \nu_e$?	60	12.3	Flavor symmetries	157	5.8	Reactor experiments	61	12.4	Testing flavour models	162	6	The solar evidence	63	13	Behind neutrino masses?	167	6.1	KamLAND	64	13.1	Neutrino electro-magnetic dipoles	168	6.2	Solar neutrinos	65	13.2	Neutrinos and light fermions	169	6.3	Solar neutrino experiments	67	13.3	Neutrinos and light scalars	174	6.4	Implications of solar data	72	13.4	Quantum corrections to neutrino masses .	176				13.5	Lepton-flavour violation and SUSY	177				13.6	Neutrinos in extra dimensions	180				14	Applications	185				A	Acronyms	186				B	Statistics	188				B.1	Statistical inference	188				B.2	Goodness-of-fit	193																																																																																																												
12.1	The problem of the flavour problem	152																																																																																																																																																																																																									
5.6	NuMI	60	12.2	In the search for a pattern	154	5.7	CHOOZ: $\nu_\mu \rightarrow \nu_e$?	60	12.3	Flavor symmetries	157	5.8	Reactor experiments	61	12.4	Testing flavour models	162	6	The solar evidence	63	13	Behind neutrino masses?	167	6.1	KamLAND	64	13.1	Neutrino electro-magnetic dipoles	168	6.2	Solar neutrinos	65	13.2	Neutrinos and light fermions	169	6.3	Solar neutrino experiments	67	13.3	Neutrinos and light scalars	174	6.4	Implications of solar data	72	13.4	Quantum corrections to neutrino masses .	176				13.5	Lepton-flavour violation and SUSY	177				13.6	Neutrinos in extra dimensions	180				14	Applications	185				A	Acronyms	186				B	Statistics	188				B.1	Statistical inference	188				B.2	Goodness-of-fit	193																																																																																																																		
12.2	In the search for a pattern	154																																																																																																																																																																																																									
5.7	CHOOZ: $\nu_\mu \rightarrow \nu_e$?	60	12.3	Flavor symmetries	157	5.8	Reactor experiments	61	12.4	Testing flavour models	162	6	The solar evidence	63	13	Behind neutrino masses?	167	6.1	KamLAND	64	13.1	Neutrino electro-magnetic dipoles	168	6.2	Solar neutrinos	65	13.2	Neutrinos and light fermions	169	6.3	Solar neutrino experiments	67	13.3	Neutrinos and light scalars	174	6.4	Implications of solar data	72	13.4	Quantum corrections to neutrino masses .	176				13.5	Lepton-flavour violation and SUSY	177				13.6	Neutrinos in extra dimensions	180				14	Applications	185				A	Acronyms	186				B	Statistics	188				B.1	Statistical inference	188				B.2	Goodness-of-fit	193																																																																																																																								
12.3	Flavor symmetries	157																																																																																																																																																																																																									
5.8	Reactor experiments	61	12.4	Testing flavour models	162	6	The solar evidence	63	13	Behind neutrino masses?	167	6.1	KamLAND	64	13.1	Neutrino electro-magnetic dipoles	168	6.2	Solar neutrinos	65	13.2	Neutrinos and light fermions	169	6.3	Solar neutrino experiments	67	13.3	Neutrinos and light scalars	174	6.4	Implications of solar data	72	13.4	Quantum corrections to neutrino masses .	176				13.5	Lepton-flavour violation and SUSY	177				13.6	Neutrinos in extra dimensions	180				14	Applications	185				A	Acronyms	186				B	Statistics	188				B.1	Statistical inference	188				B.2	Goodness-of-fit	193																																																																																																																														
12.4	Testing flavour models	162																																																																																																																																																																																																									
6	The solar evidence	63	13	Behind neutrino masses?	167																																																																																																																																																																																																						
6.1	KamLAND	64	13.1	Neutrino electro-magnetic dipoles	168	6.2	Solar neutrinos	65	13.2	Neutrinos and light fermions	169	6.3	Solar neutrino experiments	67	13.3	Neutrinos and light scalars	174	6.4	Implications of solar data	72	13.4	Quantum corrections to neutrino masses .	176				13.5	Lepton-flavour violation and SUSY	177				13.6	Neutrinos in extra dimensions	180				14	Applications	185				A	Acronyms	186				B	Statistics	188				B.1	Statistical inference	188				B.2	Goodness-of-fit	193																																																																																																																																										
13.1	Neutrino electro-magnetic dipoles	168																																																																																																																																																																																																									
6.2	Solar neutrinos	65	13.2	Neutrinos and light fermions	169	6.3	Solar neutrino experiments	67	13.3	Neutrinos and light scalars	174	6.4	Implications of solar data	72	13.4	Quantum corrections to neutrino masses .	176				13.5	Lepton-flavour violation and SUSY	177				13.6	Neutrinos in extra dimensions	180				14	Applications	185				A	Acronyms	186				B	Statistics	188				B.1	Statistical inference	188				B.2	Goodness-of-fit	193																																																																																																																																																
13.2	Neutrinos and light fermions	169																																																																																																																																																																																																									
6.3	Solar neutrino experiments	67	13.3	Neutrinos and light scalars	174	6.4	Implications of solar data	72	13.4	Quantum corrections to neutrino masses .	176				13.5	Lepton-flavour violation and SUSY	177				13.6	Neutrinos in extra dimensions	180				14	Applications	185				A	Acronyms	186				B	Statistics	188				B.1	Statistical inference	188				B.2	Goodness-of-fit	193																																																																																																																																																						
13.3	Neutrinos and light scalars	174																																																																																																																																																																																																									
6.4	Implications of solar data	72	13.4	Quantum corrections to neutrino masses .	176				13.5	Lepton-flavour violation and SUSY	177				13.6	Neutrinos in extra dimensions	180				14	Applications	185				A	Acronyms	186				B	Statistics	188				B.1	Statistical inference	188				B.2	Goodness-of-fit	193																																																																																																																																																												
13.4	Quantum corrections to neutrino masses .	176																																																																																																																																																																																																									
			13.5	Lepton-flavour violation and SUSY	177				13.6	Neutrinos in extra dimensions	180				14	Applications	185				A	Acronyms	186				B	Statistics	188				B.1	Statistical inference	188				B.2	Goodness-of-fit	193																																																																																																																																																																		
13.5	Lepton-flavour violation and SUSY	177																																																																																																																																																																																																									
			13.6	Neutrinos in extra dimensions	180				14	Applications	185				A	Acronyms	186				B	Statistics	188				B.1	Statistical inference	188				B.2	Goodness-of-fit	193																																																																																																																																																																								
13.6	Neutrinos in extra dimensions	180																																																																																																																																																																																																									
			14	Applications	185																																																																																																																																																																																																						
			A	Acronyms	186																																																																																																																																																																																																						
			B	Statistics	188																																																																																																																																																																																																						
			B.1	Statistical inference	188				B.2	Goodness-of-fit	193																																																																																																																																																																																																
B.1	Statistical inference	188																																																																																																																																																																																																									
			B.2	Goodness-of-fit	193																																																																																																																																																																																																						
B.2	Goodness-of-fit	193																																																																																																																																																																																																									